Understanding the information content of night-time light satellite data for modelling socio-economic dimensions of global change

by

Christopher Nicholas Hideo DOLL

Submitted in partial fulfilment of the requirements for the degree of
Doctor of Philosophy

Department of Geomatic Engineering,

University College London.

April 2003.

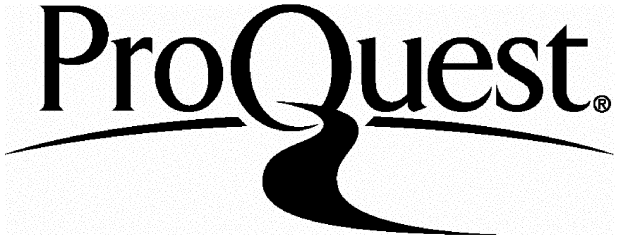

This thesis is dedicated to my parents.
They have always supported me in whatever I chose to do and have fostered a belief that subject to my best efforts, nothing is beyond me.

Acknowledgements

A great debt of thanks must firstly go to my principal supervisor Professor Jan-Peter Muller not only for his constant guidance and innumerable suggestions but also for his pro-active monitoring of the research area, which has afforded me many leads and opportunities throughout the course of the project. I am also very grateful to my second supervisor Jeremy Morley for his advice with the Geographical Information System aspects of the project and his methodical, scrupulous comments on my draft chapters. I also wish to thank the head of the Department of Geomatic Engineering, Professor Paul Cross for the financial support he has afforded me through the department to attend international conferences where I could present my research.

The night-time light data products used in this thesis were processed and supplied by Chris Elvidge and his team at NOAA-NGDC in Boulder, Colorado, USA. Thanks to their efforts, a host of scientists around the world are discovering a wide range of new applications for remotely sensed data.

This PhD was supported by the Natural Environmental Research Council (NERC) studentship award GT 04/98 188/TS.

The friendship and support of Simon Bailey, Gordon Bentley, Andrew Wayne, Tim Wilkinson and Helen Papadaki are greatly appreciated. Finally, to my family, who have supported me in every way possible and to whom I owe more than words can say.

Abstract

This thesis explores the ways in which Earth Observation data can be used to provide information about the human dimensions of global change. After setting out the key themes in global change research, attention is focused on the contribution data from satellite remote sensing systems can make to the detection of human impacts on the Earth's surface. Data sources include night-time light imagery from the Defense Meteorological Satellite Program's Operational Linescan System (DMSP-OLS), radar interferometry and new data products from the Moderate Resolution Imaging Spectroradiometer (MODIS), part of the National Aeronautic and Space Administration's Earth Observing System.

Night-time light imagery was analysed with respect to its capability to provide information on population, economic activity (via the Gross Domestic Product - GDP) and carbon dioxide emissions. Using different levels of sub-national economic data from the European Commission's statistical organisation Eurostat, relationships between radiance and GDP were established. This introduced issues concerning the Modifiable Areal Unit Problem and the Ecological Fallacy, which have been discussed in relation to the problem. These correlations were very high and anomalies could be categorized into three different types. Disaggregated maps of economic activity at 5km resolution have been produced for 11 countries in the European Union as well as for the conterminous United States using these relationships. The results gained from this exercise are highly encouraging with most countries being mapped to within 5% of the published national GDP figure.

This thesis provides a timely contribution to the debate on the human dimensions of global change at a time when international organisations are in the process of identifying the best ways to proceed with the monitoring and modelling of its impacts. The results and recommendations offer a great deal of encouragement for further research and sets the scene for the explicit monitoring of human attributes from remote sensing data.

Table of Contents

List of Figures

List of Tables

Chapter 1

Introduction

This is a broad ranging thesis incorporating the themes of global change, remote sensing and GIS technology ultimately to produce consistent datasets describing evidence of human activities, for use in global change studies. In doing so, different aspects of current remote sensing technology are presented and evaluated in terms of what they can contribute to the aims of the study. The first part of the introduction is a general discussion of the main issues considered in the thesis leading to the statement of the title and the formulation of the aims. The methods employed to investigate these aims will then be described followed by a chapter-by-chapter overview of the thesis.

Remote sensing is the science of acquiring, processing and interpreting information about an object from a sensor not directly in contact with it. This term is most often used in the context of Earth Observing (EO) satellites. A number of writers and scientists have explored how observations of the Earth's surface could be interpreted (Levy, 1990; Sagan, 1993; Lovelock, 2000). Levy's (1990) philosophical tale draws logical but incorrect conclusions about the Earth's urban environment deduced from an alien point of view. Sagan *et al.* (1993) investigated the general remotely sensed characteristics of the Earth from the perspective of treating the Earth as an unexplored planet in the solar system. Making no assumptions as to the composition of the Earth, Sagan *et al.* (1993) described how observable features such as the red edge of reflectance in the visible part of the electromagnetic (EM) spectrum, atmospheric chemistry and circulation observations strongly suggest that conditions were favourable for the presence of life on Earth. Furthermore, the detectable presence of narrow band, pulsed, amplitude modulated radio transmission was cited as uniquely attributable to intelligent life. Although the treatise of Sagan *et al.* (1993) was intended as a control experiment for the search for extra-terrestrial life

by the Galileo interplanetary spacecraft, it is the detection and inference of activities from this human element of the global environment that sets the scene for this thesis.

1.1 Anthropogenic elements of global change

Remote sensing activities have traditionally been concerned with the mapping and monitoring of physical elements of our environment. Starting with weather satellites launched in the 1960s to sensors tuned to detect biophysical land surface features, remote sensing data can make valuable contributions to large scale monitoring of physical processes whether they exist on land, sea or in the atmosphere. Archived datasets of such information are of great importance to researchers who study the causes and effects of global change. Indeed, the term global change is itself a neat description of the benefit environmental remote sensing technology can provide. Given that we can now find out so much about the physical environment, the next challenge is to develop means for remote sensing to contribute to the 'anthroposphere'. This thesis is intended to be a step in this direction.

Evidence of humanity's influence on the environment has been gradually increasing since humans first started to settle and build societies. The development of tools for agriculture and industry has resulted in this influence having an effect on every natural system on Earth. Broadly speaking anthropogenic effects on the Earth can be split into a number of areas, listed below. Although, they are listed as separate points, it will hopefully become apparent that these factors are linked together and a change in one is likely to affect at least one of the others.

1.1.1 Land use change

Vitousek *et al.* (1997) estimated that between 30-50% of the Earth's land surface has been altered by human action. The classical economic development model of a country shifting from a primarily agrarian economy to an industrial and then to a post-industrial state is largely driven through the process of urbanisation. Levels of

urban population for 2000 vary from an average of 79% for high-income countries (per-capita GNP > $9,266) to 31% for low-income countries (per-capita GNP < $755) (UNDP, 2002), although the annual growth rate at which urbanisation in low-income countries is occurring is more than 7 times that of industrialized countries for the period 1995-2015 (UN-HABITAT, 2001). Despite their increasing proportion of the total population, cities take up a small fraction of the total land surface. The bulk of human induced land alteration involves the transformation of lands for cultivation and forestry.

1.1.2 Pollution

Pollution from industrial processes takes many forms and has detrimental effects on the surrounding land and water resources as well as on air quality. The widespread use of nitrogen based fertilizers in intensive farming means that more nitrogen is artificially fixed than occurs naturally in terrestrial ecosystems. Likewise the combustion of fossil fuels releases far higher quantities of aerosols, sulphur dioxide and nitrogen oxides than would otherwise be the case. Such emissions not only have detrimental effects on human health where they contribute to smog events over urban areas but also play an increasingly important role in modifying the Earth's climate. Of most significance in a global context is the emission of carbon dioxide (CO_2) into the atmosphere from the burning of fossil fuels.

1.1.3 Resource depletion

A consequence of the pervasive aggrandisement of urban areas is that greater numbers of people are demanding resources from an area. The management of resources will therefore play an important role in the overall development of these areas. The supply of fresh water is becoming an increasingly more critical issue around the world, whilst the effectiveness of waste management schemes is also gaining in importance as the consumption of goods increases. The increase in global demand for energy rivals the availability of water as a cause for concern. The year-

on-year increase in fossil fuel usage has stimulated debates not only on increased energy efficiency but also on wholesale changes in the way we generate energy.

1.1.4 Climate change

The most important overarching theme to all these effects is that of climate change. The effect of large-scale emission of CO_2 has been estimated to result in a possible global mean temperature increase of between 1.4°C and 5.8°C (IPCC, 2002a) between 1990-2100. Climate change can be seen as a general driver for other manifestations of global change. Such an increase in temperature could lead to an array of environmental changes. Climate change in itself may cause shifts in land cover, for example semi-arid areas turning arid (desertification), and expansion of the growing season. In a warmer world sea level rise would inundate many coastal areas and low-lying islands could disappear altogether. Given that the bulk of the world's population centres have a coastal location, this implies future problems of large-scale population migration. Individual countries may be unable to cope with such an impact, which has the potential to cause political regional instability.

Individual component changes do not necessarily act in the same sense but can reinforce or offset other changes in the climate system. The role of clouds for example, can both warm and cool the Earth's atmosphere. In the case of desertification, a biogeophysical feedback mechanism exists where increasing albedo (reflectance, see chapter 4) causes a decrease in rainfall, which could induce or perpetuate drought conditions (Charney, 1975). Earth System modellers focus on trying to describe these processes in complex models, but the human dimensions of these is frequently overlooked.

The central role mankind plays on climatic and ecological processes has resulted in the term 'the anthropocene' being used by some to describe a new geological epoch, the origin of which, coincides with the Industrial Revolution (Crutzen and Stoermer, 2000). Human activity as a component of global change is under-represented in current global change research efforts. Whilst the effects on the natural environment

are investigated, there is often little consideration given to human processes which give rise to these perturbations. This is partly due to global change research stemming from a consideration of the interactions between the elements of the physical environment (land-ocean-atmosphere). It is also partly due to a paucity of data with which to provide modellers. More recently, attention is beginning to be focused on human-environment interactions. The initial questions being asked in this area will require at least a basic description of socio-economic data. Remote sensing data has the potential to provide some of these kinds of data at an enhanced resolution above what is currently available. The research presented here is set in the framework of such information making a contribution to current research efforts being made in the human dimensions of global change (HDGC). The technology combined with its application is summed up in the thesis title:

'Understanding the information content of night-time light satellite data for modelling socio-economic dimensions of global change'

This topic is investigated based on the following set of underpinning questions:

- Which aspects of remote sensing can be used in conjunction with night-time light data to detect the human fingerprints across the Earth's surface?
- How can these signals be interpreted to provide calibrated, quantitative information about human activity which is not currently available from EO data?
- How does this contribute to our understanding of global human impact on the environment?

These questions are intended to aid in the formulation of the aims, as well as to guide the interpretation of results generated from the research.

1.2 Data sources, methods and development of the aims

The wide scope of this thesis requires a number of different aspects of global change research to be reviewed. The approach used to investigate the subject of this thesis firstly involves an examination of the human dimensions of global change along with its definition, status of understanding and the political initiatives which define its data requirement. Having established a conceptual framework for the study, attention is turned to the remote sensing techniques that can contribute to the detection and analysis of anthropogenic activity. Anthropogenic activity is concentrated in urban areas. They are the nodes of human interaction and provide a focus for trade and exchange of ideas. As such they form a key element of the thesis. The potential of remotely sensed data sources to provide information about urban settlements is examined first, followed by an investigation to develop methods to infer higher-level anthropogenic information about those areas. Higher-level anthropogenic information refers to attributes of a settlement other than its spatial extent, which cannot be directly measured from satellite data, such as population, Gross Domestic Product (GDP) and CO_2 emissions.

In particular, this thesis concentrates on the use of night-time light imagery from the Defense Meteorological Satellite Programme's Operational Linescan System (DMSP-OLS). Night-time light imagery provides the most readily understandable representation of humanity's presence on Earth. From city-lights through to gas flaring in the North Sea and biomass burning in sub-Saharan Africa, human activity can be seen on every continent. To complement this uniquely human source of remotely sensed data, the use of radar interferometry to provide a different perspective on the built environment is also considered. The comprehensive array of data products from the Moderate Resolution Imaging Spectroradiometer (MODIS) are also evaluated with respect to their capacity to map anthropogenic activity, and how they relate to information derived from night-time light data. One dataset of particular interest is the BRDF/Albedo product. Albedo plays a vital role in the surface energy exchange of solar radiation and as such is crucial in evaluating the effect of urbanisation on regional climate. The creation of dedicated products from

new sensors as a means of building an archive of key land surface parameters signify the importance that remote sensing will play in the effort to study global change.

Studies have shown that night-time light imagery from the DMSP-OLS sensor has the potential to provide information on a wide range of human activities (Elvidge et al, 1997a; Doll, 1998; Doll *et al*, 2000). The remainder of the thesis (chapters 5-7) examines night-time light imagery as a means of understanding the relationship between light characteristics and socio-economic parameters (anthropogenic activity) such as population, GDP, power consumption and CO_2 mapping, with a view to estimating their values through a disaggregated map. This section will draw heavily on Geographical Information System (GIS) analysis to process and analyse the data. This is partly due to the integration of ancillary statistical data sources from the European Union (EU) and the requirement to match satellite data to administrative boundaries. The concept of spatial scale plays an important role in this section, especially in the interpretation and presentation of results. In general, the relevance of scale to HDGC is huge, not least because its meaning and treatment varies between the satellite disciplines of HDGC. The diversity of disciplines incorporated in HDGC research means that scale can have quantitative and analytical dimensions in addition to spatio-temporal domains (Gibson *et al.*, 2000). The following aims for the thesis were defined bearing this discussion in mind:

i) to examine the capability of RS data sources to contribute to the expanding toolchest of techniques for settlement mapping;
ii) to investigate the capability of night-time light imagery to infer information about human activity over and above what is currently available from existing remote sensing resources;
iii) to frame these results in a format, which can be of use to researchers investigating the human dimensions of global change.

The third aim essentially deals with making socio-economic parameters accessible to be used in conjunction with other sources of global environmental data. As a large proportion of these data are already obtained in a gridded format from EO satellites, it is desirable to generate products which are also in this format. Socio-economic data is usually provided on a national basis. Whilst this is a convenient administrative unit to collect the data, it may be an inappropriate unit on which to conduct large-scale environmental analysis. A major advancement would be to provide the scientific community with socio-economic datasets on a regular grid format. This fundamental difference in data collection methods is one of the major obstacles preventing more widespread integration of socio-economic datasets with environmental datasets. Raster datasets also offer the flexibility to perform analysis at more convenient aggregated spatial units such as ecological zones or watersheds rather than nation states. Finally, its gridding has considerable advantages for analytical studies.

In the night-time lights dataset, remote sensing stands uniquely poised to contribute to providing gridded information on socio-economic parameters. This comes at a time when debate as to what are the socio-economic drivers of global change and how these can be best represented is gaining currency amongst global change research scientists. This thesis intends to make a timely contribution to that debate.

1.3 Overview of the thesis

Chapter 2 reviews the current state of global change research highlighting what are the current themes and driving concepts within the discipline. This identifies the need and the 'end-user' of any output.

Chapter 3 reviews the different kinds of remotely sensed data, which may be used to meet the requirements set out in chapter 2. Remote sensing technology is the central theme to the whole thesis. Without it there would be nothing to feed into the

GIS analysis downstream and the global change modelling and monitoring community would be deprived of an important data-source.

Chapter 4 presents results from studies using remote sensing techniques outlined in chapter 3. These include radar interferometry and land-surface products from the MODIS sensor. These are evaluated in conjunction with night-time light imagery and other urban indicators.

Chapter 5 examines the capability of night-time light imagery to predict human population figures at the country level. Results are directly compared with those from a similar study made by Sutton *et al.* (2001). The chapter goes on to develop ideas about population morphology within cities and concludes with a description of the Landscan project, which uses night-time light imagery as an input dataset to produce a global population map at 30 arcseconds (30'').

Chapter 6 reports the results of comparing total night-time radiance to Gross Regional Product (a term used to describe a regional contribution to the Gross Domestic Product) and power consumption at the regional level for 11 European Union countries as well as the United States. This analysis is designed to derive relationships between radiance and economic activity. This process will also identify those few areas which do not fit a model. These areas can then be dealt with more suitably in the final map product.

Chapter 7 discusses results from mapping exercises using night-time light imagery. In addition to coarse resolution (1°x1°) maps of GDP and CO_2 emissions, the results of finer resolution maps derived from sub-national analysis of radiance and economic activity in chapter 6 are also presented. These represent the final products of the thesis, having been through the process of analysing the information content in relationships to produce a map that is of use to researchers working in the human dimensions of global change driven by the requirements identified in chapter 2.

Chapter 8 reports and synthesises the conclusions from each chapter and comments on further avenues of research, which would build upon the existing body of knowledge obtained from the thesis.

There are six appendices which accompany this thesis. Appendix A contains notes associated with Chapter 2. Further explanations and examples of figures from Chapters 3 and 4 are listed in Appendix B, whilst data tables from Chapters 5, 6 and 7 are in Appendices C, D and E respectively. A list of publications produced during the course of the thesis along with copies of those where C.N.H. Doll is the first-named author is to be found in Appendix F.

Chapter 2

Literature review (1): A review of global change theories and programmes

The term 'global change' is an umbrella term used to describe the wider impacts arising from, and associated with climate change. Climate change occupies a central place in global change research since it has wide-ranging impacts on both the physical and human environment. The detection of climate change and the identification of its causes have stimulated research into the description and modelling of the Earth's climate system. As we have improved our understanding of the interaction of the atmosphere, biosphere and oceans, these various disciplines have evolved into what we now term Earth System Science (ESS). Figure 2-1 shows the key elements of the Earth system and how they relate to one another.

Through a discussion of climate change, this chapter begins to explore the range of responses society can make to environmental change. The discussion of key issues such as societal vulnerability and adaptability transcends the climate change problem and forms the core of what is now being termed the 'human dimensions of global change' (HDGC). The concept of sustainability is believed to present the best chance for a society to adapt successfully or mitigate the effects of climate change. However, how this is achieved is subject to debate especially with regard to developing countries, where levels of poverty can be high. Taking sustainability as the goal, global change research programmes are presented with a view to identify what the current level of understanding is within global change research and where the focus of future research lies. This is framed by 23 questions (Schellnhuber and Sahagian, 2002) covering topics such as improving understanding of processes, integration of disciplines and the conceptual underpinning of global change research. This chapter concludes by examining two projects, which aim to use the results of global change research for wider dissemination and as an input into regional policy decision-making.

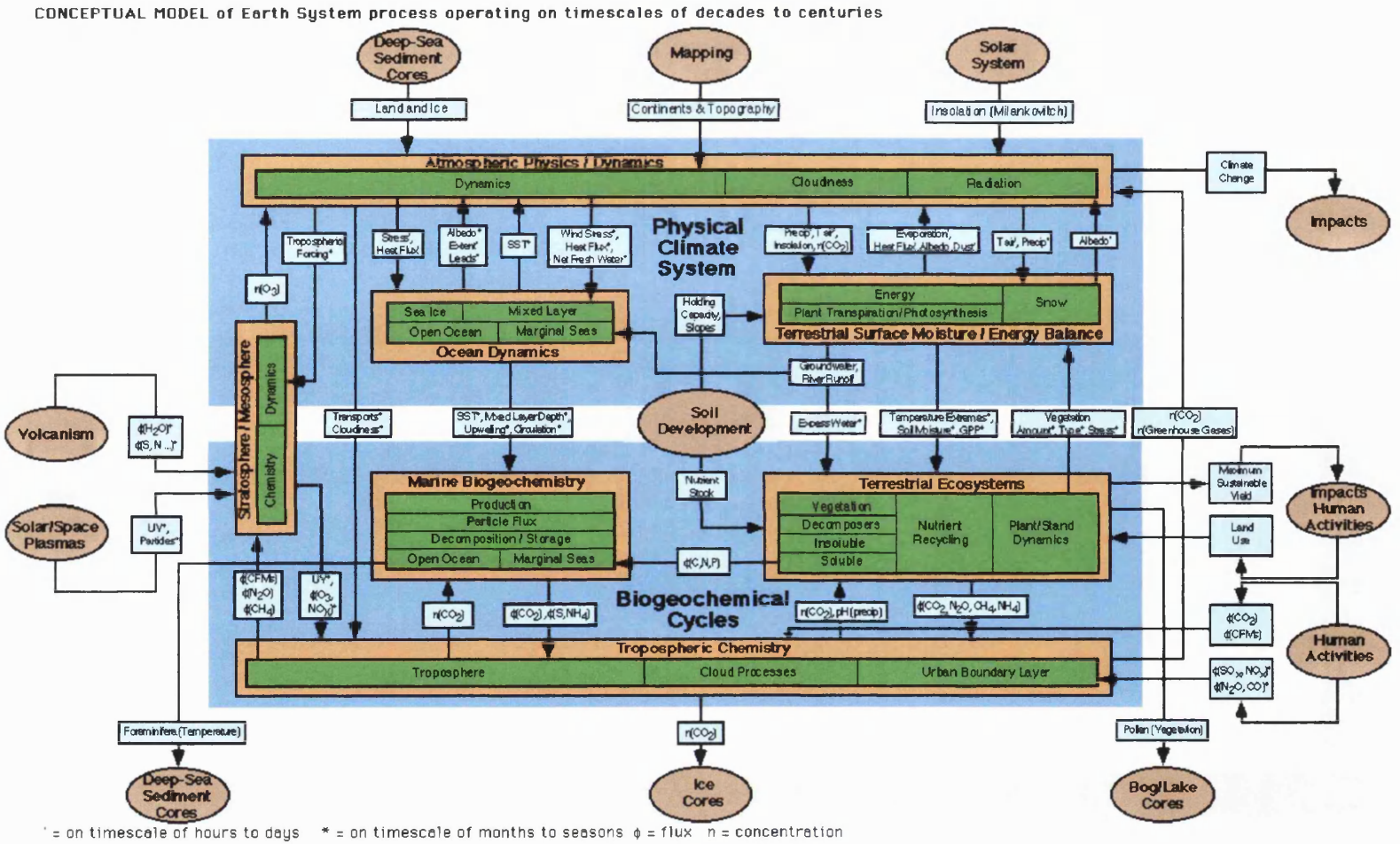

Figure 2-1 Schematic diagram of the Earth system after Bretherton in Schellnhuber (1999). Available from: http://www.usra.edu/esse/BrethColor.GIF

2.1 Climate change scenarios and responses

The potential impacts of global climate change along with concerns over the uncertainties in climate prediction prompted the establishment of the Intergovernmental Panel on Climate Change (IPCC) in 1988. This was done under the auspices of the United Nations Environment Programme (UNEP) and the World Meteorological Organization. The IPCC consists of three working groups (WG), which between them cover all aspects of climate change starting with the scientific basis (WG I), the impact, vulnerability and adaptation of both human and natural systems (WG II) through to the mitigating options available to abate climate change (WG III). The human component (causes and consequences) of climate change is a central theme of the IPCC.

2.1.1 Background

The state of the global climate system has varied throughout Earth's history. Over the last 1,000,000 years the Earth's climate has been characterised by ice ages lasting on the order of 100,000 years with inter-glacial periods of around 15,000 years. The Earth's orbit is known to vary in its eccentricity, angle of tilt and time of perihelion. These cyclic variations have periods of 100,000, 41,000 and 23,000 years respectively (Houghton, 1997). The total amount of radiation received by the Earth is largely determined by the eccentricity of the Earth's orbit, whilst the other two parameters determine how this radiation is distributed over the Earth's surface. When combined, these variables exert a profound effect on global temperatures (Lowe and Walker, 1997). Serbian geophysicist Milutin Milankovic observed the correlation between these cycles and ice ages and produced a theory of astronomically forced climatic variation.

Further information about the state of the environment during glacial periods has also been obtained from ice-cores. Data obtained from polar ice-cores have provided information on atmospheric composition by examining the gases trapped in air

bubbles. Cores drilled in both the Arctic and the Antarctic have revealed that carbon dioxide (CO_2) concentrations were significantly lower during glacial periods than during interglacial periods. More importantly there is a very strong correlation between concentrations of CO_2, methane (another important greenhouse gas) and retrieved temperatures suggesting that these parameters are very closely linked (Houghton, 1997).

Carbon dioxide is central to the current climate change debate because its atmospheric concentration is increasing at an unprecedented rate. CO_2 is released during the combustion of fossil fuels and also in the production of cement; both of these are fundamental to the industrial economy of the world. Since the beginning of the industrial revolution towards the end of the 18^{th} century, CO_2 emissions have steadily increased from 270 ppmv (parts per million by volume) towards around 380 ppmv now. Whilst there are other greenhouse gases, their emission and atmospheric concentration are minuscule in comparison. Industrial processes not only emit gases but also aerosols which, when in the stratosphere, are good reflectors of incoming solar radiation and can offset some of the warming caused by greenhouse gases. Lower down in the troposphere, aerosol particles can act as nuclei for cloud formation, which depending on their type, play key roles in both reflecting incoming and trapping outgoing radiation. Their atmospheric lifetime is short however, in contrast to CO_2 whose atmospheric lifetime can range between 50-200 years (IPCC, 2001a). This variation is caused by uncertainties in the sources and sinks of the carbon cycle. The global carbon cycle is characterised by natural fluxes between the ocean, atmosphere and terrestrial vegetation. Schimel *et al.*, (2001) have analysed temporal and spatial patterns of carbon sinks. Considerable uncertainty exists in the year-to-year variability of sinks and in particular the amount of carbon uptake of new forests as opposed to mature forest. The variable lifetime of CO_2 causes lags in the carbon cycle, which affects the stabilization time of CO_2 in the atmosphere after emissions have stopped increasing. In particular, temperature increases have been shown to lag even further behind CO_2 stabilisation, with temperatures predicted to increase for a century or more over the stabilisation time (IPCC, 2001b). Over the

last century temperatures have been rising steadily (+0.6° ± 0.2°) and there is growing evidence that the observed warming over the last 50 years is attributable to human activities with the 1990s likely to be the warmest decade of the instrumental record (IPCC, 2001b). This final observation is crucial because it launches a route of inquiry that acknowledges human activity as an agent of climate change and therefore, a means of controlling its effects.

2.1.2 The IPCC Third Assessment Report 2001 and the Kyoto Protocol

The IPCC Third Assessment Report (TAR) of climate change has come at a critical time in international solidarity on adopting mitigating measures to battle global warming. Whilst there is decreasing doubt of the fact that human activity can alter the Earth's climate, there remains a vigorous debate over what the magnitude of this change might be. This is due to the complexity of modeling the climate system resulting in a wide range of predictions from different researchers with high levels of uncertainty. The TAR concluded that an increase in temperature of between 1.4°C and 5.8°C is possible over the period 1990-2100. This range of temperature increase has been calculated according to a number of scenarios that have been developed to model future greenhouse gas emissions. These scenarios stem from four quantitative storylines (Table 2-1), which make assumptions on global population, gross world product and social organisation.

Within each family is a range of scenario groups which characterise alternative development technologies from fossil fuel intensive to predominantly non-fossil fuel regimes. Each family has an illustrative marker scenario e.g. the A1B marker scenario which describes the A1 family with balanced use of fossil and non-fossil fuels; there are 40 different emission scenarios in all. By designing such scenarios, other parameters such as the cost of adaptation and mitigation can be calculated. The economic impacts are estimated to be negative for many developing countries for all magnitudes of global mean temperature increase studied (IPCC, 2001b).

Table 2-1 Description of the four storylines used to derive emissions scenarios (IPCC, 2000).

Scenario Family	*Description*
A1	Very Rapid Economic growth, global population peaks in mid-century and then declines. Increased social and cultural interactions accompany convergence of per-capita income and rapid introduction of new and more efficient technology
A2	Heterogeneous world. Self-reliance and preservation of local identities. Continuously increasing global population. Economic development is primarily regionally orientated and per-capita economic growth and technological change are more fragmented than in other storylines
B1	Same population as in A1, rapid changes in economic structures toward a service and information economy is accompanied by the introduction of clean, resource efficient technologies. Emphasis on global solutions to economic, social and environmental sustainability but without and further climate initiatives.
B2	Emphasis on local solutions to economic, social and environmental sustainability. Continuously increasing global population but slower than A2. Intermediate levels of economic development and less rapid but more diverse technological change than B1 and A1 storylines.

The path that the global community decides to adopt depends very much on the decisions taken at key summits like the Kyoto summit in 1997, from which the Kyoto Protocol on climate change was drafted. The Kyoto Protocol was signed with the aggregate aim of reducing greenhouse gas emissions to within at least 5% of their 1990 levels during the commitment period 2008-2012 (UNFCCC, 1997). The protocol has a number of interesting features, the discussion of which has caused huge controversy with regard to its effectiveness in tackling the reduction in emissions of those countries that emit the greatest amounts of CO_2. The heavy reliance of industrialised countries (termed Annex I countries in the protocol) on fossil fuels means that a reduction in their usage will be costly to their economies.

An economic solution to this was proposed whereby a country bounded by a Quantified Emissions Limitation Reduction Objective (QELRO) could embark on a joint implementation strategy (JI). The rationale behind this is that it doesn't matter where the emission reductions come from, so long as there is an overall aggregate

reduction. Consequently, it is most efficient to seek reductions where it is cheapest to do so. There still remains differences over how freely an Annex I country can use JI, with the US favouring complete market freedom and the EU restricting JI to defined regional areas with only those countries bound by a QERLO participating. The GDP losses range from $346 billion/year if no trading is allowed to $75 billion/year if global trading is permitted for Annex I countries (Lomborg, 2001). Global emission trading is the cheapest way of reaching the emission target. However, if unrestricted trading was conducted, the United States, Canada and Japan could effectively increase their emissions by 10-15% above 1990 levels (Grubb et al, 1999).

This degree of flexibility has outraged proponents of emission reductions arguing that those who pollute most can still buy the right to pollute. Additionally by purchasing emission permits from developing countries, it may retard their own development path. The level of the reduction has also been attacked from both sides for not being stringent enough, and for costing so much for only a marginal gain. Lomborg (2001) claims the mitigation will be only 0.15°C by 2100. Lomborg himself has been widely criticized for misrepresenting the climate change problem and environmental issues in general. Rennie *et al.* (2002) attack Lomborg for selectively citing references, which are unrepresentative of the collective knowledge on a given issue. Whilst pointing to the large degree of uncertainty in future temperature increases, Lomborg confidently states the 0.15°C reduction figure with no error margin. Indeed. this figure assumes no further reductions from climate treaties beyond the Kyoto Protocol.

Those working in the energy industry are particularly vociferous about the perceived flaws in the protocol, regarding both the subjective nature of the Kyoto reduction target as well as the fundamental science published by the IPCC. Detractors point to the predominantly urban location of measuring stations as source of bias in the observation of increasing temperature. The Global Climate Coalition (GCC, 2001) is a group committed to the rejection of the Kyoto Protocol by the US Government,

preferring instead to develop new technologies to reduce emissions. Although now deactivated, it was a highly active (and ultimately effective) group lobbying the US Congress against reductions in fossil fuel consumption. The GCC was well funded by 69 energy and industrial organizations, which enabled them to spend $13 million on their anti-Kyoto advertisement campaign. This is more than the entire annual budget of Greenpeace (PRwatch, 2002). In particular, the IPCC was attacked for 'scientifically cleansing' their assessment of the human influence on climate change as being discernible (Masood, 1996). The subsequent rewording of the IPCC assessment to present a strong message to policy makers despite the lack of any new science has also been noted by others (Pearce, 2001). Lomborg (2001) has further suggested that the IPCC have a hidden agenda to subvert the political process by using climate change as a vehicle to bring about change in social and economic infrastructures.

2.1.3 Responses: Adaption versus Mitigation

The effects of climate change are not exclusively negative. Myneni *et al.* (1997) detected an increased growing season in the northern high latitudes between 1981-1991 through analysis of the normalised difference vegetation index (NDVI) measurements made from satellite data. Whilst the global effect is small, it is highly significant at the regional scale. However, Fischer *et al.* (2001) report that negative regional effects will have a disproportional impact on developing countries that have fewer adaptive choices. Whilst Canada and Russia may be able to produce an extra 130 million tonnes through cultivation of land that was once permafrost, developing countries could lose around 280 million tonnes of potential cereal production in the 2080s. The IPCC (2001b) mention that even for developed nations, negative impacts will overwhelm the positive impacts such that any economic gain would be wiped out by the cost of adaptation for other downstream effects. The IPCC TAR concludes that greater temperature increases and quicker rates of change in the

future will cause adverse effects to predominate. In the case of Europe and the US, this is most likely to manifest itself through water scarcity.

In addition to global mean temperature increase, an intensification of the hydrological cycle is also anticipated resulting in a general increase in rainfall and extreme events. Cereal crop models indicate that in some temperate areas, yields would increase in response to a small temperature increase but would decrease in response to a large temperature increase (IPCC, 2001b).

There is only medium to low confidence in the statements made about the effects of increasing temperature on Gross Domestic Product (GDP). This is one of the most difficult effects to model accurately, as the adaptations a country can make are various and not always solely under the control of its government. This is especially true for developing countries and their relationship with international financial institutions. The uncertainty associated with the predicted effects of climate change is a cause of increasing contention among policy makers; the impacts of a changing climate on the human environment can be positive in one location and negative in another.

The scientific uncertainties presented in the IPCC report have made controversy a feature of the climate change debate. These uncertainties come to the fore when any discussion is made of what action the global community should take in response to the observed increase in global mean temperature. Those opposed to cuts in greenhouse gas emissions have seized upon the admission that the magnitude and character of natural climate variability has yet to be fully understood and use this as an excuse not to adopt policies to limit the use of fossil fuels. The IPCC has produced assessments of the science, the impacts and the potential strategies we can adopt to address the issue.

The range of mitigation options is not simply limited to reducing emissions. Biological, physico-chemical and geological techniques can be employed to either

capture or store CO_2. Whilst forest areas are acknowledged by the Kyoto protocol as a carbon sink, other options include large scale seeding of the ocean with phytoplankton and bacteria that is genetically modified to trap CO_2. Alternative measures include removing CO_2 from flue gases generated by burning fossil fuels. Technology is now available for the separation, transportation and storage of CO_2 from large point sources such as power stations. Amine solvents may be used to collect the CO_2 present in the exhaust emission. The solvent can be regenerated by heating it, which separates the CO_2 for collection and storage. The IPCC (2001c) estimated between 80%-90% of CO_2 in flue gas can be removed in this way. An alternative technique involves capturing CO_2 before combustion via a reaction with oxygen or steam. This produces a fuel gas with a much higher CO_2 content, making separation easier and more efficient. IPCC (2001c) estimate the cost of CO_2 capture in power stations to be equivalent to an increase of about 50% in the cost of electricity generation.

Once separated, there is a number of ways CO_2 could be stored. Storage in the deep ocean is one possibility. This could be done either through direct injection or by the creation of a dense CO_2-seawater plume at shallower depth, which would carry the CO_2 off to deeper waters (Drange and Haugan, 1992 cited Freund, 1997). However, Freund (1997) mentions that in addition to legal and jurisdictional obstacles, the large-scale introduction of CO_2 into the marine environment will create a volume of low pH water. This could have an adverse effect on marine organisms, which generally have a low tolerance to changes in pH. An alternative method makes use of geological reservoirs. Structures such as a sedimentary basin can hold large volumes of CO_2 and minerals present in the basin act as seals. One location where this is being actively researched is in the Southern Rocky Mountains-Colorado Plateau region in the United States as its favourable geological conditions coincide with a number of power stations (Allis and Smith, 2002). An alternative to storing carbon would be to utilise it through the manufacture of other chemical products. All these options rely on the successful separation of CO_2 from fossil fuel emissions.

Whether we choose to adapt or mitigate, a substantial cost will be incurred. The decision of whether to adapt or mitigate the impacts of global change is central to the political debate surrounding climate change. The relationships between cause, effect and response can be represented in a four-point loop shown in Figure 2-2. The effect of those mitigating actions will in turn feed back into the climate system to produce a different set of impacts. The yellow arrows show the cycle of cause and effect among the four quadrants whilst the blue arrow represents the human response to the environmental impacts of climate change (IPCC, 2001b).

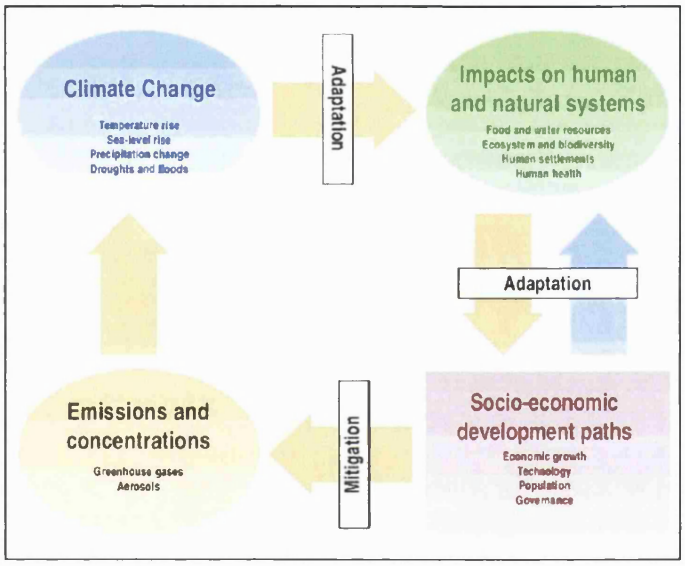

Figure 2-2 An integrated framework for climate change. Source: Figure SPM-1 in the IPCC Third Assessment Synthesis Report, Summary for Policy Makers (IPCC, 2001b).

Although Figure 2-2 describes a cause and effect loop for climate change, the model is valid for other human dimensions of global change (HDGC). There is a subtle difference between adaptation (the socio-economic response to the impact: blue arrow), and the mitigating actions taken by society. The mitigating actions are more obvious in the context of climate change. Taking the case of desertification as an example, changing agricultural practice to accommodate an encroaching desert would be an adaptive response, whereas wide-scale afforestation would be a mitigating action. The concepts of societal adaptation and mitigation are central to

HDGC research and feature in the discussion of another key theme of this thesis: sustainability. A move towards sustainability is inextricably linked to the potential to adapt adequately or ameliorate the effects of climate change.

2.2 Sustainability Science: An emergent discipline

Global environmental change is increasingly recognised as the central problem facing further societal development (IHDP, 2001). Global change research has broadened to encompass a number of disciplines. In doing so, researchers have found that the same issues keep cropping up in a variety of different scenarios. These are sometimes termed crosscutting issues as they can transcend concepts of scale (both spatial and temporal) and also subject discipline. One such issue is that of sustainable development. More generally, there is a shift towards 'sustainability science', which seeks to understand the fundamental character of interactions between nature and society (Kates *et al.*, 2001). As mentioned in the previous section, the concept of sustainability is seen as a key determinant in the societal ability to adapt or mitigate the effects of climate change. However, its definition is rather elusive. One of the earliest definitions of sustainable development was given in the World Commission on Environment and Development report (a.k.a. the Brundtland Commission) in 1987 as:

'development that meets the needs of the present without compromising the ability of future generations to meet their own needs'.

(WCED, 1987).

This is a reasonably loose definition and is subject to different interpretations. It clearly depends on the resources and population of an area and it is hard to see how resource flows in international trade and potential technological developments determine whether an area, country or region is sustainable or not. Sustainability

science develops the concept of sustainable development and aims to formalise our tentative understanding of nature-society interactions. In doing so it is realised that a whole new discipline will need to emerge. Through developing a discipline, which bridges the natural and social sciences, new methodologies that generate semi-quantitative models of qualitative data will need to be developed. This will require major advances to analyse and predict the behaviour of complex self-organising systems, characterise the irreversible impact of interacting stresses and interpret multiple scales of operation. By structure, method and content, sustainability science must differ fundamentally from science in its present form (IHDP, 2001). Techniques such as remote sensing, computer modelling and controlled experiments could all play roles in an operational model. Schellnhuber (1999) proposed that, at the highest level of abstraction, the Earth system E could be modelled by Equation 2-1.

$$E = (N, H)$$

Equation 2-1

Where: N = (a, b, c...) The ecosphere composed of planetary sub-spheres: atmosphere, biosphere, cryosphere etc.

H = (A, S) the human factor: A is the anthroposphere (human activities) and S is a metaphysical component referred to as the 'global subject' and represents the collective action of humanity as a self-aware control force.

Whilst Figure 2-1 essentially represents the *'N'* term, there is scant appreciation of how human activities influence this system. The *'S'* term in the human component of the equation may at first seem a highly abstract term to put into an equation. In recognising that the anthroposphere has a metaphysical dimension S, one also understands that the behaviour of A cannot be treated in the way as those components of the ecosphere. Instead it acknowledges that the *modis operandi* of human activities A is not fixed in time or space and can be radically altered in

unpredictable ways by mechanisms such as conflict or more helpfully, international protocols. *'S'* represents both the formulation of such choices and their implementation through networks of global institutions. Schellnhuber (1999) advocates the construction and application of macroscopes or an ever evolving Earth observation system to aid 'S' in making collective rational choices at the system level. Analysing the Earth system in such a manner has a bearing on achieving sustainable development. In this case, maximising the anthroposphere-ecosphere *N-A* welfare function. This is one of a number of paradigms of sustainable development that include developing purely adaptive or mitigative responses to anthropogenic impacts to the ecosphere. Even establishing a basic description of the Earth system can offer useful insights into understanding patterns of sustainable development.

The question remains: how does one achieve sustainable development? The traditional path of industrial development causes an increase in environmental degradation, particularly air pollution of gases and aerosols emitted in industrial processes. Environmental degradation of this nature, however, is hypothesized to follow an inverted-U shape relationship with per-capita income (Figure 2-3). Such a relationship is known as an environmental Kuznets curve (EKC) after Kuznets (1955; 1963 cited in Stern *et al.*, 1996) hypothesised such a relationship between inequality in the distribution of income and the level of income. The reasoning behind this is that as incomes increase, so to does the capacity to ameliorate the effects of environmental degradation. This is achieved through increased environmental awareness and enforcement of environmental regulations coupled with a shift from heavy industry to a more information intensive and service based industrial structure. Bartoszczuk *et al.* (2002) also cite the demand for environmental quality rising faster with income than demand for other goods or services as a factor in the downturn of pollution levels after a certain income threshold. Much research has been done into the EKC hypothesis as it may inform policy makers on development strategies. Analysis has been carried out for such pollutants as SO_2, NO_x, and also other measures of degradation such as

deforestation. The turning point in the curve tends to be around $4,000 per year (Shafik and Bandyopadhayay, 1992; Panayotou, 1993; Grossman and Kruger, 1994 all cited in Stern *et al.*, 1996), but has been shown to be as high as $11,000 per year (Selden and Song, 1994 cited in Stern *et al.*, 1996). In particular, it is noted that although this trend exists, it does not automatically follow that a country will grow out of environmental problems with economic development (Shafik and Bandyopadhayay, 1992 cited in Stern *et al.*, 1996). Arrow *et al.* (1995) discussed the relationship between economic growth, carrying capacity and the environment noting that the EKC has only been shown to hold for pollutants with short term costs such as sulphur and particulates, but not for pollutants involving long term and more dispersed effects such as CO_2. Tucker (1995) identified a positive relationship between CO_2 emissions and per capita income. Energy production is heavily reliant on the combustion of fossil fuels for most countries around the world. In this instance economic growth will have to be decoupled from combustion if an EKC is to be realised for this parameter and if Annex I countries are to take their commitment to the Kyoto protocol seriously.

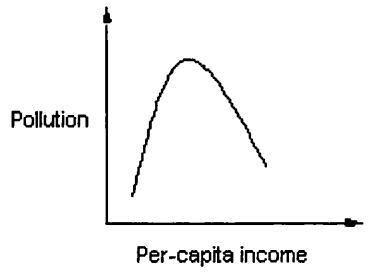

Figure 2-3 Relationship between environmental pollution and income as defined in an Environmental Kuznets Curve

The notion of ecosystem resilience was invoked by Arrow *et al.* (1995) to help predict the likely environmental effects of economic growth in a given area. When considered in conjunction with a geographically variable resource base, the implication is that the definition of sustainability will vary from location to location.

The EKC is simplified by the assumptions that there is no feedback from the quality of the environment to production possibilities and also that trade has a neutral effect on environmental degradation. In particular, the enforcement of stricter environmental regulations in developed countries may result in their polluting activities gravitating towards developing countries. These developing countries then experience increased pollution levels for marginal economic benefit. Stern *et al.* (1996) concluded that these limitations in EKC analysis restrict it to the role of a descriptive statistic rather than a tool for advising on sustainable development. However, the discussion raises interesting points regarding the scale at which one considers sustainability (local, regional or global). A local approach may render many areas unable to develop sustainably due to an inadequate resource base for the current population density. A global view may suggest that there are currently enough resources to enable sustainable development to a certain level, which some industrialised countries have already surpassed, thus implying that these countries will have to alter their energy consumption levels and lifestyles if we are to live in a truly equal world. In other words, can the entire world develop to America's level where there are 1.7 cars for each person?

At a more basic level, the unequal distribution of resources has not only allowed some areas to develop quicker than others but has also posed problems for areas which are deficient in a basic resource. Allan (1997) illustrated this point by constructing the concept of 'virtual water'. The production of every tonne of a food commodity requires a water input of approximately $1000m^3$. A tonne of wheat therefore has a virtual water value of $1000m^3$. In water stressed areas, most notably the Middle East and North Africa, countries have attempted to solve their water scarcity by importing food rather than attempting to grow the same food by expensive irrigation scheme. This relies on a country having sufficient funds (usually generated from oil reserves). In this way their available water can be used to grow less water intensive crops which can be exported. Whilst this would appear to be an ideal solution, there is still the concern that these countries, whilst fulfilling their food requirements, are not self-sufficient. Such a circumstance leave countries

at the mercy of international grain prices and is therefore a potential threat to sustainability. Allan (1997) argues that globally there is enough available water to support an expanding population. Fischer *et al.*, (2001) estimated that the current amount of cultivated lands could support a population of the 9.3 billion people projected to be living in 2050 by the United Nation's medium variant model (UN 2001, cited in Fischer, 2001). It is the distribution of the water which means that "water short" countries would be better off by concentrating on using whatever water they do have efficiently and importing the rest of their virtual water requirement instead of pursuing food self-sufficiency policies.

Economic development also has far reaching effects throughout the agricultural sector, ranging not only from how food is produced but which food is produced. Intensive farming techniques have adverse environmental effects primarily through the increased use of nitrogen-based fertilisers. Grigg (1999) observed that there is also a marked difference in the dietary consumption of people as a function of income. Besides an increase in the daily calorific intake, a reduction in the consumption of starchy staple foods and an increase in consumption of livestock and animal fat also accompany higher per-capita income. This has ramifications for agricultural production in the future, as the raising of livestock is the least efficient method of farming in terms of the area of land required to produce a unit of food.

2.3 Overview of global change research programmes

The Earth System Science Partnership (ESSP) comprises four global environmental change research programmes from which an array of science projects are undertaken to address more specific issues. Sponsorship of these programmes comes from an array of non-governmental organisations such as the International Council for Science (ICSU), inter-governmental organisations like the United Nations as well as national governments themselves. Taken together, these four research programmes represent the major elements of Earth system science. They are as follows:

- The International Geosphere-Biosphere Programme (IGBP) which carries out integrative research in areas of Earth System Science
- The World Climate Research Programme (WCRP), focusing on the biochemical and climatic processes that induce global environmental change.
- DIVERSITAS is concerned with the promotion of biodiversity science and establishing links between the biological, ecological and social sciences.
- The International Human Dimensions Programme of Global Environmental Change (IHDP) is the parallel social science programme. The IHDP aims to assess how humans contribute to global environmental change and how this feeds back into peoples' lives.

In July 2001 the Global Change Open Science conference organized by the IGBP, IHDP and WCRP culminated in the Amsterdam Declaration on Global Change made jointly by the four international global research programmes. The Amsterdam Declaration sets out a baseline of understanding from research carried out by the four programmes over the preceding decade and urges the global community to take coordinated and concerted action to address these issues. The main points are listed in Table 2-2.

Table 2-2 Main points of the Amsterdam Declaration made at the Open Science Conference, Amsterdam 10-13th July 2001 (continued on the next page).

• The Earth System behaves as a single, self-regulating system comprised of physical, chemical, biological and human components. Their interactions are multi-scale both temporally and spatially • Human activities are significantly influencing the Earth's environment in many ways in addition to greenhouse gas emissions and climate change. Anthropogenic changes are clearly identifiable beyond natural variability. • Human-driven changes cause multiple effects, which cascade through the Earth System in complex ways. These effects interact with each other and with local- and regional- scale changes in multidimensional patterns that are difficult to model and even more difficult to predict.

- Earth System changes are characterised by critical thresholds and abrupt changes (a decade or less). Human activities could inadvertently trigger such changes and have the potential to switch the Earth System to alternative modes of operation, which may prove irreversible. The probability of a human driven abrupt change has yet to be quantified but is not negligible.
- The Earth is currently operating in an unprecedented state. In terms of some key environmental parameters, the Earth System has moved well out of the range of the natural variability over the last half million years. The nature of the changes that are now occurring simultaneously is unprecedented.

On this basis, the international global change programmes urge governments, public and private institutions and the people of the world to agree that:

- An ethical framework for global stewardship and strategies for Earth system management are urgently needed. Accelerating human transformation of the environment is not sustainable and therefore the 'business as usual' way of dealing with the Earth system is not an option.
- A new system of global environmental science is required. It will draw strongly on the existing and expanding disciplinary base of global change science; integrate across disciplines, environment and development issues and the natural and social sciences. International collaboration on the basis of a shared and secure infrastructure and the intensification of the involvement of developing country scientists is needed to build an efficient international system of global environmental science.

The declaration embodies many of the observations made in the section on climate change. The development of sustainability science stems from the final point of the declaration. In the case of IGBP, eight core projects have been established to understand the various components of the Earth system and how they interact with one another. In addition to the eight core projects of IGBP are three framework activities dealing with data and information systems, integration and research and training. The most significant of these core projects from a remote sensing perspective is the Land-Use and Land-Cover Change project (LUCC).

2.3.1 Land-Use and Land-Cover Change (LUCC) Project

Land-use and land-cover change is one of the most important themes in global change research due to the wide range of impacts it has from local sustainability issues through to the alteration of global carbon sinks, biogeochemical cycles and levels of biodiversity. Expertise in both the natural and social sciences are required to understand fully the nature and ramifications of land cover change.

The global climate modelling community is one group to whom the ability adequately to map land-cover is becoming increasingly important as their models become more sophisticated. Initially, ocean-atmosphere general circulation models had very crude representations of land surface parameters. This was due to the limited processing power of the computers initially used to run the models. The coarse gridding of the models (10-20 degrees of lat/lon and 30 minute time steps) also meant that proper validation was not possible. The exponential increase in processing power over time has resulted in finer resolution grids being used, which in turn has meant that more sophisticated land surface parameterisations could be used. This completed the representation of the physical earth system as described in Figure 2-1. Land surface parameterisation stems from modelling plant physiognomy at the leaf scale and up-scaling to canopy and biome levels.

Advanced models incorporating biogeochemical and ecological processes will be able to model not only the physical, but also the biological response of the Earth system to hypothesised increases in atmospheric CO_2 concentrations (Sellers *et al.*, 1997). Remote sensing is becoming an increasingly important tool for providing land surface parameterisations such as albedo, leaf-area index, the fraction of photosynthetically active radiation (FPAR) and net primary productivity (NPP) as inputs into these models. Human activity is a major driver of global change and in order to develop biogeochemical models it is critical to account accurately for changes in the driving forces stemming from human activity (Sahagian, 1998). In order to do this there is a need for more datasets linking social and biogeochemical systems. The current dearth of these datasets arises from fundamental differences in

the diagnostic and prognostic nature of physical models and in the descriptive, qualitative nature of social models. Solutions to these problems may lie in the integration of global economic systems as well as in a more regional as opposed to global approach to analysis (Sahagian, 1998). Although the human/economic component of the Earth system is relatively small in Figure 2-1, the incorporation of human dimensions into Earth System models is a key step in the development of global change research. Remote sensing techniques can obtain information on most elements of the ecosphere. This thesis aims to assess and develop techniques for remotely assessing the state of the so-called anthroposphere. This discussion will be developed in chapter 3.

A detailed description of land-cover is required to model many of the land-atmosphere interactions and is central to understanding the global carbon cycle. Land-cover change and land management practices also have a significant effect on the strength of carbon sinks. Emissions from land-use changes could account for around 20% of anthropogenic CO_2 emissions (Schimel *et al.* 2001). Knowledge about the extent of key biomes (such as rainforests) is crucial to evaluate how much carbon the Earth can naturally sequester. Under the terms of the Kyoto protocol, such information is likely to form a key bargaining chip for those countries that have large carbon sinks in their country (see section 2.1.2).

The recognition of the interdisciplinary nature of this subject prompted the LUCC project to be established as a joint co-operation between the IGBP and the IHDP. The project aims to improve our basic understanding of global land cover dynamics. There are five overarching questions designed to meet this goal. The first two deal with the land-cover change from an historical perspective (over the last 300 years) along with the spatial and temporal nature of land-use change. The third question addresses the link between land-use and land-cover and how changes in the former will affect the latter over the next century. The impacts of human and biophysical dynamics on sustainability of specific types of land-uses and the bi-directional impact of climate and biogeochemistry on land-use and land-cover is set as the final

research question of the project. Three research foci of land-use dynamics, land-cover dynamics and regional and global models have been identified to address these questions. The issues of data classification and scalar dynamics (developing rules for crossing and linking scale) underpin these three foci and are regarded as key themes to the whole project. The 1997 IHDP-LUCC Data Requirements workshop in Barcelona identified a range of data constraints. A commonly occurring problem was uneven availability of socio-economic data and in particular spatially disaggregated data. Ancillary data of this nature can be very useful for inferring land-use from land-cover. This is important because whilst the former is a more powerful analytical tool, it is the latter which is observed from EO data. Changing land-use patterns and land management practices are the catalysts for wider land-cover change. This process is seen as a key area in which to develop understanding. Regional scale studies are seen as the optimal scale to incorporate socio-economic and biophysical models for the reasons mentioned above (IHDP-LUCC, 1997).

2.3.2 IGBP II: Global change research for the coming decade

A key function of the IGBP is to take results from its various research projects and synthesise them for dissemination amongst the wider scientific community. The Amsterdam declaration represents the culmination of research over the last decade from IGBP and other projects in the ESSP. Based on this, the IGBP entered a transition phase in 1998 towards a more Earth system orientated structure built around the three major domains of land, ocean and atmosphere (CEOS, 2001). Through its Global Analysis Integration and Modelling (GAIM) framework activity, 23 questions have been formulated to guide global change research in the next decade (Schellnhuber and Sahagian, 2002). These 23 questions are listed in Table 2-3 under four categories to represent the different fields within global change research. Reading through the questions, it becomes apparent that a wide range of disciplines will need to be involved in their response. What is also clear, is that global change research is becoming multi-disciplinary not only in terms of

Table 2-3 The 23 questions formulated by IGBP-GAIM to guide global change research in the next decade (Schellnhuber and Sahagian, 2002).

Analytic Questions:

1. What are the vital organs of the ecosphere in view of operation and evolution?
2. What are the major dynamical patterns, teleconnections and feedback loops in the planetary machinery?
3. What are the critical elements (thresholds, bottlenecks, switches) in the Earth System?
4. What are the characteristic regimes and timescales of natural planetary variability?
5. What are the anthropogenic disturbance regimes and teleperturbations that matter at the Earth- System level?
6. Which are the vital ecosphere organs and critical planetary elements that can actually be transformed by human action?
7. Which are the most vulnerable regions under global change?
8. How are abrupt and extreme events processed through nature-society interactions?

Operational Questions:

9. What are the principles for constructing "macroscopes", i.e., representations of the Earth System that aggregate away the details while retaining all systems-order items?
10. What levels of complexity and resolution have to be achieved in Earth System modelling?
11. Is it possible to describe the Earth System as a composition of weakly coupled organs and regions, and to reconstruct the planetary machinery from these parts?
12. Is there a consistent global strategy for generating, processing and integrating relevant Earth System data sets?
13. What are the best techniques for analysing and possibly predicting irregular events?
14. What are the most appropriate methodologies for integrating natural-science and social-science knowledge?

Normative Questions:

15. What are the general criteria and principles for distinguishing non-sustainable and sustainable futures?
16. What is the carrying capacity of the Earth as determined by humanitarian standards?
17. What are the accessible but intolerable domains in the co-evolution space of nature and humanity?
18. What kind of nature do modern societies want?
19. What are the equity principles that should govern global environmental management?

Strategic Questions:

20. What is the optimal mix of adaptation and mitigation measures to respond to global change?
21. What is the optimal decomposition of the planetary surface into nature reserves and managed areas?
22. What are the options and caveats for technological fixes like geo-engineering and genetic modification?
23. What is the structure of an effective and efficient system of global environment and development institutions?

understanding the problem, but also in terms of integrating these results to achieve a complete understanding of the Earth system.

Issues such as the provision and analytical capabilities of geographical information can be identified as a feature in some of the operational questions, but also some description of socio-economic characteristics would seem to be a crucial element of the operational questions (Q9-Q14). Wasson and Underdal, (2002) believe the greatest challenge lies in bridging the disciplinary divide the natural and social sciences to develop theories of human-environment interactions. A group from IGBP II has been set up to examine this area. Known as The Oslo Group, they have modified question 14 to reflect the important role of human decision-making process in environmental matters.

> What are the current theories of human-environment interactions that help identify sustainable futures?

In doing so, this question incorporates the human 'S' term in Schellnhuber model of the Earth System presented in Equation 2-1. Having identified the main areas of global change research for the next few years, the final section of this chapter examines initiatives which will make use of the knowledge gained from IGBPII and other global change research programmes.

2.4 Operational requirements for sustainability science

The concept of sustainability science has been introduced and its influence on major international research programmes examined. The previous section explored some of the data requirements needed to bridge the gap between human and natural systems. This final section outlines some initiatives which will aid this effort as well as make use of these products.

2.4.1 United Nations Environment Programme's Global Environmental Outlook 2000

The United Nations Environment Programme (UNEP) launched the Global Environmental Outlook (GEO) in 1995. It is intended to act as a global environmental assessment process incorporating regional views to build a consensus on priority issues and actions among policy makers and scientists at regional and global levels. This consultation process is intended to be as accessible as possible through the printed and electronic publication of reports for guidance in the decision-making process, as well as more technical reports. The process is undertaken by a variety of groups providing policy insight, methodology, regional perspectives and specialized inputs. Through the coordinating efforts of UNEP, a range of reports is released including technical reports, regional reports, as well as the main GEO report itself (UNEP, 2002).

The GEO is intended to be a bridging mechanism linking science to the policy agenda, a theme noted by Kates, *et al.* (2001) as a key pathway to the development of sustainability science. The general trend that is metamorphosing environmental science to sustainability science means that information is not only needed on the state of the physical environment, but also on the driving forces (e.g. population and economy), concomitant pressures (emissions), as well as the human and natural consequences (biodiversity loss and human health factors – closely related to emissions). Consideration of all these factors would result in an extremely large and almost unmanageable database. However, one can identify key datasets, which are likely to be required at all scales and at all locations. Lucht and Jaeger (2001) discussed the requirements to make the transition to sustainability. They propose the development of a Sustainability Geoscope, an instrument for observing the emerging and sustainability transition. This too would be based on a small number of parameters (less than 50), as the aim is to gather those that can be measured at many points in time and space. Such an instrument would be an example of a macroscope of Schellnhuber's *'S'* term in his equation of the Earth system. UNEP in association

with the UN Development Programme identified 10 high priority data themes, which in addition to the economy and land cover include hydrology, demographics, infrastructure, climatology, topography, soils, air and water quality. (UNDP/UNEP, 1994). Within these 10 sections, more detailed parameters can be established. Most of these data will be in raster format, though elements of the infrastructure dataset are likely to be vector data.

The regional assessments of the GEO are important to the effort of determining data requirements. Whilst the magnitude of environmental stresses varies in space, so does their regional priority. An example of this is the issue of future food supply and its distribution. Sivakumar (1998) discussed food vulnerability and climate variability and noted that different elements of climate variability (heat, rainfall) affect the yield of different crops differently. Rice can be particularly sensitive to temperature whereas wheat yield variation is more correlated to rainfall variability. This is highly significant for food supply in a changing climate for regions that are heavily dependent on one type of crop or experience a specific type of climate change.

2.4.2 Global Monitoring of Environment and Security (GMES)

The European Union's (EU) GMES project is an ambitious new initiative, which is taking global environmental research into the political domain. It is born out of the realisation that, firstly, global monitoring and environmental security are issues of high importance to the people of Europe and, secondly, Europe needs to have an independent capability to detect, analyse and ameliorate elements of environmental change and risk to society (GMES, 2001). This project is the latest development of a general trend that has seen Europe develop an independent capability from the US in many areas of science and technology.

The GMES project is an example of a political initiative that aims to link science and environmental security to the political objectives of the EU. It will draw upon

the wealth of European technological expertise to research, develop and implement operational environmental information systems. It aims to be a user-driven programme addressing the information requirements of EU environment and security policy. The role of Earth observation data is seen as key to meeting this goal, thereby making the space agencies and industry major stakeholders in the project (GMES, 2001). Existing capabilities and on-going initiatives will be integrated into the GMES project.

Environment and Security are viewed as the two distinct yet complementary themes of the project. The negative trend in environmental quality and depletion of natural resources carries the potential for conflict to occur. Issues such as food security and water resource management are likely to become the most sensitive environmental factors; in this respect Houghton (1997) comments that one of the most recent wars was fought over oil (1991 Gulf war) and that future conflicts may be fought over water. Allan (1997) cites his virtual water theory as a reason why this has not yet happened. However when water shortage is put in the context of a warmer climate of an uncertain magnitude, issues such as increased crop water requirements and changes in available growing area resulting in a decrease in food production, it is understandable why there is a growing emphasis of research in this area. Such issues are regarded by the EU as highly significant in playing a role for conflict prevention. Hence, the concept of security through sustainability has been developed. The case for sustainability to offer the most options of adaptation and/or mitigation is reinforced when these issues are considered along with the increasing risk of great floods (Milly *et al.*, 2002) and the potential damage caused by other natural disasters such as earthquakes and hurricanes. The scientific component of this is the development of Earth System analysis.

2.4.3 Exploring the anthropogenic system

The issue of security raised in section 2.4.2 is important because it not only highlights how broad and inter-connected sustainability issues are, but it also

introduces a politico-economic component to the discussion. This could prove to be the most important 'switch' between whether or not a country can embrace a sustainable future. When considered in these terms, some of the analytical questions in Table 2-3 take on a much wider context. Question 2 mentions teleconnections and feedback loops in the planetary machinery, whilst question 3 considers bottlenecks, switches and thresholds. These have been traditionally considered with respect to the physical environment. However, they could also be political, economic or technological. It is these kinds of shifts in the application of concepts that are needed if an adequate representation of the human component of the Earth system described in Equation 2-1 is to be realised. In this sense, teleconnections could mean globalisation or trading groups, whilst bottlenecks and switches include good governance, literacy levels and sanitation.

Whilst the theoretical side of sustainability science is being developed, achieving sustainable development in the modern world poses a different set of problems. The problem arises out of a need to couple sustainability with economic growth. In the present carbon economy, the use of fossil fuels as an energy source presents the cheapest means of development for a poor country. However, it will release even more CO_2 into the atmosphere. The dilemma lies in deciding whether one should try to develop as quickly as possible to reduce human suffering and hopefully find oneself of the descending limb of the EKC, or take a slower and more expensive route of implementing sustainable technologies as one develops.

These issues were discussed in a wide-ranging conference which took place in Johannesburg in September 2002. The World Summit on Sustainable Development (UN, 2003) brought world leaders together to discuss a host of environmental issues and in particular, measures for reducing poverty in developing countries. One of the most significant achievements was the ratification of the Kyoto protocol by Russia. This means that, despite the absence of the US, there are enough big producers of greenhouse gases committed to bring the treaty into effect. Other measures include agreements to halve the number of people without access to clean water and

sanitation by 2015. An increase in the use of renewable energy resources in both the developed and developing world, and "substantial improvements in market access" for food exports from developing countries were also agreed, however no firm targets have been set with respect to these resolutions.

Global trade and trade barriers play a critical role in determining paths of development. Bodies such as the Organization of Petroleum Exporting Countries (OPEC), who control oil production, can exert strong influences on developing countries. The dependence of the global economy on oil makes it the most strategically important commodity in the world. A recent report (Rifkin, 2002) mentioned that developing countries were hardest hit as a consequence of the 1973 oil embargo aimed at Israel and its allies. Developing countries have increased their dependence on oil since then. Their share of total world oil demand has increased from 26% to over 40% in the intervening 30 years. Observers warn that a second Gulf war would seriously affect developing countries with the exception of Nigeria, which is the largest oil exporter in Africa (BBC, 2003)

Formalising the links between poverty, the environment, and security is crucial to understanding the human dimensions of the Earth system. Optimising economics and the environment is potentially one of the biggest challenges since the requirements of one often conflicts with the operation of the other. A new discipline is emerging, which aims to put a greater ecological emphasis on the economics of resource management. One of the most contentious papers to come from research in ecological economics was an attempt by Costanza *et al.* (1997) to put a value on the Earth's 'ecosystem services and natural capital'. Based on 17 ecosystem services for 16 biomes, they estimate the average annual value of the biosphere to be $33 trillion. More recently, this figure has been spatially distributed by Sutton and Costanza (2002) using a satellite derived land cover map. Their results show that, whilst the northern-industrialised countries possesses more of the market value, it is those countries in tropical areas in particular, wetland and coastal areas which possess the most natural capital. Despite the controversy generated (Nature, 1998),

the use of traditional techniques applied in an alien context is likely to remain a feature of sustainability science.

2.5 Summary

This chapter has highlighted the diversity of global change issues. Global change research is a discipline in its infancy. Incorporating anthropogenic parameters into Earth system models represents the next step in achieving a truly integrated approach to studying global change. For this to be achieved, one must first accept a paradigm along the lines of the Amsterdam Declaration that the spectrum of human activity has the ability to affect our environment in a multitude of ways that will in turn impinge back onto human society in such a way that ameliorative strategies will need to be adopted. Once this has been accepted one can begin to assess the data requirements to describe and analyse what these changes are and how we can deal with them. To this end, 23 key questions have been formulated by (Schellnhuber and Sahagian, 2002) to guide global change research in the 21st Century. A recurrent theme in reviewing projects and strategies has been the need to start linking human and physical interactions at the regional scale, as this is the intermediate scale between global physical processes such as general circulation and local human population impacts. For this process to be successful, there is a need for data on the human side of the equation. This thesis aims to make a contribution to this effort by examining the role of remote sensing for providing anthropogenic information. By definition the HDGC is concerned with human presence across the Earth's surface. A key dataset is therefore the accurate definition of the location and magnitude of human settlements. The next chapter considers ways in which this can be done from Earth observation data.

Chapter 3

Literature review (2): Remote sensing techniques for inferring anthropogenic activities

This chapter reviews remote sensing techniques and assesses the contribution they can make to detecting and monitoring anthropogenic activities. Remote sensing essentially describes the collection of data from an object to a sensor that is not directly in contact with it. In the context of Earth Observation (EO), the object is the Earth's surface (or atmosphere) and the sensor is often a space-borne imaging instrument. Airborne remote sensing devices are also commonplace and extend the range of remote sensing techniques; they are less encumbered by power supply issues (as required by lidar systems for example) and the optical limitations of altitude as regards spatial scale. The temporal flexibility of an airborne campaign means that they can provide supplementary data often at an enhanced resolution to coincide with a satellite overpass. However, its limited spatial coverage and discontinuous data collection make it impractical and expensive for small scale, synoptic studies.

Remote sensing offers a range of techniques to record various properties of the land surface. The different modes of data collection can broadly be divided into those active systems, which generate their own energy to illuminate an object, against those which passively record the reflected or emitted radiation profiles of an object. Remote sensing can be conducted throughout the electromagnetic (EM) spectrum but relies on the presence of 'atmospheric windows'. These are wavelength ranges where EM waves can propagate through the atmosphere without being absorbed by the various trace gases present (Figure 3-1). Different wavelengths are sensitive to different parameters of the land surface and combining images from different wavelengths can further enhance this analysis.

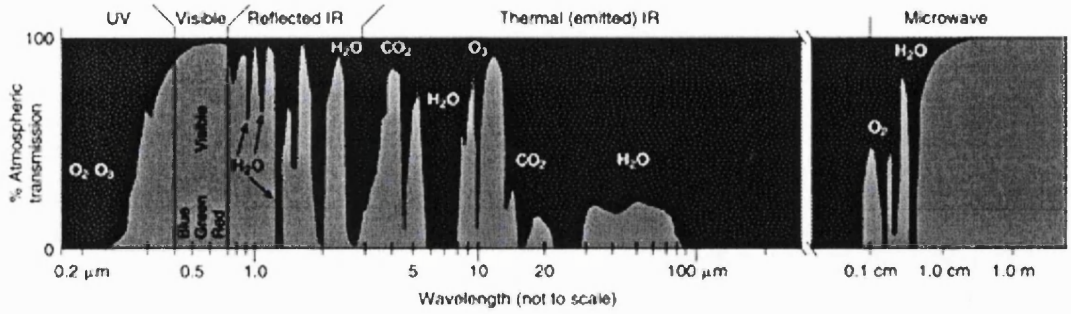

Figure 3-1 Atmospheric windows available for performing remote sensing. Source: http://earthobservatory.nasa.gov/Library/RemoteSensing/remote_04.html

This review is organised by wavelength and examines elements of remote sensing that can be used to gain information about the anthroposphere. As such, the review also focuses on key data products that are evaluated in the following chapters. These elements are as follows: night-time light imagery from the DMSP-OLS sensor (visible), thermal infrared remote sensing and interferometric SAR from the microwave region. NASA's Earth Science Enterprise will also be reviewed as an example of the production of dedicated Earth Science datasets, which can be used directly by the Earth System Science (ESS) community. Visible and Near-Infrared remote sensing from the MODIS sensor is described in section 3.4.1, as well as in the next chapter, through analysis of BRDF/Albedo measurements and their use for mapping anthropogenic activities.

3.1 The DMSP-OLS sensor and its data products

The Defense Meteorological Satellite Program, (DMSP) is the meteorological programme of the US Department of Defense, which originated in the mid-1960s with the objective of collecting worldwide cloud cover on a daily basis (Kramer, 1994). Such data was used to plan air operations during the Vietnam War. The system was officially acknowledged and declassified in 1972 and made available to the civilian/scientific community (NASA, 1997). The DMSP programme has been repeatedly upgraded over time since declassification (SMC, 1997); the latest series (Block-5D) incorporates the Operational Linescan System (OLS). The DMSP

satellite (Figure 3-2) flies in a sun-synchronous low earth orbit (833km mean altitude) and makes a night-time pass typically between 20.30 and 21.30 each night (Elvidge *et al.*, 2001a). Orbiting the Earth 14 times a day means that global coverage can be obtained every 24 hours. The OLS sensor has two broadband sensors, one in the visible/near-infrared (VNIR, 0.4 – 1.1μm) and thermal infrared (10.5 – 12.6μm) wavebands. The spectral response for the visible channel is shown in Figure 3-3). The OLS is an oscillating scan radiometer with a broad field of view (~3000km swath) and captures images at a nominal resolution of 0.56km, which is smoothed on-board into 5x5 pixel blocks to 2.8km. This is done to reduce the amount of memory required on board the satellite.

Figure 3-2 DMSP block 5 series satellite. Source: Air Force Research Laboratory Space Vehicles Directorate website. (http://www.vs.afrl.af.mil/images/pictures/dmsp.jpg)

Cross-track scanning sensors use a wide range of scan angles to acquire images and therefore suffer from two geometric problems. One is known as the bi-directional reflectance distribution function (BRDF), which describes the variation in reflectance of a surface for a given view and illumination angle. The other is a geometric distortion in pixel size as the scan moves increasingly off nadir. Low-level light amplification in the visible channel is facilitated through the use of a photomultiplier tube (PMT) so clouds illuminated by moonlight at night can be observed. The gain applied to the signal varies every 0.4 milliseconds based on the

predicted illumination of the scene from solar elevation and lunar phase and elevation. In addition to this, a BRDF algorithm further modifies the gain where the illumination angle approaches the observation angle to take advantage of the enhanced 'hot spot' of specular reflectance. The OLS employs a sinusoidal scan motion, which maintains a nearly constant pixel to pixel ground sampling distance of 0.56km at all scan angles in fine resolution data mode. The OLS has been specially designed to exploit the rotation of the scanning motion in order to reduce the expansion of the viewed area at high scan angles. Furthermore, the PMT is magnetically switched for the outer quarter of each scan to limit further the detector image on the ground surface (Elvidge *et al.*, 1997a).

These features not only permit the detection of visible band light sources down to 10^{-9} Watts/cm^2/sr/μm but also produce visually consistent imagery of clouds at all scan angles. The sensitivity of the OLS sensor is some four orders of magnitude greater than other sensors such as NOAA-AVHRR or Landsat Thematic Mapper (Elvidge *et al.*, 1997a), a feature that makes it unique amongst environmental remote sensing satellites. Although this was done with the initial aim of producing night-time cloud imagery on which to base short term cloud cover forecasts, it was also discovered that city lights as well as gas flaring, shipping fleets and biomass burning could also be detected in the absence of cloud (Croft, 1978).

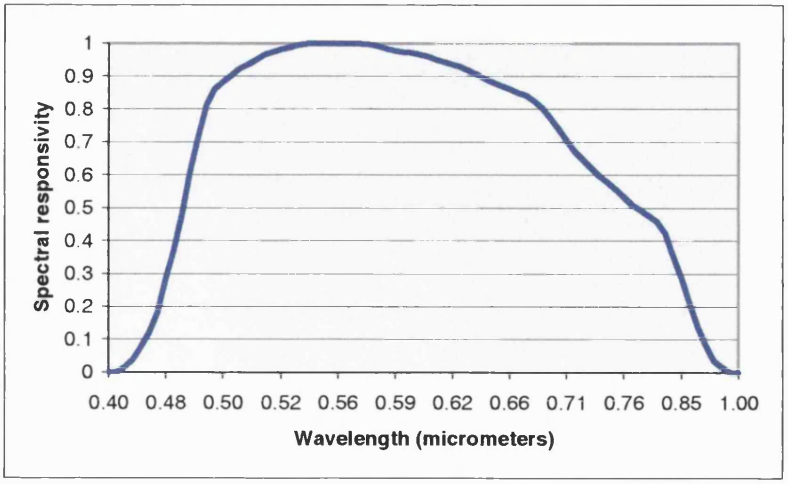

Figure 3-3 Spectral response function for the visible/near-infrared (VNIR) broadband channel of the OLS sensor

Digital OLS data was not made available by the US Department of Defense and subsequently was not archived by the National Oceanic and Atmospheric Administration's National Geophysical Data Center (NOAA-NGDC) from the time of declassification until 1992. Prior to this, scientific access to the data could only be obtained from a film archive. Despite this limitation, its potential as an indicator of human activity was noted by Croft (1978), Welch (1981), who analysed the correlation of lit area and energy consumption for selected American cities, and Sullivan (1989), who created the first global cloud free composite at a spatial resolution of 10 arc-minutes. A digital archive of night-time light imagery has been established since 1992 from which a number of global datasets has been produced.

3.1.1 The 1994-95 'City Lights' dataset

Despite the largely qualitative nature of the analysis, those studies mentioned in the previous section represent the most significant papers involving the use of OLS data for the analysis of human activity prior to the establishment of a digital archive. The digital archiving of DMSP-OLS data provided a catalyst for renewed interest in using this data source to advance the tentative observations initially made from OLS film data. The work of Christopher Elvidge and his team at NOAA-NGDC in Boulder, Colorado, in creating a 'stable lights' product represents the single greatest advance in the processing of OLS night-time light data. This product used six months worth of imagery acquired between October 1994 and March 1995 during periods of low lunar illumination. Whilst lunar illumination was crucial to imaging clouds at night, it is a hindrance to observing light sources from the ground due to the reduced contrast of light sources from the ground. Contrary to the initial mission objective of the OLS sensor, clouds now posed a problem for creating a product. The images were screened for clouds by applying a threshold to the complimentary thermal channel of the OLS sensor. Over the six-month period a temporal composite was built up of cloud free images of the earth at night. In this instance temporal compositing not only allowed clouds to be excluded, but also facilitated the analysis of 'stable lights'. The presence of stable lights is important in distinguishing

different light sources. However, the variation in brightness between orbits means that it is not possible to establish a single digital number (DN) threshold for identifying VNIR emission sources. An algorithm was developed to detect automatically light using a nested configuration of 20x20 and 50x50 pixel blocks. The light-picking algorithm applies a threshold to the central 20x20 pixel block based on the histogram of the surrounding 50x50 pixel block. Background pixels are identified by working down the frequency distribution from the brightest pixel to identify the first DN value where five consecutive DN values have greater than 0.4 % (10 pixels) of the total pixel counts. The threshold is established by calculating the mean plus four standard deviations of those background pixels. This threshold is then applied to the central 20x20 pixel block to identify pixels that are determined as being lit. There is a 60% overlap in area of the 50x50 pixel blocks used to generate the background pixels between adjacent 20x20 pixel blocks (Figure 3-4), which results in a smooth transition between threshold levels in each 20x20 pixel block (Elvidge *et al.*, 1997a).

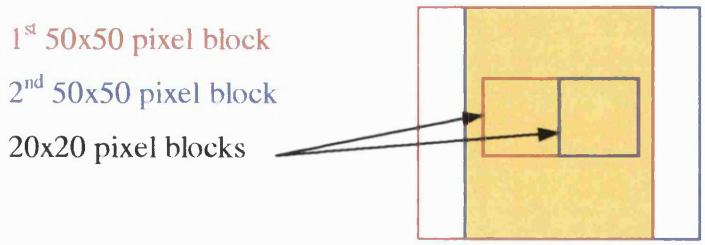

Figure 3-4 Representation of the 60% common area between adjacent blocks (shaded area) used in the light-picking algorithm.

Using this detection algorithm, the pixel value is assigned according to the percentage of times light was detected during cloud-free overpasses. Analysing the temporal frequency and stability of lights can help to distinguish their most likely source. City lights can be identified because they are temporally stable. However, an area, which is subjected to biomass burning as an agricultural process, can also be identified due to its location and lack of temporal stability over the compositing period. Through this process, the global night-time light composite can be filtered

into a variety of different products: city lights, shipping fleets, biomass burning and gas flaring. A geolocation algorithm was used to map the data onto the 1km grid developed for the NASA-USGS Global 1km AVHRR project (Eidenshink and Faundeen, 1994). City-lights accounted for most of the light emissions seen from space at night from this product. However, there were also contributions from other sources such as shipping fleets (common in the Sea of Japan and off Argentina), gas flaring and biomass burning in sub-Saharan Africa, the Amazon and SE Asia. These tended to be highly regional in nature.

Since digital archiving began, there were initially two types of night-light data available: the first is the frequency composite method outlined above. Secondly, a maximum pixel value for the cloud free orbits. The dissemination of these data allowed for more detailed and quantitative analysis than had previously been possible. Initial analysis of these images revealed a striking (though not unexpected correlation) between city-lights and human population density for the continental USA (Sutton *et al.*, 1997). The biggest problem encountered was low-light level pixel saturation. A new product was planned, which attempted to increase the detectable radiance range by varying the gain on the sensor.

3.1.2 The 1996-97 Radiance-calibrated dataset

The problems of relatively low-level pixel saturation from the 6-bit sensor over bright urban centres led to the experimentation and ultimate production of a new low-gain dataset. Elvidge *et al.* (1999) described a method for detecting a greater range of settlements than in the 1994-95 product by varying the gain of the sensor. Low gain experiments were conducted in March 1996 to identify the gain settings that produce the best results. Figure 3-5 neatly illustrates the variation in sensor saturation radiation (DN = 63) with respect to the gain setting based on pre-flight calibration. In this figure the solid diagonal line indicates the radiance at which the saturation point of the sensor is reached. The parallel dashed line indicates the radiance for DN=1, the lowest detectable radiance. Such is the effect of the gain that

sensor saturation can occur over a range of more than two orders of magnitude, likewise for the minimum detectable radiance value. Based on these experiments, two gain settings at 24dB and 50dB were selected and were alternately applied to each 24-hour set of acquisitions taken in January and February 1997. The thresholding technique used to create the stable lights dataset was found to perform poorly at identifying diffuse lighting, which is often dim and spatially scattered across the landscape. Such features were manually identified via the development of a software tool, which also provided a means of quality control for the product.

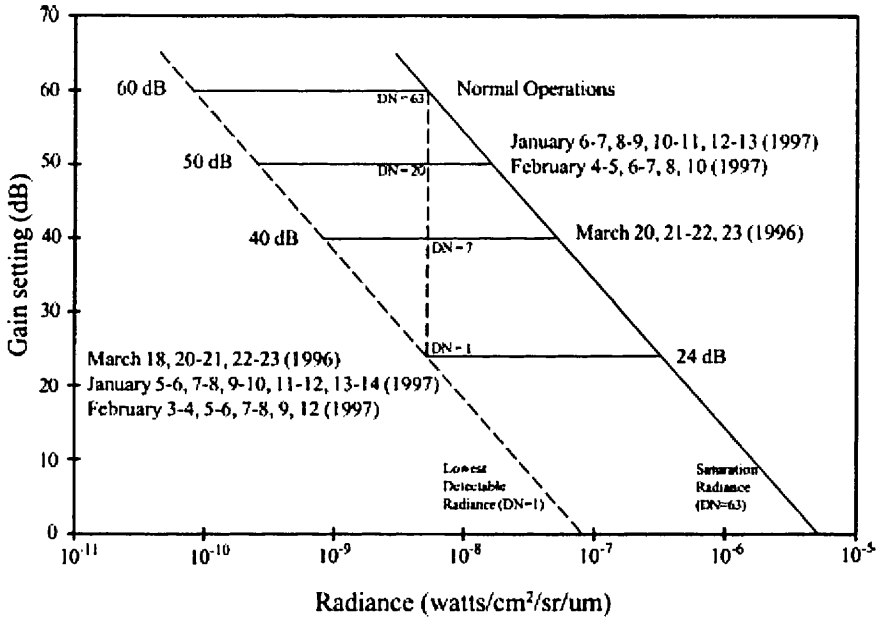

Figure 3-5. Relationship between visible band gain, digital numbers, and observed radiances derived from pre-flight calibration. Source: Figure 2 in Elvidge *et al.* (1999) © Elsevier Science.

High and low gain cloud free composites were averaged. The radiance-calibrated average DN from each image was weighted by the total number of detections. The final dataset contained calibrated radiances between 1.54 x 10^{-9} and 3.17 x 10^{-7} Watts/cm^2/sr/µm and was produced in byte (0-255) format at 30 arc-seconds (1km). The conversion from DN to radiance is given in Equation 3-1.

$$Radiance = (Digital\ Number)^{3/2}\ Watts/cm^2/sr/\mu m$$

Equation 3-1

The range was made deliberately ample on either side to allow for any future variations in gain. The radiance-calibrated night-time light dataset is the primary one used in this thesis. It is used extensively throughout and is of superior quality to the 1994-95 city lights dataset since the DN variation is a physically meaningful quantity as opposed to a 'lit-frequency' observation. This makes it a flexible dataset for use in a variety of modelling schemes subject to finding appropriate relationships between radiance and the parameters of interest.

3.2 Studies using night-time remote sensing imagery

Night-time light imagery has been used for a number of other applications in addition to estimating and mapping socio-economic parameters presented in later chapters. The examples below represent some of the most recent developments using DMSP-OLS data. The use of night-time light data for urban mapping is described in the next chapter.

3.2.1 DMSP-OLS Data for creation of a Night-time Atlas of Light Pollution

Probably the most intuitive application of night-time data is to map and quantify the amount of light pollution. Our limited view of the Universe has had a profound influence on human development. It serves as a constant reminder to consider the nature of our existence and begs questions, which we may never be able to answer. However, a clear view of the night sky for those who live in the developed world is a rapidly disappearing occurrence.

Cinzano *et al.* (2001) set about using the DMSP-OLS radiance-calibrated night-time light dataset to quantify artificial night sky brightness. Light propagation from the top of the atmosphere radiances present in the DMSP-OLS product was modelled

through Rayleigh scattering by molecules, Mie scattering by aerosols, atmospheric extinction along light paths, and Earth curvature. Hence, many areas that should appear dark in the night-time light product due to the absence of a ground level light source are in fact affected by light pollution from adjacent bright areas. Cinzano *et al.* (2001) intersected their atlas of light pollution with the Landscan 2000 global population density database (Dobson *et al.* 2000) to assess the number of people affected. The extent of this pollution is so widespread across the developed world that more than 99% of the population of the European Union and United States, and 66% of the entire world population suffer from some degree of light pollution. In particular, about half the population of the developed world do not have the possibility of viewing the Milky Way with the naked eye.

3.2.2 Modelling the Development of Night-time Lights

Modelling of the development of night-time light is of use to all of the applications discussed in this, and previous chapters. The ability to predict future scenarios of the spatial distribution of night-time lights and by association, economic activity, could greatly aid transport and energy infrastructure planning, as well as environmental impact assessments. This would be particularly beneficial for developing countries. Night-time satellite imagery is well suited for cell based modeling, not only because of its raster format, but also because it is flexible to a range of rules and assumptions which can be incorporated into a model.

Plutzar *et al.* (2000) used a cellular automata model to simulate the growth of night-time lights in China. A cellular automata model consists of a regular, discrete lattice of cells. Each cell is characterized by a state taken from a finite set of states. Evolution takes place at discrete time steps and each cell evolves according to the same rule, which depends only on the state of the cell and a finite number of neighbouring cells (Weimar, 1998). The model incorporated not only night-time lights but also terrain, population and transport infrastructure datasets. Probability surfaces of these input parameters were generated and the weighted mean was

computed to combine these surfaces. A probability surface was also generated from the night-time light data. This was based on an annular region around a cell. The higher the focal sum of this region, the higher the probability the target-cell will change. The focal sum of the region can be weighted such that cells at the edge of the region have less influence in the computation. The model was run to calculate pixels that have both intensified in value, and changed state from being unlit to lit. The generated layers of changed cells are summed with non-changing cells and compared to a predefined limit to determine whether the layer will serve as an input for the next iteration of the model or be output as the result. The model result shows an intensification of night-time light between Beijing and Shanghai, and expansion along the coast and around Hong Kong.

Dietz *et al.* (2000) conducted global simulations using global and regional GDP growth patterns of the A1B illustrative marker scenario (mentioned in chapter 2) and combined this with a simple stochastic model of spatial evolution and interaction to produce a map of future light intensity patterns. The A1 storyline and scenario family describes a future world of rapid economic growth characterised by global economic and cultural convergence. Environmental quality is sacrificed for increase in personal wealth. The model output (Figure 3-6) indicates potential changes in economic activity, which may help with future infrastructure planning. If such data are also combined with topographic data, it can also give an indication of those areas of economic activity that are susceptible to sea level rise or other regional climate change effects. The result for year 2070 shows extensive development through Eastern Europe into Russia. India is also predicted to undergo considerable development, as is China in those areas highlighted by Plutzar (1998) mentioned above. It is noted that Figure 3-6 represents only the development of lights. A key aspect of this thesis is to investigate and develop the means by which GDP can be estimated and disaggregated using DMSP-OLS night-time light imagery.

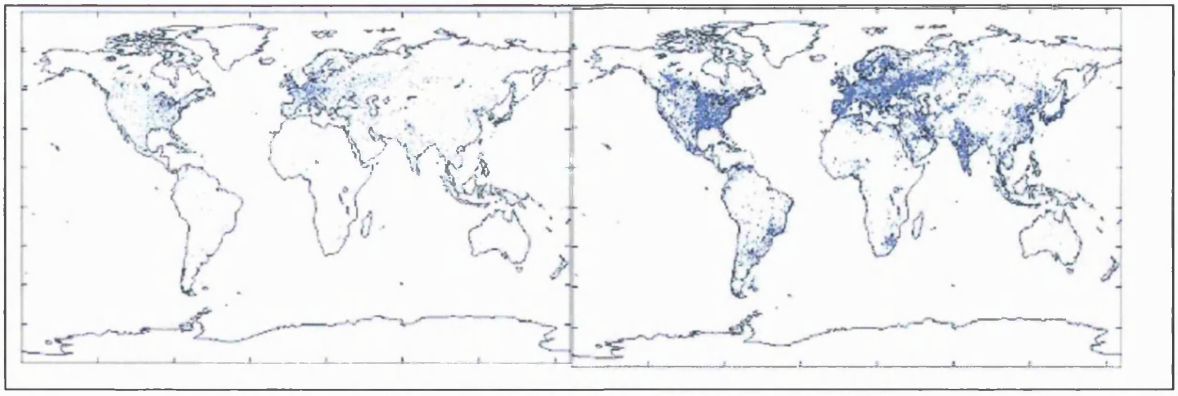

Figure 3-6 Results of a simulation of the development of night-time lights from the input 1996-97 radiance-calibrated dataset (left) to the year 2070 (right). Source: Figure 4-13 of the IPCC Special report on Emission Scenarios (IPCC, 2000) © Cambridge University Press.

3.2.3 Incorporating other sources of night-time Imagery with DMSP-OLS

MANTLE (Mapping Night-Time Light Emissions) is a EU funded project conducted amongst eight European institutions. Using the DMSP-OLS radiance-calibrated dataset as its primary data source, it aims to investigate how it can be used as a surrogate for a range of socio-economic indicators including GDP, population energy consumption, urban typology and landscape/skyscape quality. The project appears to cover the main applications of night-time data discussed in this section. Four focused study areas within the EU were chosen for their diverse environments. At the time of writing, the MANTLE project had only published (MANTLE, 2002) preliminary findings, which are discussed in chapter 8.

The Airborne Visible/Infrared Imaging Spectrometer (AVIRIS) is one such sensor that may be used to acquire high-resolution data over individual cities at night. The AVIRIS sensor is a hyperspectral imaging system that senses in 224 very narrow bands (~10nm) from 0.41-2.45 μm. It is designed to fly onboard NASA's U2 aircraft where, at an altitude of 20km, it can image 20m pixels over a 10km wide swath (Porter and Enmark, 1987). This additional data source offers not only the advantage of an enhanced spatial resolution, but also of enhanced spectral resolution too. The exclusivity of DMSP-OLS data as a source of night-time imagery has forced

researchers to use it at the continental-global level without fully understanding the contributions of different light sources at the sub-pixel level. AVIRIS data could address this issue. A test flight over Las Vegas in 1998 suggested that there are distinctive spectral signatures over the city (Elvidge and Jansen, 1999; Doll, 2003). Combining these two data sources would be of use to help understand what the DMSP-OLS data is really showing at the small scale, and therefore aid the assumptions one makes in macro-scale models using nighttime imagery. There are various types of lighting used in cities. Each has distinct spectral characteristics depending on the element used. Commonly used types of high intensity discharge lights are high pressure sodium used for street lights, mercury vapour and metal halide used in lighting car-parks and sports stadiums. Mapping spectral patterns over cities could help to identify patterns of residential, commercial and industrial land-use (Elvidge and Jansen, 1999). This could be one way of filtering out the population component if concerned with assessing areas of high economic activity.

3.3 Thermal infrared remote sensing

All bodies above absolute zero (-273°C) contain atoms in various states of random thermal motion and therefore emit EM radiation over a broad range of wavelengths. The temperature of an object affects both the quantity and also the wavelength at which radiation is at a maximum. This is known as the spectral radiant exitance peak and for blackbodies is given by Wien's displacement law (Equation 3-2).

$$\lambda_{\max} = \frac{A}{T}$$

Equation 3-2

where: λ_{max} is the maximum of spectral radiant exitance

A is a constant (2898 μmK)

T is temperature (°K)

From Equation 3-2 it can be seen that as temperature increases, the wavelength of maximum radiation decreases. The 8 –14μm is the region of peak energy emissions for most natural, terrestrial surface features. It is highly fortuitous that there is also an atmospheric window in this region, which permits thermal remote sensing. The term 'blackbody' refers to a theoretical body, which emits all its radiation. Real materials do not behave as blackbodies, but only emit a fraction of the energy of a blackbody at any given temperature. This ratio of the radiant exitance of a body over that of a blackbody at the same temperature is known as the emissivity. Different materials have different emissivities, which can vary with wavelength and viewing angle (Lillesand and Kiefer, 1993). Materials whose emissivities are sensitive to wavelength are known as selective radiators. Where emissivity is constant over all wavelengths, the object is known as a greybody. Some materials may also act like blackbodies over certain wavelength intervals. Water is one such material, whose emissivity is 0.98-0.99 over the 6-14μm wavelength range (Lillesand and Kiefer, 1993).

Bodies emit radiation over a range of wavelengths, which is known to have a peaked distribution. The radiant exitance describes a peaked curve that approaches zero as wavelength increases. The total radiant exitance from a blackbody is given by the area under the curve and is described by the Stefan-Boltzmann law (Equation 3-3).

$$M = \sigma T^4$$

Equation 3-3

where: M = total radiant exitance

σ = Stefan Boltzmann constant (5.6697×10^{-8} W.m^{-2}.K^{-4})

T = the temperature of the blackbody (K)

The remotely sensed measurement of M can therefore be used to retrieve temperature T. Although radiant exitance is measured over a discrete band of wavelengths, this is thought to have a negligible effect on the accuracy of the measurement due to the coincident peak of radiant exitance and the wavelengths used to make observations. Of more importance are the different emissivities of land

surfaces. This is incorporated into Equation 3-3 as an extra multiplicative term on the right hand side.

The importance of diurnal effects mean that the time of acquisition can have significant effects on how the detected scene elements appear relative to each other. Knowledge of these effects can be used to great effect when planning data acquisitions. Before dawn, most materials are in a state of quasi-equilibrium. After dawn, this equilibrium is upset and the materials warm up at different rates to a peak that is reached sometime after noon where maximum scene contrast usually occurs (Lillesand and Kiefer, 1993) after which cooling takes place. Urban areas are often much warmer than the surrounding environment. The man-made materials present in urban areas such as asphalt and concrete have a high thermal capacity and retain heat far longer than the surrounding vegetated environment which cools quickly by comparison. Therefore, the optimum time to detect urban areas is after dusk where the contrast between the two land surfaces should be at a maximum. This characteristic has been termed the urban heat island (UHI) effect and is observable from satellite data.

In addition to the detection of urban areas, high-resolution thermal imaging within the urban fabric can also be used to identify heat loss from buildings. In doing so, one must know the emissivity of the roof surface and also be aware that heat loss can also occur through walls, doors and windows as well as the foundations. It is recommended that these surveys be conducted some 6-8 hours after dusk on cold nights so as to minimize the effects of solar heating (Lillesand and Kiefer, 1993).

These are two examples of how thermal remote sensing can be used to gain an insight into both the extent and energy losses of urban areas. Furthermore, land surface temperature forms an important component in evaluating the net-radiation of urban areas.

3.4 NASA-EOS, MODIS and dedicated remote sensing products

The Earth Observing System (EOS) lies at the heart of NASA's Earth Science Enterprise. It consists of a science component and a data system supporting a coordinated series of Earth observation satellites (NASA, 2002a). These satellites carry a range of sensors for monitoring the land surface, biosphere, atmosphere and oceans. By collecting data on these components it facilitates the analysis of the Earth as an integrated system outlined in the previous chapter and outlined in Figure 2.2.

The Terra spacecraft is an example of one such satellite. Launched on the 19th December 1999, it carries five sensors aboard to image land surface, ocean and atmospheric processes (NASA, 2002b). Terra flies in a sun-synchronous orbit with a descending node equatorial crossing time of 10.30 am. It is complemented by its sister spacecraft Aqua (NASA, 2002c), which duplicates some of the instruments but flies with an ascending node crossing the equator around 13.30. Aqua was launched on the 3rd May 2002. Besides the improved technical specifications of the Terra and Aqua sensors, the novelty of this programme lies not only in the data processing segment but also in the fact that multiple instruments will be simultaneously gathering data. The data from each sensor will be processed into application-specific products with the aim of providing the user community with consistent high quality data products. This strategy also allows for quality control of the data in a more comprehensive manner than was previously been available. A detailed description of the quality assurance flags associated with a particular product (MODIS BRDF/Albedo) can be found in chapter 4.

3.4.1 The MODIS sensor and its products

MODIS is the flagship sensor on board the Terra spacecraft (Figure 3-7). It is a moderate resolution sensor capable of imaging at 250m, 500m and 1 km, but unlike other sensors of this type it has 36 narrowband (10nm) sensors (a full list of these can be found in Appendix B). MODIS products range from basic surface variables

of spectral reflectance, albedo and land surface temperature to 'higher order' variables such as leaf area index, vegetation indices and fraction of absorbed photsynthetically active radiation (Justice *et al.*, 1998). There are various levels of MODIS land products in order of increasing level of processing. Some products are produced on a daily basis; others are spatially and/or temporally resampled over a time period ranging from 8 days to a year. Certain products are provided at 0.5° or 1° resolution for the climate modelling community. Land product data files are produced in 10° x 10° tiles on the Integerized Sinusoidal Grid (ISG/ISIN). This is based on the sinusoidal map projection with a small adjustment made at each latitudinal row of the grid to the cell's angular width such that there are an integral number of cells covering the entire 360° in that latitudinal band (Masuoka et al, 1998). This facilitates the nesting of data at the multiple resolutions mentioned above. All in all, MODIS will provide data for 44 land, ocean and atmosphere products at a variety of resolutions in addition to basic radiance values. These products are listed in Appendix B.

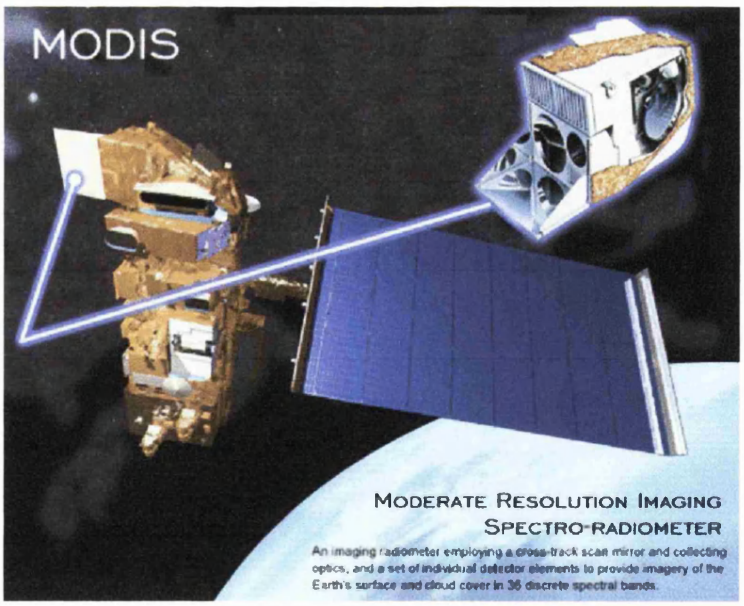

Figure 3-7 The MODIS sensor onboard the Terra spacecraft (NASA, 2002b).

The land products provide baseline information on the condition of the biosphere. Human activity also has an influence on at least two of these parameters. The albedo

is the fraction of incoming radiation that is reflected back into space. It is therefore dependent on the land surface. The albedo is an important value as it determines how much solar insolation is absorbed by the surface and how much long wave radiation is emitted into the atmosphere. Urban areas generally have a higher visible albedo due to the brighter surfaces of man-made materials present in the urban fabric than the surrounding vegetation (Taha, 1997).

MODIS also produces a daily land surface temperature product as well as an 8-day average. The components of urban structures such as concrete and asphalt are known to have a very high heat capacity which contributes to the urban heat island effect (UHI, see section 3.3). The MODIS land surface temperature product produces both day-time and night-time values, and is described by the product's Algorithm Theoretical Basis Document (Wan, 1999).

In addition to mapping the land surface components of global change, Terra also carries an instrument dedicated to measuring various gas concentrations in the lower atmosphere. Data from the MOPITT (Measurements Of Pollution In The Troposphere) sensor has provided the most detailed account of the Earth's air pollution. MOPITT uses gas correlation spectroscopy to measure upwelling and reflected infrared radiance in three absorption bands of carbon monoxide and methane (Bouchard and Giroux, 1997, Smith, 1997). Its main products include tropospheric CO and methane concentration maps and CO profiles at 3km vertical resolution and 22km horizontal (Kaufman *et al.*, 1998a).

CO is a particularly important gas in relation to anthropogenic activities as it is generated from biomass burning, industrial processes and car use. In the troposphere, it reacts with hydroxyl (OH) molecules to produce CO_2, whilst ground level CO concentrations are responsible for a number of adverse human health effects. Figure 3-8 shows the extent of the CO 'footprint' from biomass burning from the two largest rainforests on Earth. More importantly, these high concentrations are observed to be migrating westwards as it begins to be transported around the globe. The CO molecule has an average atmospheric lifetime of a few

weeks, which can be enough time for plume to travel one third of the way around the world. Sequential maps of global CO concentrations provide animations of CO transport. These can be viewed at the University of Toronto website: (http://www.atmosp.physics.utoronto.ca/MOPITT/movies.html)

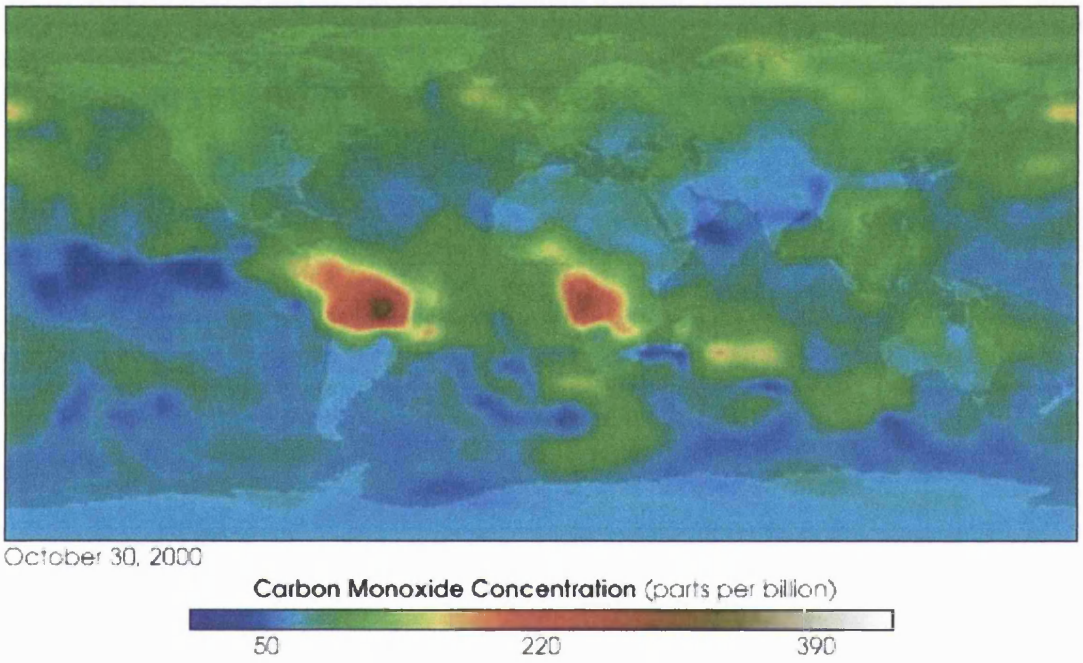

Figure 3-8 Global carbon monoxide distribution from the MOPITT sensor (http://earthobservatory.nasa.gov/Newsroom/NewImages/Images/mopitt_first_year.jpg)

Aerosols are another atmospheric constituent that instruments on board the Terra spacecraft are going to provide information on. Aerosols are very small particles (<<10μm) in the atmosphere, which can arise from industrial processes. Due to their size, they can be easily inhaled and are believed to be a significant cause of many respiratory diseases. Once in the atmosphere, they are known to aid cloud formation as well as exerting a forcing on the climate due to their interaction with incoming solar radiation. Both MODIS and the Multi-angle Imaging Spectroradiometer (MISR) are being used to produce aerosol products (Kaufman *et al.*, 1998a). MISR is an innovative new instrument employing nine looks (four either side of nadir plus nadir) in the along track direction to provide additional multi-angular as well as stereoscopic imagery. The extra information content of look angles taken through

different atmospheric path lengths provides enhanced cloud information compared to that previously available from satellite data. Although MISR is limited to the three visible bands plus the NIR, it offers an alternative measurement technique to that of MODIS, which instead relies on its wide spectral range (0.41–3.7μm) to evaluate aerosol concentrations (Kaufman *et al.*, 1998a).

3.5 Microwave remote sensing techniques

Microwave (radar) remote sensing is different from the other techniques discussed so far in the sense that it is not measuring any radiation reflected or emitted from the surface from input solar radiation, but rather a signal reflected *by* the surface, which has been emitted from the sensor itself. Due to its different mode of data collection, the information content of a radar image is conceptually different from that of an image from a passive sensor. The fact that it generates its own power to image the Earth means that the system can be used at all times regardless of solar illumination, whilst the much longer wavelength makes backscatter measurements impervious to cloud cover and therefore offers significant benefits to remote sensing in tropical and mid-latitude regions which are often cloudy. These wavelengths are summarised in Table 3-1 along with the letter associated with that band.

Table 3-1 Commonly used band names and their corresponding wavelength used in remote sensing

Band name	*Wavelength*
K	1 cm
X	3 cm
C	6 cm
S	10 cm
L	25 cm

3.5.1 Conventional radar remote sensing

Although passive microwave sensors exist, they are hampered by poor spatial resolution caused in part by the size of the antenna required but also due to the low intensity of emitted radiation in this part of the EM spectrum. By generating its own EM pulses, an active microwave system can overcome the latter of these problems. These fundamental principles, presented in this section, are based on Lewis et al. (1998).

Active microwave imaging systems differ from optical scanners in that they tend to be side looking. As such there are two components to the determination of ground resolution. These components are known as the range resolution and the azimuth resolution (Figure 3-9).

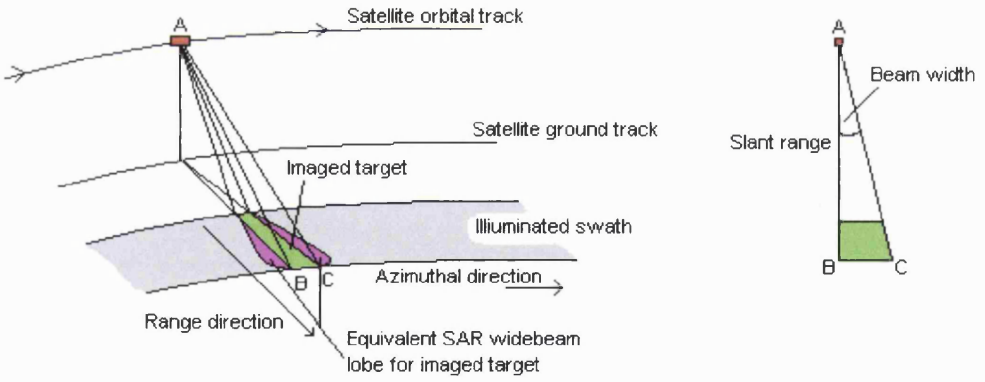

Figure 3-9 Range and azimuthal components of resolution for an active radar imaging system

The range direction runs orthogonal to the motion of the spacecraft and its resolution is defined in Equation 3-4. It is directly related to the length of the emitted pulse. The pulse strength is also proportion to its length and therefore this takes a minimum value, as the emitted pulse needs to be strong enough to reach the surface and be reflected back to the sensor. The acknowledgement of the signal return path introduces a factor of 2 in the denominator.

$$G_R = \frac{c\tau}{2\sin\theta}$$

Equation 3-4

where: c is the speed of propagation (speed of light: $3x10^8$ m.s^{-1})

τ is the pulse length

θ is the look angle

The azimuth resolution runs parallel to the flight line and therefore orthogonal to the range resolution. It is defined by the product of the beam width (β_h) and the range, R.

$$A_R = \beta_h R$$

Equation 3-5

The beam width is defined as the length of the wavelength of the pulse (λ), divided by the length of the antenna (l). Substituting Equation 3-6 into Equation 3-5, it is apparent that the azimuthal resolution is inversely proportional to the size of the antenna and therefore, fine resolution imaging can only be attained through very large antennas.

$$\beta_h = \frac{\lambda}{l}$$

Equation 3-6

The size of antenna required to produce images of comparable resolution to current optical Earth observing satellite sensors is prohibitively large to be used on space-borne sensors and can even affect the stability of aircraft when mounted on an aeroplane. This problem has been overcome through the development of synthetic aperture radar (SAR). A SAR system sends many pulses in a wide beam (lobe) to generate multiple coherent returns from a target. In doing so, it measures the

Doppler shift in the frequency of the reflected radiation as a result of the motion of the satellite relative to the ground. The signal strength and phase relationships of these return signals are stored and later combined to simulate a large antenna. The azimuthal resolution for a SAR system is altered to:

$$A_{SAR} = \frac{l}{2}$$

Equation 3-7

where: l is the length of the SAR antenna.

This makes the resolution only dependent on antenna length, where previously azimuthal resolution was also affected by the wavelength altitude and look angle (if the range is considered to be $R = H\cos\theta$ where H is the height of the sensor). Image formation results from the measurement of the intensity of reflected energy from within successive resolution cells. The intensity of the reflected energy is determined by the ground conditions within the cell. It is likely that there are multiple scattering elements (scatterers) present in the cell. The addition of coherent returns from these scatterers gives a SAR image a grainy texture referred to as speckle.

3.5.2 SAR Interferometry

A useful extension to conventional SAR imagery can be achieved by using a second SAR image to create an interferogram. By coherently combining the signals from two antennae, the interferometric phase difference between the received signals can be formed for each imaged point. As this is essentially linked to the difference in the geometric path length to the target, information is provided on topography as shown in Figure 3-10. Interferometry can be conducted in a number of ways within this basic framework depending on the environmental limitations of different configurations.

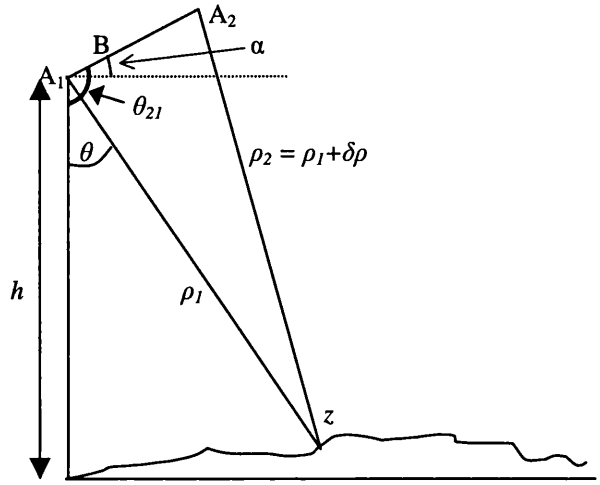

Figure 3-10 Principles imaging geometry for SAR interferometry

A resolution element in SAR imagery can be considered as a complex phasor of the coherent backscatter from ground scattering elements. An interferogram is formed by multiplying this complex phasor information from one SAR signal by the complex conjugate of the other, which has the effect of cancelling out the common backscatter phase in resolution element but leaving a phase term (φ) proportional to the differential path delay. The term *'p'* is introduced to differentiate from the scenarios where the channels share the same transmit antenna *(p = 1)*, and *(p = 2)* where each channel is receiving and transmitting on its own antenna (the case for repeat pass interferometry).

$$\varphi = \varphi_1 - \varphi_2 = \frac{2\pi p}{\lambda}(\rho_2 - \rho_1)$$

Equation 3-8

where: φ_i is the phase for signal i

λ is the wavelength

ρ_i is the range for signal i

There are three main ways to acquire SAR interferometric data depending on the position of the two received signals. These are along-track, across-track and repeat track (multi-pass) interferometry. The first two modes require two antennae on the same platform. These antennae are either mounted in such a way as to image a resolution cell in either the along-track or cross track directions. Only repeat track interferometry is readily used for space-borne interferometry. One reason for this is that it can be performed by combining signals received from an antenna mounted on two different platforms. Therefore, space-borne interferometry can be conducted using existing SAR sensors. This advantage is made possible by the precise determination and stability of orbital paths (Gens and van Genderen, 1996). This requirement of repeat-pass interferometry makes it unsuitable for use in airborne missions, where atmospheric effects can significantly affect stable flight paths and instead rely on simultaneous data capture from two antennae.

The distance between the two antenna positions is known as the baseline and is critical in the determination of the range (and therefore phase) difference between the two observations. The geometry of a generic interferometric system is shown in Figure 3-10. The two antenna positions are indicated at A_1 and A_2 represent two antennae viewing the same surface simultaneously, or a single antenna viewing the same surface on two separate passes (repeat-track). They are separated by the baseline 'B'. The look angle is denoted by θ, whilst θ_{21} denotes the total angle subtended between nadir and the baseline. The range ρ_i is slightly different between the two viewing positions. The derivation that follows is drawn from Gens and van Genderen, (1996) and Madsen and Zebker (1998).

Given this geometry, topography denoted by z in Figure 3-10 can be described by Equation 3-9.

$$z = h - \rho_1 \cos\theta$$

Equation 3-9

Using the cosine rule ρ_2 can be expressed in terms of ρ_1 thus:

$$\rho_2^2 = (\rho_1 + \delta\rho)^2 = \rho_1^2 + B^2 - 2\rho_1 B\cos(\theta_{21} - \theta)$$

Equation 3-10

From Figure 3-10, it can be seen that $\alpha = \theta_{21} - \pi/2$. Therefore the final term in Equation 3-10 can be written as a sine function owing to the two functions being even around a point separated by $\pi/2$ *i.e.* $\cos\theta = \sin(\theta + \pi/2)$.

$$\rho_2^2 = \rho_1^2 + B^2 - 2\rho_1 B\sin(\theta - \alpha)$$

Equation 3-11

Re-arranging this to make $\sin(\theta-\alpha)$ the subject gives:

$$\sin(\theta - \alpha) = \frac{\rho_1^2 - \rho_2^2 + B^2}{2\rho_1 B} \approx \frac{\rho_1 - \rho_2}{B}$$

Equation 3-12

This approximation is valid where the baseline is very much smaller than the slant range as is the case from space-borne sensors (Henderson and Lewis, 1998). This allows us to define the difference in range as a function of the baseline and relative viewing geometry. The final step is to substitute this into Equation 3-8 in order to derive an expression for the phase difference.

$$\varphi = \frac{-2\pi p}{\lambda} B\sin(\theta - \alpha)$$

Equation 3-13

Only principal values of phase (i.e. modulo 2π) can be measured from the complex valued resolution element. The phase in the interferogram is the modulus of the absolute phase.

$$2\pi i\varphi_m = W(\varphi_{top})$$

Equation 3-14

where: φ_{top} is the topographically induced phase and $W()$ is an operator that wraps phase values into the range $-\pi < \varphi < \pi$.

The process of unwrapping yields relative phase measurements between all points in the interferogram with an unknown offset of a constant multiple of 2π. Absolute phase determination is the process which determines the integer multiple of 2π that must be added to the phase measurement in order to make it proportional to the range difference.

SAR interferometry only works under coherent conditions, where the received reflections are correlated between the two SAR images (Hansen, 2001). The relationship between scattered fields received by different antenna can be statistically determined using a complex correlation function (Equation 3-15). For completely coherent scatterers (such as point scatterers) $\gamma = 1$, whilst independent scattered fields will result in $\gamma = 0$. The magnitude of this correlation is known as the coherence.

$$\gamma = \frac{\left\langle g_1 g_2^* \right\rangle}{\sqrt{\left\langle g_1 g_1^* \right\rangle \left\langle g_2 g_2^* \right\rangle}}$$

Equation 3-15

where: < > means the expectation value and * is the complex conjugation operator.

A decrease in coherence values is known as decorrelation and can be attributed to a number of different factors discussed by Zebker and Villasenor, (1992). Firstly, the baseline value must be smaller than a threshold value known as the critical effective baseline. This is the length at which there is a total loss of coherence, this is about 1100m for the ERS-1 sensor (Gens and van Genderen, 1996). Other causes stem from noise effects and speckle decorrelation due to the different viewpoints causing phase differences from scatterers located away from the centre of the resolution cell (Rosen *et al.*, 2000). Whilst these effects can be filtered (Papathanassiou, 1996),

there is another source of decorrelation that is especially pertinent to repeat-pass interferometry - temporal decorrelation.

Temporal decorrelation arises when there is a delay between the acquisitions of the two signals. The magnitude of this delay is referred to as the temporal baseline. Temporal decorrelation is primarily due to the changing position of scatterers or change in properties of scatterering mechanisms within the resolution cell. It can also be affected by a change in the atmosphere between the two passes. In this context of repeat track interferometry, coherence is largely a measure of the change in position of surface scatterers over the time difference between the two images. As such they are a useful by-product of radar interferometric and it is often used as an input to land-use classification (see section 3.5.3).

3.5.3 Radar capability for anthropogenic applications

The fundamentally different nature of radar images as opposed to optical imagery offers an alternative perspective on the remote sensing of evidence of human activities. The fact that the sensor is measuring scattered microwave radiation means that it is sensitive not only to the structural properties of the target but also to its dielectric properties, which is mainly controlled by its molecular properties and water content. As with optical imagery, radar remote sensing can be performed at a number of wavelengths. Other facets of radar imagery include the look angle, polarisation and look direction. Henderson and Xia, (1997) examined how these parameters affect the detection of urban areas and concluded that shorter wavelengths (X, C, and L) with cross polarisations and an incident angle greater than 35° are preferable. Man-made objects such as buildings (which act as corner reflectors) and metal bridges and building materials provide strong return signals to the sensor due to their high complex dielectric constant. Aside from this, the geometric relationship between the look direction and the orientation of ground features has a great deal of influence on the appearance of urban targets. The effect has been termed the cardinal effect as it often occurs on cardinal direction bearings

corresponding to the North-South, East-West settlement pattern of many urban areas (Xia and Henderson, 1997). This is due to objects acting as dihedral (double bounce) reflectors when the orientation is perpendicular to the radar look direction. Hence, areas that are orthogonal to the range direction tend to produce stronger returns than those settlements lying parallel to the range direction (Grey and Luckman, 1999).

The combination of these attributes makes radar imagery a useful tool for anthropogenic applications. In particular, its ability to detect settlements renders it highly appropriate for urban mapping and also population estimation (Lo, 1986a). Where the spatial resolution of the imagery is sufficiently high, Henderson and Xia, (1997) remarked that radar imagery can also offer intra-urban socio-economic data such as the location of residential areas and other urban land-uses, building density and the presence of major transportation routes. Furthermore, the cloud penetrating ability of radar imagery has been shown to be effective at mapping tropical forest land-use patterns as well as detecting and monitoring the extent of tropical deforestation: a manifestation of anthropogenic activity within the natural environment. Interferometric SAR data can also be used for land-cover mapping by using the coherence image, the amplitude difference and an amplitude image to create a false colour composite image with pre-defined land-cover classes (Wegmüller and Werner, 1995; 1996). This form of land-use mapping may prove to be highly appropriate for urban mapping since they tend to be highly coherent surfaces over time. It is this particular facet of radar remote sensing that is examined in the next chapter.

3.6 Summary

This chapter provides an overview of the main remote sensing techniques and data sources, which may be used to detect anthropogenically induced changes to the Earth's environment. These techniques have been presented in order of increasing wavelength and their relative features for detecting and monitoring anthropogenic

activities have been explained. These techniques will be assessed in the following chapters to understand the contribution they can make to address the needs of the global change research community outlined in Chapter 2. This chapter, in conjunction with the previous one, forms the literature review for the thesis.

The literature review has been split into two parts. The first part dealt with the wider issues of the thesis, namely global environmental change, its monitoring and modelling. The consideration of processes in isolation is less common and Earth system science is a term now widely used. A holistic approach will inevitably increase the demand for more data. These data are not only required across a broader range of disciplines but the increasing use of geographic information systems (GIS) necessitates the data to be provided in a format that is compatible with other data sources. Much of the existing data is already collected by remote sensing technologies and is therefore in a rasterised format. Night-time satellite imagery has been demonstrated to have the potential to make a significant contribution to mapping socio-economic parameters. A key element of this thesis is to investigate techniques by which satellite data may be used to provide information on such parameters.

The following chapters will examine work done with DMSP-OLS imagery to describe and map these parameters (specifically economic activity (GDP) and examine how it may be combined with other remote sensing products for human activity-environmental analysis.

Chapter 4

Assessing remote sensing techniques for potential application to HDGC issues

Human activities are largely concentrated in towns and cities. A reliable means of mapping urban areas from remote sensing data is central to realizing the aims of this thesis. Furthermore, one is not only interested in the simple description of human locations but also with the inference of the attributes associated with these locations. This chapter examines the potential of the remote sensing techniques outlined in the previous chapter to detect and map urban areas and assesses the contribution each technique can make to studies concerning the human dimensions of global change (HDGC).

4.1 Night-time lights and its relationship to urban indicators

Any regional scale image of night-time light data will reveal lit areas extending along transportation networks and along coastlines, which even the untrained observer can associate with human settlement. Using these data as a measure of urban land cover is therefore one of its most obvious applications. Doll and Muller (1999a) compared it to Digital Chart of the World urban polygons, whilst Elvidge *et al.* (1997) and Imhoff *et al.* (1997) described how DMSP-OLS data relate to urban boundaries from US census data. Urban land cover is notoriously difficult to map from conventional optical remote sensing data at the appropriate scale for global applications. There are numerous issues where an accurate map of urban areas would be hugely beneficial and night-time imagery acquired from the DMSP-OLS sensor has gone a long way to address this requirement.

Owen *et al.* (1998) used DMSP-OLS data for urban categorisation in order to correct meteorological records for urban heat island bias. In the same way, urban land cover as described by DMSP-OLS data has been used by Imhoff *et al.* (2000) to assess the impact of urbanisation on primary productivity. Using a technique the authors developed in a previous study (Imhoff *et al.*, 1997), wholly urban areas were classified as those being detected as lit 89% of the time from cloud-free observations. Peri-urban areas were classified as those lit 5-88% of the time. This map of urbanized land areas was then combined with an United States Geological Survey land cover map and a year of Normalised Differenced Vegetation Index (NDVI) data within a GIS. The NDVI is defined as the difference of the visible and near infrared channels divided by their sum and has been shown to provide a reasonable estimate of absorbed photosynthetically active radiation (Asrar *et al.*, 1984). Monthly maximum NDVI datasets over a year were averaged within the three classes of urban land cover. Each month's data were multiplied by the number of days in that month to provide a comparable unit (NDVI*days) which, when summed over the whole year, represents annual primary production. The effect of urbanization at the continental scale is generally found to cause a decrease in photosynthetic activity when compared to surrounding areas. Analysing individual cities, however, revealed that urbanization could in fact have a positive effect on primary productivity especially in cities with a strongly seasonal climate. The urban heat island effect was found to maintain a higher level of photosynthetic production for places like Chicago. Increased primary productivity in urban areas was also attributed to new species introduced and supported by irrigation in cities located in an otherwise resource-limited environment.

The effect of urbanization on primary productivity was found to be related to the climatic and physiographic environment of the city. Peri-urban areas had the highest degree of primary productivity and are also those that lie in the path of urban sprawl. Imhoff *et al.* (2000) estimated a loss of 10 NDVI*days of photosynthetic production should these lands develop into fully urbanised areas.

4.1.1 Night-time lights and the UK road network

Street lighting is a major contributor to the urban light observed at night. An experiment was devised to determine the relationship between two parameters by analysing the road network for mainland Britain within a GIS. The Bartholomew's 1:250,000-scale digital road network was used as a surrogate and a means of understanding the relationship between radiance and road transport infrastructure. This dataset was made available by the Manchester Information & Associated Services (MIMAS) facility at the University of Manchester. The road network is accessible as an ArcView line coverage. Within this coverage different road types (single/dual carriageways, tunnels etc) have their own attribute codes, which facilitates the analysis of night-time light imagery by different road types. Figure 4-1 shows a detailed map section over the Midlands. The major road types have been assigned the same colour codes as used in standard Ordnance Survey maps; these were overlaid on a greyscale radiance map. This area was selected as it displays a wide range of road types and radiance values.

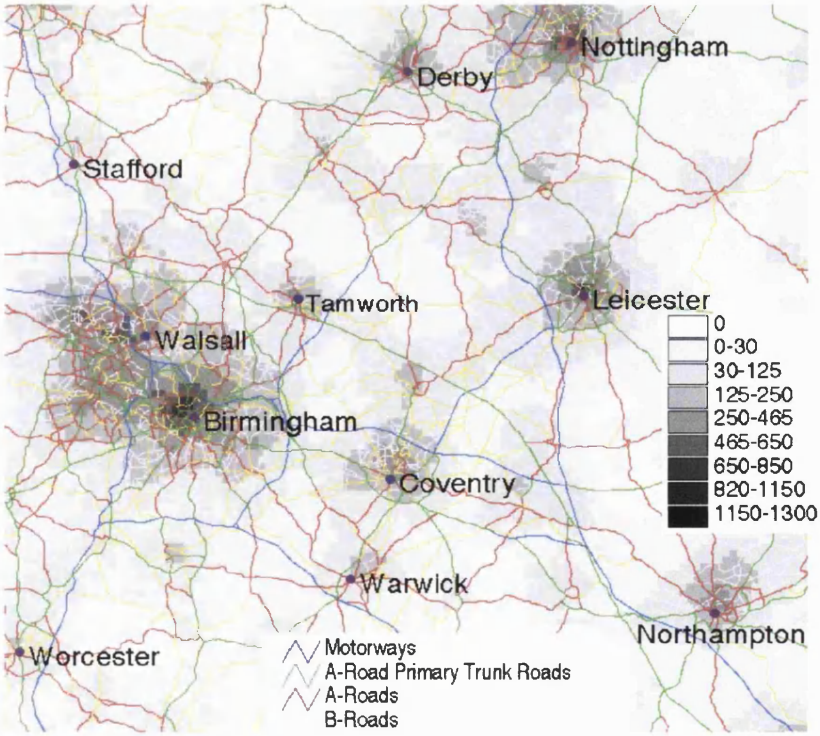

Figure 4-1 Greyscacle night-time light polygons with Road Network overlaid for the Midlands. The analysis was carried out for mainland Britain (Radiance; $x10^{-10}$ $W.cm^{2}.\mu m^{-1}.sr^{-1}$). Image size approximately 120km x 120km.

To examine the relationship between roads, road type and night-time lighting, a histogram of length of road per radiance was compiled. The data processing was done using the ArcInfo GIS package. The road network line coverage was split up into separate route topologies using the `arcroutes` command. This command splits a vector topology into separate routes according to a given attribute within the attribute table. In this case the attribute chosen was the identification code for the different road types.

The night-time radiance raster dataset was converted into a polygon coverage, such that each grid cell was represented by a discrete polygon with the radiance DN value stored as a polygon attribute. Vectorising the satellite data effectively reduces the problem to calculating the length of an arc within a polygon. The `polgonevents` command computes the geometric intersection between a polygon coverage (the night lights) and a route system (the roads). Roads were processed by four regions, depending on the prefix of the UK grid tiles used to split up the Great Britain National Grid system. The tables written out by the `polgonevents` command were merged and road lengths (classified by road types) were collated. A new table of total road length radiance and area was created. Finally, total road length was normalised by area, so road density for each road type could be plotted against radiance (Figure 4-2).

4.1.1.1 A note on graphs presented in this thesis

The graphs presented in this and subsequent chapters do not follow the standard scientific rubric of having the independent variable on the *y*-axis. In most cases this refers to some parameter of night-time light imagery (area or radiance). This has been done intentionally to make the graphs more readily understandable and, in later chapters to facilitate the derivation of relationships, where the measures from night-time light imagery are used to predict levels of economic activity.

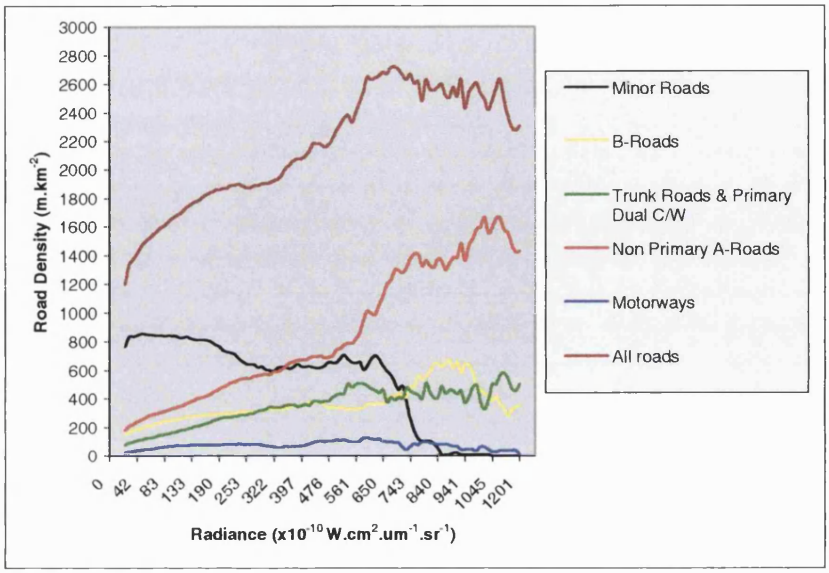

Figure 4-2 Average Road Density as a function of Radiance for Mainland Britain

Figure 4-2 shows how road density over mainland Britain varies as a function of road type. Road density is expressed here as metres per square kilometre (m/km^2). The data has been smoothed by a 10 DN (~100 x10^{-10} W.cm^2.μm^{-1}.sr^{-1}) running average to make the data more readily understandable. Non-primary A-roads dominate the plot and are observed to increase linearly up to around 560 x 10^{-10} W.cm^2.μm^{-1}.sr^{-1} (the term radiance units – r.u. is used from here on to mean 10^{-10} W.cm^2.μm^{-1}.sr^{-1}) after which the road density increases rapidly with respect to radiance until a radiance value of 800 r.u. A further peak occurs at the highest radiances in the UK at over 1000 r.u., which only occurs over London. Minor roads are densest over the lower range of radiances (0-350 r.u.). Minor roads are the densest of all roads in low radiance polygons and have a fairly constant density of around 700 m/km^2 until they drop rapidly to around 50 m/km^2 at 640 radiance units and cease to feature beyond 850 r.u. Motorways have a constant low density throughout the radiance range of around 75-100 m/km^2. Trunk roads and primary dual carriageways linearly increase to around 400 m/km^2 at 550 r.u., where it stabilises beyond higher radiance values. Meanwhile B-roads increase very gently in density (200-300 m/km^2) until they experience a broad peak of 600 m/km^2 through the 810-920 radiance unit range, suggesting that these roads are most common in the centre of towns (Doll *et al.*, 2000)

The dominance of non-primary A-roads in the higher radiance range (>620 radiance units) suggests that these road sections are concentrated in urban areas, and as such are a major source of street lighting. This study assumes that all roads are lit throughout the entire road network. This is not the case, especially in rural areas. Motorways are only lit around towns (e.g. within the M25 region in London). There exists no comprehensive list of lit road sections for the UK as this is under the control of individual Route Managers (D.Ryall, Highways Agency, personal communication). Therefore, one cannot precisely determine the quantitative effects of the road network on the night-time imagery over Britain from this study. However, despite this drawback, one can assume that most, if not all road sections within towns are lit, and in the region of the graph above 600 r.u., further increases in radiance have little effect on road density.

4.2 SAR Interferometry for urban land cover mapping

As discussed in section 3.4, imaging radar can offer distinct advantages over optical sensors when considering the mapping of urban areas. In addition to less restricted data collection limitations, the inherent difference in the information content of radar imagery makes it a potentially rich source of data.

This section examines a relatively recent application of microwave remote sensing, namely land cover mapping using interferometric coherence images and input amplitude images. The use of interferometric SAR could be especially valuable for urban mapping since urban areas are usually highly coherent land surfaces in comparison to the surrounding area. Studies have shown that urban surfaces can remain relatively coherent since surrounding vegetation will necessarily decorrelate with time as the seasonal vegetation cover alters the scattering characteristics of the target. Significant decorrelation can occur in rural areas due to changes in moisture and wind effects even at short temporal baselines (Grey and Luckman, 1999).

ERS1/2 Tandem data acquired as part of the LANDMAP project (Muller, 1999; Morley *et al.*, 2000) was processed and used to create colour composites according to the methodology proposed by Wegmüller *et al.* (1995). According to their colour scheme a RGB colour composite can be assembled from phase coherence (red), amplitude [backscatter] (green) and difference in amplitude (blue). In this way urban areas distinguish themselves as yellow pixels since there is little magnitude in the blue band and coherence and backscatter are high.

The Tandem data used were acquired in October 1995, one strip running NE-SW was processed (Table 4-1). A detailed section of the 3-band colour composite is shown in Figure 4-3a. The area over the city of Leeds was selected, as it was one of the largest cities in the processed dataset. Urban areas are easily distinguished on the image despite the very short temporal baseline. Other high coherence areas may include fields and ridges. Although, an unsupervised classification could not adequately resolve these features, a Mahalanobis Distance supervised classifier was found to improve the extraction of urban features. Two urban classes were identified from the 8 visually established classes from the 3-band composite. The classified layer was overlaid with the night-time lights radiance imagery as well as the Bartholomew's road network shown in Figure 4-3b. The densest part of the classified area compares well with the brightest area in radiance image. This area (over the centre of Leeds, UK) is assessed at 78.5% urban by the Institute of Terrestrial Ecology's 1km summarized land cover map product. This product is discussed in more detail in the next chapter (section 5.4). No other assessment of the accuracy of the classification was carried out owing to a lack of available datasets.

Table 4-1 Parameters of the two SAR scenes used to create the coherence image. Source: Landmap website: http://www.landmap.ac.uk/data/first_pass.html

Ref	*Sat1*	*Orbit1*	*Track*	*Frame*	*Date1*	*Sat2*	*Orbit2*	*Date2*	*Bpara*	*Bperp*	*Time*
23	E2	2496	137	2493	1995-10-12	E1	22169	1995-10-11	-130	-331	11:05

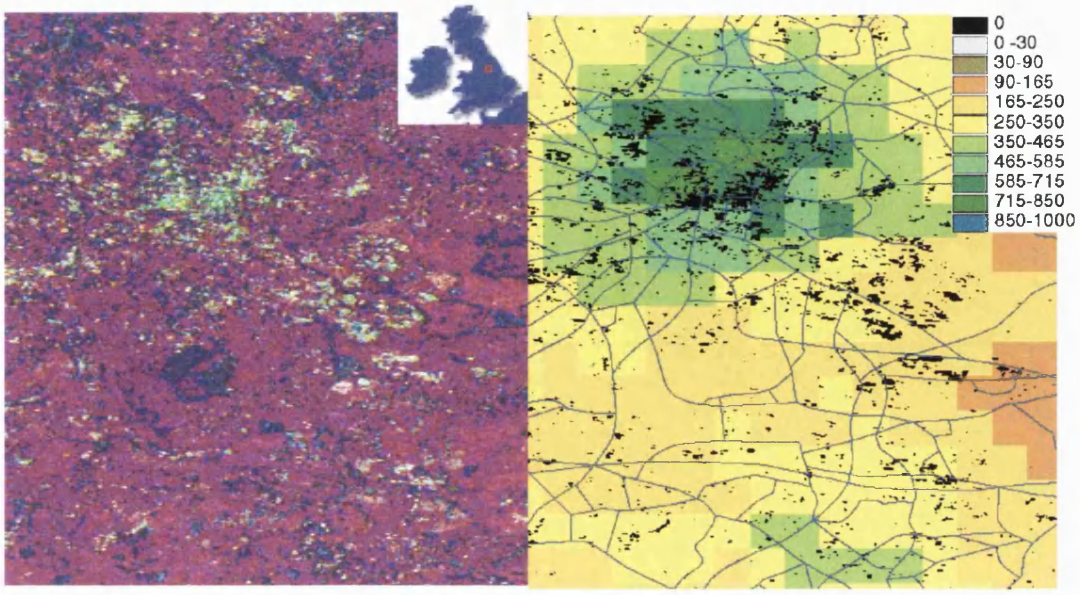

(a) (b)

Figure 4-3 Panel (a) shows a section of the three-band colour composite over Leeds, UK with phase coherence (red), amplitude (green) and phase difference (blue). Panel (b) shows the resultant classified built environment layer (black) overlaid on night-time lights with the road network overlaid (Radiance units of 10^{-10}W.cm^{-2}.μm^{-1}.sr^{-1}; Image size ~ 15km x 15km). Inset map from: www.worldatlas.com.

Wegmüller and Werner (1996) observed that the shorter acquisition time interval results in an increase in the interferometric decorrelation of fields with grass or crops. Whilst this improves the potential of discriminating fields from forests, it may serve to confuse the discrimination between fields and urban areas. Given that the Tandem data were acquired in the month of October, high surface moisture content in fields could be a likely source of error. Using a longer temporal baseline, and in particular, taking data from two different seasons (thus increasing the chance of differences in vegetated areas), may be more prudent choices for urban mapping using SAR interferometry.

The higher spatial resolution of the SAR imagery (1 arc second pixel size after INSAR processing) has many useful applications compared with the other datasets used in this study. In particular, it can help resolve our understanding of the built environment's contribution to the night-time radiance value received by the DMSP-OLS sensor. IfSAR's potential to map the built environment could be of great

benefit for mapping urbanisation in the developing world, especially if night-time lights are found to be unrepresentative of total urban area. In addition, since urban areas often stay coherent over very long time periods, it also provides a useful tool for change detection analysis. Grey and Luckman (1999) have done this over Cardiff by comparing urban classifications made between 1993 and 1995, and another made with images in 1997 and 1998. The mean coherence was found to increase with the temporal baseline, as was an increase in classification accuracy with a decreasing perpendicular baseline.

Ferretti *et al.* (2001) developed the theory of permanent scatterers based on the fact that certain elements remain highly coherent over long periods of time. Whilst this has been used as a means of minimising atmospheric effects in interferograms, most of these scatterers are found in urban areas (along with some in rocky terrain). Such a technique is likely to provide a more reliable means of mapping built settlements from interferometric data given a suitable series of interferometric pairs.

4.3 The MODIS BRDF/Albedo product and its relationship to urban features

The National Aeronautics and Space Administration's (NASA) new Moderate Resolution Imaging Spectroradiometer (MODIS) sensor on board the Terra spacecraft is producing a wealth of data products pertaining to the land surface, the oceans, and the atmosphere. Besides the spatial, temporal and spectral content, the variation of pixel reflectance with viewing and illumination angle is an additional source of information in multi-angular remotely sensed data (Wanner *et al.*, 1995). The Bi-directional Reflectance Distribution Function (BRDF) describes the nature of the anisotropic reflectance of the surface. Aside from the nature of the land surface itself, the BRDF is also a function of view and illumination angle. Therefore, it is a useful parameter to be able to quantify when dealing with satellite imagery from sensors with a large instantaneous field of view such as MODIS. Land surface BRDF and its associated products: albedo and nadir BRDF adjusted reflectance

(NBAR), are now for the first time being routinely produced on a global basis every 16 days at 1km resolution. These data sets are freely available from the Eros Data Center (EDC, 2003). This section investigates how the BRDF/Albedo product performs in relation to mapping urban areas and compares it with prototyping studies made prior to the MODIS launch.

Modelling the BRDF from satellite imagery can be done in a number of different ways. These range from physical models, which explicitly describe the scattering of light by the surface, to purely empirical models, which use mathematical functions to describe it rather than explain it. Between these two options lie hybrid semi-empirical models. Each type of model has advantages and disadvantages relative to each other as well as to the output requirements of the model. Physical models are complex and retrieving their parameters is computationally intensive, which make them unsuitable for global production of a BRDF dataset every 16 days. Empirical models on the other hand are simpler to compute but require many more observations, which can also be a problem due to cloud cover as well as the angular sampling provided by the orbital configuration of the satellite sensor (Wanner *et al.*, 1995). Semi-empirical models simplify the physical description making them less computationally intensive, whilst retaining enough complexity not to be so dependent on observations that purely empirical models require. A major advantage of linear semi-empirical models is that they can be solved analytically. Physical models generally require a numerical solution. In addition to these benefits, linear kernel driven models also have the advantage of scaling spatially as well as being able to account for sub-pixel heterogeneity due to the linear superposition of the kernels (Wanner *et al.*, 1995). A linear semi-empirical model is being used to produce the MODIS BRDF-Albedo product.

4.3.1 MOD43 description of algorithm including QA data

The BRDF/Albedo product (known as MOD43B) is one of the key land products, and is an input into other land products, such as MODIS Land Cover (MOD12). The

BRDF has a wide variety of applications and as such, the product is one of the most extensive and complex from the MODIS sensor. There are three operational products available: the BRDF parameters themselves (MOD43B1), "blacksky" (directional hemispherical) and "whitesky" (bihemispherical) albedos (MOD43B3), and NBARs (MOD43B4).

Albedo is derived by integrating the BRDF over the hemisphere (Lucht, *et al.*, 2000) at the mean solar angle over the 16 days of observations and is a crucial parameter in understanding the land-atmosphere energy balance. It is directly related to reflectance and therefore absorption of incoming solar radiation. Both the albedo and the NBAR are derived from the initial BRDF product. Each product is produced for the seven land bands (bands 1-7 of the MODIS sensor) ranging from 0.3 – 2.1μm. In addition, there are three broadband albedos, for the visible (0.3-0.7μm), Infrared (0.7-5.0μm), and shortwave (0.3-0.5μm) parts of the spectrum for the BRDF parameters, and albedo. Broadband albedos are produced by applying conversion coefficients to the spectral observations. Liang *et al.* (1999) has produced an estimate of these spectral-to-broadband conversion coefficients for MODIS and MISR.

The BRDF/albedo retrieval algorithm has been named Ambrals (Algorithm for MODIS bi-directional reflectance anisotropy of the land surface) (Wanner *et al.*, 1997). The algorithm used for characterising the BRDF uses three linear semi-empirical kernels applied over a fixed 16-day period to allow for sufficient angular sampling of the surface. The model attempts to describe the BRDF as a linear superposition of basic BRDF shapes. The kernel based BRDF model used for the MODIS product is given in Equation 4-1. Surface anisotropy can be largely explained through descriptions of volume scattering by finite elements (e.g. leaves) and by shadow casting of 3-dimensional elements within a scene (e.g. trees). According to this formulation, K_{vol} represents the volume scattering described by physically based radiative transfer theories. It is given by the RossThick kernel derived by Roujean *et al.*, (1992). K_{geo} stands for surface scattering as derived from geometrical optical theory and is sensitive to the three-dimensional structure of

objects within a scene and is described by the LiSparse kernel (Wanner *et al.*, 1995). The kernel which accompanies it, is the isotropic contribution denoted by f_{iso}, whose kernel is unity. The BRDF is determined by calculating the coefficients (weights) for each kernel based on the land surface observations for a pixel over the 16-day data collection period.

$$R(\theta,\varphi,\phi,\Lambda) = f_{iso}(\Lambda) + f_{vol}(\Lambda)K_{vol}(\theta,\varphi,\phi) + f_{geo}(\Lambda)K_{geo}(\theta,\varphi,\phi)$$

Equation 4-1

where: θ = solar zenith angle

φ = view zenith angle

ϕ = view-sun relative azimuth angle

Λ = waveband

$f_k(\Lambda)$ = BRDF kernel model parameter k in waveband Λ.

K_k = BRDF model kernel k

$R(\theta,\varphi,\phi,\Lambda)$ = BRDF in waveband Λ.

Extensive quality assurance (QA) information is provided with all MODIS data products and is an important extra dimension to image analysis. This facet of the data structure is particularly relevant to the BRDF product since knowledge about the number of looks obtained for a given pixel during the 16-day compositing period is crucial, as it is related to the way that the algorithm retrieves the BRDF parameters. The quality of a set of observations can be determined by its weight of determination. The diagonal elements of the inversion matrix may be used to compute the 'weights of determination'. The analytical properties of linear kernel driven models allow for an assessment of sampling sensitivity to be made. These factors indicate the influence of the angular sampling regime and random uncertainties in observed multiangular reflectances on the quality of BRDF model parameters, and on derived reflectances and albedo. (Lucht & Lewis, 2000). The full list of QA codes is given in Appendix 2.

BRDF parameters may be retrieved in two ways. Should there be a sufficient number of good quality observations, the algorithm will perform a full inversion, which involves analytically solving a set of linear equations obtained from minimising an appropriate error function through matrix inversion (Lewis, 1995). Where there are an insufficient number of good quality observations, the algorithm uses a look-up table of archetypal BRDF shapes based on land cover. It then fits the number of available observations to this pre-defined model before extracting the parameters. Use of information retained from the available observations introduces intra-class variation of the BRDF parameters (Strugnell and Lucht, 2001). This second mode of retrieval is known as a magnitude inversion.

BRDF archetypes have been characterised through field campaigns using ground-based instruments. From these classifications, BRDF archetypes were mapped onto existing land cover classifications. The BRDF is essentially a structural description of land cover, which differs fundamentally from ecologically based land cover classifications. BRDFs are not only influenced by land cover, but also seasonally, if one considers the annual cycle of growth and senescence of green vegetation. Two look-up tables are therefore required to map land cover to a BRDF archetype depending on whether it is winter or summer. The Olson classification (Olson, 1994 cited in Strugnell, 1998) of the United States Geological Survey (USGS) 1km land cover map was used as the underlying map from which BRDF classes were determined (Strugnell, 1998; Strugnell and Lucht, 2001). The USGS land cover classification is based on satellite measurements made from the Advanced Very High Resolution Radiometer (AVHRR).

Seven looks (over 16 days) is defined as the threshold number of looks to determine whether or not a full inversion is attempted. Where the weights of determination are inadequate, or more likely, there are less than seven available looks, a magnitude inversion is performed. Hence, there are potentially two retrieval regimes in an image of BRDF parameters. One objective of this study is to examine how well the two regimes compare with each other (i.e. do they produce similar results?). This study concentrates on the BRDF and albedo characteristics of urban areas as part of

addressing aim (1) of the thesis described in the introduction. These results also form part of the wider MODIS BRDF/Albedo beta testing of the product, the main results of which are presented by Schaaf *et al.* (2002).

The BRDF/Albedo product is produced every 16 days. Each data product is assigned a date according to the starting Julian day (JD) of the acquisition period. This notation will be used throughout section 4.3. MODIS land products use the Intergerized Sinusoidal Grid (ISG) projection (Wolfe *et al.*, 1998), which divides the Earth into tiles of 1200x1200 pixels (Figure 4-4). These data are available on a tile-by-tile basis. MODIS land products are released in a special version of the Hierarchical Data Format known as HDF-EOS (HDF-EOS, 2002), which enables storage of image and multiple levels of QA data within a single file. Tools for reading this new file format have been developed by Sadashiva Devadiga at NASA-Goddard Space Flight Center. These can either be used in conjunction with the ENVI/IDL image processing software or as stand-alone routines under a UNIX/LINUX architecture.

Various study areas (Table 4-2) were selected to evaluate the potential of the MOD43B products to detect and map urban areas. The initial site consisted of four tiles over Western Europe shown below (Area 1 in Figure 4-4). These four tiles comprise the British Isles, France, Northern Spain, Germany, Northern Italy, Denmark, and Southern Scandinavia. Other sites with large urban areas were selected according to the likely absence of cloud in order to increase the chance of full inversions occurring over these areas (Figure 4-4).

Table 4-2 Study areas for BRDF/Albedo analysis and their associated urban areas

Site # in **Figure 4-4**	*Location*	*Major Urban Centre(s)*	*Tile references*
1	Western Europe	London, Paris, Berlin, Madrid	h17v03, h18v03, h17v04, h18v04
2	California	San Francisco, Los Angeles	h08v05
3	Florida	Miami	h10v06
4	Nile Delta	Cairo	h20v05, h20v06

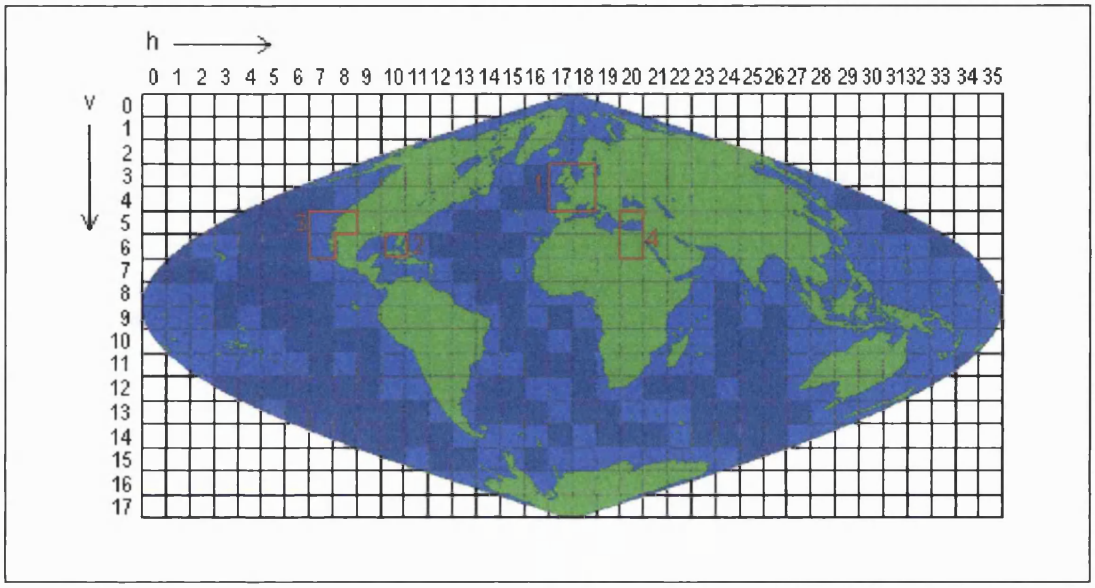

Figure 4-4 The Intergerized Sinusoidal Grid of MODIS Land Tiles (shown in green and light blue) with study areas mentioned in Table 4-2 superimposed.

4.3.2 The MODIS BRDF Parameters Product (MOD43B1)

The BRDF model can be interpreted to infer land surface properties because the angular dependence on reflectance is driven by the optical properties of the scattering medium as well as by its three-dimensional nature (Wanner *et al.*, 1997). The modelling of shadow casting given by the geometric optical parameter in the MOD43B1 algorithm suggests that it may be well suited to mapping urban areas. D'Entremont *et al.* (1999) proposed using the Normalised Difference *f*-index (NDFI) (Equation 4-2).

$$NDFI = \frac{f_{vol} - f_{geo}}{f_{vol} + f_{geo}}$$

Equation 4-2

where: f_{vol} is the weight of the volumetric kernel

f_{geo} is the weight of the geometrical optical kernel

Based on the NDVI, which is successfully used to assess the density of green vegetation, it takes the normalised difference of the two non-isotropic parameters to analyse the relative contributions of volumetric and geometric scattering. D'Entremont *et al.* (1999) used AVHRR data over New England to retrieve bi-directional reflectance parameters as a prototyping exercise for the MOD43 product. In their study, large urban areas were highly prominent, taking strongly negative NDFI values, indicating the dominance of geometric surface scattering. This section describes how a similar analysis, with MODIS data, was used to try to reproduce these results. In addition to assessing how well urban areas could be detected from the MODIS BRDF parameters, the analysis also seeks to understand what effect the method of retrieval had on the ability detect urban areas.

4.3.2.1 Magnitude inversions

The general cloudiness of Western Europe in autumn meant that the seven observations required for a full inversion was rarely obtained over the 16-day observation period. Since there were so few full inversions over the Western Europe dataset, only magnitude inverted BRDF parameters were evaluated. Although the Terra spacecraft was launched in December 1999, the initial data were mostly used to evaluate the performance of the algorithm. The final correction was to apply a realistic aerosol correction to the data. This started to be applied from JD273 (29th September 2000). Only data from after this date are evaluated here, though in time, all original data will be retrospectively processed to provide a complete dataset. The latest dataset (Collection 4) began processing in December 2002 from March 2002 onwards. Figure 4-5 shows the QA map for the four Western Europe tiles, with the corresponding image of NDFI. The NDFI colour bar was devised in recognition that most pixels take positive values (i.e. volumetric scattering > geometric scattering). More detail was therefore included in the positive range of NDFI values.

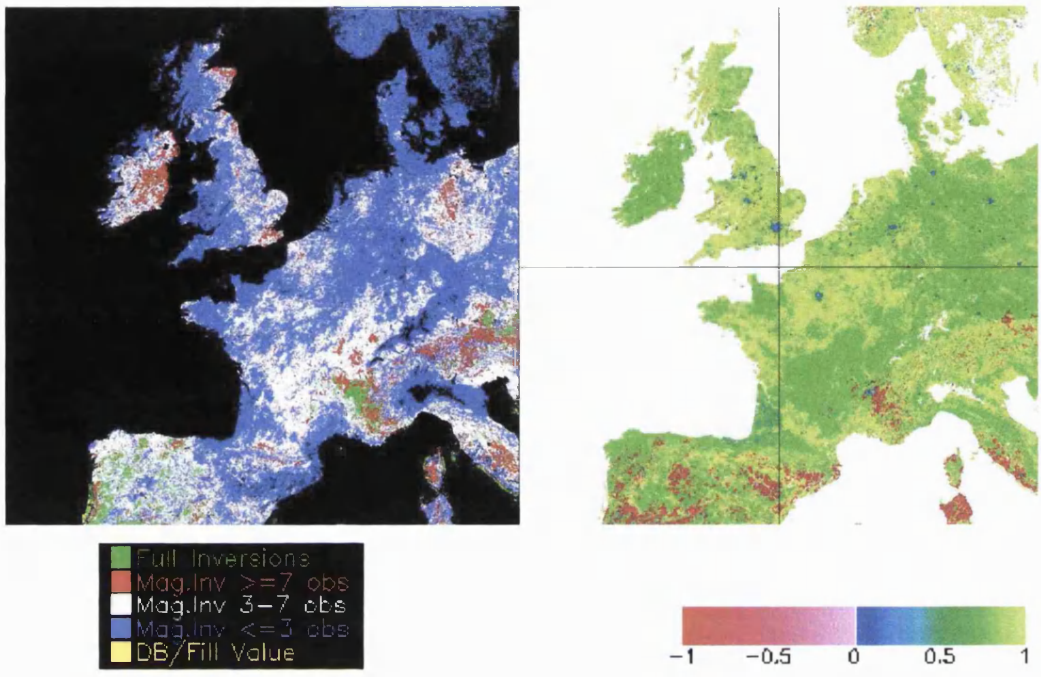

Figure 4-5 Red Band QA (left), and corresponding NDFI image (right) for JD289 (15th October 2000) Western Europe (tile boundaries shown). Image size: 2400km x 2400km).

Figure 4-5a shows that most magnitude inversions are based on fewer than 3 observations (coded blue in the image). Generally, there were more observations available towards southern Europe, as would be expected on the basis of decreasing cloud cover. JD289 had the least amount of data missing of those available dates and is the principal dataset for the Western Europe site.

Urban areas are very well highlighted in blue according to the colour scale, taking NDFI values of between 0.14-0.19 in all bands Doll *et al.* (2001). This contrasts to the strongly negative values obtained by d'Entremont (1999) (see discussion in section 4.3.2.3). The influence of the underlying land cover map is clearly visible in the image discrete patches of yellow, green and blue (urban). The Near-Infrared image of the same date (Figure 4-6) reveals that NDFI values over the image are concentrated in a smaller range. Interestingly, there is more confusion between urban and other land cover types in this part of the spectrum, especially in Southern Europe (Sardinia, Spain & Italy). These areas are the same ones that take negative

NDFI values in the red band (Figure 4-5) and correspond to shrubland in the IGBP global land cover database.

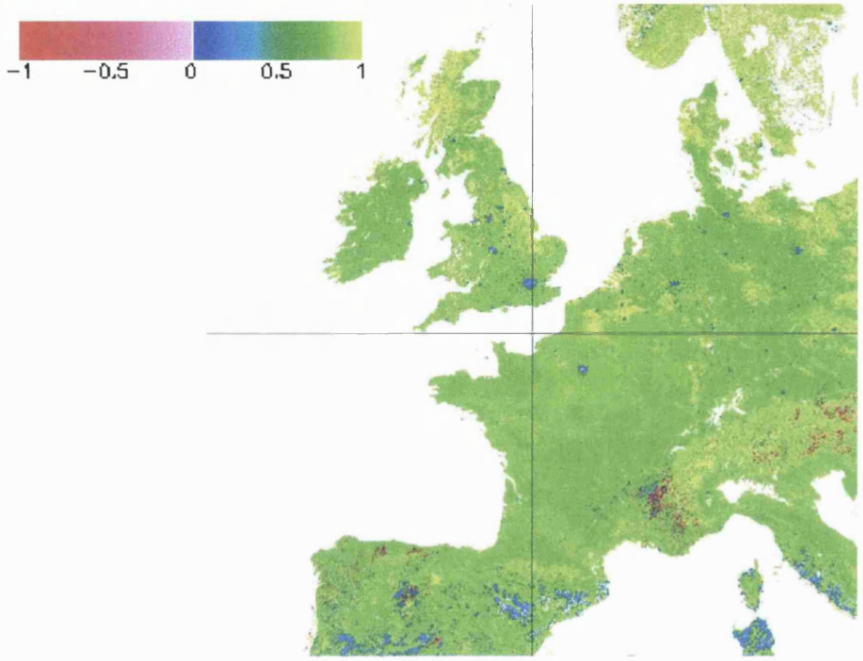

Figure 4-6 Band 2 (NIR) NDFI of Western Europe for JD289 (Image size: 2400km x 2400km).

4.3.2.2 Full Retrievals

Of the other study areas selected, Florida provided the clearest example of how the NDFI is affected by full retrievals. Figure 4-7 shows, in a similar manner to Figure 4-5, a QA and NDFI map over the Florida study area, for JD321-2000. The difference in NDFI values between areas of magnitude and full inversions is noticeable by many more negative NDFI values in areas of full inversions. The city of Miami is still visible in Figure 4-7 in the corner of South East Florida as an area of magnitude inversions. Data from JD289 had many full inversions in this area. It was compared to data from the next time period (JD305), which had mainly magnitude inversions in this area (Figure 4-8). The same area of the Floridian coastline, for two different dates with different modes of BRDF retrieval has

completely different NDFI values. Urban areas (shown in blue) are very distinctive on the magnitude inversion NDFI image. This zone of coastal development (or any other land cover unit) is completely obscured in the NDFI image of full inversions suggesting that the NDFI is not as useful as first thought for detecting urban areas as discussed further in the next section.

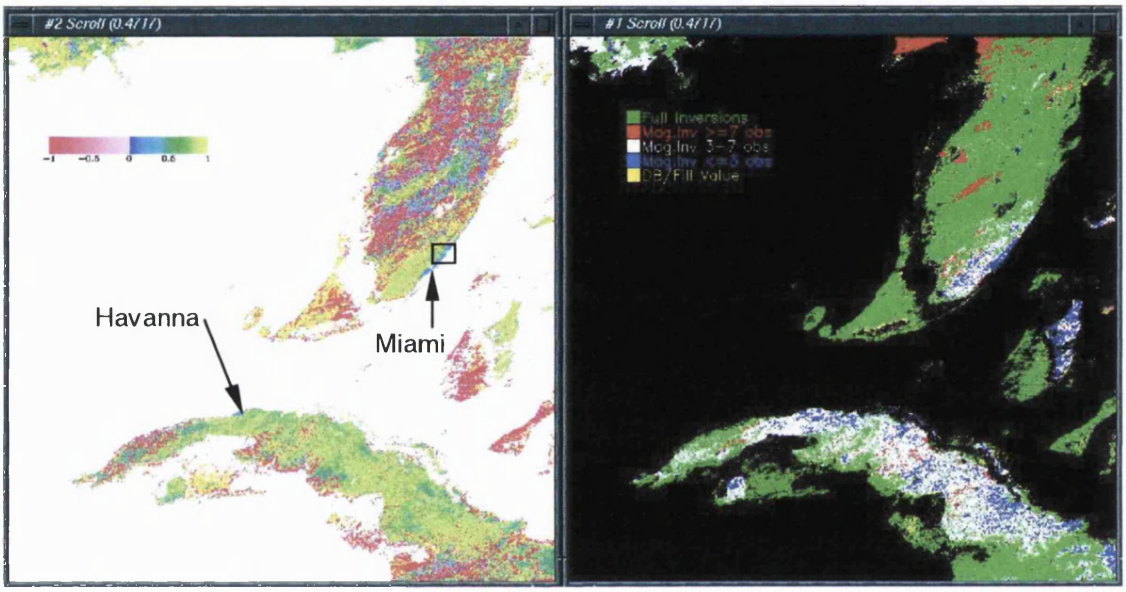

Figure 4-7 NDFI (left) and corresponding QA bits (band 1, red) for tile h10v06 for JD200-321 (16th November 2000, Image size: 1200km x 1200km). Black box refers to the inset of Figure 4-8

Analysing the Florida scene, the most obvious difference between the two retrieval regimes is that magnitude inversions tend to be dominated by volumetric scattering. whilst the opposite is true for full inversions. This can be seen in Figure 4-7 by red/pink shades in the left hand image (indicating $f_{geo} > f_{vol}$) coinciding with the green shades (full inversions) of the QA map in the right hand image. In general, the weights of the volumetric kernel take a range around twice that of the geometric kernel weights (f_{vol} 0-150, f_{geo} 0-80). A zero value volumetric parameter is commonly encountered in full inversions, whilst $f_{geo} = 0$, is more common in magnitude inverted images (seen as bright yellow in the NDFI scale). This situation is not replicated in study area 3 (California) (Figure 4-9), which has a high proportion of zero value f_{vol} pixels, especially under magnitude inversions. This is

most likely due to the desert conditions in this area resulting in an almost complete absence of vegetation and therefore, volumetric scattering. Since the balance between f_{geo} and f_{vol} are fixed for magnitude inversions (Figure 4-10), these kernel weights depend on the land cover types present in the scene. Full retrievals are observed in the coastal region north of LA towards San Francisco demonstrating the high variation in NDFI observed in the Florida scene.

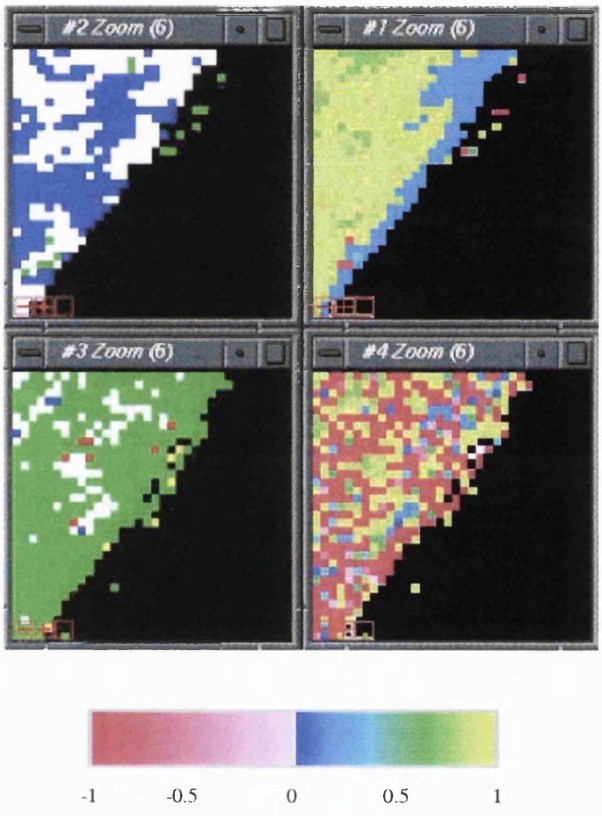

Figure 4-8 Detail from the Florida scene (see Figure 4-7) for JD305 (top) and JD289 (bottom). The two left-hand images show the QA for the MOD43B1 data (band 1, red) with the corresponding NDFI image on the right hand side. The QA images are colour coded such that green refers to pixels with full retrievals. JD 289 had a few full retrievals in this area. The large urban area to the north (West Palm Beach) and coastal development are neatly highlighted from the land cover look-up table. However when there are many full retrievals as for the JD305 product, the NDFI shows no apparent correlation to any land cover types (Image size: 35 km x 35km).

Los Angeles and San Diego are once again defined through magnitude inversions. The very high values of NDFI running down the centre of Baja California (marked '**1**' on the map) coincide with the Sierra de Juarez, whilst the lowland region around the Golfo de California is also well defined (marked '**2**'). This is due to the underlying land cover map dictating the basic shape of the BRDF for those regions (as is also the case for urban areas).

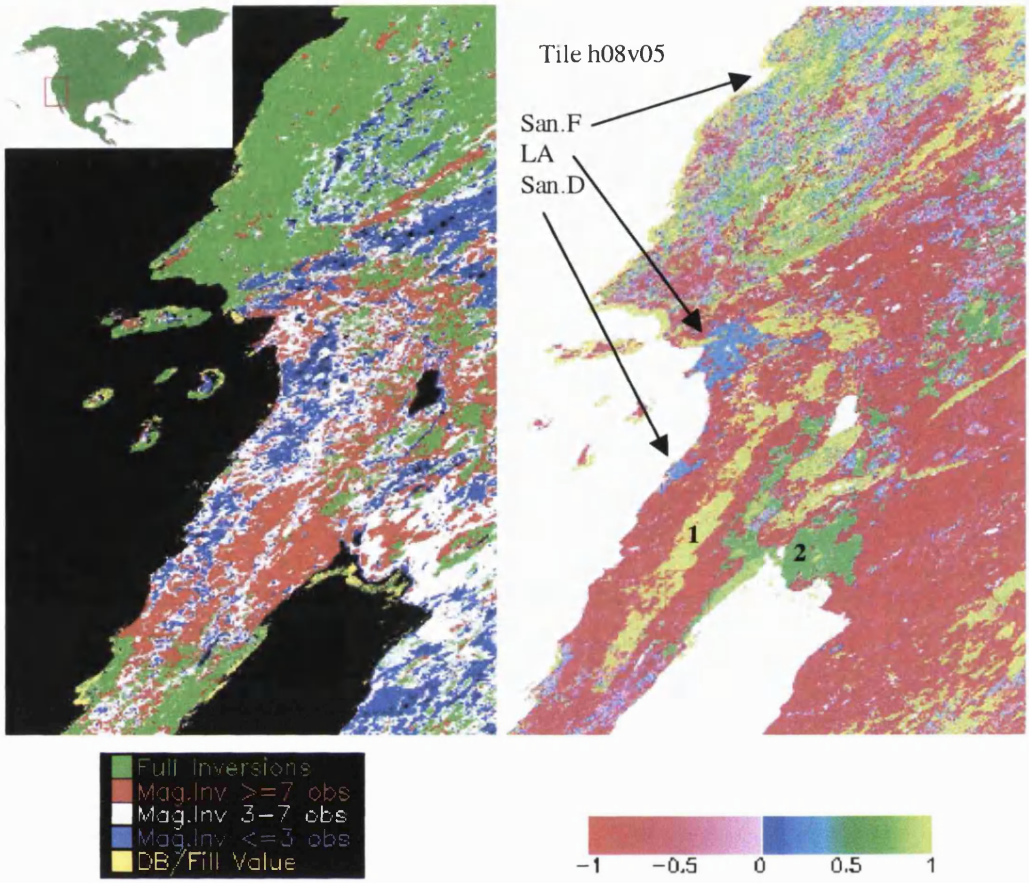

Figure 4-9 Red band NDFI, and corresponding QA for JD 2000-305 over Los Angeles and Baja California (Image size: 1000km x 600km). Inset map from: www.worldatlas.com

4.3.2.3 Comparison of kernels and retrievals

The difference in kernel weights between full and magnitude inversions is also apparent when the two parameters are plotted against each other. Figure 4-10a shows the result for the magnitude inversion areas over California (JD 2000-305, shown in Figure 4-9). Volumetric and geometric kernel weights are determined by the underlying land cover class look-up value, which determines the BRDF archetype. A magnitude inversion can have anywhere between 1-7 observations. The number of observations modulates the precise value of the two kernel weights but still conforms to the basic shape of the BRDF for that land cover. In this way, a limited number of observations can still introduce variation with a certain land cover class. The urban class is the first line of points with the shallowest gradient in Figure

4-10a, indicating that it has the most predominant geometric scattering of any of the land covers in the scene. By contrast, full inversions do not display any such patterns related to land cover. The success of the original NDVI is due to the reflectance values in the red and near infrared being largely independent of each other. However, theory and calculation suggests that the two kernels used in the NDFI are correlated to some degree (Strahler, 2001 personal communication). This correlation arises due to the fact that the two kernels are not completely orthogonal, that is to say, volumetric and geometric effects are not mutually exclusive; there are volumetric effects at the canopy level. A sparse sampling scheme only serves to further complicate the separation of these components.

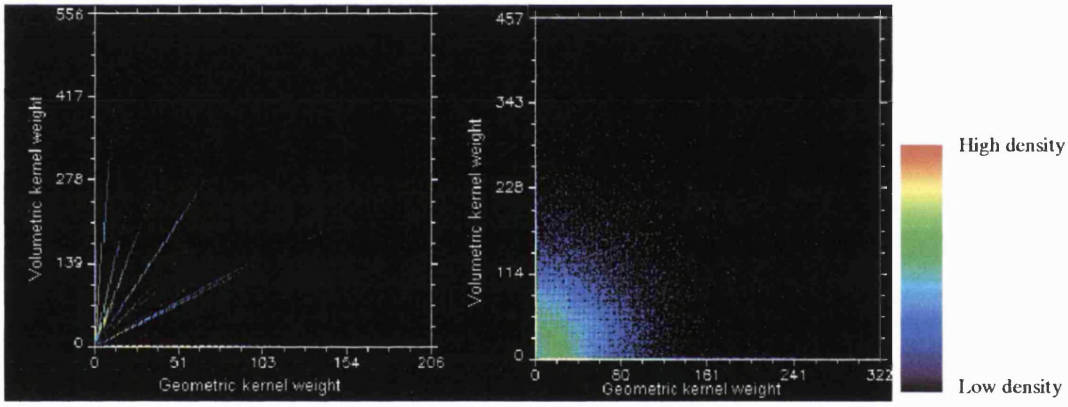

Figure 4-10 Scatterplots of geometric kernel weights versus volumetric kernel weights for the California tile (h08v05) JD2000-305 shown in Figure 4-9. Panel (a) refers to magnitude inversion areas and panel (b) refers to areas of full inversions. The colour bar on the right refers to the relative density of points at that location in feature space.

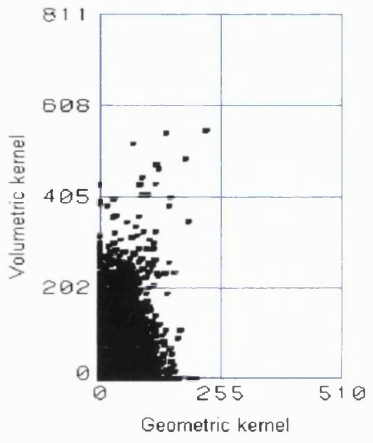

Figure 4-11 Scatterplot of full inversion kernel values over urban areas

The scatterplot for full inversions shown in Figure 4-10 applies to the whole range of land covers present in the scene. In order to assess whether there is a discernable relationship over urban areas, the radiance calibrated night-time lights dataset was used as a mask so only full retrievals in urban areas were considered. This subset is shown in Figure 4-11. The correlation

coefficient (r) is –0.013, which means there is virtually a random distribution of kernel values in these urban areas.

The operational MODIS BRDF algorithm constrains negative values in the model. The parameters used in the prototyping study of d'Entremont *et al.* (1999) were not constrained such that the kernel weights made physical sense. In addition to this, their study used 15 looks over 17 days. The fact that the operational MODIS BRDF/Albedo algorithm uses a 16-day fixed window as opposed to a moving window means that cloud free observations will only ever be used in one release of the product, when it could have been utilised for more dates under the moving window method. A large part of the discrepancy between the two studies may be due to atmospheric correction algorithm used in the MODIS products. The correction applied for aerosols has been noted to perform poorly over surfaces brighter than 0.035 at 470nm (Vermote *et al.*, 2002). It is hypothesised that these reasons are responsible for urban areas being completely obscured when full retrievals had taken place. As expected, where magnitude inversions were performed, the relationship between NDFI and land cover was good. Strugnell and Lucht (2001) mention that future models will include a separate urban BRDF. Meister (1999) has developed an urban BRDF model for application to smaller-scale remote sensing images (i.e. pixel size greater than 500m). The model is based on geometric reflection, and describes an urban area as a superposition of street structures oriented in different directions. Street structures are defined by three parameters: width of the street, height of neighbouring buildings and width of buildings.

An alternative way to visualise the three kernel parameters is to display them as RGB colour composites of the three kernel weights. Examples of temporal composites of red band QA, NDFI, and RGB colour composites of the BRDF parameters can be found in Appendix 2.

4.3.3 MODIS albedo and urban areas

Albedo may be defined as the ratio of upwelling to downwelling radiative flux at the surface and is a crucial parameter influencing land surface radiation exchange. With respect to mapping anthropogenic activities from space, the built environment is known to affect the surface albedo and net radiation transfer. Albedo values from multi-angular satellite observations are derived from integrating the BRDF model over the observable hemisphere. Albedo can be assessed in the same way as the BRDF parameters, since the QA data is the same for both products. Therefore, this presents an opportunity to test the sensitivity of the albedo product in relation to the type of the BRDF retrieval. Albedo values from full retrievals of the BRDF parameters are of particular importance as the results of section 4.3.2 suggest that there are significant differences between the two retrieval regimes.

Albedo values were analysed for the Nile Delta and parts of Florida. Figure 4-12, shows the best example of full retrievals over one area. The corresponding albedo map is shown on the right-hand side. Urban areas are clearly visible in this image of the Nile Delta (seen as light blue areas within the delta: range of values 0.12-0.14). Examining this scene in detail reveals that pixels over the centre of towns tend not to contain full retrievals. In some cases for cities over Western Europe, no data values occur in these areas. In general it is rare to find full inversions over urban areas.

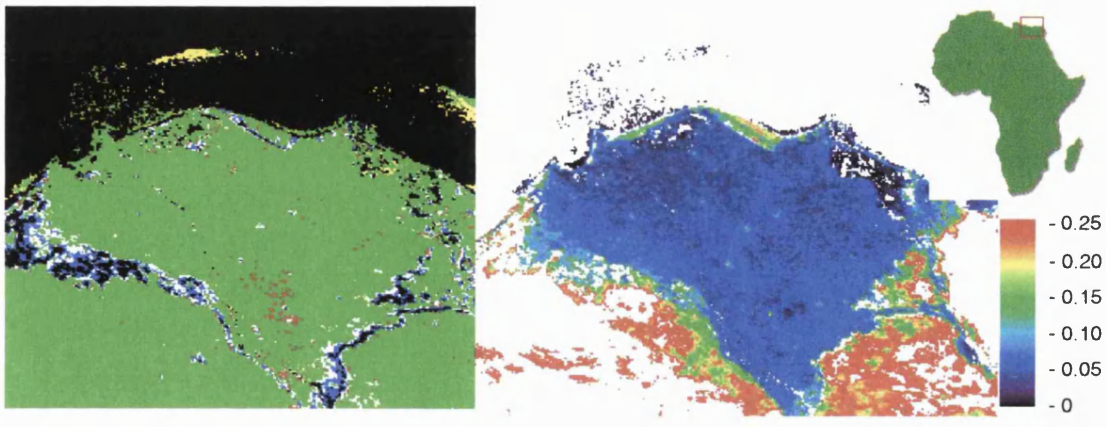

Figure 4-12 Albedo over the Nile Delta 31.10.2000 with its associated QA map on the left. Image size: 275 km x 200km. Inset map from: www.worldatlas.com

Albedo appears to be less sensitive to the inversion technique used. Figure 4-13 shows a detail of broadband visible white-sky albedo over Miami and its respective QA. The data for the 16-day period starting on 1st January 2001 had virtually all full inversions. Magnitude inversion pixels take albedo values around 25% higher than the full inversion albedo pixels. This difference was much lower in the Nile Delta. These results are in line with the prototyping study (Schaaf *et al.*, 1999) and demonstrate that anthropogenic features have a distinctly higher visible albedo than the surrounding area, and that this is detectable from the 1km product (Doll *et al.*, 2001).

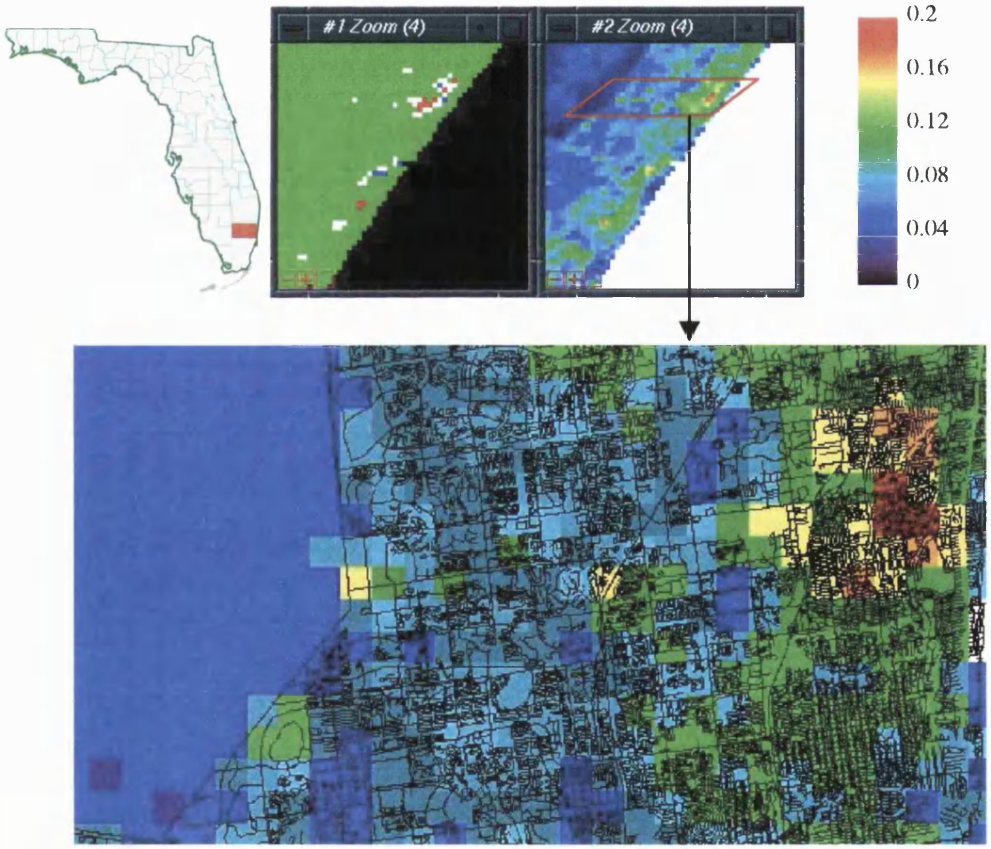

Figure 4-13 Detail from Florida study area (Broward County shown on map, top left) for date JD 001-2001. QA (left panel) is shown alongside broadband visible albedo (right panel). A section of albedo values in the red box is enlarged below and has the TIGER road network overlaid in black (Image size 30km x 16 km). Reference map from: www.worldatlas.com

Albedo values for one urbanised county in Florida were taken and compared with two indicators of urban concentration. Night-time light imagery was used in conjunction with the US TIGER (Topologically Integrated Geographic Encoding and Referencing system - (Tiger/Line®, 1997)) digital road network to investigate its relationship to albedo. A detail from Figure 4-13 is shown with the TIGER road network overlaid on the albedo raster. There is a clear boundary where the road network is confined to higher albedo values in contrast to the vegetated areas on the left of the image.

More quantitatively, Figure 4-14 shows that urban concentration indicators are observed to begin climbing at around an albedo value of 0.05 and levels off at 0.09, where both urban indicators remain constantly high beyond this value. Of the two indicators, radiance from the night-time light imagery rises most sharply in response to increasing albedo values. Figure 4-14 was produced using the same method to derive road density for the UK, described in section 4.1.1.

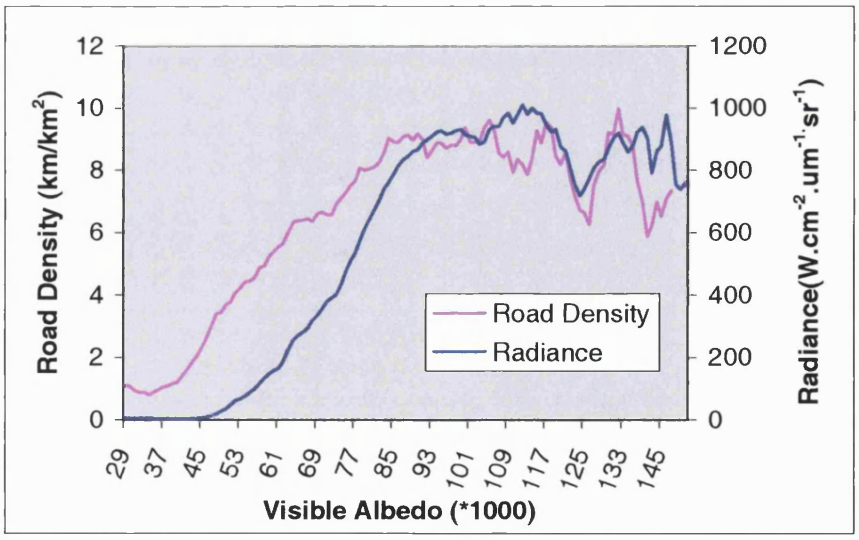

Figure 4-14 MODIS albedo values in comparison to other urban indicators Road Density & Night-time Radiance vs. Visible Albedo. Broward County, Fl.

One interesting feature of Figure 4-14 is that the magnitude of road density in this county in Florida is much higher than that of the west Midlands in Figure 4-2. This is most likely to be due to the finer scale of the TIGER dataset (1:100,000 as compared to 1:250,000 for the Bartholomew's UK dataset), which enables a more detailed representation of roads to include residential streets. The difference between the two lines between albedo values of 0.105-0.115 could be indicative of brighter street lighting in that area, but is more likely to be a source of other lighting such as an airport or industrial complex.

4.3.3.1 Albedo in conjunction with other land surface parameters

Urban albedo correlates very well with other indicators of urbanisation. The link between albedo, and anthropogenic heating was concisely explained by Taha (1997). Increasing the albedo of building materials can have dramatic decreases in the surface temperature of those surfaces. This, in turn, helps keeps cities cooler, and reduces the power demands made by air conditioning units. Power usage of this nature is particularly high in cities with a hot climate. Taha *et al.* (1997) reported that afternoon air temperatures on summer days could be lowered by as much as 4 degrees by increasing the surface albedo from 0.25 to 0.40. One sixth of the total energy used in the US is spent on cooling, at a cost of $40bn a year. In addition to which are the climatic implications associated with the localised heating over urban areas (BBC, 2000). Figure 4-15 is an example of the 8-day land surface temperature product from MODIS. Cities (as well as rivers) can be clearly identified in the imagery as warmer tones in the image.

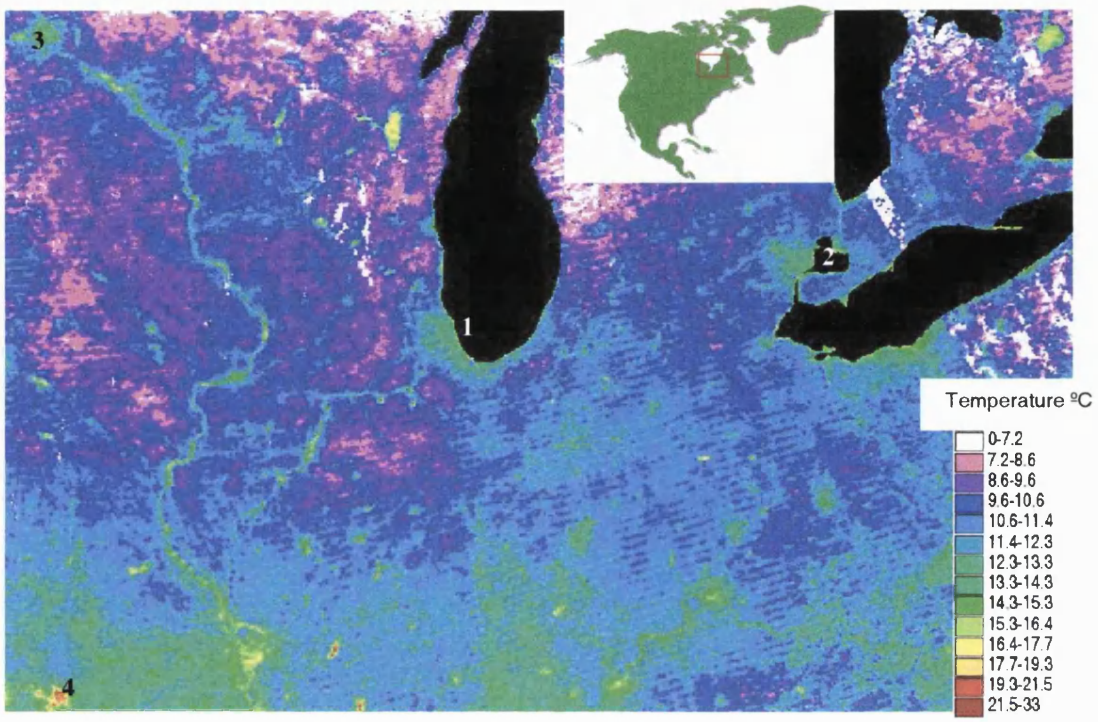

Figure 4-15 A land surface temperature scene from MODIS over the Great Lakes area of the United States.). Image size ~1200km x 850km. Inset map from: www.worldatlas.com

Thermal anomalies are detectable throughout the scene in Figure 4-15 and many of the bright concentrations of higher temperature do correlate with urban areas such as those of Chicago (1), Detroit (2) and the twin cities of Minneapolis & St.Paul (3). However, not all anomalies correspond to urban areas (4) and conversely not all urban areas demonstrate the heat island effect. Such issues complicate the analysis of thermal imagery in relation to urban areas. Figure 4-15 is included here as an example of the land-surface temperature product although no further analysis was carried out.

Both MODIS BRDF/Albedo and LST products rely to some degree on an underlying land cover map. The LST product uses a classification-based emissivity look-up table derived from land-cover types as part of the LST algorithm (Wan, 1999). However, this does not mean that information over urban areas cannot be independently derived from these datasets. The use of night-time light imagery in conjunction with global databases of physical parameters such as MODIS albedo and land surface temperature should nonetheless aid the interpretation of these

products in a HDGC context and it is hoped that they could ultimately play an important role in understanding the human footprint on the Earth, and how to manage our urban environments.

4.4 Summary

This chapter has sought to give examples of how different remote sensing datasets can offer different kinds of information about urban environments. Night-time light imagery provides a very obvious form of urban detection, which has been shown to correlate with other urban indicators. The coherence information from interferometric SAR images can yield higher spatial resolution results but requires complex processing of images. Notwithstanding this, radar applications can find important applications subject to temporal baseline considerations.

The MODIS products discussed above represent the nascence of a continuous stream of high quality datasets describing numerous facets of our environment, some of which have detectable elements of human activity. The BRDF/Albedo product has been evaluated in the light of previous studies; the BRDF parameters themselves were not found to be able to detect independently urban areas due to the model constraints and the possible poor performance of the atmospheric correction used for MODIS products. The associated albedo product was found to be less affected by the type of inversion. Albedo appears to correlate well with urban areas under both full and magnitude inverted retrieval regimes. MODIS albedo has been shown to correlate with both night-time light imagery and road density as urban indicators and has the potential to be incorporated with datasets of other land surface parameters.

Chapter 5

Night-time light imagery as a proxy for mapping human population

The accurate location and determination of the magnitude of human population in a format which is compatible with other remote sensing data is one of the key data requirements in the quest to link human and physical systems together within a single model. A detailed description of human population across the Earth's surface is essential for identifying locations of population which may be at risk from environmental change. Moreover, in recognizing that the anthropogenic component of the Earth system has the potential to stress the environment, it also serves as a means of identifying areas most susceptible to human influence. Whilst census data has been available for decades in many countries, it is not generally available for others, nor is its format readably integrated with other geo-datasets. Recently, efforts have been made to take census data and represent the data as a surface. The advent of night-time light data has also stimulated research into using satellite data to map populated areas. This chapter explores the application of night-time light imagery to mapping human population both globally and at the city level. Starting with a review of early remote sensing methods to map population, this chapter explores the characteristics of the light-population relationship and the refinements possible to estimate population by using radiance calibrated night-time light data. The chapter concludes with a discussion of the LANDSCAN database, the first satellite-based global database of human population.

5.1 Representing population on a grid

In general, socio-economic data are usually reported at the national or regional level. Whilst these administrative units are convenient for collecting data, it may be an

inappropriate unit to perform large-scale environmental analysis. An alternative scheme might be to use ecological zones or watersheds rather than nation states. Since satellite sensors collect much global environmental data, the representation of population on a compatible raster would seem to be a sensible way to proceed in order to maximise the usefulness of these data in terms of both compatibility and flexibility to different methods of analysis. This section outlines two projects undertaken to construct gridded representations of the human population.

5.1.1 The global demography project

The first attempt to map population density globally onto a grid was made by Tobler *et al.* (1995) in the Global Demography Project. The project aimed at creating a gridded population density map at the medium resolution of 5' (5 arc-minutes corresponds to an area of approximately 7,900 km^2). The input to this map was based on census data from over 19,000 administrative units worldwide. Global census data were obtained with a reference year ranging from 1979-1994. Estimates for 1994 were derived based on the implementation of a standard growth model based on growth rates provided by the United Nations (Tobler *et al.*, 1995). The algorithm used to create the map employed a method called pycnophylactic interpolation developed by the project's lead investigator, Waldo Tobler, in 1979. Pycnopylactic interpolation is a volume preserving smoothing function, which works on the assumption that one geographical area affects an adjacent area (Tobler, 1979). Hence an area with a low population density lying adjacent to an area with a higher population density will be represented as having a higher than average density at the boundary between the two areas. This will be compensated by areas further away from the boundary having a lower than average density in order to preserve the volume of the area. In this way pycnopylactic interpolation smoothes out the often large discontinuities present in standard chloropleth maps.

The interpolation function used is a purely mathematical one and doesn't take into account the spatial arrangement of entities *within* an administrative area. The

variation of population density produced by the model in a given area is solely a consequence of the magnitude of the densities of the bounding areas. Returning to the example mentioned above, if the area of lower population density were the result of population being concentrated in a city in the centre of its administrative area, population density would be incorrectly allocated to cells along the border of the higher density area. The magnitude of these errors can be minimised by using data from smaller and smaller administrative areas. However due to differences in the collection and availability of data between countries, the map is likely to be more accurate in some places than in others. The raster datasets produced by the Global Demography Project are distributed by CIESIN and can be viewed on their website (CIESIN, 2000).

The product known as the Gridded Population of the World (GPW) was recently updated in a second version to include a number of improvements. More recent data were collected from a vastly increased number of administrative boundaries (127,105). This permitted the increase of the map resolution to 2.5' and its production for 1990 and 1995 rather than the 1994 estimate of GPW version 1. User feedback determined that the pycnophylactic interpolation, which had been a key feature of the first version, was dropped as users preferred to work with unsmoothed data.

An example of the application of a global population density map was given by Small and Cohen (1999) who used the GPW (v.1) dataset to analyse the climatic and physiographic distribution of human population. They concluded that whilst human population is spatially dispersed it occupies narrow ranges of continental physiographic features such as elevation and distance from coastlines or permanent rivers. The amount of available land for each of these parameters is also limited throughout its range (i.e. there is more land at lower elevations than at higher ones). Normalising population data by the amount of available land provided a means of visualising the most densely populated range for a given parameter. Population was found to be less constrained by climatic parameters than by physiographic parameters.

5.1.2 Gridding the UK Census

A larger-scale mapping project than the GPW to turn the data from the 1991 UK Census into a surface was developed by David Martin at Southampton University. This was a particularly useful undertaking since the administrative zones of the UK census are subjected to more frequent alteration than in other countries. Whilst countries such as France have relatively stable commune boundaries, which contain a wide range of population size, the UK's desire to retain population parity between boundaries results in frequent boundary changes. This makes the separation of boundary change from population change particularly difficult (Martin, 2000). The gridding algorithm uses a set of distance decay functions generated from the population-weighted centroid for each enumeration district (ED). This allows each cell to be allocated a weight to which the population of the ED will be distributed. Greater detail on this method can be found at the SURPOP website (Crown, 1999). The output resolution of the grid was set at 200m. The SURPOP dataset was evaluated in comparison to night-time light imagery by Doll and Muller (2000) described below in section 5.4.

5.2 Methods of estimating population from remote sensing data

Population estimation based on measured land areas can be conducted at all scales subject to appropriate discriminatory features being found in the data to delimit a settled area. This can be notoriously difficult to do from normal spectral data since the variety of land-cover surfaces give rise to indistinct spectral signals. This problem is compounded for small scale, coarse spatial resolution imagery. Once a technique for delimiting settled areas is established, the estimation process centres on the mathematical model used to relate area and population. The allometric growth model is frequently used as a means of estimating population as it has been empirically observed to relate population and the area of a settlement.

5.2.1 The allometric growth model

The allometric growth model has been widely used to model the relationship between area and population. Stewart and Warntz (1958) demonstrated the link between the radius of a built up area and the population living within. On the basis of their empirical results they established the relationship:

$$r = aP^b$$

Equation 5-1

where: r is the radius of a circle of equivalent area to the settlement

P is the Population

a, b are coefficients

More formally, Equation 5-1 expresses the law of allometric growth, which states that the rate of relative growth of an organ is a constant fraction of the rate of relative growth of the total organism (Nordbeck, 1965). It is observed in a host of geographic features from river morphology to volcanoes, and densely populated areas. Generally expressed as $y = ax^b$, taking logs will linearise the equation thus:

$$Log\ y = Log\ a + b\ Log\ x$$

Equation 5-2

Nordbeck (1965) tested the model for cities in Sweden, the US, and Japan, but considered the problem from the viewpoint of estimating area from known population values. The correlation coefficients were determined at greater than 0.9; in particular the coefficient, r, between area and population for towns in southern Sweden was 0.98.

The allometric growth model allows the estimation of a variable y, by means of another proxy variable x, which is easier to measure than y. Since the equivalent area of the circle can be established, the population for a given area is easily

computed. Tobler (1969) was the first to survey the role of satellites for monitoring population from space combining established theory with space-borne photography from the Gemini missions to assess population on much larger scales. The satellite data were only used in a geometrical context to ascertain the area (and hence, the radius of an equivalent circle) of the settlements in question. Whilst a degree of spatial variation in the coefficients was found between the regions sampled, the correlation coefficient was found to be as high as 0.99 in some areas. Further investigations by others support this relationship. Lo and Welch (1977 cited in Lo, 1986b) used Landsat data to assess settlements in China. The boundaries of cities with a population range of 500,000 to 3,000,000 were found to be easily delineated in the near infrared band 7 images. The Equation 5-1 was modified to read

$$P = cA^d$$

Equation 5-3

where: P is the population

A is the area of the settlement

c,d are coefficients

Although the coefficients (c and d) will be different from those in Figure 5-3, the fundamental relationship will be the same since area and radius are related by a power law. In this case, $c = a^{-1/b}\pi^{-d}$ and $d = 1/2b$; a derivation for this equivalence is given in Appendix C. A single regression for the 124 cities in the sample revealed that certain cities were over- or underestimated. Cities of over 2,500,000 inhabitants were found to be particularly underestimated. The model was refined by grouping cities by regions and applying a separate model for each region. A linear growth model was applied for those excessively large cities. These ideas have been re-tested and extended by a number of other researchers using night-time imagery and are explored in the section 5.3.

5.2.2 Early approaches to population estimation

Population estimation from remotely sensed data has been attempted in a number of ways and its early development was summarised by Lo (1986b). His chapter identified four main ways of estimating population from remote sensing data:

i. estimation based on measured land area;
ii. estimation based on the number of dwelling units;
iii. estimation based on measured land use areas;
iv. estimation based on spectral radiance characteristics of individual pixels.

Land areas can be assessed from many different sources of remotely sensed data. In addition to optical remote sensing, radar imagery can often be more useful in detecting the presence of settlements. Radar data are very efficient at identifying man-made features as they often provide a high return because of the high dielectric properties of some of the materials used in their construction, most notably metal. The geometric shape of urban features also contributes to the high return by acting as corner reflectors. Haack and Slonecker (1994) used the Shuttle Imaging Radar-B (SIR-B) synthetic aperture radar (SAR) to identify villages in Southern Sudan. Lo (1986a) used SIR-A data to analyse settlement, population and land use in northern China and observed that settlements down to 1.6 km^2 in size could be delineated, corresponding to populations of between 1,000 and 2,000 people. Population was assessed in two ways depending on the size of the area. Small villages were estimated using overall population density figures, whilst urban estimates were produced via allometric growth models. Both methods were judged to provide accurate estimates.

Harris (1985) also identified a linear relationship between population and area of settlement. In this limited study of small settlements in Tunisia, towns away from the coast were observed to take a circular form as their growth was uninhibited by topography. Settlements ranged in population from 1,000-34,000 and were observed

from SIR-A imagery. The relationship derived was noted to have limits in extrapolation. In particular, it was observed that larger towns will have multi-storied buildings allowing for an increase in population without commensurate increase in settlement area. Henderson and Anuta (1980) recognised the inconsistent detection of settlements below 1,000 people, thus preventing extrapolation below this level. Whilst these points are most pertinent to large-scale urban mapping exercises, it highlights the shortcomings of reliance on area as a surrogate measure of population, with no consideration being given to varying density.

Method (ii) could only really be done from aerial photographs and more recently, from very high spatial resolution satellite imagery such as the IKONOS satellite operated by Space Imaging (Space Imaging, 2002). The use of such large-scale data restricts the spatial extent to which this technique can be practically employed. It also requires extensive manual intervention, which can be time consuming. This is becoming less of an issue with advances in automated feature extraction techniques. However, large amounts of ground truth data are needed to calibrate the technique e.g. average number of people to a dwelling.

An extension to estimating population based solely on land areas is to consider land use as a sub division of an urban area. In this way one may attempt to account for a distribution of population densities. Use of the allometric growth model assumes a uniform population density within the defined urban area. By classifying an area into residential classes one can compute the population of the area using Equation 5-4.

$$P = \sum_{i=1}^{n} (A_i D_i)$$

Equation 5-4

where: P is population

A_i is the area devoted to residential land use over n categories

D_i is the corresponding population density of that area

Population density values can be obtained from sample surveys of each residential class or indeed from census data. This approach first requires that the individual land classes be accurately represented. Lo (1979 cited in Lo, 1986b) encountered difficulties in differentiating between single family, and multi-family residential use, and though less accurate than the dwelling count method, it has the advantage of being used at smaller scales (whole urban areas). The method is best applied to suburban, as opposed to inner city locations and areas that are slowly changing urban environments. These two techniques work best for large scale, high spatial resolution and are therefore inappropriate for global population estimation. In the same way as for population estimation based on dwelling units, this technique has been essentially restricted to aerial photography as it is hard to obtain such a fine level of classification within an urban area from space borne satellite imagery. However, the advent of high spatial resolution satellite imagery is stimulating innovative classification techniques, such as analysis of the structural composition of urban land-use informing graph based models (Barnsley *et al.*, 2003)

Whilst these two techniques are perhaps best suited to aerial photography (and now very high spatial resolution satellite data), a similar multi-spectral technique can be employed using regular satellite data. Using the rationale that radiance values differ over spectral bands for different land covers, it is possible to develop a linear mixture model such that:

$$P = Ax_1 + Bx_2 + Cx_3 + Dx_4 + E$$

Equation 5-5

where: P is population

x_1, x_2, x_3, x_4 are the radiance values for the multispectral bands

A, B, C, D, E are fitted coefficients.

Iisaka and Hegedus (1982) used this methodology to estimate population of the Kanto district of Tokyo from Landsat MSS data. It was found that the presence of non-residential built structures near the central business district (CBD) affects the

reliability of this technique (multiple regression coefficients increased from 0.84 to 0.94 and 0.78 to 0.9 when these non-residential cells were excluded from the analysis). However, it serves as an early example of how the spectral properties of remote sensing data may be used to estimate population. Recently, Harvey (2003) evaluates an improved pixel based estimation method using data from the 6 reflective bands of the Thematic Mapper instrument. This method uses a classification of residential and non-residential areas make an initial population estimate. This is iteratively re-estimated based on the spectral characteristics of these areas.

There are essentially two ways in which to estimate population from remote sensing data. One is to use a zone-based model, the other is to use a pixel-based model. Whilst the former is more practical as census data is usually published by zone, the latter minimizes the Modifiable Areal Unit problem (MAUP) (Lo, 2003), which arises as a consequence of using different sized zones and aggregations. The MAUP is further discussed in Chapter 6, whilst the spatial disaggregation and dasymetric mapping (Langford, 2003) is discussed in Chapter 7. The following sections of this chapter examine how these ideas can be applied to night-time light imagery for population estimation.

5.3 Population estimation from night-time light imagery

The total area of light at night observed by the DMSP-OLS 'city-lights' product has been observed to correlate with population figures for countries regardless of economic development (Elvidge 1997b; 1997c). Doll (1998) extended these observations to analyse the relationship between the lit-area in a country and population. Firstly, a graph of lit-area versus city population was produced. The graph relied upon the collation of a global database of city location and corresponding population figures. This database was obtained from the University of Iowa's Center for Global and Regional Environmental Research (CGRER). However, much of the population data was deemed to be inaccurate, so this element

of the database was augmented with the latest available data from the Philip's Geographical Digest 1998-99 (Philip, 1998). Despite the title of the book, the city population figures from Philip (1998) largely pertained to the mid-1990s time-period. An additional source of georeferenced data was included from the United Nation's demographic Yearbook for 1995 (UN, 1995), which provided a database for every city with more than 100,000 inhabitants. This resulted in a global database of 2954 cities with which to compare against the night-time light clusters. The analysis relied on the matching of city locations to clusters of light; both continental and individual country level analysis was performed. Clusters were converted into polygons using a GIS (`gridpoly` command in Arc/Info) so they could be matched to population data stored as attribute data in the point coverage of city locations. Large conurbations often contained multiple population points (Figure 5-1). In this case, the populations were summed and attributed to the entire lit-area of the polygon. Lit-area versus population relationships were analysed in log-log space as has been advocated in previous studies by Tobler (1969), Elvidge *et al.* (1997b; 1997c).

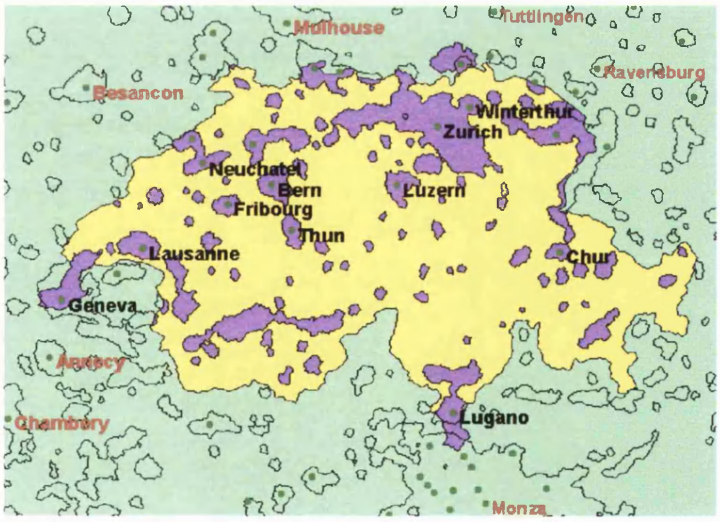

Figure 5-1. Frequency Composite Image of Switzerland. (Note how Swiss polygons purple = populated are intersected by the European coverage (green)).

At the continental scale the relationship exhibits an essentially linear (in log-log space) distribution, which becomes ever more spread out at lower area/population levels as is shown for Europe in Figure 5-2. This suggests that there is a wide range of population densities for low population towns. Other error sources contributing to

this effect include the inaccurate city population statistics and the assumption that all population is accounted for within the polygon. Care was taken to use the population figures pertaining to the urban agglomeration rather than the individual town where possible. The individual country relationships tend to be a linear subset of this distribution.

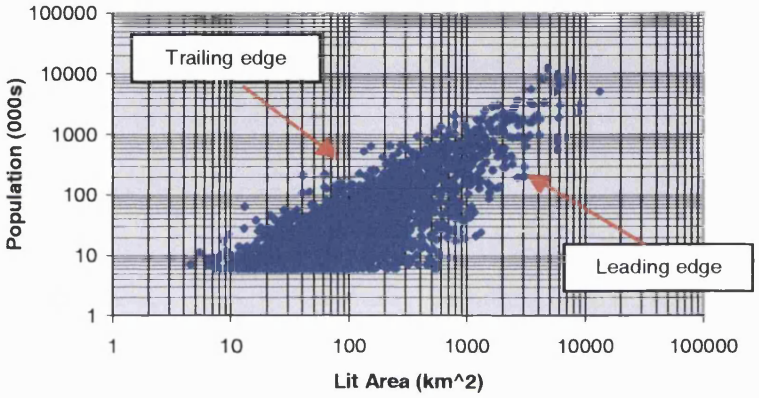

Figure 5-2. Lit-area/population scatterplot for European cities with annotations referred to in the text below.

The individual country relationships were used to predict the urban population for each country by estimating the population of lit areas which had no population data associated with them. This was then compared to the urban population figure published by the World Resources Institute (WRI, 1996). Forty-six countries were tested in all; these results are presented in Doll *et al.* (2000) along with a complementary study for carbon dioxide emissions. The population results from this study are shown in Appendix C and described later in this section. These methods and results were replicated and extended by Sutton *et al.* (2001) who went on to calculate a figure for the global population. By taking the estimated population of a country and assuming that it was equal to the known urban population, it was possible to adjust this estimated figure and retrieve a value for the total population of a country by using the accompanying national urban population percentage figure. Sutton *et al.* (2001) also observed a broad based distribution to points in his lit-area

population scatterplot similar to that shown in Figure 5-1. These points could be largely resolved by dividing them into three categories based on the per-capita income of the country to which it belonged. Low-income countries (per capita GNP < $1000) occupied a band of points on the trailing edge of the distribution. Medium income countries ($1000 < p.c.GNP < $5000) occupied the middle part of the cluster, whilst high-income countries' points were located further to the right and composed the leading edge. The further to the left of the graph a point is, the smaller the settlement was observed from the night-time light imagery. This implies one of two things: either that the low income countries have the highest population densities, or that much of the population may be undetected due to low lighting in informal settlements. This classification of countries by income was also used to apply different frequency thresholds to the night-time light data in order to help define urban areas. A threshold of 40% was applied to low-income countries and 80% to medium and high-income countries.

The difference in methodology and Sutton's use of population data for 1997 (some 2-3 years after the imagery was taken) to calibrate his relationships as opposed to the 1995 data used by Doll (1998) means it is not possible to compare directly the results of the two studies. However, it is possible to make some general comparisons between the two studies. The range of 'error' or disparity between the observed and predicted populations is similar with both over and underestimations as high as 68% for Sutton and 108% (Iran) for Doll. Despite this, both studies were accurate to within 10% of the total official figures. Sutton *et al.* (2001) estimated a global population figure of 6.3 billion versus the published figure of 5.9 billion whilst Doll *et al.* (2000) accounted for 1.77 billion of the 1.96 billion urban dwellers in the 46 countries studied. A notable point is that many countries poorly estimated by Doll *et al.* (2000) were also notable disparities in Sutton's study. In particular, both methods heavily overestimated the population of China by 22 and 24% respectively. Iran was also another country overestimated by both studies, whilst Germany and the UK were countries whose populations were consistently underestimated by the studies. Russia and South Korea were two countries both underestimated by 36% and 42% respectively by Doll but this was reduced to disparities of just 5% and 2% in

Sutton's study suggesting that the 80% threshold applied was highly effective for these countries. Despite the use of a 40% threshold for India and Indonesia, Doll and Sutton's results are both within 9% of the published figures. The omission of a threshold increases the likelihood of allocating more area than is represented by the population statistic. In this case there will be a general tendency to underestimate population, as has been the case with the results presented by Doll *et al.* (2000). The employment of a variable threshold as used by Sutton *et al.* (2001) however has not been shown to provide consistently more reliable results either in terms of individual countries or total population counts.

The use of satellite data offers many advantages in comparison to conventional census collection techniques, not least of which is the homogeneous method of collection. In addition to this, it is far easier to revise estimates over both space and time. The result of an exercise in estimating population is precisely that: an estimate. The figures that are used to calibrate and compare against are themselves estimates based on projections of a growth rate from the last census of that country. In this sense, one can only talk of relative accuracy rather than absolute error. The techniques outlined here rely on census data to calibrate the models. It is not intended that satellite data completely replace the census in its traditional form. However the benefits it offers makes it a potentially useful tool for intercesnal population estimation as well as for monitoring urbanisation in developing countries.

5.3.1 Refinements using radiance calibrated data

Population estimation from night-time lights was attempted by Doll *et al.* (2000) using the frequency composite (FC) version of the night-time data. As the global radiance-calibrated (RC) dataset became available, the study was repeated to ascertain firstly what kind of methodology could be developed to integrate lit-area and radiance with population, and secondly what advantages radiance-calibrated

data had over the frequency composite data for population estimation. These two datasets are described in chapter 3.

The methodology of Doll (1998) considered population to be a function of area only, and therefore ascribes a uniform population density to the urban area in question. A preliminary analysis of the relationship between lit area and radiance shows this for all countries. Low intensity lighting covers the majority of the area with very little area covered by the highest radiance values. An approach was developed to use the extra information contained in the radiance calibrated imagery by calculating a country specific coefficient, which was then used to calculate population for 'unknown' polygons in much the same way as the allometric relationships before. The coefficient is derived by taking the product of area and radiance for a given urban area, and then dividing by the population contained within that area. This is based on a set of urban polygons which have population associated with the lit area (the same polygons as used in the frequency-composite study). The polygons from the 1994/5 dataset were firstly intersected with a country mask so polygons and fractions of polygons could be attributed to a specific country. This is a major improvement to the crude version used with the FC data that selected the entire polygon if it intersected with the country mask. These new sets of urban polygons were overlaid on the radiance-calibrated image and used to mask out an area of the radiance image (Figure 5-3).

Using the ArcView GIS function of tabulating areas of grids within polygons, a table of area (A_r) under each radiance value (r) was produced. A set of calibration polygons was established from those polygons enclosing population points. The total population value associated with these polygons is known as the calibration population (P_{cal}). The following model applied for each calibration polygon with a radiance range r:

$$\frac{\sum_r (rA_r)}{P_{cal}} = NARC\,(W/cm^2/sr/\mu m/m^2/person) \qquad \textbf{Equation 5-6}$$

For each of the calibration polygons the Normalised Areal-Radiance Coefficient (NARC) was calculated and averaged at the country level. Population was then determined for the rest of the 'unknown' lit polygon areas by calculating $\Sigma(rA_r)$ and dividing by the NARC. These new values along with the existing calibration data were summed to obtain the total urban population for the country in question.

Preliminary results were presented for 12 countries by Doll and Muller (1999b). These results differ slightly than those presented here (in Appendix C) because the segmentation of night-time light polygons across country borders was not applied in this limited study. In all but one of the cases (Germany), the result was not severely affected by this. Countries that were not well estimated by the use of the frequency composite data were of particular interest. China, Iran and Russia fell into this category whilst India, New Zealand and Bulgaria were accurately estimated under the old methodology. The new technique improves the accuracy of estimation for over half of the countries tested (26/44). China has gone from being substantially over estimated to similarly underestimated. Iran and Russia were previously significant outliers but are now more accurately accounted for. Urban population was also calculated using the total recalculation scheme used for the frequency composite data. This was found to be less accurate overall, only improving the accuracy of 4 countries.

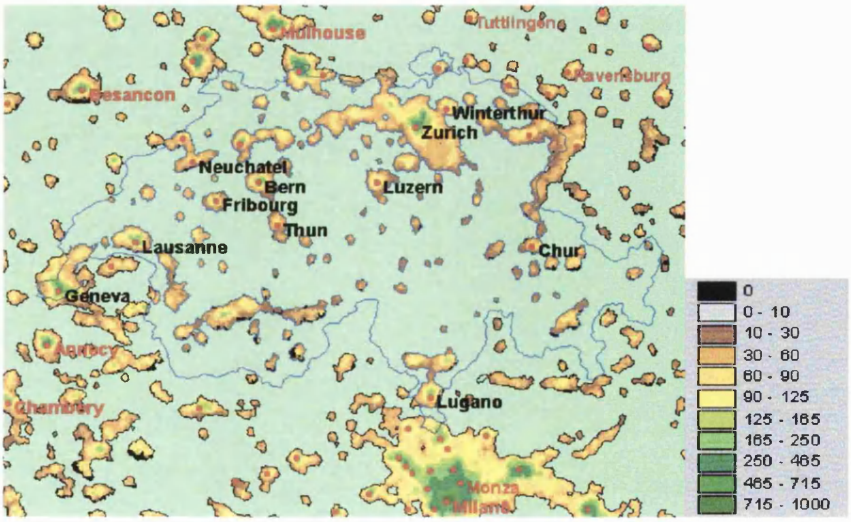

Figure 5-3. Radiance Calibrated Image of Switzerland masked by the 1994/5 urban polygons (as in Figure 5-1). Radiance (x 10^{-10}W.cm^{-2}.sr^{-1}.µm^{-1}) Blue outline indicate Swiss urban polygons

Overall, the frequency composite experiment is still the most accurate, accounting for 1.75 out of 1.95 billion people (90%), whereas the radiance calibrated experiment using the existing city data only accounted for 1.57 billion (81%). The maximum percentage disagreement using the RC method was 61.4% (Cameroon) compared to 108% with the previous FC results (Iran). The RC results tended to underestimate urban population even though city calibration data was used to compute the total.

The results obtained in the first limited study of 12 countries (Doll and Muller, 1999b) appeared to be better at population estimation than using frequency-composite data. However, the FC data had a very good overall agreement with the urban population published by the WRI. This is largely attributed to outlying countries, which have been over- and under-estimated canceling each other out when summed and compared to the total. If absolute percentage disagreement is analysed, the standard deviation for the RC results (12%) is far lower than for the FC results (22%) indicating that there is less variation in the RC discrepancies. Whilst the overall accuracy for the total number of countries has gone down slightly, this technique appears to model individual countries more accurately than before, which makes it more robust and ultimately more reliable. In using the calibration city population data as part of the estimation, its accuracy is a function of the percentage of city data known.

Accurate city population data is clearly a major pre-requisite in trying to perform such an analysis. Whilst a key assumption with both methods is that all population is accounted for, the advantage of using RC data is that population density can be modelled within polygons. However, to exploit fully this feature, one must have some idea of the population morphology within a city. The methodology outlined proposes that:

i. Population density is directly related to radiance
ii. This model is correct for all countries in the analysis

The results seem to suggest that countries like Russia, Korea and Vietnam fit this model whereas countries like China, Sweden and Cuba do not. However, there is no apparent correlation between the percentage difference between the estimated and the true urban population figure and the NARC for each country. The NARCs range over three orders of magnitude with the values for Finland, Canada, Sweden and the US being much higher than the rest of the countries. The coefficients themselves are correlated to per-capita GDP (Figure 5-4) indicating that the amount of light per person is related to the economic development. If population morphology is dependent on GDP, then one could rank countries by GDP and apply different models to groups of countries as was suggested by Sutton *et al.* (2001). Another scenario is that population morphology is more a function of size, as larger cities tend to have low-density commercial centres.

Population morphology will be discussed in section 5.4. The advantages of a radiance-calibrated dataset are manifold. As urban sprawl further encroaches onto undeveloped lands, the increasing light pollution will be mapped. As these are likely to be lower density suburban housing, it is likely to be quite low intensity light. Owen *et al.*, (1998) assigned urban/suburban/rural classifications to DMSP-OLS frequency data, based on the correlation of night-time lights to housing density for rural areas, and on the assessment made by Imhoff *et al.* (1997) for urban areas.

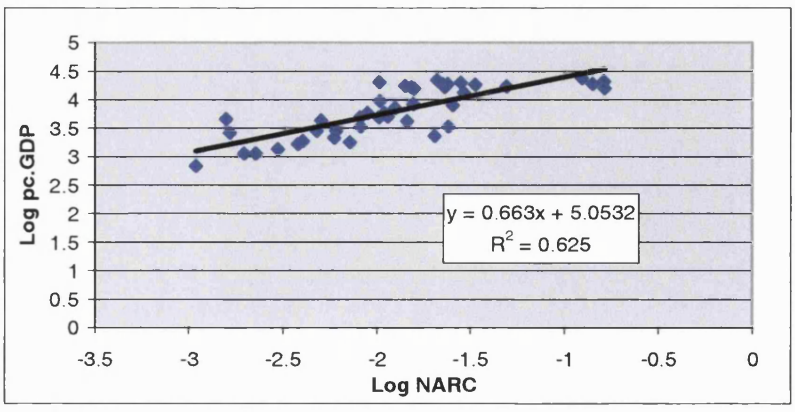

Figure 5-4. Correlation of NARCs to per-capita GDP for the 44 countries tested

The method described above has the potential for further refinement; some of these are discussed in section 5.3.3. It demonstrates the potential for modelling and estimating population from radiance calibrated night-time data. The RC dataset is a technically superior product, and is the benchmark to be used in future studies. Identifying the population morphology of a city is regarded here to be a key factor affecting the success of this technique. In addition, there may be more subtle relationships between NARCs for different settlement sizes, which if implemented could model population better. Any such detail has been effaced through the averaging of the city coefficients to produce a single figure for each country.

5.3.2 Other studies

Nakayama and Elvidge (1999) compared the city-lights frequency composite data and the radiance calibrated datasets to population density. They found the radiance calibrated data set to be better correlated than the city-lights dataset due to its broader dynamic range. However, the relationship is confused by lit pixels which have no population associated with them, such as sections of road or port facilities. The radiance dataset was also found to be more sensitive to the presence of population, with a pixel having the lowest detectable population density (8 people.km^{-2}) being 50% more likely to be detected by the radiance dataset than the city-lights dataset. This compares with a mean population density range of 10 - 41 persons.km^{-2} over the first 63 DN values reported by Sutton *et al.*, (1997) for the USA. However, this value leaps to 321 persons.km^{-2} for the highest DN value (64 for a 6-bit sensor) highlighting the relatively low-level at which the sensor becomes saturated in the frequency composite product. Based on these figures, 80% of the population is classified as occupying 10% of the area in the United States.

Konami *et al.* (1998) used the FC dataset to compare different models for China. They found that neither linear nor exponential models could be satisfactorily applied to estimate population for the whole of China, though it was possible to represent the population distribution in large Chinese cities. A further interesting point was

that models tended to fit better in flat rather than mountainous provinces. However, this may be due to the largely non-urban population found in mountain areas.

A more detailed analysis of RC night-time imagery to estimate population for China is provided by Lo (2001). Lo's detailed study derived a number of variables from the night-time light imagery from which different models could be established at different spatial scales. These variables not only took into account the light intensity of pixels but also considered the percentage lit-area within a region and mean pixel values. A variety of population data was obtained at city, county and provincial level. In calibrating his models, some population data was withheld by Lo so as to provide a means of accuracy assessment. When the results are considered aggregated to the total for the given spatial unit, Lo's results are easily the most accurate. However, the magnitude of errors for individual entities within each spatial scale were frequently on the order of 30-50% and occasionally more than double the published figure. Different models were found to be more appropriate for modeling different elements of the population at different spatial scales. Overall, the allometric growth model using light volume (essentially area weighted by the radiance similar to the approach by Doll and Muller (1999b)) was found to be useful for estimating the non-agricultural (urban) population at the provincial, county and city level. The best results occurred for cities, where light area or light volume may be used as the independent variable. Mean pixel values were only found to predict population density at the provincial level, whereas percent light area was found to be more appropriate at predicting city level densities. Urban populations were predicted by the radiance imagery much more reliably than total population counts. In this case it seems that the approach of Doll (1998) and Sutton *et al.* (2001) to use the imagery just for estimating urban population would seem to be most appropriate, particularly in developing countries. Whilst adjusting this figure based on the percentage of population in urban areas to obtain a figure for the total population is feasible, it does not help in identifying the location of these populations within the country.

5.3.3 Theoretical and empirical models

The results presented in this section compared the results from two empirical models and proposed a model for use with radiance-calibrated night-time light data. Sutton (2003) discusses a number of theoretical models that can be used with DMSP-OLS night-time data. These theoretical models use different distance-decay functions to model population density as a function of distance to the edge of a cluster (lit-area polygon). Such models only rely on night-time light data to delimit an urban area through the identification of lit clusters. With the exception of constant density model, all models assume that population density is highest at the center of the cluster. The models include linear, parabolic, exponential and Gaussian functions to describe the variation in population density from the center to the edge of a cluster. The distance to the edge of a cluster was calculated for each pixel in a cluster. This served as the starting point from which different models could be applied. Pixels over water and/or lying in another country were also evaluated in this way and then discarded to take account of the fact that the highest population density is at the edge of a coast or border for cities like Chicago (Lake Michagn) or Los Angeles (Pacific Ocean). Empirically, the distance grid can be overlaid on to census-block level population density data and then derive a relationship between population density and distance to the center of the cluster. None of these models tested by Sutton (2003) produced a R^2 value greater than 0.30 when tested against the original census. Besides the need for accurate co-registration between the two datasets Sutton (2003) suggests that varying population density at constant distances from the centre of a cluster is responsible for the low correlation.

Sutton (2003) also proposes a method to estimate intra-urban population density from low-gain DMSP-OLS imagery using Equation 5-7.

$$EPD = ECP \times \frac{pv_i}{\sum_{Cluster}(pv_i)}$$

Equation 5-7

where: EPD = Estimated population density

ECP = Estimated cluster population

pv_i = low-gain radiance calibrated pixel value

In this example, ECP is determined from a regression of the log-log relationship between area and population. There are potentially two sources of error in this, firstly arising from the error in the ECP and secondly, with the allocation of population within the cluster. Spatial aggregation can reduce errors of misregistration and the fact that there is a fundamental mismatch between brightness and recorded population. This will be explored further in the next section.

5.4 Radiance calibrated dataset for population morphology analysis

Doll and Muller (1999b) noted the importance of understanding the nature of the population morphology in order to model accurately intra-urban population. The radiance calibrated night-time light dataset was therefore compared to the SURPOP population data for the UK. The 200m SURPOP data was aggregated to 1km pixels to facilitate comparison with the night-time light imagery. On first inspection, a comparison between the night-time lights and the original SURPOP data reveals the similarity in distribution between the two datasets (Figure 5-5) at the national level. The next step involved investigating this apparently good relationship at finer scales. The fact that both datasets were gridded allowed this to be undertaken down to the pixel level.

A land cover map produced by the Institute of Terrestrial Ecology (Fuller, *et al.*, 1994) was also used to try to understand the precise relationship of the night-time light data to the land surface. The land cover map was derived from a mosaic of Landsat Thematic Mapper (TM) images acquired between 1987 and 1990. The original map was produced at a resolution of 25m but the ITE also created a 'summary' dataset at 1km. This dataset differs from conventional land cover maps

since individual land cover classes are presented as individual layers with the value of a given cell being the percentage coverage of that land cover class. In this way, the classic resampling problem of having to assign the majority land cover class to a larger area is avoided. An assessment of accuracy for the land cover map is put at between 80-85% (Fuller, 1995). This format was particularly convenient for analysis with night-time lights since different land cover classes can be combined. In particular since urban and suburban classes are distinct, there was a good opportunity to examine how these two individual classes contributed to light-time light emissions and also the gridded population data. As a point of note, the urban class is defined as *'all developments which are large enough to fill individual pixels* [at 25m], *to the exclusion of significant quantities of permanent vegetation'* (Fuller, 1995). The suburban/rural development category` includes *'all land where pixels of the Landsat image have recorded a mixture of built-up land and permanent vegetation'* (Fuller, 1995).

Figure 5-5 Comparison of night-time lights (left hand image) with 200m SURPOP population counts on the right. Source: The 1991 Census, Crown Copyright. ESRC/JISC purchase. The surface data used in this work were generated by David Martin, Ian Bracken and Nick Tate, and obtained from Manchester Computing

Figure 5-6 shows a section of the three datasets over London. Urban areas are characterised in the land cover map by a core of high percentage urban cover surrounded by an annulus of high percentage 'suburban/rural development' (Figure 5-6 a,b). Population (Figure 5-6c) is observed to follow a similar pattern, though in London the ring of high population density is much closer to the centre than the 'suburban/rural development' ring suggesting that the highest population densities are to be found around the central business district; the population density of the centre is in fact very low. The highly prominent suburban ring 15km from the centre of London coincides with population densities about one third of those found in the high-density zones around the centre. The night-time radiance image has similar characteristics to the population grid with suburban areas less bright than the high population density inner city areas. However, there are also disparities caused by airports (Heathrow Airport is prominent on the middle-left of the radiance image) and bright city centres.

The correlation between radiance and population was stronger for the suburban land-cover class than for the rural class. There is a substantial spread of points in the urban land cover class. Combining the ITE dataset and the SURPOP datasets with the DCW urban polygons revealed that in general, a DCW polygon corresponded to approximately 43% of urban and suburban land cover classes (combined) and 2000 people/km^2. However, no single radiance threshold could be identified (Doll and Muller, 2000).

The results highlighted the difficulty in trying to use just the satellite imagery as a proxy for mapping human population. In particular, the lack of an exact one-to-one correspondence between population density and light (radiance) was attributed to the fact that light does not explicitly emanate from residential housing but is hypothesised to come mainly from street lighting along roads and major highways, airports and commercial 'downtown' areas. Whilst airports have no residential population, it does have a transient population, which is absent in a census. Likewise, city centres have high daytime populations due to the number of people

who work there, whilst the annular residential areas are depleted of population in the day.

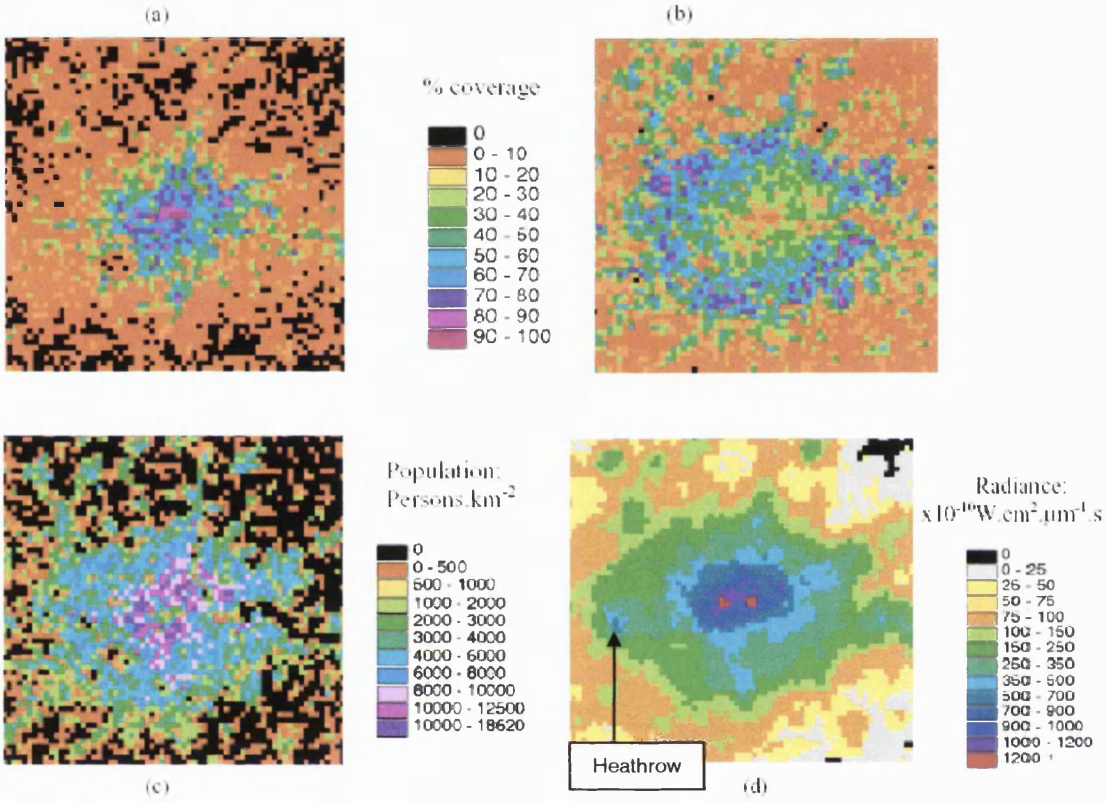

Figure 5-6. Different datasets over London, Urban land cover (a), Suburban land cover (b), and 1km resolution population generated from SURPOP (see Figure 5-5) (c) as compared to the Radiance Calibrated Night-time lights Imagery (d). Image size 65 x 60 km.

These complications are made more acute as the resolution of analysis increases. Night-time light imagery has been shown to be excellent for identifying the location of population centres (towns). Its ability to model the population morphology within a town is less assured and as such give rise to notions of day and night-time populations. Such considerations are starting to be addressed in the latest (2001) releases of the LANDSCAN database described below in the next section.

5.5 The Landscan population mapping project

The increasing body of research concerning the relationship between night-time light imagery and population stimulated the development of the Landscan database. Landscan is a global database of human population counts at 30'' resolution. It is the first such data set to be derived in part from the DMSP-OLS city-lights dataset. Sub-national census data was apportioned to grid cells based on probability coefficients generated from the proximity of the cell to roads, slopes, land cover and night-time lights. The database was developed by the Oak Ridge National Laboratory (ORNL) as part of their Global Population Project for estimating ambient populations at risk of accidental or terrorist releases of noxious substances or radioactivity. As such, the population distribution within the database aims to represent ambient population, which integrates diurnal movements and collective travel habits into a single measure (Dobson *et al.* 2000). The foundation of the Landscan population database is worldwide census data obtained from the 1994 Global Demography Project (Tobler *et al.*, 1995) described in section 5.1 earlier in this chapter. Aggregate census data and demographic characteristics (age/sex) by country and sub-national area were obtained from the United Nations Statistical Division, and updated to the year 2000 through the International Programs Center of the United States Bureau of the Census.

The source data of the four input datasets were largely obtained from the National Imagery and Mapping Agency (NIMA). Slope data were used to weight a cell by building categories of slopes most favourable to human occupation. The slope data were derived from NIMA's Digital Terrain Elevation Data Level-1 product at 3''. DTED-0 (30'') was used where the finer resolution product was not available. Road data were sourced from NIMA's Vector Smart Map (VMAP – developed from the Digital Chart of the World). Again, two resolutions were used (1:1,000,000 and 1:250,000) as coverage allowed. The land cover map was produced by the U.S. Geological Survey's Global Land Cover Characteristics (GLCC) database. Land cover can be a highly effective indicator of population density. This data set is derived from the National Oceanic and Atmospheric Administration's (NOAA)

Advanced Very High Resolution Radiometry (AVHRR) instrument providing satellite imagery at 1 km resolution (Loveland, 1991). However, this dataset has been shown to have misclassified areas by as much as 52% in some regions (Dunderdale *et al.*, 1998). The urban layer in this product is not derived from satellite imagery and is instead a rasterised version of the VMAP-0 populated places polygons. Finally, the Landscan database employed the frequency-composite night-time light dataset. The combination of these datasets permitted the generation of composite probability coefficients, which express the relative likelihood of population to exist in a cell due to road proximity, slope, land cover, and night-time lights. These coefficients are weighted values, independent of census data, which are then used to apportion a share of the actual population count within the area of interest. Coefficients vary considerably from country to country even within a particular region. Whilst the generic model remains the same, the probability weights of individual variables are customised for each area based on physical, economic and cultural factors. Control totals can be based on any administrative unit. The resulting population distribution is normalized and compared with appropriate control totals to ensure that aggregate distributions are consistent with census control totals (Dobson *et al.* 2000).

Landscan 2001 has also recently been released (August, 2002, Personal communication by King, 2002). This latest release includes a substantially increased number of second order administrative boundaries used for population distribution, greater use of NIMA's Controlled Image Base for verification and refining built up areas and the incorporation of new and improved VMAP-1 and DTED-1 tiles of roads, populated places and elevation. The project aims to release year on year updates to make use of the latest census and vector data as it becomes available. It is anticipated that the MODIS land cover map will replace the USGS product in the next version. (King, 2002 personal communication).

LandscanUSA is in development to produce both night-time and daytime population distributions at an enhanced 3' (~90m) resolution. (Dobson *et al.*, 2003). The model includes the development of spatial distributions for "residential or nighttime population" as well as for "daytime population". Locating daytime populations

requires not only census data, but data on places of work, journey to work, and other mobility factors. Block-to-block worker flows from the US Census along with locations of schools, student populations and their age structure are incorporated in to the model. Estimates of people engaged in shopping and other daytime activates are allocated to transportation and commercial land-use areas (Dobson *et al.*, 2003). LandscanUSA is currently being tested on a prototype area over Houston, Texas.

No comparison of the Landscan database was made with the RC dataset. The inclusion in the model of night-time light data, along with an array of other variables, would make it particularly difficult to ascertain precisely what the relationship between light and population without 'reverse engineering' the database. The Landscan project represents the forefront of global medium resolution population mapping in a raster format. The demand for improved information about the human population in both spatial and temporal dimensions is increasing in the light of recent security threats to civilian populations. Whilst the applications of such datasets are numerous, it should also be noted that the model itself has significant potential to be adapted for other applications such as estimating the spatial distribution of pesticide usage in urban watersheds (ORNL, 2002).

The distribution between daytime as well as night-time population distributions becomes more acute at higher spatial resolutions. The results of section 5.4 show that there are fundamental differences between the brightest areas in a city and the recorded residential population as given in a census. Paradoxically, night-time light data provides a good representation of *daytime* population distribution with respect to airports and city centres. The theoretical models proposed by Sutton (2003) are likely to be more akin to daytime population distributions than residential census counts. Hence, one issue that must be made clear from the start is which facet of population distribution is being modeled. The experiences from the LandscanUSA experiment suggest that such high spatial and temporal resolution population data products would only be available for those countries where high quality input data exists.

5.6 Summary

The estimation of human population from remote sensing data has been comprehensively examined from its conception to present day techniques using DMSP-OLS night-time imagery. Two studies using the frequency composite product to estimate urban population have compared favourably to each other. The results presented by Doll *et al.* (2000) have been independently re-produced by Sutton *et al.*, (2001). The radiance-calibrated dataset offers an intriguing dimension to population estimation using the night-time lights dataset. The implicit assumption in its use, however, is that population is related to the observed radiance. In the absence of radiance, theoretical models can be used to infer population density across a cluster.

Further studies using the radiance-calibrated night-time lights product have found that although it offers more modelling possibilities, there is no fundamental relationship between radiance and population density. This problem arises due to the fact that residential population is recoded in a census and differs considerably from the daytime population distribution. Night-time lights can, and will play a significant role in mapping population as the Landscan project has demonstrated although the data requirement increases rapidly for higher spatial resolution products.

Chapter 6

Night-time light imagery and Its relationship to non-population parameters

Night-time light imagery can be intuitively perceived to be indicative of a range of socio-economic parameters other than human population. Socio-economic data are collected at irregular spatial units. Night-time light imagery potentially offers a means to disaggregate these data to a constant spatial resolution. Non-population parameters such as Gross Domestic Product (GDP), power consumption and even greenhouse gas emissions have all been identified as correlates of lit-area or total radiance (Elvidge *et al.*, 1997; 1999; 2000; Doll *et al.*, 2000). Previous work used country level aggregations of light and GDP to build a global relationship. This chapter takes an in-depth look at the nature of sub-national relationships and discusses the implications for producing disaggregated maps of these parameters (the results of which are presented in chapter 7).

6.1 Issues surrounding multi-scale analysis of night-time light data.

The use of multi-scale data introduces issues, which ought to be taken into consideration when results are analysed. In particular the Modifiable Areal Unit Problem (MAUP) and the ecological fallacy are two complementary themes which frequently occur in GIS analysis, but are usually overlooked due to the lack of general robust solution. These two issues are particularly pertinent in this analysis since the relationships derived from the data will be used as an input to the map production procedure.

The MAUP consists of two separate but closely related components, which have been observed to cause a variation in statistical results depending on the spatial

arrangement of zones or the scale used to analyse the data. These are known as scale and zoning effects. The scale effect occurs when different results are observed from the same data at different spatial resolutions (Wrigley *et al.*, 1996). This arises due to the aggregation of the data into larger units (e.g. enumeration districts – wards – counties – regions). In addition to this, different results can also be produced where the scale of analysis remains constant but constituent areas are aggregated in a different way or zone boundaries are altered.

A practical application of using the zoning effect can be seen as far back as the early 19th century, where it was observed that voting districts could be divided in such a way so as to concentrate the power of the ruling party. This occasionally gave rise to bizarrely shaped districts epitomised by that of a former governor of Massachusetts, Elbridge Gerry, whose party created a salamander shaped district in 1812. The term gerrymander was coined to describe the elected member from such a district as well as the action of altering district boundaries to gain an electoral advantage.

The MAUP has only been intermittently studied. It was identified by Gehlke and Biehl (1934 cited in Openshaw, 1984) and was again revisited in 1984 by Stan Openshaw. Whilst its effect has been well documented, it is also an issue that is frequently overlooked in spatial analysis, since its effect can take many forms. Openshaw (1984) remarked that 'the aggregational variability is not susceptible to a statistical approach since no systematic regularities could be found'. A corollary to the MAUP is the ecological fallacy.

In an analytical environment where results are known to vary depending on the scale or zoning structure, it follows that erroneous inferences can be made from data that are generalised from one scale to another. It has three manifestations depending on the direction of the scale change. The individualistic fallacy occurs when a macro-level relationship is imputed from a micro-level (individual) relationship. Cross-level fallacies describe those inferences made about one sub-population from another at the same scale of analysis. The final fallacy, the ecological fallacy is the opposite of the individualistic fallacy and describes those inferences made about the

fine resolution from the coarse resolution (Cao and Lam, 1997). In this sense, the cross-level fallacy arises from the zoning effect, whilst the individual and ecological fallacies are derived form the scale effect.

The aim of this chapter is to produce and examine a set of relationships which can be applied to night-time light data in order to produce a disaggregated map of GDP. In order to do this, the radiance-GDP relationship will be examined across a range of sub-national scales. A multi-scale approach is anticipated to facilitate the identification of MAUP effects that exist with this type of analysis and what implications this has with respect to creating an accurate map.

6.2 Sub-national correlation characteristics: The United States

The correlations between socio-economic parameters and night-time light imagery have been demonstrated to be strong at the country level (Doll *et al.*, 2000). Studies of these correlations at the sub-national level are scarce due to the paucity of disaggregated socio-economic data. A pilot study examined the variation in the correlation between light and GDP at two sub-national units for the UK (Doll, 2003). The strength of the correlation was found to be stronger at the county level than the regional level. It is hypothesized that in aggregating to the regional level, there is a commensurate aggregation of economic sectors, which confuses the correlation. These effects are smoothed out when comparing countries at the international scale. This effect is believed to be a manifestation of the MAUP.

This section describes the MAUP for correlations involving night-time light imagery and socio-economic parameters. It will also make inferences about why these variations occur, and secondly what it can tell us about the overall relationship between light and the parameter in question. In building an understanding of the smaller scale issues, it is hoped that a further insight will be gained into modelling socio-economic data from night-time lights.

6.2.1 State and regional correlations

Economic data were downloaded from the US Bureau of Economic Analysis (BEA, 2002) and state power consumption data from US Energy Information Administration (EIA, 2003). Multi-scale relationships between light parameters and Gross State Product (GSP – a state's contribution to national GDP), and Power consumption were tested for the USA. These analyses were carried out at the state level. For each state, the total amount of radiance was calculated and plotted against the corresponding power consumption or GSP figure. A more general term for GSP would be the GRP (Gross Regional Product). It is introduced here to define the contribution of a sub-national areal unit such as generic administrative region or even square pixel areas to the national GDP total. The term GSP will only be used when explicitly referring to a state as opposed to aggregations of states.

An image of the night-time lights of the United States with its state boundaries is shown in Figure 6-1. Data are also presented aggregated up to the regional level as defined by the US Census regions (see Figure 6-2). Examining the relationship between energy consumption and night-time lights (Table 6-1), the state level relationship is consistently better than the regional level one. The intra-state relationship is better still for 6 out of 9 regions having a linear R^2 value greater than 0.9.

Table 6-1 Correlation of energy consumption and night-time lights at state and aggregated US Census Division level.

	US Census Divisions	*US States*
Lit-area	0.499	0.699
Log lit-area	0.641	0.729
Total Radiance	0.652	0.844
Log radiance	0.784	0.900

The same pattern is evident for the economic activity (GRP) with the regional-level correlations being much lower than for the power consumption figures (Figure 6-2).

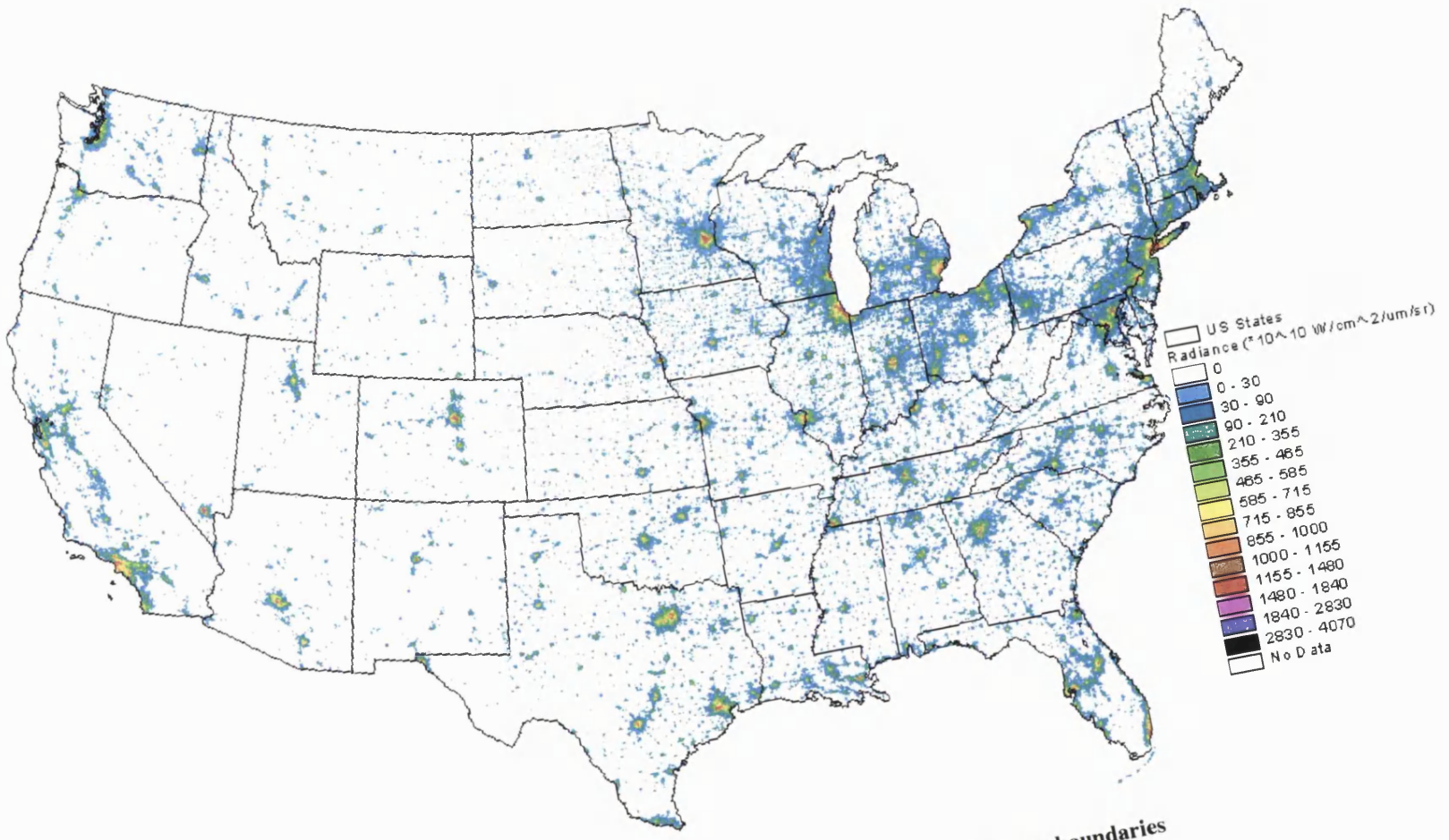

Figure 6-1Night-time lights of the United Sates with state boundaries

However, intra-regional state correlations reveal that some regions are highly correlated ($R^2 > 0.9$ for the southern states), though other regions (Mid-Atlantic and East-North Central) have such a small sample size so as not to be statistically valid. For all cases, correlations using the total (summed) radiance figures perform better than the lit-area figures.

Table 6-2 Correlation of GRP and night-time lights at state and aggregated US Census Division level.

	US Census Divisions	*US States*
Lit-area	0.328	0.563
Log area	0.373	0.467
Total Radiance	0.49	0.751
Log radiance	0.55	0.790

6.2.2 Regional aggregations

The variation in the correlation of parameters at a given scale depends on how regions are aggregated. In having data at two hierarchical sub-national scales, it is possible to test the national correlation at the smaller scale (regions), by using different aggregations of larger scale units (states). Economic data from the BEA was also presented using their regional classification. Their grouping of states is similar to that of the US Census using traditional aggregations based on states' locations with respect to the various geographical regions (e.g. Plains, Great Lakes, Mountain Division, South Atlantic). In addition to these two classical aggregations, three others were devised. One was a geographical aggregation, which established five regions according to their latitudinal position. The other two consisted of a random aggregation based on seven alphabetical divisions and one, which divided the states after they had been ranked by GSP. The five aggregations are shown in (Figure 6-2). Two of the aggregation methods produce 'regions' which are composed of non-contiguous states. Examining how different aggregations affect the correlation of total radiance with the GRP, it appears that a wide range of results can be obtained depending on how one assembles the regions.

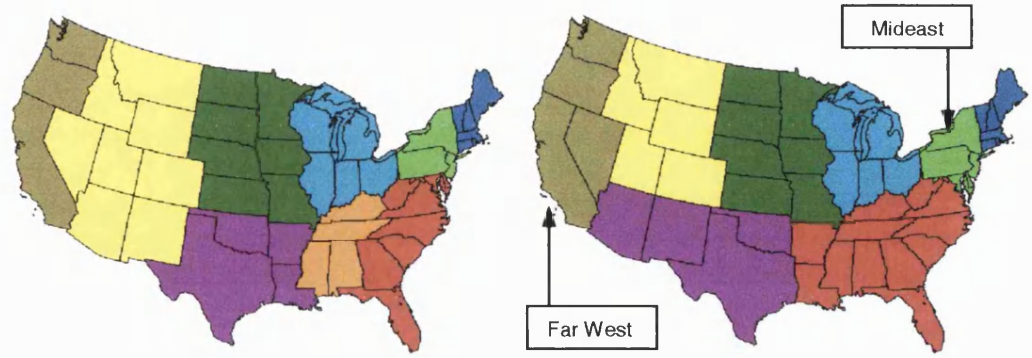

US Census Divisions (9 regions)

US BEA (8 regions)

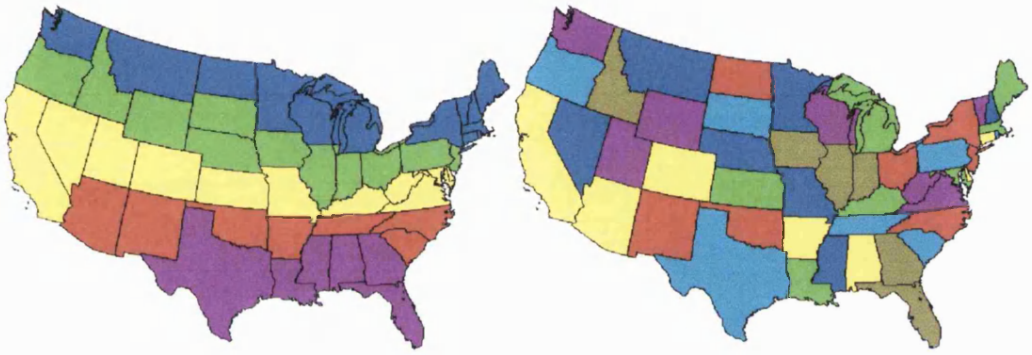

Latitudinal Division (5 regions)

Alphabetical zones (7 regions)

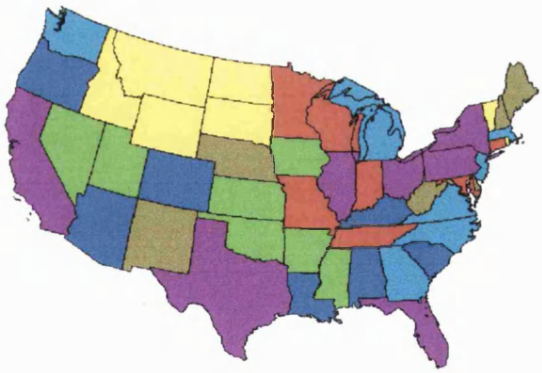

Ranked by Gross State Product (7 regions)

Figure 6-2 Aggregation of US states into larger zones according to 5 different criteria.

In addition to comparing the r-squared value at this scale, the intra-regional correlation was also computed to see if any discernable patterns were present. The

intra-regional correlation here refers to the average correlation of states within a given zone. Figure 6-3 shows firstly that a regional correlation of different strengths (0.4 –0.95) can be obtained depending on how regions are arranged. Secondly, that the intra-regional correlation (i.e. those states which when summed form one point on the regional level scatter plot) declines as the regional level correlation increases.

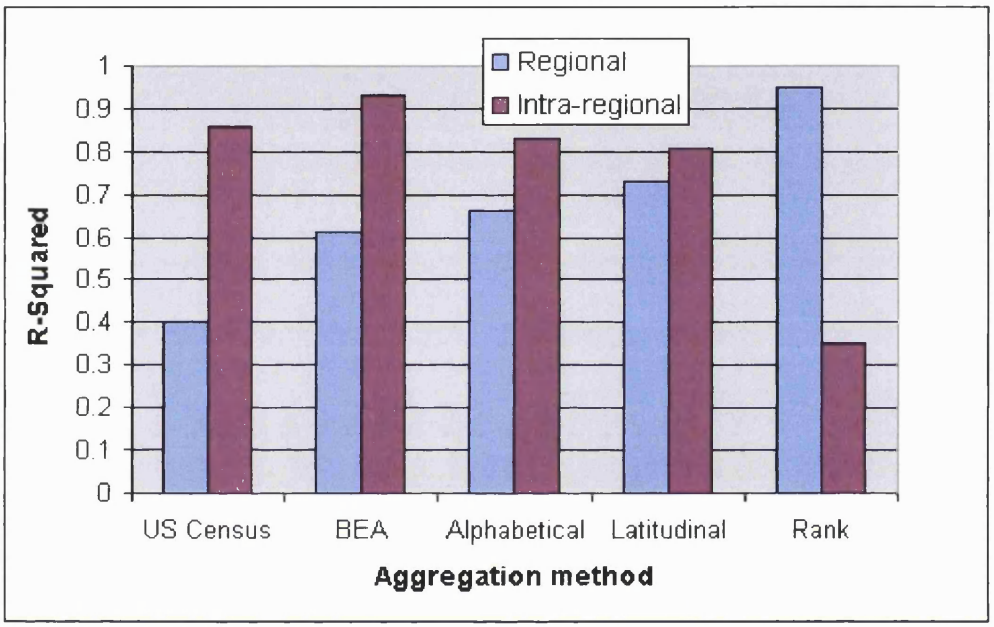

Figure 6-3 Comparison of regional and (mean) intra-regional correlation coefficients (of total radiance vs. GDP by state) for different aggregation methods.

These results suggest that the US Census divisions seem to be completely unsuitable for building a national scale correlation, but ideal for intra-regional analysis. By shifting one or two states here and there to build the BEA regions, the correlations improve in both measures, though these geographical divisions are generally unsuitable. Even something as random as an alphabetical classification provides a better regional correlation result than the two traditional geographically regional zones. By using a geographical criterion to aggregate states, the latitudinal divisions provide a regional and intra-regional correlation that is most similar to each other. However, ranking states based on their GSP gives the best regional correlation, but the worst intra-regional correlation, despite the component states being of roughly

equal magnitude to each other. The same pattern of results was also observed for the power consumption data.

6.2.3 Derived relationships

One further point to examine is what effect different aggregations have on the magnitude of relationships associated with these correlations. Figure 6-4 shows the trajectory of the relationship for each aggregation method. Also plotted (bold in red) is the relationship derived from state level radiance-GRP plot. Two points on the plot are of particular interest. Firstly, there is a point around 1E+07 radiance units (point A), where the all-state relationship intersects that of the US Census and BEA relationships. Secondly, further along around 1.75E+07 radiance units (point B) is a point where all the relationships converge *except* the all-state relationship. Despite their divergence at high radiance values, all models would produce similar results if the input values were between these points. The results show that the US Census and BEA relationships are markedly different from those of the other three aggregation schemes. More importantly, it also shows that the overall state-level relationship is most similar to these simulated aggregation schemes and not to those of the conventional US regions. This has important implications for extending this technique to areas that have only one level of sub-national data.

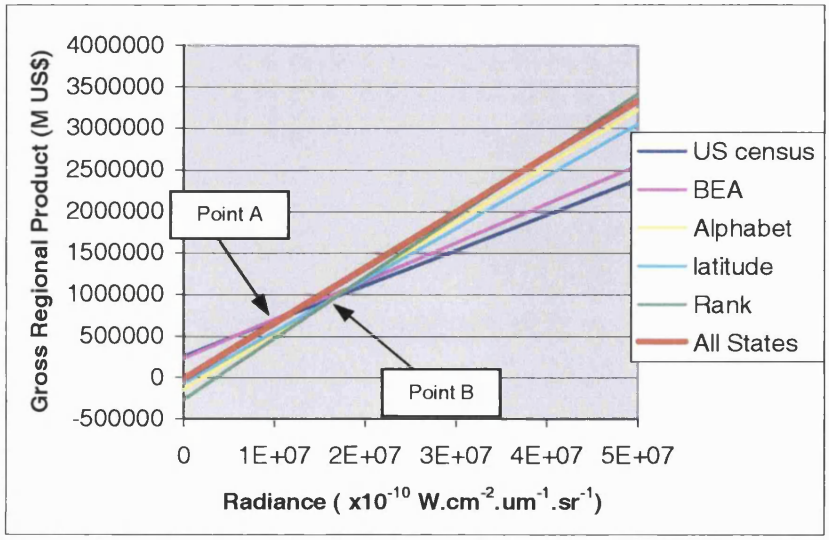

Figure 6-4 Comparison of different relationships derived from the five aggregation schemes displayed in Figure 6-3

Taking these points into consideration it is suggested that the US has a number of regional sub-economies, hence the high intra-regional correlation coefficients of the US Census and BEA divisions. However, the regions themselves vary greatly and bear little relationship to each other. This is not to say that there is no general nationwide correlation. The reason why the intra-regional correlation is so poor for the ranked states goes back to the nature of the individual regional economies. Assembling regions by ranking states puts the most economically productive states (California, Texas, Florida, Illinois, Ohio, Pennsylvania, and New York) together. However, they apparently bear little resemblance to each other. This trend continues for each group of states. BEA (and US Census) regions by contrast usually consist of one dominant state and a number of less economically productive satellite states. Working down the list of states, each BEA region generally has a good mix of members from each group of (ranked) states. The exceptions are the Plains and Mideast regions which contain Ohio and Illinois, and New York and Pennsylvania respectively, and conversely the Rocky Mountain region, which has no member from the most economically active group of states. However, when viewed in totality their component states fit a single nationwide model as shown in Figure 6-5.

The graph of total state radiance and GRP (Figure 6-5) reveals that there are two major outliers: California and New York. Their effect can be seen to be carried through to their respective regions of the Far West and Mideast. Whilst amongst the most radiant states, neither has a total radiance value higher than that of Texas, whilst Florida and Illinois are also of comparable total radiance. These three all lie along the main trendline with the other states. The regression has excluded California, New York and their regions. This gives a gradient of 0.0499, which is the lowest of any country analysed and therefore, assuming parity between the US Dollar and the Euro, the United States has the lowest amount of economic activity per unit radiance for those states in the regression. When this revised relationship is plotted along with those in Figure 6-4, it is much more in-line with those from the BEA and the US Census Bureau rather than the simulated regions. This relationship is fitted through the origin. The reasons for doing this are discussed in the next section.

The range of radiance-GRP relationships encountered is examined in the next section of this chapter. The United States fits into the major outlier category described below in section 6.3.3.1.

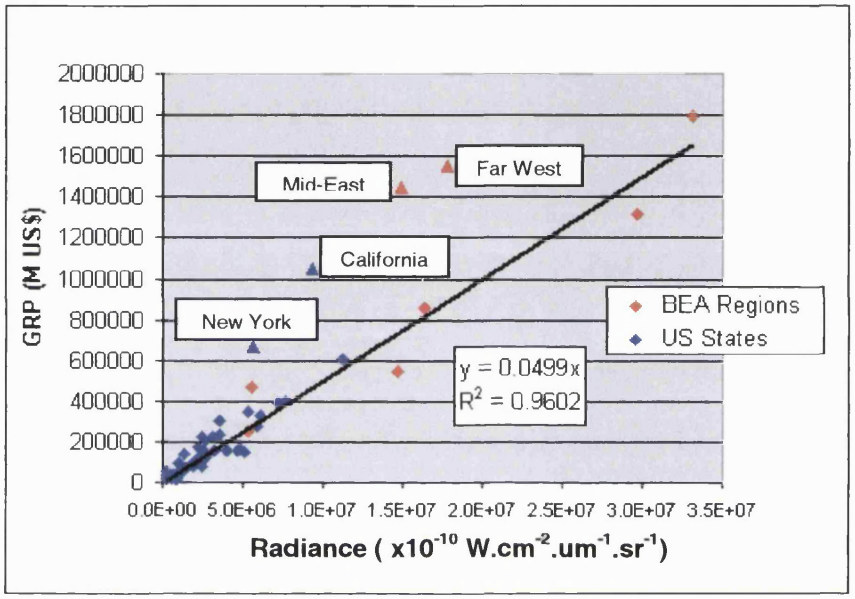

Figure 6-5 Total radiance – GRP scatterplot US States and aggregated regions defined by the Bureau of Economic Analysis (BEA), (n = 55). The outlying BEA regions are shown in Figure 6-2.

Simulating regions only helps to identify those areas that can be grouped together to improve the correlation between the two parameters. It does not mean that using this relationship to disaggregate a parameter will be any more accurate. This is due to the fact that applying one model to a set of states will never account for the inherent variability within the relationship. In this sense, using the MAUP as an analytical tool is limited to describing variation. However, it is this variability which must be critically evaluated if one is to minimise these errors further down the processing chain of map production. An in-depth analysis of its key characteristics has been shown here to be a useful tool for developing theories about the spatial nature of relationships.

6.3 Sub-national correlation characteristics: Europe

6.3.1 The NUTS regional reference system

Statistical reporting in the European Union is done according to the Nomenclature of Units for Territorial Statistics (NUTS) system. The NUTS is a five-level hierarchical classification based on three regional levels and two local levels. Each member state is divided into a number of NUTS-1 regions which in turn are divided into a number of NUTS-2 regions and so on. There are 78 NUTS-1 regions, 210 NUTS-2 and 1093 NUTS-3 units within the 15 EU countries (Eurostat, 2002a). In spite of the desire to create a single, coherent structure of territorial distribution across Europe, NUTS regions of a given level can differ substantially between countries. For instance, mainland Portugal is regarded as a NUTS-1 region along with Madeira and the Azores, which are much smaller both in terms of size and economic importance. France by contrast, divides mainland France into 8 NUTS-1 regions whilst including its overseas territories all aggregated as an additional NUTS-1 region and individually at the NUTS-2 level. Most countries already have a series of administrative regions, which need only be assigned a NUTS level. This can result in significant differences between countries. At the NUTS-3 level, Germany has many more regions than any other country. With around 450 regions (Kreise), it has 5 times as many NUTS-3 regions as either France or Italy. Consequently, these regions are much smaller than equivalent NUTS-3 regions in other countries.

There are essentially two methods available to subdivide a national territory into regions. Normative regions are units that are the result of political decisions. They are derived according to the function of that area and the population required to carry those functions out. They are largely determined according to political, historical and cultural factors (Eurostat, 2002b). The alternative is to have analytical regions, which are determined by homogeneity of some geographical factor; this may be human or physical. Hence regions may be determined by factors such as altitude, land cover type or homogeneous economy types. NUTS regions are

primarily based on the normative classification and favour units of a general character; that is to say, one not dominated by a single activity (Eurostat, 2002b).

In this study, data were collected for the three regional NUTS levels (1-3). The 1961 Brussels Conference on regional economies found that the NUTS-2 level was the level generally used by member states for the application of their regional policies, whereas NUTS-1 regions should be used for analysing regional community problems. By contrast NUTS-3 regions may be used to identify where specific measures need to be taken (Eurostat, 2002c).

The digital boundaries of these regions were downloaded from UNEP's Global Resource Information Database (GRID) data collection in Geneva (UNEP, 2003a). GRID is a worldwide network of 15 environmental data centres managed by UNEP's Division of Early Warning and Assessment. The principal aim of GRID-Geneva is to support environmental decision-making within UNEP and the UN. GRID-Geneva specialises in handling and analysing spatial and statistical data on environmental and natural resource issues. Since its establishment in 1985, GRID-Geneva has compiled an archive of global, European and other geo-spatial databases through the use of GIS and remotely sensed imagery (UNEP, 2003b). The collection of such datasets is a key component of UNEP's flagship publication, the Global Environmental Outlook mentioned in section 2.4 of this thesis.

6.3.2 European Economic data

European economic data were purchased from Eurostat, the statistical body of the European Commission. Regional accounts were compiled in accordance with the European System of Integrated Economic Accounting (ESA). The ESA is fully consistent with the world-wide guidelines on national accounting, the 1993 System of National Accounts (SNA). The 1993 SNA (UNSD, 2003) has been prepared under the auspices of the United Nations, the International Monetary Fund, the Commission of the European Communities, the Organisation for Economic

Cooperation and Development and the World Bank. The UN statistical commission has unanimously approved the system and it is the international standard for the compilation of national accounts statistics (Eurostat, 2002d).

Due to the incomplete nature of the data-tables, data from a range of years around the time of acquisition for the night-time light imagery were obtained. The total GDP dataset was the most complete both temporally and spatially. GDP by sector and power consumption data were only available down to the NUTS-2 level but was found to be incomplete both in terms of the number of countries with data and omissions of values for some sectors within these countries. These statistical data were only useful to the analysis if they could be matched to the corresponding digital boundary data obtained from UNEP. In all, there were 11 countries for which there were compatible digital NUTS boundaries and socio-economic data. A summary of the available data is presented in Table 6-3.

Table 6-3 Summary of Data Acquisitions from Eurostat where: Belgium (B), Germany (D), Denmark (Dk), Spain (E), France (F), Greece (Gr), Italy (I), Ireland (Irl), The Netherlands (Nl), Portugal (Pt) and the UK

Parameter	*Year*	*NUTS Level*	*Countries*
GDP (total)	1997, 98, 99	1-2-3	EU-11 (above)
GDP by sector	1998	1-2	Nl, F, I, Pt, B, D (NUTS-1)
	1999	1	D
	1997	1-2	UK (from ONS)
Energy Consumption	1996	1-2	B, E, Gr, I
	1997	1-2	F, E

The night-time light imagery was geo-rectified to the digital boundaries dataset by matching the projection parameters of each dataset. The Lambert Equal Area Azimuthal projection was chosen for the two continental scale datasets of North America and Europe. In each case the dataset of vectorised boundaries was intersected with the night-time light data in order to identify those pixels which intersect and are contained within the administrative boundary under consideration. This scheme minimises the inclusion of those pixels which are affected by blooming

from coastal areas. Blooming is a phenomenon of night-time light imagery where illuminated areas are overestimated as a result the large pixel size from the OLS sensor being unable to resolve sub-pixel light sources. Geolocation errors in the compositing process and illuminated radiance values recorded over water bodies as a consequence of reflection from adjacent illuminated land area also contribute to the blooming effect (Elvidge *et al.*, 1997a; 2001). The latter is the most obvious manifestation of blooming, the inclusion of these pixels result in an overestimation of both lit area and radiance of administrative boundaries in coastal zones.

6.3.3 Total radiance - GRP correlation results

Each country was tested for at least one NUTS level depending on the availability of data and the NUTS configuration of that country. Denmark and the Republic of Ireland only consist of NUTS-1 regions.

One way of visualising the MAUP effect on the derived relationship at the different spatial resolutions is to plot each relationship throughout the radiance range to see how and where they differ. A consequence of disaggregating a relationship to map a parameter at a finer scale is that the input radiance will be smaller than that which went into creating the relationship. Using a linear relationship with a slope and an intercept can cause erroneous results where the magnitude of the intercept is high. In cases where the intercept is negative this can cause areas to have a negative GRP. The results considered here therefore refer to regression lines constrained to pass through the origin. Hence, pixels with zero radiance are assumed to have no GRP associated with them.

Based on the US analysis, simulated NUTS-1 regions have also been computed to examine whether a higher degree of correlation produces a different relationship. These simulated NUTS-1 regions have been created based on the ranked radiance method, which yielded the highest regional correlation based for the US.

The results refer to the 1997 set of economic data as this is co-temporal with the night-time light data. Strong linear positive correlations between total radiance and GRP were observed for all the countries tested at the finest level of observation. A number of variations were identified around this basic model. Results are presented here for the 11 EU countries listed in the caption of Table 6-3. These countries have been divided into four categories based on the type of scatter identified in their radiance-GRP relationship. The four types of relationship are listed as follow:

i) Major outlier: where there is at least one point lying well away from the main trendline. These points are not the most radiant on the graph.
ii) Those countries where the bulk of economic activity is concentrated in one area and thus have a point that is far more radiant than the rest of the country and is offset from the main trendline.
iii) Those countries where two distinct regional relationships can be identified in the data.
iv) Those countries where all points fitted a single linear model.

In the figures that appear throughout section 6.3.3, triangles denote those points that were excluded from both the regression and the associated statistics that accompany the graphs. The number of valid points (n) used to derive the relationship shown on the graph is given in the caption for each graph. Full figures and results for these results are given in Appendix D.

6.3.3.1 Major Outlier

Countries: France, Denmark (and the United States)

The radiance-GRP relationships for both these countries exhibit more than one point that is so far away from the main trendline that those points in question cannot be assumed to belong to the same model. More importantly, these points are not the most radiant, compared to others at the same NUTS level.

In France, NUTS-3 regions correspond to the département level. Every part of the country is represented at the NUTS-3 level. The NUTS-3 scatterplot (Figure 6-6) exhibits a strong, positive correlation of total radiance with GRP. Paris and an adjacent département (Hauts-de-Seine) are outlying areas from the main scatter. When these two areas are excluded from the analysis the R^2 value rises from 0.26 to 0.75 for the remaining 94 départements.

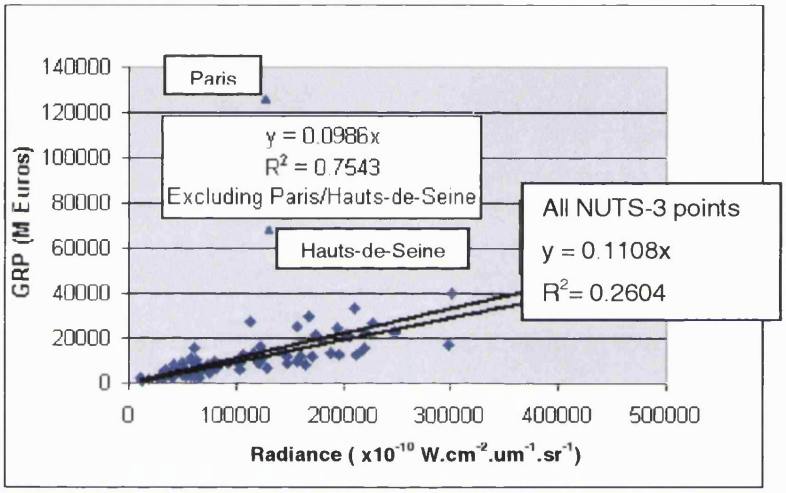

Figure 6-6 Total Radiance-GRP scatterplot for NUTS-3 regions of France (*n = 94*).

Figure 6-7 shows how the two outlying Parisian départements (shown as blue triangles in Figure 6-6) have combined to produce the anomalous Ile-de-France NUTS-1 region, which has a GRP far higher than other regions of similar radiance. The Parisian region is absent at the NUTS-2 level, its NUTS-1 Ile de France region is instead directly composed of eight départements around Paris. The Ile-de-France region is outlined in red in the map in Figure 6-7. In this case, the two outlying regions have been carried through the aggregation process. Excluded from Figure 6-7 are NUTS-1 points of the French overseas territories: Ile de la Réunion; Martinique; Guadeloupe and French Guyana.

The presence of such extreme outliers considerably influenced the unconstrained NUTS-1 relationship, where there were fewer points to mitigate its impact. In such instances the intercept can be very high, which prevents extrapolation to smaller

scales. Without the constraint, all but the highest radiance values would have negative GRP values in the output map. It is for this reason that the derived relationships were constrained to go through the origin. Considering just the gradient of the slopes, the NUTS-1 and all NUTS-3 regions are most similar (y = 0.111x) whereas NUTS-2 is virtually identical to the GDP/total-radiance figure computed for the whole of France (y = 0.128x). The actual NUTS-1 gradient lies in between these lines.

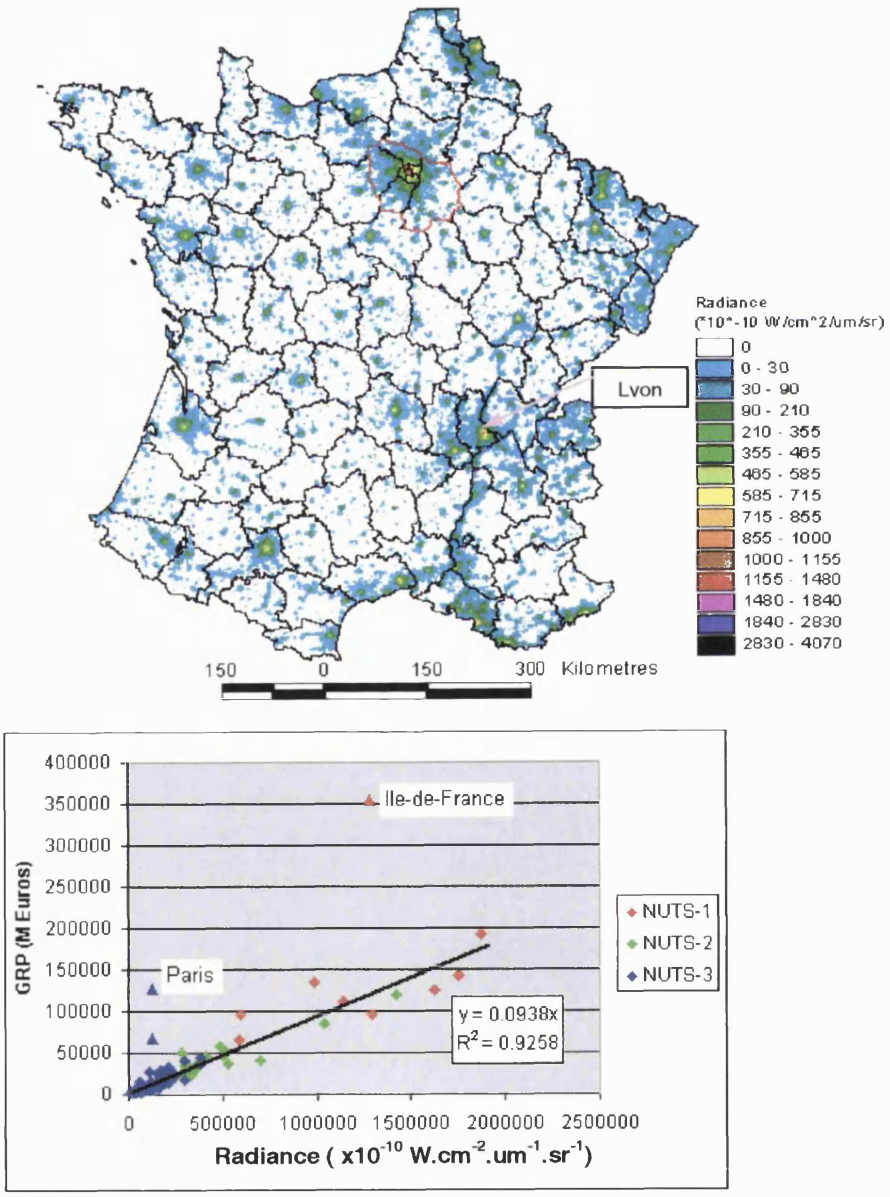

Figure 6-7 Night-time lights of France with NUTS-3 regions and corresponding Total Radiance-GRP scatterplot. Ile-de-France NUTS-1 region is outlined in red. (*n = 121*)

There was only one set of regional-level spatial units (Amter) available with which to analyse Denmark. Like France it has two outlying areas – the centre (København og Frederiksberg Kommuner) and the hinterland of Copenhagen (Københavns) shown in Figure 6-8. The much smaller city centre is the greater of two outliers. The specific properties of these outlying areas are discussed in section 6.4 below.

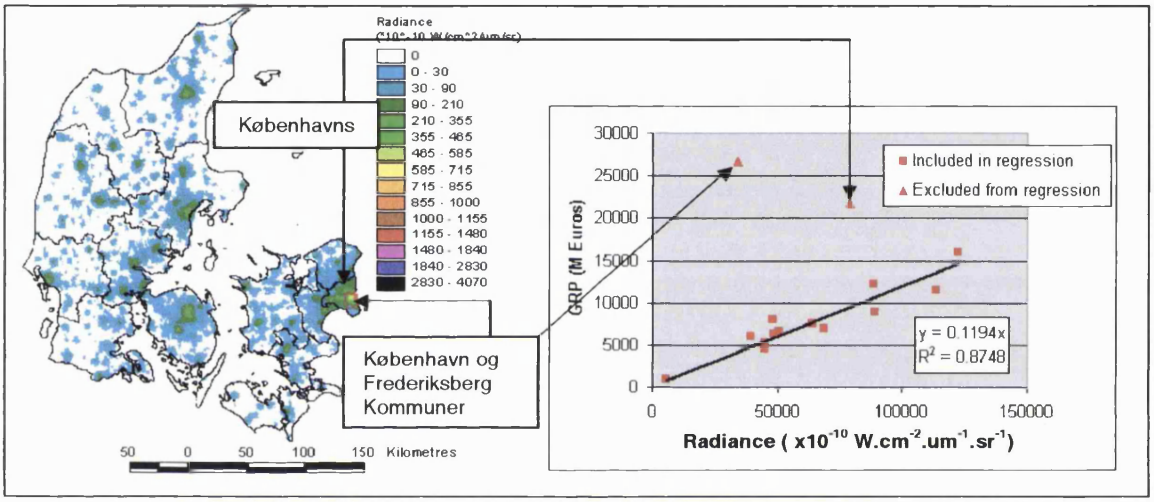

Figure 6-8 Night-time lights of Denmark with its administrative boundaries and total radiance – GRP scatterplot (NUTS-1 only available, *n=13*).

If these countries obeyed the hypothesized relationship of total radiance within a region being proportional to GRP then these points would lie far away from the other points in the scatterplot but remain along the trendline. Occasionally, this point is slightly offset from the others. This is the case for the next type of graph.

6.3.3.2 Offset point

Countries: Portugal, Italy, Spain, Ireland, England

Some countries are well modelled by a single regression model with the exception of one point. This point need not necessarily be the capital city but has a higher GRP/radiance ratio than any other place in the country. This is most acutely

demonstrated for Portugal (Figure 6-9) where the capital Lisbon (Grande Lisboa) is observed to be offset from the linear alignment of the other points in the plot. The effect of this point can be seen to be carried through the aggregation process, where the corresponding NUTS-1 point (Lisboa e Vale do Tejo) is also offset by the same margin. This suggests that it is only the NUTS-3 area of Lisbon, which is responsible for the position of its NUTS-1 region on the scatterplot. Portugal was only tested at two NUTS level since mainland Portugal was itself a NUTS-1 region along with Madeira and the Azores.

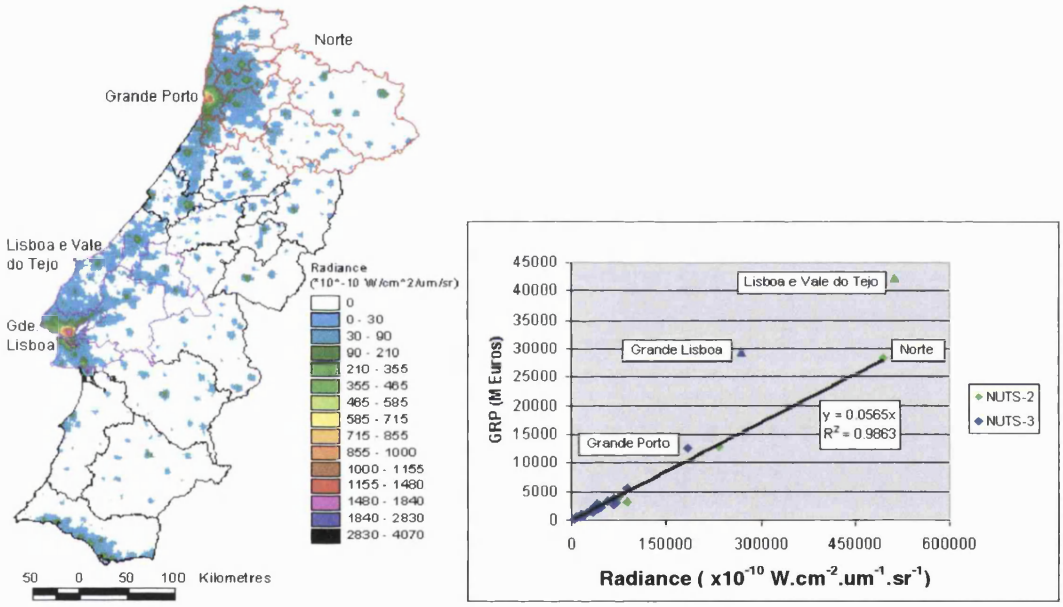

Figure 6-9 Night-time lights of Portugal with its NUTS-3 boundaries and its total radiance – GRP scatterplot. The outlying area of Lisbon and its region (Lisboa e Vale do Tejo) is outlined in magenta, whilst Porto and its region (Norte) is outlined in red on the map (*n=30*).

A similar pattern is observed for Italy (Figure 6-10), where despite more scatter, the NUTS-3 point of Milan lies higher up the plot-space than its fellow NUTS-3 points. This is again preserved through the aggregation process.

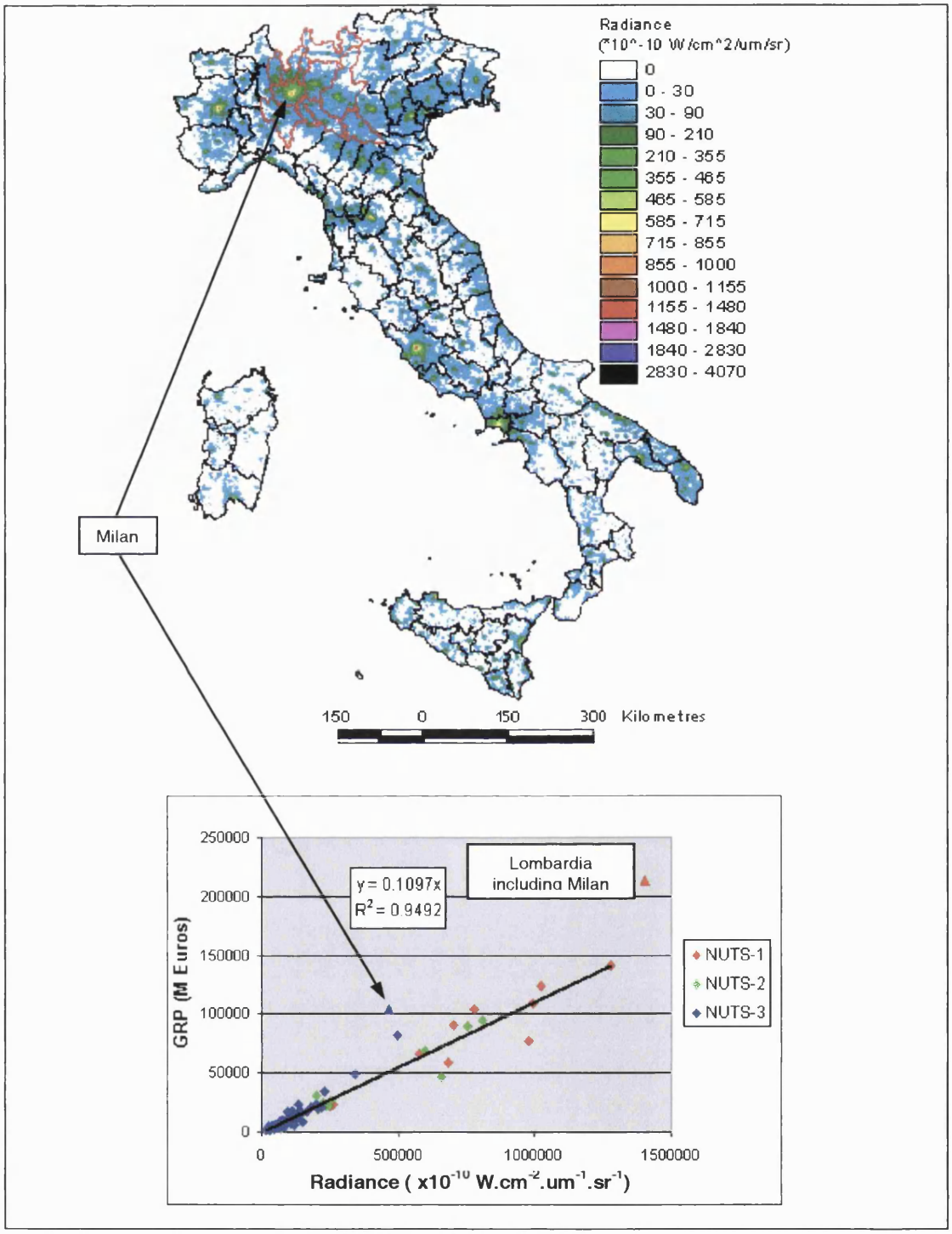

Figure 6-10 Night-time lights of Italy with its NUTS-3 boundaries and its total radiance – GRP scatterplot. The region containing Milan (Lombardia) is outlined in red on the map (*n=118*).

Spain is one of the most interesting cases to be studied, as it seemed to exhibit all of the features mentioned for other countries. The relationships derived at each NUTS

level were found to vary more than any other country. The gradient becomes progressively shallower as larger areas are considered in the analysis ranging through $y = 0.069x$, $0.059x$ and $0.056x$ for NUTS levels-3, 2 and 1 respectively. These values are for relationships constrained to run through the origin and include the outlying points, whose effect becomes less influential as the spatial units become larger in size. The generally good correlation in Figure 6-11 masks much of the detail. Despite the standard deviation of the GRP/radiance quotients being relatively low compared to other countries (Table 6-4), the individual NUTS-3 zones have been combined in such a way as to result in vastly different relationships at different NUTS levels and confuse the base-level correlation.

Table 6-4 Summary of statistics for NUTS-3 quotients for European countries in section 6.3.3

Country	*Min*	*Max*	*Mean*	*Std.dev*	*Range*
Denmark	0.100	0.783	0.180	0.172	0.683
France	0.033	0.993	0.117	0.109	0.959
Portugal	0.037	0.109	0.056	0.015	0.072
Italy	0.053	0.224	0.102	0.032	0.171
Spain	0.032	0.094	0.056	0.014	0.062
Ireland	0.131	0.265	0.173	0.047	0.134
Great Britain	0.107	0.404	0.191	0.066	0.296
East Germany	0.087	0.101	0.092	0.005	0.014
West Germany	0.095	0.428	0.213	0.075	0.332
Belgium	0.015	0.391	0.078	0.059	0.376
Greece	0.052	0.334	0.120	0.056	0.282
Netherlands	0.053	0.284	0.142	0.050	0.231

The NUTS-3 area of Barcelona is far more radiant than other NUTS-3 regions and is observed to be an outlier. The capital, Madrid is a NUTS-1 region and is about one third brighter than Barcelona. Barcelona is part of Cataluña, which is itself part of the Este NUTS-1 region. The other regions of Este have anomalously low GRP for the total radiance in the region. Barcelona dominates this region to such an extent that not only does it pull its NUTS-2 point away from the trendline but it has also pulled its NUTS-1 point *towards* it. In fact, it is only due to the presence of Barcelona in the region that its NUTS-1 point is anywhere near the regression line. Its position without Barcelona's contribution is also shown in Figure 6-11. In this

case, due to the magnitude of these modifiable areal unit effects, it is most prudent to just use the original NUTS-3 relationship and treat Barcelona and Madrid as separate outliers. This is the relationship displayed on the graph in Figure 6-11. This is the most extreme example of an outlying point's effect being carried throughout the aggregation process encountered for any of the countries analysed.

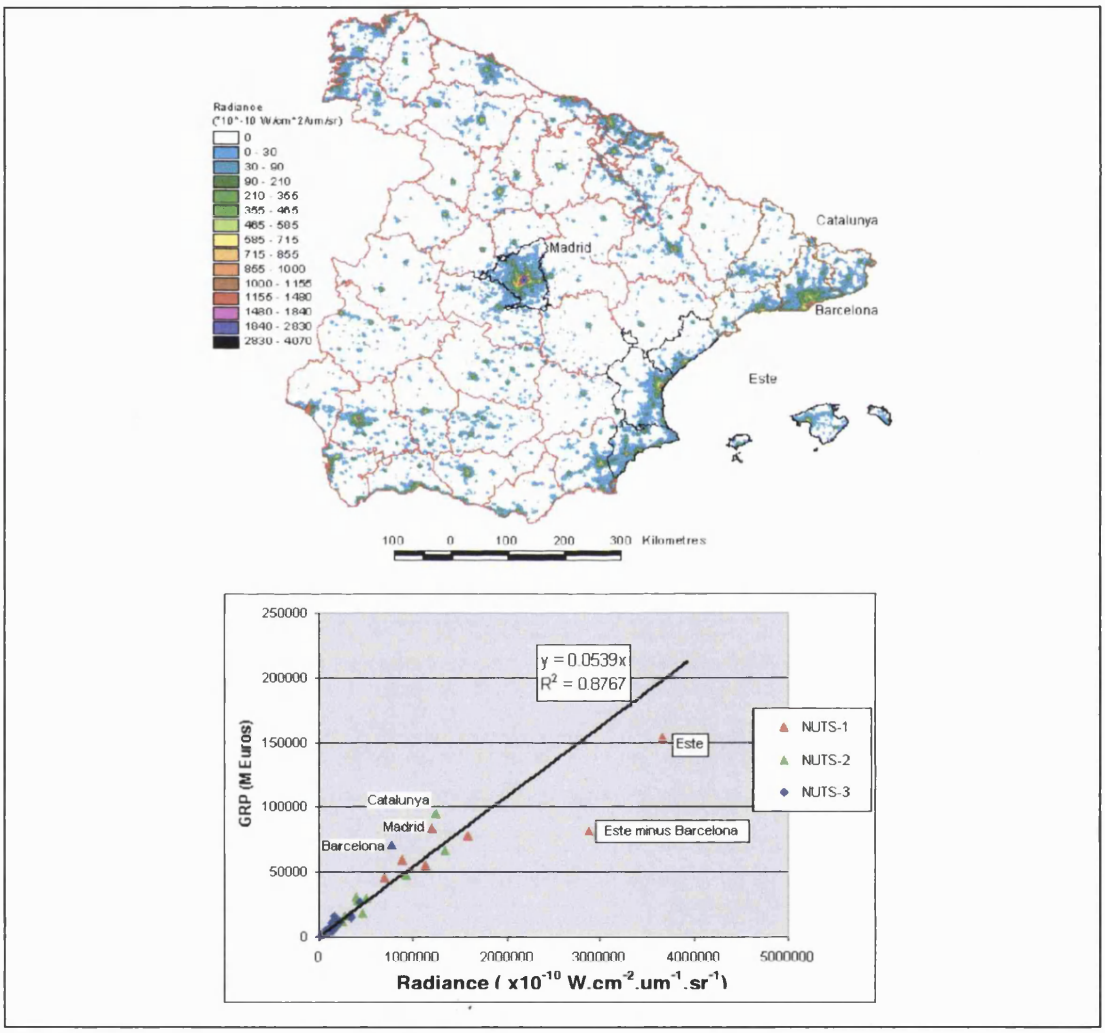

Figure 6-11 Night-time lights of Spain with its NUTS-3 boundaries and total radiance – GRP scatterplot. The relationship is based on NUTS-3 points only, excluding Barcelona and Madrid. The NUTS-1 regions of Madrid and Este are outlined in black on the map. Cataluña lies within the region of Este and is outlined in brown (*n=40*).

In the case of Ireland (Figure 6-12), there were only two levels of regional units available for analysis, the top level consisting of two regions. The NUTS-2 region around the capital Dublin is far more radiant than any of its counterparts. Although the Dublin point appears to be slightly offset from the rest, its aggregated NUTS-1

point has a GDP/radiance quotient lower than Dublin indicating that, in contrast to Portugal and Italy, the regions surrounding Dublin have a much lower GRP/radiance ratio so as to push its NUTS-1 point back towards the trendline in a similar fashion to that of 'Grande Porto' and its 'Norte' NUTS-2 region indicated in Figure 6-9 of Portugal. As with Spain, the relationship displayed only applies to NUTS-2 points – excluding Dublin.

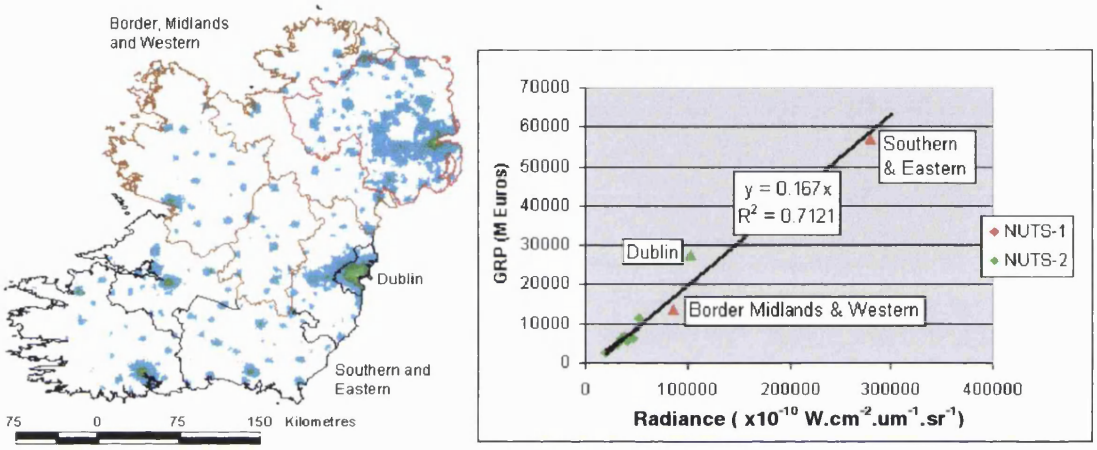

Figure 6-12 Night-time lights of Ireland with its NUTS-2 boundaries and its total radiance – GRP scatterplot. The relationship applies to NUTS-2 points only excluding Dublin (*n*=7).

When examining Great Britain, London was not split into its inner and outer London NUTS-2 boundaries due to a lack of digital boundary data and appears here only as the NUTS-1 'Greater London' unit. Therefore, like Madrid in the previous example, although it appears as a red point, it represents a part of the country which is not represented in any other part of the graph. Had the NUTS-2 boundaries been available for London, it is possible that Great Britain could be classified along with France and Denmark as a member of the major outlier model. The other most prominent outlier (South East) lies further along the x (radiance) axis nearer to the trendline. The total-radiance/GDP relationship for Great Britain (Figure 6-13) has, along with Germany (Figure 6-14) one of the noisiest distributions. This is caused in part, by a number of NUTS-2 points, which lie above the trendline each having a GRP of around 50 billion Euros. These points refer to the other main economic centres of the Great Britain (Greater Manchester and the West Midlands) as well as most of the component

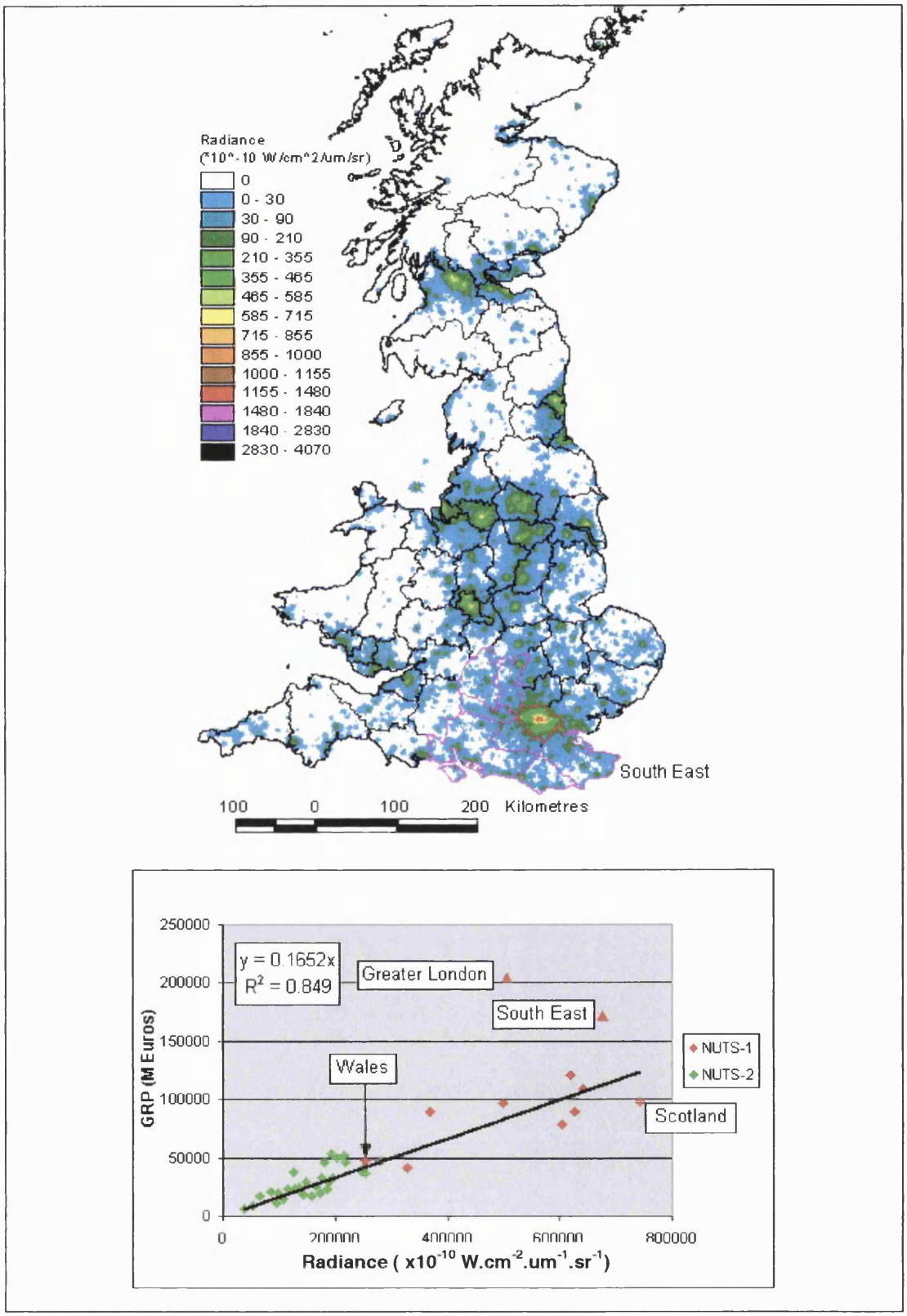

Figure 6-13 Night-time lights of the Great Britain with its county boundaries (approximately NUTS-2). London is outlined in red and the South East in magenta. The total radiance – GRP scatterplot includes the NUTS-1 points of Scotland and Wales (*n*=38).

NUTS-2 regions of the South East, which are heavily influenced by London. The increased spread within the points make identification of outliers more difficult than for cases where outliers and their up-scale effects can be easily identified and removed. In this case, all but the most obvious outlying points are included in the regression.

6.3.3.3 Two relationships in one country

Countries: Germany, Belgium

Two countries were found each to have two distinct relationships operating within its border. Germany (Figure 6-14) was studied at NUTS-1 and NUTS-2 levels. NUTS-3 regions were very small and there was a problem with accurately matching the names from each of the datasets. Furthermore, their sizes were so small that they would approach the resolution of the imagery, where inaccuracies in measurement would become significant. Examining the two levels of data there is an interesting distribution of NUTS-1 regions, which appear to describe a sigmoidal curve whilst the NUTS-2 regions remain largely linear. In particular, there are two sets of two NUTS-1 points, which have similar GRP for different total radiance values. The first set refers to the regions of Rheinland-Pfalz (western Germany) and Sachsen (eastern Germany including Dresden and Liepzig) and the second to Hessen and Niedersachsen (both in Western Germany). Hessen includes the financial capital (Frankfurt) whilst Niedersachsen is mainly agricultural and surrounds the city of Bremen, which is itself a NUTS-1 area. Examining the GRP/radiance quotient of the constituent NUTS-2 areas reveals consistently higher quotients in Hessen than in Niedersachsen. This would suggest that this is an actual feature of the relationship rather than an artifact of the MAUP.

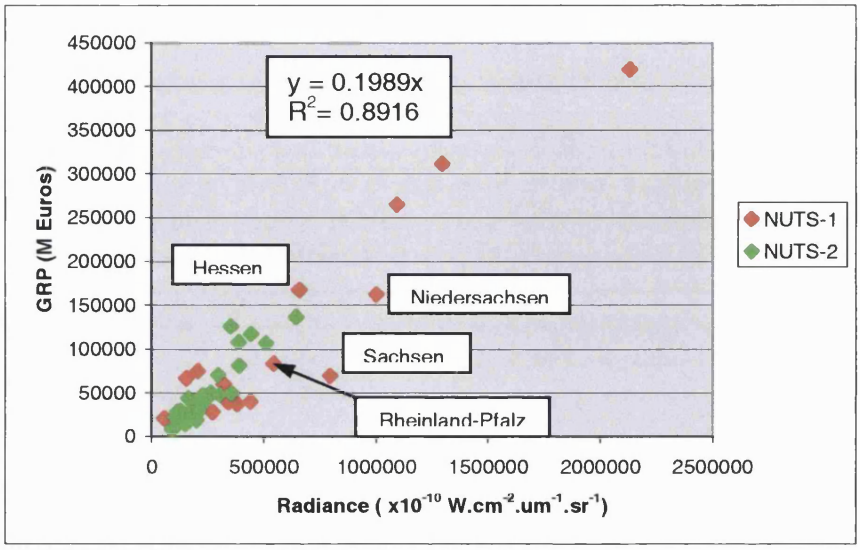

Figure 6-14. Total radiance – GRP scatterplot NUTS-1&2 regions of Germany

Since reunification in 1990, Germany has had to integrate two very different economies under one political system. This difference in economic productivity still existed during the mid-1990s, which can be seen in the data. If one re-analyses the data in Figure 6-14 in the context of its Cold War boundaries, then it becomes apparent that there are two separate relationships at work within the unified Germany. The points lying in the former East Germany occupy a fraction of the radiance range (Figure 6-15). It has a gradient half the magnitude of the West German points and is more similar to the GDP-radiance relationship of Greece. In fact, the distribution of points for the former East Germany is of the same type as France and Denmark. Berlin is the outlying point, whose position lies amongst the points of West German cities. Despite its location, Berlin (specifically West Berlin) has always been economically more akin to West German cities due to its subvention from West Germany for much of the Cold War. An interesting feature of the radiance map of Germany is that it has a relatively small range of radiance values for a country with such a large economy. Radiance values peak at around 715 $W.cm^{2}.\mu m^{-1}.sr^{-1}$, which is considerably less than other large countries in Europe or America. It is due to this relatively small amount of radiance that West Germany has the steepest gradient of any country tested.

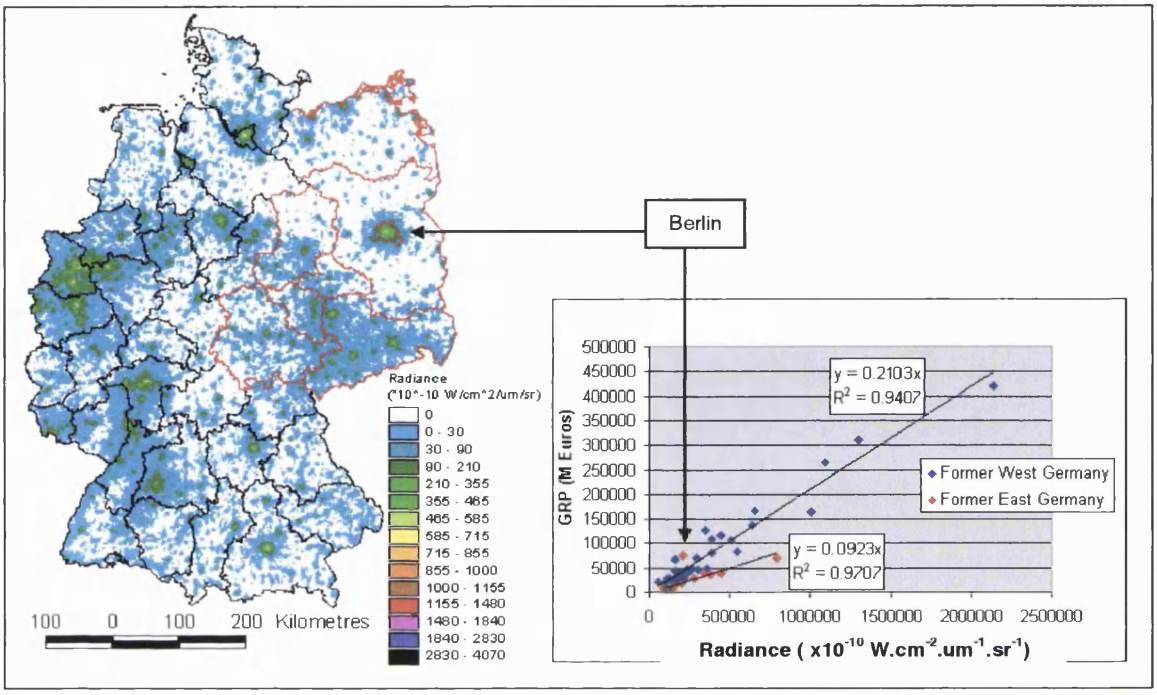

Figure 6-15 Night-time lights of Germany with NUTS-2 boundaries and its total radiance – GRP scatterplot divided according to the boundaries of the former East Germany (*n=8*) and West Germany (*n=37* including Berlin).

In the case of Belgium (Figure 6-16), there are only three NUTS-1 regions. Brussels, the capital, is only included at the NUTS-1 level. It occupies the position of a major outlier and Belgium could be classified as one of the countries belonging to those in the major outlier model of section 6.3.3.1. However, when Brussels was excluded from the analysis, it became apparent that there are two distinct relationships present. Investigating this further, it transpired that the two lines corresponded to the French speaking Wallonia region (outlined in black in Figure 6-16), and the Flemish speaking Vlaams Gewest region (outlined in red in Figure 6-16).

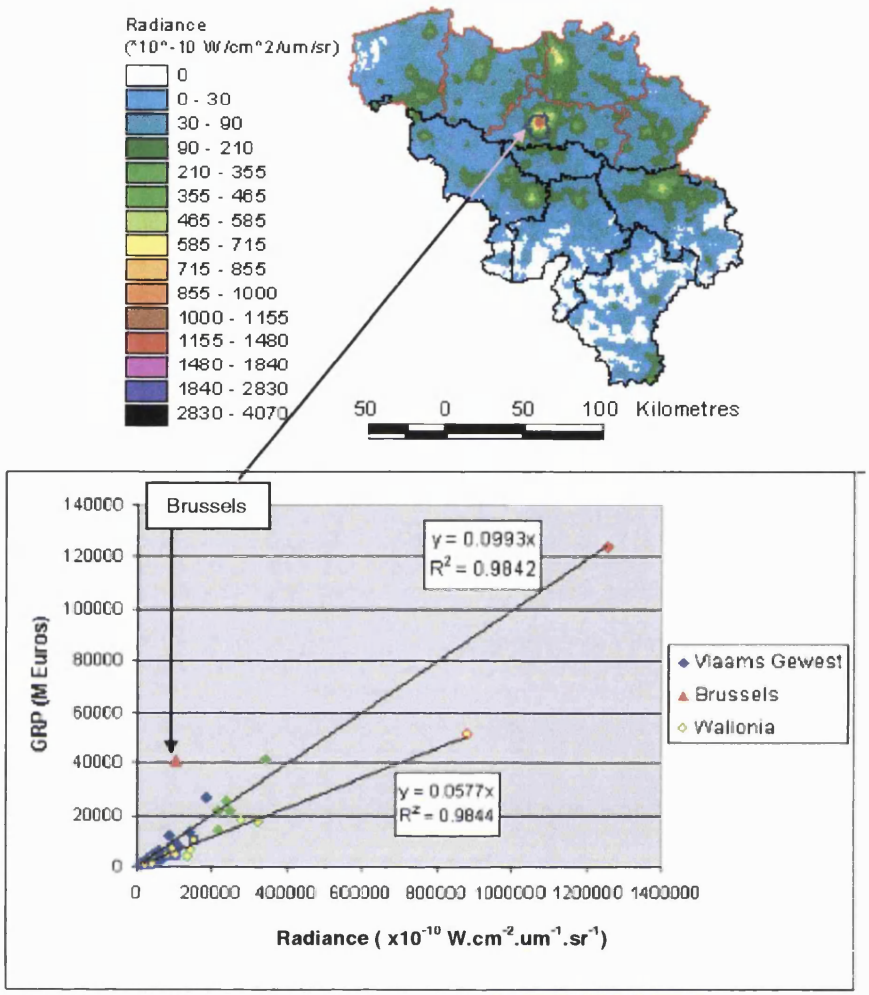

Figure 6-16 Night-time lights of Belgium with NUTS-2 administrative boundaries for Vlaams Gewest (red) and Wallonia (black) and its total radiance – GRP scatterplot for all NUTS regions in Belgium (Vlaams Gewest *n=22*, Wallonia *n=19*)

6.3.3.4 One relationship

Countries: Greece, The Netherlands

Two countries, however, did not exhibit any of the features mentioned so far. Greece has the smallest NUTS-3 areas of those countries where NUTS-3 units were analysed. This can be seen in Figure 6-17, where points occupy a narrow radiance range. There is a clear distinction between NUTS-3 and NUTS-2 points with the exception of Thessaloniki, which is some three times more radiant than the next

most radiant NUTS-3 point. Athens, the capital, is a NUTS-1 region and lies at the extreme top-right of the scatterplot just above the trendline. The night-time lights image of Greece reveals that apart from Greece and Thessaloniki, there are not many highly radiant areas. Nonetheless a very strong correlation is present.

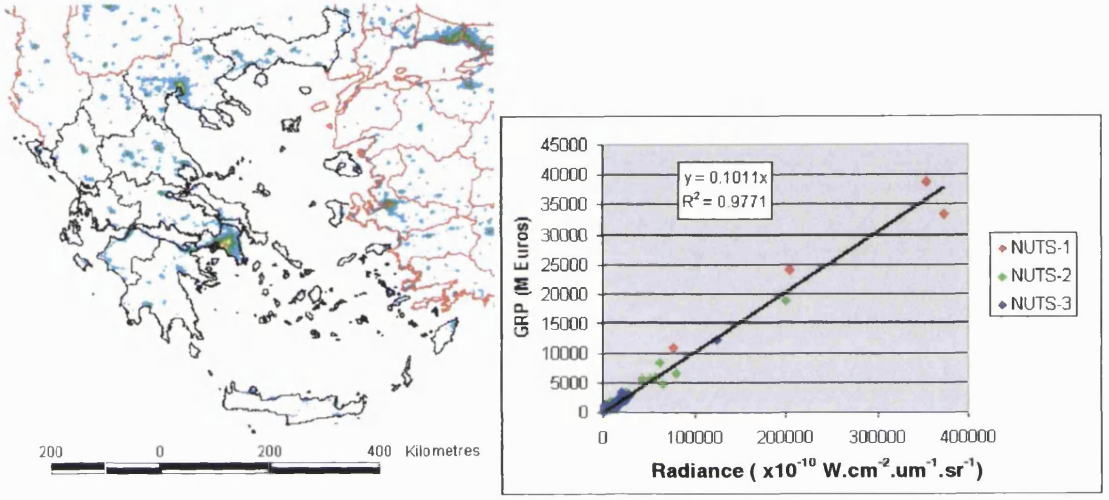

Figure 6-17 Night-time lights of Greece with NUTS-2 regions outlined in black and its total radiance – GRP scatterplot (*n=61*).

The 11th country – the Netherlands, was as close to the ideal result as might be expected. The Netherlands exhibits the strongest relationship of all the countries tested in the sense that the relationships at different NUTS levels are very similar (Figure 6-18). This suggests Dutch NUTS areas seem to be less susceptible to MAUP effects than other countries examined. The corollary to this is that for countries which have a large amount of scatter at the lowest regional level of analysis (usually NUTS-3) will have a greater chance of different relationships being derived at higher levels of aggregation. Clearly, if there is a perfect $R^2 = 1$ linear relationship at NUTS-3 then this will be preserved no matter how these regions are aggregated. Crucially however, the same thing cannot be said when disaggregating a relationship since the $R^2 = 1$ result could have arisen by chance. Whilst the likelihood may be small, examples presented here of how areal units can combine

together to give spurious results should be considered when drawing conclusions about regions at different scales.

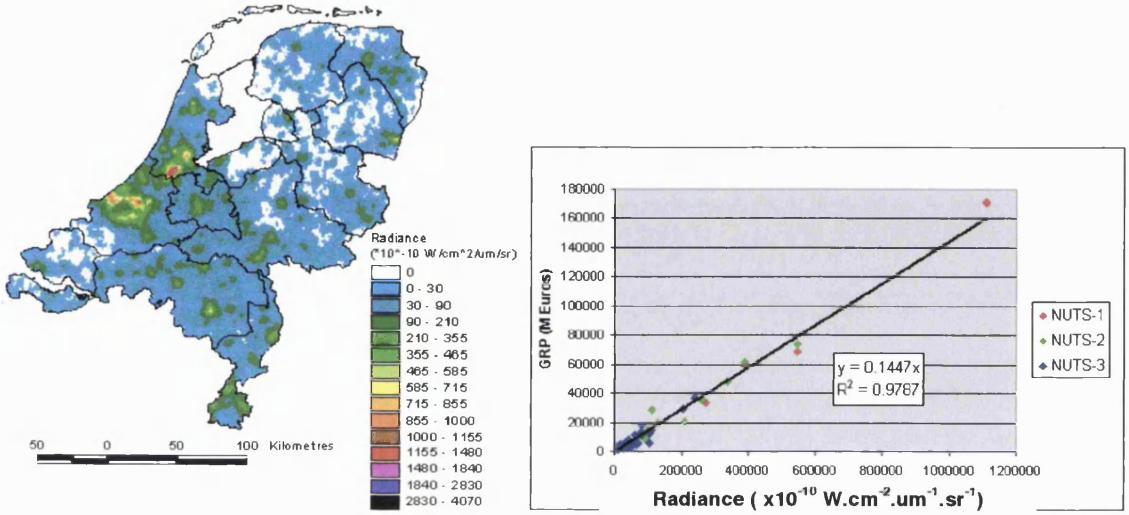

Figure 6-18. Night-time lights of The Netherlands with its NUTS-2 boundaries and its total radiance – GRP scatterplot (*n=54*).

In addition to this, examining the NUTS-2 gross regional product by sector (Figure 6-19) reveals that these regions are also well balanced with respect to their distribution of GRP generating sectors. That is, in order to obtain such a graph, each region must have the same proportion of each type of economic sector.

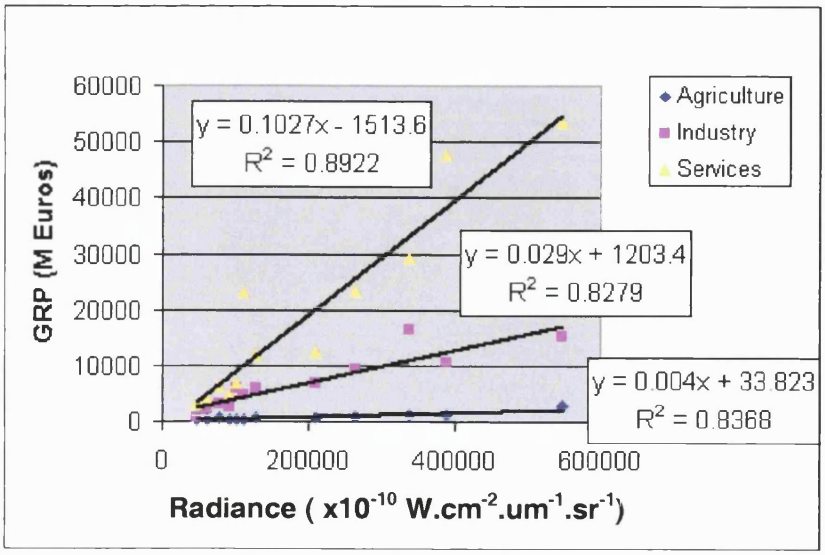

Figure 6-19 Netherlands NUTS-2 GRP by sector versus total radiance.

6.3.3.5 Summary

At a general level one can conclude that the relationship between radiance and economic activity holds across sub-national regional scales. Whilst some of the relationships are not perfect, there are different types of outliers that can be identified from the scatterplots. The nature of these outlying points is further discussed in the next section. A summary table of the results presented in this section can be found in the summary (section 6.5).

6.3.4 Correlations with energy consumption data

Similarly strong relationships exist between total radiance and power consumption figures. These figures were only available for a smaller number of countries (5) and extend down to the NUTS-2 level (see Table 6-5). Power consumption figures are sub-divided into 8 contributory sectors, which enable an analysis to be carried out as function of different energy consuming sectors. These data are not universally available for all countries but a selection is shown in Table 6-5. Overall, there is a good correlation between total radiance and total energy consumption, however this is not the case for all sectors.

Table 6-5 Summary of correlation coefficients (R^2) between total radiance and energy consumption at NUTS-2 level for different energy consuming sectors ('-' denotes no data available)

Country	*n*	*Total*	*Industrial*	*Transport*	*Household*	*Agricultural*	*Services*
Spain	16	0.810	0.394	0.703	0.975	0.301	0.925
Greece	13	0.870	0.249	-	0.960	0.110	0.935
France	21	0.891	0.654	0.472	0.719	0.005	0.590
Italy	20	0.929	-	-	0.936	0.743	-
Belgium	10	0.560	-	-	-	-	-

Country level correlations have been shown to be high for the relationship between lit-area and total electrical power consumption (Elvidge *et al.*, 1997c). In this more detailed analysis, the industrial sector had weak – medium positive correlations with

total radiance. In the case of Greece, this was due to one point (Central Greece) being an extreme outlier (very high energy consumption in this sector) from what was otherwise a very good correlation (R^2 = 0.85 without this point). The services sector and, in particular, household energy consumption were found to be highly correlated with total radiance for those countries where data were available. The R^2 figure for Italy's agricultural sector is affected by one outlying area (Emilia-Romagna) in the same manner as the industrial correlation was affected in Greece.

Figure 6-20 compares the scatterplots between total radiance and energy consumption for the services sector and total consumption at the NUTS-2 level. The two additional NUTS-1 regions of Ile-de-France and Nord-Pas de Calais are also included in order to cover the whole country. Whilst the Ile-de-France region is a major outlier when compared to the service sector, its position is not so anomalous in the adjacent graph of total energy consumption. However, it is the Rhône-Alpes region containing the cities of Lyon (shown in Figure 6-7), which has the highest amount of both total energy consumption and night-time radiance.

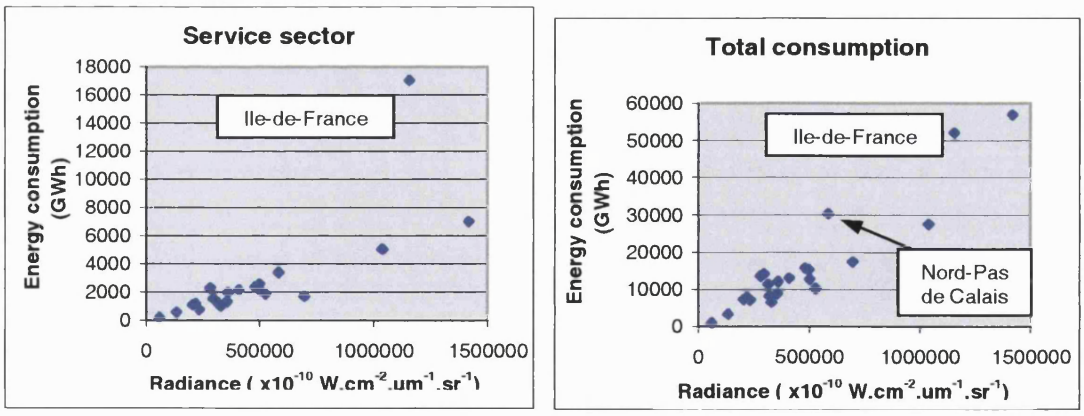

Figure 6-20 Comparison of service sector versus total energy consumption correlation with NUTS-2 total radiance (plus the Ile de France region)

Total GRP and energy consumption figures are very well correlated, especially when comparing the services sector figures (R^2 = 0.996).

6.4 Outlying points

For a few of the countries tested in the analysis of European countries, there is a number of points which deviated from the derived regression line. These points invariably represent heavily urbanised areas, usually a capital city or its hinterland. From the position of these points on their respective graphs, it doesn't appear that they are related to each other. Therefore other metrics are sought from the data to help understand why these points deviate from other points in the total-radiance/GDP scatterplots.

In seeking other discriminating metrics, it is worthwhile first to appreciate what the graphs presented in section 6.3 are showing. The scatterplots are a visualisation of how the total amount of radiance in a NUTS region is related to its GDP output on a national scale. It is a more sophisticated measure than a simple lit-area versus GDP plot since pixels of equal areas can have very different radiances. It was hoped that this feature might help to reduce the magnitude of outlying regions but it appears that this is still not sufficient for some countries.

6.4.1 Radiance distributions within NUTS regions

Figure 6-21 illustrates the difference in radiance distribution between Paris, Hauts-de-Seine and another NUTS-3 point from near the regression line. Loire-Atlantique is a typical French département. It is substantially larger in area than the major outliers for France and has one of the main cities in France (Nantes) within its borders. It has a distinctive negatively skewed distribution of radiance values with a low mean. By contrast, Paris has a far more evenly distributed radiance-frequency profile with no obvious modal class. The frequency values on the y-axis have been normalised by dividing pixels counts by the total number of lit pixels. Zero radiance (unlit) pixels have been excluded from the graph. The distribution for Paris shown in Figure 6-21 is the same for the two outlying Copenhagen amter in Denmark and has been found to be a unique feature to outlying points tested in the analysis. However, the distribution of radiance for those points which have much higher radiances

compared to the other NUTS regions in its group but are not outliers, (e.g. Thessaloniki and Lisbon) are more in keeping with other NUTS-3 areas by having a clearly peaked distribution. This includes Berlin, which, although outlying with respect to those points in the former East Germany, is well in line with West German NUTS regions.

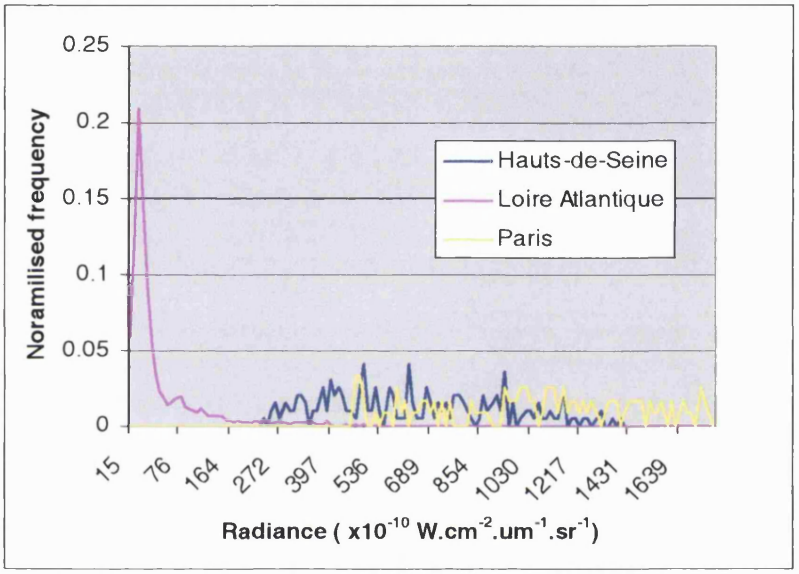

Figure 6-21 Radiance Distribution for the two outlying French NUTS-3 départements Paris and Hauts-de-Seine) in comparison with a regular département - Loire Atlantique.

There is a number of similarities between the French and Danish outliers. Firstly both Paris and Copenhagen city centres are themselves NUTS regions. They are of the order of 100 km^2, when the average NUTS-3 region is 5700km^2 in France and 2800 km^2 in Denmark. The Ile-de-France region around Paris is also a NUTS-1 region a fraction of the size of its sister NUTS-1 regions in France. It is highly urbanised and has a high proportion of higher radiance pixels. The Ile-de-France region is still an obvious outlier even after aggregation. However, if it is further combined with the much larger annular Bassin Parisien region, it begins to align with the other NUTS-1 regions. If a single scale independent relationship exists however, then it shouldn't matter what spatial units are employed to construct the relationship. The difference in size of NUTS regions is an important issue.

Contrasting Spain's NUTS-3 boundaries with that of France or Denmark, Spanish areas are reasonably large and uniform in size – even for Madrid and Barcelona. It begs the question whether a correlation is only as good as the spatial units it is based on. Would Barcelona's NUTS-3 point be an outlier of the magnitude of Paris or Brussels, if it had a small administrative boundary in the centre of the city? If so, then the disaggregation will underestimate the centre of the city and overestimate the surrounding area by virtue of not having an appropriate spatial unit to describe its radiance relationship to economic activity. The same can be said for Milan or Rome, which also have large NUTS-3 areas when compared to the concentrated zones of Paris or Copenhagen. Whilst the problem can be "aggregated away", the application of a 'macro-relationship' to create a disaggregated map would be a misrepresentation of the finer points of the data.

An example of this is presented by Doll (2003) who investigated the characteristic of the radiance-GDP relationship in England and found that the Greater London area had disproportionate levels of lit-area (1.7%) and radiance (8.6%) compared to its 16% share of GDP. This was mirrored by certain regions having greater amounts of light than their contribution to the national economy. If one hypothesises that increasing radiance is linearly related to GDP, then one way to disaggregate the statistic is to divide the GDP by the total radiance to establish a 'GDP per unit radiance' coefficient and apply this to lit pixels. Comparing coefficients across NUTS-1 regions, there is a difference of a factor of 3 between the lowest (NorthEast) and the highest (Greater London). A single coefficient was calculated for the UK and applied to the eleven NUTS-1 regions. The result confirmed the existence of a North/South divide with the greatest disparities of over and underestimation seen between those regions furthest apart.

6.4.2 Scale dependencies in resolving outliers

From this discussion, two additional metrics may be identified as being potentially helpful. Firstly, the radiance distributions shown in Figure 6-21 suggests that the

mean radiance of a region could be a useful feature to discriminate those areas, which, while having equal total radiance, have different GRP. Secondly, the proportion of area lit in a NUTS region can give an indication of how urbanised that region is and therefore an inference can be made as to which sector of the economy is contributing to its GDP. Figure 6-19 has shown that tertiary sector industries have a higher GDP per unit radiance contribution which could be used to weight that region. This is more formally discussed below.

Figure 6-22 shows the result of plotting *mean* radiance against GRP for four countries. A logarithmic function is observed to fit to the data well for Danish Amter. The outlying points of the two Parisian départements also have much higher mean radiance than other NUTS-3 regions in France. However two other départements surrounding Paris now manifest themselves as outliers from the main cluster. NUTS regions containing a major economic centre were distinguished by having a much higher mean radiance than other areas.

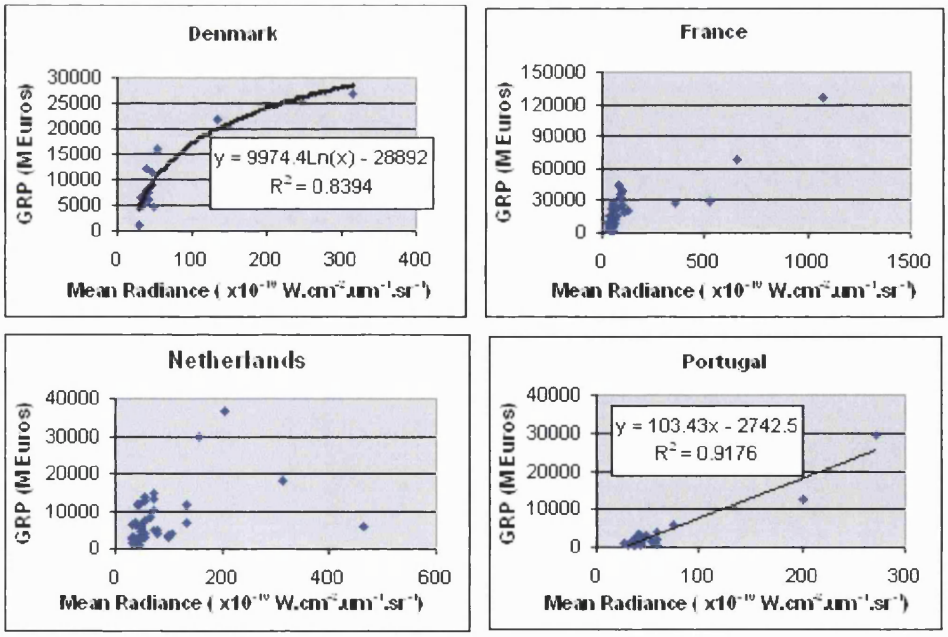

Figure 6-22 Mean-radiance vs. GRP for the smallest available NUTS regions of Denmark, France, The Netherlands and Portugal.

Whilst the result for Denmark offered encouragement for this route of enquiry, this parameter generated more ambiguous results for the other countries tested. This ranged from Denmark's logarithmic relationship to a linear relationship for Portugal, which was almost identical to its total radiance-GRP relationship. The mean radiance result for Netherlands NUTS-3 areas was highly ambiguous at low mean radiance levels despite the best result for total radiance against GRP being seen for this country.

The results presented in Figure 6-22 are for NUTS-3 points only. Over the full range of NUTS-3 points, mean radiance can be said to be a discriminating feature of radiance for GRP. However, it is not a predictive tool because it is scale independent - i.e. the relationship doesn't scale unlike total radiance, equal mean radiances can have different GDPs at different scales. Consider, for example the situation where the equal mean radiance has been drawn from a set of 40 pixels as opposed to 4000 pixels. The size of different NUTS regions has been shown to vary greatly even at NUTS-3 level. The relationship derived between mean radiance and GRP at one scale cannot be assumed to be valid at another level. This is crucial if the relationship is to be used to disaggregate its correlate. The same can be said for the other measures of radiance such as the standard deviation and range, where the result can be the same for a 5x5 window of pixels or a region of 10^3 pixels. In this context, the radiance distribution discussion in section 6.4.1 can also be considered to be a scale dependent feature, as radiance distributions of Paris and Hauts-de-Seine will tend towards that of the Loire-Atlantique as NUTS-3 regions are aggregated together. Although mean radiance is not of use here because the relationship doesn't scale (and hasn't been found to produce a consistent form of relationship), it may be a useful measure from night-light imagery for other applications.

Weighting total radiance by the proportion of lit area in a region does not seem to help resolve the presence of outliers. In the case of France and Denmark, the magnitude of the outliers is so extreme that the weighting has no discernible effect. However, an altogether more robust approach would be to weight both the radiance and the GRP by the lit-area. Plotting these normalized values against each other

essentially gives some idea of how the radiance per unit area is related to the GRP per unit area. Plotting 'densities' in this way provides a scale independent metric of the radiance-GRP relationship. Figure 6-23 shows how points from different NUTS levels are mixed together in the plot space.

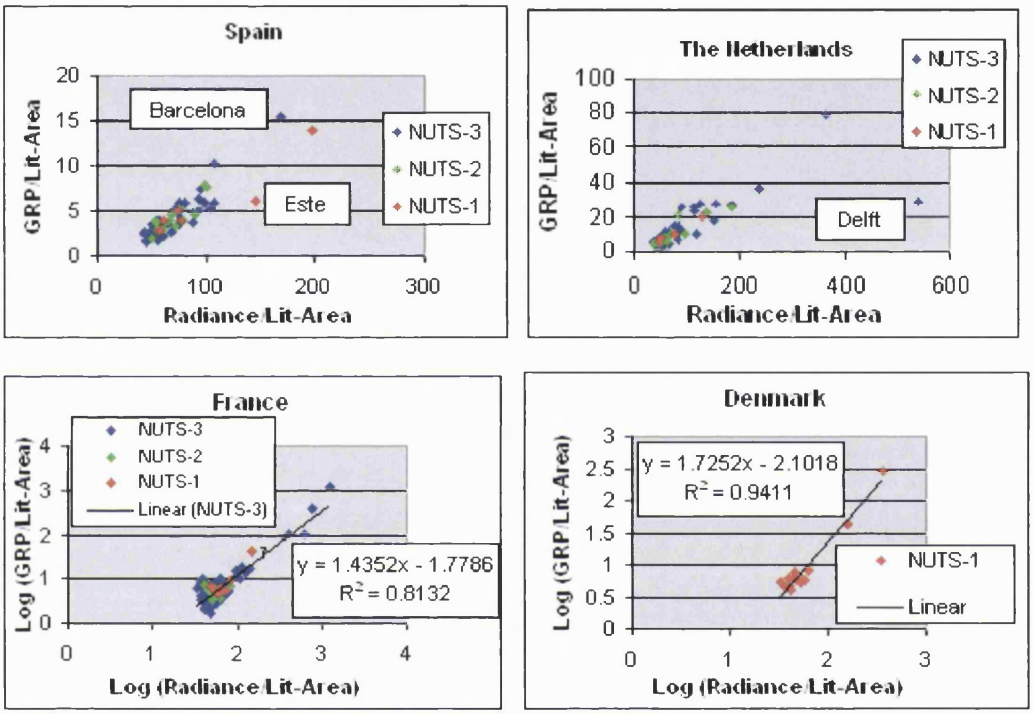

Figure 6-23 Radiance/GRP density plots for four countries (Clockwise from top-left: Spain, The Netherlands, France and Denmark)

These area-normalised graphs make it easier to visualise how the points at different NUTS levels differ from each other. Interesting results are generated for the four countries shown. The NUTS-1 regions of Spain still have a shallower gradient than either the NUTS-2 or NUTS-3 points. Barcelona's NUTS-1 point (Este) is less affected by Barcelona now, and its position in the graph relative to the other points is more similar to that indicated in Figure 6-11 when Barcelona's radiance is subtracted. Applying the analysis to The Netherlands, which exhibited the strongest relationship between radiance and GRP, generates an outlier (Delft-im-Westland). This point is also observed in the mean-radiance-GRP graph in Figure 6-22.

The analysis improves the relationship for countries classed as having major outliers. In this case, the outlying points are pushed further along the x-axis, enabling the derivation of a log-log relationship. The graphs for France and Denmark in Figure 6-23 are shown in log-log space. The strength of the relationship for those countries is largely due to the presence of formerly outlying points aligning themselves away from the main cluster. As regards the main cluster of points, it is much less correlated than the same set of points in Figure 6-7. The NUTS-2 R^2 of this main cluster for France is 0.01 in 'density space' compared with 0.84 for the same points in radiance-GRP space. Similarly, those Danish points used to derive the relationship in Figure 6-8, has a R^2 value of 0.87 compared with 0.31 in density space. Normalising points by lit-area does appear to help in the quest for a single relationship that is valid for all points in a country. This is an encouraging development for those countries whose most economically productive area is not necessarily its brightest area.

6.4.3 Incorporating economic sector breakdowns with land-use patterns

One of the most potentially useful observations is shown in Figure 6-19 and illustrates how the three economic sectors of The Netherlands have different relationships to radiance. In this sense different sectors of the economy can be seen to be more productive than others for a given amount of radiance. The scatterplots for each country shown in section 6.3 are essentially the combination of these sub-relationships. The general trend reported for each country exists because the administrative units used are a combination of different land-use types and therefore different sectors of the economy. Outliers occur where the administrative unit in question is heavily dominated by one single sector. This is usually the service sector of an urban area. Large urban areas tend to dominate their respective NUTS region because the normative criteria used to define NUTS regions (see section 6.3.1) will necessarily take the city as a region. The NUTS-3 region of Paris is very small compared to other NUTS-3 regions in France. These areas are exceptions; most

NUTS-3 areas adhere to the preference for generality (Eurostat, 2002b) and incorporate towns, industrial and rural areas. They are therefore less likely to be outliers. In this sense, traditional political boundaries can be quite useful for identifying areas where a relationship would not be applicable.

Figure 6-19 suggests that the main sectors of an economy are related differently to night-time radiance through the comparison of *total* radiance to sector GRP figures. If this theory were to be fully validated, radiance would have to be classified according to whether it is predominantly urban or rural. This could be done in one of two ways. A radiance threshold could be applied to the data as has been commonly used in studies (Imhoff *et al.*, 1997; 2000) using the frequency-composite version of the night-time lights product described in chapter 3. Alternatively, one could attempt to classify night-time lights based on an underlying land-use map. A broad correlation has been performed using the CORINE land-use map from the European Environment Agency. The CORINE land cover database provides a 44 class biophysical inventory across the European and parts of North Africa. It is represented at a spatial resolution of 250m, a quarter of nominal resolution of the night-time light data. The breadth of land cover classes extends to include 11 categories of urban land-use. From these 44 classes, it was possible to re-map them into more economically meaningful urban/services, industrial, agricultural and non-GDP generating (forests, marshes, estuaries etc) classes.

A preliminary analysis of these classes with the night-time radiance imagery is shown in Figure 6-24. The four lines on the graph refer to the relative percentage of these remapped classes occurring in each radiance value across Europe (shown in Appendix D). As would be expected, the proportion of the urban/services class to be found in a radiance class rises with increasing radiance, which is mirrored by a commensurate decrease in the agricultural class. Two things are important to note about this graph however. Firstly, the urban content of a radiance pixel is observed to level off at around 60% in the radiance range of 500-1650 $W.cm^{-2}.\mu m^{-1}.sr^{-1}$ before climbing towards 100% at very high radiance range, indicating that high radiance pixels can still have a substantial proportion of non-urban land-uses. Secondly, the

crossing point of the urban/services and agricultural traces (Radiance = 200 W.cm^{-2}.μm^{-1}.sr^{-1}) indicates where urban/services becomes the dominant GDP generator, but not necessarily greater than the sum of the others. The data presented in Figure 6-24 is for the whole of Western Europe and again subject to aggregation effects. It is intended more to give an overview of the radiance/land-use characteristics of Western Europe rather than be representative of one specific area. The local statistics for a given area could be substantially different than this 'global' statistic.

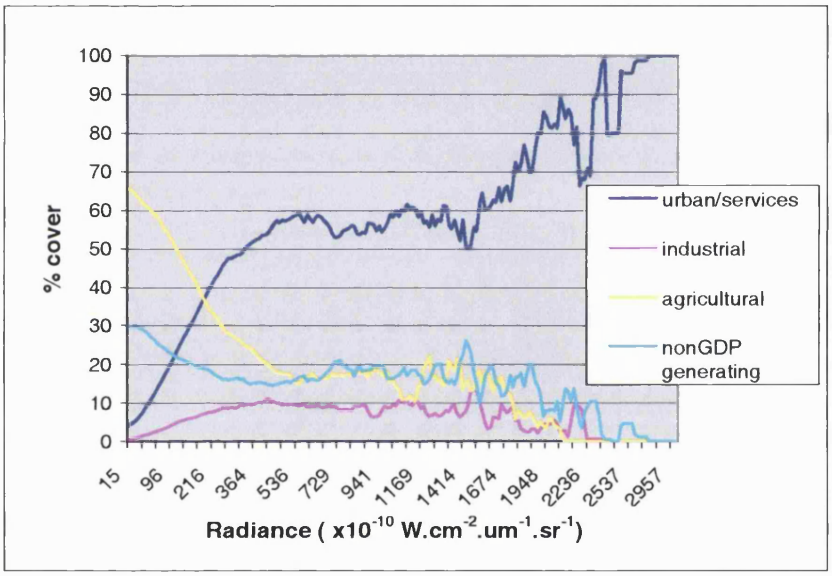

Figure 6-24 Proportion of economic land-use classes occurring in the range of radiance values for Western Europe.

Figure 6-24 highlights the problem of attempting to attribute radiance values to specific types of GDP generating land-use areas. Performing the analysis the other way round (i.e. by examining those radiance values occurring in specific land-use areas) could be a more effective way to visualise the data. Clearer results may be obtained by looking at smaller areas.

6.5 Summary

The results presented in this chapter are summarized in Table 6-6. In general, it can be said that total radiance is related to regional economic activity as expressed by the gross domestic product. Whilst there were variations in the magnitude of the relationship, a linear relationship could be derived for the majority of the points for all the countries tested. Within this framework, some countries had two regionally definable relationships at work. Others displayed outlying points, whose position varied from being just offset (i.e still the most radiant point but appreciably away from the main trendline) to points that lay well away from the main trendline.

Table 6-6 Summary of Results for Europe and the United States. The outliers column refers to the number of outliers with the total number of points including aggregated points given in brackets (e.g. Paris,Hauts-de-Seine and its higher level NUTS region)

Country	*# Valid points*	*Gradient*	*R^2*	*Outliers (all)*
Germany (West incl. Berlin)	37	0.2103	0.94	-
Ireland	10	0.2026	0.97	-
UK	38	0.1652	0.85	1 (2)
Netherlands	54	0.1447	0.98	-
Denmark	13	0.1194	0.87	2
Italy	118	0.1097	0.95	1 (2)
Greece	61	0.1011	0.98	-
Belgium (Vlaams)	22	0.0993	0.98	(1 Brussels)
France	94	0.0986	0.75	2 (3)
Germany (East excl. Berlin)	8	0.0923	0.97	(1 Berlin)
Spain	40	0.0539	0.88	2 (3)
Belgium (Wallonia)	19	0.0577	0.98	(1 Brussels)
Portugal	30	0.0565	0.99	1 (2)
USA	55	0.0499	0.96	2 (4)

It is not anticipated that the variations identified and presented in this chapter constitute an exhaustive list of the different types of relationships. Other variations may exist, most probably from the countries in the developing world. Relationships have been derived for the countries tested but questions still remain as how best to deal with outlying areas, as they appear not to conform to the model tested. The outliers themselves bear no relationship to each other on a GRP-radiance graph (R^2

= 0.11). Although the tendency for countries to have only one or at most two outliers points towards the consideration of outlying points as special cases. Efforts have also been made to analyse these relationships under a single model.

The modifiable areal unit problem is acknowledged to have potentially serious effects on the results and its effects have been noted to operate in two ways. The first effect occurs when an outlier is carried through the aggregation process to make the higher level NUTS zone also an outlier. The second effect is caused by aggregating an outlying area (highly economically active in terms of radiance/GRP) with surrounding areas of substantially lower radiance/GRP values. This has the effect of mitigating the impact of the outlier in higher-level aggregations. Both these effects were observed for the Barcelona-Cataluña-Sur NUTS aggregation discussed in section 6.3.3.2. Experiences such as these suggest that caution should be exercised when interpreting the higher-level aggregations. The blanket application of a single relationship may have serious implications for the accuracy of the disaggregation in certain areas.

The results presented in this chapter have raised a number of important issues regarding the nature of the radiance-GRP relationship and the most appropriate way to proceed for disaggregating a national GDP figure. Anomalies in the relationship can be explained by the prevailing statistical geography. The analysis has largely concentrated on using just one dependent variable, night-time light radiance. However, the incorporation of other data such as land-use data has also been shown to be potentially useful in understanding outlying areas and ultimately accommodating all areas within a single model.

Chapter 7

Mapping socio-economic parameters from night-time iight imagery

This chapter presents results from various ways at mapping socio-economic parameters from night-time light data. The first section deals with the creation of coarse resolution maps of Carbon Dioxide (CO_2) and GDP maps at the global scale. This work was originally published in Doll *et al.* (2000) who created global 1°x1° resolution maps of CO_2 emissions and GDP by applying relationships derived from the correlation of total lit-area at the country level and the parameter under consideration. These maps were derived from relationships based on the frequency composite night-time light product described in section 3.1. The experiences from this study led to further investigations on the use of radiance-calibrated data, the results of which are presented in chapter 6. These results will be used to create a higher spatial resolution regional map, which is anticipated to be more accurate now that different archetypes of relationships have been identified from sub-national analysis of the Eurostat data.

7.1 Spatial disaggregation of statistics

The work presented in this chapter concerns the efficacy of using dasymetric mapping techniques to map economic activity from night-time satellite imagery. Dasymetric mapping has been defined as the subdivision of source zones into smaller spatial units that possess greater internal consistency in the density of the variable being mapped (Langford, 2003). The simplest method of doing this is to assume a uniform distribution of the parameter concerned across the source zone and reassign this to the target zone using the relative proportion of overlap between the source and target zones to assign values (binary dasymetric mapping). This can be improved through *intelligent area interpolation,* where a second set of attribute

data of known distribution can be used to reallocate values (Flowerdew and Green, 1989).

Li *et al.* (1996) used a map of cultivation intensity at 1° x 1° resolution (Matthews, 1983) to disaggregate country level estimates of pesticide (Hexachlorocyclohexane - HCH) usage. The cultivation map was used to identify five intensity levels, which in turn, was used to weight the HCH concentration of that cell. Instead of deriving a global correlation between cultivation intensity and HCH concentrations, the 1-degree grid (segmented by political boundaries) was used to distribute the national total into the grid cells lying within a national boundary. This is further discussed in section 7.2.4. Other methods of disaggregating data (distance-decay functions) are also discussed in chapter 5 of this thesis (section 5.3.3).

An example of the use of satellite data for dasymetric mapping is provided by Walker and Mallawaarachchi (1998) who used a multivariate approach in conjunction with NOAA-AVHRR NDVI data to disaggregate agricultural statistics. In this chapter, night-time lights in one form or another (lit-area or radiance) will be used as the density measure to disaggregate spatially a number of socio-economic statistics.

7.2 Global mapping using the frequency composite night-time lights product

Global relationships between country level lit-area and a number of socio-economic and environmental parameters have been established by Elvidge *et al.* (1997a;b) and Doll (1998). Doll (1998) derived relationships between lit-area and GDP and CO_2 emissions. These relationships were used to create maps at 1°x1° resolution (Doll, *et al.*, 2000). The geographical projection (platte carée) was used because it is a common projection used for global modelling studies such as climate change and land-use. In addition to this, the Carbon Dioxide Information Analysis Center (CDIAC) had already produced a map of CO_2 emissions at 1° resolution (Brenkert,

1998), so it made sense to produce a map in the same projection to facilitate comparison. However, the choice of this projection imposes the problem of how to account for changing areas with latitude. The east-west (E/W) distance for every degree decreases as a function of latitude due to converging lines of longitude towards the poles. In other words, a square degree at high latitude will be less in area than a square degree at the equator. This conversion is required because the global relationships are based on the correlation between lit-area and CO_2 or GDP. The decrease in E/W distance is shown in Table 7-1.

Table 7-1 Distance in metres of 30 arc-seconds (30'', 1/120 of degree) for increasing latitudes (Muller, 1999).

Latitude	*E/W (@30'')*	*N/S (@30'')*
0	927.7	921.4
10	913.7	921.7
20	872.1	922.5
30	804.1	923.8
40	711.6	925.4
50	597.5	927.0
60	465.0	928.5
70	318.3	929.7

The global night-light data (at 30'' ~ 1km) were resampled to 1 degree. From this, the percentage of 'lit' cells was calculated for each 1° cell. Area calculations were approximated into ten zones - (i) a 20° equatorial zone, from the equator to 10° of latitude, (ii) 10°-30°, (iii) 30°-40°, (iv) 40°-50°, (v) 50°-60°, and (vi) 60°+ for the Northern Hemisphere. Neither map extends beyond 60° South since there are negligible lit areas in these high latitude regions. Using the values in Table 7-1, areas for a one-degree cell could be calculated (see Table 7-2 below). The percentage lit value in each one-degree cell could then be converted into an areal value and inserted into the relationship to retrieve the cell value of the parameter being mapped. These areal approximations for bands of latitude mean that area will be over and underestimated around the mean value of the zone. A more elegant method would be to derive the function to plot area against latitude and then use this to calculate an unique area for each cell for its given latitude value.

Table 7-2 Dimensions of the Latitudinal Zones used to create maps

Latitudinal Zone	*Dimension (m) at 30'' (E/W x N/S)*	*Area (km^2) at 1 Degree*
60º+ (Northern Hemisphere)	400 x 929	5351.040
50º-60º	531.25 x 927.5	7095.375
40º-50º	655 x 926.1	8734.975
30º-40º	755 x 924.6	10052.251
10º-30º	850 x 922.5	11291.400
-10º-10º	920 x 921.5	12208.032

This approximation for area has been used for the global maps of both CO_2 emissions and GDP presented in this section (7.2).

7.2.1 Identifying correlations from night-time light data

Country level lit-area values were matched to CO_2 emission figures published by the World Resources Institute (WRI) in their biennial publication, World Resources 1996-97 (WRI, 1996). Despite a temporal disparity between the two datasets (the CO_2 emissions data published is for 1992), a strong log-log relationship is present between the two parameters (Figure 7-1). Saxon *et al.* (1997) reproduced the same result using emission data for 1994 obtained from the Carbon Dioxide Information Analysis Center (CDIAC). This is the same body as the WRI uses to produce its estimate. The total of the emissions data is assessed as being accurate to within 10% of the global figure though it is acknowledged that individual country estimates may deviate significantly from this figure. Saxon *et al.* (1997) also identifies North Korea and Somalia as major outliers in the same position as is identified in Figure 7-1 and used the correlation of night-time lights with electricity consumption data to help resolve outliers. Where one bright outlier was not detected in the other correlation, it was concluded that one or other dataset has been underestimated as in the case of Somalia's CO_2 emissions. Where a country is observed to be outlying in both graphs, it is possible that economic disruption combined with an unusually small proportion of energy production goes into lighting (Saxon *et al.*, 1997). North Korea in particular is well known to be a particularly 'dark' country as regards the amount

of lit area in relation to any of the parameters tested. The lack of detectable light in this region is particularly apparent when compared to its very well illuminated neighbour, South Korea.

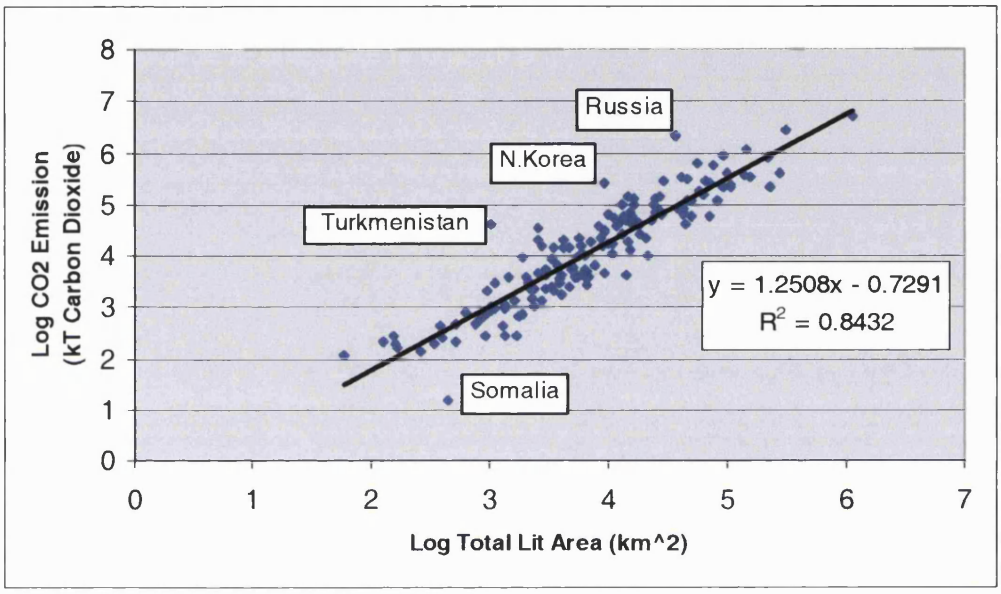

Figure 7-1 Country level lit-area versus CO_2 emission data from the WRI

Figure 7-1 essentially provides a baseline correlation from which it may be possible to undertake further monitoring. The theory being that those countries which have signed up to the Kyoto protocol should be able to have their emissions predicted over time as they converge to their emission limits. Their position on the graph should then be predictable and a deviation from this predicted value would imply that an under-reporting has taken place. In this way night-time light imagery may be able to help monitor countries' compliance with the protocol. However, it is also recognised that countries have different light/energy consumption patterns or could develop different regimes of energy efficiency, both of which can severely affect the strength of the relationship. In this case the relationship cannot be regarded as static and further research is needed into other discriminatory factors which can be used to identify countries which have signed up to specific Quantified Emission Limitation and Reduction Objectives (QELROs) described in chapter 2 (section 2.1.1). Given

the complications currently associated with these methods, it is most likely that it could only be used as a preliminary assessment to identify those countries meriting further investigation.

7.2.2 Carbon dioxide emission mapping from night-time light data

Relationships were derived for both CO_2 (Equation 7.1) emissions and GDP (Equation 7-2 discussed in section 7.2.3). Having calculated the area of 1 degree for each latitudinal zone, these figures could be inserted directly into the relationship for CO_2 to obtain the emissions estimate for that cell.

$$CO_2 = 10\text{^}(1.2508*(\text{Log } A) - 0.7291)$$

Equation 7-1

Where CO_2 is the emissions estimate for the cell of area A.

The approximations made for area with changing latitude means that it does not necessarily follow that a one-degree cell with the highest percentage of lit area would also be the cell with the highest GDP or CO_2 emission. Although the one-degree cell with the highest percentage of lit 30'' cells (75.5%) lies on the eastern seaboard of the US around New York, another cell over Tokyo has a value of 66.4% lit but lies in the 30°-40° zone. A square degree in this zone of latitude has an area 15% larger than the 40°-50° zone of the New York cell. Thus, the highest values of CO_2 emissions and GDP occur over Tokyo.

The resultant map of CO_2 emissions based on Equation 7-1 is shown in Figure 7-2. It was compared to a map prepared by the Carbon Dioxide Information and Analysis Center (CDIAC, 1998) shown in Figure 7-3. CDIAC express their emissions estimates in terms of kilotonnes of elemental carbon (ktC), whilst the WRI figures on which Equation 7-1 is based on is expressed in the actual mass of CO_2. This introduces a factor of 3.664 (WRI, 1996), which has been accounted for in Figure 7-2. A difference map [CDIAC] – [OLS] is also presented in Figure 7-4. The most

notable feature of the maps is the similarity of the distribution of emissions especially for high areas of GDP. The satellite-based product only maps the location and distribution of CO_2 emissions based on the presence of city-lights. This results in more grid-cells having 'no data' values than CDIAC's map, which provides an estimate for each land cell. Most of the 'no-data' cells over the land surface in the OLS map coincide with zero value cells in the CDIAC map. Out of 17,636 land cells in the map, 9,552 cells have a defined value in the OLS compared with 11,275 cells greater than zero in the CDIAC map. The values in the CDIAC map were distributed according to a gridded population map (Li, 1996). The city-lights map uses only the lit area to distribute spatially the relationship. The night-light CO_2 map occupies a much smaller range of emissions and generally magnitudes are below the CDIAC estimates.

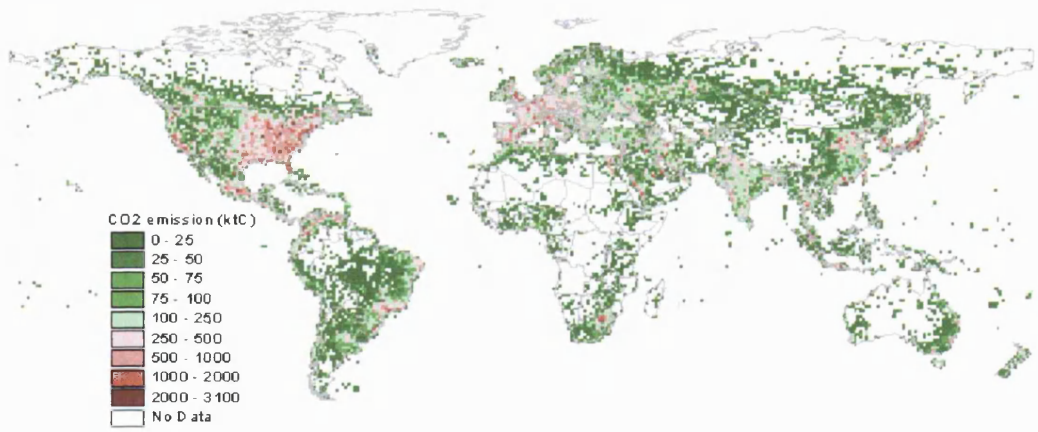

Figure 7-2 Global CO_2 emissions map derived from CO_2/lit-area relationship (CO_2 in ktC)

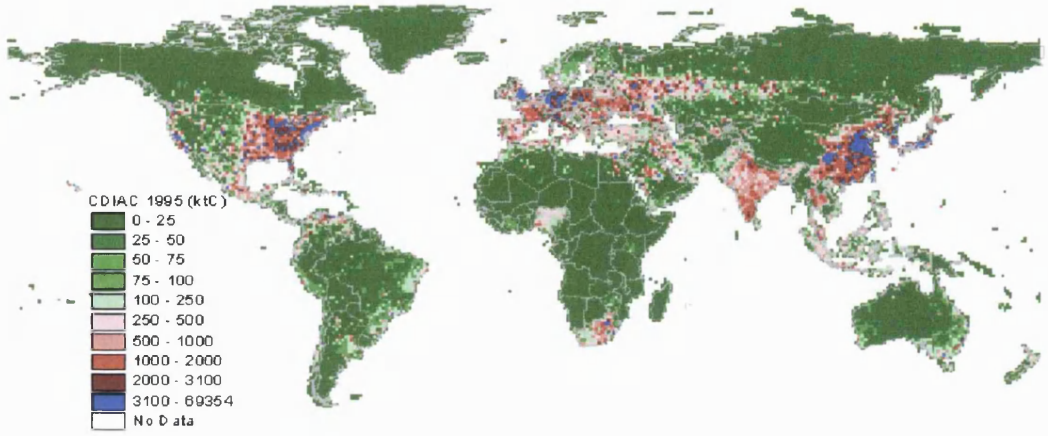

Figure 7-3 CDIAC 1995 global CO_2 emissions map (CO_2 in ktC)

The most populous class is that of the lowest emissions category (0 – 25 ktC). The very highest class of emission values (where the CDIAC map values exceed the night-light CO_2 map) covers three areas: The United States, Europe and the Far East. Whilst these areas account for only 2.1% of the 17,268 one-degree cells, they contribute 45% of the total global emissions.

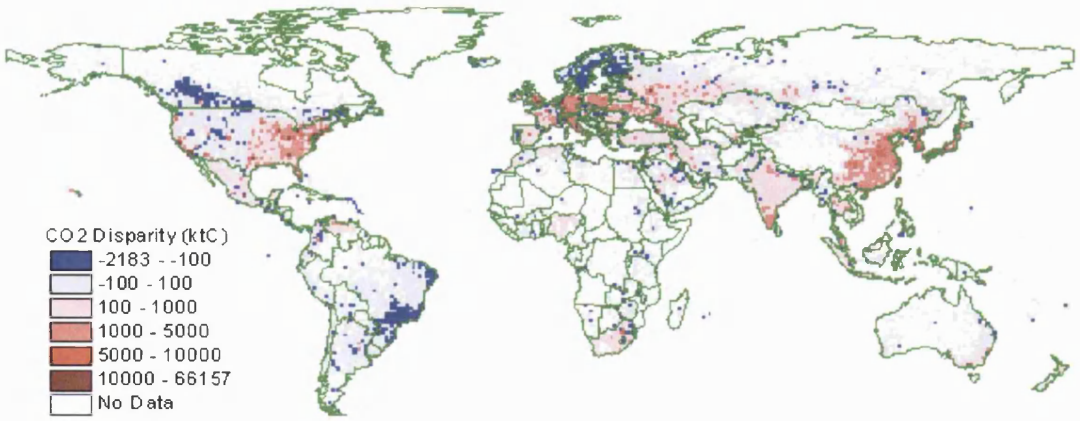

Figure 7-4 Difference map [CDIAC'95] – [OLS] (CO_2 in ktC)

The difference map reveals that the night-light map generally has lower emissions than CDIAC, this is most appreciable in the eastern US, Europe, India and China. Over 5,000 (54%) of the cells in the OLS map are within 100ktC of those in the CDIAC map. In addition to the underestimation of emission values in major industrial areas, emissions over Scandinavia, parts of Canada and the Brazilian State of Minas Gerais appear to have been overestimated from the night-light data.

The global emission value from the satellite-based map is 1.53 billion tonnes of carbon, which is around a quarter of the sum of the CDIAC map. However, the use of the city-lights dataset to map the emission data highlighted the same regions to have the maximum values as identified in the CDIAC map. A time series of data is needed to evaluate fully the contribution that night-time lights can make to the monitoring of CO_2 emissions.

One reason for the low magnitudes of the satellite-derived CO_2 map may be due to emissions not explicitly manifesting themselves in terms of street lights reflecting transport infrastructure, whereas the hub of any country's economy is the cities. Russia for example is shown as a significant outlier in the CO_2-lit area relationship (Figure 7-1). However, its national emission total is much higher than the relationship would have predicted. 51% of its GDP is generated from industry compared with only 9% from Somalia, the outlying country below the main trendline. Tucker (1995) cites the dependency on countries for imports of fossil fuel resulting in differing patterns of energy consumption and energy policies as other factors which affect the GDP- CO_2 relationship.

7.2.3 Global GDP mapping

The relationship between night-time light and economic activity as expressed by GDP can be mapped in the same way as for CO_2 emissions in the last section. The Purchasing Power Parity (PPP) measure for GDP was used as it attempts to account for bias in the exchange rate by assessing how much of a group of goods and

services each currency can purchase locally. PPP-GDP is measured in International dollars (I$) and is obtained using conversion factors (PPP), which equalise the purchasing powers of different currencies thus making national GDP figures more intercomparable. Since these can change over time, the international dollar is continually being reassessed and is set on a year-by-year basis. The relationship between PPP-GDP and lit-area is given by Equation 7-2 (Doll *et al.*, 2000). The PPP-GDP figure refers to 1992, which was the latest available figure published in The World Resources Institute publication (WRI, 1996) at the time of analysis.

$$GDP = 10^{(0.9735*(\log A) + 0.7124)}$$

Equation 7-2

Where *GDP* is the emissions estimate for the cell of area *A*.

It seems that night-time lights reflect economic activity better than CO_2 despite the similarly strong correlation between lit area and CO_2 emission and the correlation between CO_2 emissions and GDP (Doll *et al.*, 2000). The total figure of the PPP-GDP map (Figure 7-5) is 22.1 trillion Intl$ compared with 27.7 trillion I$, in other words around 80% of the WRI figure. The 1 degree cells have an average value of 2311 million I$, but range as high as 27275 MI$ (Tokyo area). Similarly in the CO_2 map (Figure 7-2), a relatively small number of cells take the highest values. The top two classes account for less than 3% of the cells, but contain more than 16.4% of global GDP. With the exception of Japan and the US, there only appears to be one or two hubs of high productivity per country. In Russia for example, Moscow stands out as node of the economy, with only a thin line of higher value economic productivity cells along the Trans-Siberian railway. The principal development in China is observed to occur in the north between Beijing and Shanghai.

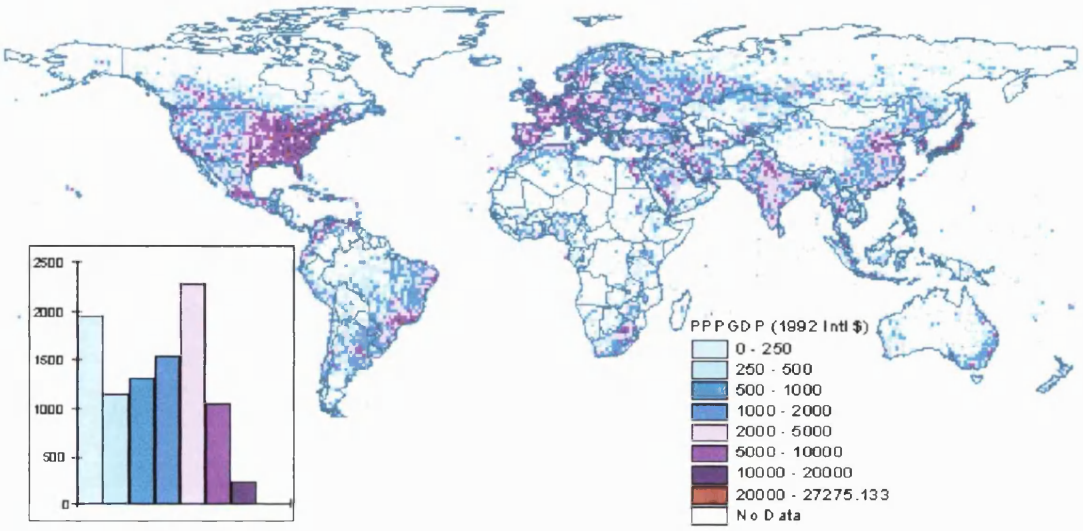

Figure 7-5 Global PPP-GDP economic activity map derived from GDP/lit-area relationship with bar chart distribution of values (1992 International $).

Being the first map of its kind, there is no similar map with which to make comparisons, hence it is difficult to test whether the disaggregation is correct. Preliminary tests were carried out at the country level by intersecting the country outlines layer with the map. Errors associated with this method are discussed in the section 7.2.4 below. Those countries and regions identified as having overestimated CO_2 emissions (Brazil, Canada and Scandinavia) in the CO_2 difference map (Figure 7-4) were also found to have greatly overestimated GDP as well. This would seem to indicate that national policies on light usage differ substantially even between neighbouring countries. Canada for example is overestimated by 88%, whereas the United States is underestimated by 26%. Chile was the only country in South America to be underestimated. All in all, the map was found to have overestimated GDP for 56 out of 137 countries tested.

7.2.4 Considerations for global mapping studies

The results and analysis of the mapping exercises has raised a number of important issues pertaining to the methodology and accuracy assessment. The non-linear

characteristics of the log-log relationship means that in the context of retrieving a disaggregated component of a country total, the whole is greater than the sum of its parts. That is, disaggregated mapping based on relationships established in log space tends to underestimate the parameter, as has been the experience with global CO_2 and to a lesser extent global GDP mapping.

In view of the observations made in section 7.2.2, one must also give consideration to other ancillary data sources which may be used to help weight the night-time lights since they have been shown to be effective in mapping the distribution of global carbon emissions. Elvidge *et al.* (2000) noted a strong positive correlation between cumulative brightness and energy related carbon emissions for the 48 conterminous states of the US. The use of radiance-calibrated data is certainly one area which can offer greater modelling flexibilities as it provides the added dimension of intensity instead of simply the lit-area. Furthermore, criteria need to be identified for grouping countries together. Although there is a broad correlation, this may be further divided into countries which share the same energy utilisation patterns such as those most dependent on fossil fuels. Whilst the bulk of night-time lights come from populated places, it can also provide information on two other sources of CO_2 emission: gas flaring and biomass burning. These practices have distinctive spatio-temporal characteristics, which distinguish themselves from other light sources present in the raw data. In addition to the luminescent detection of forest fires from DMSP-OLS data (Elvidge *et al.*, 2001b), other studies have concentrated on establishing the relationship between the thermal properties of the fire, its rate of biomass consumption and emission properties from satellite data (Kaufman *et al.*, 1998b).

High quality ancillary data is a key requirement in undertaking such mapping exercises. The International Energy Agency provides breakdowns of fossil fuel usage by final use sector (Elvidge *et al.*, 2000). The availability of such figures classified by residential, commercial, transportation and industrial use presents the possibility of incorporating a wealth of other digital map data to help distribute emissions more accurately. Relationships between road networks linking cities may

be constructed to estimate the flow of traffic which could be weighted towards bright urban centres, whilst the spatial distribution from air travel may be distributed according to those sectors which experience the densest traffic (Penner *et al.* 1999). Working with data classified by final energy use would facilitate the task of mapping emissions by reducing the problem to the creation of four separate emission maps at a higher spatial resolution than is currently considered here. These 'sub-maps' could then be combined using standard GIS functions. Elvidge (2002) observes that it is the modelling of CO_2 emissions from these distributed sources as opposed to emissions from major point sources such as power stations, where night-time light data can potentially make the most significant contribution.

In the absence of a validation map with which to compare directly the results, country level comparisons have been used as a substitute. The coarse resolution of the map has ramifications on this approach as approximations have to be made in intersecting a vector country mask with raster grid cells. These approximations become more important as the resolution of the raster becomes coarser and the country in question becomes smaller. The ArcView 'Summarize Zones' algorithm appears to make the distinction based on whether or not the majority of the cell is intersected by the country mask. This can have major implications for countries that have large proportions of their light in coastal or border areas. Chile was identified as the only country in South America underestimated by this calculation procedure. However, there is a number of cells intersecting with its country mask which is believed to have been omitted from the assessment suggesting that, like its neighbouring countries, it too is overestimated.

Li *et al.* (1996) (described in section 7.1) used Equation 7-3 to calculate the contribution of a cell to the total disaggregation within a political unit as a solution to the problem of cells split by boundaries.

$$V_{ij} = \frac{C_i R_{ij}}{\sum_i C_i R_{ij}} V_j$$

Equation 7-3

where for a cell i and political unit j;

V_{ij} is the zone parameter component in cell i for political unit j,

C_i is the intensity value (e.g. lit-area, radiance) for cell i,

R_{ij} is the fraction of total area of unit j in cell i, and

V_j is total value of the parameter to be mapped (GDP/ CO_2)

In order to calculate the zone parameter for a cell, the intensity component multiplied by the ratio of the cell's intersection is divided by the sum of this product for all cells in the region and multiplied by the total of the zone parameter. Clearly, where a cell is not split by a boundary the R_{ij} term is unity. In their example, C_i is the cultivation intensity expressed as a decimal fraction (there are five classes 0, 0.25, 0.5, 0.75 and 1), so likewise radiance would also have to be expressed as a ratio of the total radiance of a region. Since the equation is built around the political unit rather than the cell, it does not matter if more than two regions intersect the split cell since the method is only interested in the contribution of the cell to the region as a whole.

This method assumes that the quantity is evenly distributed within a cell. This is unlikely to be the case for night-time imagery as lights tend to be clustered. The problem of splitting allocated proportions in a cell by intersecting it with a vector or polygon coverage is a fundamental problem in geographic information science. The error involved in allocating data to cells is inversely proportional to the resolution of the cells in the grid and is an example of the ecological fallacy.

7.3 Mapping results from radiance-calibrated data

The sub-national analysis presented in chapter 6 revealed linear relationships between cumulative brightness and GDP. Whilst this was observed for all countries, only two countries could have a single relationship applied to all its regions. Other countries exhibited at least one outlier, which did not appear to fit the derived

model. Further analysis for some countries revealed the presence of two regional relationships. In those cases, outlying points were excluded from the application of the derived relationship and dealt with separately.

In producing a map of this nature, one must consider how sensible it is create a map at a spatial resolution where the subject of the map starts to loose its intuitive credibility. Addressing socio-economic issues such as economic activity is one such application where such concerns become important.

The main factors in choosing a spatial resolution for the map were based not only on what the map aimed to display but also on the technical specifications of the DMSP-OLS sensor. Firstly, although the night-time data has a nominal resolution of 1km, this is resampled from 2.7km. It therefore makes sense to aggregate up rather than use the finer resolution data, which would also reduce any noise effects present in the fine resolution data. Whilst the relationship between cumulative radiance and GRP has been demonstrated to be consistent from the NUTS-3 level up to NUTS-1, an unknown factor is how far the relationship can be extrapolated in the other direction (NUTS-3 to finer scales) before it becomes invalid. Besides the unquantified micro-scale relationship, there is a desire to maintain an aggregate nature to the GDP figures in the map. As has been shown in Figure 6-18 and discussed in section 6.4.3, different relationships exist between the different economic sectors and total night-time radiance. The relationships derived are an aggregate of these sector combinations. Keeping the map resolution sufficiently coarse avoids issues of sector specific GDP representations at finer scales where the aggregate relationship may not be valid. This is further discussed below in section 7.4.3.

Taking these considerations in mind, a choice of 5km for the output resolution was based on the ability of this resolution to provide a detailed map at the continental scale whilst being coarse enough to generalise the nigh-time light emissions to a level which shows detail in large cities without making too much distinction within

small towns. In addition to this is the advantage of making the mapping process less computationally intensive.

7.3.1 Methods employed

Each country's map was produced in ArcView using the cell-based modelling tools in the Spatial Analyst module, whilst the Arc/Info GRID module was used for pre- and post processing of the data. The terms in bold/italics included in following description refer to the output at different stages of the process and accompany the schematic diagram shown in Figure 7-6.

The first task to be performed involved resampling the night-time data to produce a 5km input file on which the output maps would be based. The data were stored in their 8-bit DN format. These values were converted to radiances using Equation 3-1 given in chapter 3 and then aggregated (summed) up to 5km resolution (***radiance-grid***). The DN-radiance conversion equation is non-commutative and therefore the processing must be done in this order since conversion and then aggregation is not the same as aggregation and then conversion. A 5x5 focal sum kernel was applied to the input radiance-calibrated data. 5km is referred to as the nominal resolution of the maps although the exact value is 4.6km. This is because the input data does not have an exact resolution of 1km but 926.5m. Upon resampling on a 5x5 cell basis, the output resolution becomes 4.6km.

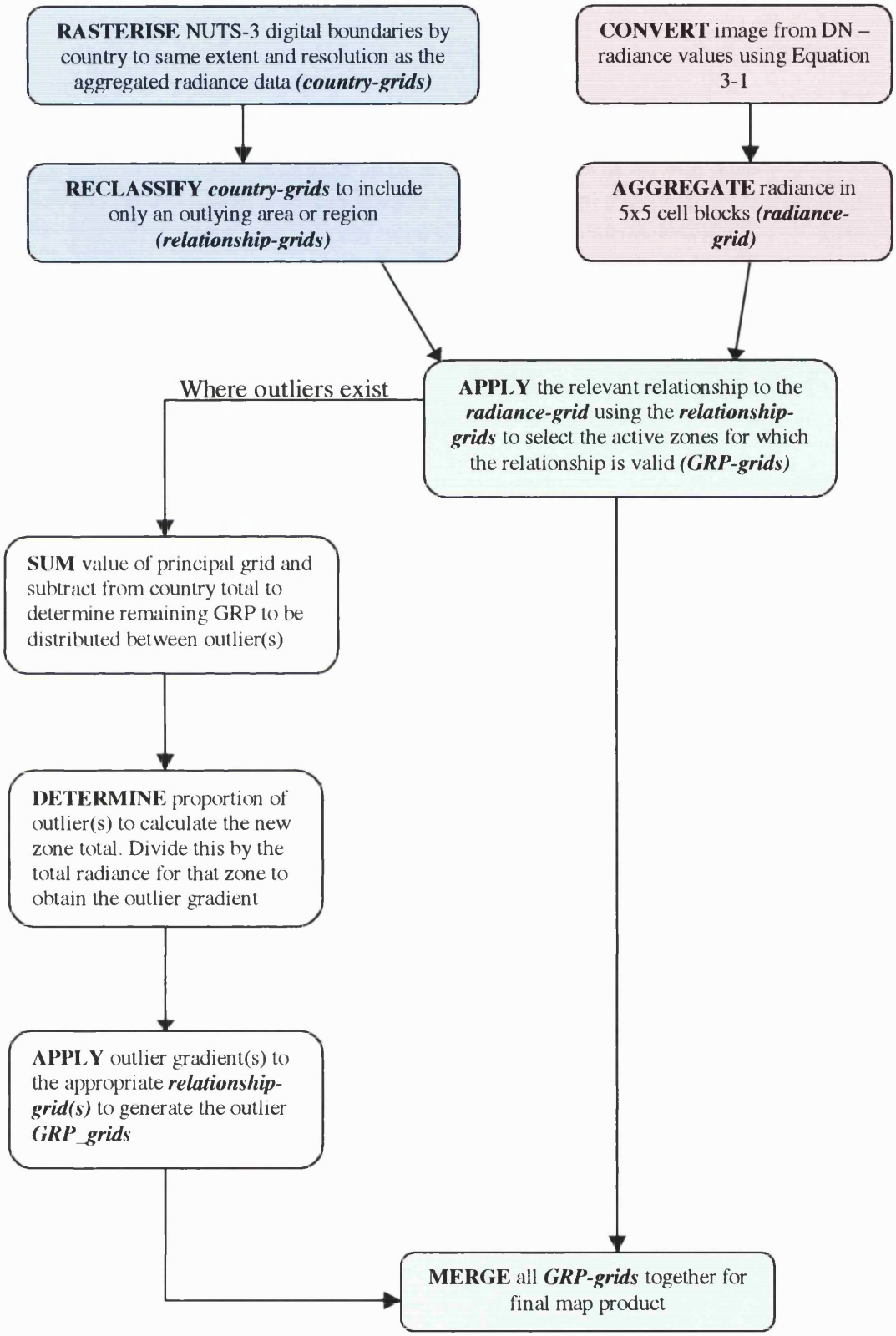

Figure 7-6 Overview of the processing chain for producing the GDP map of Europe.

In order to allocate these new cells to their respective countries, the polygon coverage of NUTS boundaries was rasterised to the same extent and resolution as the aggregated radiance data (***country-grids***). Whole cells were allocated to countries based on the majority intersection discrimination described in section 7.2.4 and no allocation of sub-cell entities as outlined in Equation 7-3 occurred. These errors are most appreciable at coarser resolutions and the decision to proceed in the prescribed manner was based on evaluations of increased accuracy in relation to the magnitude of national GDP and the desire to keep the processing methodology as simple as possible. The polygon coverage contained both region-name and country-name attribute data, which facilitated the construction of individual country raster files. These rasters now contained the NUTS-3 regions, which could be combined with the aggregated radiance data to apply the radiance-GDP relationship by NUTS zone. Furthermore, having NUTS-3 regions as separate entities within the file permitted the exclusion of certain areas which had not fitted the regression model and conversely, allowed the selection of those areas for individual treatment. The reclassification of the country mask was achieved through entering 'NODATA' values for the excluded areas, which meant that processing only occurred in defined areas (***relationship-grids***). In reality, this reclassification occurred solely to select outlying regions and ignore the rest of the country. Each relationship was then applied to the respective grid in order to obtain a disaggregated map of GDP for the area under consideration.

These processes resulted in the production of a ***GRP-grid*** per relationship, each of which was then combined using the MERGE command in Arc-GRID. Again, 'No Data' values were ignored so the grids were merged in order with the main grid first and then subsequent grids of the outlying regions. This ensured that the data contained in outlying area grids would overwrite those areas in the main grid whilst leaving other areas intact. Finally these grids were merged together to produce one map for Europe and another for the US shown in Figure 7-7 and Figure 7-8 respectively.

7.3.2 Treatment of outlying areas

Outlying areas identified for certain countries in chapter 6 were excluded from the main relationship of that country. However, values were attributed to the radiance cells in these areas. Firstly, the main relationship was applied to the regions and compared to the corresponding NUTS-3 GRP figures published by Eurostat. For those areas that had been classified as being valid for the relationship, the map total was compared to the published total. The map total was then subtracted from the published total for the whole country. This figure refers to the remaining amount of GRP to be disaggregated throughout the outlying area(s). It is divided by the total radiance in the outlying area to obtain a density and then used to calculate the GRP for those pixels in the anomalous zone. Where more than one outlier existed for a country, the remaining GRP for the regions was split in the same proportion as the corresponding published data and then distributed according to the radiance ratio for that zone. There were no instances where more than two outliers were encountered. This may not be the best way to deal with outliers; there is no reason (other than an intuitive one) to suggest that the radiance-GRP relationship for these areas is of the same nature as has been demonstrated for the other regions of that country. It is however, a quick and simple technique to ensure that all the cells of the map have a value and that the value bears some relation to the published figure for its region.

In doing so, it also acts to constrain the map total for that country to the published total and thereby produce a map, which, whatever the individual errors between estimated and published totals of its regions will at least sum to the correct value for the whole country.

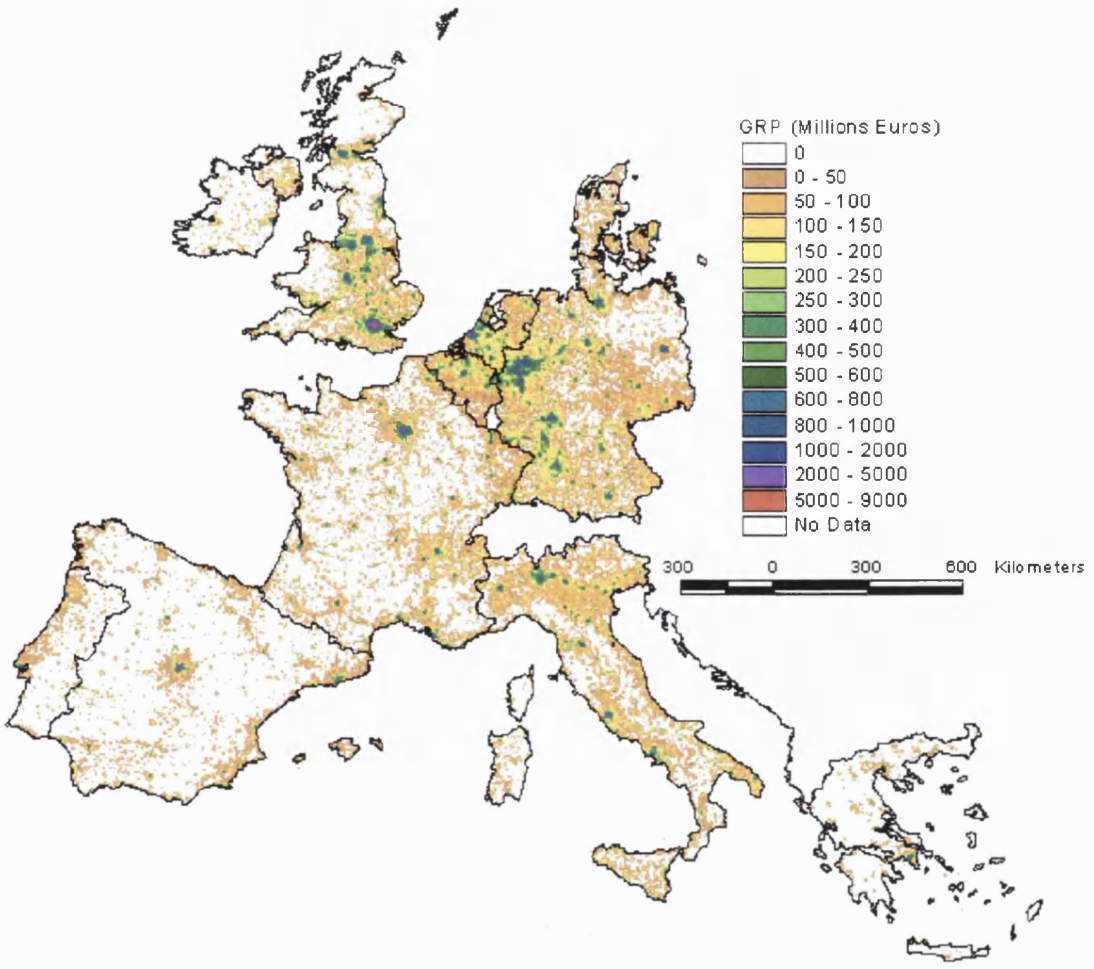

Figure 7-7 Map of estimated economic activity based on DMSP-OLS radiance-calibrated night-time lights for 11 countries in the European Union

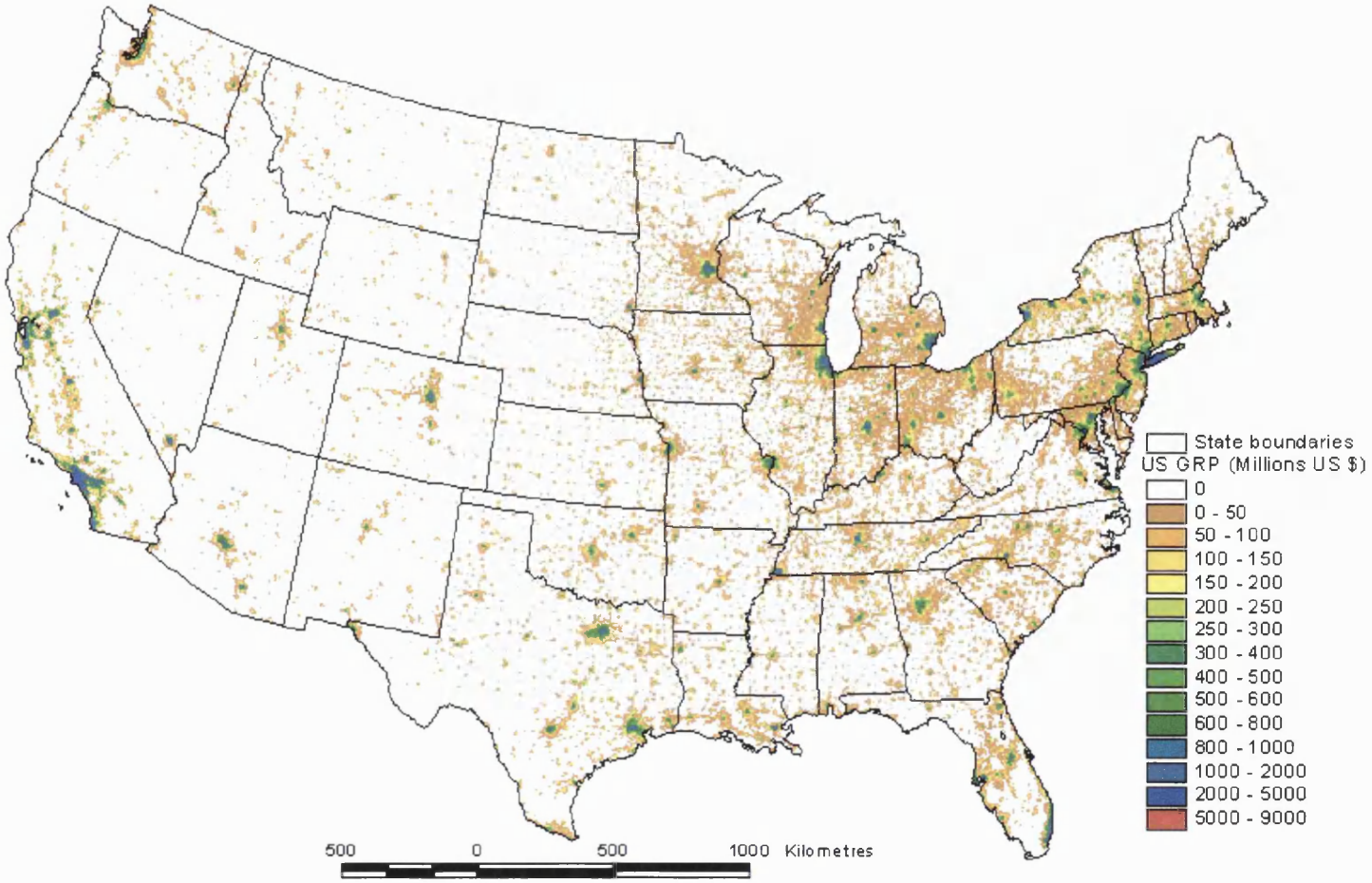

Figure 7-8 Map of estimated economic activity based on DMSP-OLS radiance-calibrated night-time lights for the United States

7.3.3 Results

The results will be presented for the countries as they were classified in chapter 6. The results of the mapping exercise are generally excellent. The results are presented in tables by archetype. The 'Map Estimate' figure quoted for each country refers to the GRP for those areas valid for the main relationship (i.e. outliers excluded). Outliers are listed in italics separately underneath. For these areas, the 'Map Estimate' figure refers to the published total for the whole country minus the map estimate for all areas excluding outliers. Where there is more than one outlying area, the percentage next to the name of the region refers to that outlier's proportion of the remainder. The '% difference' column shows the difference between the two totals. Percentage difference is calculated relative to the published value as shown by Equation 7-4.

$$\left(\frac{\sum_{zone} x_{ij} - E_{zone}}{E_{zone}} \right) \times 100$$

Equation 7-4

where x_{ij} is the GRP value for cell ij in the zone calculated by the model, and

E_{zone} is the expected (published) value of GRP for the zone

The bracketed figure to the right of this refers to the average absolute percentage difference from the expected value and the estimated NUTS-3 areas for that country and is shown in Equation 7-5.

$$\frac{1}{n} \times \sum_{zones=i}^{n} \left| \left(\frac{\sum_{zone} x_{ij} - E_{zone}}{E_{zone}} \right) \times 100 \right|$$

Equation 7-5

where n is the total number of zones valid for the model.

This is intended to give some idea of how much variation there is at this scale since aggregate country total figures can mask the detail of NUTS-3 level agreement. Most countries (outliers excluded since these have been constrained to agree with the country total) were estimated to within 5% of the published total, although average NUTS-3 estimations were usually between 20%-30% of the published figure. A full list of results for each country can be found in Appendix E.

7.3.3.1 Major Outliers

Countries classified as having major outliers have points in their distribution which are far less radiant than their GRP would suggest. As a result, the point of an outlying region lies well above the main trend of points in the midst of the radiance range. The results for each country in this section are shown in Table 7-3.

The total GDP for France (for 94/96 départements) was underestimated by 5.6% using the all-points relationship (Figure 6-7). This resulted in a substantially larger amount to disaggregate between Paris and Hauts-de-Seine (the two outliers) such that the individual error on these two départements approaches 30%. As an alternative, higher-level aggregations were ignored and the NUTS-3 relationship was used instead (Figure 6-6). The gradient increased from 0.0938 to 0.0986 and the difference between totals was less than 1%. As a result, the error for the two outliers fell to around 4%.

There was only one NUTS level with which to analyse the Danish regions (Figure 6-8). This yielded a map which was reasonably accurate compared to the other countries tested. The 13 amter in the main relationship had a percentage mean absolute difference of 16.6%, whilst they summed together to leave the two amter belonging to the capital with very close agreement to the published figures.

The United States is included here and like the other countries in this section, it had two outlying points in its radiance-GRP graph (Figure 6-5). California and New York are offset by a similar magnitude to each other, which is well over twice the

figure for the rest of the country. The total GRP for the remaining 48 states is underestimated by just over 5%. In order to constrain the country total, the methodology requires the remainder to be disaggregated amongst the remaining outliers. This has resulted in both outliers being overestimated by 22%. This is however, still less than the mean percentage difference for those states modelled by the main relationship, which was the highest of any country analysed. A comparison is made between this, and other results in the next section.

Table 7-3 Map estimate and accuracy assessment for countries in the major outlier model

Area	*Gradient*	*Map Estimate*	*Published Figure*	*% Difference*
France	0.0938	970,022.8	1,027,701.1	-5.6 (32.8)
(Paris (65%)		*163,919.2*	*126,239.1*	*29.8*
Hauts-de-Seine (35%)		*88,264.2*	*68,266.0*	*29.3*
France (NUTS-3 only)	0.0986	1,019,661.4	1,027,701.1	-0.8 (32.1)
Paris (65%)	*1.1957*	*131,654.1*	*126,239.1*	*4.3*
Hauts-de-Seine (35%)	*0.6439*	*70,890.7*	*68,266.0*	*3.8*
Denmark	0.1194	99,681.6	100,780.2	-1.1 (16.6)
Kobenhavn og Frederiksberg Kommuner (55%)	*0.7681*	*27,218.2*	*26,755.6*	*1.8*
Kobenhavns amt (45%)	*0.2731*	*22,269.4*	*21,633.2*	*2.9*
United States	0.0499	6,142,244	6,516,332	-5.7 (33.4)
California (61%)	*0.1369*	*1,274,102*	*1,045,254*	*21.9*
New York (39%)	*0.1432*	*808,617*	*663,377*	*21.9*

7.3.3.2 Offset point

Countries belonging to the offset point model are characterised by a distribution of points in the plot space, which have monotonically increasing values of radiance and GRP. The most radiant of these points is observed to be offset from the main trendline. The results for the countries in this section are shown in Table 7-4.

The three Southern European countries in this section performed well, with low mean percentage differences between the individual NUTS-3 zones. It is interesting to note that although Italy (Figure 6-10) had the closest overall agreement between

the predicted and published figures, it had the highest individual zone differences of the three.

Table 7-4 Map estimate and accuracy assessment for countries in the offset point model

Area	*Gradient*	*Map Estimate*	*Published Figure*	*% Difference*
Portugal	0.0565	63,784.0	61,085.6	+4.4 (19.9)
Lisbon	*0.0978*	*26,694.9*	*29,393.5*	*- 9.2*
Italy	0.1097	923,095.0	925,360.6	-0.3 (28.4)
Milan	*0.2447*	*106,896.2*	*104,630.6*	*+2.2*
Spain (NUTS-3)	0.0539	309,842.9	319,919.3	-3.2 (18.5)
Barcelona (46%)	*0.0962*	*74,395.4*	*71,203.3*	*4.5*
Madrid (54%)	*0.0760*	*90,927.7*	*84,043.4*	*8.2*
Ireland (NUTS-3)	0.167	43,917.3	43,077.4	1.9 (14.8)
Dublin	*0.2573*	*26,680.5*	*27,530.4*	*-3.1*
England	0.1652	830,060.4	795,909.3	+4.3 (26.8)
Greater London	*0.2883*	*169,891.6*	*204,042.7*	*-20.1*
Scotland	0.1652	144496.11	98071.1	47.3
Wales	1.1652	48060.47	46841.5	2.6

Even if a single model including the main outlying point (Milan) is used, the total estimated value is to within 1% of what it should be. Treating Milan separately yields even better results as the individual NUTS-3 regions are more accurately estimated and their total is only a quarter of a percentage point less than the Eurostat figure. The Italian case provides the clearest example of how agreement with the national total can be achieved within a single model but relies on overestimation and underestimation of component regions to cancel each other out. It is the nature of using an inexact regression as has been observed with the results for estimating population in chapter 5. This process operates for all the countries throughout the tables of results in this section, which explains why the total percentage error is always substantially lower than the percentage mean absolute difference of component NUTS-3 regions quoted in brackets. There is considerable variation in the Radiance/GDP quotients of Italy's NUTS-3 points. They have standard deviation twice as that of Portugal's NUTS-3 regions and more than double the range.

Spain (Figure 6-11) was the only European country to have two offset points (Barcelona and Madrid). There is a large difference in the derived relationship at

different spatial scales but the all-points relationship with components of the outlying NUTS-1/2 regions removed ($y = 0.0531x$) compares well to the main NUTS-3 relationship ($y = 0.0539x$). Applying the different NUTS-1/2 relationships underestimates the country total by 23% and 8% respectively, whilst the blanket application of the NUTS-3 relationship overestimates the total by 7%. These differences arise from the effect of aggregating outlying points described in section 6.3.3.2. At the NUTS-3 level, Barcelona exerts such a major influence on the derived gradient that most areas are overestimated. As this point is aggregated with others, its effect is less severe. At the NUTS-1 level, Barcelona's aggregation with many surrounding areas of below average economic activity means that its NUTS-1 point in the graph (Figure 6-11) is causing the derived gradient to underestimate economic activity. These effects become more acute due to the ever-decreasing number of points with which to derive a relationship (41 at NUTS-3 compared with 6 at NUTS-1).

As discussed in chapter 6, Ireland (Figure 6-12) posed somewhat of a dilemma with regard to which category it should belong. The low number of points for Ireland hampered a definitive assessment although there are facets of the relationship, which suggest it could belong to the offset point model. One interesting feature of the relationship was that the origin-constrained regression did not appear to fit the points at all well. An unconstrained model is observed to pass through virtually all the points, but it yields an intercept value of around –5000 (Million Euros), which when used to produce a map would lead to all but the most radiant cells returning negative GRP values. In this case the constrained linear model does not appear able to describe accurately GRP from radiance at a finer scale and the unconstrained model cannot be used to disaggregate GRP due to the generation of negative values below a certain threshold. Despite the perceived difficulty in assigning Ireland to a relationship class, the results are no worse than for other countries. In fact, the individual differences at the finest spatial scale (NUTS-2) are the lowest of any country in this section. The problem of classification is likely to occur for a subset of the same number of points (7 used for the relationship) from another country.

There are similarities between the US result in the last section and England here. England is referred to rather than Great Britain as this is the region where the remaining GRP is disaggregated. In this case, London is the sole outlier to mitigate the overestimation of the rest of England by 4%. Consequently the Greater London region is underestimated by 20%. Portugal on the other hand is also estimated to a similar degree, but the effect of accommodating the shortfall in the Lisbon area is not as severe as for England or the US because Lisbon accounts for over 30% of the total GDP for Portugal, where as the figure is 20% for both the English and American outliers. Although the overestimation for Ireland is less than half the percentage value of these countries, the fact that Dublin accounts for nearly 40% of Irish economic production means that the difference between the estimated and published total for Dublin is only $1/7^{th}$ of that for American outliers. Section 7.4.3 discusses some of the implications associated with this method.

7.3.3.3 Two relationships in one country

The two-relationships model identifies the presence of two distinct relationships, which can be spatially defined. Whilst it may be argued that Spain contains two relationships, the fact that Barcelona and Madrid are non-contiguous areas prevents it from inclusion in this section.

Table 7-5 Map estimate and accuracy assessment for countries in the two-relationship model

Area	*Gradient*	*Map Estimate*	*Eurostat Figure*	*% Difference*
Belgium (one model – all points)	0.085	187,658.5	175,550.3	6.9 (29.4)
Belgium (two models)		179,851.8	175,550.3	2.5
Vlaams Gewest	*0.0993*	*125,234.6*	*123,772.8*	*1.2 (30.3)*
Wallonia	*0.0577*	*54,617.3*	*51,777.5*	*5.5 (56.1)*
Brussels	*0.3785*	*36,552.9*	*40,854.4*	*-10.5*
West Germany	0.2103	1,600,794.1	1,651475.8	-3.1 (26.8)
East Germany	0.0923	205,139.1	212016.8	-3.2 (6.6)
Germany		1,805,933.2	1,863,492.6	-3.1 (23.2)

Belgium (Figure 6-16) exhibits a range of features, which could give it membership to other archetypes. Brussels, the capital, is an extreme outlier and was dealt with separately from the two identified relationships. There are three NUTS-1 areas in Belgium, of which Brussels is one. Analysing the other two regions by themselves revealed two different relationships at work. The economic dominance of the Vlaams Gewest region exerts a bias on the derived relationship of the single relationship model shown in the first line of Table 7-5. This causes the errors for individual NUTS-2 regions to be high. Applying two separate relationships is much more accurate than the result of the single model approach. There is however a considerable difference in the overall accuracy between the two regions. The more productive Flemish speaking Vlaams Gewest region has a much lower average percentage difference for its component NUTS-3 areas than for French speaking Wallonia. The high levels of error at NUTS-3 were reduced by half when the disparity of NUTS-2 regions were analysed. Both regions are overestimated, which results in the estimated GRP for Brussels being relatively low.

The relationships for Germany (Figure 6-15) had many similarities with those of Belgium. Germany's capital is also an extreme outlier with respect to the regions of the former East Germany. Due to its historical support by West Germany, its position in the scatterplot fell in line with the distribution of West German regions and was therefore evaluated as part of that relationship. Like Belgium, there is a considerable difference between the accuracy of the two regions. East Germany (minus Berlin) has the lowest mean regional differences of any of the countries tested, whereas West German NUTS-2 points have nearly four times the mean absolute percentage difference. However, both areas are aggregated to the same level of accuracy (3%). There is a considerable difference in the magnitude of these two regional relationships with West Germany having a GRP more than twice that of East Germany per unit radiance.

7.3.3.4 Single relationship model

The two remaining countries were each modelled using one relationship for all parts of the country. The result for Greece underestimated total GDP by a comparatively large margin (6.5%) and it had the highest mean percentage difference amongst its NUTS-3 areas. A reason for this is that although there exists a single relationship, there is considerable noise around this trendline at low radiance levels where the bulk of the points are. The R^2 value drops to 0.72 for those NUTS-3 points excluding the main economic centers of Athens and Thessaloniki but the relationship for these points (0.1) is virtually identical to that for all the points (0.1011). Greece has the smallest NUTS-3 regions of any country examined and also the lowest mean GRP at just over 2 billion Euros. Furthermore many of these are small islands, which can be sensitive to errors of omission due to the coastal location of many lights outlined in section 7.2.4. These errors have been noted for at least two islands (Lefkada and Crete).

Table 7-6 Map estimate and accuracy assessment for countries in the single relationship model

Area	*Gradient*	*Map Estimate*	*Eurostat Figure*	*% Difference*
Greece	0.1011	100,132.9	107,102.4	-6.51 (36.4)
Netherlands	0.1447	337,999.0	332,653.9	1.61 (22.5)
Perfect Netherlands	0.1429	332,653.9	332,653.9	---- (22.3)

A refinement of the single relationship model is to simply use a GDP/radiance quotient for the whole country. The relationship model derived from all points includes aggregated points that have been subjected to some modifiable areal unit effect. Since the mapping is set at a fixed resolution and therefore fixed radiance range, it may be just as well to ensure that the country total is reached exactly by using a simple radiance ratio. The so-called 'perfect gradient' was tested for the Netherlands. Its gradient was very close to that one derived across the three levels of NUTS regions in Figure 6-18 and the results show a negligible improvement in the

accuracy of component regions. The analysis presented in chapter 6 is still relevant because this method should only be applied if there are no outlying points.

7.4 Analysis

This section presents a discussion of the various methods that can be used to analyse the results of section 7.3.3.

7.4.1 Density Mapping

The results from those countries where a density model (described in section 6.4.2, Figure 6-23) was also evaluated did not offer any improvement. The two main reasons why this method was unsuitable concern the strength and nature of the relationship. A summary of the results is presented in Table 7-7. Different relationships were applied as dictated by the best fit to the points.

Table 7-7 Results from density mapping experiment for countries with outliers.

Country	*Type of relationship*	*Map Estimate*	*Eurostat*	*% Difference*
France	2nd order polynomial in log-log space	1,623,397.6	1,222,206.2	32.8 (47.4)
Paris		*87,112.6*	*126,239.1*	*-31*
Hauts-de-Seine		*55,505.1*	*68,266.4*	*-18.7*
Denmark	Log-log	187,359.4	149,169.0	25.6 (48)
Kobenhavn og Frederiksberg Kommuner		*21,474.6*	*26,755.6*	*-19.7*
Kobenhavns Amt		*28,822.6*	*21,633.2*	*33.2*
England	2nd order polynomial	2,486,860.0	999,952.0	148.7 (281.8)
Greater London		*429,175.5*	*204,042.7*	*110.3*

For the two countries with the major outliers, the aggregated total was overestimated by density mapping techniques by 25-30% whilst their outliers were consistently underestimated by 20-30%. The experience for Denmark revealed that whilst outliers were more accurately modelled than using the linear model, other NUTS

areas sometimes had wildly inaccurate estimates with mean errors of 47% and 42% for French NUTS-3 and Danish NUTS-1 regions respectively.

The large spread in values at the lower levels of the plot means that, whilst previously outlying points may be accommodated in a single model, the other regions are far more susceptible to gross errors of estimation. The crux of the problem is that there is simply not the same strength of the relationship in the value range where the majority of the input values lie. Figure 7-9 shows the difference between the general plot and the area of the graph where most of the points are. Higher-level NUTS regions (green and red points) are virtually randomly distributed. The relationship appears to be deceptively strong because the outlying points extrapolate the relationship into something that looks acceptable. In reality, the range of values that forms the input from the resampled radiances falls into the cloud of points where there is no effective relationship. The relationship gets less accurate at lower values of radiance/lit-area. The important thing to note is that the 5km ***radiance-grid*** is supplying most of its input values in this range of lower radiance/lit-area values shown in Figure 7-9.

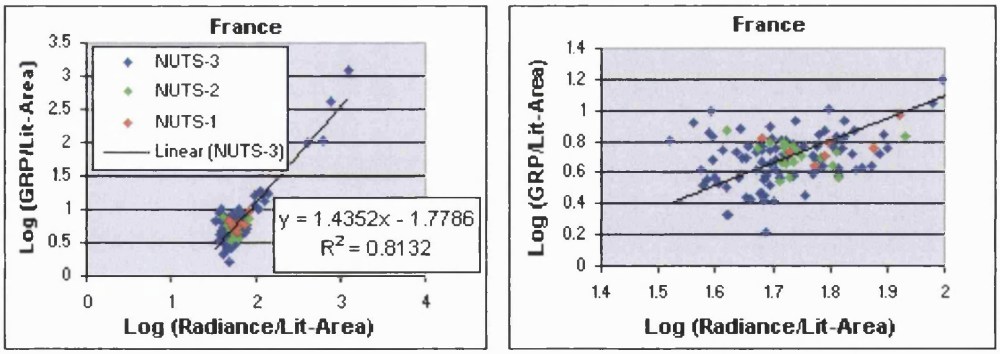

Figure 7-9 Comparison between overall density relationship (left) and zoomed-in portion (right) where most of the points lie.

It is clearly desirable to be able to account for all areas with one model but the high level of variability at low radiance levels means that a model which accounts for most of the points with a linear relationship and treats outliers as special cases is easily the most accurate method tested. This does not necessarily discount the

applicability of other methods. More sophisticated models that analyse the clusters might help account for currently outlying areas under one model. These developments are further discussed under further work in the concluding chapter (chapter 8).

7.4.2 Simulated regions as an analysis tool

A key problem with the map results is that there is no independent way of checking whether the disaggregation is correct. The relationships presented in the previous chapter were constructed from the finest scale data available. Analysing MAUP effects has been shown to offer insights into the nature of relationships. Whilst it may not be possible to assess the sub-NUTS-3 accuracy of the map, it is still worthwhile to examine how robust the map result is to aggregation. Simulated regions have been shown to provide an alternative means of aggregating lower levels of data to compare against conventional NUTS classifications (see the analysis for the US in section 6.1 of this thesis). It was therefore proposed to use simulated regions based on ranked GRP and alphabetical divisions as a cross-check against the conventional NUTS-1 regions. This analysis has been performed for four countries: France, Spain, Italy and Greece. These countries were selected based on their range of errors presented in section 7.3.3 and their capacity to be aggregated into different units (i.e. a sufficient number of zones and sub-zones to work with).

Table 7-8 shows the results of these aggregation tests. The figure in brackets next to the name of each country refers to the NUTS-3 mean accuracy presented in respective results table in section 7.3.3. The two simulated regions were determined by dividing the component NUTS-3 areas into groups with an equal number of members in each. These are given in the '# Group' and '# Members' columns. The next column shows the percentage mean absolute difference for the conventional NUTS-1 units of each country. The column tilted 'Ranked GRP/Estimates' refers to the aggregations of NUTS-3 areas ranked firstly by their GRP and then by ranking on the estimated values rather than the published values. The result for aggregation

by alphabetical division is presented in the last column. A full list of these groups and can be found in Appendix E.

Table 7-8 Mean percentage difference for different aggregation strategies of NUTS-3 regions

Country	*# Group*	*# Members*	*NUTS-1*	*Ranked GRP/Estimates*		*Alphabet*
France (32)	8	12	17.1	14.9	5.4	8.7
Italy (28.4)	10	10	13.4	19	13.4	10.9
Spain (18.5)	8	6	11	6.9	7.5	4.8
Greece (36.4)	10	5	23	20.8	31.4	14.8

The results show that mean accuracy is improved from the NUTS-3 level for each country regardless of aggregation strategy but that different aggregation methods do have an effect on accuracy assessments. Generally, the greatest discrepancy is to be found in the conventional NUTS-1 units, followed by the ranked aggregations and then alphabetical (random) aggregations. Italy is the exception, where NUTS-1 regions are more accurate than the ranked aggregation. However, there are large disparities between the regions. Half of Italy's 10 NUTS-1 regions are estimated to within 5% of the published figure and three of these are less than 1.5% out. Comparing aggregations based on ranking the estimated figure tends to be more accurate than comparisons made on the published figure. Of those countries tested, none of them had identical published and estimated NUTS-3 rankings.

7.4.3 General comments

In order to understand how these results may be translated to global scale mapping of socio-economic parameters one first needs to understand the finer scale effects before going on to make judgments at the larger spatial scales. As such, the EU and USA were selected due to the availability and quality of data present for these regions. Despite the emphasis of this study being regional scale relationships in the developed world, it is neither implied nor anticipated that this is the full geographical scope of these results.

Although split into four different sections, the difference between the models essentially comes down to whether or not a country had outlying areas or not. The basic model is the same for all countries once the decision has been made as to which areas are to be excluded. Assuming this decision has been made correctly, there is no advantage in the type of model used. The use of a tailored quotient to deal with outliers implies that economic activity is enhanced by the same magnitude throughout the whole outlying region. Figure 7-10 shows a comparison of New York State as part of the single model for the US and then with its special quotient applied. Whilst all areas in the right-hand image have much higher GRP values, the size of the state brings into question whether it is necessarily the case that the upstate towns of Albany, Rochester and Buffalo contribute the same amount of GRP/per unit radiance as Manhattan in the South East. The area in and around New York City now takes the top class of GRP values (shown in red), but in reality, this could is still be an underestimation.

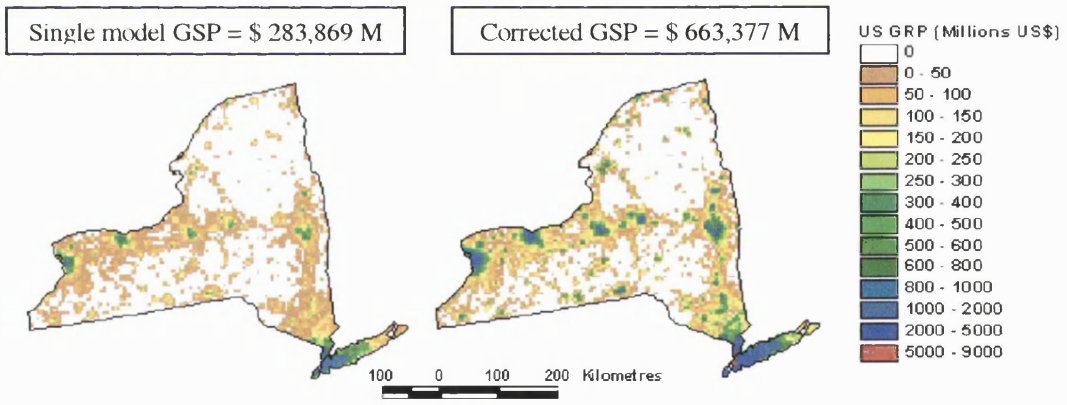

Figure 7-10 Comparison of New York state as part of a single relationship (left) for the US and using a tailored quotient as an outlier (right).

This has been less of a problem for other countries such as France and Denmark because their outlying areas have been far smaller in area (of the order of 100km^2) and more homogeneous. In addition to the physical size of the outlying area having an influence on how homogeneous the area is, and hence how accurate the disaggregation is likely to be within the area, the proportion of the outlier with respect to the total GDP of the country is also important. Comparing the example of

London and Lisbon in, it is apparent that the smaller the proportion of total GDP of the outlier, the larger the error will be between the predicted and published total.

The accuracy of the map is therefore only as good as the spatial units on which it is based. Outliers exist where one sector dominates all others, whether it is in the agricultural or service sectors. The only difference between so-called major outliers and some of the offset point countries is that the spatial units are sufficiently small to concentrate high-level economic activity with radiance. Given the example of New York, it is likely that if GRP data were available for Manhattan County, it too would be a major outlier in the same way that Paris, Copenhagen and Brussels are for their respective countries. However, outliers also exist in the opposite sense. Compare the underestimation of obvious outliers mentioned above with the situation where agricultural states such as Wyoming and the Dakotas are *overestimated* by the main US model by between 77% and 190%. In this case, they are not detected because they are of relatively low economic importance and less conspicuous amongst other points on the graph. Whilst these are extreme examples, the success of this method is partially reliant upon obtaining a sufficient mix of economic sectors within each zone. Overcoming such issues is discussed in section 8.3.1 of the conclusions (chapter 8).

In analysing the results, it is important not to lose sight of what the map is attempting to show. It displays values of aggregate economic activity over a number of cells. There are some issues related with how to 'read' the map, especially outside of urban areas. For instance, the map does not explicitly display the economic activity of a unit of agricultural land. This income is represented as a node rather than dispersed throughout fields. Similarly, the income generated from the fishing industry is concentrated in coastal towns. Recent work published by Sutton and Costanza (2002) has attempted to map these so-called non-market values to provide an ecosystem valuation (also mentioned in section 2.4.3 of this thesis) known as the ecosystem services product (ESP). Concentrating on the land-surface they used the IGBP land-cover map to obtain the distributions of different ecosystems across the Earth's surface. Using unit ecosystem service values developed by Costanza et al.

(1997), the entire land surface can be assessed according to its value to the ecosystem. In this scheme of valuation some of the traditionally 'poor' countries have the highest ESP valuations in the world. The concept of ESP has interesting research potential with respect to its influence on the growth of GDP and conversely what impacts market economic growth can have on a country's ESP. Such issues are central to the debate on sustainability and paths of sustainable development. However, opinion is still divided on the best method to value services which cannot be traded.

7.5 Summary

Night-time lights have been used here to produce the first ever maps of CO_2 emissions and economic activity derived exclusively from satellite imagery. This has been achieved by identifying relationships between lit area and total CO_2 emission, and GDP and using the night-light imagery to distribute these relationships at 1-degree resolution. The estimated GDP map has a closer global to the published figures total than the CO_2 map, though both have underestimated magnitudes. This is believed to be a consequence of disaggregating a relationship established at one spatial scaled in log-log space to a finer resolution. Nonetheless the map agrees very well with the spatial distribution of CO_2 from the map produced by CDIAC.

A more detailed map of economic activity has also been produced for 11 countries in the European Union. Despite identifying a range of different characteristics from individual country correlations, all but one of the 11 countries was estimated to within 5% of the published value for those areas which were valid for the relationship. Errors at the finest scale (NUTS-3) were found to vary considerably between countries and decreased substantially as the scale of analysis increased towards the country level.

The map will over estimate and under estimate certain areas. This is an inevitable consequence of the method. The only way to avoid this is to use individual quotients

for each region, but this rather defeats the object of trying to seek relationships that are valid for a whole country or region. Nonetheless it is encouraging to see that very little adjustment to the value of outlier(s) was required to constrain the map to a country total.

This is a highly encouraging result when considering that the map is based on just one variable and re-affirms night-time light data as a promising tool for mapping socio-economic parameters. In the case of CO_2 emission mapping, night-time lights will be one of many datasets to go into a final model. Economic activity mapping could also benefit from the inclusion of other variables as has been shown with respect to human population mapping from the Landscan project. The importance of other variables such as land-use and transportation networks is likely to become more acute as the spatial resolution of the map increases.

Chapter 8

Conclusions and future work

This final chapter draws out the main findings from each chapter and attempts to bring them together in the context of the research questions and aims of the thesis. Future lines of research are also discussed. As stated in the introduction, this thesis has been guided by a number of research questions, which were formalised into the three aims listed below. The relevant chapter(s) whose conclusions address each aim are listed alongside in bold.

i) To examine the capability of RS data sources to contribute to the expanding toolchest of techniques for settlement mapping. **(Chapter 4)**
ii) To investigate the capability of night-time light imagery to yield information about human activity over and above what is currently available from existing remote sensing resources. **(Chapters 5, 6)**
iii) To frame these results in a format, which can be of use to researchers investigating the human dimensions of global change. **(Chapters 2, 7)**

8.1 Chapter conclusions

The wider issues of this study as regards current global change research activities and remote sensing techniques used to address these issues have been reviewed in Chapters 2 and 3 respectively. The main body of results and analysis is contained in Chapters 4-7. A key point to note from the review of Chapter 2 is the palpable acknowledgement that anthropogenic processes play a vital role in global change and that an understanding of how they fit into the Earth System is a major challenge to the advancement of the research field. To investigate this hypothesis, 23 key

questions have been devised by Schellnhuber and Sahagian, (2002), from which it is clear that some description of socio-economic processes is required. This not only helps to confer legitimacy to the thesis but also identifies an end-user for the knowledge gained from this experience.

8.1.1 Chapter 4: Remote sensing techniques for application to HDGC issues

This chapter investigated three potential sources of remote sensing data for analysis of human environments. Digital road data in the UK and US were used as an indicator of urban concentration to help assess the suitability of a method to detect urban areas. The conclusions are as follows:

i. The road network in the UK was found to correlate with radiance from night-time lights. In general, road density was found to plateau beyond a certain radiance value for both UK (~700 x 10^{-10} $W.cm^2.\mu m^{-1}.sr^{-1}$) and US (900 x$10^{-10}$ $W.cm^2.\mu m^{-1}.sr^{-1}$).

ii. Interferometric land cover mapping has the potential to offer a perspective on the built environment at a higher spatial resolution. However, better results are more likely to be obtained through the use of longer temporal baselines preferably in a different season.

iii. BRDF parameters as produced by the MODIS BRDF-Albedo product were not found to be a reliable means of detecting urban areas. A normalized difference index between the volumetric and geometric kernels was used to assess the relative contribution of each one on a pixel-by-pixel basis. A 'full' inversion of the model was performed where a sufficient number of looks were available over the 16-day collection period. These results did not display a correlation with any land cover types. Results from areas where magnitude inversions had been performed were much better. This was due to the magnitude inversion process being linked to a land-cover map, which pre-

determined the underlying BRDF shape and therefore cannot be considered as an independent means of urban detection.

iv. The lack of a clear result with full inversions was attributed to the poor performance of the atmospheric correction algorithm over bright surfaces in addition to the use of a constrained model unlike that of the control study (d'Entremont *et al.*, 1999).

v. The associated albedo values were also examined as a means of detecting urban areas. Albedo values were found to be more robust to the inversion method used. Although the magnitude inversion still gave higher albedo values, full inversions were also found to give similar albedo values over urban areas.

vi. Albedo values were further analysed in conjunction with the US TIGER road-line dataset and night-time light imagery. Albedo was found to be correlated to both and displayed the same 'plateau' feature for road density vs. albedo as was found for road density vs. night-time light (see (i)).

8.1.2 Chapter 5: Night-time light as a proxy for mapping human population

Night-time light imagery was used in this chapter to map population distribution. Firstly using frequency composite and then radiance calibrated data, this chapter examined different ways in which night-time data could contribute to the remote sensing human of population. The conclusions are as follows:

i. Population was found to correlate with lit-area from frequency composite night-time light data according to an allometric growth model. Urban population was estimated for 44 countries and overall, 90% of the urban population was accounted for. High magnitude errors of different sign cancelled each other out and help to explain the good agreement for the total number of countries.

ii. A similar study carried out at the global scale, published by Sutton *et al.* (2001) confirmed these findings. The two studies found that many of the same countries were difficult to estimate accurately.

iii. Radiance-calibrated night-time light data offered the potential to model intra-urban population density. In the study by Doll and Muller (1999b), it was found to underestimate consistently urban population and overall, it was less accurate over the total number of countries investigated. However, the errors of individual countries occupied a smaller range than for the frequency composite data. It improved the accuracy of estimation for 26 out of 44 countries tested compared to the frequency composite method mentioned in point (i). In this sense, the radiance-calibrated data can be said to provide a more robust method for estimating urban population.

iv. There is no one-to-one correspondence between radiance and residential population density. The brightest areas tend not to coincide with the areas of highest population density as recorded by census data. Further analysis with a gridded population dataset derived from the 1991 UK census reveals that the population morphology of a British city resembles a high-density annulus around a lower density urban core. It is this core where the highest radiance values are to be found.

v. Nonetheless, the fact that population is not static over the diurnal time period means that night-time imagery may be highly useful for modelling ambient daytime population distribution.

8.1.3 Chapter 6: Night-time light imagery and its relationship to non-population parameters

This chapter focused on the sub-national characteristics of the relationship between radiance from night-time light imagery and GDP in the US and EU. The principal conclusions are as follows:

i. Total radiance is directly correlated to GDP at every sub-national scale tested; at the state level for the US; and down to NUTS-3 level in the EU. These correlations were statistically significant at 99.9%.

ii. A systematic set of features was identified within the 12 countries analysed. Most countries had one or two outlying points in the graph of total-radiance against GRP at the finest scale of analysis. This could range from being slightly offset at the end of the distribution to being grossly outlying and positioned well away from the main trend-line. Such points could be masked through aggregation with other points as the analysis became more generalised or the outlier(s) may be carried through the aggregation depending on the comparative economic activity of the zones used in the aggregation.

iii. Aggregation of zones and different zoning strategies has been shown to produce different correlations for the same data. This is a manifestation of the modifiable areal unit problem.

iv. Whilst the nature of the relationship was the same (linear in normal space), its magnitude varied considerably (by up to a factor of 4) between countries. Assuming a conversion rate of unity between the US Dollar and the Euro, the United States produces the least amount of economic output per unit radiance; Germany produces the most. An alternative way to consider this is that the US consumes more energy in the form of light emissions per unit GDP than any other country.

v. Some countries have been shown to have two different relationships operating within them; which could be spatially defined.

vi. Outlying regions were characterised by a higher mean radiance value and a distinctive radiance profile, which was less peaked and therefore more evenly distributed throughout its radiance range.

vii. Normalising both radiance and GRP axes by lit-area resolved outlying points to the detriment of the majority of points, which formed an uncorrelated cloud. This is often masked in the correlation

coefficient, which was biased by two or so former outliers that extended the relationship.

viii. On the basis of these experiments, the results point towards a methodology where outlying points are considered as special cases rather than trying to incorporate them within a single model.

ix. The urban/service-sector land-use class is positively correlated to radiance, other land-use classes are observed to decrease in percentage cover as radiance increases.

8.1.4 Chapter 7: Mapping socio-economic parameters from night-time light correlations

The final results chapter examined how night-time lights can be used to map socio-economic parameters and in particular, map economic activity based on the results from the Chapter 6. The conclusions are as follows:

i. Night-time lights were found to be an accurate means of spatially disaggregating carbon dioxide emissions data. The poor agreement with the CDIAC dataset is believed to be largely due to methodological shortcoming with the model as opposed to a limitation of the remotely sensed data (i.e. the use of a log-log relationship for spatial disaggregation).

ii. Estimating country level GDP in the EU from the relationships derived in Chapter 6 was found to be accurate to within 5% for most countries and within 7% for all.

iii. For a given country-level percentage error, the method used for the treatment of outliers will yield an increasing amount of error between its predicted and observed value(s) as the outlier(s) form(s) a decreasing percentage of total GDP for that country.

iv. The method used to construct the economic activity map from a given relationship has the inevitable consequence of over- and

underestimation. However, alternative aggregations of the finest-scaled zones data did not appear to give substantially different results compared to the administrative NUTS-1 aggregation from the original data.

8.2 Overall conclusions

After initially evaluating night-time lights in comparison to other potentially valuable data sources, this thesis has presented the results of a series of studies designed to investigate the potential of night-time light imagery to provide information on socio-economic data. Starting with a bulk estimate at the country level (Chapter 5) and through a consideration of the finer scale components of the radiance-GDP relationship (Chapter 6) it culminates in the production of a disaggregated map (Chapter 7). The important thing to do is to link these findings together to make some general statements about the title of the thesis:

'Understanding the information content of night-time light satellite data for modelling socio-economic dimensions of global change'

Although other data sources were evaluated, night-time light imagery appears to provide the best means of obtaining data on anthropogenic activity as well as being a highly versatile as a tool with which to analyse other datasets. The information content of night-time imagery for applications to mapping anthropogenic activity is hugely significant and has not been completely explored in this thesis (see section 8.3). The method used in Chapter 6, to combine night-time data with sub-national economic data provided a means of investigating the MAUP and this in itself is one of the most significant elements of Chapter 6. The difference in the relationship between countries is an interesting feature to observe and will be useful when extending the technique to countries where there is no finer scale data available other than the aggregated national value, especially with regard to developing countries.

8.2.1 Original aspects of the thesis

It is believed that there are a number of original aspects associated with the research presented here. The Chapter 6 results, for the first time, relate economic activity (an element of the anthroposphere) to a calibrated physical quantity as measured from an Earth observing satellite. In particular the analysis presented in Chapter 6 is the first systematic analysis of the radiance-GDP relationship at the sub-national level with the identification of variation between relationships and provisional outlier analysis. The analysis of outliers has laid the groundwork for future more pointed studies of certain countries.

The maps produced in Chapter 7 are in themselves a first attempt at using night-time imagery to map globally anthropogenic parameters. Sutton and Costanza (2002) have very recently published a paper briefly outlining a global map of the market economy at 1km resolution. However, this has been based on simple GDP/radiance quotient applied to all countries regardless of the more subtle considerations discussed in Chapter 6 and how these relate to creating a map in Chapter 7.

Economic output is conventionally reported at the national or regional level. The creation of a gridded GDP map allows, for the first time, GDP figures to be aggregated and analysed according to whichever spatial units are most convenient for the user. This opens up the possibility for spatial economic analysis to be carried out in units not previously considered such as by biome, by catchment area, or other ecological unit, which cross administrative boundaries. The question of which river basin has the greatest economic activity is an example of such a query where a GDP map would be useful. Apart from the analytical flexibility of the GDP map, its spatially explicit description of economic activity offers much greater detail than normal chloropleth maps.

It is not just sufficient to understand where people are but also to understand what their potential is to perturb the surrounding environment. A large population with high economic activity surrounded by desert can bring very different problems as

opposed to a large population with low economic activity surrounded by forest. A GDP map could help identify areas of potential stress and/or areas where mitigation potential may be greatest. An extension to this would be an adaptability map as discussed in Chapter 2, where countries are classified according to their ability to absorb and respond to environmental perturbations. A related issue is how one defines high and low economic activity. This could be done in a comparative manner, though the inclusion of economic growth data.

8.3 Avenues for future work

The conclusions highlight the considerable developments that have been made, but also suggest areas which might benefit from further work. In considering this aspect of the thesis it appears that advancements can be made on two fronts. The first consideration is given to the improvement of the existing body of results through alternative or complementary methods. Secondly, recommendations are made regarding future lines of inquiry, which would develop the subject area as a whole. Within this division is the issue of whether developments lie on the conceptual side of what is trying to be achieved or with the technical capabilities of obtaining further information from night-time light imagery. Often these two strands cannot be easily broken apart, as it is the conceptualisation of the problem which drives the technical innovation and therefore future work is presented under different themes.

8.3.1 Improvements to current work

This section considers ways in which the current results may be improved upon. The estimation of socio-economic parameters has relied on just one dependent variable. Three possibilities exist to improve on these results. Firstly, one accepts these results and sets about working out how to identify and quantify the magnitude of outliers. Secondly, consider whether or not there is any extra information which may be sought from night-time light data to further understand what makes a zone anomalously economically active. Finally, one accepts that the results represent the

best that can be achieved with night-time light data and seeks other data sources to make further progress.

8.3.1.1 Detection of outliers

The results presented in Chapter 6 reveal that most countries have at least one economically dominant (outlying) region. Two questions arise in connection with outliers. Firstly, assuming the same kind of relationship applies to other countries how can one automatically detect the features, which identify it as an outlying area? The radiance histogram has been shown to be different for outlying areas than in conventional areas, though metrics from this graph relating to the degree of economic anomaly need to be determined.

8.3.1.2 Alternative techniques

An alternative approach to detecting outliers from the data is to use a previously unmentioned facet of night-time light data. Within each administrative boundary the light is arranged in clusters of bright pixels. Analysis of the size, number and distribution of these clusters within an administrative unit could provide valuable extra information about the economic characteristics of each zone. The results in Chapter 6 and the economic activity maps are based on the hypothesis that radiance is related to GDP by a constant factor irrespective of scale. This hypothesis therefore assumes that two zones of equal total radiance will have the same GDP regardless of how radiance is distributed. Figure 7-10 showed the effect of using a special coefficient for large-area outliers such as New York. Issues such as whether clusters of radiance pixels are more economically productive than individual ones come into play. The decision on how to handle these issues strike at the heart of the conceptual side of the project. One method could involve the use of kernel density estimators for weighting clusters within a zone. This may be the single most useful technique in resolving outliers as it would allow pixels of equal radiance to have different GDP values based on their position within the a cluster. Conclusion (iii) of Chapter 7 (section 8.1.4) also raises the question of whether using the outlier to constrain the

county-level map total is always the best method. If it appears that the method would yield an unacceptably high level of error for the outlier, this could be modified to a pre-determined level of accuracy at the expense of not preserving the country level total.

Taken together, these suggestions will go some to addressing the problems encountered with the map results in Chapter 7. Whilst possibly improving the NUTS-3 accuracy, these measures will not resolve the outstanding problem with validation. There is no guarantee that the disaggregation below NUTS-3 will be correct due to the ecological fallacy of assuming a finer scale relationship from a coarser scale. The lack of independent validation data for the map is a problem, although the consistently strong relationship at higher NUTS levels should engender a high degree of confidence that the disaggregation is accurate.

8.3.1.3 Other data sources

What other variables need to be brought into the analysis? Chapter 6, briefly discussed land-use maps as an extra source of information relating light emission to economic sectors. Figure 6-19 has shown the variation in the GDP/radiance between the agricultural and service sectors subject to the caveat that in terms of agriculture, the map represents economic activity as nodes rather than spread over the farmland. A more sophisticated approach could involve a combination of these factors perhaps where cluster size and underlying land-use combine to determine a conversion factor for that country. This could be undertaken in a manner similar to that of the Landscan project discussed at the end of Chapter 5, where probability surfaces are generated according to light intensity, a cluster attribute, prevailing land-use and so on. Such an approach may facilitate higher resolution mapping, as the economic generality could then be broken apart.

8.3.2 Next steps

This section briefly outlines some of the current innovations within this field of research as well as some ideas on ways to further utilize the results.

8.3.2.1 Temporal development of night-time lights

The biggest question posed by the results presented in this thesis concerns the potential of night-time lights to accurately monitor and detect change. In particular, an assessment of how sensitive lights are to seasonal variation and annual changes would be highly desirable. Results from the MANTLE project (Figure 8-1) over tourist areas in Greece suggest that night-time light imagery from the DMSP-OLS sensor has the capability of providing this information.

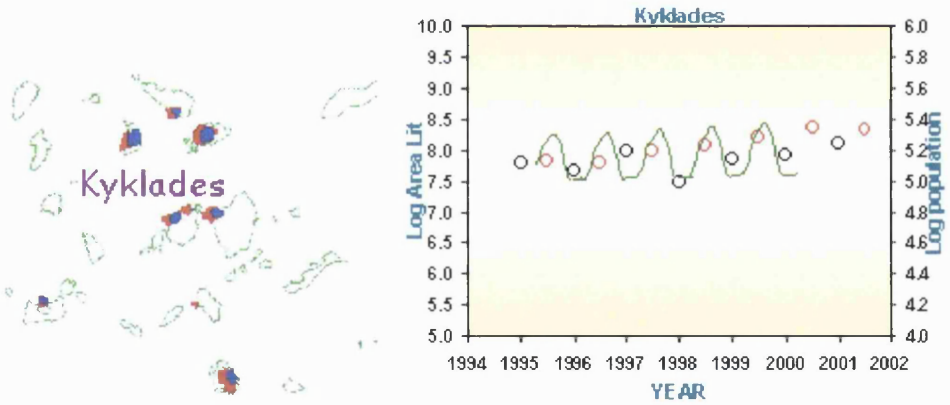

(a) (b)

Figure 8-1 Panel (a) shows the seasonal increase in night-time lights of the Kyklades island group in Greece. Red areas shows DMSP-OLS detected lights in summer 2001 compared to Winter 2001 shown in blue. Panel (b) shows how these increases in light correlates with population (Summer OLS measurement shown as red circles, winter OLS measurement shown as black circles). (Source: MANTLE project website: http://www.mantle-project.com/)

Figure 8-1 shows that light can be observed to change over seasons, so DMSP-OLS data has a temporal resolution of at least 6 months. A change-detection version of DMSP-OLS data between 1992-93 and 2000 has been completed for the USA and East Asia. This involves differencing the average DN values between the two dates to detect areas of expanding light, the occurrence or disappearance of light in an area

or a change in intensification of existing light. However, the absence of low-gain data in the early years of the archive prevented change being detected in certain areas, most notably urban centers (Elvidge, 2002). How sensitive light is to changes in economic activity is still unknown and in particular, what are the leads and lags in the system. Obtaining such answers is paramount in order to work towards a truly comprehensive understanding of what light is showing in relation to economic activity. This is probably the most important next step to take in the field of night-time light research for mapping of socio-economic data.

8.3.2.2 Linking human and physical environments

Ultimately, this thesis is looking toward linking the two strands of economic activity and human impact on the environment. The work presented in this thesis facilitates global monitoring of the human environment from satellite data as well as information on the human dimensions of current global change issues. Progress is needed in both these areas. For instance, considering the assumptions of Environmental Kuznets Curves in Chapter Two, does it necessarily follow that richer countries pollute more? Environmental Kuznets curves suggest this is an oversimplification and that the situation varies depending on the type of pollution under consideration. The globalisation of commerce and industry may also have impacts on using the methods presented in this thesis. Increasing flows of investment between countries raises the question of whether the light detected in one location necessarily contributes fully to the economy of that country. This may not be the case for countries which are in receipt of large amounts of foreign investment. Such considerations pose obstacles to the present technique but also point toward areas of further investigation for more sophisticated models.

From the physical environmental standpoint, questions remained unanswered regarding urban heat islands and the relationship between lighting and thermal emissions from buildings. Potentially useful data could be obtained by simultaneously flying a thermal scanner with a low-light radiometer. These are considerations are more pertinent to high spatial resolution imagery such as the

AVIRIS sensor discussed in Chapter 3. Furthermore, there is also the issue of incorporating light (and associated socio-economic data), land-surface temperature and albedo data to help understand the net radiation of urban areas in relation to anthropogenic activity.

8.4 Closing remarks

The greatest step forward of this project is that satellite data is explicitly being used to address the human dimensions of global change. This comes at a time when it is increasingly being recognised that the human dimensions are currently under-reported in a format that is compatible with other data sources pertaining to the numerous physical elements of global change. In this context, it is believed that this thesis provides a timely contribution to this debate and the results and recommendations offer a great deal of encouragement for further research. Whilst the results presented here are largely concerned with economic activity, the discussion about outliers and how to deal with them is generic to any other parameter correlating with night-time light data.

The unique low-light imaging capability of the OLS sensor is set to continue until at least the end 2010 under DMSP (Elvidge, 2002). A new programme is currently being set up to integrate existing polar-orbiting satellite systems for the US under one programme. NOAA, NASA and the Department of Defense will jointly manage the National Polar Orbiting Environmental Satellite System (NPOESS). Elements from the OLS and AVHRR sensors will be incorporated into the Visible/Infrared Imager/Radiometer Suite (VIIRS) (NOAA, 2002). NPOESS current mandate extends to 2018, so the collection of night-time light data across the Earth's surface is assured for many years to come. The continuing production of this uniquely human source of remote sensing data bodes well for remote sensing to make a significant impact to understanding the human dimensions of global change as it currently does to the understanding the physical components of global change.

Whilst the production of OLS-style data may be assured for the next 15 years, it is also worthwhile to consider whether any other sources of night-time light data may emerge in the coming years. Figure 8-2 shows an image taken with a digital camera by Dan Petit, a crewmember on the International Space Station. The image, whilst un-calibrated for radiance values, has a dramatically increased resolution (estimated to be around 50m) compared to the OLS sensor.

Features such as Hyde Park and Regent's Park are visible as two dark areas to the West of the very bright centre. There is also sufficient resolution in the image to identify the lit sections of major highways (the M25 Orbital motorway is annotated), which was an issue in Chapter Four. The crew of the International Space Station acquired this image shortly after 7:22 p.m. local time on the evening of February 4, 2003 (NASA, 2003).

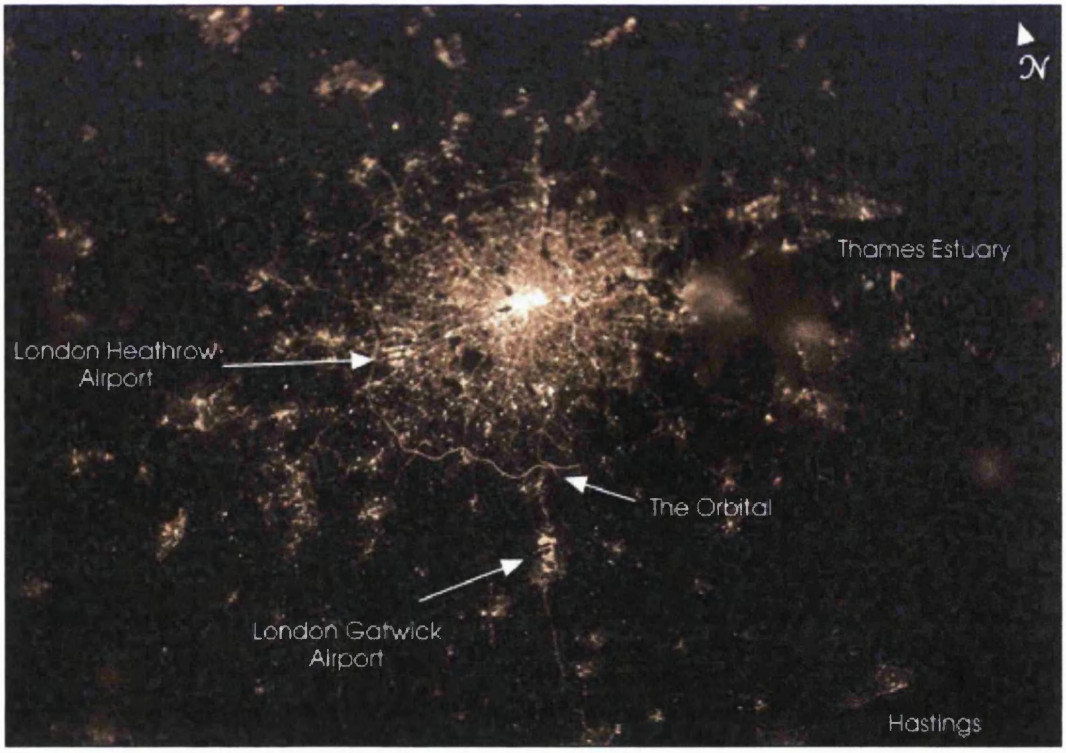

Figure 8-2 London at night as seen from the International Space Station on 4th February 2003 (NASA, 2003).

Currently, the DMSP-OLS sensor dominates night-time light remote sensing. Many researchers around the world have taken this data to exploit its potential for applications to the human environment. Through this effort, night-time light imagery is gaining currency as a valuable component of the remote-sensing toolchest within the wider scientific community. This thesis forms part of this effort and along with glimpses of what new sensors could offer such as that shown in Figure 8-2, night-time light remote sensing is well placed to provide a major contribution to urban and HDGC studies.

References

Allan, J.A., 1997. 'Virtual water': a long term solution for water short Middle Eastern economies? *Paper presented at the 1997 British Association Festival of Science, Water and Development Session.* 9 September 1997. Available from: http://www.kcl.ac.uk/kis/schools/hums/geog/water/occasionalpapers/acrobatfiles/occ03.pdf

Allis, R.G and White, S.P. 2002. Geological storage of CO_2 beneath the Southern Rocky Mountains-Colorado Plateau region. *Eos. Trans. AGU, 83*(47), Fall Meeting . Suppl., Abstract U22A-05. Available from: http://www.agu.org/meetings/fm02/fm02-pdf/fm02_U22A.pdf

Arrow, K., Bolin, B., Costanza, R., Dasgupta, P., Folke, C., Holling, C.S., Jansson, B-O., Levin, S., Mäler, K-G., Perrings, C. and Primentel, D., 1995. Economic growth, carrying capacity and the environment. *Ecological Economics,* **15**, 91-95.

Asrar, G., Fuchs, M., Kanemasu, E.T. and Hatfield, J.L., 1984. Estimating absorbed photosynthetic radiation and leaf-area index from spectral reflectance in wheat. *Agronomy Journal,* **76** (2), 300-306.

Barnsley, M.J., Steel., A.M. and Barr, S.L., 2003. Determining urban land use through an analysis of the spatial composition of buildings identified in LIDAR and multispectral image data. *In*: Mesev, V. (Ed.) *Remotely Sensed Cities.* Taylor & Francis: London, UK, 83-108.

Bartoszczuk, P., Nakamori, Y. and Tieju, M., 2002. Environmental Kuznets Curve for Some Countries- Regression and Agent-based Approach. *In:* Brebbia C.A. and Martin-Duque, J.F. (Eds.), *Air Pollution X. International Conference on Modelling, Monitoring and Management of Air Pollution.,* Segovia, Spain 1-3 July. WITPress: Southampton, UK, 93-102.

Bouchard, R. and Giroux, J., 1997. Test and qualification results on the MOPITT flight calibration sources. *Optical Engineering,* **36** (11), 2992-3000.

Brenkert, A.L., 1998. *Carbon Dioxide Emission Estimates from Fossil-Fuel Burning, Hydraulic Cement Production, and Gas Flaring for 1995 on a One Degree Grid Cell Basis.* ORNL/CDIAC data product NDP-058A. Carbon Dioxide Analysis Center, Oak Ridge, Tennessee, USA. Available from: http://cdiac.esd.ornl.gov/ndps/ndp058a.html

BBC, 2000. *Cities make their own weather.* 22nd February. Available from: http://news.bbc.co.uk/1/hi/sci/tech/specials/washington_2000/652679.stm

BBC, 2003. *Iraq war 'devastating for African growth'.* 29th January. Available from: http://news.bbc.co.uk/1/hi/business/2703249.stm

BEA, 2002. *Bureau of Economic Analysis: Gross State Product data.* Available from: http://www.bea.doc.gov/bea/regional/gsp/

Cao, C. and Lam, N, S-N., 1997. Understanding the Scale and Resolution Effects in Remote Sensing and GIS. *In:* Quattrochi, D.A. and Goodchild, M.F. (Eds.) *Scale in Remote Sensing and GIS.* CRC Lewis: Boca Raton, FL, USA, 57-72.

CDIAC, 2002. *Carbon Dioxide Information and Analysis Center.* Available from: http://cdiac.esd.ornl.gov/home.html

CEOS, 2001. *IGBP Report: 2001.* Available from: http://ceos.esa.int/igosp9/docs/doc20_IGBP.doc

Charney, J., Stone, P.H. and Quirk, W.J., 1975. Drought in the Sahara: A Biogeophysical Feedback Mechanism. *Science*, **187**, 434-435.

CIESIN, 2000. *Gridded Population of the World (GPW).* Available from: http://sedac.ciesin.columbia.edu/plue/gpw/index.html

Cinzano, P., Falchi, F. and Elvidge, C.D., 2001. The first world atlas of the artificial night sky brightness. *Monthly Notices of the Royal Astronomical Society,* **328** (3), 689-707.

Costanza, R., d'Arge, R., de Groot, R., Farber, S., Grasso, M., Hannon, B., Limburg, K., Naeem, S., Oneill, R.V., Paruelo, J., Raskin, R.G., Sutton, P. and van den Belt, M., 1997. The value of the world's ecosystem services and natural capital. *Nature,* **387**, 253-260.

Croft, T.A., 1978, Nighttime images of the Earth from space. *Scientific American,* **239**, 68-79.

Crown, 1999. 1991 Population census surface dataset. Available from: http://census.ac.uk/cdu/software/surpop/

Crutzen, P. J. and Stoermer, E. F., 2000. The "Anthropocene". *IGBP Newsletter,* **41**, 12-13.

d'Entremont, R.P., Schaaf, C.B., Lucht, W. and Strahler, AH., 1999. Retrieval of red spectral albedo and bidirectional reflectance using AVHRR HRPT and GOES satellite observations of the New England region. *Journal of Geophysical Research – Atmospheres,* **104** (D6), 6229-6239.

Dobson, J.E,, Bright, E.A., Coleman, P.R., Durfee, R.C. and Worley, B.A., 2000. LandScan: A global population database for estimating populations at risk. *Photogrammetric Engineering and Remote Sensing.* **66** (7), 849-857.

Dobson, J.E., Bright, E.A., Coleman, P.R. and Bhaduri, B.L., 2003. Landscan. A global population database for estimating populations at risk. *In*: Mesev, V. (Ed.) *Remotely Sensed Cities.* Taylor & Francis: London, UK, 267-280.

Doll, C.N.H., 1998. *Assessing the potential for quantitative estimation of socio-economic parameters from DMSP-OLS imagery.* Dissertation (MSc). University of London.

Doll, C.N.H. and J-P Muller., 1999a. An evaluation of global urban growth via comparison of DCW and DMSP-OLS satellite data. *In: Proceedings of IEEE International Geoscience and Remote Sensing Symposium (IGARSS'99).* Hamburg, Germany 28 June – 2 July. 1134-1136.

Doll, C.N.H. and Muller, J-P., 1999b. The use of radiance calibrated night-time imagery to improve remotely sensed population estimation. *In: Proceedings of the 25th Annual Conference of the Remote Sensing Society.* University of Wales, Cardiff, UK 9 – 11 September. Nottingham, UK: Remote Sensing Society, 127-133.

Doll, C.N.H. and Muller, J-P., 2000. A comparison of different techniques applied to the UK to map socio-economic parameters: implications for modelling the human dimensions of global change. *In: International Archives of Photogrammetry and Remote Sensing,* GITC bv: Amsterdam, The Netherlands, **33** (B4), 222-229.

Doll, C.N.H., Muller, J-P. and Elvidge, C.D., 2000. Night-time imagery as a tool for global mapping of socio-economic parameters and greenhouse gas emissions. *Ambio*, **29** (3), 157-162.

Doll, C.N.H., Muller, J-P., Schaaf, C., Strahler, A.H. and Gao, F., 2001. Mapping Urban Landcover Using the BRDF/Albedo Product from the EOS/MODIS Instrument. *In: Proceedings of IEEE International Geoscience and Remote Sensing Symposium (IGARSS'01),* University of New South Wales, Sydney, Australia July 9 - 13 2001. Available on supplementary CD-ROM of the conference proceedings.

Doll, C.N.H., 2003. Estimating non-population parameters from night-time satellite imagery. *In*: Mesev, V. (Ed.) *Remotely Sensed Cities.* Taylor & Francis: London, UK, 335-354.

Dunderdale, M., Muller, J.-P. and Gapare, N., 1998. Assessment of the IGBP-DIS 1km land cover map using the Vegetation Resources Information System (VegRIS) project of Zimbabwe. *In: Proceedings of the 24th Annual Conference of the Remote Sensing Society.* University of Greenwich, UK 9 – 11 September 1998. Remote Sensing Society: Nottingham UK, 518-526.

EDC, 2003. *Eros Data Center.* United States Geological Survey. Available from: http://edcdaac.usgs.gov

Eidenshink, J.C. and Faundeen, J.L., 1994. The 1km AVHRR global land dataset – 1st stages in implementation. *International Journal of Remote Sensing.* **15** (17), 3443-3462.

Elvidge, C.D., Baugh, K.E., Kihn, E.A., Kroehl, H.W. and Davis, E.R., 1997a. Mapping city lights with nighttime data from the DMSP operational linescan system. *Photogrammetric Engineering and Remote Sensing,* **63** (6), 727-734.

Elvidge, C.D., Baugh, K.E., Hobson, V.R., Kihn, E.A., Kroehl, H.W., Davis, E.R. and Cocero, D., 1997b. Satellite inventory of human settlements using

nocturnal radiation emissions: A contribution for the global toolchest. *Global Change Biology*, **3** (5), 387-395.

Elvidge, C.D., Baugh, K.E., Kihn, E.A., Kroehl, H.W., Davis, E.R. and Davis, C.W., 1997c. Relation between satellite observed visible-near infrared emissions, population, economic activity and electric power consumption. *International Journal of Remote Sensing,* **18** (6), 1373-1379.

Elvidge, C.D., Baugh, K.E., Dietz, J.B., Bland, T., Sutton, P.C. and Kroehl, H.W., 1999. Radiance calibration of DMSP-OLS low-light imaging data of human settlements. *Remote Sensing of Enviroment,* **68** (1), 77-88.

Elvidge, C.D. and Jansen, W.T., 1999. *AVIRIS observations of nocturnal lighting.* AVIRIS Airborne Geosciences Workshop Proceedings, JPL. Available from: http://popo.jpl.nasa.gov/docs/workshops/99_docs/16.pdf

Elvidge, C.D., Imhoff, M.L. and Sutton, P.C., 2000, Relation between fossil fuel trace gas emissions and satellite observations of nocturnal lighting. *International Archives of Photogrammetry and Remote Sensing,* GITC bv: Amsterdam, The Netherlands, **33** (B7), 397-401.

Elvidge, C.D., Imhoff., M.L., Baugh, K.E., Hobson, V-R., Nelson., I., Safran, J., Dietz, J.B. and Tuttle., B.T., 2001a. Night-time lights of the world: 1994-1995. *ISPRS Journal of Photogrammetry & Remote Sensing,* **56**, 81-99.

Elvidge, C.D., Hobson, V.R., Baugh, K.E., Dietz, J.B., Shimabukuro, Y.E., Krug, T., Novo, E.M.L.M. and Echavarria, F.R., 2001b. DMSP-OLS estimation of tropical forest area impacted by surface fires in Roraima, Brazil: 1995 versus 1998. *International Journal of Remote Sensing,* **22** (14), 2661-2673.

Elvidge, C.D., 2002. Global observations of urban areas based on nocturnal lighting. *LUCC Newsletter,* **8**, 10-12.

EIA, 2003. *Energy Information Administration: Multi-state data.* Available from: http://www.eia.doe.gov/emeu/states/multi_states.html

Eurostat, 2002a, *Main characteristics of the NUTS.* Available from: http://europa.eu.int/comm/eurostat/ramon/nuts/mainchar_regions_en.html

Eurostat, 2002b. *Basic principles of the NUTS.* Available from: http://europa.eu.int/comm/eurostat/ramon/nuts/basicnuts_regions_en.html

Eurostat, 2002c. *Application of the NUTS.* Available from: http://europa.eu.int/comm/eurostat/ramon/nuts/application_regions_en.html

Eurostat, 2002d. *CODED: Eurostat Concepts and Definitions Database.* Available from: http://forum.europa.eu.int/irc/dsis/coded/info/data/coded/en/gl000060.htm

Ferretti, A., Prati, C. and Rocca, F. 2001. Permanent scatterers in SAR interferometry. *IEEE Transactions on Geoscience and Remote Sensing,* **39** (1), 8-20.

Fischer, G., Shah, M., van Velthuizen, H. and Nachtergaele, F.O., 2001. *Global agro-ecological assessment for agriculture in the 21st Century.* Joint report by International Institute for Applied Systems Analysis and the Food and Agriculture Organisation. Vienna, Austria: Remaprint. Available from: http://www.iiasa.ac.at/Research/LUC/Papers/gaea.pdf

Flowerdew, R. and Green, M., 1989. Statistical methods for inference between incompatible zonal systems. *In*: Goodchild, M.F. and Gopal, S. (Eds.), *Accuracy of Spatial Databases.* Taylor and Francis: London, UK, 239-247.

Freund, P., 1997. International collaboration on capture, storage and utilisation of greenhouse gases. *Waste Management,* **17** (5-6), 281-287.

Fuller, R.M., Groom, G.B. and Jones, A.R. 1994. The land-cover map of Great-Britain – An automated classification of Landsat Thematic Mapper data. *Photogrammetric Engineering and Remote Sensing,* **60** (5), 553-562.

Fuller, R.M., 1995. *The Land cover Map of Great Britain – A Description, Annex A.* Monks Wood, Cambridgeshire, UK: Institute of Terrestrial Ecology.

GCC, 2001. *Global Climate Coalition.* Available from: http://www.globalclimate.org/

Gens, R. and van Genderen, J.L., 1996. SAR interferometry - Issues, techniques, applications. *International Journal of Remote Sensing,* **17** (10), 1803-1835.

Gibson, C.C., Ostrom, E. and Ahn, T.K., 2000. The concept of scale and the human dimensions of global change: a survey. *Ecological Economics,* **32** (2), 217-239.

GMES, 2001. A European Approach to Global Monitoring for Environment and Security (GMES): Towards Meeting Users' Needs. *Joint document from Commission services and the European Space Agency* European Commission Staff Working Paper SEC(2001) 993. Available from: http://gmes.jrc.it/download/SEC_2001_993_EN1.pdf

Grey, W.M.F. and Luckman, A.J., 1999. Using SAR interferometric phase coherence to detect urban change. *In: Proceedings of the 25th Annual Conference of the Remote Sensing Society.* University of Wales, Cardiff, UK 9 – 11 September 1999. Remote Sensing Society: Nottingham, UK, 457-464.

Grigg, D, 1999. The changing geography of world food consumption in the second half of the twentieth century. *The Geographical Journal,* **165** (1), 1-12.

Grubb, M., Vrolijk, C. and Brack. D., 1999. *The Kyoto protocol - A guide and assessment.* Royal Institute of International Affairs & Earthscan: London, UK.

Haack, B.N. and Slonecker, E.T., 1984. Merged spaceborne radar & TM digital data for locating villages in Sudan. *Photogrammetric Engineering and Remote Sensing,* **60** (10), 1253-1257.

Hanssen, R.F., 2001. *Radar Interferometry, Data interpretation and error analysis.* Thesis (PhD). Technical University of Delft, The Netherlands.

HDF-EOS, 2002. *HDF-EOS tools and information center.* NASA. Available from: http://hdfeos.gsfc.nasa.gov/hdfeos/index.cfm

Harris, R., 1985. SIR-A imagery of Tunisia and its potential for population estimation. *International Journal of Remote Sensing,* **6** (7), 975-978.

Henderson, F.M. and Anuta, M.A., 1980. Effects of radar system parameters, population and environmental modulation on settlement visibility. *International Journal of Remote Sensing,* **1** (2), 137-151.

Henderson, F.M. and Xia, Z.G., 1997. SAR applications in human settlement detection, population estimation and urban land use pattern analysis: A status report. *IEEE Transactions on Geoscience and Remote Sensing,* **35** (1), 79-85.

Houghton, J.T., 1997. *Climate Change: The complete briefing.* 2nd edition. Cambridge University Press: Cambridge, UK.

IHDP, 2001. *International Human Dimensions Programme on Global Environmental Change Annual Report 2000.* IHDP: Bonn, Germany.

IHDP-LUCC, 1997. *LUCC Data Requirements Workshop. Survey of needs, gaps and priorities on data for land-use/land-cover change research.* Organised by IGBP/IHDP-LUCC and IGBP-DIS, Barcelona, 11-14 November 1997. Available from: http://www.geo.ucl.ac.be/LUCC/publications/reportseries/series3/contents.html

Iisaka, J. and Hegedus, E., 1982. Population estimation from Landsat imagery. *Remote Sensing Environment,* **12**, 259-272.

Imhoff, M.L., Lawrence, W.T., Stutzer, D.C. and Elvidge, C.D. 1997. A Technique for using composite DMSP-OLS "City Lights" satellite data to map urban area. *Remote Sensing of Enviroment,* **61**, 361-370.

Imhoff, M.L., Tucker, C.J., Lawrence, W.T. and Stutzer, D.C. 2000. The use of multisource satellite and geospatial data to study the effect of urbanization on primary productivity in the United States. *IEEE Transactions on Geoscience and Remote Sensing,* **38** (6), 2549-2556.

IPCC, 2000. *Emissions Scenarios 2000; Special Report of the Intergovernmental Panel on Climate Change.* Cambridge University Press: Cambridge, UK.

IPCC, 2001a. *Climate change 2001: Impacts, Adaptation and Vulnerability - Contribution of Working Group II to the Third Assessment Report of the Intergovernmental Panel on Climate Change (IPCC).* Cambridge University Press: Cambridge, UK.

IPCC, 2001b. *Climate change 2001: Synthesis Report, Summary for Policy Makers.* Geneva, Switzerland: IPCC. Available from: http://www.ipcc.ch/pub/SYRspm.pdf

IPCC, 2001c. *Climate change 2001: Mitigation - Contribution of Working Group III to the Third Assessment Report of the Intergovernmental Panel on Climate Change (IPCC).* Cambridge University Press: Cambridge, UK.

Justice, C.O., Vermote, E., Townshend, J.R.G., Defries, R., Roy, D.P., Hall, D.K., Salomonson, V.V., Privette, J.L., Riggs, G., Strahler, A., Lucht, W., Myneni, R.B., Knyazikhin, Y., Running, S.W., Nemani, R.R., Wan, Z.M., Huete, A.R., van Leeuwen, W., Wolfe, R.E., Giglio, L., Muller, J-P., Lewis P. and Barnsley, M.J. 1998. The Moderate Resolution Imaging Spectroradiometer (MODIS): Land remote sensing for global change research. *IEEE Transactions on Geoscience and Remote Sensing,* **36** (4), 1228-1249.

Kates, R.C., Clark, W.C., Corell, R., Hall, J.M., Jaeger, C.C., Lowe, I., McCarthy, J.J., Schellnhuber, H.J., Bolin, B., Dickson, N.M., Faucheux, S., Gallopin, G.C., Grübler, A., Huntley, B., Jäger, J., Jodha, N.S., Kasperson, R.E., Mabogunje, A., Matson, P., Mooney, H., Moore, B., O'Riordan, T. and Svedlin, U., 2001. Environment and Development: Sustainability Science. *Science,* **292**, 641-642.

Kaufman, Y. J., Herring, D. D., Ranson, K. J. and Collatz, G. J., 1998a. Earth Observing System AM1 Mission to Earth. *IEEE Transactions on Geoscience and Remote Sensing,* **36** (4), 1045-1055.

Kaufman, Y.J., Justice, C.O., Flynn L.P., Kendall, J.D., Prins, E.M., Giglio, L., Ward, D.E., Menzel, W.P. and Setzer, A.W., 1998b, Potential global fire monitoring from EOS-MODIS. *Journal of Geophysical Research-Atmospheres,* **103** (D24), 32215-32238.

Konami, K., Shibasaki, R. and Tan, G., 1998. Using nighttime DMSP/OLS images of Citylights to Estimate District-level Population Distribution in

Developing Countries. *In: Proceedings of the 19th Asian Conference on Remote Sensing,* 16-20 November, Manila, The Philippines. Available from: http://www.gisdevelopment.net/aars/acrs/1998/ps2/ps2021.shtml

Kramer, H. J. 1994. *Observation of the Earth and its Environment - Survey of Missions and Sensors,* 2nd Edition, Springer-Verlag: Berlin & New York.

Langford, M., 2003. Refining methods for dasymetric mapping using satellite remote sensing. *In:* Mesev, V. (Ed.) *Remotely Sensed Cities.* Taylor & Francis: London, UK, 137-156.

Levi, P., 1990. *In:* Levi, P. *The sixth day and other tales* translated by Raymond Rosenthal. Michael Joseph: London. 155-162.

Lewis, A.J., Henderson, F.M and Holcomb, D.W., 1998. Radar Fundamentals: The Geoscience Perspective. Chapter 3: *In:* Henderson, F.M. and Lewis, A.J. (Eds.) *Principles and Applications of Imaging radar.* John Wiley & Sons: New York, USA, 131-182.

Lewis, P., 1995. The utility of kernel-driven BRDF models in Global BRDF and albedo studies. *In: Proceedings of IEEE International Geoscience and Remote Sensing Symposium (IGARSS'95).* Firenze, Italy, 10-14 July 1995, 1186-1188.

Li, Y-F., 1996. *Global population distribution (1990), Terrestrial area and country name information on a one by one degree grid cell basis.* ORNL/CDIAC Data product DB1016, Carbon Dioxide Analysis Center, Oak Ridge, Tennessee, USA. Available from: http://cdiac.esd.ornl.gov/ndps/db1016.html

Li, Y-F., McMillan, A. and Scholtz, M.T., 1996. Global HCH with 1° x 1° longitude/latitude resolution. *Environmental Science and Technology*, **30**, 3525-3533.

Liang, S., A. H. Strahler, A.H. and Walthall, C.W., 1999. Retrieval of land surface albedo from satellite observations: A simulation study. *Journal of Applied Meteorology,* **38**, 712–725.

Lillesand, T.M. and Kiefer, R.W., 1993. *Remote Sensing and Image Interpretation.* Third Edition. John Wiley & Sons: New York, NY, USA.

Lo, C.P. and Welch, R., 1977. Chinese urban population estimates. *Annals of the Association of American Geographers,* **67**, 246-253.

Lo, C.P., 1986a. Settlement, Population & Land Use Analysis of N.China Plain using SIR. *Professional Geographer,* **38** (2), 141-149.

Lo, C.P., 1986b. The human population. *In: Applied remote sensing.* Longman: London, UK, 40-78.

Lo, C.P., 2001. Modeling the population of China using DMSP Operational Linescan nighttime data. *Photogrammetric Engineering and Remote Sensing,* **67** (9), 1037-1047.

Lomborg, B. 2001. *The skeptical environmentalist. Measuring the real state of the world.* Cambridge University Press: Cambridge, UK.

Loveland, T.R., Merchant, J.W., Ohlen, D.O. and Brown, J.F., 1991. Development of a land-cover characteristics database for the conterminous United States. *Photogrammetric Engineering and Remote Sensing,* **57** (11), 1453-1463.

Lovelock, J., 2000. *Gaia: A new look at life on Earth,* Oxford University Press: Oxford, 148p.

Lowe, J.J. and Walker, M.J.C., 1997. *Reconstructing quaternary environments.* Longman: London, UK. pp. 12-16.

Lucht, W., Schaaf, C.B. and Strahler, A.H., 2000. An algorithm for the retrieval of albedo from space using semiempirical BRDF models. *IEEE Transactions on Geoscience and Remote Sensing,* **38** (2), 977-998.

Lucht, W. and Lewis, P., 2000. Theoretical noise sensitivity of BRDF and albedo retrieval from the EOS-MODIS and MISR sensors with respect to angular sampling. *International Journal of Remote Sensing,* **21** (1), 81-98.

Lucht, W. and Jaeger, C.J., 2001. The sustainability Geoscope: A proposal for a global observation instrument for the anthropocene. *In:* Heinen, D., Hoch, S., Krafft, T., Moss, Scheidt, P. and Welshhoff (Eds.). *Contributions to global change research.* German National Committee on Global Change Research: Bonn, Germany. 134-140.

Madsen, S.N. and Zebker, H.A., 1998. Imaging radar interferometry. Chapter 6. *In:* Henderson, F.M. and Lewis, A.J (Eds). *Principles and Applications of Imaging radar.* John Wiley & Sons: New York, USA. 359-380.

MANTLE, 2001. *MANTLE project – Home.* Available from: http://www.mantle-project.com/

Martin, D., 2000. Census 2001: Making the best use of zonal geographies. *Paper presented at The census of population: 2000 and beyond,* University of Manchester 22-23 June. Available from: http://www.ccsr.ac.uk/conference/Martinpap.doc

Masood, E., 1996. Climate report 'subject to scientific cleansing'. *Nature*, **381**, 546.

Masuoka, E., Fleig, A., Wolfe, R.E. and Patt, F., 1998. Key characteristics of MODIS data products. *IEEE Transactions on Geoscience and Remote Sensing,* **36** (4), 1313-1323.

Matthews, E., 1983. Global vegetation and land-use - new high-resolution data-bases for climate studies. *Journal of climate and applied meteorology,* **22** (3), 474-487.

Meister, G. 2000. *Bidirectional reflectance of urban surfaces.* Thesis (PhD). University of Hamburg, Germany.

Milly, P.C.D., Wetherald, R.T., Dunne, K.A. and Delworth, T.L., 2002. Increasing risk of great floods in a changing climate. *Nature,* **415**, 514-517.

MIMAS, 2003. *Manchester Information and Associated Services.* Available from: http://www.mimas.ac.uk

Morley, J.G., Muller, J-P.A.L., Walker, A.H., Kitmitto, K., Mitchell, K.L., Chugani, K., Smith, A., Barnes, J., Cross, P.A. and Dowman, I.J., 2000. LANDMAP: Creating a DEM of the British Isles by SAR Interferometry. *In: International Archives of Photogrammetry and Remote Sensing,* GITC bv: Amsterdam, The Netherlands, **33** (B4), 686-693.

Muller, J-P., 1999. *Final Report on EOS/AM1 DEM data-sets: DEM and DEM auxiliary datasets in support of the EOS/Terra platform by the NASA/EOS DEM Science Working Group.* JPL Technical Publication D-13508, Pasadena, CA, USA.

Muller, J.-P., Morley, J.G., Walker, A., Barnes, J.B., Cross, P.A., Dowman, I.J., Mitchell, K., Smith, A., Chugani, K. and Kitmitto, K., 1999. The LANDMAP project for the creation of multi-sensor geocoded and topographic map products for the British Isles based on ERS-tandem interferometry. *In: Proceedings of the 2nd*

International Workshop on ERS SAR Interferometry, Liege, Belgium 10–12 November 1999. Available from: http://earth.esa.int/pub/ESA_DOC/fringe1999/Papers/muller.pdf

Myneni, R.B., Keeling, C.D., Tucker, C.J., Asrar, G. and Nemani, R.R., 1997. Increased plant growth in the northern high latitudes form 1981 to 1991. *Nature,* **386**, 698-702.

Nakayama, M. and Elvidge, C.D., 1999. Applying Newly Developed Calibrated Radiance DMSP/OLS Data for Estimation of Population. *In: Proceedings of 20th Asian Conference on Remote Sensing,* 22-25th November 1999, Hong Kong. Available from: http://www.gisdevelopment.net/aars/acrs/1999/ts7/ts7091pf.htm

NASA, 1997. *DMSP F8 Source/Platform Document.* Available from: http://eosweb.larc.nasa.gov/GUIDE/source_documents/dmsp_f8.html

NASA, 2002a. *EOS: Earth Observing System.* Available from: http://eos.gsfc.nasa.gov/main.html

NASA, 2002b. *Terra EOS-AM Project Homepage.* Available from: http://eos-am.gsfc.nasa.gov/

NASA, 2002c. *Aqua Homepage.* Available from: http://aqua.gsfc.nasa.gov/

NASA, 2003, *EO Newsroom: New images – London by night.* Available from: http://earthobservatory.nasa.gov/Newsroom/NewImages/images_topic.php3?topic=life&img_id=10929

Nature, 1998. Audacious bid to value the planet whips up a storm. *Nature,* **395**, 430.

Nordbeck, S., 1965. The Law of Allometric Growth. *Michigan Inter-University Community of Mathematical Geographers Discussion Paper 7,* Department of Geography, University of Michigan, Ann Arbor, USA.

NOAA, 2002. *NPOESS Instruments – VIIRS.* Available from: http://www.ipo.noaa.gov/Technology/viirs_summary.html

Openshaw, S., 1984. The modifiable areal unit problem. *Concepts and Techniques in Modern Geography 38,* GeoBooks: Norwich, UK.

ORNL, 2002. *Geographic Information Science & Technology*, Available from: http://www.ornl.gov/gist

Owen, T.W., Gallo, K.P., Elvidge, C.D. and Baugh, K.E., 1998. Using DMSP-OLS light frequency data to categorize urban environments associated with US climate observing stations. *International Journal of Remote Sensing,* **19** (17), 3451-3456.

Papathanassiou, K.P., Reigber, A and Coltelli, M., 1996. On the Interferometric Coherence: A Multifrequency and Multitemporal Analysis. *In: Proceedings of Fringe'96, Workshop on ERS SAR Interferometry.* Zürich, Switzerland, 30 September - 2 October. 1996, ESTEC, Noordwijk, The Netherlands: ESA Publications Division (ESA SP-406) Available from: http://earth.esa.int/workshops/fringe_1996/papathan/

Pearce, F., 2001. We are all guilty! It's official, people are to blame for global for global warming! *New Scientist*, **169** (2275), 5.

Penner, J. (ed.), Lister, D. (ed.), Griggs, D.J. (ed.), Dokken, D. and McFarland, M., 1999. *Aviation and the global atmosphere: Special report of the*

Intergovernmental Panel on Climate Change. Cambridge University Press: Cambridge, UK.

Philip, G., 1998. *Philip's Geographical Digest 1998-99.* Heinemann Educational in assoc. with George Philip: Oxford, UK.

Plutzar, C., Grubler, A., Stojanovic, V., Reidl, L. and Pospishil, W., 2000. A GIS approach for modelling the spatial and temporal development of night-time lights. *In*: Stobl, Blasshke and Griesebner (Eds.) *Angewandte Geographische Inforamtionsverarbeitung XII*, Beitrage zum AGIT-Symposium, Salzburg 2000. Wichman Verlag: Heidelberg, Germany, 389-394.

Porter, M. and Enmark, H.T., 1987, *A system overview of the Airborne Visible/Infrared Imaging Spectrometer (AVIRIS).* JPL Publication 87-38. Available from: http://popo.jpl.nasa.gov/docs/aviris87/A-PORTER.PDF

PRwatch, 2002. *Inpropaganda review: Global Climate Coalition.* Available from: http://www.prwatch.org/improp/gcc.html

Rennie, J., Schneider, S., Holdren, J.P., Bongaarts, J. and Lovelock, T., 2002. Misleading Math about the Earth. *Scientific American*, **January,** 59-70.

Rifkin, J., 2002. Pumping up the pressure. *The Guardian*, 26 April. Available from: http://www.guardian.co.uk/oil/story/0,11319,690851,00.html

Rosen, P.A., Hensley, S., Joughin, I.R., Li, F.K., Madsen, S.N., Rodriguez, E. and Goldstein, R.M., 2000. Synthetic aperture radar interformetry. *Proceedings of the IEEE,* **88** (3), 333-382.

Roujean, J-L., Leroy, M. and Deschamps, P.Y., 1992. A bi-directional reflectance model of the Earth's surface for the correction of remote-sensing data. *Journal of Geophysical Research – Atmospheres,* **97** (D18), 20455-20468.

Sagan, C., Thompson, W.R., Carlson, R., Gurnett, D. and Hord, C., 1993. A Search for life on Earth from the Galileo spacecraft. *Nature,* **365**, 715-721.

Sahagian, D. 1998. Incorporating human dimensions into Earth system models. *Research GAIM,* **2** (1), 8. Available from: http://gaim.unh.edu/Products/News/Summer98/rgsum98.pdf

Saxon, E.C., Parris, T and Elvidge, C.D., 1997. Satellite Surveillance of National CO_2 Emissions from Fossil Fuels. *Development Discussion Paper No. 608.* Harvard Institute for International Development, Harvard University, USA. Available from: http://www.cid.harvard.edu/hiid/608.pdf

Schaaf, C. B., Lucht, W., Tsang, T., Gao, F., Strugnell, N., Chen, L., Liu, Y. and Strahler, A.H., 1999. Prototyping the MODerate Resolution Imaging Spectroradiometer (MODIS) BRDF and Albedo Product. *In: Proceedings of IEEE International Geoscience and Remote Sensing Symposium (IGARSS'99),* Hamburg, Germany, 28 June - 2 July, 1506-1508,

Schaaf, C.B., Gao, F., Strahler, A.H., Lucht, W., Li, X.W., Tsang, T., Strugnell, N.C., Zhang, X.Y., Jin, Y.F., Muller, J.P., Lewis, P., Barnsley, M., Hobson, P., Disney, M., Roberts, G., Dunderdale, M., Doll, C., d'Entremont, R.P., Hu, B.X., Liang, S.L., Privette, J.L. and Roy, D., 2002. First operational BRDF, albedo nadir reflectance products from MODIS. *Remote Sensing of Environment,* **83** (1-2), 135-148.

Schellnhuber, H.J. 1999. 'Earth system' analysis and the second Copernican Revolution. *Nature,* **402 Supplement**, C19-C23.

Schellnhuber, J and Sahagian, D., 2002. Integration: The twenty-three GAIM questions. *IGBP Newsletter,* **49**, 20-21.

Schimel, D.S., House J.I., Hibbard, K.A., Bousquet, P., Ciais, P., Peylin, P., Braswell, B.H., Apps, M.J., Baker, D., Bondeau, A., Canadell, J., Churkina, G., Cramer, W., Denning, A.S., Field, C.B., Friedlingstein, P., Goodale, C., Heimann, M., Houghton, R.A., Melillo, J.M., Moore, B., Murdiyarso, D., Noble, I., Pacala, S.W., Prentice, I.C., Raupach, M.R., Rayner, P.J., Scholes, R.J., Steffen, W.L., Wirth, C., 2001. Recent patterns and mechanisms of carbon exchange by terrestrial ecosystems. *Nature,* **414**, 169-172.

Sellers, P.J., Dickinson, R. E., Randall, D. A., Betts, A. K., Hall, F. G., Berry, J. A., Collatz, G. J., Denning, A. S., Mooney, H. A., Nobre, C. A. Sato, N., Field, C. B. and Henderson-Sellers, A., 1997. Modeling the exchanges of energy, water and carbon between continents and the atmosphere. *Science,* **275**, 502-509.

Sivakumar, M.V.K., 1998. Climate variability and food vulnerability. *IGBP Newsletter,* **35**, 14-17.

Small, C. and Cohen, J.E., 1999. Continental Physiography, Climate and the Global Distribution of Human Population. *In: Proceedings of the International Symposium on Digital Earth,* Beijing, China, 29 November – 2 December 1999, 965-971.

SMC, 1995. *SMC Historical Overview Satellite Systems. Space and Missile System Center.* Available from: http://www.losangeles.af.mil/SMC/HO/Smchov10.htm

Smith, M.W., 1997. Method and results for optimizing the MOPITT methane bandpass. *Applied Optics,* **36** (18), 4285-4291.

Space Imaging, 2002. *Space Imaging – Visual Information.* Visual results. http://www.spaceimaging.com

Stern, D.I., Common, M.S. and Barbier, E.B., 1996. Economic growth and environmental degradation: The environmental Kuznets curve and sustainable development. *World Development,* **24** (7), 1151-1160.

Stewart, J. and Warntz, W., 1958. Physics of Population Distribution. *Journal of Regional Science,* **1**, 99-123.

Strugnell, N.C., 2001. *Retrieval of land surface albedos from satellite measurements.* Thesis (PhD). University of Boston, Massachusetts, USA.

Strugnell, N.C. and Lucht, W., 2001. An algorithm to infer continental-scale albedo from AVHRR data, land cover class and field observations of typical BRDFs. *Journal of Climate,* **14** (7), 1360-1376.

Sullivan, W.T. III., 1989. A 10-km resolution image of the entire night-time Earth based on cloud free satellite photographs in the 400-1100nm band. *International Journal of Remote Sensing,* **10** (1), 1-5.

Sutton, P., Roberts, C., Elvidge, C. and Meij, H., 1997. A comparison of nighttime satellite imagery and population density for the continental united states. *Photogrammetric Engineering and Remote Sensing,* **63** (11), 1303-1313.

Sutton P.C., Roberts D, Elvidge C,D. and Baugh, K., 2001. Census from Heaven: An estimate of the global human population using night-time satellite imagery, *International Journal of Remote Sensing,* **22** (16), 3061-3076.

Sutton, P.C. and Costanza, R., 2002. Global estimates of market and non-market values derived from nighttime satellite imagery, landcover and ecosystem service valuation. *Ecological Economics,* **41**, 509-527.

Sutton, P.C., 2003. Estimation of human population parameters using night-time satellite imagery. *In:* Mesev, V. (Ed.) *Remotely Sensed Cities.* Taylor & Francis: London, UK, 301-334.

Taha, H., 1997. Urban climates and heat islands: Albedo, evapotranspiration and anthropogenic heat. *Energy and Buildings.* **25** (2), 99-103.

Tiger/Line®, *1997. Tiger/Line® Files, 1997 Technical Documentation.*Washington, DC, USA: US Bureau of the Census. Available from: ftp://ftp.mapshots.com/Tiger/Tiger97D.pdf

Tobler, W., 1969. Satellite Confirmation of Settlement Size Coefficients. *Area,* **1**, 30-34.

Tobler, W., 1979. Smooth pychnoplactic interpolation for geographic regions. *Journal of the American Statistical Association,* **74**, 519-530.

Tobler, W., Deichmann, U., Gottsegen, J. and Maloy, K., 1995. *The Global Demography Project.* National Center for Geographic Information and Analysis, Technical Report 95-6. University of California, Santa Barbara, USA.

Tucker, M., 1995. Carbon dioxide emissions and global GDP. *Ecological Economics*, **15**, 215-223.

UN, 2003. *United Nations: Johannesburg Summit 2002.* Available from: http://www.johannesburgsummit.org/

UN, 1995. *UN Statistical Division Demographic Yearbook 1995.* United Nations, (Sales No. E/F.97.XIII.1): New York, USA.

UNDP, 2002. *Human Development Report 2002, Demographic trends.* Available from: http://www.undp.org/hdr2002/indicator/pdf/hdr_2002_table_5.pdf

UNDP/UNEP, 1994. *Report on the International Symposium on Core Data Needs for Environmental Assessment and Sustainable Development Strategies,* Volume I & II. Bangkok, Thailand, 15 - 18 November, 1994. Nairobi, Kenya: UNEP/EAP. (MR/94-10).

UNEP, 2002. *Global Environmental Outlook: Prospectus.* Available from: http://www.unep-wcmc.org/geo/pdfs/prospectus_november.pdf

UNEP, 2003a. *UNEP-GRID GNV158 - Administrative Regions/Boundaries of Europe.* Available from: http://www.grid.unep.ch/data/grid/gnv158.php

UNEP, 2003b. *GRID Geneva Data collections.* Available from: http://www.grid.unep.ch/data/grid/index.php

UNFCCC, 1997. *Kyoto Protocol to the United Nations framework convention on climate change.* Available from: http://unfccc.int/resource/docs/convkp/kpeng.pdf

UN-HABITAT, 2001. *The state of the world's cities report 2001; An urbanized world.* Available from: http://www.unchs.org/Istanbul+5/10-11.pdf

UNSD, 2003. *United Nations Statistical Division: National Accounts.* Available from: http://unstats.un.org/unsd/sna1993/introduction.asp

Vermote, E.F., El-Saleous, N.Z. and Justice, C.O., 2002. Atmospheric correction of MODIS data in the visible to middle infrared: first results. *Remote Sensing Enviroment,* **83**, 79-111.

Vitousek, P.M., Mooney, H.A., Lubchenco, J. and Melillo, J.M., 1997. Human domination of Earth's ecosystems, *Science,* **277**, 494-499.

Walker, P.A. and Mallawaarachchi, T. 1998. Disaggregating agricultural statistics using NOAA-AVHRR NDVI. *Remote Sensing Environment,* **63** (2), 112-125.

Wan, Z., 1999. *MODIS Land-Surface Temperature Algorithm Theoretical Basis Document Version 3.3.* Contract Number: NAS5-31370. Available from: http://modis-land.gsfc.nasa.gov/pdfs/atbd_mod11.pdf

Wanner, W., Li, X. and Strahler, A.H., 1995. On the derivation of kernels for kernel-driven models of bi-directional reflectance. *Journal of Geophysical Research – Atmospheres,* **100** (D10), 21077-21089.

Wanner, W., Strahler, A.H., Hu, B., Lewis, P., Muller, J.P., Li, X., Schaaf, C.L.B. and Barnsley, M.J., 1997. Global retrieval of bidirectional reflectance and albedo over land from EOS MODIS and MISR data: Theory and algorithm. *Journal of Geophysical Research – Atmospheres,* **102** (D14), 17143-17161.

Wasson, B and Underdal, A., 2002. Human-environment interactions: Methods and theory. *IGBP Newsletter,* **49**, 22-23.

WCED, 1987. *Our common future.* Oxford, UK: Oxford University Press.

Wegmüller U., Werner, C. L., Nüesch, D. and Borgeaud, M., 1995. Land-surface analysis using ERS-1 SAR interferometry. *ESA Bulletin,* **81**, 30-37.

Wegmüller U. and C. L. Werner, 1996. Land applications using ERS- 1/2 Tandem data. *In: Proceedings of Fringe'96, Workshop on ERS SAR Interferometry.* Zürich, Switzerland, 30 September - 2 October., ESTEC, Noordwijk, The Netherlands: ESA

Publications Division (ESA SP-406). Available from: http://earth.esa.int/workshops/fringe_1996/wegmuell/

Weimar, J., 1998. *Simulations with cellular automata.* Available from: http://www.tu-bs.de/institute/WiR/weimar/Zascriptnew/intro.html

Welch, R. and Zupko, S., 1981. Urbanized area energy utilization patterns from DMSP data. *Photogrammetric Engineering and Remote Sensing,* **45** (2), 201-207.

WRI, 1996. *World Resources 1996-97, A Guide to the Global Environment.* A Report by The World Resources Institute, UNEP, UNDP, The World Bank. Oxford, UK: Oxford University Press. Available from: http://www.wri.org/wri/wr-96-97/

Wrigley, N., Holt, T., Steel, D. and Tranmer, M., 1996. Analysing, modelling and resolving the ecological fallacy. *In:* Longley, P. and Batty, M. (Eds.). *Spatial Analysis: Modelling in a GIS Environment.* New York, USA: Wiley, 25-41.

Wolfe, R.E., Roy, D.P. and Vermote, E. 1998. MODIS land data storage, gridding and compositing methodology: Level 2 grid. *IEEE Transactions on Geoscience and Remote Sensing,* **36** (4), 1324-1338.

Xia, Z.G. and Henderson, F.M. 1997. Understanding the relationships between radar response patterns and the bio- and geophysical parameters of urban areas. *IEEE Transactions on Geoscience and Remote Sensing,* **35** (1), 93-101.

Zebker, H.A., Villasenor, J., 1992. Decorrelation in interferometric radar echoes. *IEEE Transactions on Geoscience and Remote Sensing,* **30** (5), 950-959.

Appendix A

ANNEX I Countries of the Kyoto Protocol

Australia
Austria
Belarus a/
Belgium
Bulgaria a/
Canada
Czechoslovakia a/
Denmark
European Economic Community
Estonia a/
Finland
France
Germany
Greece
Hungary a/
Iceland
Ireland
Italy
Japan
Latvia a/
Lithuania a/
Luxembourg
Netherlands
New Zealand
Norway
Poland a/
Portugal
Romania a/
Russian Federation a/
Spain
Sweden
Switzerland
Turkey
Ukraine a/
United Kingdom of Great Britain and Northern Ireland
United States of America

a/ Countries that are undergoing the process of transition to a market economy.

Taken from http://cop3.unfccc.int/fccc/climate/annex1.htm

Appendix B

MODIS Technical Specifications (http://modis.gsfc.nasa.gov/about/specs.html)

Data Products (http://modis.gsfc.nasa.gov/data/dataproducts.html)

MOD43 QA Specifications (http://geography.bu.edu/brdf/userguide/param.html)

Colour composites of MOD43 BRDF parameters.

The Nile delta	JD 321-2000; 16/11/2000
Florida	JD 321-2000; 16/11/2000
Western Europe	JD 001-2001l 01/01/2001

Full sequences for October – December 2000 can be found at the following sites:

Western Europe:	www.ge.ucl.ac.uk/~cdoll/WE.html
Florida:	www.ge.ucl.ac.uk/~cdoll/florida.html
East Mediterranean/Nile:	www.ge.ucl.ac.uk/~cdoll/nile.html

MODIS Technical Specifications

Orbit:	705 km, 10:30 a.m. descending node (Terra) or 1:30 p.m. ascending node (Aqua), sun-synchronous, near-polar, circular
Scan Rate:	20.3 rpm, cross track
Swath Dimensions:	2330 km (cross track) by 10 km (along track at nadir)
Telescope:	17.78 cm diam. off-axis, afocal (collimated), with intermediate field stop
Size:	1.0 x 1.6 x 1.0 m
Weight:	228.7 kg
Power:	162.5 W (single orbit average)
Data Rate:	10.6 Mbps (peak daytime); 6.1 Mbps (orbital average)
Quantization:	12 bits
Spatial Resolution:	250 m (bands 1-2) 500 m (bands 3-7) 1000 m (bands 8-36)
Design Life:	6 years

Primary Use	Band	Bandwidth	Spectral Radiance	Required SNR
Land/Cloud/Aerosols Boundaries	1	620 - 670	21.8	128
	2	841 - 876	24.7	201
Land/Cloud/Aerosols Properties	3	459 - 479	35.3	243
	4	545 - 565	29.0	228
	5	1230 - 1250	5.4	74
	6	1628 - 1652	7.3	275
	7	2105 - 2155	1.0	110
Ocean Color/ Phytoplankton/ Biogeochemistry	8	405 - 420	44.9	880
	9	438 - 448	41.9	838
	10	483 - 493	32.1	802
	11	526 - 536	27.9	754
	12	546 - 556	21.0	750
	13	662 - 672	9.5	910
	14	673 - 683	8.7	1087
	15	743 - 753	10.2	586
	16	862 - 877	6.2	516
Atmospheric Water Vapor	17	890 - 920	10.0	167
	18	931 - 941	3.6	57
	19	915 - 965	15.0	250

[1] Bands 1 to 19 are in nm;
[2] Spectral Radiance values are (W/m^2 -μm-sr)
[3] SNR = Signal-to-noise ratio

Note: Performance goal is 30-40% better than

MODIS Technical Specifications continued

Primary Use	Band	Bandwidth	Spectral Radiance[2]	Required NE[delta]T(K)[4]
Surface/Cloud Temperature	20	3.660 - 3.840	0.45(300K)	0.05
	21	3.929 - 3.989	2.38(335K)	2.00
	22	3.929 - 3.989	0.67(300K)	0.07
	23	4.020 - 4.080	0.79(300K)	0.07
Atmospheric Temperature	24	4.433 - 4.498	0.17(250K)	0.25
	25	4.482 - 4.549	0.59(275K)	0.25
Cirrus Clouds Water Vapor	26	1.360 - 1.390	6.00	150(SNR)
	27	6.535 - 6.895	1.16(240K)	0.25
	28	7.175 - 7.475	2.18(250K)	0.25
Cloud Properties	29	8.400 - 8.700	9.58(300K)	0.05
Ozone	30	9.580 - 9.880	3.69(250K)	0.25
Surface/Cloud Temperature	31	10.780 - 11.280	9.55(300K)	0.05
	32	11.770 - 12.270	8.94(300K)	0.05
Cloud Top Altitude	33	13.185 - 13.485	4.52(260K)	0.25
	34	13.485 - 13.785	3.76(250K)	0.25
	35	13.785 - 14.085	3.11(240K)	0.25
	36	14.085 - 14.385	2.08(220K)	0.35

[1] Bands 20 to 36 are in μm
[2] Spectral Radiance values are (W/m^2 -μm-sr)
[4] NE(delta)T = Noise-equivalent temperature difference

Note: Performance goal is 30-40% better than

Data Products

Primary Use	Product Number	Data Product
Calibration	MOD 01	Level-1A Radiance Counts
	MOD 02	Level-1B Calibrated Geolocated Radiances
	MOD 03	Geolocation Data Set
Atmosphere	MOD 04	Aerosol Product
	MOD 05	Total Precipitable Water (Water Vapor)
	MOD 06	Cloud Product
	MOD 07	Atmospheric Profiles
	MOD 08	Gridded Atmospheric Product
	MOD 35	Cloud Mask

Data Products continued

Primary Use	Product Number	Data Product
Land	MOD 09	Surface Reflectance
	MOD 11	Land Surface Temperature & Emissivity
	MOD 11	Land Cover/Land Cover Change
	MOD 13	Gridded Vegetation Indices (Max NDVI & Integrated MVI)
	MOD 14	Thermal Anomalies, Fires & Biomass Burning
	MOD 15	Leaf Area Index & FPAR
	MOD 16	Evapotranspiration
	MOD 17	Net Photosynthesis and Primary Productivity
	MOD 43	Surface Reflectance
	MOD 44	Vegetation Cover Conversion
Cryosphere	MOD 10	Snow Cover
	MOD 29	Sea Ice Cover
Ocean	MOD 18	Normalized Water-leaving Radiance
	MOD 19	Pigment Concentration
	MOD 20	Chlorophyll Fluorescence
	MOD 21	Chlorophyll_a Pigment Concentration
	MOD 22	Photosynthetically Available Radiation (PAR)
	MOD 23	Suspended-Solids Concentration
	MOD 24	Organic Matter Concentration
	MOD 25	Coccolith Concentration
	MOD 26	Ocean Water Attenuation Coefficient
	MOD 27	Ocean Primary Productivity
	MOD 28	Sea Surface Temperature
	MOD 31	Phycoerythrin Concentration
	MOD 36	Total Absorption Coefficient
	MOD 37	Ocean Aerosol Properties
	MOD 39	Clear Water Epsilon

MOD43 QA Specifications

Quality Assurance information is contained in two bit-words; each one is 32 bits in length.

Bit-word #1 holds band-averaged quality and inversion status information and band-independent data (bits 00-01 are the MODLAND mandatory QA)

Bit Number range / QA category	**Bit number/ information**
00-01 Mandatory QA	0 = processed, good quality 1 = processed, see other QA 2 = not processed due to cloud effects 3 = not processed due to other effects
02-03 Period used	0 = 16 days 1 = 32 days
04-07 land/water	0 = Shallow ocean 1 = Land (Nothing else but land) 2 = Ocean coastlines and lake shores 3 = Shallow inland water 4 = Ephemeral water 5 = Deep inland water 6 = Moderate or continental ocean 7 = Deep ocean
08-10 AM/MISR/PM	0 = AM 1 = AM/PM 2 = AM/PM/MISR 3 = AM/MISR 4 = PM 5 = PM/MISR 6 = MISR
16-17 snow/no snow	0 = no Snow 1 = Snow present
18-30	TBD
31 I	Qafil

Bit-word #2 holds band-specific quality and inversion status information.

Bit Number range / QA category	Bit number/ information
00-03 Band1 Quality	0 = RMSE good, WoD(ref) good, WoD(WSA) good 1 = RMSE good, WoD(ref) good, WoD(WSA) moderate 2 = RMSE good, WoD(ref) moderate, WoD(WSA) good 3 = RMSE good, WoD(ref) moderate, WoD(WSA) moderate 4 = RMSE moderate, WoD(ref) good, WoD(WSA) good 5 = RMSE moderate, WoD(ref) good, WoD(WSA) moderate 6 = RMSE moderate, WoD(ref) moderate, WoD(WSA) good 7 = RMSE moderate, WoD(ref)moderate, WoD(WSA)moderate 8 = magnitude inversion (numobs >=7) 9 = magnitude inversion (numobs >3&<7) 10 = magnitude inversion (numobs <=3) 11 = Bus-in DB parameters (not currently used) 15 = Fill value
04-07	Band2 Quality (see explanation for band1)
08-11	Band3 Quality (see explanation for band1)
12-15	Band4 Quality (see explanation for band1)
16-19	Band5 Quality (see explanation for band1)
20-23	Band6 Quality (see explanation for band1)
24-27	Band7 Quality (see explanation for band1)
28-30	TBD
31	QAFill

Note that while the RMSE indicates the fit of the full inversion, the Weights of Determination (WoD) give some indication of noise expected in the full retrieval and are dependent on the angular sampling of the available surface reflectances.

Colour composites of MOD43 BRDF parameters – The Nile Delta

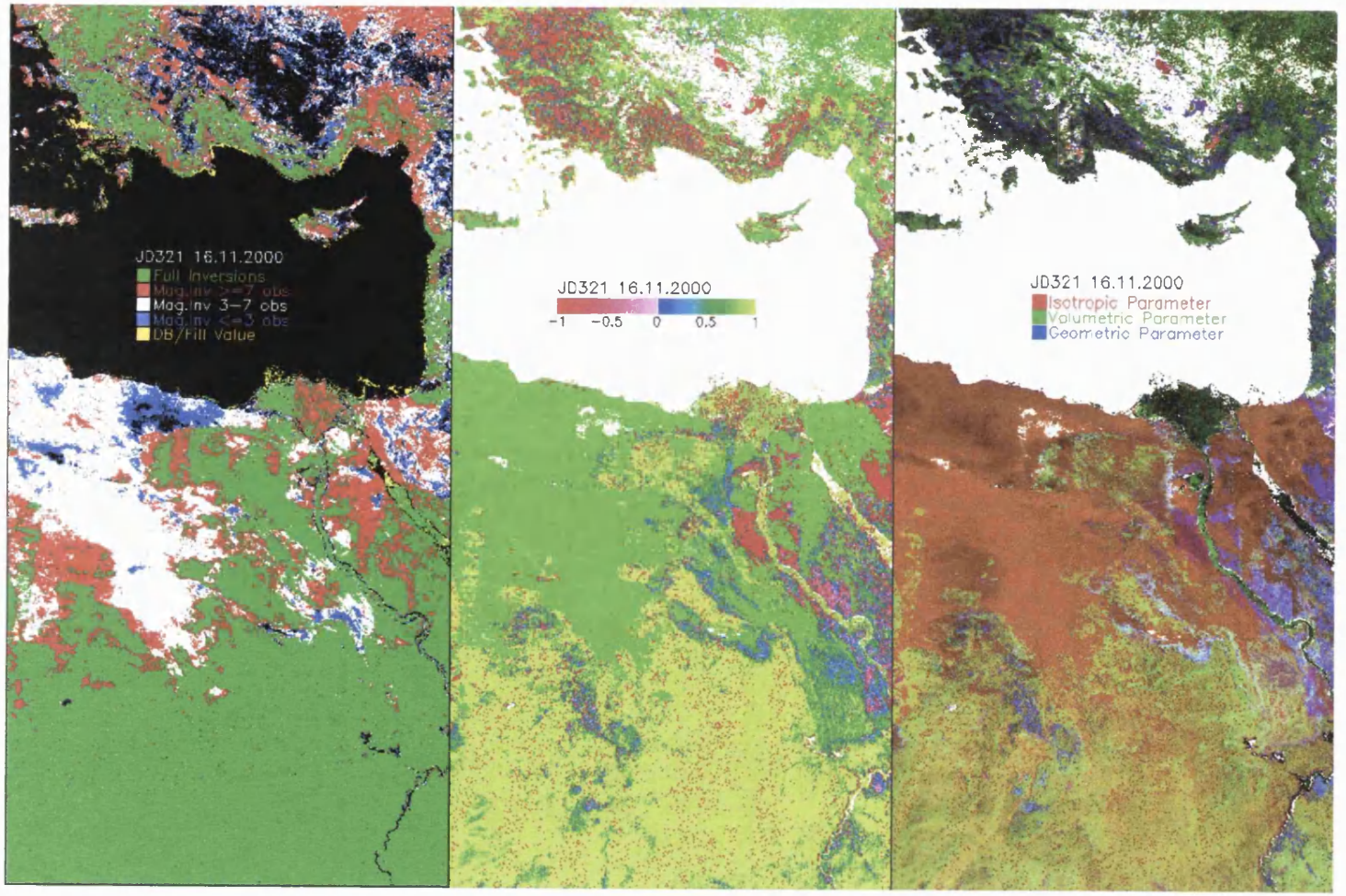

NOTES

The RGB colour composties are of parameters 0,1,2 (isotropic, volumetric, geometric). Each image has been been linearly stretched between the following ranges:

Isotropic (red): 0-700
Volumetric (green): 0-200
Geometric (blue): 0-100

Colour composites of MOD43 BRDF parameters - Florida

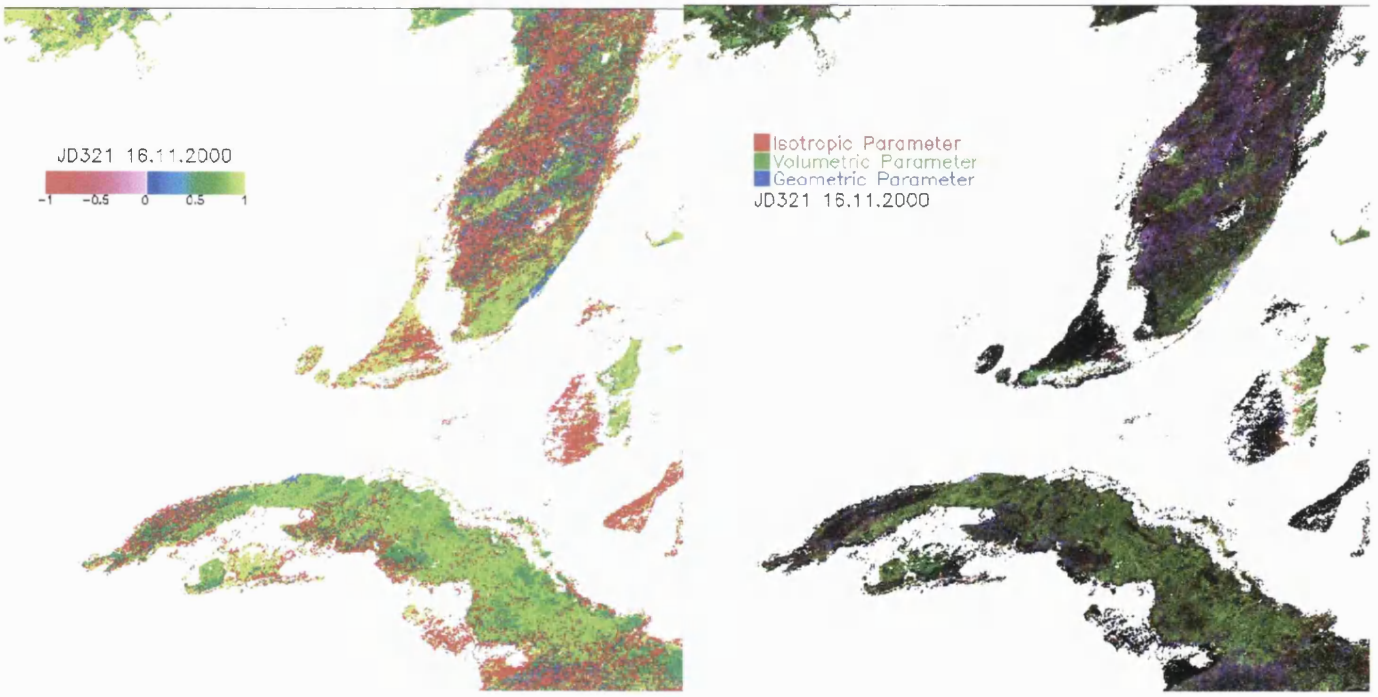

NOTES

The Normalised Difference f Index is defined as:

(fvol - fgeo)/(fvol + fgeo) where:

fvol = the weight of the volumetric kernel
fgeo = the weight of the geometric kernel

The QA image for this date can be seen in Figure 4-7. The RGB colour composties are of parameters 0,1,2 (isotropic, volumetric, geometric). Each image has been been linearly stretched between the following ranges:

Isotropic (red): 0-200 Volumetric (green): 0-100
Geometric (blue): 0-50

Colour composites of MOD43 BRDF parameters – Western Europe

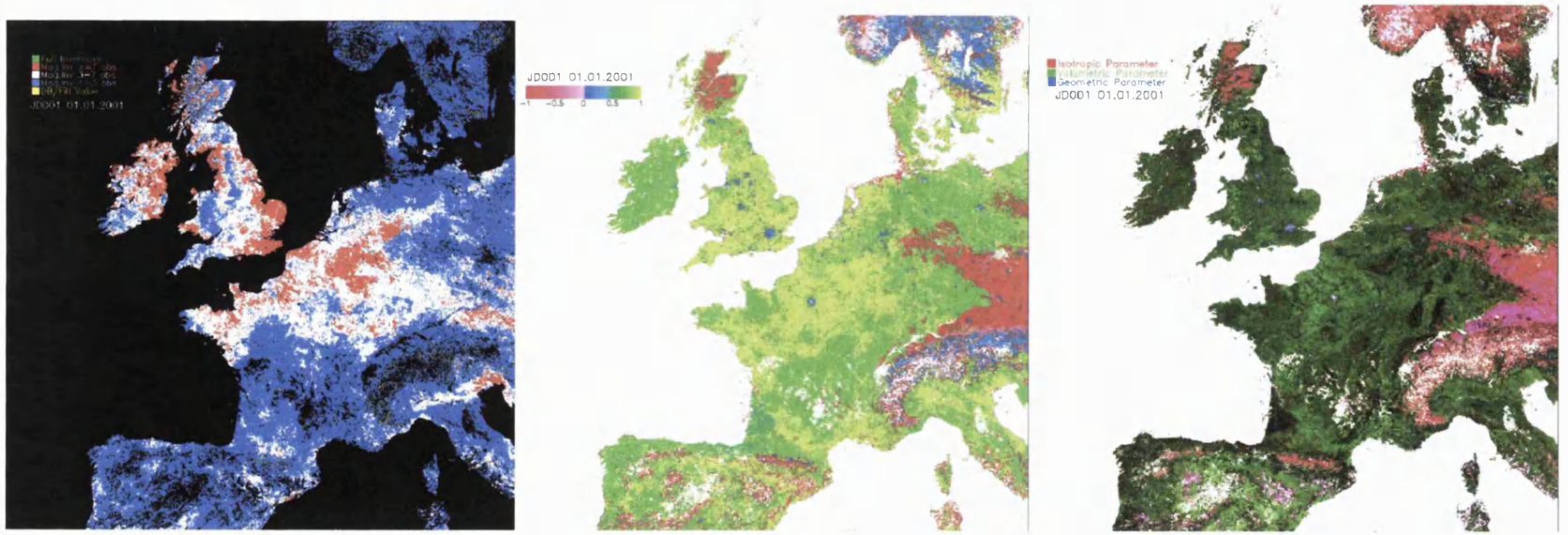

NOTES

The Normalised Difference f Index is defined as:

(fvol - fgeo)/(fvol + fgeo)

where: fvol = the weight of the volumetric kernel
fgeo = the weight of the geometric kernel

The RGB colour composties are of parameters 0,1,2 (isotropic, volumetric, geometric). Each image has been been linearly stretched between the following ranges:

Isotropic (red): 0-200
Volumetric (green): 0-100
Geometric (blue): 0-50

Appendix C

Equivalence of allometric growth model equations

(Equations 5-3 and 5-5)

Result and comparison of population estimation using radiance-calibrated and frequency composite DMSP-OLS data

Equation 5-3 states:

$$r = aP^b$$

r = radius of a circle of the same area as the settlement

P = Population density

a, b are coefficients

Equation 5-5 states:

$$P = cA^d$$

P is the population

A is the area of the settlement

c,d are coefficients

Given that area is related to radiance by:

$$A = \pi r^2$$

Equation 5-5 can be written:

$$P = c\left(\pi r^2\right)^d \Rightarrow P = c\pi^d r^{2d}$$

Equation 5-3 can be re-arranged to make *P* the subject:

$$P = \left(\frac{r}{a}\right)^{1/b} \Rightarrow P = \left(\frac{1}{a}\right)^{1/b} r^{1/b}$$

Setting constants equal to each other:

$c\pi^d = \left(\frac{1}{a}\right)^{1/b}$	$2d = \frac{1}{b}$
$c = \frac{a^{-1/b}}{\pi^d}$	$d = \frac{1}{2b}$

Country	NARC	pc PPP GDP	WRI Urban Pop,	RC Urban Pop.	% out	RC Urban Pop Recalc.	% out	Freq.comp Urban Pop.	% out	Calibration Population	% known
Finland	0.17924	15619	3225	2560.59	20.6	1935.76	40.0	2004	37.9	1439	44.6
Canada	0.16262	20970	22593	24619.3	9.0	14695.9	35.0	22704	0.5	20462	90.6
Sweden	0.14133	18387	7296	4664.92	36.1	3152.46	56.8	10270	40.8	3217	44.1
US	0.12454	23220	200695	160998	19.8	94817.2	52.8	139113	30.7	120944	60.3
France	0.03366	18232	42203	30120.9	28.6	20768.2	50.8	34836	17.5	23480	55.6
Spain	0.02931	12986	30292	19519.9	35.6	20643.9	31.9	42729	41.1	14296	47.2
Japan	0.02801	19920	97120	70550.3	27.4	42386.3	56.4	36859	62.0	63605	65.5
Mexico	0.02532	7867	70535	49574.7	29.7	34539.7	51.0	50543	28.3	40463	57.4
Uzbekistan	0.02403	3334	9430	6166.98	34.6	2989.67	68.3	8029	14.9	5559	59.0
Denmark	0.02386	18730	4414	3526.62	20.1	2617.84	40.7	3202	27.5	2662	60.3
Italy	0.02300	16724	38101	35124.9	7.8	33238.1	12.8	27146	28.8	22405	58.8
Australia	0.02255	18500	15318	16707.4	9.1	10404	32.1	14482	5.5	13590	88.7
Switzerland	0.02091	21631	4379	3708.14	15.3	2393.29	45.3	5215	19.1	3064	70.0
Egypt	0.02033	2274	28170	19164.8	32.0	11707	58.4	30919	9.8	17418	61.8
Austria	0.01988	16989	4424	5309.44	20.0	4577.44	3.5	4344	1.8	2703	61.1
NewZealand	0.01578	15502	3077	2750.9	10.6	2408.49	21.7	3196	3.9	2283	74.2
Russia	0.01572	8320	111736	106191	5.0	91376.8	18.2	75368	32.5	95270	85.3
UK	0.01529	16302	52119	42220.4	19.0	33264.4	36.2	28758	44.8	39026	74.9
Iran	0.01453	4161	39716	33135.1	16.6	32842.2	17.3	82563	107.9	20969	52.8
Holland	0.01415	17373	13801	8654.36	37.3	10239.6	25.8	7952	42.4	7843	56.8
Malaysia	0.01253	7191	10814	6331.19	41.5	6874.86	36.4	8981	17.0	5052	46.7
Syria	0.01145	4955	7676	8559.18	11.5	6252.29	18.5	8437	9.9	6411	83.5
Hungary	0.01094	5780	6541	5784.22	11.6	5949.56	9.0	6392	2.3	4252	65.0
Korea	0.01037	9565	36572	34308.4	6.2	29229	20.1	25751	29.6	29297	80.1
Germany	0.01035	20197	70616	80233.1	13.6	81656.3	15.6	46101	34.7	39933	56.5
Poland	0.01027	4907	24853	20954.5	15.7	19716.5	20.7	21405	13.9	16872	67.9
Ukraine	0.00892	5768	36099	29987.6	16.9	23305.4	35.4	40665	12.6	24430	67.7
Iraq	0.00821	3347	15258	9898.65	35.1	8865.7	41.9	25927	69.9	7342	48.1
Turkey	0.00813	4893	42598	40699.5	4.5	25021.2	41.3	33885	20.5	31813	74.7
Pakistan	0.00724	1793	48742	37490.8	23.1	27506.5	43.6	37741	22.6	26521	54.4
Morocco	0.00610	2777	13071	10700.3	18.1	8474.21	35.2	15700	20.1	7899	60.4
Romania	0.00597	2130	12650	10758.7	15.0	8928.59	29.4	10849	14.2	8942	70.7
Cuba	0.00505	4266	8389	5123.35	38.9	3260.9	61.1	5518	34.2	4685	55.8
SriLanka	0.00480	2783	4108	3407.31	17.1	2444.88	40.5	2134	48.1	2953	71.9
Bulgaria	0.00474	6774	6210	4965.42	20.0	4927.98	20.6	5610	9.7	3984	64.2
China	0.00404	1838	369492	277217	25.0	250258	32.3	459652	24.4	173337	46.9
India	0.00381	1633	250681	209292	16.5	190044	24.2	234462	6.5	97735	39.0
Coted'Ivoire	0.00299	1315	6211	4323.33	30.4	2864.81	53.9	3670	40.9	3842	61.9
Nigeria	0.00228	1132	43884	31162.8	29.0	20114.4	54.2	25581	41.7	19616	44.7
Cameroon	0.00197	1122	6201	2392.16	61.4	1803.44	70.9	1855	70.1	2242	36.2
Indonesia	0.00166	2601	69992	53873.1	23.0	55361.9	20.9	66478	5.0	23592	33.7
Georgia	0.00159	4495	3190	2657.15	16.7	2699.88	15.4	2796	12.4	2461	77.1
Philippines	0.00151	2172	37741	23089.7	38.8	30375.2	19.5	16878	55.3	21636	57.3
Vietnam	0.00110	665	15479	14460	6.6	18925.9	22.3	12392	19.9	10581	68.4
TOTAL			1945712	1572938	19.2	1305860	33	1749092	10.1	1096126	

Appendix D

Chapter 6 Data tables

Economic Activity (GDP) by region

	Units
United States	
State GSP data	millions (US$)
Simulated regions	
Energy consumption data	trillion Btu
Denmark	millions ECU
France	
Portugal	
Italy	
Spain	
Ireland	
United Kingdom	
Germany	
Belgium	
Greece	
Netherlands	

Energy Consumption

Spain	GWh
Greece	
France	
Itlay	
Belgium	

CORINE Land use dataet

Land cover use mapping to economic sector
Percentage land-use by radiance

Radiance values are given in $W.cm^{-2}.um^{-1}.sr^{-1}$
Lit-area values are given in km^2
1 Gigawatt hour (GWh) = 3,413,000 Btu (Britsh thermal Units)

United States

Economic Activity

	Total Radiance	Lit-area	GSP	GSP/Radiance
Alabama	2300226.394	26349.89577	104213	0.04530554
Alaska	936332.2583	8119.899217	26575	0.028382019
Arizona	2196363.764	15396.07808	122273	0.055670651
Arkansas	1350029.823	16597.10673	59141	0.04380718
California	9325220.337	64056.37659	1045254	0.112088933
Colorado	2401355.58	16044.32443	129575	0.053959106
Connecticut	1317239.71	10777.43649	134968	0.102462748
Delaware	409867.9685	3373.972231	31263	0.076275782
District of Columbia	247704.93	166.3801989	50546	0.204057303
Florida	7181162.972	45415.43004	389473	0.054235366
Georgia	3579232.836	35654.45837	235733	0.06586132
Hawaii	202846.4536	2017.47356	38537	0.189981138
Idaho	667417.8482	10655.60618	29388	0.044032386
Illinois	7675700.989	47958.41046	400327	0.052155106
Indiana	4803400.928	46754.65426	162953	0.033924505
Iowa	2415629.037	31212.19797	81695	0.033819348
Kansas	1445600.528	15980.68173	72998	0.050496661
Kentucky	2400632.472	28029.15384	101535	0.042295104
Louisiana	2638111.679	26316.25606	123549	0.046832362
Maine	636948.0902	9221.827092	30409	0.047741724
Maryland	2591560.528	16756.21348	154646	0.059672926
Massachusetts	2428529.313	15727.9293	223571	0.092060244
Michigan	5924909.586	58229.4329	279503	0.047174222
Minnesota	4659695.688	48904.86831	152334	0.032691834
Mississippi	1307072.607	16538.91912	58743	0.044942415
Missouri	3199286.029	29756.59853	155811	0.048701804
Montana	781435.9856	12249.4012	18907	0.0241952
Nebraska	1169312.525	13021.29622	49275	0.042140146
Nevada	1305202.873	7098.888488	59248	0.045393709
New Hampshire	607964.0633	7597.119903	37470	0.061631932
New Jersey	3596943.662	16762.57775	299986	0.08340025
New Mexico	1031864.981	11055.64601	47829	0.046351995
New York	5674919.091	48212.98125	663377	0.116896292
North Carolina	3141155.807	35998.12894	221629	0.070556513
North Dakota	876629.9736	12128.48008	15910	0.018149049
Ohio	6144859.467	62222.55768	326451	0.053125869
Oklahoma	1927785.761	22056.74113	79423	0.04119908
Oregon	977491.9054	11206.57012	97510	0.099755302
Pennsylvania	5285533.438	56831.11189	347306	0.065708789
Rhode Island	370582.6333	2311.139157	29409	0.079358819
South Carolina	1842028.187	25621.64145	95447	0.051816254
South Dakota	868152.1522	11506.59999	19767	0.02276905
Tennessee	4024578.267	34908.92961	151738	0.037702832
Texas	11203933.07	81237.17779	608622	0.054322174
Utah	974786.4374	9710.966693	55070	0.056494426
Vermont	233776.8424	4751.382075	15510	0.066345322
Virginia	2651277.896	25616.18637	212105	0.080001044
Washington	2186773.301	27029.96347	175242	0.080137251
West Virginia	718922.8196	10741.97842	38281	0.053247719
Wisconsin	5080407.177	62583.5027	148194	0.029169709
Wyoming	555595.5305	7485.290589	16244	0.029237096

BEA Regions

	Total Radiance	GRP	Member states
Plains	14634305.93	547790	Minnesota, Missouri, Nebraska, N & S Dakota
Rocky Mountain	5380591.382	249183	Colorado, Idaho, Montana, Utah, Wyoming
Great Lakes	29629278.15	1317428	Illinois, Indiana, Michigan , Ohio, Wisconsin
New England	5595040.652	471336	Connecticut, Maine, Massachusetts, New Hampshire, Rhode Island, Vermont
Mideast	17806529.62	1547124	Delaware, DC, Maryland, New Jersey, New York , Pennsylvania
Southeast	33134431.76	1791586	Florida, Georgia, Kentucky, Louisiana, Mississippi, N & S Carolina, Tennessee, Virginia, W Virginia
Southwest	16359947.58	858147	Arizona, New Mexico, Oklahoma, Texas,
Far West	14933867.13	1442365	Alaska, California, Hawaii, Nevada, Oregon, Washington

US Census Regions

	Total Radiance	GRP	Member states
Pacific	13628664.26	1383118	Alaska, Washington, Oregon, California, Hawaii
mountain	9914023	478534	Montana, Idaho,. Wyoming, Utah, Nevada, Colorado, Arizona, New Mexico
W-N Central	14634305.93	547790	Minnesota, N & S Dakota, Iowa, Nebraska, Missouri, Kansas
E-N Central	25900047.72	1072672	Ohio, Illionois, Indiana
New England	5595040.652	471337	Maine, New Hampshire, Vermont, Massachusetts, Connecticut, Rhode Island
Middle Atlantic	14557396.19	1310669	New York, Pennsylvania, New Jersey
South Atlantic	22362913.94	1429123	West Virginia, Delaware, Maryland, Virginia, DC, N & S Carolina, Georgia, Florida
E-S Central	10032509.74	416229	Tennessee, Alabama, Mississippi
west South central	17119860.33	870735	Oklahoma, Texas, Arkansas, Louisiana

Simulated Regions

Alphabetically

	Total Radiance	GRP
Alaska - Delaware	20236635.83	1653262
DC - Iowa	26773095.99	1388652
Kansas - Michigan	18066292.2	986211
Minnesota - New Hampshire	13029969.77	531788
New Jersey - Oklahoma	22394158.74	1654605
Oregon - Texas	24572299.65	1349799
Utah - Wyoming	12401540	660646

Latitudunal divisions

		Total Radiance	GRP
zone 1		31716143.71	1951379
	Alaska	26575	936332.2583
	Connecticut	134968	1317239.71
	Maine	30409	636948.0902
	Massachusetts	223571	2428529.313
	Michigan	279503	5924909.586
	Minnesota	152334	4659695.688
	Montana	18907	781435.9856
	New Hampshire	37470	607964.0633
	New York	663377	5674919.091
	North Dakota	15910	876629.9736
	Rhode Island	29409	370582.6333
	Vermont	15510	233776.8424
	Washington	175242	2186773.301
	Wisconsin	148194	5080407.177
zone2		34160037.48	1830902
	Idaho	29388	667417.8482
	Illinois	400327	7675700.989
	Indiana	162953	4803400.928
	Iowa	81695	2415629.037
	Nebraska	49275	1169312.525
	New Jersey	299986	3596943.662

		Total Radiance	GRP
	Ohio	326451	6144859.467
	Oregon	97510	977491.9054
	Pennsylvania	347306	5285533.438
	South Dakota	19767	868152.1522
	Wyoming	16244	555595.5305
zone 3		27671418.4	2106332
	California	1045254	9325220.337
	Colorado	129575	2401355.58
	Delaware	31263	409867.9685
	District of Columbia	50546	247704.93
	Kansas	72998	1445600.528
	Kentucky	101535	2400632.472
	Maryland	154646	2591560.528
	Missouri	155811	3199286.029
	Nevada	59248	1305202.873
	Utah	55070	974786.4374
	Virginia	212105	2651277.896
	West Virginia	38281	718922.8196
zone4		15513806.59	777480
	Arizona	122273	2196363.764
	Arkansas	59141	1350029.823
	New Mexico	47829	1031864.981
	North Carolina	221629	3141155.807
	Oklahoma	79423	1927785.761
	South Carolina	95447	1842028.187
	Tennessee	151738	4024578.267
zone 5		28412586.01	1558870
	Alabama	104213	2300226.394
	Florida	389473	7181162.972
	Georgia	235733	3579232.836
	Hawaii	38537	202846.4536
	Louisiana	123549	2638111.679
	Mississippi	58743	1307072.607
	Texas	608622	11203933.07

Division by rank

		Total Radiance	GRP
group 1		5289923.224	171710
	Alaska	26575	936332.2583
	Idaho	29388	667417.8482
	Montana	18907	781435.9856
	North Dakota	15910	876629.9736
	Rhode Island	29409	370582.6333
	South Dakota	19767	868152.1522
	Vermont	15510	233776.8424
	Wyoming	16244	555595.5305
group 2		5025431.831	323610
	Delaware	31263	409867.9685
	District of Columbia	50546	247704.93
	Hawaii	38537	202846.4536
	Maine	30409	636948.0902
	Nebraska	49275	1169312.525
	New Hampshire	37470	607964.0633
	New Mexico	47829	1031864.981
	West Virginia	38281	718922.8196
group3		10726107.07	466318
	Arkansas	59141	1350029.823

		Total Radiance	GRP
	Iowa	81695	2415629.037
	Kansas	72998	1445600.528
	Mississippi	58743	1307072.607
	Nevada	59248	1305202.873
	Oklahoma	79423	1927785.761
	Utah	55070	974786.4374
group4		14756209.98	774102
	Alabama	104213	2300226.394
	Arizona	122273	2196363.764
	Colorado	129575	2401355.58
	Kentucky	101535	2400632.472
	Louisiana	123549	2638111.679
	Oregon	97510	977491.9054
	South Carolina	95447	1842028.187
group5		25676168.33	1060644
	Connecticut	134968	1317239.71
	Indiana	162953	4803400.928
	Maryland	154646	2591560.528
	Minnesota	152334	4659695.688
	Missouri	155811	3199286.029
	Tennessee	151738	4024578.267
	Wisconsin	148194	5080407.177
group6		23508822.4	1647769
	Georgia	235733	3579232.836
	Massachusetts	223571	2428529.313
	Michigan	279503	5924909.586
	New Jersey	299986	3596943.662
	North Carolina	221629	3141155.807
	Virginia	212105	2651277.896
	Washington	175242	2186773.301
group7		52491329.36	3780810
	California	1045254	9325220.337
	Florida	389473	7181162.972
	Illinois	400327	7675700.989
	New York	663377	5674919.091
	Ohio	326451	6144859.467
	Pennsylvania	347306	5285533.438
	Texas	608622	11203933.07

Energy Consmption (Quad BtU)

	Total Radiance	Total Lit area	Consumption
Alabama	2300226.394	26349.89577	2004.8
Alaska	936332.2583	8119.899217	694.7
Arizona	2196363.764	15396.07808	1219.8
Arkansas	1350029.823	16597.10673	1203.7
California	9325220.337	64056.37659	8375.4
Colorado	2401355.58	16044.32443	1155.5
Connecticut	1317239.71	10777.43649	839.3
Delaware	409867.9685	3373.972231	278.8
District of Columbia	247704.93	166.3801989	169.8
Florida	7181162.972	45415.43004	3852.9
Georgia	3579232.836	35654.45837	2798.1
Hawaii	202846.4536	2017.47356	241.4
Idaho	667417.8482	10655.60618	518.3
Illinois	7675700.989	47958.41046	3882.6
Indiana	4803400.928	46754.65426	2735.8
Iowa	2415629.037	31212.19797	1121.7
Kansas	1445600.528	15980.68173	1050
Kentucky	2400632.472	28029.15384	1830.2

	Total Radiance	Total Lit area	Consumption
Louisiana	2638111.679	26316.25606	3615.4
Maine	636948.0902	9221.827092	528.6
Maryland	2591560.528	16756.21348	1378.2
Massachusetts	2428529.313	15727.9293	1569.1
Michigan	5924909.586	58229.4329	3239.6
Minnesota	4659695.688	48904.86831	1675.3
Mississippi	1307072.607	16538.91912	1208.5
Missouri	3199286.029	29756.59853	1768
Montana	781435.9856	12249.4012	412.4
Nebraska	1169312.525	13021.29622	602
Nevada	1305202.873	7098.888488	615.3
New Hampshire	607964.0633	7597.119903	335.4
New Jersey	3596943.662	16762.57775	2588.7
New Mexico	1031864.981	11055.64601	635
New York	5674919.091	48212.98125	4283
North Carolina	3141155.807	35998.12894	2446.9
North Dakota	876629.9736	12128.48008	365.7
Ohio	6144859.467	62222.55768	4323.4
Oklahoma	1927785.761	22056.74113	1377.5
Oregon	977491.9054	11206.57012	1109.2
Pennsylvania	5285533.438	56831.11189	3715.5
Rhode Island	370582.6333	2311.139157	261.1
South Carolina	1842028.187	25621.64145	1493
South Dakota	868152.1522	11506.59999	239
Tennessee	4024578.267	34908.92961	2070.5
Texas	11203933.07	81237.17779	11501
Utah	974786.4374	9710.966693	693.9
Vermont	233776.8424	4751.382075	165
Virginia	2651277.896	25616.18637	2227.3
Washington	2186773.301	27029.96347	2240.8
West Virginia	718922.8196	10741.97842	735.4
Wisconsin	5080407.177	62583.5027	1810.5
Wyoming	555595.5305	7485.290589	421.8

US Census Divisions

	Total Radiance	Total Lit area	Energy Consumption
Pacific	13628664.26	112430.283	12661.5
Mountain	9914023	89696.20167	5672
West North Central	14634305.93	162510.7228	6821.7
E.N. Central	29629278.15	277748.558	15991.9
New England	5595040.652	50386.83402	3698.5
South Atlantic	22362913.94	199344.3895	15380.4
E.S.Central	10032509.74	105826.8983	7114
W.S.Central	17119860.33	146207.2817	17697.6
Middle Atlantic	14557396.19	121806.6709	10587.2

Denmark

Region	Total Radiance	GRP	GRP/Radiance
dk001 København og Frederiksberg Kommuner	34178.26808	26755.6	0.782824921
dk002 Københavns amt	78940.88244	21633.2	0.274043048
dk003 Frederiksborg amt	48044.72766	7990.9	0.1663221
dk004 Roskilde amt	44983.97092	4551.1	0.101171593
dk005 Vestsjællands amt	68558.66513	7005.8	0.102186937
dk006 Storstrøms amt	45223.94457	5224.8	0.115531718
dk007 Bornholms amt	5876.4188	938.7	0.159740146
dk008 Fyns amt	113522.1916	11455.5	0.100909785
dk009 Sønderjyllands amt	50461.9088	6668.2	0.132143238
dk00a Ribe amt	48871.60039	6265.7	0.128207383
dk00b Vejle amt	89046.50501	8929	0.100273447
dk00c Ringkøbing amt	63913.99571	7597.6	0.118872243
dk00d Århus amt	122133.492	15908.7	0.130256654
dk00e Viborg amt	39190.55272	6091.5	0.155432868
dk00f Nordjyllands amt	88545.13858	12152.7	0.137248642

Region	Lit-area	Radiance/Lit-area	GRP/Lit-area	Mean Radiance
dk001 København og Frederiksberg Kommuner	93.59682276	365.1648323	285.8601308	313.5620924
dk002 Københavns amt	508.3423769	155.2907765	42.55635765	133.3460851
dk003 Frederiksborg amt	1032.14111	46.54860387	7.74206155	39.97065527
dk004 Roskilde amt	783.9807265	57.3789245	5.8051172	49.27050482
dk005 Vestsjællands amt	1677.873318	40.86045376	4.175404617	35.08631786
dk006 Storstrøms amt	1122.303187	40.29565727	4.655426503	34.60133477
dk007 Bornholms amt	179.4654675	32.74400854	5.23053272	28.11683635
dk008 Fyns amt	2067.716965	54.90219093	5.540168307	47.14376726
dk009 Sønderjyllands amt	1417.691325	35.5944259	4.703562675	30.56445111
dk00a Ribe amt	1008.097889	48.47902263	6.215368633	41.6282797
dk00b Vejle amt	1677.873318	53.07105372	5.321617492	45.57139456
dk00c Ringkøbing amt	1315.507637	48.58504344	5.775413068	41.71931833
dk00d Århus amt	1926.892388	63.38365999	8.256143466	54.42668979
dk00e Viborg amt	979.7612365	40.00010539	6.217331093	34.34754837
dk00f Nordjyllands amt	1965.533278	45.04891347	6.182902185	38.68289145

France

NUTS-3

	Total Radiance	GRP	GRP/Radiance
fr101 Paris	127160.0078	126239.1	0.992757882
fr102 Seine-et-Marne	203930.6126	21741.4	0.106611753
fr103 Yvelines	209952.742	33110.8	0.157705966
fr104 Essonne	156643.0507	25382.2	0.162038468
fr105 Hauts-de-Seine	129407.8227	68266	0.527526069
fr106 Seine-Saint-Denis	167429.5188	29309.3	0.175054556
fr107 Val-de-Marne	113445.5532	27738.5	0.244509364
fr108 Val-d'Oise	174479.7986	21299.4	0.122073731
fr211 Ardennes	61138.88258	4719.6	0.077194738
fr212 Aube	62646.42505	5345.7	0.085331286
fr213 Marne	159540.5732	12218.7	0.076586788
fr214 Haute-Marne	37891.68578	3440.2	0.090790365
fr221 Aisne	92346.11412	8957.6	0.097000292
fr222 Oise	143522.6995	13424.8	0.093537817
fr223 Somme	80284.7021	9699	0.120807573

	Total Radiance	GRP	GRP/Radiance
fr231 Eure	103314.7543	8972.8	0.086849164
fr232 Seine-Maritime	194431.9265	24734.1	0.127212133
fr241 Cher	77233.7583	5505.4	0.071282301
fr242 Eure-et-Loir	65721.55972	7292.1	0.110954457
fr243 Indre	43972.90854	3899.2	0.088672779
fr244 Indre-et-Loire	62444.58307	10145.4	0.162470458
fr245 Loir-et-Cher	46332.63609	5586.9	0.12058239
fr246 Loiret	115967.8643	13397.7	0.115529419
fr251 Calvados	116229.527	11483.2	0.098797614
fr252 Manche	50794.63703	8631.1	0.169921482
fr253 Orne	38737.81881	4993.9	0.128915364
fr261 Côte-d'Or	147261.2722	11600.8	0.078776992
fr262 Nièvre	49604.85632	3716.4	0.074920084
fr263 Saône-et-Loire	100668.4752	9467.4	0.09404533
fr264 Yonne	60293.59275	5734.7	0.095112926
fr411 Meurthe-et-Moselle	211859.7595	12815.1	0.060488599
fr412 Meuse	57917.37444	3109	0.05367992
fr413 Moselle	298254.4551	17344.2	0.058152359
fr414 Vosges	129217.0241	6715.4	0.051969932
fr421 Bas-Rhin	219634.8984	22771.3	0.103677968
fr422 Haut-Rhin	142524.8765	14019.1	0.098362478
fr431 Doubs	101470.8761	9829	0.096865232
fr432 Jura	52940.95956	4457.1	0.084190012
fr433 Haute-Saône	53551.32693	3256.3	0.060807083
fr434 Territoire de Belfort	28642.18448	2440.3	0.085199507
fr511 Loire-Atlantique	201619.8906	21376	0.106021286
fr512 Maine-et-Loire	106534.8523	12338.5	0.115816559
fr513 Mayenne	32864.93772	5156.4	0.156896692
fr514 Sarthe	59936.05883	9380.1	0.156501782
fr515 Vendée	80016.68957	8872.8	0.110886867
fr521 Côte-du-Nord	42180.48195	8273.9	0.196154705
fr522 Finistère	61345.65447	15459.6	0.25200807
fr523 Ille-et-Vilaine	121933	16256.5	0.133323218
fr524 Morbihan	58416.89756	10792	0.184741067
fr531 Charente	51063.35044	6341.1	0.124181041
fr532 Charente-Maritime	73406.06309	8419.8	0.114701697
fr533 Deux-Sèvres	34187.74619	5851.9	0.171169517
fr534 Vienne	62019.36475	6928	0.111707046
fr611 Dordogne	40619.5737	5541.9	0.136434224
fr612 Gironde	226800.6694	26977.3	0.11894718
fr613 Landes	68032.08645	5725.3	0.084155878
fr614 Lot-et-Garonne	39774.84799	4916.9	0.123618323
fr615 Pyrénées-Atlantiques	124089.5901	10810	0.087114479
fr621 Ariège	41144.61371	2116.3	0.051435651
fr622 Aveyron	34944.46099	4392.8	0.125708049
fr623 Haute-Garonne	247618.4052	22206.7	0.089681137
fr624 Gers	29708.58984	2762.5	0.092986574
fr625 Lot	10634.82298	2459.5	0.231268542
fr626 Hautes-Pyrénées	62853.81918	3800.1	0.060459333
fr627 Tarn	45647.37663	5155.3	0.112937487
fr628 Tarn-et-Garonne	29760.97726	3305	0.111051461

	Total Radiance	GRP	GRP/Radiance
fr631 Corrèze	34353.84408	3799.7	0.110604798
fr632 Creuse	18271.35829	1705.4	0.093337341
fr633 Haute-Vienne	81731.03073	6541.7	0.080039367
fr711 Ain	157330.6041	9323.5	0.059260562
fr712 Ardèche	45015.04792	4362.5	0.096912037
fr713 Drôme	119926.8238	8686.8	0.07243417
fr714 Isère	247335.6312	22941.1	0.092752912
fr715 Loire	195358.7894	12688.3	0.064948703
fr716 Rhône	301664.842	39908.5	0.13229417
fr717 Savoie	164232.8434	8242.5	0.050187891
fr718 Haute-Savoie	187339.3822	13236.6	0.070655726
fr721 Allier	69668.49103	5755.2	0.082608363
fr722 Cantal	29135.49913	2232.7	0.076631603
fr723 Haute-Loire	61446.92795	3092.3	0.050324729
fr724 Puy-de-Dôme	171622.4508	11537.6	0.067226636
fr811 Aude	75028.46381	4574.3	0.060967528
fr812 Gard	120898.8924	10166.2	0.084088446
fr813 Hérault	217612.6556	14720.7	0.067646341
fr814 Lozère	12285.5562	1038	0.084489459
fr815 Pyrénées-Orientales	102724.3233	5895.6	0.057392444
fr821 Alpes-de-Haute-Provence	40136.37431	2327	0.057977335
fr822 Hautes-Alpes	65895.76735	2204.9	0.033460419
fr823 Alpes-Maritimes	179249.2398	19177.9	0.106990133
fr824 Bouches-du-Rhône	386874.8739	36043.5	0.093165782
fr825 Var	219736.106	15607.7	0.071029292
fr826 Vaucluse	147257.6764	8691.3	0.059021032
fr831 Corse-du-Sud	28271.14186	2012.2	0.071175052
fr832 Haute-Corse	32242.19629	2137.3	0.066288908

	Lit-area	Radiance/Lit-area	GRP/Lit-area	Mean Radiance
fr101 Paris	101.3250008	1254.971693	1245.88304	1077.627184
fr102 Seine-et-Marne	2931.555532	69.56396029	7.416335719	59.7336299
fr103 Yvelines	2108.075228	99.59452069	15.7066501	85.52046511
fr104 Essonne	1380.767807	113.4463375	18.38267076	97.41483246
fr105 Hauts-de-Seine	168.3025437	768.8999815	405.6147846	660.2439932
fr106 Seine-Saint-Denis	273.9209767	611.2329214	106.9991074	524.8574256
fr107 Val-de-Marne	273.9209767	414.1543102	101.2646068	355.6286931
fr108 Val-d'Oise	1224.486874	142.4921755	17.39455151	122.3560999
fr211 Ardennes	1250.247467	48.90142486	3.774932662	41.99099076
fr212 Aube	942.8377193	66.4445469	5.66979862	57.0550319
fr213 Marne	2306.431798	69.1720316	5.297663695	59.39708605
fr214 Haute-Marne	765.9483111	49.47029092	4.491425792	42.47946834
fr221 Aisne	1725.959759	53.50421041	5.189924013	45.94334034
fr222 Oise	2730.622903	52.56042472	4.916387388	45.13292435
fr223 Somme	1527.60319	52.5559927	6.349161918	45.12911864
fr231 Eure	2728.046843	37.87132709	3.289093082	32.5195953
fr232 Seine-Maritime	2898.925447	67.07034384	8.53216147	57.59239525
fr241 Cher	1495.831791	51.6326493	3.680494045	44.33625618
fr242 Eure-et-Loir	1323.235815	49.66730718	5.51080912	42.64864354
fr243 Indre	937.6856006	46.89515175	4.158323427	40.26823124

	Lit-area	Radiance/Lit-area	GRP/Lit-area	Mean Radiance
fr244 Indre-et-Loire	997.7936519	62.5826622	10.16783378	53.73888385
fr245 Loir-et-Cher	1176.400433	39.38508929	4.749148201	33.81944238
fr246 Loiret	1916.588151	60.50745133	6.990390708	51.9569284
fr251 Calvados	2223.997899	52.26152734	5.163314231	44.87626523
fr252 Manche	1287.170985	39.46222968	6.705480548	33.88568179
fr253 Orne	854.3930152	45.33957807	5.844968195	38.9324812
fr261 Côte-d'Or	2412.908917	61.03059721	4.807806841	52.40614668
fr262 Nièvre	1025.271618	48.38216082	3.624795551	41.54510578
fr263 Saône-et-Loire	1981.848321	50.7952471	4.777055792	43.61719026
fr264 Yonne	1132.607424	53.23432592	5.063272479	45.71159418
fr411 Meurthe-et-Moselle	2958.174811	71.61840425	4.332096924	61.49775309
fr412 Meuse	1197.867594	48.35039759	2.595445453	41.51783112
fr413 Moselle	3980.011684	74.93808532	4.357826403	64.34831823
fr414 Vosges	2571.76591	50.24447351	2.611201888	43.14424844
fr421 Bas-Rhin	3882.980115	56.56348781	5.864387487	48.57030038
fr422 Haut-Rhin	2685.971208	53.06269705	5.219378361	45.5642188
fr431 Doubs	1694.188361	59.89350323	5.801598115	51.42973949
fr432 Jura	1215.90001	43.54055362	3.665679715	37.38768329
fr433 Haute-Saône	1123.161873	47.67908189	2.899225906	40.94138142
fr434 Territoire de Belfort	436.2127153	65.66104901	5.594289012	56.38225289
fr511 Loire-Atlantique	3116.173118	64.70111994	6.859695913	55.5579748
fr512 Maine-et-Loire	2211.976289	48.16274607	5.578043519	41.35669731
fr513 Mayenne	662.047251	49.64137782	7.78856795	42.62637834
fr514 Sarthe	1087.955729	55.09053102	8.621766264	47.30549234
fr515 Vendée	2138.129254	37.42369149	4.149795894	32.13521668
fr521 Côte-du-Nord	1278.58412	32.9899936	6.471142469	28.32806039
fr522 Finistère	1574.830945	38.95380306	9.816672738	33.44910275
fr523 Ille-et-Vilaine	2450.691121	49.75453618	6.633434895	42.7235459
fr524 Morbihan	1502.701283	38.87459086	7.181733404	33.38108431
fr531 Charente	980.619923	52.07251989	6.466419712	44.71396709
fr532 Charente-Maritime	1563.668021	46.94478759	5.384646797	40.31085286
fr533 Deux-Sèvres	777.1112349	43.99337528	7.530324794	37.77651511
fr534 Vienne	1136.900856	54.55125168	6.093759153	46.84242048
fr611 Dordogne	987.4894145	41.13418646	5.612110792	35.32136842
fr612 Gironde	3679.471427	61.63947019	7.331841144	52.92897766
fr613 Landes	1563.668021	43.50801164	3.661454941	37.35973993
fr614 Lot-et-Garonne	827.7737353	48.05038659	5.939908202	41.26021574
fr615 Pyrénées-Atlantiques	2100.34705	59.08051724	5.146768482	50.73163944
fr621 Ariège	985.7720416	41.73846688	2.146845224	35.84025583
fr622 Aveyron	808.8826335	43.20090399	5.430701338	37.09603076
fr623 Haute-Garonne	3158.248754	78.4037055	7.031333417	67.3241993
fr624 Gers	750.491955	39.58548742	3.680918871	33.99152154
fr625 Lot	291.0947057	36.53389351	8.449140269	31.37115921
fr626 Hautes-Pyrénées	1394.506791	45.07243679	2.725049477	38.70309061
fr627 Tarn	903.3381427	50.53188222	5.706943786	43.3910424
fr628 Tarn-et-Garonne	672.3514883	44.26401633	4.915583675	38.00891091
fr631 Corrèze	764.2309382	44.95217658	4.97192643	38.59982479
fr632 Creuse	475.7122919	38.40842165	3.58493995	32.98079112
fr633 Haute-Vienne	1348.996409	60.58654433	4.849308684	52.02484449

	Lit-area	Radiance/Lit-area	GRP/Lit-area	Mean Radiance
fr711 Ain	3240.682653	48.54859948	2.877017283	41.6880244
fr712 Ardèche	941.1203464	47.83134069	4.63543267	41.07212399
fr713 Drôme	1956.087727	61.30953234	4.440905118	52.64566449
fr714 Isère	3885.556175	63.65514229	5.904199803	54.65980797
fr715 Loire	2986.511464	65.41370818	4.248535508	56.16986466
fr716 Rhône	2539.135825	118.8061068	15.71735533	102.0171937
fr717 Savoie	2883.46909	56.95668594	2.858535931	48.90793428
fr718 Haute-Savoie	3431.311044	54.59702713	3.857592573	46.88172724
fr721 Allier	1375.615689	50.64531584	4.183726637	43.48844631
fr722 Cantal	698.9707682	41.68343005	3.19426806	35.79299645
fr723 Haute-Loire	1469.212512	41.82303613	2.104732961	35.9128743
fr724 Puy-de-Dôme	2922.109981	58.73237212	3.948379793	50.43269194
fr811 Aude	1562.809334	48.00871236	2.926972536	41.22443064
fr812 Gard	2040.238999	59.25722057	4.9828476	50.88337219
fr813 Hérault	2814.774175	77.31087542	5.229797876	66.38580093
fr814 Lozère	303.9750024	40.41633719	3.414754476	34.70496099
fr815 Pyrénées-Orientales	1572.254885	65.33566806	3.749773688	56.10285267
fr821 Alpes-de-Haute-Provence	875.8601764	45.82509331	2.656816765	39.34938656
fr822 Hautes-Alpes	1353.289841	48.69301856	1.629288814	41.8120351
fr823 Alpes-Maritimes	1434.865054	124.92411	13.36564714	107.2706402
fr824 Bouches-du-Rhône	3664.873758	105.5629469	9.834854454	90.64547181
fr825 Var	2767.54642	79.39744187	5.639544069	68.17750726
fr826 Vaucluse	2101.205737	70.08246448	4.136339363	60.17886242
fr831 Corse-du-Sud	473.994919	59.64439856	4.245193185	51.21583668
fr832 Haute-Corse	650.8843272	49.53598504	3.28368638	42.535879

NUTS-2

	Total Radiance	GRP	GRP/Radiance
fr21 Champagne-Ardenne	321217.5666	25724.2	0.080083416
fr22 Picardie	316153.5157	32081.4	0.101474121
fr23 Haute-Normandie	297746.6808	33706.9	0.113206636
fr24 Centre	411673.31	45826.7	0.111318123
fr25 Basse-Normandie	205761.9828	25108.2	0.122025457
fr26 Bourgogne	357828.1965	30519.2	0.085290093
fr41 Lorraine	697248.6132	39983.8	0.057345112
fr42 Alsace	362159.7749	36790.4	0.101586102
fr43 Franche-Comté	236605.347	19982.7	0.084455826
fr51 Pays de la Loire	480972.4291	57123.8	0.118767307
fr52 Bretagne	283876.034	50782	0.178887944
fr53 Poitou-Charentes	220676.5245	27540.7	0.124801222
fr61 Aquitaine	499316.7676	53971.4	0.108090502
fr62 Midi-Pyrénées	502313.0658	46198.1	0.091970731
fr63 Limousin	134356.2331	12046.7	0.089662383
fr71 Rhône-Alpes	1418203.964	119389.9	0.084183871
fr72 Auvergne	331873.3689	22617.9	0.068152199
fr81 Languedoc-Roussillon	528549.8912	36394.8	0.068857833
fr82 Provence-Alpes-Côte d'Azur	1039150.038	84052.3	0.080885625
fr83 Corse	60513.33816	4149.5	0.068571659

	Lit-area	Radiance/Lit-area	GRP/Lit-area
fr21 Champagne-Ardenne	5265.465296	61.00459287	4.885456186
fr22 Picardie	5984.185852	52.83150015	5.36103002
fr23 Haute-Normandie	5626.97229	52.91418998	5.990237425

	Lit-area	Radiance/Lit-area	GRP/Lit-area
fr24 Centre	7847.535443	52.45892968	5.839629567
fr25 Basse-Normandie	4365.561899	47.13298943	5.751424578
fr26 Bourgogne	6552.63628	54.60827996	4.657545253
fr41 Lorraine	10707.82	65.11583247	3.734074723
fr42 Alsace	6568.951323	55.13205337	5.600650422
fr43 Franche-Comté	4469.462959	52.93820515	4.470939839
fr51 Pays de la Loire	9216.28164	52.1872538	6.198139578
fr52 Bretagne	6806.807469	41.70472506	7.46047251
fr53 Poitou-Charentes	4458.300035	49.49790789	6.177399409
fr61 Aquitaine	9158.749648	54.51800593	5.892878621
fr62 Midi-Pyrénées	8964.686511	56.03241844	5.1533425
fr63 Limousin	2588.939639	51.8962401	4.653140544
fr71 Rhône-Alpes	21863.87432	64.86517179	5.460601274
fr72 Auvergne	6465.908949	51.32663814	3.498023275
fr81 Languedoc-Roussillon	8294.052396	63.72637476	4.388060054
fr82 Provence-Alpes-Côte d'Azur	12197.64099	85.19270562	6.890865217
fr83 Corse	1124.879246	53.79540814	3.688840393

NUTS-1

	Total Radiance	GRP	GRP/Radiance
fr1 Île de France	1282449.106	353086.6	0.275322115
fr2 Bassin Parisien	1910381.252	192966.6	0.101009471
fr3 Nord - Pas-de-Calais	585321.8862	65128.9	0.111270228
fr4 Est	1296013.735	96756.9	0.074657311
fr5 Ouest	985524.9876	135446.5	0.137435886
fr6 Sud-Ouest	1135986.066	112216.3	0.098783166
fr7 Centre-Est	1750077.333	142007.8	0.081143729
fr8 Méditerranée	1628213.267	124596.6	0.076523514

	Lit-area	Radiance/Lit-area	GRP/Lit-area
fr1 Île de France	8462.354939	151.5475439	41.72439026
fr2 Bassin Parisien	35642.35706	53.59862282	5.413968545
fr3 Nord - Pas-de-Calais	7037.794123	83.16837292	9.254163856
fr4 Est	21746.23428	59.59715684	4.449363451
fr5 Ouest	20481.38914	48.11807347	6.613150067
fr6 Sud-Ouest	18123.43616	62.68050145	6.19177837
fr7 Centre-Est	28329.78327	61.77517547	5.012668068
fr8 Méditerranée	21616.57263	75.3224526	5.763938722
fr7 Centre-Est	28329.78327	61.77517547	5.012668068
fr8 Méditerranée	21616.57263	75.3224526	5.763938722

Portugal

NUTS-3

	Total Radiance	GRP	GRP/Radiance
pt111 Minho-Lima	33587.31209	1551.4	0.046190061
pt112 Cávado	45331.85179	2629.2	0.057998954
pt113 Ave	66702.66819	3758.4	0.056345572
pt114 Grande Porto	184763.3881	12468.4	0.067483066
pt115 Tâmega	67123.22859	2693.6	0.040129178
pt116 Entre Douro e Vouga	34826.41212	2168	0.062251604
pt117 Douro	30005.88886	1547	0.051556546
pt118 Alto Trás-os-Montes	34197.59955	1337.5	0.039110932
pt121 Baixo Vouga	58039.20889	3277.3	0.056467
pt122 Baixo Mondego	41294.21778	2811.1	0.068074906
pt123 Pinhal Litoral	42436.92812	2017.6	0.047543498

	Total Radiance	GRP	GRP/Radiance
pt124 Pinhal Interior Norte	8518.710948	740.4	0.086914558
pt125 Dão-Lafões	31121.33152	1685.6	0.054162207
pt126 Pinhal Interior Sul	5076.290997	285.4	0.056222151
pt127 Serra da Estrela	5575.138866	246.9	0.044285892
pt128 Beira Interior Norte	18595.25413	685.3	0.036853489
pt129 Beira Interior Sul	13657.83827	550	0.040269916
pt12a Cova da Beira	9570.222283	556.1	0.058107323
pt131 Oeste	72580.64422	3195.3	0.044024134
pt132 Grande Lisboa	270075.4704	29393.5	0.108834393
pt133 Península de Setúbal	87887.4005	5680.4	0.0646327
pt134 Médio Tejo	35494.75933	1845.1	0.051982322
pt135 Lezíria do Tejo	47640.5669	2205.8	0.046300876
pt141 Alentejo Litoral	16089.65604	1108.6	0.068901411
pt142 Alto Alentejo	18747.61951	876.6	0.046757936
pt143 Alentejo Central	24898.22169	1292	0.051891256
pt144 Baixo Alentejo	16064.83124	818.8	0.050968478

	Lit-area	Radiance/Lit-area	GRP/Lit-area	Mean Radiance
pt111 Minho-Lima	765.9483111	43.85062491	2.025463047	37.6539373
pt112 Cávado	849.2408965	53.37926138	3.095941341	45.8360483
pt113 Ave	964.3048805	69.17176252	3.897522533	59.39685499
pt114 Grande Porto	794.2849639	232.6159961	15.69764073	199.7442032
pt115 Tâmega	1382.48518	48.55258453	1.948375316	41.69144631
pt116 Entre Douro e Vouga	517.7879278	67.25999246	4.187042385	57.75524395
pt117 Douro	674.0688612	44.51457497	2.295017748	38.22406222
pt118 Alto Trás-os-Montes	549.5593264	62.22731179	2.433768177	53.43374926
pt121 Baixo Vouga	1214.182637	47.80105327	2.699182068	41.04611659
pt122 Baixo Mondego	751.3506415	54.95998207	3.741395621	47.19339173
pt123 Pinhal Litoral	1005.52183	42.20388544	2.006520336	36.23990444
pt124 Pinhal Interior Norte	274.7796632	31.00197027	2.694522555	26.6209717
pt125 Dão-Lafões	789.1328452	39.43737953	2.136015514	33.86434331
pt126 Pinhal Interior Sul	145.1180096	34.98043427	1.966675265	30.03722482
pt127 Serra da Estrela	132.2377129	42.15997648	1.867092183	36.20220041
pt128 Beira Interior Norte	425.9084779	43.66021127	1.609031131	37.49043169
pt129 Beira Interior Sul	200.0739423	68.26395341	2.74898367	58.61733161
pt12a Cova da Beira	192.3457642	49.75530562	2.891147628	42.7242066
pt131 Oeste	1885.675439	38.4905285	1.694512181	33.05129516
pt132 Grande Lisboa	855.2517016	315.78478	34.36824498	271.1601107
pt133 Península de Setúbal	1008.097889	87.18141505	5.634770254	74.86149953
pt134 Médio Tejo	853.5343287	41.58562595	2.161717388	35.70901339
pt135 Lezíria do Tejo	1099.118653	43.34433483	2.00688069	37.21919287
pt141 Alentejo Litoral	323.7247907	49.70164937	3.42451376	42.67813271
pt142 Alto Alentejo	440.5061475	42.55926874	1.989983579	36.54506726
pt143 Alentejo Central	522.9400465	47.61200037	2.470646508	40.88377943
pt144 Baixo Alentejo	337.4637738	47.60460969	2.426334509	40.87743315
pt15 Algarve	1429.712935	61.96798059	2.135953257	53.21106508

NUTS-2

	Total Radiance	GRP
pt11 Norte	496538.3493	28153.4
pt12 Centro (P)	233885.1418	12855.6
pt13 Lisboa e Vale do Tejo	513678.8414	42320.1
pt14 Alentejo	75800.32848	4096
pt15 Algarve	88596.4234	3053.8

Italy

NUTS-3

	Total Radiance	GRP	GRP/Radiance	Mean Radiance
it111 Torino	343229.7531	49109.4	0.143080253	74.59894652
it112 Vercelli	61384.2724	3578.9	0.058303208	35.56446835
it113 Biella		3885.9		
it114 Verbano-Cusio-Ossola		2709.5		
it115 Novara	78636.70501	7087.4	0.090128395	36.42274431
it116 Cuneo	139661.6151	11439.8	0.081910838	39.72173352
it117 Asti	49994.01289	3643.7	0.072882727	37.98937148
it118 Alessandria	81055.10963	8292	0.102300768	40.02721461
it131 Imperia	31427.56395	4232.9	0.134687499	60.20606117
it132 Savona	47744.89135	5481.9	0.114816472	54.94233755
it133 Genova	97080.52983	17070.6	0.175839584	86.98972202
it134 La Spezia	24581.2166	4157.5	0.169133207	69.43846494
it201 Varese	109530.5243	16606.1	0.151611618	73.41187954
it202 Como	123904.2461	10886.6	0.08786301	66.04703947
it203 Lecco		6432.6		
it204 Sondrio	55545.06722	3293.6	0.059295994	39.59021183
it205 Milano	467867.053	104630.6	0.223633187	148.3879013
it206 Bergamo	178198.6225	20343	0.114159132	67.0423711
it207 Brescia	202437.836	23473.7	0.115955102	51.48469885
it208 Pavia	97356.4372	9115.1	0.093626064	38.38976228
it209 Lodi		3750.2		
it20a Cremona	73902.90866	6752.4	0.091368528	38.9167502
it20b Mantova	97986.88425	8556	0.087317809	37.34256258
it311 Bolzano-Bozen	99930.59166	11548.2	0.11556221	33.73753937
it312 Trento	144120.9742	10263.8	0.07121656	37.7972657
it321 Verona	164590.0322	17139.5	0.104134496	52.10194115
it322 Vicenza	134096.3269	17642.7	0.131567362	50.90976722
it323 Belluno	56771.81776	4457.2	0.078510785	32.29341168
it324 Treviso	129911.526	16378.2	0.126071955	48.1332071
it325 Venezia	117638.4385	16873.6	0.14343611	56.3402483
it326 Padova	146538.9788	17623.8	0.120266977	64.2151528
it327 Rovigo	58232.29457	4364.1	0.074942951	36.739618
it331 Pordenone	62414.59173	6009.3	0.09628037	41.03523451
it332 Udine	114115.6964	10421.1	0.091320479	40.49527903
it333 Gorizia	25578.22207	2654.2	0.103767963	56.33969616
it334 Trieste	25101.95857	4949.9	0.197191784	102.8768793
it401 Piacenza	47351.5452	5471.2	0.115544276	36.06362923
it402 Parma	81506.22636	9302.3	0.114129931	50.97324973
it403 Reggio nell'Emilia	74828.70825	10316.9	0.137873555	49.00373819
it404 Modena	114926.5871	15239	0.13259769	61.26150694
it405 Bologna	134398.8175	22905.1	0.170426351	56.37534288
it406 Ferrara	56307.47053	6647.6	0.118058935	35.93329323
it407 Ravenna	81406.43033	7030.5	0.086362956	52.38509028
it408 Forlì-Cesena	111313.632	7378.5	0.066285682	63.10296595
it409 Rimini		5794.8		
it511 Massa-Carrara	28423.50536	3034.8	0.106770786	54.45115966
it512 Lucca	68110.71193	6830.4	0.100283785	56.47654386
it513 Pistoia	41717.735	4811.3	0.115329847	59.68202428
it514 Firenze	222280.1771	21165.7	0.095220817	80.41974564
it515 Prato		5054.5		
it516 Livorno	49162.52482	6149.4	0.125083079	63.8474348
it517 Pisa	68625.76804	7694.8	0.112126978	56.57524155
it518 Arezzo	55225.40674	5861.3	0.106134121	42.64510171
it519 Siena	34710.70906	4820.2	0.138867806	37.97670573
it51a Grosseto	26485.39432	3377.3	0.127515564	42.64958826
it521 Perugia	101535.9253	10861	0.106967066	42.09615475
it522 Terni	43846.6663	3647.1	0.083178502	49.93925544

	Total Radiance	GRP	GRP/Radiance	Mean Radiance
it531 Pesaro e Urbino	54286.57131	6087.9	0.112143756	38.12259219
it532 Ancona	72015.43002	8574.2	0.119060596	47.47226762
it533 Macerata	55070.99721	5281.2	0.095898027	36.37450276
it534 Ascoli Piceno	71961.86883	6288	0.08737961	43.66618252
it601 Viterbo	57251.78234	4561.4	0.079672629	35.1022577
it602 Rieti	34055.84035	2316.2	0.068011829	35.21803551
it603 Roma	496120.0353	81656	0.164589201	94.01554577
it604 Latina	94301.7214	8275	0.087750254	47.43547352
it605 Frosinone	94473.04146	7903.8	0.083661962	39.71124061
it711 L'Aquila	69738.23117	4417.8	0.063348323	41.0708075
it712 Teramo	44247.86154	4401.2	0.099466954	37.21434947
it713 Pescara	35714.87355	4412.8	0.123556366	47.93942757
it714 Chieti	60026.09323	5890.6	0.098133989	35.56048175
it721 Isernia	14885.34002	1508.1	0.101314448	28.73617763
it722 Campobasso	34100.7492	3194.1	0.093666564	37.06603172
it801 Caserta	119636.7833	9727.1	0.081305262	57.21510437
it802 Benevento	44309.91487	3372.2	0.076104863	32.50910847
it803 Napoli	230611.832	34613	0.150092039	159.0426426
it804 Avellino	75434.18513	5224	0.069252422	39.24775499
it805 Salerno	107024.9034	13318.7	0.124444868	42.87856706
it911 Foggia	107120.1884	7449.3	0.069541513	46.07319928
it912 Bari	207377.8007	19333.1	0.093226468	68.98795762
it913 Taranto	121442.4887	6720.1	0.055335658	62.69617377
it914 Brindisi	69589.44466	5004.6	0.071916079	43.93273019
it915 Lecce	149606.7221	8356.4	0.055855779	51.73123168
it921 Potenza	54816.60707	5096.7	0.092977298	33.06188603
it922 Matera	34736.26046	2602.6	0.074924588	39.2500118
it931 Cosenza	92660.19832	8004.8	0.086388764	33.01040195
it932 Crotone		1635.2		
it933 Catanzaro	85148.46967	4495.6	0.052797191	33.41776673
it934 Vibo Valentia		1722.8		
it935 Reggio di Calabria	56272.86732	6413.9	0.113978553	38.7821277
ita01 Trapani	82106.47706	4863.9	0.059238932	55.21619167
ita02 Palermo	128115.6264	14303.5	0.111645241	71.33386766
ita03 Messina	63401.01301	8440	0.133120901	42.29553901
ita04 Agrigento	74491.0474	4782.4	0.064201004	52.60667186
ita05 Caltanissetta	46927.02304	3062	0.06525025	64.02049524
ita06 Enna	29092.51572	1810.8	0.062242812	39.26115479
ita07 Catania	132766.0015	12083.8	0.091015771	77.86862253
ita08 Ragusa	63416.65106	3798.9	0.059903826	52.36717673
ita09 Siracusa	62219.26857	5759.3	0.092564573	59.48304831
itb01 Sassari	83000.04649	6383.6	0.0769108	48.90986827
itb02 Nuoro	38480.25933	3480.7	0.090454172	35.335408
itb03 Oristano	24365.72684	2023	0.083026458	36.15093001
itb04 Cagliari	106810.9898	10330.3	0.096715703	49.13109003

NUTS-2

	Total Radiance	GRP
it11 Piemonte	753961.4682	89746.7
it12 Valle d'Aosta	69920.78851	2761.7
it13 Liguria	200834.2017	30942.9
it31 Trentino-Alto Adige	244051.5659	21812
it32 Veneto	807779.4147	94479.1
it33 Friuli-Venezia Giulia	227210.4687	24034.5
it51 Toscana	594741.9323	68799.8
it52 Umbria	145382.5916	14508.1
it53 Marche	253334.8674	26231.3
it71 Abruzzo	209727.0595	19122.3
it72 Molise	48986.08922	4702.2
it91 Puglia	655136.6445	46863.5
it92 Basilicata	89552.86753	7699.3
it93 Calabria	234081.5353	22272.3

NUTS-1

	Total Radiance	GRP
it1 Nord Ovest	1024716.458	123451.3
it2 Lombardia	1406729.579	213839.9
it3 Nord Est	1279041.449	140325.6
it4 Emilia-Romagna	702039.4172	90086.1
it5 Centro (I)	993459.3913	109539.2
it6 Lazio	776202.4208	104712.4
it7 Abruzzo-Molise	258713.1487	23824.5
it8 Campania	577017.6187	66254.9
it9 Sud	978771.0473	76835.1
ita Sicilia	682535.6237	58904.7
itb Sardegna	252657.0225	22217.6

Spain

NUTS-3

	Total Radiance	GRP	GRP/Radiance
es111 La Coruña	170385.4893	11970.3	0.070254222
es112 Lugo	49416.40653	3496.4	0.070753829
es113 Orense	52398.49071	3101.9	0.05919827
es114 Pontevedra	130868.572	8825.3	0.067436359
es211 Álava	91033.8678	4957.5	0.054457754
es212 Guipúzcoa	135226.3414	10518.6	0.077785141
es213 Vizcaya	165183.9806	15522.7	0.093972188
es241 Huesca	49611.47085	2695.1	0.05432413
es242 Teruel	34214.80674	1912.4	0.05589393
es243 Zaragoza	182867.7406	11550.6	0.063163683
es411 Avila	28465.53655	1744.1	0.061270582
es412 Burgos	69042.99137	4940.2	0.07155252
es413 León	137100.3873	5559.1	0.040547661
es414 Palencia	40521.99608	2148.5	0.053020587
es415 Salamanca	50634.43981	3638.8	0.071864131
es416 Segovia	35502.86158	1826.2	0.051438107
es417 Soria	19773.18299	1198.1	0.060592167
es418 Valladolid	95559.22669	6376.2	0.066725111
es419 Zamora	24395.18915	1895	0.07767925
es421 Albacete	64216.51325	3243.3	0.050505701
es422 Ciudad Real	141591.5295	4815.9	0.034012628
es423 Cuenca	58296.52375	1989.1	0.034120388
es424 Guadalajara	58897.46708	1903.3	0.032315481
es425 Toledo	146332.1046	5386.2	0.036808054
es431 Badajoz	111440.2992	5003.6	0.044899377
es432 Cáceres	52367.20511	3481.4	0.066480539
es511 Barcelona	777368.4858	71203.3	0.0915953
es512 Gerona	171518.8905	8279.8	0.0482734
es513 Lérida	119807.9889	5256.2	0.043871866
es514 Tarragona	171121.5871	9295.8	0.054322778
es521 Alicante	342895.4802	14763.6	0.043055686
es522 Castellón de la Plana	137277.8482	6472.1	0.04714599
es523 Valencia	441581.4147	26180.9	0.059288954

	Total Radiance	GRP	GRP/Radiance
es611 Almería	97363.48069	5146.9	0.052862736
es612 Cadiz	187784.9867	9933.2	0.052896667
es613 Córdoba	119344.0676	6658.6	0.055793305
es614 Granada	135579.1274	6765.8	0.049902962
es615 Huelva	110192.0028	4289.9	0.038931137
es616 Jaén	135050.4503	5673	0.042006524
es617 Málaga	215493.3741	11536.4	0.053534825
es618 Sevilla	330846.7299	16374.9	0.049493915

	Lit-area	Radiance/Lit-area	GRP/Lit-area	Mean Radiance
es111 La Coruña	3098.999389	54.98080765	3.862633869	47.21127179
es112 Lugo	986.6307281	50.08602015	3.543777728	43.00818434
es113 Orense	1195.291535	43.83741471	2.595099112	37.64259182
es114 Pontevedra	2300.420993	56.88896618	3.836384744	48.84978157
es211 Álava	1042.445347	87.32723308	4.755644997	74.98670739
es212 Guipúzcoa	1415.115265	95.55853487	7.433034084	82.05481429
es213 Vizcaya	1534.472682	107.6486943	10.11598329	92.43646977
es241 Huesca	1013.250008	48.96271449	2.659856875	42.04361704
es242 Teruel	789.9915316	43.31034621	2.420785443	37.19000527
es243 Zaragoza	2462.712731	74.25459668	4.690193807	63.7614123
es411 Avila	522.08136	54.52318111	3.340667056	46.8183141
es412 Burgos	847.5235236	81.46439532	5.828982751	69.95236835
es413 León	2382.854892	57.53618811	2.33295784	49.40554224
es414 Palencia	620.8303015	65.270648	3.460688041	56.04701776
es415 Salamanca	704.9815733	71.8237777	5.161553348	61.67410111
es416 Segovia	652.6017	54.40203661	2.798337791	46.71428897
es417 Soria	373.5286046	52.93619482	3.207518742	45.45559056
es418 Valladolid	1023.554245	93.36019768	6.229469546	80.16713205
es419 Zamora	322.8661042	75.55822314	5.869306115	64.88081862
es421 Albacete	1227.92162	52.29691554	2.641292366	44.90665014
es422 Ciudad Real	2327.898959	60.82374365	2.068775357	52.22852147
es423 Cuenca	1300.909968	44.81211243	1.529006656	38.4795515
es424 Guadalajara	1067.347254	55.181167	1.783205974	47.38331764
es425 Toledo	3268.160619	44.77506514	1.648083013	38.4477395
es431 Badajoz	2000.739423	55.69955685	2.500875398	47.82845195
es432 Cáceres	935.9682277	55.94976791	3.719570704	48.04330479
es511 Barcelona	4624.026519	168.1150578	15.39854923	144.3581138
es512 Gerona	3048.336888	56.26638287	2.716169604	48.31517774
es513 Lérida	2357.952985	50.81016869	2.229136897	43.63000084
es514 Tarragona	2198.237305	77.84491088	4.228751817	66.84436628
es521 Alicante	3929.349183	87.26520964	3.757263432	74.93344871
es522 Castellón de la Plana	1811.828404	75.76757707	3.572137397	65.06058799
es523 Valencia	4508.962535	97.93415032	5.806413292	84.09472298
es611 Almería	1649.536666	59.02474478	3.120209516	50.68374561
es612 Cadiz	2010.184973	93.41676971	4.941435804	80.21570968
es613 Córdoba	1936.337939	61.63390447	3.438759251	52.92419555
es614 Granada	1805.817599	75.0790819	3.746668547	64.46938655
es615 Huelva	1610.037089	68.44066113	2.664472781	58.76906492
es616 Jaén	2549.440062	52.97259281	2.225194498	45.48684502
es617 Málaga	1992.152558	108.1711203	5.790921962	92.8850699
es618 Sevilla	3185.72672	103.8528282	5.140083077	89.17701121

NUTS-2

	Total Radiance	GRP
es11 Galicia	403068.9586	27393.9
es12 Principado de Asturias	173468.0557	11780.6
es13 Cantabria	123092.2413	6130
es21 Pais Vasco	391444.1898	30998.8

	Total Radiance	GRP
es22 Comunidad Foral de Navarra	169576.1744	8547.1
es23 La Rioja	51113.10223	3779.7
es24 Aragón	266694.0182	16158
es41 Castilla y León	500995.8115	29326.3
es42 Castilla-la Mancha	469334.1382	17337.8
es43 Extremadura	163807.5043	8484.9
es51 Cataluña	1239816.952	94035.1
es52 Comunidad Valenciana	921754.7432	47416.7
es53 Baleares	176036.383	11831.1
es61 Andalucia	1331654.219	66378.7

	Lit-area	Radiance/Lit-area	GRP/Lit-area
es11 Galicia	7581.342644	53.16590708	3.613330947
es12 Principado de Asturias	2301.279679	75.37895426	5.119151795
es13 Cantabria	1586.852555	77.57005587	3.862992804
es21 Pais Vasco	3992.033294	98.05634397	7.765165698
es22 Comunidad Foral de Navarra	2749.514005	61.67496296	3.10858573
es23 La Rioja	942.8377193	54.21198281	4.008855313
es24 Aragón	4265.954271	62.51684881	3.787663668
es41 Castilla y León	7450.822304	67.24033818	3.935981668
es42 Castilla-la Mancha	9192.23842	51.05765503	1.886134716
es43 Extremadura	2936.70765	55.77930248	2.889255932
es51 Cataluña	12228.5537	101.3870473	7.689797365
es52 Comunidad Valenciana	10250.14012	89.92606268	4.625956273
es53 Baleares	2585.504893	68.08588276	4.575934097
es61 Andalucia	16739.23361	79.55287863	3.965456338
es62 Murcia	3493.136468	71.31528743	3.299040878

NUTS-1

	Total Radiance	GRP
es1 Noroeste	699629.2556	45304.6
es2 Noreste	878827.4846	59483.5
es3 Comunidad de Madrid	1197490.175	84043.4
es4 Centro (E)	1134137.454	55149
es5 Este	3669262.298	153282.9
es6 Sur	1580768.251	77902.7
este - Barcelona	2891893.812	82079.6

	Lit-area	Radiance/Lit-area	GRP/Lit-area
es1 Noroeste	11469.47488	60.99924042	3.950015191
es2 Noreste	11950.33929	73.53996095	4.97755742
es3 Comunidad de Madrid	6067.478438	197.3620817	13.85145425
es4 Centro (E)	19579.76837	57.92394641	2.81663189
es5 Este	25064.19871	146.3945582	6.115611424
es6 Sur	20232.37007	78.13065127	3.850399123

Ireland

NUTS-2

	Total Radiance	GRP	GRP/Radiance
ie011 Border	35582.20424	6104.4	0.171557669
ie012 Midlands	19896.80862	2659.8	0.13367973
ie013 West	30692.12833	4937.1	0.160858835
ie021 Dublin	103740.3919	27530.4	0.265377829
ie022 Mid-East	46258.48323	6059.3	0.130987866
ie023 Midwest	40411.10623	5590	0.138328309
ie024 South-East (IE)	38507.28554	6470.2	0.168025347
ie025 South-West (IE)	51629.56284	11256.6	0.21802625

	Lit-area	Radiance/Lit-area	GRP/Lit-area
ie011 Border	903.3381427	39.38968428	6.757602399
ie021 Dublin	830.3497947	124.9357711	33.15518373
ie022 Mid-East	1261.410391	36.67203279	4.803591315
ie012 Midlands	556.4288179	35.75804844	4.780126252
ie023 Midwest	856.9690745	47.15585128	6.522989179
ie024 South-East (IE)	928.2400497	41.48418887	6.970395214
ie025 South-West (IE)	1028.706364	50.18882419	10.94248115
ie013 West	829.4911082	37.00115411	5.951962536

NUTS-1

	Total Radiance	GRP	Radiance/Lit-area	GRP/Lit-area
ie01 Border, Midlands and Western	86171.14119	13701.3	37.64151467	5.985039514
ie02 Southern and Eastern	280546.8297	56906.6	57.18821389	11.60015537

United Kingdom

NUTS-2

	Total Radiance	GRP	GRP/Radiance
Northumb., T&W	185279.3241	22459.7	0.121220757
TeesVal & Durham	142243.3059	18012.9	0.12663443
Cumbria	52108.91407	9050.8	0.173690052
North Yorkshire	108796.2873	14177.8	0.130315109
Lancashire	136444.1257	23612.2	0.173053987
E.Riding&N.Lincs	158747.6012	17048.8	0.107395639
West Yorkshire	245557.33	38328.6	0.156088193
Merseyside	96938.8749	19727.2	0.203501433
Greater Manchest	217306.5954	46047.7	0.21190199
South Yorkshire	173515.3465	19380.4	0.111692714
Lincolnshire	95603.24707	10677.1	0.111681353
Derbs & Notts	253344.3464	36113.2	0.142545908
Cheshire	116051.2045	22658.9	0.195249158
Shrops & Staffs	166201.4223	24950.8	0.150123866
East Anglia	279814.4767	46802.5	0.167262611
Leics&Northants	194931.1078	32242.9	0.165406642
H'fd,Worcs&Warwk	128944.8027	22759.4	0.176504981
West Midlands	203964.1564	48919.7	0.239844593
Beds & Herts	174674.5951	32538	0.186277804
Berks,Bucks&Oxo	214457.5239	51561	0.240425232
Gloucs,Wilts&NS	180929.7629	45916.9	0.253783011
Essex	188120.0162	29327.2	0.155896223
Kent	147160.4292	29246	0.19873549

	Total Radiance	GRP	GRP/Radiance
Surrey,E&W Sussx	192163.8319	52791	0.27471871
Hants & IoW	124565.0493	37872.3	0.304036327
Dorset&Somerset	85211.25388	20119.2	0.236109658
Devon	66262.09633	17223.6	0.259931408
Cornwall	36490.73824	6343.5	0.173838632
Greater London	505365.5115	204042.7	0.40375272

	Lit-area	Radiance/Lit-area	GRP/Lit-area
Northumb., T&W	1411	131.3106478	15.91757619
TeesVal & Durham	1992	71.40728208	9.042620482
Cumbria	1542	33.79307008	5.869520104
North Yorkshire	3245	33.52736127	4.369121726
Lancashire	2429	56.1729624	9.720955126
E.Riding&N.Lincs	2799	56.71582752	6.091032512
West Yorkshire	2034	120.7263176	18.8439528
Merseyside	664	145.9922815	29.70963855
Greater Manchest	1284	169.2418967	35.8626947
South Yorkshire	1538	112.8188209	12.60104031
Lincolnshire	2843	33.62759306	3.755575097
Derbs & Notts	4384	57.78840019	8.2375
Cheshire	2071	56.03631312	10.94104297
Shrops & Staffs	3347	49.65683368	7.454675829
East Anglia	7119	39.30530646	6.574308189
Leics&Northants	3854	50.57890707	8.366087182
H'fd,Worcs&Warwk	2982	43.24104718	7.632260228
West Midlands	902	226.1243419	54.23470067
Beds & Herts	2625	66.54270288	12.39542857
Berks,Bucks&Oxo	4430	48.41027628	11.63905192
Gloucs,Wilts&NS	3845	47.05585511	11.94197659
Essex	2952	63.72629276	9.934688347
Kent	3076	47.84149194	9.507802341
Surrey,E&W Sussx	4166	46.12669992	12.6718675
Hants & IoW	2648	47.04118175	14.3022281
Dorset&Somerset	2220	38.38344769	9.062702703
Devon	1541	42.99941358	11.17689812
Cornwall	1215	30.03352942	5.220987654
Greater London	1586	318.6415583	128.652396

NUTS-1

	Total Radiance	GRP
Scotland	743420.3441	98079.1
North East	327522.63	40472.6
North West	618701.5524	121096.9
Yorks. & The Hum	627088.1777	88935.7
East Midlands	603939.8257	79033.2
Wales	253741.0493	46841.5
West Midlands	499110.3814	96629.9
East of England	642582.088	108667.7
South East	678346.8343	171470.2
South West	368893.8513	89603.2
Greater London	505365.5115	204042.7

Germany

West Germany

NUTS-2

	Total Radiance	GRP	GRP/Radiance
de11 Stuttgart	386820.5782	107710	0.278449509
de12 Karlsruhe	296052.4661	69945.9	0.236261839
de13 Freiburg	225960.3587	46691.1	0.206634032
de14 Tübingen	184144.3084	40548.8	0.220201213

	Total Radiance	GRP	GRP/Radiance
de21 Oberbayern	351954.8544	125785.9	0.357392144
de22 Niederbayern	175294.7807	24499.9	0.139764002
de23 Oberpfalz	140177.3548	23469.4	0.167426472
de24 Oberfranken	161020.4137	24720.9	0.153526497
de25 Mittelfranken	161453.724	43584.9	0.269952894
de26 Unterfranken	127683.7996	29112.9	0.228007782
de27 Schwaben	177401.7022	40153.6	0.226342811
de71 Darmstadt	441777.0736	117255.7	0.265418255
de72 Gießen	102634.7898	21706	0.211487743
de73 Kassel	113526.808	28101.8	0.247534485
de91 Braunschweig	223034.8999	36176.9	0.162202866
de92 Hannover	263752.2219	49995.2	0.189553664
de93 Lüneburg	210643.8757	28620	0.135869129
de94 Weser-Ems	303735.9012	47197.5	0.155389929
dea1 Düsseldorf	643316.1125	136491.7	0.212168944
dea2 Köln	508221.065	106801.5	0.210147724
dea3 Münster	355843.581	49006.9	0.137720343
dea4 Detmold	236600.0841	46179.4	0.195179136
dea5 Arnsberg	390235.4011	80830.7	0.207133181
deb1 Koblenz	192631.6794	29376.6	0.152501396
deb2 Trier	100347.9045	9581.2	0.095479821
deb3 Rheinhessen-Pfalz	251190.819	44282.3	0.176289485

NUTS-1

	Total Radiance	GRP	GRP/Radiance
de1 Baden-Württemberg	1092977.711	264895.8	0.242361575
de2 Bayern	1294986.629	311327.5	0.240409818
de3 Berlin	205108.3914	74786.5	0.364619407
de5 Bremen	57598.69569	20367.3	0.353606966
de6 Hamburg	155387.9175	66441.1	0.427582151
de7 Hessen	657938.6713	167063.5	0.253919563
de9 Niedersachsen	1001166.899	161989.7	0.161800895
dea Nordrhein-Westfalen	2134216.244	419310.2	0.196470344
deb Rheinland-Pfalz	544170.4029	83240.1	0.152966974
dec Saarland	143785.1024	22672.7	0.157684625
def Schleswig-Holstein	322573.4693	59381.4	0.184086435

East Germany

NUTS-2

	Total Radiance	GRP	GRP/Radiance
dee1 Dessau	89311.31685	7729.1	0.086541104
dee2 Halle	150936.9645	13671	0.090574234
dee3 Magdeburg	200155.5013	18141.5	0.090637029

NUTS-1

	Total Radiance	GRP	GRP/Radiance
de4 Brandenburg	342944.7534	39071.5	0.113929429
de8 Mecklenburg-Vorpommern	273129.7108	27454.6	0.100518541
ded Sachsen	794048.6	69454.3	0.087468576
dee Sachsen-Anhalt	440403.7827	39541.6	0.089784878
deg Thüringen	381807.5517	36494.8	0.09558428

Belgium

NUTS-3

	Total Radiance	GRP	GRP/Radiance
be211 Antwerpen (Arrondissement)	185427.1361	26640.8	0.143672607
be212 Mechelen	60249.57534	6465.3	0.10730864
be213 Turnhout	94914.79753	8355	0.088026316
be221 Hasselt	94779.608	8322.1	0.087804752
be222 Maaseik	58436.51048	3213.7	0.054994728
be223 Tongeren	61137.56469	2301.1	0.037638071
be231 Aalst	36223.28795	3663.1	0.101125552
be232 Dendermonde	29982.12377	2655.2	0.088559437
be233 Eeklo	16200.39337	1081	0.066726775
be234 Gent (Arrondissement)	83904.74466	11813.8	0.140800142
be235 Oudenaarde	21883.89376	1927.9	0.088096754
be236 Sint-Niklaas	52432.3213	4039.3	0.077038359
be241 Halle-Vilvoorde	141658.1722	13224.6	0.093355715
be242 Leuven	106385.1852	8165.7	0.076755988
be251 Brugge	45735.73699	5356.1	0.117109734
be252 Diksmuide	10751.56677	660.2	0.061405004
be253 Ieper	24155.74732	1671.3	0.069188503
be254 Kortrijk	59746.59825	6233.5	0.1043323
be255 Oostende	16834.36838	2115.8	0.125683361
be256 Roeselare	25482.28927	2928.2	0.114911183
be257 Tielt	21992.70356	1904.5	0.086596902
be258 Veurne	9756.064402	1034.7	0.10605711
be321 Ath	20131.18965	875	0.043464893
be322 Charleroi	93140.10024	6951.4	0.074633804
be323 Mons	39063.03155	3433.8	0.087904084
be324 Mouscron	20759.7277	1096.9	0.05283788
be325 Soignies	34148.06841	2111.4	0.06183073
be326 Thuin	30027.35513	1338.4	0.04457269
be327 Tournai	39924.2692	2032.6	0.050911389
be331 Huy	44072.59168	1477	0.033512892
be332 Liège (Arrondissement)	154109.9815	10372.2	0.067303882
be333 Verviers	102125.5933	4291.4	0.042020809
be334 Waremme	24864.81231	758.4	0.030500934
be341 Arlon	28656.80117	982	0.034267607
be342 Bastogne	35323.40874	525.5	0.01487682
be343 Marche-en-Famenne	24291.43325	791.1	0.032567037
be344 Neufchâteau	27401.03332	811.4	0.029612022
be345 Virton	19403.95216	676.2	0.034848571
be351 Dinant	40875.6959	1255.4	0.030712627
be352 Namur (Arrondissement)	82186.0663	4670	0.056822284
be353 Philippeville	20418.14115	692.6	0.033920816

	Lit-area	Radiance/Lit-area	GRP/Lit-area	Mean Radiance
be211 Antwerpen (Arrondissement)	991.7828468	186.9634433	26.86152527	160.5429749
be212 Mechelen	516.9292414	116.5528481	12.50712764	100.082351
be213 Turnhout	1355.007214	70.04744812	6.166018833	60.14879435
be221 Hasselt	911.9250072	103.9335551	9.125860059	89.24633517
be222 Maaseik	875.0014899	66.78446968	3.672793746	57.34691899
be223 Tongeren	631.9932253	96.73768996	3.641020042	83.06734328
be231 Aalst	476.5709783	76.00817003	7.686368173	65.26718546
be232 Dendermonde	346.9093248	86.42639916	7.653873247	74.21317762
be233 Eeklo	319.4313584	50.71635249	3.384138631	43.54944452

	Lit-area	Radiance/Lit-area	GRP/Lit-area	Mean Radiance
be234 Gent (Arrondissement)	941.1203464	89.15410763	12.55291105	76.55542392
be235 Oudenaarde	415.6042406	52.65560749	4.638788087	45.21465651
be236 Sint-Niklaas	476.5709783	110.0199628	8.475757408	94.47265094
be241 Halle-Vilvoorde	947.1311515	149.5655296	13.962797	128.4298932
be242 Leuven	1160.944077	91.63678712	7.033672131	78.68726715
be251 Brugge	661.1885645	69.17200243	8.100714815	59.397061
be252 Diksmuide	306.5510617	35.07267831	2.153637949	30.11643353
be253 Ieper	524.6574194	46.0409906	3.185507225	39.53477464
be254 Kortrijk	416.462927	143.4619852	14.96771884	123.1888623
be255 Oostende	279.0730954	60.32243401	7.581526255	51.79805654
be256 Roeselare	283.3665277	89.92695604	10.33361288	77.21905837
be257 Tielt	322.0074178	68.29874825	5.914460024	58.64720947
be258 Veurne	196.6391965	49.61403717	5.261921421	42.6029013
be321 Ath	508.3423769	39.60163577	1.721280853	34.00538791
be322 Charleroi	559.0048773	166.617688	12.4353119	143.0723505
be323 Mons	593.3523352	65.83446165	5.787118035	56.53115996
be324 Mouscron	110.7705517	187.4119734	9.902451356	160.9281216
be325 Soignies	506.625004	67.40304593	4.167579538	57.87808203
be326 Thuin	684.3730986	43.87570931	1.955658401	37.67547694
be327 Tournai	631.1345389	63.25793747	3.220549463	54.31873357
be331 Huy	656.8951323	67.09227929	2.248456302	57.61123092
be332 Liège (Arrondissement)	792.567591	194.4439607	13.08683337	166.9663938
be333 Verviers	1481.234122	68.94628728	2.897178736	59.20324246
be334 Waremme	369.2351724	67.34139694	2.053975506	57.82514487
be341 Arlon	312.5618669	91.68361278	3.14177801	78.72747571
be342 Bastogne	732.4595397	48.2257474	0.717445772	41.41079569
be343 Marche-en-Famenne	628.5584795	38.64625814	1.25859411	33.18501809
be344 Neufchâteau	676.6449206	40.49543932	1.199151838	34.77288491
be345 Virton	474.8536054	40.86301954	1.424017828	35.08852107
be351 Dinant	1083.662297	37.71995762	1.158478987	32.38961639
be352 Namur (Arrondissement)	1136.04217	72.34420383	4.110762896	62.12098734
be353 Philippeville	518.6466143	39.36811808	1.335398672	33.80486944
be1 Région Bruxelles-capitale/Brussels hoofdstad gewest	165.7264843	631.1729986	246.5170257	541.9796996

NUTS-2

	Total Radiance	GRP
be21 Antwerpen	340591.5089	41461.1
be22 Limburg (B)	214353.6832	13836.9
be23 Oost-Vlaanderen	240626.7648	25180.3
be24 Vlaams Brabant	248043.3575	21390.3
be25 West-Vlaanderen	214455.075	21904.2
be31 Brabant Wallon	77664.41448	6634.8
be32 Hainaut	277193.7419	17839.5
be33 Liège	325172.9788	16899
be34 Luxembourg (B)	135076.6286	3786.1
be35 Namur	143479.9034	6618.1

NUTS-1

	Total Radiance	GRP
be1 Région Bruxelles-capitale/Brussels hoofdstad gewest	104602.0821	40854.4
be2 Vlaams Gewest	1258070.389	123772.8
be3 Région Wallonne	958587.6672	51777.5

Greece

NUTS-3

	Total Radiance	GRP	GRP/Radiance	Mean Radiance
gr111 Evros	14267.92696	1273.5	0.089256134	36.39777284
gr112 Xanthi	12603.56666	796.2	0.063172594	38.54301727
gr113 Rodopi	7428.673072	716.2	0.096410219	35.71477436
gr114 Drama	13346.23372	698.2	0.052314384	36.07090193
gr115 Kavala	17474.72909	1216.2	0.069597645	30.81962801
gr121 Imathia	16060.83593	1254.8	0.078127938	31.00547475
gr122 Thessaloniki	124233.166	12219.7	0.098361013	72.65097426
gr123 Kilkis	8924.959966	904.1	0.101300174	26.24988224
gr124 Pella	14576.64042	1128	0.077384086	27.34829346
gr125 Pieria	8050.057334	937.3	0.116433953	37.26878393
gr126 Serres	19317.75676	1383.2	0.071602517	29.22504803
gr127 Chalkidiki	8648.810323	1093.9	0.126479823	25.36308011
gr131 Grevena	1381.859575	319.1	0.230920714	29.40126754
gr132 Kastoria	7294.031368	500.1	0.068562908	39.21522239
gr133 Kozani	15292.88506	1788.3	0.116936732	36.76174291
gr134 Florina	4154.017674	471.9	0.113600865	27.32906363
gr141 Karditsa	11822.26969	983.9	0.08322429	37.17694869
gr142 Larisa	28762.01719	2654.7	0.092298811	42.67361598
gr143 Magnisia	24484.40271	1967.4	0.080353196	49.36371511
gr144 Trikala	15575.39122	993.3	0.063773679	34.5352355
gr211 Arta	6916.409533	470.4	0.068012167	35.46876682
gr212 Thesprotia	3565.04602	303.3	0.085076041	34.95143155
gr213 Ioannina	14074.43299	1351.9	0.096053603	57.91947729
gr214 Preveza	1731.891363	449.8	0.259716059	25.09987481
gr221 Zakynthos	3347.956686	290.3	0.086709604	32.82310475
gr222 Kerkyra	1154.589068	1059.3		31.20510992
gr223 Kefallinia	2452.013971	316.1	0.128914437	34.05574958
gr224 Lefkada	54.00000003	222		27
gr231 Aitoloakarnania	13299.59345	1723	0.129552832	35.75159527
gr232 Achaia	28010.9941	2859.7	0.102092057	50.56136117
gr233 Ileia	16977.22566	1185.9	0.069852403	31.79255739
gr241 Voiotia	21067.7259	3409.9	0.161854204	33.70836143
gr242 Evvoia	18834.9854	2182.3	0.115864173	34.18327657
gr243 Evrytania	695.6160549	232.3	0.333948589	23.18720182
gr244 Fthiotida	17598.48476	2032.4	0.115487215	38.93470077
gr245 Fokida	3434.730335	462	0.134508376	32.71171746
gr251 Argolida	10550.43264	910.1	0.086261865	35.88582528
gr252 Arkadia	6563.709677	966.9	0.147309989	31.86266832
gr253 Korinthia	19356.41583	1749.8	0.090398967	42.91888208
gr254 Lakonia	3353.469404	728.1	0.217118426	30.48608548
gr255 Messinia	11622.34792	1236.8	0.106415675	42.57270298
gr3 Attiki	354434.288	38757.4	9.144944915	135.3836088
gr411 Lesvos	4366.584782	1021.3	0.233889882	26.95422704
gr412 Samos	2476.997055	360.8	0.145660246	30.96246317
gr413 Chios	3114.138042	412.9	0.132588856	33.84932653
gr421 Dodekanisos	16252.91375	2221.9	0.136707795	39.25824574
gr422 Kyklades	8537.192565	1153.1	0.135067821	33.87774826
gr431 Irakleio	19349.95135	2700.5	0.139561074	44.68810932
gr432 Lasithi	6506.839585	846.3	0.130063142	32.69768634
gr433 Rethymni	4633.057509	766.5	0.165441503	45.8718565
gr434 Chania	11962.75945	1419.2	0.118634836	45.83432735

NUTS-2

	Total Radiance	GRP
gr11 Anatoliki Makedonia, Thraki	65121.1295	4700.3
gr12 Kentriki Makedonia	199812.2268	18921.1
gr13 Dytiki Makedonia	28122.79367	3079.5
gr14 Thessalia	80644.0808	6599.2
gr21 Ipeiros	26287.7799	2575.3
gr22 Ionia Nisia	7008.559725	1887.8
gr23 Dytiki Ellada	58287.81321	5768.5
gr24 Sterea Ellada	61631.54245	8319
gr25 Peloponnisos	51446.37546	5591.8
gr41 Voreio Aigaio	9957.719879	1794.9
gr42 Notio Aigaio	24790.10631	3375
gr43 Kriti	42452.60789	5732.5

NUTS-1

	Total Radiance	GRP
gr1 Voreia Ellada	373700.2308	33300.2
gr2 Kentriki Ellada	204662.0707	24142.4
gr3 Attiki	354434.288	38757.4
gr4 Nisia Aigaiou, Kriti	77200.43408	10902.4

Netherlands

NUTS-3

	Total Radiance	GRP	GRP/Radiance
nl111 Oost-Groningen	29713.59717	2029.1	0.068288602
nl112 Delfzijl en omgeving	11068.10809	997.7	0.090141874
nl113 Overig Groningen	61822.96226	11628.9	0.188100013
nl121 Noord-Friesland	41077.35275	6246.9	0.152076499
nl122 Zuidwest-Friesland	9551.661785	1443.5	0.151125535
nl123 Zuidoost-Friesland	28928.68804	3134.9	0.108366477
nl131 Noord-Drenthe	26539.12967	2805.1	0.105696759
nl132 Zuidoost-Drenthe	46811.51879	2798.1	0.05977375
nl133 Zuidwest-Drenthe	18714.78126	2451.5	0.130992715
nl211 Noord-Overijssel	43439.46308	6590.9	0.151726093
nl212 Zuidwest-Overijssel	15999.05589	2542.3	0.158903126
nl213 Twente	69692.56001	10281.5	0.147526508
nl221 Veluwe	81878.80479	11765.8	0.14369775
nl222 Achterhoek	58209.739	6498.2	0.11163424
nl223 Arnhem/Nijmegen	78257.93274	13390.7	0.17110981
nl224 Zuidwest-Gelderland	46279.62332	3597	0.077723191
nl321 Kop van Noord-Holland	51268.81714	5437.9	0.106066422
nl322 Alkmaar en omgeving	28054.2928	3764.3	0.134179109
nl323 Ijmond	17272.83869	3502.1	0.20275185
nl324 Agglomeratie Haarlem	18577.6934	4085.6	0.219919659
nl325 Zaanstreek	12679.76476	2787.5	0.219838463
nl326 Groot-Amsterdam	242872.8913	36716.7	0.151176608
nl327 Het Gooi en Vechtstreek	17747.18053	5047.1	0.284388835
nl331 Agglomeratie Leiden en Bollenstreek	39316.22581	6975.4	0.177417844
nl332 Agglomeratie 's - Gravenhage	81822.63851	17884.9	0.218581316
nl333 Delft en Westland	105725.0923	5614.2	0.053101869
nl334 Oost-Zuid-Holland	71959.63118	5725.4	0.079564054
nl335 Groot-Rijnmond	207012.3103	29542.4	0.142708421
nl336 Zuidoost Zuid-Holland	42080.40999	8198	0.194817493

	Total Radiance	GRP	GRP/Radiance
nl341 Zeeuwsch-Vlaanderen	25360.03438	2520.8	0.099400496
nl342 Overig Zeeland	35460.72241	4523.2	0.127555213
nl411 West-Noord-Brabant	83395.03468	13466.6	0.161479638
nl412 Midden-Noord-Brabant	62812.88511	7502	0.119434094
nl413 Noordoost-Noord-Brabant	81041.63718	12571.3	0.155121496
nl414 Zuidoost-Noord-Brabant	112010.5688	14756.3	0.131740247
nl421 Noord-Limburg	66008.9479	5079.3	0.076948659
nl422 Midden-Limburg	40917.28202	3880.5	0.094837678
nl423 Zuid-Limburg	103280.2998	11872.8	0.114957064

	Lit-area	Radiance/Lit-area	GRP/Lit-area
nl111 Oost-Groningen	594.2110216	50.00512627	3.414780147
nl112 Delfzijl en omgeving	217.2476712	50.94695849	4.592454292
nl113 Overig Groningen	1086.238356	56.91472955	10.70566136
nl121 Noord-Friesland	1127.455305	36.43368615	5.540707441
nl122 Zuidwest-Friesland	261.04068	36.5907022	5.529789456
nl123 Zuidoost-Friesland	812.3173793	35.61254354	3.859205872
nl131 Noord-Drenthe	683.5144122	38.82746171	4.103936874
nl132 Zuidoost-Drenthe	726.4487345	64.43884691	3.851751496
nl133 Zuidwest-Drenthe	533.2442839	35.09607477	4.597330106
nl211 Noord-Overijssel	980.619923	44.29796098	6.721156531
nl212 Zuidwest-Overijssel	330.5942823	48.39483543	7.690090653
nl213 Twente	1292.323103	53.92812357	7.955827744
nl221 Veluwe	1537.048741	53.27014207	7.654799543
nl222 Achterhoek	1370.46357	42.47448839	4.74160725
nl223 Arnhem/Nijmegen	947.989838	82.55144687	14.12536239
nl224 Zuidwest-Gelderland	779.6872943	59.35664677	4.613387991
nl23 Flevoland	779.6872943	61.6885168	5.703825152
nl31 Utrecht	1344.702977	83.98980606	21.23167755
nl321 Kop van Noord-Holland	895.6099647	57.24458097	6.071727889
nl322 Alkmaar en omgeving	313.4205533	89.51006084	12.01038018
nl323 Ijmond	149.4114419	115.6058631	23.43930262
nl324 Agglomeratie Haarlem	148.5527554	125.057885	27.50268744
nl325 Zaanstreek	109.0531788	116.2713906	25.56092385
nl326 Groot-Amsterdam	1018.402127	238.4842735	36.05324364
nl327 Het Gooi en Vechtstreek	195.78051	90.64835172	25.77937916
nl331 Agglomeratie Leiden en Bollenstreek	251.5951291	156.2678338	27.72470208
nl332 Agglomeratie 's - Gravenhage	224.9758492	363.695209	79.49697739
nl333 Delft en Westland	195.78051	540.018474	28.67599027
nl334 Oost-Zuid-Holland	596.787081	120.5783997	9.593706336
nl335 Groot-Rijnmond	1130.031365	183.19165	26.14299118
nl336 Zuidoost Zuid-Holland	561.5809366	74.93204852	14.59807388
nl341 Zeeuwsch-Vlaanderen	625.1237337	40.5680236	4.032481674
nl342 Overig Zeeland	762.5135653	46.5050381	5.931960041
nl411 West-Noord-Brabant	1281.16018	65.09337084	10.51125395
nl412 Midden-Noord-Brabant	1016.684754	61.78206655	7.378885119
nl413 Noordoost-Noord-Brabant	1299.192595	62.37846298	9.676240496
nl414 Zuidoost-Noord-Brabant	1373.039629	81.57854031	10.74717705
nl421 Noord-Limburg	810.6000064	81.43220748	6.266099136
nl422 Midden-Limburg	662.047251	61.80417177	5.861364116
nl423 Zuid-Limburg	672.3514883	153.6105765	17.65862083

NUTS-2

	Total Radiance	GRP
nl11 Groningen	102604.6675	14655.7
nl12 Friesland	79557.70257	10825.3
nl13 Drenthe	92065.42971	8054.7
nl21 Overijssel	129131.079	19414.7
nl22 Gelderland	264626.0999	35251.7
nl23 Flevoland	48097.75275	4447.2
nl31 Utrecht	112941.3422	28550.3
nl32 Noord-Holland	388473.4786	61341.3
nl33 Zuid-Holland	547916.308	73940.3
nl34 Zeeland	60820.75679	7044
nl41 Noord-Brabant	339260.1257	48296.2
nl42 Limburg (NL)	210206.5297	20832.5

	Lit-area	Radiance/Lit-area	GRP/Lit-area
nl11 Groningen	1897.697049	54.06799129	7.722887069
nl12 Friesland	2200.813365	36.1492273	4.918772384
nl13 Drenthe	1943.207431	47.3780762	4.145054138
nl21 Overijssel	2603.537309	49.59832093	7.457046971
nl22 Gelderland	4635.189443	57.09067625	7.605233924
nl23 Flevoland	779.6872943	61.6885168	5.703825152
nl31 Utrecht	1344.702977	83.98980606	21.23167755
nl32 Noord-Holland	2830.230531	137.2585994	21.6736055
nl33 Zuid-Holland	2960.750871	185.0599162	24.97349599
nl34 Zeeland	1387.637299	43.83044246	5.07625444
nl41 Noord-Brabant	4970.077158	68.26053499	9.717394412
nl42 Limburg (NL)	2144.998746	97.99843944	9.712126891

NUTS-1

	Total Radiance	GRP
nl1 Noord-Nederland	274227.7998	33535.6
nl2 Oost-Nederland	393757.1788	59113.6
nl3 West-Nederland	1110151.886	170875.9
nl4 Zuid-Nederland	549466.6554	69128.7

	Lit-area	Radiance/Lit-area	GRP/Lit-area
nl1 Noord-Nederland	6041.717844	45.38904445	5.550672982
nl2 Oost-Nederland	8018.414046	49.10661592	7.372230925
nl3 West-Nederland	8523.321677	130.2487372	20.04804071
nl4 Zuid-Nederland	7115.075903	77.22569131	9.7158064

NUTS-2 GRP by Sector (excluding extra-territorial organizations and bodies)

	All branches - Total	Agriculture, hunting, forestry and fishing	Industry	Services
nl Netherlands	321825.8	9886.2	85810.1	226129.6
nl1 Noord-Nederland	30975.3	1472.6	11541.4	17961.7
nl11 Groningen	13125.8	304.1	5836	6985.7
nl12 Friesland	10370.9	759.7	3263.5	6347.8
nl13 Drenthe	7479	408.8	2441.8	4628.2
nl2 Oost-Nederland	56550.3	2055.3	16186.6	38308.4
nl21 Overijssel	18564	716.4	5991.4	11855.8
nl22 Gelderland	33641	1005.6	9423	23212.5
nl23 Flevoland	4346.1	333.3	772.6	3240.1
nl3 West-Nederland	164848.4	4513.3	32509.3	127825.8
nl31 Utrecht	27949.7	349.3	4743	22857.5
nl32 Noord-Holland	59041.2	1107.2	10429	47505.3
nl33 Zuid-Holland	71171.4	2744.3	15100.4	53326.8
nl34 Zeeland	6686.1	312.4	2237.3	4136.2
nl4 Zuid-Nederland	66613.5	1845	23126.9	41641.8
nl41 Noord-Brabant	46761	1194.7	16404.2	29162
nl42 Limburg (NL)	19853	650.3	6722.2	12480.2

Enegy Consumption Data

Spain 1997

	Total Radiance	Total electricity consumption	Consumption by industrial sector	Consumption by transport sector	Consumption by households	Consumption by agriculture	Consumption by services sector
es3 Comunldad de Madrid	1197490.2	17511	3473	806	5845	31	5703
es11 Galicia	403069.0	12944	7762	44	2621	53	1952
es12 Principado de Asturias	173468.1	7583	5257	72	1019	8	813
es13 Cantabria	123092.2	3240	2214	35	480	19	445
es21 Pais Vasco	391444.2	13701	9000	215	2182	27	1758
es22 Comunidad Foral de Navarra	169576.2	3034	1823	49	576	56	487
es23 La Rioja	51113.1	1051	462	20	300	19	230
es24 Aragón	266694.0	6500	3233	173	1394	168	1204
es41 Castilla y León	500995.8	8745	3241	254	2491	360	1935
es42 Castilla-la Mancha	469334.1	6840	2052	249	1730	534	1420
es43 Extremadura	163807.5	2039	425	3	769	146	641
es51 Cataluña	1239817.0	31808	15129	766	6960	284	7906
es52 Comunidad Valenciana	921754.7	15868	6041	193	4204	509	4583
es53 Baleares	176036.4	3071	257	161	980	58	1604
es61 Andalucia	1331654.2	20807	6884	351	6395	830	5564
es62 Murcia	249114.0	3820	1118	10	986	473	993
		186	9	0	97	0	80
		0.810128918	0.39397274	0.703238955	0.975165519	0.301213925	0.925106286
es1 Noroeste	699629.3	23767	15233	151	4120	80	3210
es2 Noreste	878827.5	24286	14518	457	4452	270	3679
es3 Comunidad de Madrid	1197490.2	17511	3473	806	5845	31	5703
es4 Centro (E)	1134137.5	17624	5718	506	4990	1040	3996
es5 Este	2337608.1	50747	21427	1120	12144	851	14093
es6 Sur -es63	1580768.3	24627	8002	361	7381	1303	6557

Greece 1996

	Total Radiance	Total electricity consumption	Consumption by industrial sector	Consumption by transport sector	Consumption by households	Consumption by agriculture	Consumption by services sector
gr11 Anatoliki Makedonia, Thra	65121.1	1498	388	0	512	216	380
gr12 Kentriki Makedonia	199812.2	6313	2380	0	2164	377	1390
gr13 Dytiki Makedonia	28122.8	714	164	0	318	55	175
gr14 Thessalia	80644.1	2718	1043	0	678	507	489
gr21 Ipeiros	26287.8	663	115	0	276	52	218
gr22 Ionia Nisia	7008.6	528	43	0	226	8	249
gr23 Dytiki Ellada	58287.8	943	338	0	324	53	226
gr24 Sterea Ellada	61631.5	5970	4697	0	559	300	413
gr25 Peloponnisos	51446.4	1487	291	0	575	222	397
gr3 Attiki	354434.3	11458	2296	70	5401	143	3545
gr41 Voreio Aigaio	9957.7	404	29	0	205	12	156
gr42 Notio Aigaio	24790.1	909	62	0	336	17	492
gr43 Kriti	42452.6	1440	148	0	543	140	609

France 1996

NUTS-2	Total Radiance	Total electricity consumption	Consumption by industrial sector	Consumption by transport sector	Consumption by households	Consumption by agriculture	Consumption by services sector
fr1 Île de France	1155289.1	51984	**8733**	3443	20410	**95**	**17040**
fr21 Champagne-Ardenne	321217.6	8134	**3458**	207	2753	**51**	**1161**
fr22 Picardie	316153.5	11172	**5493**	345	3825	**89**	**1243**
fr23 Haute-Normandie	297746.7	14035	**7273**	198	3656	**45**	**1535**
fr24 Centre	411673.3	12992	**3719**	521	5719	**494**	**2156**
fr25 Basse-Normandie	205762.0	7117	**2496**	42	3335	**41**	**1086**
fr26 Bourgogne	357828.2	8742	**2894**	857	3427	**44**	**1345**
fr3 Nord - Pas-de-Calais	585321.9	30218	**18533**	788	6840	**88**	**3370**
fr41 Lorraine	697248.6	17315	**9520**	420	4464	**30**	**1713**
fr42 Alsace	362159.8	11960	**5964**	186	3524	**27**	**1956**
fr43 Franche-Comté	236605.3	6989	**3814**	120	2211	**14**	**728**
fr51 Pays de la Loire	480972.4	15631	**5023**	288	6912	**344**	**2388**

	Total Radiance	Total electricity consumption	Consumption by industrial sector	Consumption by transport sector	Consumption by households	Consumption by agriculture	Consumption by services sector
fr52 Bretagne	283876.0	13490	**3903**	146	6456	**428**	**2294**
fr53 Poitou-Charentes	220676.5	7850	**2224**	209	3733	**276**	**1162**
fr61 Aquitaine	499316.8	15200	**5017**	289	5971	**248**	**2545**
fr62 Midi-Pyrénées	502313.1	12598	**4413**	251	5335	**123**	**2123**
fr63 Limousin	134356.2	3282	**1145**	85	1445	**11**	**548**
fr71 Rhône-Alpes	1418204.0	56881	**35643**	1128	11635	**139**	**6998**
fr72 Auvergne	331873.4	6450	**2517**	39	2769	**34**	**997**
fr81 Languedoc-Roussillon	528549.9	10175	**2511**	304	5144	**129**	**1869**
fr82 Provence-Alpes-Côte d'Azur	1039150.0	27335	**9496**	597	10363	**139**	**5055**
fr83 Corse	60513.3	858	**28**	1	582	**5**	**197**

NUTS-1	Total Radiance	Total electricity consumption	Consumption by industrial sector	Consumption by transport sector	Consumption by households	Consumption by agriculture	Consumption by services sector
fr1 Île de France	1155289.1	51984	**8733**	3443	20410	**95**	**17040**
fr2 Bassin Parisien	1910381.3	62192	**25333**	2170	22715	**764**	**8526**
fr3 Nord - Pas-de-Calais	585321.9	30218	**18533**	788	6840	**88**	**3370**
fr4 Est	598765.1	36264	**19298**	726	10199	**71**	**4397**
fr5 Ouest	985525.0	36971	**11150**	643	17101	**1048**	**5844**
fr6 Sud-Ouest	1135986.1	31080	**10575**	625	12751	**382**	**5216**
fr7 Centre-Est	1750077.3	63331	**38160**	1167	14404	**173**	**7995**
fr8 Méditerranée	1567699.9	38368	**12035**	902	16089	**273**	**7121**

Italy 1996

	Total Radiance	Total electricity consumption	Consumption by industrial sector	Consumption by transport sector	Consumption by households	Consumption by agriculture	Consumption by services sector
		245954 :		:	57997	**4107**	
NUTS-2							
it11 Piemonte	753961.5	22955 :		:	4418	**218**	
it12 Valle d'Aosta	69920.8	749 :		:	176	**3**	
it13 Liguria	200834.2	5929 :		:	1764	**35**	
it2 Lombardia	1406729.6	50988		:	9258	**636**	
it31 Trentino-Alto Adige	244051.6	4558		:	897	**125**	
it32 Veneto	807779.4	23714		:	4295	**434**	
it33 Friuli-Venezia Giulia	227210.5	7560		:	1222	**96**	
it4 Emilia-Romagna	702039.4	20056		:	4168	**665**	
it51 Toscana	594741.9	16439		:	3714	**180**	
it52 Umbria	145382.6	4747		:	782	**80**	
it53 Marche	253334.9	5251		:	1285	**80**	
it6 Lazio	776202.4	17362		:	6062	**237**	
it71 Abruzzo	209727.1	5206		:	1104	**67**	
it72 Molise	48986.1	1040		:	256	**17**	
it8 Campania	577017.6	13731		:	5300	**188**	
it91 Puglia	655136.6	13911		:	3721	**408**	
it92 Basilicata	89552.9	2078		:	449	**51**	
it93 Calabria	234081.5	4522		:	1915	**114**	
ita Sicilia	682535.6	15214		:	5333	**333**	
itb Sardegna	252657.0	9944		:	1878	**140**	

NUTS-1	Total Radiance	Total electricity consumption	Consumption by industrial sector	Consumption by transport sector	Consumption by households	Consumption by agriculture	Consumption by services sector
it1 Nord Ovest	1024716.5	29633	:	:	6358	**256**	
it2 Lombardia	1406729.6	50988	:	:	9258	**636**	
it3 Nord Est	1279041.4	35832	:	:	6414	**655**	
it4 Emilia-Romagna	702039.4	20056	:	:	4168	**665**	
it5 Centro (I)	993459.4	26437	:	:	5781	**340**	
it6 Lazio	776202.4	17362	:	:	6062	**237**	
it7 Abruzzo-Molise	258713.1	6246	:	:	1360	**84**	
it8 Campania	577017.6	13731	:	:	5300	**188**	
it9 Sud	978771.0	20511	:	:	6085	**573**	
ita Sicilia	682535.6	15214	:	:	5333	**333**	
itb Sardegna	252657.0	9944	:	:	1878	**140**	

Belgium 1996

	Total Radiance	Total electricity consumption
be21 Antwerpen	340591.5	17084
be22 Limburg (B)	214353.7	6433
be23 Oost-Vlaanderen	240626.8	9930
be24 Vlaams Brabant	248043.4	4584
be25 West-Vlaanderen	214455.1	7364
be31 Brabant Wallon		
be32 Hainaut	277193.7	8541
be33 Liège	325173.0	6832
be34 Luxembourg (B)	135076.6	1499
be35 Namur	143479.9	2692
be1 Région Bruxelles-capitale/Brussels	104602.1	4784
be2 Vlaams Gewest	1258070.4	45395
be3 Région Wallonne	880923.3	21226

CORINE Land cover classes and Economic classification

Radiance/Land-use class	Classification
CONTINIOUS URBAN FABRIC	urban/service
DISCONTINUOUS URBAN FABRIC	urban/service
INDUSTRIAL OR COMMERCIAL UNTS	industiral
ROAD AND RAILNETWORKS AND ASSOCIATED LAND	urban/service
PORT AREAS	urban/service
AIRPORTS	urban/service
MINERAL EXTRACTION SITES	industiral
DUMP SITES	industiral
CONSTRUCTION SITES	industiral
GREEN URBAN AREAS	urban/service
SPORT AND LEISURE FACILITIES	urban/service
NON-IRRIGATED ARABLE LAND	agriculture
PERMANENTLY IRRIGATED LAND	agriculture
RICE FIELDS	agriculture
VINEYARDS	agriculture
FRUIT TREES AND BERRY PLANTATIONS	agriculture
OLIVE GROWES	agriculture
PASTURES	agriculture
ANNUAL CROPS ASSOCIATED WITH PERMANENT CROPS	agriculture
COMPLEX CULTIVATION PATTERNS	agriculture
LAND PRINCIPALLY OCCUPIED BY AGRICULTURE, WITH SIGNIFICANT AREAS OF NATURAL VEGETATION	agriculture
AGRO-FORESTRY AREAS	agriculture
BROAD-LEAVED FOREST	non GDP Generating
CONIFEROUS FOREST	non GDP Generating
MIXED FOREST	non GDP Generating
NATURAL GRASSLAND	non GDP Generating
MOORS AND HEATHLAND	non GDP Generating
SCLEROPHYLLOUS VEGETATION	non GDP Generating
TRANSITIONAZL WOODLAND-SHRUB	non GDP Generating
BEACHES, DUNES, AND SAND PLAINS	non GDP Generating
BARE ROCK	non GDP Generating
SPARSELY VEGETATED AREAS	non GDP Generating
BURNT AREAS	non GDP Generating
GLACIERS AND PERPETUAL SNOW	non GDP Generating
INLAND MARSHES	non GDP Generating
PEATBOGS	non GDP Generating
SALT-MARSHES	non GDP Generating
SALINES	non GDP Generating
INTERTIDAL FLATS	non GDP Generating
WATER COURSES	non GDP Generating
WATER BODIES	non GDP Generating
COASTAL LAGOONS	non GDP Generating
ESTUARIES	non GDP Generating
SEA AND OCEAN	non GDP Generating

Percentage of Landuse by radiance value

Radiance	urban/service	industrial	agriculture	nonGDP generating
15	3.25	0.34	65.17	31.24
19	3.71	0.45	66.55	29.29
23	3.97	0.55	66.27	29.21
27	4.35	0.71	65.12	29.82
32	4.89	0.85	64.56	29.7
36	5.64	1	63.53	29.84
42	6.44	1.25	62.98	29.33
47	7.59	1.39	62.17	28.85
52	8.33	1.63	61.38	28.66
58	9.59	1.9	60.28	28.23
64	10.94	2.15	59.7	27.21
70	12.17	2.36	59.58	25.9
76	13.22	2.8	58.62	25.36
83	14.68	2.81	57.31	25.2
89	16.17	3.23	56.61	23.98
96	16.83	3.29	55.45	24.43
103	18.72	3.75	54.01	23.52
110	19.98	4.19	52.6	23.23
118	21.05	4.6	52.36	22
125	22.9	4.8	50.59	21.71
133	24.38	4.99	48.75	21.88
140	25.59	5.35	47.77	21.28
148	27.36	5.42	46.58	20.65
156	28.36	6.01	44.45	21.19
164	29	5.86	45	20.14
173	31.25	6.41	42.43	19.91
181	32.82	6.48	40.86	19.83
190	33.84	6.23	41	18.93
198	35.17	6.9	39.04	18.89
207	37.17	7.2	36.61	19.02
216	37.97	8.17	34.99	18.88
225	39.68	6.97	34.37	18.98
234	40.32	7.72	33.8	18.16
244	41.96	7.84	32.84	17.36
253	43.67	7.78	32.57	15.97
263	45.01	8.87	29.86	16.26
272	45.31	8.68	29.48	16.53
282	45.55	9.17	28.48	16.8
292	48.35	9.44	27.28	14.93
302	48.93	8.09	26.69	16.29
312	49.42	8.01	27.62	14.94
322	44.6	10.07	27.19	18.15
333	48.38	8.44	26.36	16.83
343	50.23	9.63	23.9	16.24
354	49.84	9.9	26.14	14.12
364	51.79	8.72	23.73	15.77
375	51.04	10.67	23.76	14.53
386	50.73	10.08	24.5	14.7
397	53.96	8.36	22.66	15.02
408	51.75	9.84	22.53	15.87
419	54.05	11.12	19.68	15.15

Radiance	urban/service	industrial	agriculture	nonGDP generating
430	52.56	11.42	20.2	15.83
442	55.37	9.85	20.28	14.49
453	53.99	10.78	20.9	14.33
465	54.36	12.89	18.48	14.26
476	59.48	8.88	17.76	13.88
488	58.15	9.37	16.77	15.71
500	60.68	7.61	16.14	15.58
512	51.39	11.72	20.68	16.21
524	58.1	9.67	17.16	15.07
536	57.84	10.02	17.66	14.47
548	60.04	7.88	15.89	16.19
561	61.71	9.47	14.85	13.97
573	54.39	11.26	14.68	19.67
586	59.55	9.61	14.96	15.88
598	60.3	7.85	14.39	17.45
611	54.42	8.75	19.64	17.19
624	55.93	10.13	18.75	15.18
637	64.09	8.7	15.4	11.8
650	54.94	9.83	16.83	18.41
663	55.18	9.06	17.67	18.09
676	60.61	8.75	14.91	15.72
689	58.33	10.71	15.41	15.55
702	61.98	6.23	17.14	14.65
716	51.07	9.49	17.28	22.16
729	51.2	10.53	16.48	21.79
743	56.05	9.83	16.36	17.76
756	49.31	8.82	21.03	20.84
770	57.67	7.04	14.36	20.93
784	51.24	8.05	18.4	22.3
798	52.91	6.85	16.76	23.48
811	62.25	10.7	15.49	11.55
826	50.77	9.32	21.03	18.88
840	59.18	6.78	16.07	17.97
854	55.72	6.71	16.23	21.34
868	50.52	12.31	22.76	14.4
882	52.79	10.85	13.26	23.1
897	50	9.4	20.54	20.06
911	62.75	7.77	17.06	12.42
926	54.25	6.52	17.28	21.95
941	63.88	5.52	14.83	15.78
955	51.64	3.05	22.29	23.02
970	49.07	9.3	17.21	24.42
985	54.25	8.51	26	11.24
1000	60.7	7.99	8.81	22.49
1015	56.11	11.1	14.96	17.83
1030	57.39	8.99	16.81	16.81
1045	55.4	7.32	24.04	13.24
1061	65.54	9.38	12.61	12.46
1076	56.49	11.18	11.18	21.16
1091	64.17	9.76	5.63	20.45
1107	50.25	15.87	15.7	18.18
1122	65.25	7	9	18.75
1138	62.35	6.57	13.75	17.33
1154	66.16	13.5	10.08	10.27

Radiance	urban/service	industrial	agriculture	nonGDP generating
1169	57.88	4.91	10.85	26.36
1185	52.46	14.78	12.17	20.58
1201	62.78	13.42	5.06	18.73
1217	51.76	4.52	32.91	10.8
1233	71.7	5.66	14.34	8.3
1249	44.03	8.21	31.72	16.04
1266	55.76	5.07	17.05	22.12
1282	54.41	8.81	13.68	23.1
1298	68.51	6.57	6.23	18.69
1315	56.61	7.73	16.96	18.7
1331	53.13	5.21	23.96	17.71
1348	52.43	5.34	20.39	21.84
1364	75.94	12.03	4.51	7.52
1381	66.2	10.56	11.27	11.97
1398	33.16	5.1	45.41	16.33
1414	48.19	12.44	16.58	22.8
1431	63.28	7.81	14.06	14.84
1448	63.18	0.5	19.9	16.42
1465	52.46	5.74	8.2	33.61
1482	60.65	8.33	7.87	23.15
1499	15.03	16.34	26.14	42.48
1517	58.29	16.04	17.65	8.02
1534	67.88	18.13	5.7	8.29
1551	76.07	7.69	10.26	5.98
1569	54.89	9.02	25.56	10.53
1586	51.35	0	33.11	15.54
1604	72.07	5.59	0	22.35
1621	45.54	1.98	21.78	30.69
1639	78.38	0	9.46	12.16
1657	58.82	10.59	12.94	17.65
1674	58.37	13.88	18.66	9.09
1692	69.07	4.12	19.59	7.22
1710	65.38	0.96	9.62	24.04
1728	59.57	18.09	22.34	0
1746	75.45	4.55	0	20
1764	61.41	9.78	12.5	16.3
1782	50	8.33	15.97	25.69
1800	87.6	4.65	0	7.75
1819	87.5	0	0	12.5
1837	63.81	3.81	11.43	20.95
1856	70.77	0	7.69	21.54
1874	74.53	5.59	11.8	8.07
1893	75	2.63	0	22.37
1911	64.29	0	7.14	28.57
1930	66.67	8.33	6.67	18.33
1948	100	0	0	0
1967	94.64	0	3.57	1.79
1986	72.73	7.39	7.95	11.93
2005	92.86	4.76	2.38	0
2024	60.53	10.53	2.63	26.32
2043	87.5	0	12.5	0
2062	92.86	0	3.57	3.57
2081	78.13	12.5	0	9.38
2100	87.5	0	0	12.5

Radiance	urban/service	industrial	agriculture	nonGDP generating
2119	100	0	0	0
2139	76.32	1.32	0	22.37
2158	76.47	0	0	23.53
2178	89.86	4.35	0	5.8
2197	81.67	18.33	0	0
2217	60	22.5	0	17.5
2236	100	0	0	0
2256	0	0	0	0
2275	100	0	0	0
2295	79.55	0	0	20.45
2315	75	0	0	25
2335	90	3.33	0	6.67
2355	100	0	0	0
2375	100	0	0	0
2395	97.5	0	0	2.5
2415	100	0	0	0
2435	100	0	0	0
2455	0	0	0	0
2476	100	0	0	0
2496	100	0	0	0
2516	100	0	0	0
2537	100	0	0	0
2557	79.55	0	0	20.45
2578	97.37	0	0	2.63
2598	100	0	0	0
2640	100	0	0	0
2681	100	0	0	0
2702	93.75	0	0	6.25
2723	100	0	0	0
2744	100	0	0	0
2786	100	0	0	0
2828	100	0	0	0
2871	100	0	0	0
2892	100	0	0	0
2914	100	0	0	0
2935	100	0	0	0
2957	100	0	0	0
3043	100	0	0	0
4072	100	0	0	0

Appendix E

Chapter 7 Data tables

France	NUTS-3, Density Mapping (NUTS-3), Simulated Regions
Denmark	NUTS-3, Density Mapping (NUTS-3)
United States	State
Portugal	NUTS-3
Italy	NUTS-3, Density Mapping (NUTS-3), Simulated Regions
Spain	NUTS-3, Density Mapping (NUTS-3), Simulated Regions
Great Britain	NUTS-3, Density Mapping (NUTS-3)
Ireland	NUTS-3
Belgium	NUTS-3
Germany	NUTS-2
Greece	NUTS-3, Simulated Regions
Netherlands	NUTS-2

France

Outiers: Paris, Ile-de-France

NUTS-3 Region	Estimated GRP	Official GRP	Percentage Difference
Ain	15417.61	9323.50	65.36
Aisne	9105.23	8957.60	1.65
Allier	6819.21	5755.20	18.49
Alpes-de-Haute-Provence	3971.57	2327.00	70.67
Alpes-Maritimes	17693.06	19177.90	-7.74
Ardèche	5430.78	4362.50	24.49
Ardennes	5939.20	4719.60	25.84
Ariège	4171.40	2116.30	97.11
Aube	6107.18	5345.70	14.24
Aude	7571.30	4574.30	65.52
Aveyron	3442.40	4392.80	-21.64
Bas-Rhin	21681.47	22771.30	-4.79
Bouches-du-Rhône	37603.93	36043.50	4.33
Calvados	11664.56	11483.20	1.58
Cantal	2861.76	2232.70	28.17
Charente	4930.77	6341.10	-22.24
Charente-Maritime	6919.18	8419.80	-17.82
Cher	7816.97	5505.40	41.99
Corrèze	3423.71	3799.70	-9.90
Corse-du-Sud	2877.32	2012.20	42.99
Côte-d'Or	14329.54	11600.80	23.52
Côte-du-Nord	4351.90	8273.90	-47.40
Creuse	1833.32	1705.40	7.50
Deux-Sèvres	3108.02	5851.90	-46.89
Dordogne	4143.35	5541.90	-25.24
Doubs	10002.50	9829.00	1.77
Drôme	11269.67	8686.80	29.73
Essonne	15584.81	25382.20	-38.60
Eure	10260.26	8972.80	14.35
Eure-et-Loir	6659.77	7292.10	-8.67
Finistère	6116.16	15459.60	-60.44
Gard	13566.21	10166.20	33.44
Gers	2955.07	2762.50	6.97
Gironde	22246.85	26977.30	-17.53
Haute-Corse	3223.53	2137.30	50.82
Haute-Garonne	24080.05	22206.70	8.44
Haute-Loire	6098.38	3092.30	97.21
Haute-Marne	4063.86	3440.20	18.13
Hautes-Alpes	6484.15	2204.90	194.08
Haute-Saône	5103.87	3256.30	56.74
Haute-Savoie	19129.46	13236.60	44.52
Hautes-Pyrénées	6022.98	3800.10	58.50
Haute-Vienne	8125.67	6541.70	24.21
Haut-Rhin	14427.58	14019.10	2.91
Hauts-de-Seine	70890.66	68266.00	3.84
Hérault	21355.96	14720.70	45.07
Ille-et-Vilaine	11881.15	16256.50	-26.91
Indre	4328.05	3899.20	11.00
Indre-et-Loire	6194.77	10145.40	-38.94
Isère	24321.95	22941.10	6.02
Jura	4998.66	4457.10	12.15
Landes	6561.61	5725.30	14.61
Loire	18468.16	12688.30	45.55
Loire-Atlantique	20166.95	21376.00	-5.66
Loiret	11307.58	13397.70	-15.60

NUTS-3 Region	Estimated GRP	Official GRP	Percentage Difference
Loir-et-Cher	4500.00	5586.90	-19.45
Lot	994.79	2459.50	-59.55
Lot-et-Garonne	4126.98	4916.90	-16.07
Lozère	1196.67	1038.00	15.29
Maine-et-Loire	10559.46	12338.50	-14.42
Manche	5208.98	8631.10	-39.65
Marne	15160.52	12218.70	24.08
Mayenne	3354.65	5156.40	-34.94
Meurthe-et-Moselle	20698.39	12815.10	61.52
Meuse	5930.46	3109.00	90.75
Morbihan	5713.40	10792.00	-47.06
Moselle	28454.16	17344.20	64.06
Nièvre	4752.37	3716.40	27.88
Nord	38910.11	44079.40	-11.73
Oise	14826.35	13424.80	10.44
Orne	3726.36	4993.90	-25.38
Paris	131654.09	126239.10	4.29
Pas-de-Calais	18973.19	21049.40	-9.86
Puy-de-Dôme	16998.44	11537.60	47.33
Pyrénées-Atlantiques	12600.32	10810.00	16.56
Pyrénées-Orientales	10523.97	5895.60	78.51
Rhône	30099.09	39908.50	-24.58
Saône-et-Loire	10333.78	9467.40	9.15
Sarthe	5771.39	9380.10	-38.47
Savoie	15890.20	8242.50	92.78
Seine-et-Marne	22417.04	21741.40	3.11
Seine-Maritime	19261.70	24734.10	-22.12
Seine-Saint-Denis	19777.62	29309.30	-32.52
Somme	8069.75	9699.00	-16.80
Tarn	4595.63	5155.30	-10.86
Tarn-et-Garonne	2811.45	3305.00	-14.93
Territoire de Belfort	3083.81	2440.30	26.37
Val-de-Marne	10603.84	27738.50	-61.77
Val-d'Oise	14799.02	21299.40	-30.52
Var	22020.09	15607.70	41.08
Vaucluse	12473.23	8691.30	43.51
Vendée	7621.00	8872.80	-14.11
Vienne	6087.95	6928.00	-12.13
Vosges	12829.95	6715.40	91.05
Yonne	5963.78	5734.70	3.99
Yvelines	19721.20	33110.80	-40.44
Percentage Mean Absolute Difference			32.07
Standard Deviation			42.08

Density relationship

Best fit: 2nd order polymonial on log-log space $y = 0.7495x^2 - 1.8688x + 1.6814$; $R^2 = 0.8573$

NUTS-3 Region	Estimated GRP	Official GRP	Percentage Difference
Ain	15534.56	9323.50	66.62
Aisne	9621.46	8957.60	7.41
Allier	7449.68	5755.20	29.44
Alpes-de-Haute-Provence	3795.18	2327.00	63.09
Alpes-Maritimes	34242.82	19177.90	78.55
Ardèche	5371.81	4362.50	23.14
Ardennes	6237.63	4719.60	32.16

NUTS-3 Region	Estimated GRP	Official GRP	Percentage Difference
Ariège	3889.35	2116.30	83.78
Aube	8001.63	5345.70	49.68
Aude	8272.15	4574.30	80.84
Aveyron	3528.39	4392.80	-19.68
Bas-Rhin	29091.84	22771.30	27.76
Bouches-du-Rhône	66833.81	36043.50	85.43
Calvados	14570.32	11483.20	26.88
Cantal	2862.67	2232.70	28.22
Charente	5650.93	6341.10	-10.88
Charente-Maritime	7400.74	8419.80	-12.10
Cher	8817.68	5505.40	60.16
Corrèze	3584.19	3799.70	-5.67
Corse-du-Sud	3122.49	2012.20	55.18
Côte-d'Or	21831.26	11600.80	88.19
Côtes-d'Armor	4256.40	8273.90	-48.56
Creuse	1810.49	1705.40	6.16
Deux-Sèvres	3232.92	5851.90	-44.75
Dordogne	4516.85	5541.90	-18.50
Doubs	12317.63	9829.00	25.32
Drôme	12570.70	8686.80	44.71
Essonne	25724.45	25382.20	1.35
Eure	9588.92	8972.80	6.87
Eure-et-Loir	6870.23	7292.10	-5.79
Finistère	6360.99	15459.60	-58.85
Gard	17240.67	10166.20	69.59
Gers	2842.89	2762.50	2.91
Gironde	33807.82	26977.30	25.32
Haute-Corse	3282.11	2137.30	53.56
Haute-Garonne	44636.85	22206.70	101.01
Haute-Loire	5872.06	3092.30	89.89
Haute-Marne	4528.77	3440.20	31.64
Hautes-Alpes	6450.38	2204.90	192.55
Haute-Saône	5160.05	3256.30	58.46
Haute-Savoie	20168.76	13236.60	52.37
Hautes-Pyrénées	6023.26	3800.10	58.50
Haute-Vienne	11396.41	6541.70	74.21
Haut-Rhin	17311.81	14019.10	23.49
Hauts-de-Seine	55505.05	68266.00	-18.69
Hérault	35302.65	14720.70	139.82
Ille-et-Vilaine	14593.55	16256.50	-10.23
Indre	5124.43	3899.20	31.42
Indre-et-Loire	8162.67	10145.40	-19.54
Isère	29208.02	22941.10	27.32
Jura	4853.48	4457.10	8.89
Landes	6394.56	5725.30	11.69
Loire	28269.14	12688.30	122.80
Loire-Atlantique	29505.83	21376.00	38.03
Loiret	13769.90	13397.70	2.78
Loir-et-Cher	4671.56	5586.90	-16.38
Lot	965.99	2459.50	-60.72
Lot-et-Garonne	4208.53	4916.90	-14.41
Lozère	1201.03	1038.00	15.71
Maine-et-Loire	12669.09	12338.50	2.68
Manche	5155.44	8631.10	-40.27
Marne	21703.82	12218.70	77.63
Mayenne	3508.56	5156.40	-31.96
Meurthe-et-Moselle	31665.17	12815.10	147.09
Meuse	6158.99	3109.00	98.10
Morbihan	5791.80	10792.00	-46.33
Moselle	43142.40	17344.20	148.74

NUTS-3 Region	Estimated GRP	Official GRP	Percentage Difference
Nièvre	4712.60	3716.40	26.81
Nord	72850.80	44079.40	65.27
Oise	14873.08	13424.80	10.79
Orne	3846.10	4993.90	-22.98
Paris	87112.62	126239.10	-30.99
Pas-de-Calais	22997.02	21049.40	9.25
Puy-de-Dôme	25825.26	11537.60	123.84
Pyrénées-Atlantiques	15404.97	10810.00	42.51
Pyrénées-Orientales	12507.07	5895.60	112.14
Rhône	71890.54	39908.50	80.14
Saône-et-Loire	10539.00	9467.40	11.32
Sarthe	7199.03	9380.10	-23.25
Savoie	15993.40	8242.50	94.04
Seine-et-Marne	28172.82	21741.40	29.58
Seine-Maritime	26765.67	24734.10	8.21
Seine-St-Denis	98071.34	29309.30	234.61
Somme	8932.15	9699.00	-7.91
Tarn	4712.36	5155.30	-8.59
Tarn-et-Garonne	2776.17	3305.00	-16.00
Territoire-de-Belfort	3694.84	2440.30	51.41
Val-de-Marne	36200.94	27738.50	30.51
Val-d'Oise	31278.88	21299.40	46.85
Var	30265.20	15607.70	93.91
Vaucluse	14943.56	8691.30	71.94
Vendée	7447.43	8872.80	-16.06
Vienne	7080.06	6928.00	2.19
Vosges	13444.75	6715.40	100.21
Yonne	6225.29	5734.70	8.55
Yvelines	30420.00	33110.80	-8.13
Percentage Mean Absolute Difference			47.38
Standard Deviation			54.40

Simulated Regions

NUTS-1

	Estimated GRP	Official GRP	Percentage Difference
fr1 Île de France	305448.28	353086.60	-13.49
fr2 Bassin Parisien	189580.56	192966.60	-1.75
fr3 Nord - Pas-de-Calais	57883.30	65128.90	-11.13
fr4 Est	127210.85	96756.90	31.47
fr5 Ouest	96581.98	135446.50	-28.69
fr6 Sud-Ouest	112135.55	112216.30	-0.07
fr7 Centre-Est	172804.72	142007.80	21.69
fr8 Méditerranée	160560.97	124596.60	28.86
Percentage Mean Absolute Difference			17.15
Standard Deviation			21.83

Ranked by Official GRP

NUTS-3 Regions	Estimated GRP	Official GRP	Percentage Difference
Lozère, Creuse, Corse-du-Sud, Ariège, Haute-Corse, Hautes-Alpes, Cantal, Alpes-de-Haute-Provence, Territoire-de-Belfort, Lot, Gers, Haute-Loire	39751.76	26528.40	49.85
Meuse, Haute-Saône, Tarn-et-Garonne, Haute-Marne, Nièvre, Corrèze, Hautes-Pyrénées, Indre, Ardèche, Aveyron, Jura, Aude	57879.87	46112.60	25.52
Ardennes, Lot-et-Garonne, Orne, Tarn, Mayenne, Aube, Cher, Dordogne, Loir-et-Cher, Landes, Yonne, Allier	63654.92	64137.20	-0.75
Deux-Sèvres, Pyrénées-Orientales, Charente, Haute-Vienne, Vosges Eure-et-Loir,, Vienne, Savoie, Côtes-d'Armor, Charente-Maritime, Manche, Drôme	95906.01	87819.90	9.21
Vaucluse, Vendée, Aisne, Eure, Ain, Sarthe, Saône-et-Loire, Somme, Doubs, Indre-et-Loire, Gard, Morbihan	114529.12	114297.10	0.20
Pyrénées-Atlantiques, Calvados, Puy-de-Dôme, Côte-d'Or, Marne, Maine-et-Loire, Loire, Meurthe-et-Moselle, Haute-Savoie, Loiret, Oise, Haut-Rhin	180170.38	149570.40	20.46
Hérault, Finistère, Var, Ille-et-Vilaine, Moselle, Alpes-Maritimes, Pas-de-Calais, Val-d'Oise, Loire-Atlantique, Seine-et-Marne, Haute-Garonne, Bas-Rhin	229638.30	229010.80	0.27
Isère, Seine-Maritime, Essonne, Gironde, Val-de-Marne, Seine-St-Denis, Yvelines, Bouches-du-Rhône, Rhône, Nord, Hauts-de-Seine, Paris	440675.85	504729.80	-12.69
Percentage Mean Absolute Difference			14.87
Standard Deviation			19.79

Ranked by estimates

NUTS-3 Regions	Estimated GRP	Official GRP	Percentage Difference
Lot, Lozère, Creuse, Tarn-et-Garonne, Cantal, Corse-du-Sud, Gers, Territoire de Belfort, Deux-Sèvres, Haute-Corse, Mayenne, Corrèze	31724.09	34900.90	-9.10
Aveyron, Orne, Alpes-de-Haute-Provence, Haute-Marne, Lot-et-Garonne, Dordogne, Ariège, Indre, Côte-du-Nord, Loir-et-Cher, Tarn, Nièvre	50173.85	54360.70	-7.70
Charente, Jura, Haute-Saône, Manche, Ardèche, Morbihan, Sarthe, Meuse, Ardennes, Yonne, Hautes-Pyrénées, Vienne	67102.21	71511.60	-6.17
Haute-Loire, Aube, Finistère, Indre-et-Loire, Hautes-Alpes, Landes, Eure-et-Loir, Allier, Charente-Maritime, Aude, Vendée, Cher	80969.68	82392.80	-1.73
Somme, Haute-Vienne, Aisne, Doubs, Eure, Saône-et-Loire, Pyrénées-Orientales, Maine-et-Loire, Val-de-Marne, Drôme, Loiret, Calvados	121826.25	133007.80	-8.41
Ille-et-Vilaine, Vaucluse, Pyrénées-Atlantiques, Vosges, Gard, Côte-d'Or, Haut-Rhin, Val-d'Oise, Oise, Marne, Ain, Essonne	167896.30	159907.90	5.00
Savoie, Puy-de-Dôme, Alpes-Maritimes, Loire, Pas-de-Calais, Haute-Savoie, Seine-Maritime, Yvelines, Seine-Saint-Denis, Loire-Atlantique, Meurthe-et-Moselle, Hérault	228134.32	221998.30	2.76
Bas-Rhin, Var, Gironde, Seine-et-Marne, Haute-Garonne, Isère, Moselle, Rhône, Bouches-du-Rhône, Nord, Hauts-de-Seine, Paris	474379.49	464126.20	2.21
Percentage Mean Absolute Difference			5.38
Standard Deviation			2.91

Alphabet

NUTS-3 Regions	Estimated GRP	Official GRP	Percentage Difference
Ain - Bas-Rhin	107350.41	93823.70	14.42
Bouches-du-Rhone - Deux Sevres	123402.45	126040.90	-2.09
Dordogne - Haute Garonne	133216.25	151266.30	-11.93
Haute-Loire - Indre	201991.81	174940.30	15.46
Indre-et-Loire - Maine-et-Loire	117725.62	120969.90	-2.68
Manche - Paris	288949.28	274858.60	5.13
Puy-de-Dome - Somme	322370.57	328014.00	-1.72
Tarn - Yvelines	130680.70	155298.20	-15.85
Percentage Mean Absolute Difference			8.66
Standard Deviation			11.22

Denmark

Outliers: København og Frederiksberg Kommuner, Københavns amt

NUTS-1 Region	Estimated GRP	Official GRP	Percentage Difference
dk001 København og Frederiksberg Kommuner	*4231.08*	*26755.60*	*-84.19*
dk002 Københavns amt	*9734.59*	*21633.20*	*-55.00*
dk007 Bornholms amt	527.50	938.70	-43.81
dk003 Frederiksborg amt	5472.83	7990.90	-31.51
dk00e Viborg amt	5070.22	6091.50	-16.77
dk009 Sønderjyllands amt	5656.56	6668.20	-15.17
dk00a Ribe amt	5738.05	6265.70	-8.42
dk00f Nordjyllands amt	11169.84	12152.70	-8.09
dk00d Århus amt	14665.71	15908.70	-7.81
dk006 Storstrøms amt	5163.27	5224.80	-1.18
dk00c Ringkøbing amt	8222.82	7597.60	8.23
dk00b Vejle amt	10301.93	8929.00	15.38
dk004 Roskilde amt	5296.82	4551.10	16.39
dk008 Fyns amt	13816.35	11455.50	20.61
dk005 Vestsjællands amt	8579.70	7005.80	22.47
Percentage Mean Absolute Difference			16.60
Standard Deviation			32.70

Density Mapping

Best fit: linear in log-log space $y = 1.7252x - 2.1018$; $R^2 = 0.9411$

NUTS-1 Region	Estimated GRP	Official GRP	Percentage Difference
Kobenhavn og Frederiksberg Kommuner	21474.57	26755.60	-19.74
Kobenhavns Amt	28822.60	21633.20	33.23
Frederiksborg Amt	250.26	7990.90	-96.87
Roskilde Amt	8191.96	4551.10	80.00
Vestsjællands Amt	9941.08	7005.80	41.90
Storstroms Amt	5557.33	5224.80	6.36
Bornholms Amt	309.47	938.70	-67.03
Fyns Amt	25276.10	11455.50	120.65
Sonderjyllands Amt	4601.50	6668.20	-30.99
Ribe Amt	7008.36	6265.70	11.85
Vejle Amt	14536.14	8929.00	62.80
Ringkobing Amt	9757.62	7597.60	28.43
Århus Amt	31862.87	15908.70	100.29
Viborg Amt	4856.06	6091.50	-20.28
Nordjyllands Amt	14913.46	12152.70	22.72
Percentage Mean Absolute Difference			48.05
Standard Deviation			57.75

United States

Outliers: New York, California

State	Estimated GSP	Official GSP	Percentage Difference
New York	*283868.84*	*663377.00*	*-57.21*
California	*464509.63*	*1045254.00*	*-55.56*
Alaska	47093.05	26575.00	77.21
District of Columbia	11177.48	50546.00	-77.89
Hawaii	9200.55	38537.00	-76.13
Connecticut	65342.20	134968.00	-51.59
Oregon	48648.73	97510.00	-50.11
Massachusetts	118602.45	223571.00	-46.95
New Jersey	178078.05	299986.00	-40.64
Virginia	133901.27	212105.00	-36.87
Washington	111513.72	175242.00	-36.37
Delaware	20208.25	31263.00	-35.36
Rhode Island	19261.02	29409.00	-34.51
North Carolina	157337.08	221629.00	-29.01
Georgia	179584.39	235733.00	-23.82
Pennsylvania	264704.53	347306.00	-23.78
Vermont	12374.23	15510.00	-20.22
Maryland	130951.22	154646.00	-15.32
Utah	48836.70	55070.00	-11.32
Arizona	109993.39	122273.00	-10.04
New Hampshire	33963.30	37470.00	-9.36
Florida	356502.31	389473.00	-8.47
Texas	558163.69	608622.00	-8.29
Colorado	119794.39	129575.00	-7.55
West Virginia	35585.41	38281.00	-7.04
Ohio	308250.50	326451.00	-5.58
Illinois	384799.22	400327.00	-3.88
South Carolina	91814.78	95447.00	-3.81
Kansas	73943.93	72998.00	1.30
Missouri	158746.67	155811.00	1.88
Louisiana	131354.42	123549.00	6.32
Michigan	298788.84	279503.00	6.90
Maine	32655.75	30409.00	7.39
New Mexico	51606.53	47829.00	7.90
Mississippi	64371.39	58743.00	9.58
Alabama	114494.02	104213.00	9.87
Nevada	65218.64	59248.00	10.08
Idaho	33326.87	29388.00	13.40
Arkansas	67195.61	59141.00	13.62
Kentucky	120655.87	101535.00	18.83
Nebraska	59510.27	49275.00	20.77
Oklahoma	96397.73	79423.00	21.37
Tennessee	206881.50	151738.00	36.34
Iowa	119031.01	81695.00	45.70
Indiana	238983.41	162953.00	46.66
Minnesota	232156.44	152334.00	52.40
Wyoming	27638.93	16244.00	70.15
Wisconsin	266997.03	148194.00	80.17
Montana	39035.59	18907.00	106.46
South Dakota	43349.75	19767.00	119.30
North Dakota	44221.74	15910.00	177.95
Percentage Mean Absolute Difference			33.38
Standard Deviation			48.42

Portugal

Outlier: Grande Lisboa

NUTS-3 Region	Estimated GRP	Official GRP	Percentage Difference
Grande Lisboa	*15420.89*	*29393.50*	*-47.54*
Pinhal Interior Norte	517.47	740.40	-30.11
Baixo Mondego	2168.49	2811.10	-22.86
Alentejo Litoral	882.65	1108.60	-20.38
Peninsula de Setúbal	4629.41	5680.40	-18.50
Grande Porto	10806.75	12468.40	-13.33
Entre Douro E Vouga	1886.07	2168.00	-13.00
Cavado	2549.94	2629.20	-3.01
Cova da Beira	549.34	556.10	-1.22
Pinhal Interior Sul	291.94	285.40	2.29
Ave	3864.72	3758.40	2.83
Dao-Lafoes	1745.79	1685.60	3.57
Baixo Vouga	3419.15	3277.30	4.33
Medio Tejo	1967.67	1845.10	6.64
Alentejo Central	1397.56	1292.00	8.17
Douro	1686.04	1547.00	8.99
Baixo Alentejo	916.16	818.80	11.89
Pinhal Litoral	2264.86	2017.60	12.26
Minho-Lima	1876.85	1551.40	20.98
Oeste	3890.46	3195.30	21.76
Alto Alentejo	1089.35	876.60	24.27
Serra da Estrela	319.33	246.90	29.34
Leziria Do Tejo	2890.33	2205.80	31.03
Tamega	3755.45	2693.60	39.42
Beira Interior Sul	773.76	550.00	40.68
Alto Tras-Os-Montes	1930.90	1337.50	44.37
Beira Interior Norte	1018.63	685.30	48.64
Algarve	4694.92	3053.80	53.74
Percentage Mean Absolute Difference			19.91
Standard Deviation			22.92

Italy

Outlier: Milano

NUTS-3 Region	Estimated GRP	Official GRP	Percentage Difference
Milano	*47929.94*	*104630.60*	*-54.19*
Agrigento	8487.00	4782.40	77.46
Alessandria	8909.72	8292.00	7.45
Ancona	7519.34	8574.20	-12.30
Aosta	7650.65	2761.70	177.03
Arezzo	6544.55	5861.30	11.66
Ascoli Piceno	8041.95	6288.00	27.89
Asti	5177.62	3643.70	42.10
Avellino	8335.46	5224.00	59.56
Bari	22766.63	19333.10	17.76
Belluno	6237.40	4457.20	39.94
Benevento	5058.59	3372.20	50.01
Bergamo	18783.12	20343.00	-7.67
Biella	3036.17	3885.90	-21.87
Bologna	15182.86	22905.10	-33.71
Bolzano	11173.94	11548.20	-3.24
Brescia	22290.49	23473.70	-5.04
Brindisi	8531.63	5004.60	70.48
Cagliari	11311.89	10330.30	9.50
Caltanissetta	5096.01	3062.00	66.43

NUTS-3 Region	Estimated GRP	Official GRP	Percentage Difference
Campobasso	3859.89	3194.10	20.84
Caserta	13153.84	9727.10	35.23
Catania	14443.05	12083.80	19.52
Catanzaro	5948.11	4495.60	32.31
Chieti	5634.38	5890.60	-4.35
Como	8607.58	10886.60	-20.93
Cosenza	10149.00	8004.80	26.79
Cremona	8000.30	6752.40	18.48
Crotone	1324.52	1635.20	-19.00
Cuneo	15734.71	11439.80	37.54
Enna	3270.57	1810.80	80.61
Ferrara	6300.38	6647.60	-5.22
Firenze	20094.21	21165.70	-5.06
Foggia	11717.18	7449.30	57.29
Forlì-Cesena	6803.86	7378.50	-7.79
Frosinone	10462.73	7903.80	32.38
Genova	10879.72	17070.60	-36.27
Gorizia	2004.01	2654.20	-24.50
Grosseto	2950.19	3377.30	-12.65
Imperia	3335.96	4232.90	-21.19
Isernia	1588.54	1508.10	5.33
La Spezia	3198.36	4157.50	-23.07
L'Aquila	7500.26	4417.80	69.77
Latina	10386.45	8275.00	25.52
Lecce	16028.06	8356.40	91.81
Lecco	4828.03	6432.60	-24.94
Livorno	4902.00	6149.40	-20.28
Lodi	4802.77	3750.20	28.07
Lucca	7501.96	6830.40	9.83
Macerata	6006.22	5281.20	13.73
Mantova	10293.07	8556.00	20.30
Massa-Carrara	3041.17	3034.80	0.21
Matera	3993.14	2602.60	53.43
Messina	6258.98	8440.00	-25.84
Modena	12270.62	15239.00	-19.48
Napoli	24692.73	34613.00	-28.66
Novara	5331.11	7087.40	-24.78
Nuoro	4029.65	3480.70	15.77
Oristano	2711.18	2023.00	34.02
Padova	16731.06	17623.80	-5.07
Palermo	11857.40	14303.50	-17.10
Parma	9334.02	9302.30	0.34
Pavia	10580.13	9115.10	16.07
Perugia	10969.26	10861.00	1.00
Pesaro e Urbino	6270.66	6087.90	3.00
Pescara	3894.01	4412.80	-11.76
Piacenza	5606.09	5471.20	2.47
Pisa	8397.38	7694.80	9.13
Pistoia	4591.05	4811.30	-4.58
Pordenone	6941.88	6009.30	15.52
Potenza	5752.81	5096.70	12.87
Prato	3717.00	5054.50	-26.46
Ragusa	6799.43	3798.90	78.98
Ravenna	8597.65	7030.50	22.29
Reggio di Calabria	5755.73	6413.90	-10.26
Reggio nell Emilia	8654.11	10316.90	-16.12
Rieti	3792.74	2316.20	63.75
Rimini	4787.60	5794.80	-17.38
Roma	53179.71	81656.00	-34.87
Rovigo	5496.10	4364.10	25.94
Salerno	11720.99	13318.70	-12.00
Sassari	8817.20	6383.60	38.12
Savona	4448.91	5481.90	-18.84
Siena	3817.45	4820.20	-20.80
Siracusa	6567.56	5759.30	14.03

NUTS-3 Region	Estimated GRP	Official GRP	Percentage Difference
Sondrio	5893.47	3293.60	78.94
Taranto	12767.76	6720.10	89.99
Teramo	5249.14	4401.20	19.27
Terni	4661.14	3647.10	27.80
Torino	38081.58	49109.40	-22.46
Trapani	8686.85	4863.90	78.60
Trento	15412.69	10263.80	50.17
Treviso	15104.86	16378.20	-7.77
Trieste	2601.63	4949.90	-47.44
Udine	12598.19	10421.10	20.89
Varese	11014.11	16606.10	-33.67
Venezia	12546.24	16873.60	-25.65
Verbano-Cusio-Ossola	3233.78	2709.50	19.35
Vercelli	3968.74	3578.90	10.89
Verona	17516.97	17139.50	2.20
Vibo Valentia	1921.51	1722.80	11.53
Vicenza	14107.16	17642.70	-20.04
Viterbo	6477.72	4561.40	42.01
Percentage Mean Absolute Difference			28.44
Standard Deviation			36.61

Simulated Regions

NUTS-1

NUTS-1 Region	Estimated GRP	Official GRP	Percentage Difference
it1 Nord Ovest	112987.03	123451.20	-8.48
it2 Lombardia	211989.27	213839.90	-0.87
it3 Nord Est	138472.13	140325.60	-1.32
it4 Emilia-Romagna	77537.19	90085.90	-13.93
it5 Centro (I)	109025.52	109539.10	-0.47
it6 Lazio	84299.36	104712.40	-19.49
it7 Abruzzo-Molise	27726.22	23824.60	16.38
it8 Campania	62961.60	66255.00	-4.97
it9 Sud	106656.10	76835.10	38.81
ita Sicilia	71466.85	58904.60	21.33
itb Sardegna	26869.92	22217.60	20.94
Percentage Mean Absolute Difference			13.36
Standard Deviation			17.70

Rank by Official GRP

NUTS-3 Regions	Estimated GRP	Official GRP	Percentage Difference
Isernia, Crotone, Vibo Valentia, Enna, Oristano, Rieti, Matera, Gorizia, Verbano-Cusio-Ossol, Aosta, Massa-Carrara	34531.82	24778.90	39.36
Caltanissetta, Campobasso, Sondrio, Benevento, Grosseto, Nuoro, Vercelli, Asti, Terni, Lodi, Ragusa	52297.49	38198.70	36.91
Biella, La Spezia, Imperia, Rovigo, Teramo, Pescara, L'Aquila, Belluno, Catanzaro, Viterbo, Agrigento	58860.24	48168.80	22.20

NUTS-3 Regions	Estimated GRP	Official GRP	Percentage Difference
Pistoia, Siena, Trapani, Trieste, Brindisi, Prato, Potenza, Avellino, Macerata, Piacenza	57646.19	50577.50	13.98
Savona, Siracusa, Rimini, Arezzo, Chieti, Pordenone, Pesaro e Urbino, Livorno, Ascoli Piceno, Sassari	62956.69	59706.10	5.44
Reggio di Calabria, Lecco, Ferrara, Taranto, Cremona, Lucca, Ravenna, Novara, Forlì-Cesena, Foggia	77603.96	68742.70	12.89
Pisa, Frosinone, Cosenza, Latina, Alessandria, Lecce, Messina, Mantova, Ancona, Pavia	98984.86	83212.10	18.95
Parma, Caserta, Trento, Reggio nell'Emilia, Cagliari, Udine, Perugia, Como, Cuneo, Bolzano-Bozen	116950.23	105097.10	11.28
Catania, Salerno, Palermo, Modena, Treviso, Varese, Venezia, Genova, Verona, Padova	134085.02	156636.80	-14.40
Vicenza, Bari, Bergamo, Firenze, Bologna, Brescia, Napoli, Torino, Roma, Milano	336074.70	394872.30	-14.89
Percentage Mean Absolute Difference			19.03
Standard Deviation			18.18

Rank by estimates

NUTS-3 Regions	Estimated GRP	Official GRP	Percentage Difference
Crotone, Isernia, Vibo Valentia, Gorizia, Trieste, Oristano, Grosseto, Biella, Massa-Carrara, La Spezia, Verbano-Cusio-Ossol	27611.07	31658.20	-12.78
Enna, Imperia, Prato, Rieti, Siena, Campobasso, Pescara, Vercelli, Matera, Nuoro, Savona	42128.06	40985.60	2.79
Pistoia, Terni, Rimini, Lodi, Lecco, Livorno, Benevento, Caltanissetta, Asti, Teramo, Novara	54485.07	52151.90	4.47
Rovigo, Piacenza, Chieti, Potenza, Reggio di Calabria, Sondrio, Catanzaro, Macerata, Belluno, Messina	58589.31	53204.10	10.12
Pesaro e Urbino, Ferrara, Viterbo, Arezzo, Siracusa, Ragusa, Forlì-Cesena, Pordenone, L'Aquila, Lucca	67708.26	57352.40	18.06
Ancona, Aosta, Cremona, Ascoli Piceno, Avellino, Pisa, Agrigento, Brindisi, Ravenna, Como	82168.92	64999.20	26.42

NUTS-3 Regions	Estimated GRP	Official GRP	Percentage Difference
Reggio nell'Emilia, Trapani, Sassari, Alessandria, Parma, Cosenza, Mantova, Latina, Frosinone, Pavia,	96273.29	81013.40	18.84
Genova, Perugia, Varese, Bolzano-Bozen, Cagliari, Foggia, Salerno, Palermo, Modena, Venezia,	115461.34	133600.30	-13.58
Udine, Taranto, Caserta, Vicenza, Catania, Treviso, Bologna, Trento, Cuneo, Lecce	144533.19	125938.10	14.77
Padova, Verona, Bergamo, Firenze, Brescia, Bari, Napoli, Torino, Roma, Milano	341032.71	389087.80	-12.35
Percentage Mean Absolute Difference			13.42
Standard Deviation			14.55

Alphabet

NUTS-3 Regions	Estimated GRP	Official GRP	Percentage Difference
Agrigento - Benevento	94728.90	72589.80	30.50
Bergamo - Catania	126862.88	125557.80	1.04
Catanzaro - Foggia	96780.94	86178.40	12.30
Forli-Cesena - Latina	59110.09	60975.70	-3.06
Lecce - Messina	67655.40	59433.60	13.83
Milano - Pavia	204434.12	217418.40	-5.97
Perugia - Ragusa	62939.57	59298.40	6.14
Ravenna - Savona	115250.75	143076.60	-19.45
Siena - Treviso	116242.51	109256.80	6.39
Trieste - Viterbo	85986.04	96205.50	-10.62
Percentage Mean Absolute Difference			10.93
Standard Deviation			14.11

Spain

Outliers: Barcelona, Madrid

NUTS-3 Region	Estimated GRP	Official GRP	Percentage Difference
Barcelona	*41689.70*	*71203.30*	*-41.45*
Madrid	*64463.68*	*84043.40*	*-23.30*
Álava	4936.51	4957.50	-0.42
Albacete	3474.38	3243.30	7.12
Alicante	17440.68	14763.60	18.13
Almería	5090.32	5146.90	-1.10
Asturias	8879.33	11780.60	-24.63
Avila	1501.25	1744.10	-13.92
Badajoz	5996.96	5003.60	19.85
Baleares	8647.84	11831.10	-26.91
Burgos	3885.17	4940.20	-21.36
Cáceres	2830.07	3481.40	-18.71
Cadiz	10111.52	9933.20	1.80
Cantabria	5827.45	6130.00	-4.94
Castellón de la Plana	7139.36	6472.10	10.31
Ciudad Real	7856.78	4815.90	63.14
Córdoba	6325.40	6658.60	-5.00
Cuenca	2790.88	1989.10	40.31

NUTS-3 Region	Estimated GRP	Official GRP	Percentage Difference
Gerona	8522.42	8279.80	2.93
Granada	7271.57	6765.80	7.48
Guadalajara	2795.21	1903.30	46.86
Guipúzcoa	7315.29	10518.60	-30.45
Huelva	5567.57	4289.90	29.78
Huesca	2612.13	2695.10	-3.08
Jaén	7295.78	5673.00	28.61
La Coruña	9348.69	11970.30	-21.90
León	7402.39	5559.10	33.16
Lérida	6408.19	5256.20	21.92
Lugo	2655.87	3496.40	-24.04
Málaga	10942.91	11536.40	-5.14
Murcia	14492.24	11524.00	25.76
Navarra	8697.14	8547.10	1.76
Orense	2842.81	3101.90	-8.35
Palencia	2189.57	2148.50	1.91
Pontevedra	7032.25	8825.30	-20.32
Rioja	3129.08	3779.70	-17.21
Salamanca	2823.91	3638.80	-22.39
Segovia	1653.40	1826.20	-9.46
Sevilla	17766.31	16374.90	8.50
Soria	1058.74	1198.10	-11.63
Tarragona	8852.85	9295.80	-4.77
Teruel	1865.66	1912.40	-2.44
Toledo	8571.40	5386.20	59.14
Valencia	22706.50	26180.90	-13.27
Valladolid	5140.50	6376.20	-19.38
Vizcaya	8952.61	15522.70	-42.33
Zamora	1237.53	1895.00	-34.70
Zaragoza	9958.49	11550.60	-13.78

Simulated Regions

NUTS-1

NUTS-1 Region	Estimated GRP	Official GRP	Percentage Difference
es1 Noroeste	21879.62	27393.90	-20.13
es2 Noreste	62173.69	77394.30	-19.67
es3 Comunidad de Madrid	90927.69	84043.40	8.19
es4 Centro (E)	61208.15	55149.00	10.99
es5 Este	145465.39	141451.70	2.84
es6 Sur	93511.47	89733.80	4.21
Percentage Mean Absolute Difference			11.00
Standard Deviation			13.96

Ranked by Official GRP

NUTS-3 Regions	Estimated GRP	Official GRP	Percentage Difference
Soria, Ávila, Segovia, Zamora, Guadalajara, Teruel	10111.79	10479.10	-3.51
Cuenca, Palencia, Huesca, Orense, Albacete, Cáceres	16739.84	16659.30	0.48
Lugo, Salamanca, La Rioja, Huelva, Ciudad Real, Burgos	25918.38	24960.90	3.84
Alava, Badajoz, Almería, Lérida, Toledo, León	38405.77	31309.50	22.66
Jaén, Cantabria, Valladolid, Castellón de la Plana, Córdoba, Granada	39000.06	38075.70	2.43

NUTS-3 Regions	Estimated GRP	Official GRP	Percentage Difference
Gerona, Navarra, Pontevedra, Tarragona, Cádiz, Guipúzcoa	50531.47	55399.80	-8.79
Murcia, Málaga, Zaragoza, Asturias, Baleares, La Coruña	62269.50	70193.00	-11.29
Alicante, Viscaya, Sevilla, Valencia, Barcelona, Madrid	232189.17	228088.80	1.80
Percentage Mean Absolute Difference			6.85
Standard Deviation			10.33

Ranked by estimates

NUTS-3 Regions	Estimated GRP	Official GRP	Percentage Difference
Soria, Zamora, Ávila, Segovia, Teruel, Palencia	9506.15	10724.30	-11.36
Huesca, Lugo, Cuenca, Guadalajara, Salamanca, Cáceres	16508.07	17204.10	-4.05
Orense, La Rioja, Albacete, Burgos, Alava, Almería	23358.28	25169.50	-7.20
Valladolid, Huelva, Cantabria, Badajoz, Córdoba, Lérida	35266.08	33714.50	4.60
Pontevedra, Castellón de la Plana, Granada, Jaén, Guipúzcoa, León	43456.64	43813.90	-0.82
Ciudad Real, Gerona, Toledo, Baleares, Navarra, Tarragona	51148.43	48155.90	6.21
Asturias, Viscaya, La Coruña, Zaragoza, Cádiz, Málaga	58193.55	72293.80	-19.50
Murcia, Alicante, Sevilla, Valencia, Barcelona, Madrid	237728.80	224090.10	6.09
Percentage Mean Absolute Difference			7.48
Standard Deviation			9.18

Alphabet

NUTS-3 Regions	Estimated GRP	Official GRP	Percentage Difference
Alava - Avila	41322.46	41636.00	-0.75
Badajos - Cadiz	105866.95	106392.80	-0.49
Cantabria - Gerona	38462.29	34345.50	11.99
Granada - Jaen	32857.56	31845.70	3.18
La Coruna - Malaga	127685.74	121861.80	4.78
Murcia - La Rioja	38383.09	37926.50	1.20
Salamanca - Teruel	34020.89	34246.20	-0.66
Toledo - Zaragoza	56567.03	66911.60	-15.46
Percentage Mean Absolute Difference			4.81
Standard Deviation			7.71

Great Britain

Outlier: Greater London

NUTS-2 Regions	Estimated GRP	Official GRP	Percentage Difference
Greater London	97784.56	*204042.70*	*-52.08*
Northumberland, Tyne and Wear	36280.61	22459.70	61.54
Tees Valley and Durham	26163.61	18012.90	45.25
Cumbria	9534.59	9050.80	5.35
North Yorkshire	21107.64	14177.80	48.88
Lancashire	26198.68	23612.20	10.95
East Riding and North Lincolnshire	29603.45	17048.80	73.64
West Yorkshire	47010.22	38328.60	22.65
Merseyside	15630.24	19727.20	-20.77
Greater Manchester	41451.60	46047.70	-9.98
South Yorkshire	33546.21	19380.40	73.09
Lincolnshire	18516.52	10677.10	73.42
Derbyshire and Nottinghamshire	48713.15	36113.20	34.89
Cheshire	21890.98	22658.90	-3.39
Shropshire and Staffordshire	30919.70	24950.80	23.92
East Anglia	53695.23	46802.50	14.73
Leicestershire, Rutland and Northants	37065.95	32242.90	14.96
Herefordshire, Worcestershire and Warks	25287.77	22759.40	11.11
West Midlands	39819.40	48919.70	-18.60
Bedfordshire, Hertfordshire	32594.33	32538.00	0.17
Berkshire, Bucks and Oxfordshire	41521.94	51561.00	-19.47
Gloucestershire, Wiltshire and North Somerset	34241.87	45916.90	-25.43
Essex	36128.55	29327.20	23.19
Kent	28361.16	29246.00	-3.03
Surrey, East and West Sussex	36126.43	52791.00	-31.57
Hampshire and Isle of Wight	22827.15	37872.30	-39.73
Dorset and Somerset	16632.17	20119.20	-17.33
Devon	12882.09	17223.60	-25.21
Cornwall and Isles of Scilly	6309.15	6343.50	-0.54
Percentage Mean Absolute Difference			26.88
Standard Deviation			33.14
Scotland	144496.11	98079.10	47.33
Wales	48060.47	46841.50	2.60

Density Mapping

Best fit: Second order polynomial $y = 0.7659x^2 - 1.8685x + 1.8901$; $R^2 = 0.8513$

NUTS-2 Regions	Estimated GRP	Official GRP	Percentage Difference
Northumberland, Tyne and Wear	139469.59	22459.70	610.98
Tees Valley and Durham	52079.34	18012.90	279.12
Cumbria	74140.30	9050.80	809.16
North Yorkshire	89995.52	14177.80	624.76
Lancashire	35954.04	23612.20	142.27
East Riding and North Lincolnshire	59799.04	17048.80	340.75

NUTS-2 Regions	Estimated GRP	Official GRP	Percentage Difference
West Yorkshire	84603.67	38328.60	210.73
Merseyside	23814.58	19727.20	110.72
Greater Manchester	87977.83	46047.70	181.06
South Yorkshire	58200.96	19380.40	290.31
Lincolnshire	61558.65	10677.10	566.55
Derbyshire and Nottinghamshire	76133.43	36113.20	200.82
Cheshire	30042.49	22658.90	122.59
Shropshire and Staffordshire	73304.33	24950.80	283.80
East Anglia	135244.11	46802.50	278.97
Leicestershire, Rutland and Northants	66266.52	32242.90	195.52
Herefordshire, Worcestershire and Warks	62227.40	22759.40	263.41
West Midlands	107214.99	48919.70	209.17
Bedfordshire, Hertfordshire	40012.83	32538.00	112.97
Berkshire, Bucks and Oxfordshire	71292.77	51561.00	128.27
Gloucestershire, Wiltshire and North Somerset	85294.30	45916.90	175.76
Essex	54717.82	29327.20	176.58
Kent	42800.50	29246.00	136.35
Surrey, East and West Sussex	59387.64	52791.00	102.50
Hampshire and Isle of Wight	45959.58	37872.30	111.35
Dorset and Somerset	65433.83	20119.20	315.23
Devon	74496.48	17223.60	422.53
Cornwall and Isles of Scilly	36652.96	6343.50	567.80
Greater London	429175.50	204042.70	200.34
Percentage Mean Absolute Difference			281.74
Standard Deviation			185.52

Ireland

Outlier: Dublin

NUTS-1 Region	Estimated GRP	Official GRP	Percentage Difference
Dublin	*17324.65*	*27530.40*	*-37.07*
Border	5942.23	6104.40	-2.66
Mid-East	7725.17	6059.30	27.49
Midlands	3322.77	2659.80	24.93
Midwest	6748.65	5590.00	20.73
South-East (IE)	6430.72	6470.20	-0.61
South-West (IE)	8622.14	11256.60	-23.40
West	5125.59	4937.10	3.82
Percentage Mean Absolute Difference			14.80
Standard Deviation			18.33

Belgium

Outlier: Brussels

Vlaams Gewest

NUTS-3 Region	Estimated GRP	Official GRP	Percentage Difference
Antwerpen (Arrondissement)	18365.43	26640.80	-31.06
Mechelen	5907.89	6465.30	-8.62
Turnhout	9310.50	8355.00	11.44
Hasselt	9860.18	8322.10	18.48
Maaseik	5257.00	3213.70	63.58
Tongeren	6411.53	2301.10	178.63
Aalst	3419.19	3663.10	-6.66
Dendermonde	3087.97	2655.20	16.30
Eeklo	1246.46	1081.00	15.31
Gent (Arrondissement)	8714.42	11813.80	-26.24
Oudenaarde	2055.52	1927.90	6.62
Sint-Niklaas	4725.77	4039.30	16.99
Halle-Vilvoorde	14243.62	13224.60	7.71
Leuven	11319.48	8165.70	38.62
Brugge	4311.08	5356.10	-19.51
Diksmuide	1140.32	660.20	72.72
Ieper	2201.12	1671.30	31.70
Kortrijk	5284.67	6233.50	-15.22
Oostende	1415.22	2115.80	-33.11
Roeselare	2289.80	2928.20	-21.80
Tielt	2316.20	1904.50	21.62
Veurne	979.82	1034.70	-5.30
Percentage Mean Absolute Difference			30.33
Standard Deviation			46.05

Wallonia

Ath	1329.97	875.00	52.00
Charleroi	5269.49	6951.40	-24.20
Mons	2174.37	3433.80	-36.68
Mouscron	1045.54	1096.90	-4.68
Soignies	2263.94	2111.40	7.22
Thuin	1526.70	1338.40	14.07
Tournai	2401.66	2032.60	18.16
Huy	2672.79	1477.00	80.96
Liège (Arrondissement)	8598.82	10372.20	-17.10
Verviers	5910.57	4291.40	37.73
Waremme	1353.91	758.40	78.52
Arlon	1335.44	982.00	35.99
Bastogne	1979.01	525.50	276.60
Marche-en-Famenne	1305.25	791.10	64.99
Neufchâteau	1612.56	811.40	98.74
Virton	1033.17	676.20	52.79
Dinant	2390.83	1255.40	90.44
Namur (Arrondissement)	4774.19	4670.00	2.23
Philippeville	1195.32	692.60	72.58
Percentage Mean Absolute Difference			56.09
Standard Deviation			68.73

Germany

West Germany (including Berlin)

NUTS Region	Estimated GRP	Official GRP	Percentage Difference
Stuttgart	81304.32	107710.00	-24.52
Karlsruhe	62737.50	69945.90	-10.31
Freiburg	47640.63	46691.10	2.03
Tübingen	38064.92	40548.80	-6.13
Oberbayern	74237.28	125785.90	-40.98
Niederbayern	36448.81	24499.90	48.77
Oberpfalz	29294.33	23469.40	24.82
Oberfranken	33878.71	24720.90	37.04
Mittelfranken	34200.69	43584.90	-21.53
Unterfranken	26572.35	29112.90	-8.73
Schwaben	38068.79	40153.60	-5.19
Berlin	41442.98	74786.50	-44.58
Bremen	11339.73	20367.30	-44.32
Hamburg	32538.00	66441.10	-51.03
Darmstadt	93536.84	117255.70	-20.23
Gießen	21733.78	21706.00	0.13
Kassel	23611.84	28101.80	-15.98
Braunschweig	47616.83	36176.90	31.62
Hannover	55009.49	49995.20	10.03
Lüneburg	45084.14	28620.00	57.53
Weser-Ems	64153.79	47197.50	35.93
Düsseldorf	135226.00	136491.70	-0.93
Köln	106747.45	106801.50	-0.05
Münster	73662.80	49006.90	50.31
Detmold	50040.55	46179.40	8.36
Arnsberg	83278.41	80830.70	3.03
Koblenz	40333.84	29376.60	37.30
Trier	21210.24	9581.20	121.37
Rheinhessen-Pfalz	52507.78	44282.30	18.58
Saarland	30679.08	22672.70	35.31
Schleswig-Holstein	68592.20	59381.40	15.51
Percentage Mean Absolute Difference			26.84
Standard Deviation			36.03

East Germany

NUTS Region	Estimated GRP	Official GRP	Percentage Difference
Brandenburg	32729.00	39071.50	-16.23
Mecklenburg-Vorpommern	24655.43	27454.60	-10.20
Sachsen	73286.98	69454.30	5.52
Dessau	8323.23	7729.10	7.69
Halle	13611.23	13671.00	-0.44
Magdeburg	18123.76	18141.50	-0.10
Thüringen	34409.47	36494.80	-5.71
Percentage Mean Absolute Difference			6.55
Standard Deviation			8.52

Greece

NUTS-3 Region	Estimated GRP	Official GRP	Percentage Difference
ACHAIA	2013.78	2859.70	-29.58
AITOLOAKARNANIA	1132.58	1723.00	-34.27
ARGOLIDA	1075.15	910.10	18.14
ARKADIA	669.05	966.90	-30.80
ARTA	687.34	470.40	46.12
ATTIKI	35058.72	38757.40	-9.54
CHALKIDIKI	732.51	1093.90	-33.04
CHANIA	806.55	1419.20	-43.17
CHIOS	278.97	412.90	-32.44
DODEKANISOS	1104.49	2221.90	-50.29
DRAMA	1330.54	698.20	90.57
EVROS	1400.54	1273.50	9.98
EVRYTANIA	70.33	232.30	-69.73
EVVOIA	1368.81	2182.30	-37.28
FLORINA	428.63	471.90	-9.17
FOKIDA	327.70	462.00	-29.07
FTHIOTIDA	1687.41	2032.40	-16.97
GREVENA	135.55	319.10	-57.52
ILEIA	1676.96	1185.90	41.41
IMATHIA	1628.66	1254.80	29.79
IOANNINA	1422.93	1351.90	5.25
IRAKLEIO	765.29	2700.50	-71.66
KARDITSA	1204.41	983.90	22.41
KASTORIA	743.90	500.10	48.75
KAVALA	1796.77	1216.20	47.74
KEFALLINIA	236.61	316.10	-25.15
KERKYRA	169.69	1059.30	-83.98
KILKIS	905.07	904.10	0.11
KORINTHIA	1607.33	1749.80	-8.14
KOZANI	1530.57	1788.30	-14.41
KYKLADES	603.31	1153.10	-47.68
LAKONIA	350.97	728.10	-51.80
LARISA	2922.92	2654.70	10.10
LASITHI	568.67	846.30	-32.80
LEFKADA	28.06	222.00	-87.36
LESVOS	320.66	1021.30	-68.60
MAGNISIA	2277.34	1967.40	15.75
MESSINIA	1132.92	1236.80	-8.40
PELLA	1507.94	1128.00	33.68
PIERIA	812.30	937.30	-13.34
PREVEZA	158.94	449.80	-64.66
RETHYMNI	143.05	766.50	-81.34
RODOPI	756.27	716.20	5.59
SAMOS	194.53	360.80	-46.08
SERRES	1951.61	1383.20	41.09
THESPROTIA	332.62	303.30	9.67
THESSALONIKI	11635.85	12219.70	-4.78
TRIKALA	1565.49	993.30	57.61
VOIOTIA	1912.56	3409.90	-43.91
XANTHI	1208.91	796.20	51.84
ZAKYNTHOS	385.93	290.30	32.94
Percentage Mean Absolute Difference			36.38
Standard Deviation			42.05

Simulated Regions

NUTS-1

NUTS-1 Region	Estimated GRP	Official GRP	Percentage Difference
gr1 Voreia Ellada	38460.38	33300.10	15.50
gr2 Kentriki Ellada	19023.84	24142.40	-21.20
gr3 Attiki	37405.82	38757.40	-3.49
gr4 Nisia Aigaiou, Kriti	5242.81	10902.40	-51.91
Percentage Mean Absolute Difference			23.02
Standard Deviation			28.65

Ranked by Official GRP

NUTS-3 Regions	Estimated GRP	Official GRP	Percentage Difference
LEFKADA, EVRYTANIA, ZAKYNTHOS, THESPROTIA, KEFALLINIA, GREVENA	1189.09	1683.10	-29.35
SAMOS, CHIOS, PREVEZA, FOKIDA, ARTA,	1647.48	2475.00	-33.44
FLORINA, KASTORIA, DRAMA, RODOPI, LAKONIA	3610.30	3584.90	0.71
RETHYMNI, XANTHI, LASITHI, KILKIS, ARGOLIDA	3900.85	4951.30	-21.22
PIERIA, ARKADIA, KARDITSA, TRIKALA, LESVOS	4571.91	5812.80	-21.35
KERKYRA, CHALKIDIKI, PELLA, KYKLADES, ILEIA	4690.40	6641.50	-29.38
KAVALA, MESSINIA, IMATHIA, EVROS, IOANNINA	7381.82	7519.10	-1.83
SERRES, CHANIA, AITOLOAKARNANIA, KORINTHIA, KOZANI	7028.64	9415.40	-25.35
MAGNISIA, FTHIOTIDA, EVVOIA, DODEKANISOS, LARISA	9360.97	12847.00	-27.13
IRAKLEIO, ACHAIA, VOIOTIA, THESSALONIKI, ATTIKI	51386.20	62601.90	-17.92
Percentage Mean Absolute Difference			20.77
Standard Deviation			11.54

Ranked by Estimates

NUTS-3 Regions	Estimated GRP	Official GRP	Percentage Difference
LEFKADA, EVRYTANIA, GREVENA, RETHYMNI, PREVEZA, KERKYRA	705.61	3049.00	-76.86
SAMOS, KEFALLINIA, CHIOS, LESVOS, FOKIDA	1358.47	3632.40	-62.60
THESPROTIA, LAKONIA, ZAKYNTHOS, FLORINA, LASITHI	2066.82	3101.90	-33.37
KYKLADES, ARKADIA, ARTA, CHALKIDIKI, KASTORIA	3436.10	5030.70	-31.70
RODOPI, IRAKLEIO, CHANIA, PIERIA, KILKIS	4045.48	7177.40	-43.64

NUTS-3 Regions	Estimated GRP	Official GRP	Percentage Difference
ARGOLIDA, DODEKANISOS, AITOLOAKARNANIA, MESSINIA, KARDITSA	5649.55	7979.80	-29.20
XANTHI, DRAMA, EVVOIA, EVROS, IOANNINA	6731.73	7286.00	-7.61
PELLA, KOZANI, TRIKALA, KORINTHIA, IMATHIA	7839.99	8266.10	-5.15
ILEIA, FTHIOTIDA, KAVALA, VOIOTIA, SERRES	9025.32	10482.40	-13.90
ACHAIA, MAGNISIA, LARISA, THESSALONIKI, ATTIKI	53908.60	59842.10	-9.92
Percentage Mean Absolute Difference			31.39
Standard Deviation			24.09

Alphabetical

NUTS-3 Regions	Estimated GRP	Official GRP	Percentage Difference
Achaia - Athens	40636.62	45687.50	-11.06
Chalkidiki - Drama	4253.05	5846.10	-27.25
Evros - Fokida	3596.01	4622.00	-22.20
Fthiotida - Ioannina	6551.50	6144.10	6.63
Irakleio - Kefallinia	4746.98	5716.80	-16.96
Kerkyra - Kyklades	4815.96	6654.60	-27.63
Lakonia - Lesvos	4191.28	5472.40	-23.41
Magnisia - Preveza	5889.44	5719.30	2.97
Rethymni - Thesprotia	3378.08	3530.00	-4.30
Thessaloniki - Zakynthos	16708.75	17709.40	-5.65
Percentage Mean Absolute Difference			14.81
Standard Deviation			12.47

Netherlands

NUTS-2 Regions	Estimated GRP	Official GRP	Percentage Difference
Groningen	15213.54	14655.70	3.81
Friesland	11104.00	10825.30	2.57
Drenthe	12908.95	8054.70	60.27
Overijssel	18304.27	19414.70	-5.72
Gelderland	38404.44	35251.70	8.94
Flevoland	6613.20	4447.20	48.70
Utrecht	17653.11	28550.30	-38.17
Noord-Holland	51363.19	61341.30	-16.27
Zuid-Holland	77558.45	73940.30	4.89
Zeeland	9421.13	7044.00	33.75
Noord-Brabant	49362.97	48296.20	2.21
Limburg	30091.75	20832.50	44.45
Percentage Mean Absolute Difference			22.48
Standard Deviation			28.83

Appendix F

List of Publications

First named author (copies in this section)

Doll, C.N.H. and J-P Muller., 1999a. An evaluation of global urban growth via comparison of DCW and DMSP-OLS satellite data. *In: Proceedings of IEEE International Geoscience and Remote Sensing Symposium (IGARSS'99).* Hamburg, Germany 28 June – 2 July. 1134-1136. © IEEE.

Doll, C.N.H. and Muller, J-P., 1999b. The use of radiance calibrated night-time imagery to improve remotely sensed population estimation. *In: Proceedings of the 25th Annual Conference of the Remote Sensing Society.* University of Wales, Cardiff, UK 9 – 11 September. Nottingham, UK: Remote Sensing Society, 127-133.

Doll, C.N.H. and Muller, J-P., 2000. A comparison of different techniques applied to the UK to map socio-economic parameters: implications for modelling the human dimensions of global change. *In: International Archives of Photogrammetry and Remote Sensing,* GITC bv: Amsterdam, The Netherlands, **33** (B4), 222-229.

Doll, C.N.H., Muller, J-P. and Elvidge, C.D., 2000. Night-time imagery as a tool for global mapping of socio-economic parameters and greenhouse gas emissions. *Ambio*, **29** (3), 157-162. © Royal Swedish Academy of Sciences.

Doll, C.N.H., Muller, J-P., Schaaf, C., Strahler, A.H. and Gao, F., 2001. Mapping Urban Landcover Using the BRDF/Albedo Product from the EOS/MODIS Instrument. *In: Proceedings of IEEE International Geoscience and Remote Sensing Symposium (IGARSS'01),* University of New South Wales, Sydney, Australia July 9 - 13 2001. Available on supplementary CD-ROM of the conference proceedings. © IEEE.

Doll, C.N.H., 2003. Estimating non-population parameters from night-time satellite imagery. *In*: Mesev, V. (Ed.) *Remotely Sensed Cities.* Taylor & Francis: London, UK, 335-354. © Taylor and Francis.

Other:

Schaaf, C.B., Gao, F., Strahler, A.H., Lucht, W., Li, X.W., Tsang, T., Strugnell, N.C., Zhang, X.Y., Jin, Y.F., Muller, J.P., Lewis, P., Barnsley, M., Hobson, P., Disney, M., Roberts, G., Dunderdale, M., Doll, C., d'Entremont, R.P., Hu, B.X., Liang, S.L., Privette, J.L. and Roy, D., 2002. First operational BRDF, albedo nadir reflectance products from MODIS. *Remote Sensing of Environment,* **83** (1-2), 135-148.

An Evaluation of Global Urban Growth via Comparison of DCW and DMSP-OLS Satellite Data

Christopher N H Doll, Jan-Peter Muller
Department of Geomatic Engineering, University College London,
Gower Street, London, WC1E 6BT, United Kingdom
Tel: (+44) 171 504 2742 Fax: (+44) 171 380 0453 Email: cdoll@ge.ucl.ac.uk

ABSTRACT

Whilst urbanised areas account for the smallest land cover class, it is arguably the most important in that knowledge of the size and spatial distribution of our cities is a key parameter on a number of fronts from resource management to economic development planning.

An evaluation has been performed comparing satellite assessments of urban land area extent at two different times. The 1:1,000,000 Digital Chart of the World (DCW) dataset originally collected in the 1960s and 1970s mapped many physical, social and cultural features. A populated places layer is included in this. This has been quantitatively compared using a geographic information system (GIS) to the 1994-5 Defence Meteorological Satellite Programme Operational Linescan (DMSP-OLS) city lights dataset at 1km prepared by Chris Elvidge and others at the National Oceanic & Atmospheric Administration National Geophysical Data Center (NOAA-NGDC)[1]. The city-lights dataset is a temporal composite of nocturnal VIS-NIR emissions. Once processed into a "stable lights" product a map of electrified human settlements is derived.

The city-lights are observed to envelop the DCW polygons suggesting many of these areas have merged into larger conurbations. By using the International Geosphere-Biosphere Programme (IGBP) global land cover map (derived from 1km satellite data) it has also been possible to assess which land cover types have been misidentified in the IGBP land cover map. This raises important questions regarding the diminishing extent of agricultural land and its human carrying capacity.

INTRODUCTION

Global population has experienced unprecedented growth in the post-war period. Our population currently stands at around 6 billion, the last billion of which was added in little over a decade. Over half these of these people live in cities [2]. Urbanisation continues unbounded, with developing countries catching up fast to their industrialised counterparts, especially in Asia.

The aim of this study was to investigate the extent to which urban areas have increased in recent times, and to identify which classes of land use have been misidentified in a recently compiled global land cover map.

Traditionally, settlements have developed in areas of good communication or near to prime agricultural lands. The importance of the immediate surrounding to a city has always meant that it will have important effects on, and will be affected by the state of the city. A study specific to the US [3] found that in the most agriculturally productive states, the best soils were being taken for urbanisation. Urban areas have experienced massive increases in recent times. In the developing world, the rapid expansion of cities has been accompanied by rural-urban migration. Decentralisation of the population in industrialised countries has had the effect of sprawling suburban landscapes with a low overall density. These cannot be easily identified in coarse resolution satellite imagery, but are more likely to be identified by night-time lights.

THE DATASETS

Urban detection from satellites is hampered by the heterogeneity in land cover giving rise to complex spectral signatures. This has long been a problem for optical remote sensing, and is further exacerbated by the scale required for practical global mapping. The DMSP-OLS sensor takes VIS-NIR images at night. Night-time images are very useful for urban mapping as only light sources are present on cloud free images. These include city lights, gas flaring and biomass burning. A temporal composite of these images was acquired over the six month period October '94 to March '95[1]. Using the thermal channel to screen out clouds, the time series of images was used to filter out other light sources and create a stable lights dataset. The city-lights product prepared at NOAA-NGDC maps global settlements at 30" (1km) remapped from an initial pixel size of 2.7km.

The city-lights image was made into a binary image of lit/unlit pixels and then converted into polygons from the raster image. This method results in the maximum lit area being under consideration. The city-light polygons were overlaid with the DCW polygons to identify the differences between the two datasets.

The DCW populated places layer features all urbanised/built up areas that can be represented at the 1:1,000,000 scale. The date of the dataset varies by geographical area and is most up to date for Russia and the US. Most of the data was collected in the 1960s and early 1970s, however, resulting in a thirty-year gap between the two sets of urban area data.

The IGBP land cover map at 1km comprises 17 classes of forests, croplands and savannahs mapped from overpasses of the NOAA Advanced Very High Resolution Radiometer (AVHRR) taken between 1992 and 1993 [4]. The urban/built up layer is taken directly from the DCW populated places.

The processing and analysis was done in a GIS which facilitates the overlaying of multiple themes for analysis. The analysis was carried out on a continent by continent basis. Lambert's Azimuthal Equal Area projection was used for the analysis.

A country mask derived from the DCW coastlines and political boundaries was used to assign urban area polygons from both the DCW and OLS datasets to countries and hence calculate total urban area within a country. The total area of the country was also taken from this data.

URBAN GROWTH

The city lights are observed to substantially buffer the DCW polygons as illustrated in fig.1. Often several DCW polygons exist within a lit area and occasionally the DCW polygon may lie outside or partially within a larger area. It is not clear whether the DCW polygons have grown in size, or if new settlements have developed in between to fill the area. DCW polygons only account for around 5% of the lit area. Many lit area polygons have no DCW polygons within them suggesting the emergence of new urban areas.

Country level assessments were made for a selection of 46 countries shown in fig.2. The greatest proportions of urbanised areas exist in the developed world. Most of these countries (largely in western Europe) have around 20% of the land area covered by city lights. The Russian republics have experienced the least amount of increase, with more than 10% of the lit area accounted for by the DCW. Other countries have experienced huge shifts of area towards urbanisation. Over half of the countries listed have less than 0.5% of total land area devoted to DCW urban area. Only one country (Cameroon) remained in this situation when urban area was considered through lit area.

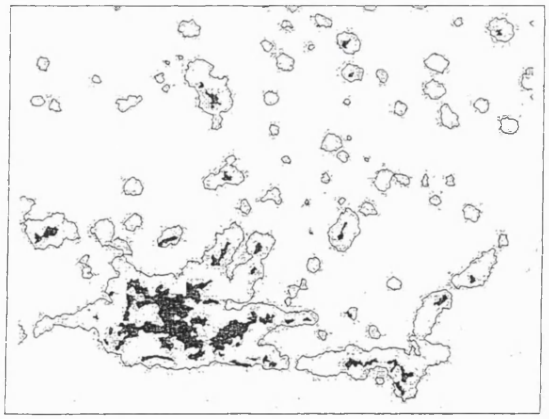

Fig.1. City light Polygons (lines) enveloping DCW Urban Areas (dark). Area around Rio de Janeiro, Brazil

Fig.2. Table of % Urban Area by Country Derived From DCW-OLS with Increase

Country	DCW %	OLS %	DCW-OLS % Increase
Finland	0.05	12.22	24440
Spain	0.18	18.01	10006
Mexico	0.11	8.05	7318
Iran	0.09	6.34	7044
Egypt	0.05	3.17	6340
Syria	0.13	7.59	5838
Italy	0.5	26.59	5318
Turkey	0.14	7.12	5086
Canada	0.06	2.87	4783
Philippines	0.1	3.78	3780
Cote d'Ivoire	0.03	1.08	3600
Morocco	0.11	3.9	3545
India	0.2	6.79	3395
Pakistan	0.15	4.71	3140
Nigeria	0.06	1.8	3000
Switzerland	0.81	21.73	2683
Korea	0.91	23.95	2632
France	0.73	18.7	2562
Iraq	0.17	4.32	2541
Poland	0.47	11.8	2511
Malaysia	0.24	5.6	2333
Austria	0.67	14.99	2237
Japan	1.49	32.79	2201
Cuba	0.4	8.58	2145
Sweden	0.64	12.84	2006
Sri Lanka	0.34	6.68	1965
Denmark	1.83	25.4	1388
US	0.88	12.17	1383
Azerbaijan	0.95	11.88	1251
Vietnam	0.21	2.39	1138
Cameroon	0.04	0.43	1075
Bulgaria	0.85	9.11	1072
Australia	0.08	0.83	1038
Indonesia	0.27	2.57	952
Russia	0.25	2.28	912
New Zealand	0.46	4.14	900
Netherlands	3.88	34.17	881
Kazakhstan	0.17	1.49	876
Uzbekistan	0.58	5.07	874
Hungary	1.72	12.95	753
Germany	2.76	18.79	681
UK	4.35	27.12	623
Georgia	0.84	5.06	602
China	0.57	3.4	596
Romania	1.06	6.12	577
Ukraine	2.95	8.91	302

MISIDENTIFICATION OF AREAS IN IGBP LAND COVER MAP

The city lights polygon layer was intersected with the IGBP 1km land cover grid used to summarise the different land cover classes present within the lit. In all continents, the cropland cover classes occupied the greatest proportions of the 17 categories. Africa had the largest proportion of the urban area in the lit areas at 15% (fig.3).

Croplands formed the major land cover class in every continent. Asia, in particular had the greatest amount of pure cropland covered by lights at over 45%. This translates into well over 500,000 km^2. Europe and Asia had the highest rates of total cropland misidentification from the two classes with 60% each. North America has equal amounts (30%) of cropland and forests under the night-time lights. Africa's major non urban land cover class is the woody savannahs (20%≡60,000 km^2).

There is also a high contribution from water bodies. Night-time imagery is very sensitive to reflection of moonlight from water bodies, which results in an overestimation of city area. As most cities are coastal in location, this may explain why there is such a large contribution. Errors in registration between the two datasets is another possible explanation. However, most of the large differences may be accounted for by the misclassification in the land cover map which [5] have shown to be as high as 52%.

The very high contribution of croplands to the land cover classes under city-lights suggests that urbanised areas are encroaching onto existing farmlands around cities. However, the IGBP land cover map was assembled only 2-3 years before the OLS dataset. The urban layer in IGBP was taken directly from the DCW dataset. Given the magnitude of difference between that and the more recent night-time data, the non urban areas within the city lights highlight which have been misidentified in the IGBP map.

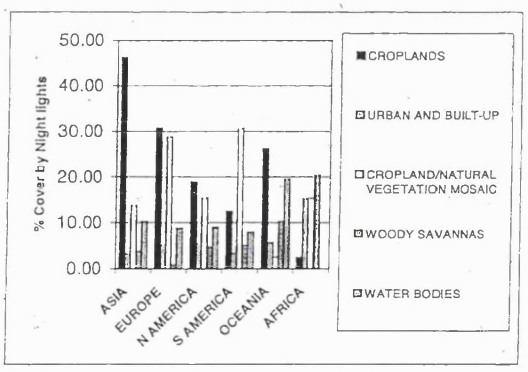

Fig.3. Percentage of Land Cover Classes Intersecting with DMSP-OLS Imagery

CONCLUSION

The DMSP-OLS data offers a unique view of urbanisation from satellites. The potential frequency of acquisition of a stable lights dataset make it a highly appropriate tool for urban mapping and monitoring.

The results reveal that urban areas are severely under represented in the IGBP land cover map. Urban area as assessed from the DCW is generally around 5% of the figure when considered at the continental scale. Others [5] have noted the poor correlation of the IGBP to complementary maps. It is suggested that subject to a more rigorous study, night-time imagery could be used as the urban input to land cover maps. The use of a city-lights image may be considered a proxy for the underlying built environment.

Studies with a radiance calibrated dataset [6] are the best way to gain an understanding of what the city-lights image is really showing. Establishing the conditions under which a pixel is observed to be lit will better enable us to understand the limitations of using night-time data for such analyses. The urban fringes are of particular importance as they are frontiers of land cover change.

ACKNOWLEDGMENTS

The authors would like to thank Christopher Elvidge and Kimberly Baugh for processing the DMSP-OLS night-time light data at NOAA-NGDC. This work is supported under a NERC studentship, number GT 04/98/ 188/TS.

REFERENCES

[1] C.Elvidge "Mapping City Lights with the night-time data from the DMSP Operational Linescan System" Phot.Eng.& Rem.Sens. 63(3) 1996.

[2] W. Meyer "Human Impact on the Earth" Cambridge University Press pp 74-76 (1996).

[3] M. Imhoff "Can Urban Sprawl Reduce Human Carrying Capacity? Evaluating Land Use Change with Nighttime Views of the Earth" In Press

[4] T.Loveland and A.Belward "The IGBP-DIS Global 1km Land Cover Dataset, DISCover: First Results IJRS 18(15), 3291-3295 (1997).

[5] M.Dunderdale, J-P Muller, N Gapare "Assessment of IGBP-DIS 1km Land Cover Map Using The Vegetation Resources Information System (VegRIS) Project of Zimbabwe. Proc. RSS98. Greenwick, UK pp.518-526

[6] C.Elvidge "Radiance Calibration of DMSP-OLS Low-light imaging data of Human Settlements. Remote Sensing Environments 68:77-88 (1999).

The Use of Radiance Calibrated Night-time Imagery to Improve Remotely Sensed Population Estimation

C N H Doll and J-P Muller

Department of Geomatic Engineering
University College London
Gower Street
LONDON
WC1E 6BT

Telephone: +44 (0) 171 504 2742
Fax: +44 (0) 171 380 0453
Email: cdoll@ge.ucl.ac.uk, jpmuller@ge.ucl.ac.uk

Abstract

Night-time imagery showing the occurrence of night-lights due to urbanisation has been demonstrated to produce significant new socio-economic and environmental information (Doll et al. 1999). The study compared areal coverage of night-lights to a variety of socio-economic and environmental statistics. Good relationships between area, GDP and CO_2 emissions were observed. However, there was a wide range of agreement to the allometric growth model between area and population observed in other studies. It is believed that areal analysis by itself is insufficient to provide a sound basis for modelling of these parameters, and that extra information may be gained through the analysis of a radiance calibrated dataset. This analysis focuses on 12 countries that were split between weak and strong allometric relationships. The radiance-calibrated dataset was used to determine if improvements could be made to the population estimation capability of night-time light data. The technique used provided a significantly more robust way of quantifying urban population. The advent of radiance calibrated datasets will provide an extra dimension by which to assess such parameters often considered outside the realm of conventional remote sensing.

1 Introduction

Urban areas are nodes of anthropogenic activity and as such are of great importance to scientists concerned with global change. Much global change research is focussed towards discerning and documenting the impacts on natural systems (Houghton et al., 1995). Whilst human population has been identified as a key parameter for improved modelling of environmental impacts on natural resources, it remains poorly defined across the earth's surface (Clark & Rhind, 1992). Attempts at producing a global population map have suffered from inhomogeneous data collection techniques, poor spatial resolution and the fact that they are extremely difficult to update (Tobler, 1995). The use of satellite data for identification and assessment of human

settlements have been hampered by the lack of a clear, discriminating spectral signature when compared to surrounding land cover types. Although-high resolution satellites can provide clear discrimination of urban features such as roads; it is impractical to use at a global scale for synoptic mapping of urban areas. Night-time imagery distinguishes itself in this respect in that only light sources emanating from cities are considered.

The use of night-time imagery as collected by the Defense Meteorological Satellite Program's Operational Linescan System (DMSP-OLS) has recently undergone a revival since the digital archiving system implemented by the National Oceanic & Atmospheric Administration's National (NOAA) and the US Air Force at NOAA's National Geophysical Data Center (NOAA-NGDC). This allowed for more accurate assessment of lit areas than previously afforded by the photographic archive, which had poor geometric qualities. Doll et al.(1999) have shown the potential of using DMSP-OLS frequency composite imagery to map population, GDP and CO_2 emissions. This paper presents a methodology for estimating urban population with a radiance calibrated dataset.

2 Datasets

A number of supporting datasets was required to perform this analysis besides the satellite data. Most importantly, population data was required both at the national and individual city scale. The database of world city locations and population was required to calibrate the area-radiance relationship for each country. This was obtained from the Center for Global & Regional Environmental Research (CGRER), part of the University of Iowa. However, the population data was taken from the latest edition of Philip's Geographical Journal. Country level statistics were obtained from the World Resources Institute's (WRI) biennial digest. The WRI collate data from the UN and the World Bank on a host of different socio-economic and environmental parameters. Digital country boundaries were required to segment the night-lights imagery into individual country files.

2.1 Night-time Imagery

This study contrasts two different data products produced by NOAA-NGDC. The frequency value composite image was acquired between October 1994 and March 1995. From this sequence of images a 'stable lights' dataset was created. Stable lights refer to light sources that are spatially and temporally stable throughout the period of observation. In this way city lights may be distinguished from transient features such as bush fires. The OLS channel used to acquire the images is a broad band visible – near infrared (0.4-1.1μm) capable of sensing light emissions down to 10^{-9} W/cm^2/sr/μm. Clouds were screened via use of the thermal channel of the OLS sensor. The DN value associated with a pixel refers to the percentage frequency with which lights were detected during cloud free overpasses (Elvidge et al., 1997). This was thresholded to minimise the effects of reflection from adjacent water bodies (blooming).

The radiance calibrated dataset was collected during the period March 1996 and January-February 1997. It differs from the stable lights product in that a variable gain control was used to acquire images. Previously high gain settings were used to amplify the signal from faint light sources. This also had the effect of saturating the data received from much brighter cities. In order to accommodate the wide range of light intensities encountered, a variable gain of 24dB and 50dB was used and then composited (Elvidge et al., 1999). All data was taken when lunar illumination was low so as to minimise its effects. By conducting an initial variable gain

experiment, thresholds of minimum detectable light were established and used to calibrate the output from of the sensor.

3 Methodology

The methodology used by Doll et al.(1999) derived the allometric growth model for each country and estimated the urban population based on the lit area within that country. The satellite data was vectorised into discrete polygons within a Geographical Information System (GIS). Using the set of 'calibration cities' the total population, P was matched to a polygon of area, A (figure 1).

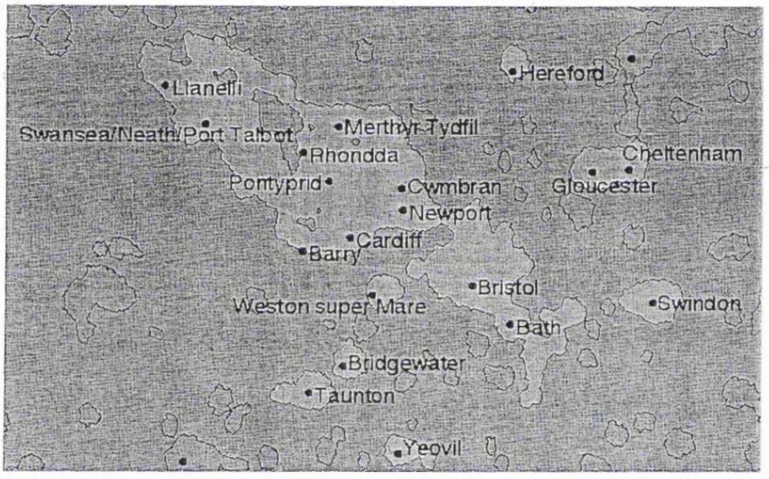

Figure 1: Points (towns) lying within polygons around the South Wales area.

As can be seen in figure 1, there are polygons that have multiple points lying within them. In this case the total population of the towns are plotted against the area of the polygon. The relationship of total population to lit area was plotted according to the allometric growth model, which has been observed in other area-population studies (Nordbeck 1965, Tobler 1969):

$$P=aA^b \quad (1)$$

Where P = Population, A = Area

Plotting the logarithms of P and A, we have:

$$\log P = b.\log A + \log a \quad (2)$$

A linear regression was fitted to the points, and used to estimate population for polygons, which had no population data, associated with it. Most countries fitted this model well with R^2 values between 0.6-0.7. This method considers population to be a function of area only, and therefore ascribes a uniform population density to the urban area in question.

3.1 A Technique for Handling Radiance Calibrated Datasets

A preliminary analysis of the relationship between lit area and radiance shows that for all countries, the majority of area is covered by low intensity lighting with very little area covered by the highest radiance values. The relationship between DN and radiance obeys the following relationship:

$$\text{Radiance} = DN^{(3/2)*}10^{-10}\ \text{W/cm}^2\text{/sr/}\mu\text{m} \qquad (3)$$

Over an 8-bit range (0-255), this relationship covers three orders of magnitude. The methodology adopted, sums the product of area and radiance to estimate population via calculation of a country specific coefficient. This is based on a set of urban polygons which have population associated with it. The polygons from the 1994/5 dataset were overlaid on the radiance calibrated image and used to mask out an area of the radiance image (figure 2).

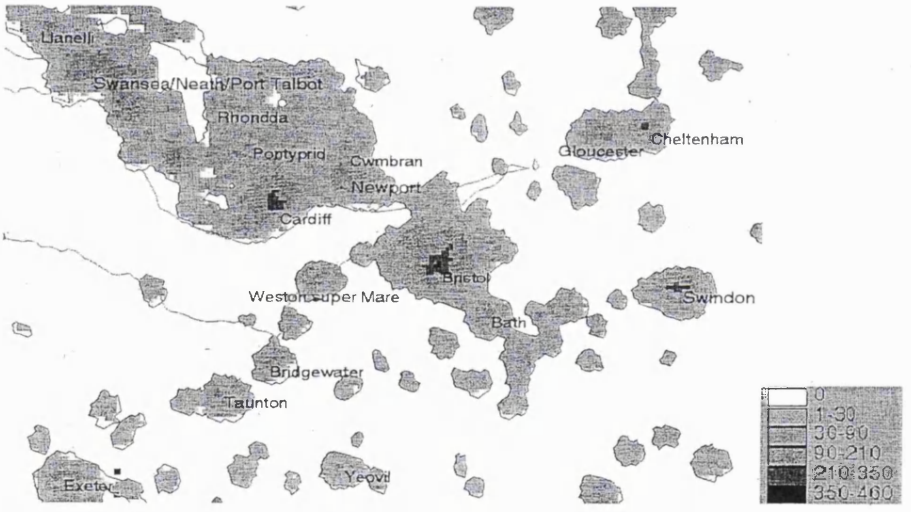

Figure 2: Radiance Calibrated Image of South Wales (as in Fig.1) with under the 1994/5 Urban polygons. Radiance in 10^{-10}W/cm^2/sr/μm

Using the GIS function of tabulating areas of grids within polygons, a table of area under each DN value was produced. For polygons which had population points (cities) lying within, a set of calibration polygons were established and the following model applied:

$$\Sigma \frac{(\text{Radiance})(\text{Area})}{\text{Population}} = \text{NARC}\ (\text{W/cm}^2\text{/sr/}\mu\text{m/m}^2\text{/person}) \qquad (4)$$

For each of the calibration polygons the Normalised Areal-Radiance Coefficient (NARC) was calculated and averaged. Population was then determined for the rest of the 'unknown' polygons by calculating the Σ(Radiance)(Area) and dividing by the NARC. These were summed to obtain the urban population for that country.

4 Results

The results presented are for the 12 countries selected for the study. The selection of these countries was based on the strength of the allometric relationship derived and the degree of accuracy to which urban population was estimated. Countries, which were not well estimated by the use of frequency composite images, were of particular interest. China, Iran and Russia fell into this category whilst India, New Zealand and Bulgaria were well estimated under the old methodology.

Table 1: Summary of Results

Country	WRI Urban Population	Frequency Composite Population	Accuracy (%)	Radiance Population	Accuracy (%)
Bulgaria	6201	5610.0	90.47	4973.1	80.20
Cameroon	5938	1854.0	31.22	2582.1	43.48
China	369492	459652.0	124.40	292453.0	79.15
Germany	70616	46101.0	65.28	56410.0	79.88
India	250681	234462.0	93.53	212468.0	84.76
Iran	39716	82569.5	207.90	39184.0	98.66
Iraq	15258	25927.0	169.92	11771.0	77.15
Japan	97120	36858.7	37.95	72935.0	75.10
Korea	36572	25751.0	70.41	30399.9	83.12
New Zealand	3077	3195.0	103.83	3107.0	100.97
Russia	111736	75368.0	67.45	115466.0	103.34
UK	52119	28758.3	55.18	43687.2	83.82
TOTAL	**1058526**	**1026106.5**	**96.94**	**885436.3**	**83.65**

The new technique improves the accuracy of estimation for 10 out of 12 of the countries. China has gone from being hugely over estimated to well underestimated, but is still closer to the published total. Iran and Russia were previously significant outliers but are now accurately accounted for.

5 Discussion

The results obtained in the first study had a very good overall agreement with the urban population as quoted by the WRI. This can be largely attributed to outlying countries, which have been over, and underestimated canceling each other out when summed and compared to the total. Whilst the overall accuracy has gone down slightly, this technique appears to model individual countries more accurately than before which makes it more robust and ultimately more reliable. It would seem that there is still some way to go with this approach. The reasons as to why some countries perform much better than others is still unclear, though accurate city population data is clearly a major pre-requisite in trying to perform such an analysis. It is perhaps understandable that Japan was not modelled at all well under the previous method since it has such a large population for a small set of islands and a uniform population density was assumed. However, the key assumption with both methods is that all population is accounted for with a polygon used to derive a relationship for the other 'unknown' polygons. In countries such as China, which has experienced unprecedented rates of urbanisation, migration between cities is also a factor to consider and one that is not accounted for here, but highlights the need for high quality ancillary data.

The advantages of a radiance calibrated dataset are manifold. As urban sprawl further encroaches onto undeveloped lands, the increasing light pollution will be mapped. As these are likely to be suburban housing, it is likely to be quite low intensity light. Figure 2 highlights how well urban centres are identified through their higher radiance values. The UK in particular has vast swaths of low intensity light across the country with urban centres lying within. At the very least, the presence of lights can be used as a proxy for the underlying built environment.

6 Summary & Conclusions

A technique for handling radiance calibrated night-time data is presented. The application of which appears to estimate urban population more robustly than previously attempted. Countries which were had been grossly over/underestimated are more accurately estimated, and countries which previously enjoyed good agreement with the allometric growth model are not severely affected by the new technique.

This is a simple method, and has potential for refinement. For instance, one could assign weightings to different radiance values thereby altering the relationship between area and radiance, thought there ought to be a sound rationale behind it. (Owen et al., 1998) assigned urban/suburban/rural classifications to DMSP-OLS frequency data, based on the correlation of night-time lights to housing density for rural areas, and on the assessment made by Imhoff et al. (1997) for urban areas. In addition, there maybe more subtle relationships between the NARCs and different settlement sizes, which if implemented could model population better. This is an encouraging step towards modelling urban population at a global scale.

7 Acknowledgements

The authors wish to thank Chris Elvidge and Kimberly Baugh of NOAA-NGDC for processing and supplying the night-time lights datasets. This work is supported by the NERC studentship GT 04/98 188/TS.

References

CLARK, J.T., and RHIND D.W., (Eds), 1992, *Population Data and Global Environmental Change*, International Social Science Council, Human Dimensions of Global Environmental Change Programme, Report No.3, Paris

DOLL, C.N.H., MULLER, J-P., and ELVIDGE, C.D., 1999, Night-time Imagery as a Tool for Mapping Socio-Economic Parameters. *Submitted to Ambio.*

ELVIDGE, C.D., BAUGH, K.E., KIHN, E.A., KROEHL, H.W., DAVIS, E.A., 1997, Mapping City Lights with Nighttime Data from the DMSP-OLS Operational Linescan System. *Photogrammetric Engineering & Remote Sensing.* **63:** 727-734.

ELVIDGE, C.D., BAUGH, E., DIETZ, J.B., BLAND, T., SUTTON, P.C., KROEHL., H.W., 1999, Radiance Calibration of DMSP-OLS Low-Light Imaging Data of Human Settlements. *Remote Sensing of Environment* **68:** 77-88.

HOUGHTON J.T., MEIRA-FILHO L.G., BRUCE J., LEE H, CALLANDER, B.A., HAITES E., HARRIS N, MASKELL K, 1995 *Climate Change 1994: Radiative Forcing of Climate Change and an Evaluation of the IPCC IS92 Emission Scenarios.* Press Syndicate of the University of Cambridge, Cambridge.

IMHOFF, M.L., LAWRENCE, W.T., STUTZER, D.C., ELVIDGE, C.D., 1997. A Technique for Using DMSP-OLS 'City-Lights' Satellite Data to Map Urban Areas. *Remote Sensing of Environment,* **61,** 361-370.

NORDBECK, S. 1965. *The Law of Allometric Growth.* Inter-University Community of Mathematical Geographers, Department of Geography, University of Michigan: Ann Arbor, Michigan.

OWEN, T.W., GALLO, K.P., ELVIDGE, C.D., BAUGH, K.E., Using DMSP-OLS Light Frequency Data to Categorize Urban Environments Associated with US Climate Observing Stations. 1998, *International Journal of Remote Sensing* **19(17):** 3451-3456

Philip G, *Philip's Geographical Digest 1998-99*, 1998 Heinemann Educational in assoc. with George Philip.

TOBLER, W.R. 1969. Satellite Confirmation of Settlement Size Coefficients. *Area,* 1: 31.

TOBLER, W.R, DEICHMANN, J., and MALLOY, K, 1995. *The Global Demography Project,* Technical Report No. 95-6, National Center for Geographic Information and Analysis, UCSB, Santa Barbara, California, 75p.

WRI, *World Resources 1996-97, A Guide to the Global Environment.* 1996 The World Resources Institute, UNEP, UNDP, The World Bank, OUP, Oxford, UK. Chapters 7,8,14

IAPRS, Vol. XXXIII, Amsterdam, 2000

A COMPARISON OF DIFFERENT TECHNIQUES APPLIED TO THE UK TO MAP SOCIO-ECONOMIC PARAMETERS: IMPLICATIONS FOR MODELLING THE HUMAN DIMENSIONS OF GLOBAL CHANGE

Christopher N.H. DOLL, Jan-Peter MULLER
Department of Geomatic Engineering,
University College London,
London WC1E 6BT,
United Kingdom.

cdoll@ge.ucl.ac.uk, jpmuller@ge.ucl.ac.uk

KEY WORDS: Global Change, Mapping, Interferometry, Remote Sensing

ABSTRACT

This paper focuses on the potential of remotely sensed imagery to map the parameters important to aid our understanding and modelling of the interactions between anthropogenic activity and the natural environment. Urban areas are nodes for commerce, industry, habitation and the exchange of ideas. As such they are areas which are of greatest importance to scientists studying human induced global change. Urban areal extent is one parameter that is readily mapped from remote sensing data, and is already a component of global land use maps. This paper considers to what extent remote sensing can provide information on other parameters, and how different techniques may compliment each other.

Night-time imagery over the UK has been analysed with respect to a number of other datasets. Street lighting is hypothesised to be a major contributor to night-light data, so a detailed map of the road network was used to analyse which road types were the largest contributors to "light pollution" over the UK. The UK is highly visible from space at night, urban centres being clearly visible as foci of bright light. A 1km land-use map provided by the Institute of Terrestrial Ecology (ITE) was used as a more quantitative measure of correlation between light and land cover class. Varying proportions of urban/suburban cover against radiance were tested to establish the threshold radiance for different land cover proportions. Night-light data has been previously demonstrated to be useful for estimating urban population (84% accurate for the UK). A 200m gridded census map was resampled and summed to 1km and used to better understand the radiance-population relationship. Features such as airports were found to affect the correlation of light to population. Night-time light imagery is limited however, in that the light emissions are used as a proxy for the underlying built environment. SAR interferometric composite images of phase coherence, amplitude, and difference in amplitude and its urban classified component may also be used to elucidate the night-light data and assess the accuracy of the built environment components of the ITE land use map. A preliminary example of this is shown here.

1 INTRODUCTION

Apart from natural hazards, human activity has the greatest potential to inflict unplanned changes on the natural environment. However, the feedbacks between human activity, the natural environment and the climate system are so complex, it is one of the least well understood aspects of the subject despite being a major (if not the primary) driver for global change. There is a dearth of suitable datasets to link the effects of human activity to the well-established biogeochemical processes leading to global change.

Conventional optical imagery is not well suited to urban area detection and delimitation as it suffers from mixed signals arising from the heterogeneous land-cover, particularly due to green spaces within the urban fabric, which is a feature of these areas. Night-time imagery overcomes this problem by solely considering light emissions from the ground. In the absence of industrial processes such as gas flare burn off, this contribution is primarily from cities and transport networks; the hubs of human concentration.

1.1 Night-time Imagery

Night-time imagery has great potential not only for mapping urban areas, but also deriving other socio-economic parameters. (Doll et al., 2000) have demonstrated its utility for mapping Carbon Dioxide emissions, economic activity and, estimating national populations (Doll & Muller, 1999). A radiance calibrated image of the UK at 30" (~1km) captured by the Defense Meteorological Satellite Program Operational Linescan System (DMSP-OLS) was processed and supplied by Chris Elvidge at NOAA-NGDC. The radiance-calibrated night-time light product supercedes the frequency composite dataset acquired between October 1994 and March 1995 from which a 'stable lights' dataset was created. Stable lights refer to light sources that are spatially and temporally stable throughout the period of observation. In this way city lights may be distinguished from transient features such as bush fires. The OLS channel used to acquire the images is a broad band visible – near infrared (0.4-1.1μm) capable of sensing light emissions down to 10^{-9} $W.cm^2sr^{-1}.\mu m^{-1}$. Clouds were screened via use of the thermal channel of the OLS sensor. The DN value associated with a pixel refers to the percentage frequency with which lights were detected during cloud free overpasses (Elvidge et al., 1997). This was thresholded to minimise the effects of reflection from adjacent water bodies (blooming).

The radiance-calibrated dataset was collected during the period March 1996 and January-February 1997. It differs from the preliminary stable-lights product in that a variable gain control was used to acquire the constituent images. Previously high gain settings were used to amplify the signal from faint light sources. This also had the effect of saturating the data received from much brighter cities. In order to accommodate the wide range of light intensities encountered, a variable gain of 24dB and 50dB was used and then the individual images composited (Elvidge et al., 1999). All data were taken when lunar illumination was low so as to minimise its effects, especially over water bodies close to terrestrial light sources. By conducting an initial variable gain experiment, thresholds of minimum detectable light were established and used to calibrate the output from the sensor. Work done by Chris Elvidge at NOAA-NGDC based in the US, suggests that towns of only 150 inhabitants can be detected (Elvidge, pers. com.)

1.2 Other Datasets

Studies up until now have concentrated on night-time lights at a global scale and have been used to infer parameters like population via derivation of areal, and areal-radiance log-log relationships. An aim of this paper is to establish to what degree night-time imagery represents light sources on the ground, and how well the coarse resolution of the imagery compares to the expected classes found in land use maps (namely, the urban and suburban classes) and gridded census data. The UK was selected for this study, as there were many ancillary datasets available and almost all similar previous work has only focused on the US. The UK offers a European perspective, and access to comparative data was easily available from the Manchester Information and Associated Services website [1].

City-lights over the UK was compared against the following datasets which are described in more detail below:

- Bartholomew's 1:250,000 road network
- Institute of Terrestrial Ecology's 1km land-cover map
- 1991 Population census data gridded to 200m (SURPOP)

1.2.1. The ITE Land Cover Map. The map used was produced by the ITE and is itself derived entirely from satellite data, specifically a mosaic of 46 Landsat TM images taken between 1987 and 1990. The product was produced on a 25m grid and there is also a 1km 'summary' dataset. In resampling from 25m to 1km, the relative % coverage of each of the 25 classes is represented in each 1-km cell. Each land cover class is represented as an ArcView coverage, thus the urban layer is essentially a map of the UK with the % urban value in each cell. A realistic assessment of accuracy for the Land Cover map is put at between 80-85% (Fuller, 1995)

The format of the landcover map was such that it could be used with the radiance calibrated night-time data to test whether there is any obvious relationship between radiance and land cover exist for the UK. In particular since urban and suburban classes are distinct, there is a good opportunity to examine how these two individual classes affect night-time light emissions. It is hypothesised that light should only come from cells that have some component of urban or suburban infrastructure therein and that radiances are higher where urban infrastructure predominates. As a point of note, the urban class is defined as *'all developments which are large enough to fill individual pixels* [at 25m], *to the exclusion of significant quantities of permanent vegetation'* (Fuller, 1995). The suburban/rural development category includes *'all land where pixels of the Landsat image have recorded a mixture of built-up land and permanent vegetation'* (Fuller, 1995). However, this study is only concerned with which part of the built environment is covered by lights. In this case, one need not make the distinction too rigorously.

IAPRS, Vol. XXXIII, Amsterdam, 2000

1.2.2 Gridded Census Data. A complementary element of the analysis involves a gridded dataset of the census taken in 1991. Census data is collected at the smallest level, by enumeration districts (ED, ~200 households in 1991) of irregular shape and size. This data was then gridded to 200m via identifying the centroids of each ED and then running a re-distribution algorithm that generates a distance decay function, whose extent is determined by the local density of centroids. Weights are assigned to the surrounding cells, which receive a proportion of the count at the centroid [2]. The initial dataset has a resolution of 200m, though this was aggregated to 1km so as to match with the other datasets.

2 NIGHT-LIGHTS AND THE UK ROAD NETWORK

Street lights generate most of the urban light observed at night. The Bartholomew's road network at 1:250,00 is available as an ArcView coverage from MIMAS. Arcs (roads) were assigned identification numbers based on road classes (single/dual carriageways, tunnels etc). These in turn could be grouped into the major road types displayed in road atlases namely; A-roads; B-roads; motorways; and minor roads. These categories were overlaid onto a greyscale night-time image map of the UK, using the standard colour map from OS maps (Figure 1). The distance of each road type was calculated for the range of radiances occurring with mainland Britain.

2.1 Methodology

Processing of the data was done using ArcInfo. The arc line coverage was split up into separate route topologies using the ***ARCROUTES*** command that splits an arc topology up into separate routes according to a given attribute within the attribute table. The id-code codes for the road types were selected enabling the GIS to recognise different road types. The night-light grid was vectorised such that each square grid cell was made into a discrete polygon. By vectorising the satellite data, it effectively reduces the problem to calculating the length of an arc within a polygon. The ***POLYGONEVENTS*** command was invoked to compute the geometric intersection of a polygon coverage (the night-lights) and a route system (the roads). Roads were processed by four regions, depending on the prefix of the UK grid tiles used to split up the Great Britain National Grid system. The tables written out by the ***POLYGONEVENTS*** command were merged and road lengths (classified by road types) were collated. A new table of total road length radiance and area was created. Finally total road length was normalised by area so road density for each road type could be plotted against radiance.

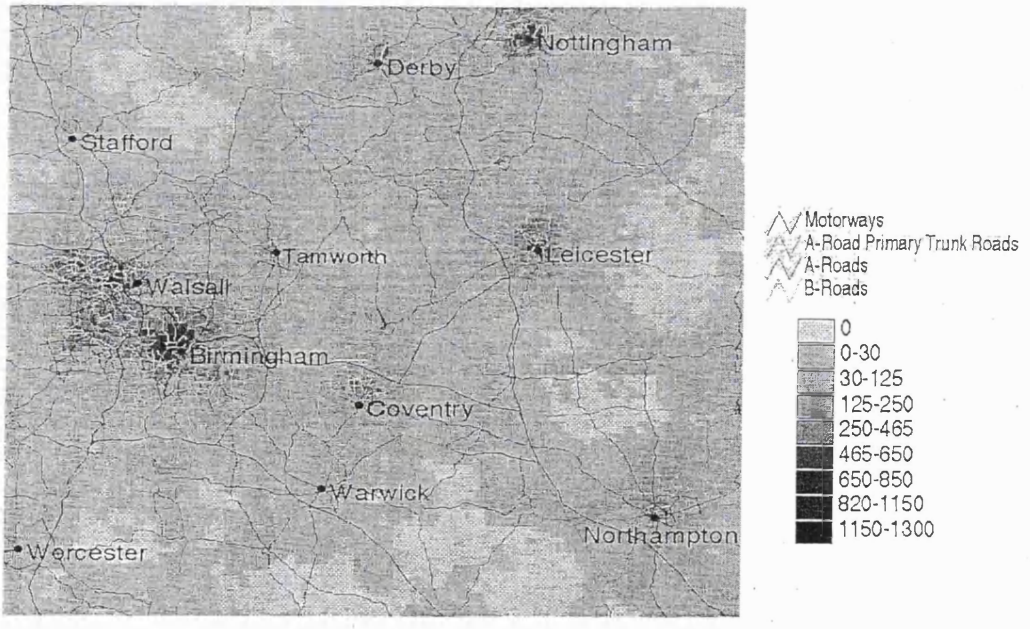

Figure 1. Greyscale Night-time light polygons with Road Network overlaid for the Midlands.
(Radiance; $x10^{-10}$ $W.cm^{2}.\mu m^{-1}$)

2.2 Results

Figure 2 shows how road density over mainland Britain varies as a function of road type. Road density is expressed as metre lengths per square kilometre and the data has been smoothed by a 10 DN (~32 $W.cm^2.um^{-1}.sr^{-1}$) running average to make the data more readily understandable. Non primary A-roads dominate the plot and are observed to linearly increase up to around $560x10^{-10}$ $W.cm^2.um^{-1}.sr^{-1}$ where upon the road density increases rapidly until it reaches 800 $W.cm^2.um^{-1}.sr^{-1}$. A further peak occurs at the highest radiances in the UK at over 1000 $W.cm^2.um^{-1}.sr^{-1}$ which only occurs over London. Minor roads are densest over the lower range of radiances (0-350 $W.cm^2.um^{-1}.sr^{-1}$). Minor roads are the densest of all roads in low radiance polygons and have a fairly constant density of around 700 $m.km^{-2}$ until they drop rapidly to around 50 $m.km^{-2}$ at 640 $W.cm^2.um^{-1}.sr^{-1}$ and cease to feature beyond 850 $W.cm^2.um^{-1}.sr^{-1}$. Motorways have a constant low density throughout the radiance range of around 75-100 $m.km^{-2}$. Trunk roads and primary dual carriageways linearly increase to around 400 $m.km^{-2}$ at 550 $W.cm^2.um^{-1}.sr^{-1}$ where it stabilises throughout the higher radiances. Meanwhile B-roads increase very gently in density (200-300 $m.km^{-2}$) until they experience a broad peak of 600 $m.km^{-2}$ through the 810-920 $W.cm^2.um^{-1}.sr^{-1}$ radiance range, suggesting that these roads are most common in the centre of towns.

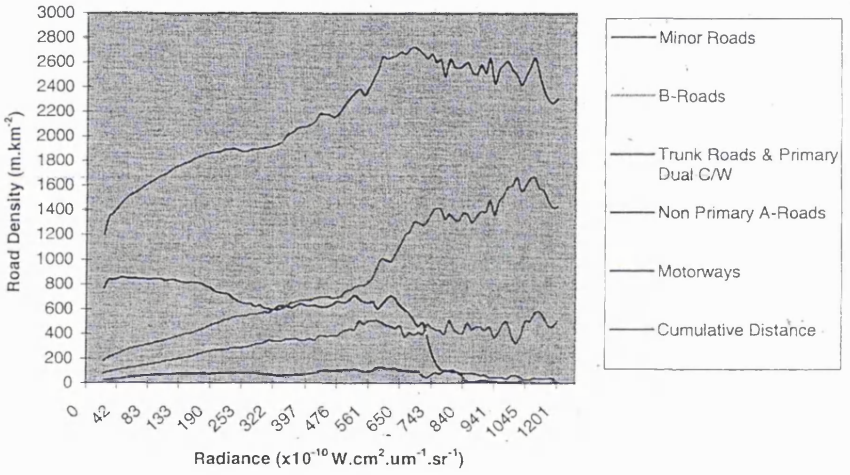

Figure 2. Average Road Density as a function of Radiance for Mainland Britain

2.3 Discussion. The cumulative distance trace is most akin to the non-primary A-roads, showing it is the most dominant of all the road types displayed. Cumulative distance increases roughly linearly with radiance until it reaches a peak of 2700 $m.km^{-2}$ at 600 $W.cm^2.um^{-1}.sr^{-1}$ beyond which road density gently falls to around 2400 $m.km^{-2}$. It is therefore true to say that overall, night-time light imagery and the road network, taken as a proxy for street lighting are correlated. However there is variation within different road classes. The dominance of non-primary A-roads in the higher radiance range (>620 $W.cm^2.um^{-1}.sr^{-1}$) suggests that these road sections are concentrated in urban areas, and as such are a major source of street lighting. This study assumes that all roads are lit throughout the entire road network. This is not the case, especially in rural areas. Motorways are only lit around towns (e.g. within the M25 region in London). There exists no comprehensive list of lit road sections for the UK as this is under the control of individual Route Managers (D.Ryall, Highways Agency, personal communication). Thus, it is not immediately clear what are the quantitative effects of road network on the night-time image over Britain.

3 NIGHT-LIGHTS, LAND COVER & POPULATION

The night-light map of Great Britain is observed to have a wide covering of low intensity lighting with urban centres lying within distinguished by their higher radiances. Low level light is far more widespread in this version of the night-time light product than in the frequency composite product produced some 18 months to two years earlier. This is not to

say urban area has increased during this time interval, rather that the incorporation of low–gain imagery has identified many more faint light sources which are non-urban, and as such raw night-time imagery cannot be taken as an absolute measure for urban area. The contribution of low radiance light around the urban periphery is of great importance in its interpretation for global urban land cover mapping. In order to assess this situation for mainland Britain, the land cover map was required to identify; firstly if there was a radiance threshold which corresponded to the urban (and suburban) classes of the land cover map.

3.1 Results and Discussion

The first item to be tested was whether there can be a proportion of the built environment, which can be said to be urban. At a first attempt the DCW (Denko, 1992) populated places polygons were used as the urban layer (as opposed to the night-lights). This was tested against proportions of the built environment as defined by a threshold of summed urban and suburban land cover. Assessments were made both visually and with respect to cell counts.

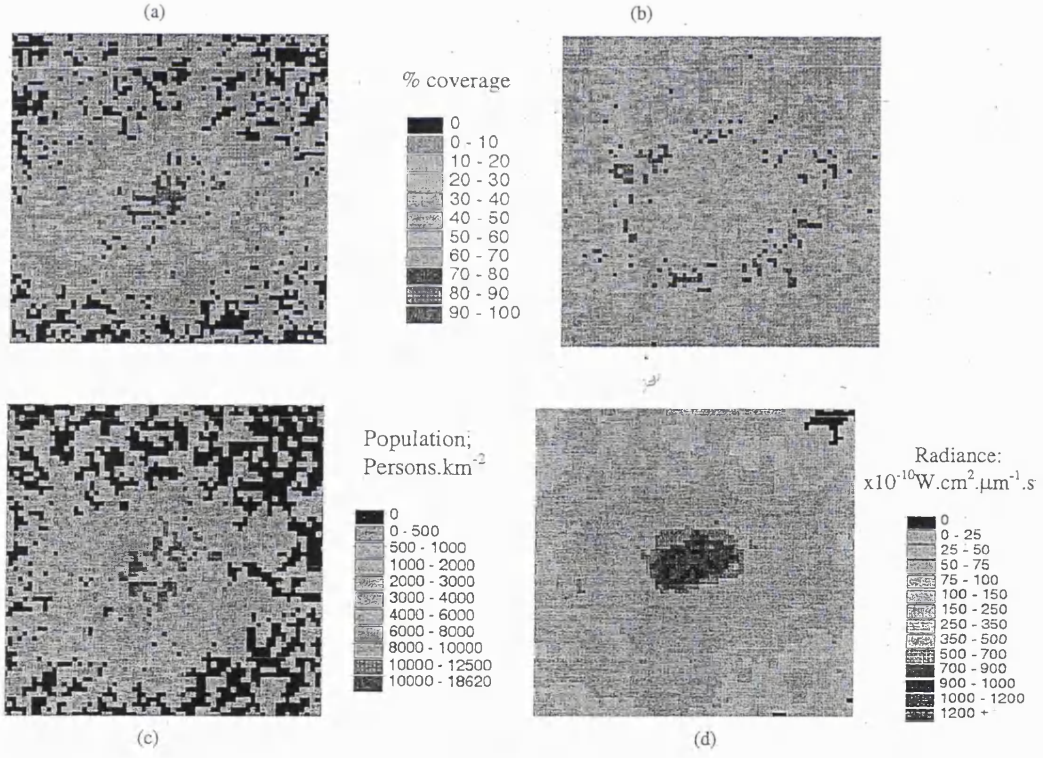

Figure 3. Different Datasets over London, Urban land cover (a), Suburban land cover (b), and Population (c) as compared to the Radiance Calibrated Night-time lights Imagery (d). Image 65 x 60 km.

Urban areas are characterised in the land cover map by a core of high percentage urban cover surrounded by a ring of high percentage 'suburban/rural development' (Figure 3 a,b). Population (Figure 3c) can be observed to follow a similar pattern though in London, the ring of high population density is much closer to the centre. The night-lights image (Figure 3d) has much less detail even though it has the same 1km resolution. This is partly due to the image having been resampled from a nominal resolution of 2.7km. A threshold of 43% for combined urban+suburban land cover was found to be consistent with the DCW urban polygons. This also approximated to a population density of 2000 people.km^{-2}. However, no single radiance threshold could be easily determined in the same way. One reason for this is illustrated in Figures 3c and 3d. The bright patch in the radiance image towards the west of London is Heathrow

Airport, though it has no *recorded* population. The fact that light-sources may be attributable to human activity other than habitation results in the poor correlation between radiance and population (Figure 4a). A given radiance threshold was found to overestimate the area for some settlements, and underestimate for others. In some cases settlements were totally omitted. The spread of population at low radiance values in the scatterplot supports this. Smaller settlements and urban fringes are noted to be omitted when invoking a single threshold. This suggests an adaptive threshold approach whereby the radiance threshold is a function of settlement size, though not helpful in the London Airport case, would generally help to elucidate a relationship between these two parameters. Population was found to be better correlated with suburban land cover (Figure 4b) than with the urban land cover class. Summing urban and suburban land cover helps to define the built environment, but effaces (?) the correlation between a 'built' cover percentage and population. The DCW urban polygons intersected with 33.4 million people out of a total 54.45 million from the 1991 census, giving a 61.3% urban percentage compared with 89% from the WRI. The WRI urban population figure for 1995 (WRI, 1996) for the UK is 52.1 million.

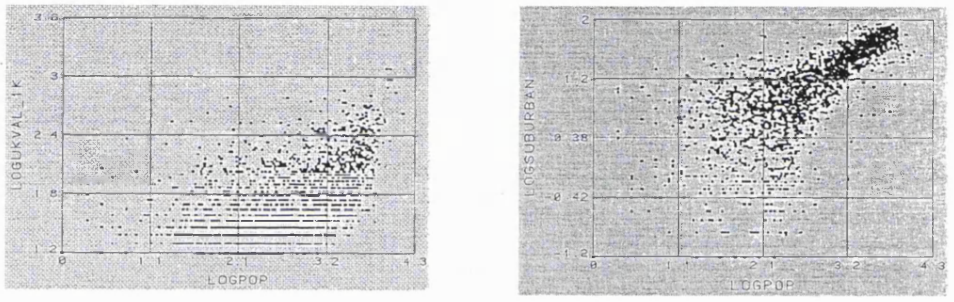

(a) (b)

Figure 4. Scatterplot of Log population and Log radiance (a), and Log Suburban land cover (b)

The gridded population dataset has the potential to identify the population morphology outlined as being a key component of accurate population estimation in the previous section. Once a criterion for urban area delimitation has been agreed, the population morphology within these areas can be assessed and used in population estimation models. The lack of such census datasets for most other parts of the world is a disadvantage for ascertaining how population morphologies differ and to what extent they can be generalised for global mapping.

4 INTERFEROMETRIC COMPOSITES

Imaging radar can offer distinct advantages over optical sensors when considering the mapping of urban area. The inherent nature of radar imagery being more related to the physical properties of the target as opposed to the molecular resonances of surface materials more akin associated with optical imagery (Henderson & Xia, 1997). The structural/physical nature of radar imagery has meant that the backscatter in an image is dependent on the geometric relationship between the look angle of the antenna, and the orientation of the buildings (targets) (Bryan, 1979). In this respect the use of interferometric SAR is particularly valuable for urban mapping. Since urban areas are highly coherent land surfaces when compared to the surrounding area, they tend to appear as bright patches on the image. Studies have shown that urban surfaces can remain relatively coherent since surrounding vegetation will necessarily decorrelate with time as the seasonal vegetation cover alters the scattering characteristics of the target. Significant decorrelation can occur in rural areas due to changes in moisture and wind effects even at short temporal baselines (Grey & Luckman, 1999).

ERS1/2 tandem data was acquired as part of the LANDMAP project (Muller et al., 1999, Morley et al., 2000) was processed and used to create colour composites according to the methodology proposed by Wegmuller & Werner (1995). According to the colour scheme the three bands are assembled into a RGB colour composite as phase coherence (red), amplitude [backscatter] (green) and difference in amplitude (blue). In this way urban areas distinguish themselves as yellow pixels since there is little magnitude in the blue band and coherence and backscatter are high. One strip was processed running diagonally across the British Isles from NE-SW. An example of the 3 band colour composite is shown in Figure 5. Urban areas are easily distinguished on the image despite the very short temporal baseline. Other high coherence areas include fields and ridges. An unsupervised classification could not adequately resolve these

features, however a Mahalanbois Distance supervised classifier (Figure 6) was found to markedly improve the extraction of urban features from the 3 band composite. Two supervised urban classes were identified. Both were found to contribute to urban cover in the classification, though one (yellow) was noted to also misclassify some 'bright' pixels on the crest of hills.

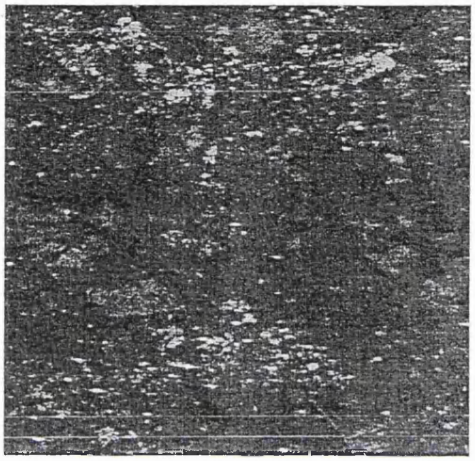

Figure 5. Section of the three-band colour composite phase coherence (red), amplitude (green) and phase difference (blue)

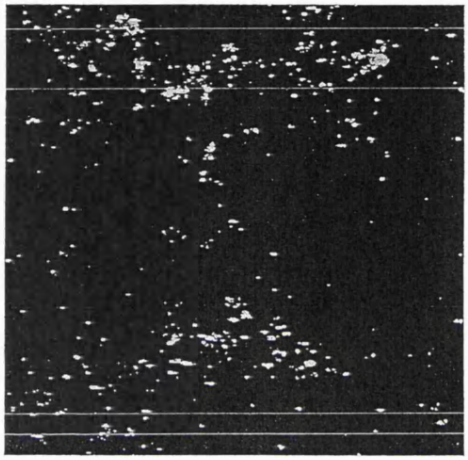

Figure 6. Classified urban layers (2) from the Figure 5. (Mahalanbois distance supervised classification (8 classes)

Urban areas are very apparent on the image at all scales, though the supervised classification still misclassifies some pixels belonging to other high coherent features at this temporal baseline. The result is expected to significantly improve with use of interferometric data with a longer temporal baseline. The higher resolution of this imagery (1 arc second pixel size) has many useful applications with respect to the other datasets used in this study. The lack of a one-to-one correspondence between population and radiance means that there needs to be a more subjective investigation into what the effective ground conditions are to produce a given radiance. The adaptive threshold approach mentioned in the previous section would benefit from the incorporation of a high-resolution urban layer, since pixels of equal radiance but in different positions (i.e. isolated or part of a large cluster). This new layer would also provide a source of validation for the urban components in the ITE land use map, given that interferometric techniques are more reliable than classifications from optical data as displayed in the land cover map.

Aside from the potential to classify night-time data, it is highly valuable in areas where settlements are not reliably detected by night-time imagery. Doll & Muller (1999) used night-time imagery to estimate the urban component of population, but considered the data to be unrepresentative of total settled areas. IfSAR's ability to map the built environment should be of great potential to map urbanisation in the developing world. In addition, since there is urban areas can stay coherent over very long time periods, it also provides a useful tool for change detection analysis as has been attempted by Grey and Luckman (1999) for an area over Cardiff.

5 SUMMARY & CONCLUSIONS

Population, and land cover have been combined with night-time radiance data over mainland Britain to analyse the relationship between these parameters which have, up until now been considered individually. The radiance-calibrated night-light image is over-sensitive to urban land cover. Unlike the land cover data, there appeared to be no single radiance threshold that corresponds to the urban delimitation as described by DCW map layer. This was attributed to the lack of a one-to-one correspondence between population density and radiance for low radiance values. It is hypothesised that this is can be modelled by analysing the population morphology within an urban area, which may be dependent on the size of the settlement in question. The SURPOP dataset will be used to test this hypothesis, along with the previous city lights polygons will be used to test this hypothesis. Higher resolution classified interferometric composites of urban area may be combined to assess how much of the built environment is present to produce a night-

light pixel of a given radiance and also to assess the urban layers of the land cover map. The preliminary results presented here are positive and set to become more so with the use of longer temporal baselines for increased delimitation of urban areas.

ACKNOWLEDGEMENTS

The authors acknowledge and wish to thank Alec Walker from the Department of Geomatic Engineering, UCL, for processing the SAR data as part of the LANDMAP project. The authors also wish to thank Chris Elvidge and Kimberly Baugh of NOAA-NGDC for processing and supplying the night-time lights datasets. All processing was done at the Manchester Computing Facility, MIMAS. We thank Dr. Kamie Kimitto for provision of the computing facilities. This work is supported by the NERC studentship GT 04/98 188/TS.

REFERENCES

Bryan, M. 1979. The Effect of Radar Azimuth Angle on Cultural Data. Photogrammetric Engineering and Remote Sensing, 45, 1097-1107

Denko, D.M. 1992. The Digital Chart of the World Project. PERS 58(8): 1125-1128

Doll, C.N.H., Muller, J-P., Elvidge, C.D. 2000. Night-time Imagery as a Tool for Global Mapping of Socio-Economic Parameters and Greenhouse Gas Emissions. AmbioVol.29 No.3 159-164.

Doll, C.N.H. and Muller, J-P. 1999. The Use of Radiance Calibrated Night-time Imagery to Improve Remotely Sensed Population Estimation. Proc. RSS99, Cardiff, 8-10th Sept. 1999 pp.127-133

Elvidge, C.D., Baugh, K.E., Kihn, E.A., Kroehl, H.W., Davis, E.R. 1997. Mapping City Lights with Nighttime data from the DMSP-OLS. *Photogrammetric Engineering and Remote Sensing 63 (6): 727-734*

Elvidge, C.D., Baugh, E., Dietz, J.B., Bland, T., Sutton, P.C., Kroehl., H.W. 1999. Radiance Calibration of DMSP-OLS Low-Light Imaging Data of Human Settlements. *Remote Sensing of Environment* 68: 77-88.

Fuller, R.M., 1995. The Land cover Map of Great Britain – A Description, Annex A. Pub. ITE Monks Wood, Abbots Ripton, Huntington, Cambs. PE17 2LS.

Grey, W.M.J., Luckman, A.J., 1999. Using SAR Interferometric Phase Coherence to Detect Urban Change. Proc. RSS99, Cardiff, 8-10th Sept. 1999. 457-464.

Henderson, F.M., and Xia, Z-G. 1997. SAR Applications in Human Settlement Detection, Population Estimation and Urban Land Use Pattern Analysis: A Status Report. IEEE Transactions on Geoscience and Remote Sensing, Vol.35. No.1 79-85

Morley, J.G., Walker, A.H., Muller, J-P., Kimitto. K, Mitchell., K, Chagani, K., Smith., A., Barnes, J., Cross. P.A., Dowman, I.J. 2000. LANDMAP: Creating a DEM of the British Isles by SAR interferometry. ISPRS 2000. Amsterdam.

Muller, J-P, Morley, J.G., Walker, A.H., Barnes, J., Cross, P.A., Dowman, I.J., Mitchell, K., Smith, A, Chagani, K, Kimitto, 1999. The LANDMAP Project for the Creation of multi-sensor Geocoded and Topographic Map Products for the British Isles based on Tandem Interferometry. Fringe '99 ESA Workshop, Liege 10th Sept. – 12th November 1999. www.esa.int/fringe99.

Wegmuller, U., Werner, C.L. 1995. Land Surface Analysis using ERS-1/2 Tandem Data. ESA Bulll. No.81, Feb. 1995. 30-37.

World Resources 1996-97, 1996. A Guide to the Global Environment. Joint Publication by; The World Resources Institute, UNEP, UNDP, The World Bank, *OUP.*

URL References

[1] http://www.mimas.ac.uk
[2] http://census.ac.uk/cdu/surpop/

Report

Christopher N.H. Doll, Jan-Peter Muller and Christopher D. Elvidge

Night-time Imagery as a Tool for Global Mapping of Socioeconomic Parameters and Greenhouse Gas Emissions

Night-time satellite imagery acquired between October 1994 and March 1995 is here exploited to derive economic and energy-related global maps. By considering the lit area of a city, and combining this with ancillary statistical information, an analysis was performed designed to investigate the potential of night-time imagery for quantitative estimation of global socioeconomic parameters. An attempt to estimate global urban population using correlations of lit area and urban populations to derive country-level relationships accounted for over 90% of the quoted total. Furthermore, the total lit area of a country has a statistically significant high correlation value with other parameters, specifically Gross Domestic Product (GDP) and total carbon dioxide (CO_2) emission. The new technique is limited by the spatial resolution of the sensor and the poorer correlation using night-time lights for centrally-planned economies. These findings offer great potential for synoptic global mapping of such parameters in the future.

INTRODUCTION

The Earth's population has doubled from 2.5 to 5 billion over the period 1950–85, and currently stands at around 6 billion (1). Levels of development are so diverse and trends so transient that projections of how human population will progress vary greatly (2). However, it is well documented that since 1945, the percentage of human population living in urban areas has grown from 30% to 47% in 2000 and is projected to reach 60% in 2025 (3, 4). It is increasingly being recognized that anthropogenic activity poses the largest threat in terms of forced inputs into the natural system.

Knowledge of the size and spatial distribution of urban areas is vital to many of the global issues confronting society today, in particular, to what extent human activity influences the magnitude and rate of global warming we are currently experiencing. CO_2 has been identified as the most important of the greenhouse gases accounting for around 64% of anthropogenic radiative forcing (5). The need for global monitoring of our urban environments could not be more necessary.

Imagery has been obtained from the broadband visible-near infrared (0.4–1.1μm) channel of the Defense Meteorological Satellite Program Operational Linescan System (DMSP-OLS). This sensor distinguishes itself from the rest of passive, optical remote sensing in that the data can be acquired at night and are sensitive to light sources down to a minimum detectable radiance of 10^{-9} W m^{-2} sr^{-1} μm^{-1} (6). Work performed by Elvidge and colleagues at the National Oceanic and Atmospheric Administration's National Geophysical Data Center (NOAA-NGDC) in Colorado, USA has indicated that towns with only 150 inhabitants can be detected. Dr. P. Cizano at Padua Observatory, Italy (pers. comm., 1999) has calculated that two unshielded light fixtures of the "globe" kind, with clean transparent glass equipped with 250 W high pressure sodium lamps with 125 lm W^{-1} efficiency and placed at every km^2 could be sufficient to produce this luminance. In essence, the only radiance detected by the sensor, after masking out clouds using the OLS Infra-Red channel are man-made light sources, primarily from cities, but also from oil-field gas-flare burnoff, biomass burning, and shipping fleets (7). In the analysis, these temporally varying night-time lights have been screened out so that only urban lights remain.

The first use of night-time lit areas, albeit using photographic products, was reported by Croft in the late 1970s (7, 8). Attempts were then made to correlate these lit areas derived manually from photographic products with energy and population (9), and with population and land use in China (10). The first global map was produced using photographic products (11). The first use of global digital mapped data looked at lit areas and compared these with population, energy usage, and economic activity (6, 12, 13). However, these data are restricted to the USA and a few other countries. Studies have also looked at the accuracy of the night-time lit areas and population census data but only for the conterminous USA (14, 15). The work reported here represents the first attempt to obtain global maps of socioeconomic parameters and CO_2 emission.

METHOD

A 6-month 1 km composite taken between October 1994 and March 1995 was assembled from a time series of images. The brightness value associated with our global 1 km composite refers to the percentage of times the pixel had been viewed (lit) on the cloud-free night-time overpasses made by the satellite. From this composite, a 'stable lights' dataset was produced eliminating transient light sources such as migrating bush fires and shipping fleets, to reveal a city-lights only dataset. This was further thresholded (at 7%) to try to minimize the effects of blooming; e.g. reflection of light from waterbodies and around urban peripheries.

A number of supporting datasets have been used to help to interpret and compare against the satellite data. A comprehensive dataset of human population location centers ca 1990 was obtained from the University of Iowa's Center for Global and Regional Environmental Research (CGRER). Population figures were taken from the latest edition of the Philip's Geographical Digest for data collected around 1995 (16). The aggregated country-level statistics were taken from the World Resources Institute (WRI) biennial publication (17). The WRI compiles data directly from the World Bank and the United Nations environment and development programs to produce what are widely regarded as the standard statistics on the human environment. Global country polygons were acquired from ESRI based on the Digital Chart of the World (18).

The data processing and analysis was performed within a geographic information system (GIS). The global 30 arc-second (≈ 1 km) dataset was processed on a continent by continent basis due to its large size (> 1 Gb). The perimeters of lit areas were traced by vectorizing the raster image into discrete polygons. Upon projection to an equal-area representation (Lambert-Azimuthal), lit areas could be calculated accurately. In order to assess the nature of, and quantify any relationship between lit area and population, city population locations were used to geolocate

and reference into corresponding city-light polygons. Where a country level figure for lit area was required, a country mask was overlaid over the lit area polygons, and a spatial intersection algorithm used to assign lit polygons to countries. For countries that had more than 10 lit-area polygons with associated population figures, a linear log-log relationship was tested and extrapolated to the other polygons within that country. The individual urban populations were then summed and compared with the WRI urban population figure. The differences between the WRI, and the lit area-derived populations for 46 countries where there were sufficient lit area polygons to do a comparison are shown in Table 1. An assessment of the linearity of the log-log relationship between lit area and the other variables was also tested at the continental scale.

Country-level relationships between lit area, and Gross Domestic Product (GDP) (Fig. 1a), and total CO_2 emissions (Fig. 1b) were used to create global maps of these parameters on a 1° x 1° grid (Figs 2 and 3, respectively). The resultant CO_2 emissions map was compared to the 1995 map (Fig. 4) produced by the Carbon Dioxide Information Analysis Center (19) (CDIAC). In order to compare values from CDIAC on a geographic (Plate Carée) grid with those from DMSP-OLS, an approximation was needed to account for the difference in projection. The OLS data was approximated into 10 zones; an equatorial zone, from the equator to 10° of latitude; 10°–30°; 30°–40°, 40°–50°; 50°–60°; and 60°+ for the Northern Hemisphere. The map does not extend beyond 60° South and there were very few lit areas above 60° North. The percentage lit per square degree could then be converted into area and inserted into the relationship to derive the required parameter.

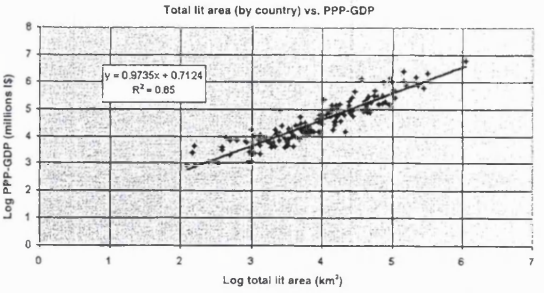

Figure 1a. Relationship between PPP-GDP and total lit area (for all countries).

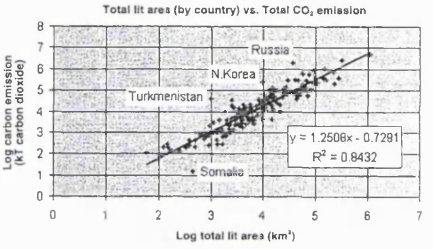

Figure 1b. Relationship between total CO_2 emissions and total lit area (for all countries).

Table 1. Summary of WRI urban population and total CO_2 emissions with predicted values from relationships for 46 countries with at least 10 identified urban polygons.

Country	Total lit area (km²)	Urb. pop WRI 1995 (000s)	Predicted urban population (000s)	WRI Total CO_2 (ktonnes carbon)	Predicted CO_2 (ktonnes carbon)
Austria	71 714	15 318	14 482	267 937	220 947
Australia	15 688	4424	4344	56 572	33 015
Azerbaijan	10 200	9340	8029	63 878	19 269
Bulgaria	11 493	6201	5611	54 359	22 372
Cameroon	2334	5938	1855	2231	3045
Canada	280 557	22 593	22 704	409 862	1 216 984
China	317 239	369 492	459 652	2 667 982	1 419 170
Cote d'Ivorie	3691	6211	3670	6309	5404
Cuba	9406	8389	5518	28 623	17 412
Denmark	13 682	4414	3202	53 897	27 823
Egypt	43 095	28 170	30 919	83 997	116 853
Finland	44 613	3225	2004	41 176	122 025
France	142 838	42 203	34 836	362 076	523 093
Georgia	4220	3190	2796	13 839	6389
Germany	92 580	70 616	46 101	878 136	304 101
Hungary	13 685	6541	6392	59 910	27 830
India	220 644	250 681	234 462	769 440	901 136
Indonesia	57 953	69 992	66 478	184 585	169 259
Iran	108 616	39 716	82 563	235 478	371 361
Iraq	28 164	15 258	25 927	64 527	68 641
Italy	99 215	38 101	27 146	407 701	331 604
Japan	146 886	97 120	36 859	1 093 470	541 700
Kazakhstan	46 800	10 218	14 418	297 982	129 552
Korea	29 835	36 572	25 751	289 833	73 772
Malaysia	24 766	10 814	8981	70 492	58 442
Mexico	157 758	70 535	50 543	332 852	592 308
Morocco	18 407	13 071	15 700	27 344	40 322
Netherlands	27 005	13 801	7952	139 027	65 124
New Zealand	16 787	3077	3196	26 179	35 932
Nigeria	13 185	43 884	25 581	96 513	26 563
Pakistan	42 315	48 742	37 741	71 902	114 213
Philippines	14 065	36 614	16 878	49 698	28 799
Poland	40 840	24 853	21 405	341 892	109 256
Romania	16 703	12 650	10 849	122 103	35 708
Russia	37 000	111 736	75 368	2 103 132	96 562
Spain	105 917	30 292	42 729	223 196	359 855
Sri Lanka	5063	4108	2134	4972	8024
Sweden	71 754	7296	10 270	56 796	221 103
Switzerland	17 898	4379	5215	43 701	38 932
Syria	16 145	7676	8437	42 407	34 223
Turkey	63 675	42 598	33 885	145 490	190 415
UK	75 930	52 119	28 758	566 246	237 313
Ukraine	56 702	36 099	40 665	611 342	164 704
US	1 120 050	200 695	139 113	4 991 349	6 875 213
Uzbekistan	8547	9430	8029	21 522	15 447
Vietnam	24 865	15 479	12 392	123 253	58 736
TOTAL	3 790 525	1 963 961	1 771 538	18 495 208	16 079 952

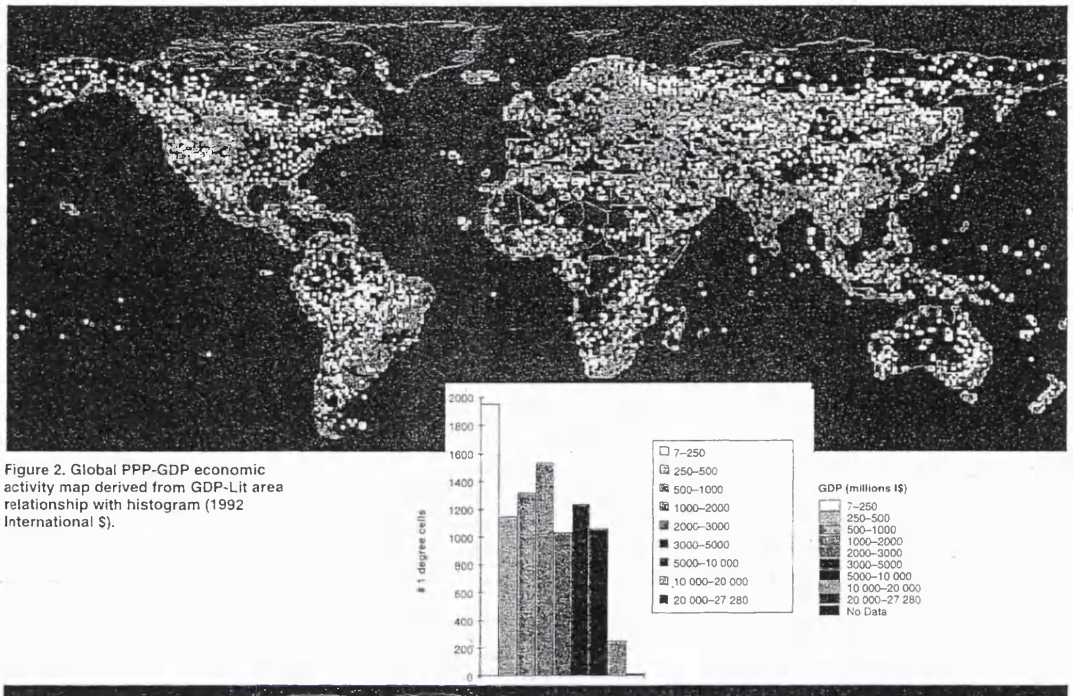

Figure 2. Global PPP-GDP economic activity map derived from GDP-Lit area relationship with histogram (1992 International $).

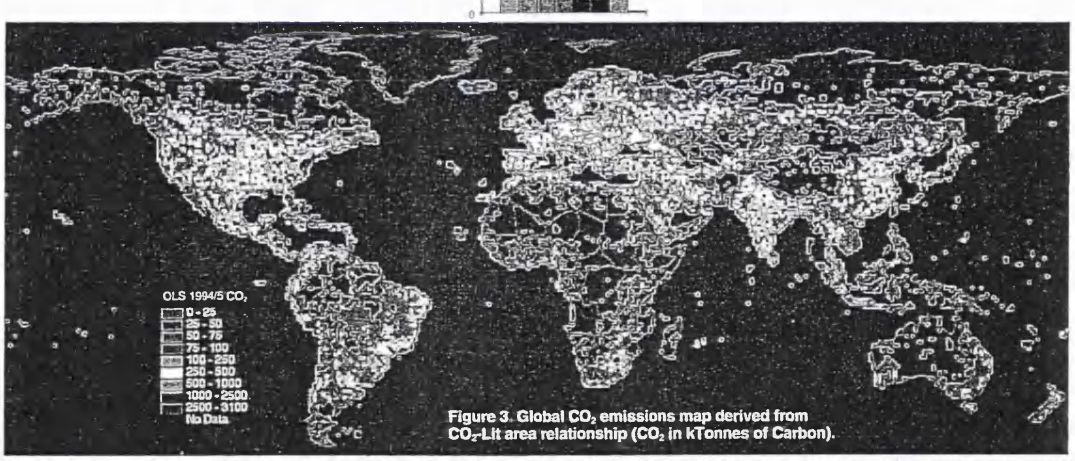

Figure 3. Global CO_2 emissions map derived from CO_2-Lit area relationship (CO_2 in kTonnes of Carbon).

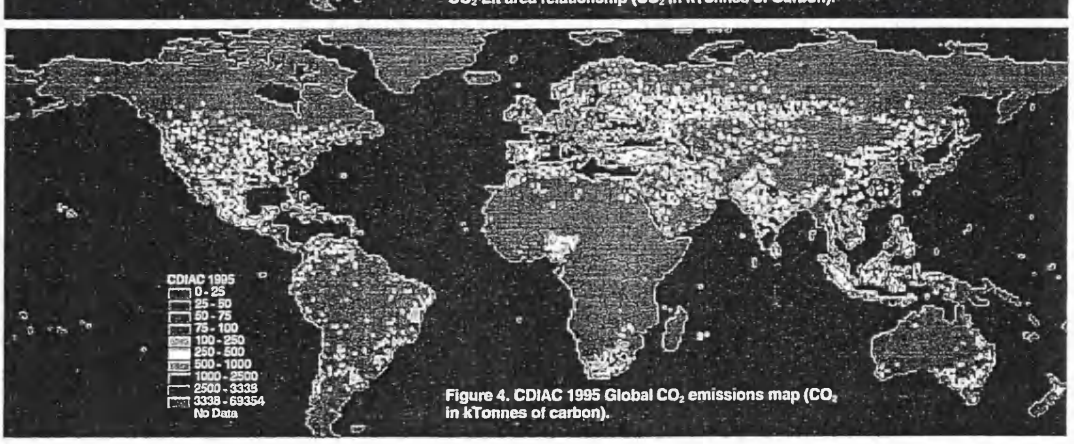

Figure 4. CDIAC 1995 Global CO_2 emissions map (CO_2 in kTonnes of carbon).

Comparison of economic statistics on an international basis requires conversion to a common currency, and is therefore limited by the market exchange rate. The market exchange rate often does not reflect the purchasing power at home. Government intervention through interest rates, import tariffs, and export subsidies can further distort the accuracy of market-based exchange rates. In an attempt to improve this, another method was devised based on the purchasing power of an individual currency in its country. The Purchasing Power Parity (PPP) attempts to account for bias in the exchange rate by assessing how much of a group of goods and services each currency can purchase locally. PPP-GDP is measured in international dollars (I$) and is obtained using conversion factors (PPP), which equalize the purchasing powers of different currencies. The PPP figure makes international comparisons more meaningful and is increasingly being adopted by international organisations (17).

RESULTS

Continental plots do not appear to strictly conform to the allometric growth model observed in other studies (20–22); $P = ax^b$, but occupy a triangular region with the apex at the largest lit area. Country-level plots also exhibited the same pattern in log-log space, whilst there were only 5 countries at $R^2 > 0.8$ (Denmark, New Zealand, India, Bulgaria, and Finland) which fit the allometric growth model. Attempts to calculate urban population generally tended to underestimate the figure quoted by the WRI. Table 1 shows that the major exceptions to this were Iran, Iraq, China, Russia, and Spain, while the US, Japan, Germany, and the UK were significantly underestimated (by over 20 million). When the WRI urban population aggregated to the country level is plotted against the OLS estimated population, a very strong positive correlation ($R^2 = 0.91$) is observed with the OLS derived figures, the correlation being significant at 0.1%. At the polygon level, a relationship was not found to be adequate to offer a reasonable estimate of population. However, these variations were found to significantly cancel each other out when a country was considered as a whole. This effect was also found to operate at a global level. The estimate for the global total urban population, accounted for 90.2% of the total urban population for the 46 countries. Where population was overestimated, the value never fell outside that for the total population from the WRI. The cancellation effect is due to the fact that the linear least-squares fit to the log-log plot of population against polygon size will necessarily result in both over- and underestimation of the population figures for those polygons which have population figures available.

Country-level total lit area was found to correlate highly with other WRI statistics such as GDP and national power consumption supporting previous more regional studies (13). The relationship between GDP and total CO_2 emission (Fig. 5) supports the hypothesis that CO_2 emission is more a function of economic wealth than shear population numbers. Less-developed countries use less energy per capita than industrialized nations but extract marginal economic income with each additional energy unit when compared to industrialized countries (23). The relationship between total lit area and total CO_2 emissions is also very highly correlated (Fig. 1b). The centrally planned economies of China, Russia, and North Korea are the most significant outliers, with their values above that of the regression line. From this, it would appear these countries have less streetlighting than the main cluster of countries for their level of CO_2 emission. When an analysis was carried out by looking at the nature of the relationship for different sectors of fossil fuels (not shown here), it was revealed that the 'Total CO_2' relationship appears to be dominated by the liquid

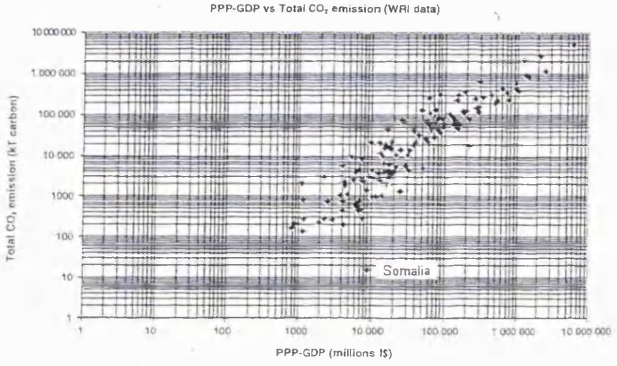

Figure 5. Relationship between PPP-GDP and total CO_2 emissions (WRI Data).

Figure 6. Difference map [CDIAC'95]–[OLS] (CO_2 in kTonnes of carbon).

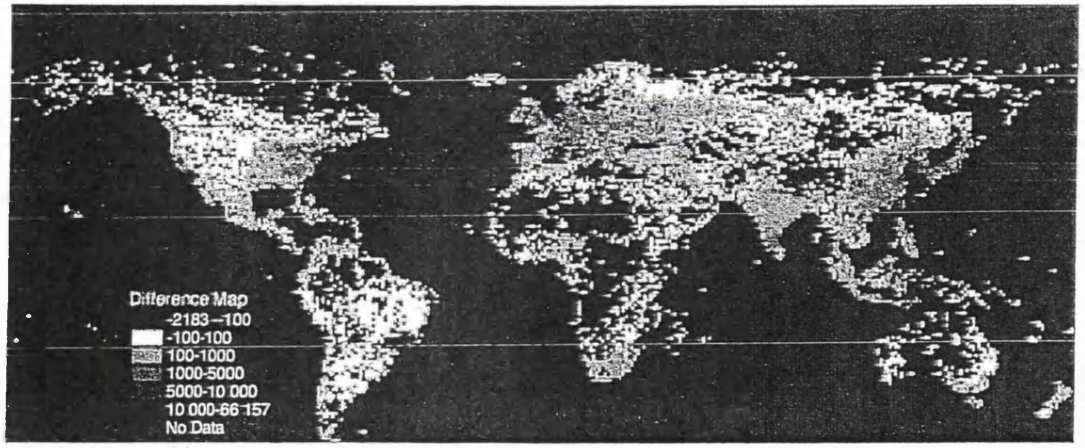

(oil) component. The CO_2 relationship accounts for 86.9% of the total recorded by WRI for the 46 countries listed in Table 1.

DISCUSSION

A difference map [CDIAC]—[OLS] (Fig. 6) accompanies the two CO_2 maps. The most notable feature of the maps is the similarity of the distribution of emissions especially for high areas of GDP. The satellite derived CO_2 data only map the location and distribution of city-lights. This results in fewer grid cells taking values than CDIAC's map which provides an estimate for each land cell. The values in the CDIAC map were distributed according to a gridded population map (24), the city-lights map uses only the lit area to extrapolate and spatially distribute the relationship. The night-light CO_2 map occupies a much smaller range of emissions, and generally magnitudes are below the CDIAC estimates. However, there is a striking degree of similarity between the histograms of the two maps (Figs 7a, b). Both exhibit a bimodal distribution, which may be interpreted as identifying the division between developing and developed nations. In this case, the 4 classes of the lowest emissions (0–100 kilotonnes of Carbon (ktC)) belong mainly the developing nations. The very highest class of emission values belong to just three or four urban centers. The largest class being that of lowest emissions (0–25 ktC) for both maps, indicating that the bulk of emissions are confined to a few regions (Eastern US, Europe, India, and the Far East, particularly Japan).

The difference map reveals that the night-light map, generally, has lower emissions than CDIAC, this being most appreciable in the eastern US, Europe, India, and China. The modal class of the difference map histogram (Fig. 7c) is that centered around 0 difference (–100–100 ktC, 5100 cells) with only 45 1° cells in the highest class (over 10 000 ktC error). CDIAC emissions over Scandinavia, parts of Canada, and southwestern Brazil are lower than the night-light data suggest. This may be attributable to the use of hydroelectric power to light towns rather than conventional fossil fuels. The world's most powerful hydroelectric dam is situated in Paraguay near the Brazilian border. The Itaipu Dam provides enough power for Paraguay and the neighboring states of Brazil.

The total CO_2 emission of our map (i.e. sum of 1° cells) is 1.53 billion tonnes of carbon, just under 25% of the CDIAC map. The use of city lights to map the emission data highlighted the same regions to have the maximum values as identified in the CDIAC map. The CO_2 map produced from the data essentially aims to quantify the contribution of urban areas to greenhouse gas emissions. A time series of images is needed to evaluate fully the impact of mapping CO_2 emissions from city-light data. However, if current urbanization trends continue, the relationship is likely to get stronger as rapidly developing countries such as China and India experience high rates of urban growth assuming the "business as usual" scenario (3).

The PPP-GDP map appears to model economic activity very well (Fig. 2). The total GDP figure is 22.1 trillion I$ compared with 27.7 trillion I$, around 80% of the WRI figure. It seems that night-time lights reflect economic activity better than CO_2 despite the similarly strong correlation between lit area and CO_2 emission and the correlation between the two statistics themselves. The 1° cells have an average value of 2311 million I$, but range as high as 27 275 M I$ (Tokyo area). Similarly, in the CO_2 map, a relatively small number of cells take the highest values, though there is a much greater range of values in the GDP map caused by the higher intercept of the allometric relationship. With the exception of Japan and the US, there only appear to be one or two hubs of high productivity per country. In Russia, for example, Moscow stands out as node of the economy, with only a thin line of higher productivity along the Trans-Siberian railway which tails off rapidly away from there. The principal development in China is observed to occur in the north be-

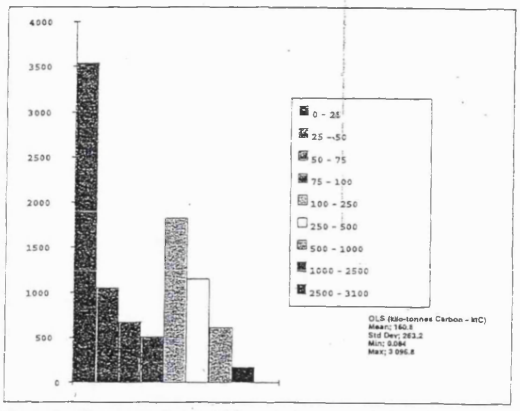

Figure 7a. Histogram of global CO_2 emissions map derived from DMSP-OLS imagery value class *vs.* cell count.

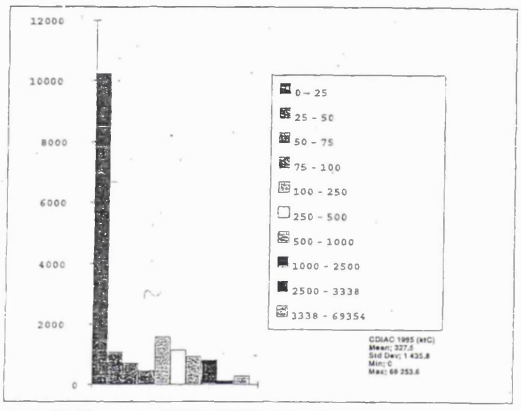

Figure 7b. Histogram of CDIAC 1995 global CO_2 emissions map value class *vs.* cell count.

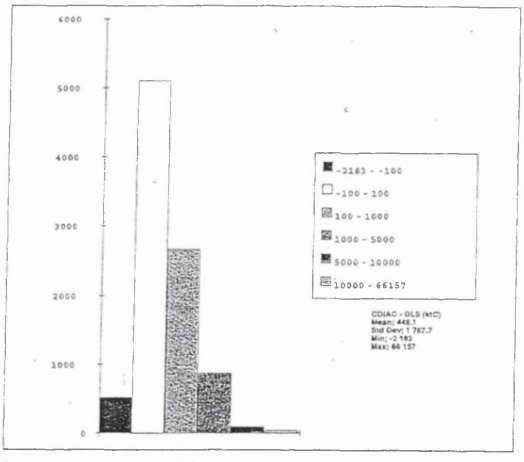

Figure 7c. Histogram of difference map value class *vs.* cell count.

tween Beijing and Shanghai. The economic activity map has a highly modal histogram in the lowest value class, though the CO_2 map identifies more of a continuum in emissions.

A reason for the low magnitudes of the CO_2 map may be due to emissions not explicitly manifesting themselves in terms of street lights reflecting transport infrastructure (e.g. cement production), whereas the hub of any country's economy is the cities. Russia, for example, is shown as a significant outlier in the CO_2 lit-area relationship (Fig. 1b). Russia's national CO_2 total is much higher than the relationship would have predicted. 51% of its GDP is generated from industry compared with only 9% from Somalia, the outlying country below the main trendline. Other major factors include the dependency on countries for imports of fossil fuel resulting in differing patterns of energy consumption and energy policies (23).

CONCLUSION

We have attempted to show how the use of night-time data to map socioeconomic and CO_2 emission parameters does have significant advantages. The most obvious advantage is the potential frequency of acquisition of the data. Given the data were compiled over just a 6-month period it should be possible to produce such a dataset annually. The inherent differentiation of urban area and transportation routes' location are major advantages of this type of data over other remotely sensing imagery. The use of a city-lights map as a global dataset can offer significant advantages for the mapping of urban areas for global land-cover maps or when the knowledge of the magnitude and/or location of urban areas are needed as input into a wider environmental analysis. City lights represent a first attempt to map the human dimensions of global change which has been neglected in most studies to date. In this case, the night-time data have been taken as a proxy for development and urbanization. The anomalies in the magnitude of the CO_2 map may be attributed to the exclusive use of area as the parameter to derive relationships. A radiance-calibrated dataset recently created (25) is likely to improve the ability of night-time lights to map such parameters at the subnational level. A radiance value recorded at the sensor could be used to further modulate the magnitudes associated with each cell by acting as a weighting function. In addition, the incorporation of percentage contribution to GDP from the agricultural, industrial and service sectors could yield significant improvements to the findings presented here. This study has also highlighted the huge importance of accurate statistics in trying to model the parameters associated with the socioeconomic domain compared with the physical-natural applications usually attempted in remote sensing. The use of city lights will also prove a valuable tool to map the shifts in land use as more rural land is encroached upon by the city (14). In future, it may be possible to create such night-time datasets at 250 m from the National Aeronautics and Space Administration's Moderate-resolution Imaging Spectro-Radiometer (NASA-MODIS) instrument (26); displaying the creeping urbanization of green spaces as well as map urbanization and development on an annual timescale. It can also be used to better define the error in areal measurements from earth observation data.

References and Notes

1. Meyer, W.B. 1996. *Human impact on the Earth*. Cambridge University Press, Cambridge, UK, Chapters 1, 2.
2. United Nations Population Division (UNDP), 1992. *Long Range World Projections: Two Centuries of Population Growth 1950–2150*. UNDP, New York. (http://www.wri.org/wri/enved/trends/pop-1b.html).
3. Gardner, G. 1996. *Shrinking Fields: Cropland Loss in a World of Eight Billion*. World Watch Institute: Washington, DC, USA. p. 56.
4. World Resources Institute. 1998. *World Resources 1998–1999. A Guide to the Global Environment*. UNEP, UNDP, The World Bank, OUP, Oxford, UK, Chpt. 9.
5. Climate Change 1995: *The Science of Climate Change*. 1996. Cambridge University Press, Cambridge, UK. Chapter 2.
6. Elvidge, C.D., Baugh, K.E., Kihn, E.A., Kroehl, H.W. and Davis, E.R. 1996. Mapping city lights with night-time data from the DMSP operational linescan system., *Photogram. Eng. Remote Sens. 63*, 727–734.
7. Croft, T.A. 1978. Nighttime images of the earth from space. *Sci. Amer. 239*, 68–79.
8. Croft, T.A. 1979. *The Brightness of Lights on Earth at Night, Digitally Recorded by DMSP Satellite*. Stanford Research Institute. Prepared for the U.S. Geological Survey, Menlo Park.
9. Welch, R. 1980. Monitoring urban population and energy utilization patterns from satellite data., *Remote Sens. Env. 9*, 1–9.
10. Lo, C.P. 1986. Settlement, population and land use analyses of the North China Plain using Shuttle Imaging Radar-A data. *Prof. Geographer 38*, 141–149.
11. Sullivan, W.T.I. 1989. A 10 km resolution image of the entire night-time Earth based on cloud-free satellite photographs in the 400–1100 nm band. *Int. J. Remote Sens. 10*, 1–5,
12. Elvidge, C.D., Baugh, K.E., Hobson, V.H., Kihn, E.A., Kroehl, H.W., Davis, E.R. and Cocero, D. 1997. Satellite inventory of human settlements using nocturnal radiation emissions: A contribution for the global toolchest. *Global Change Biol. 3*, 387–395.
13. Elvidge, C.D., Baugh, K.E., Kihn, E.A., Kroehl, H.W., Davis E.R. and Davis, C.W. 1997. Relation between satellite observed visible-near infrared emissions, population, economic activity and electric power consumption. *Int. J. Remote Sens. 18*, 1373–1379.
14. Imhoff, M.L., Lawrence, W.T., Elvidge, C.D., Paul T., Levine E., Prevalsky, M. and Brown, V. 1997. Using nighttime DMSP/OLS images of city lights to estimate the impact of urban land use on soil resources in the U.S. *Remote Sens. Env. 59*, 105–117.
15. Imhoff, M.L., Lawrence, W.T., Stutzer, D.C. and Elvidge, C.D. 1997. A technique for using composite DMSP/OLS 'city lights" satellite data to accurately map urban areas. *Remote Sens. Env. 61*, 361–370.
16. Philip's. 1998. *Philip's Geographical Digest 1998–1999*. Heinemann Educational in assoc. with George Philip.
17. The World Resources Institute. 1996. *World Resources 1996–97, A Guide to the Global Environment*. UNEP, UNDP, The World Bank, OUP, Oxford, UK. Chapters 7, 8, 14.
18. Denko, D.M. 1992. The digital chart of the world project. *Photo. Eng. Remote Sens. 58*, 1125–1128.
19. Brenkert, A.L. 1998. *Carbon Dioxide Emission Estimates From Fossil Fuel Burning, Hydraulic Cement Production, and Gas Flaring for 1995 on a 1 Degree Cell Basis*. CDIAC Numerical Data Package 058a. 1998 CDIAC (http://cdiac.esd.ornl.gov/ndps/ndp058a.html).
20. Stewart, J. and Warntz, W. 1958. Physics of population distribution. *J. Regional Sci. 1*, 99–123.
21. Norbeck, S. 1965. *The Law of Allometric Growth*. Inter-University Community of Mathematical Geographers, Department of Geography, University of Michigan, Ann Arbor, Michigan.
22. Tobler, W.R. 1969. Satellite confirmation of settlement size coefficients. *Area, 1*, 31–34.
23. Tucker, M. 1997. Carbon dioxide emissions and global GDP. *Ecol. Econ. 15*, 215–223.
24. Li, Y-F. 1990. *Global Population Data, Terrestrial Area and Country Name Information on a 1 Degree Grid Cell Basis*. CDIAC Numerical Data Package 1016 (http://cdiac.esd.ornl.gov/ndps/db1016.html).
25. Elvidge, C.D., Baugh, K.E., Dietz, J.B., Bland, T., Sutton P.C. and Kroehl. H.W. 1999. Radiance calibration of DMSP-OLS low-light imaging data of human settlements. *Remote Sens. Env. 68*, 77–88.
26. Justice, C.O., Vermote, E., Townshend, J.R.G., Defrires, R., Roy, D.P., Hall, D.K., Salomonson, V.V., Privette, J.L., Riggs, G. and Strahler, A. 1998. The moderate resolution imaging spectroradiometer (MODIS): land remote sensing for global change research 1998. *IEEE Trans. Geosci. Remote Sens. 36*, 1228–1249.

27. The authors wish to thank Kimberly Baugh at NOAA-NGDC for processing the night-time data, and Glenn Larson at CGRER, University of Iowa for assistance with the world cities dataset. We are also very grateful to two referees for their constructive comments. This work is supported by NERC studentship GT04/98/ 188/TS.
28. First submitted 26 July 1999. Accepted for publication after revision 21 Dec. 1999.

Christopher Doll is a research student reading for his doctorate at University College London (UCL). He did his first degree in geography and mathematics at Royal Holloway, University of London, in 1997, before completing a MSc in remote sensing at UCL in 1998. His address: Department of Geomatic Engineering, University College London, Gower Street, London WC1E 6BT, United Kingdom.
E-mail: cdoll@ge.ucl.ac.uk

Jan-Peter Muller is professor of image understanding and remote sensing at the Department of Geomatic Engineering, UCL. He did his first degree in physics at Sheffield University, before completing his PhD in planetary meteorology at UCL in 1981. He has a wide variety of research interests and is a NASA Science Team member for MODIS and MISR instruments on the forthcoming EOS-Terra mission. His address: Department of Geomatic Engineering, University College London, Gower Street, London, WC1E 6BT, United Kingdom.
E-mail: jpmuller@ge.ucl.ac.uk

Christopher Elvidge works at the Department of Solar Terrestrial Physics at NOAA-NDGC in Boulder, Colorado, USA. He is chiefly responsible for the developing the algorithms for creating the night-time imagery dataset used in this paper. His address: Department of Geomatic Engineering, University College London, Gower Street, London WC1E 6BT, United Kingdom. Solar-Terrestrial Physics Division, NOAA National Geophysical Data Center, 325 Broadway, Boulder, Colorado 80303, USA.
E-mail: cde@ngdc.noaa.gov

Mapping Urban Landcover using the Bidirectional Reflectance Distribution Function BRDF/Albedo Product from the Moderate Resolution Imaging Spectroradiometer (MODIS)

Christopher N H Doll[1*], Jan-Peter Muller[1], Crystal Schaaf[2], Alan H Strahler[2], Feng Gao[2]

1. Department of Geomatic Engineering, University College London, Gower Street, London, WC1E 6BT, United Kingdom
2. Center for Remote Sensing, Department of Geography, Boston University, Boston, MA 02215, USA.

Abstract – This paper reports on the results of an evaluation study on using the Bidirectional Reflectance Distribution Function (BRDF)/Albedo product for global urban mapping. Results over Western Europe and Florida look promising, and are evaluated with respect to the extensive quality assurance (QA) information which accompanies the product. The QA information provides information on the number of full versus magnitude inversions which are sourced from a look-up table. Better sampling will soon be available with the launch of the Terra's sister spacecraft 'Aqua' which will complement Terra with afternoon views, and after incorporating data from the Muti-angle Imaging Spectroradiometer (MISR) instrument.

I. Introduction

The National Aeronautics and Space Administration's (NASA) new Moderate Resolution Imaging Spectroradiometer (MODIS) sensor onboard the Terra spacecraft is producing a wealth of data products pertaining to the land surface, the oceans, and the atmosphere. The Bidirectional Reflectance Distribution Function (BRDF) is of importance as it describes the intrinsic properties of anisotropic reflectance of the surface. Aside from the nature of the land surface itself, the albedo is also a function of view and illumination angle. Therefore it is a useful parameter to be able to quantify when dealing with satellite imagery from sensors with a large instantaneous field of view such as MODIS. Land surface BRDF and as its associated products (albedo and nadir BRDF adjusted reflectance (NBAR)) are now for the first time being routinely produced on a global basis every 16 days. These data sets are freely available from the DAAC at EROS Data Center (http://edcdaac.usgs.gov).

II. The BRDF/Albedo Product (MOD43B)

The BRDF/Albedo product (known as MOD43B) is one of the key land products, as well as is an input into other land products, such as the MODIS Land Cover product. The BRDF has a wide variety of applications and as such, the product is one of the most extensive and complex from the MODIS sensor. There are three operational products available; the BRDF parameters themselves (MOD43B1), "blacksky" (directional hemispherical) and "whitesky" (bihemispherical) albedos (MOD43B3), and (nadir BRDF adjusted reflectance) NBARs (MOD43B4).

Albedo is derived from integrating the BRDF over the hemisphere [1] at the mean solar angle over the 16 days of observations. It is a crucial parameter in understanding the land-atmosphere energy balance. It is directly related to reflectance and absorption of incoming solar radiation. Both the albedo and the NBAR are derived from the initial BRDF product. Each product is produced for the seven land spectral bands (bands 1-7 of the MODIS sensor) ranging from 0.3 – 2.1μm. In addition, there are three broadband albedos, for the visible (0.3-0.7μm), Infrared (0.7-5.0μm), and shortwave (0.3-0.5μm) parts of the spectrum.

A. The BRDF Algorithm

The algorithm used for characterising the BRDF uses three linear semi-empirical kernels applied over a fixed 16-day period to allow for sufficient angular sampling of the surface. The three kernels describe the BRDF in its isotropic, volumteric and geometric components as shown in equation (1). The volumetric kernel models leaf level volume scattering and is given by the RossThick kernel [2] whilst the geometric kernel is sensitive to the three-dimensional structure of objects within a scene and is described by the LiSparse kernel [3].

$$R(\theta,\varphi,\phi,\Lambda) = f_{iso}(\Lambda) + f_{vol}(\Lambda)K_{vol}(\theta,\varphi,\phi) + f_{geo}(\Lambda)K_{geo}(\theta,\varphi,\phi) \quad (1)$$

where: θ = solar zenith angle
φ = view zenith angle
ϕ = view-sun relative azimuth angle
Λ = waveband
$f_k(\Lambda)$ = BRDF kernel model parameter k in waveband Λ.
K_k = BRDF model kernel k
$R(\theta,\varphi,\phi,\Lambda)$ = BRDF in waveband Λ.

* This work is supported by NERC Studentship GT 04/98 188/TS

B. The Normalised Difference f-index (NDFI)

The geometric kernel lends itself well to urban mapping, as it is has been postulated to be closely related to the amount of shadow casting from objects in the scene. Previous work [4] has shown that taking the normalised difference of the two non-isotropic parameters as shown in equation (2) augments urban area detection.

$$NDFI = \frac{f_{vol} - f_{geo}}{f_{vol} + f_{geo}} \quad (2)$$

C. Quality Assurance

Extensive quality assurance information accompanies all MODIS land products. For the BRDF/Albedo product there is both band independent and band dependent information stored in two bit words. Band dependent information refers to the quality of a full inversion, or where a full inversion was not performed, the number of looks over that point during the compositing period.

Successful BRDF retrieval relies on there being enough cloud free looks to sample a given point on the land surface. Seven looks (over 16 days) define the threshold number of looks to determine whether or not a full inversion is attempted. Out of these, only those with reasonable weights of determination [5], a measure based on the available angular samples for a pixel are fully inverted. Where these weights are inadequate, or more likely, there are less than seven available looks, a magnitude inversion is performed. Magnitude inversions fit the available looks to an archetypal shape for a given land cover class. By using the available observations, it introduces variation within a class [6].

II. Results

Western Europe was the initial study area selected as it has many large urban conurbations, in addition to smaller towns. Full atmospheric correction was only applied to the data after Julian Day (JD) 273 (29th September 2000) which meant that only data after this date was analysed. Due to the typically cloudy conditions experienced during a Northern European autumn most of the data had less than seven clear looks and many took magnitude-inverted values. Fig.1. shows a NDFI image for JD289 (15th October 2000). The blue areas highlight the major urban areas in Western Europe. The other colours in the image also correspond to major landcover types in Europe, indicating that the retrieved values from the available looks correspond to the landcover lookup table.

Figure 1. NDFI red band for Western Europe JD289 (15th October 2000)

In order to test how well full inversions can detect urban (and other land cover types), other areas were selected based on the likelihood of having clear sky conditions to permit a full inversion, and the presence of large urban areas within the scene. Fig.2. shows a detail from the east coast of Florida for JD305 (top) and JD289 (bottom). The two left-hand images show the QA for the BRDF parameters (band 1, red, 250m) with the corresponding NDFI images. The QA images are colour coded such that green refers to pixels with full retrievals, white 3-7 observations, and blue less than three observations. JD289 had a few full retrievals in this area. The large urban area to the north (West Palm Beach) and coastal development are clearly highlighted from the land cover look-up table. However when there are many full retrievals as for the JD305 (31st October 2000) product, the NDFI shows no apparent correlation to any land cover types. The NDFI value is largely negative however indicating a dominance of the geometric kernel weight over the volumetric kernel.

Visible albedo appears to be more robust to the inversion technique used. Results over Florida show distinct landcover features that have both types of inversion regime at work within. Fig.3. shows a detail of broadband visible whitesky albedo over Miami and its respective QA. The data for the 16 day period starting on 1st January 2001 had virtually all full inversions. It is interesting to note however, that it is rare to find urban centres with full inversions. Pixels which have magnitude inversions at urban centres take albedo values around 25% higher than the full inversion albedo pixels.

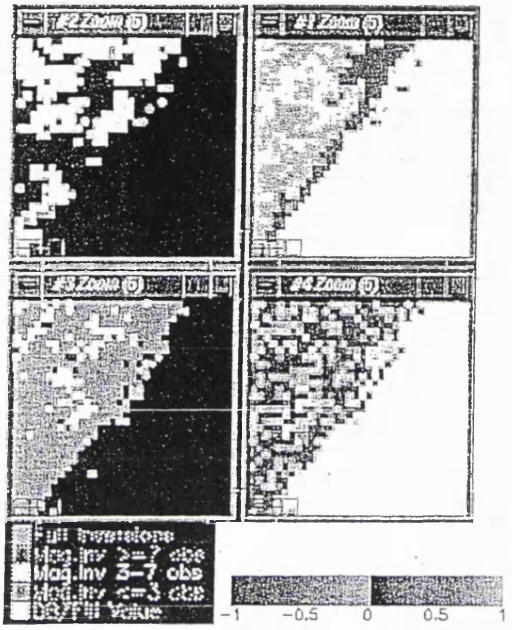

Figure 2. QA and NDFI for full magnitude inversions (top: JD305, 31st October 2000) versus full inversions (bottom: JD289, 15th October 2000)

These results are in line with the prototyping study [7] and demonstrate that anthropogenic features have a distinctly higher albedo than the surrounding area, and that this is detectable from the 1km product.

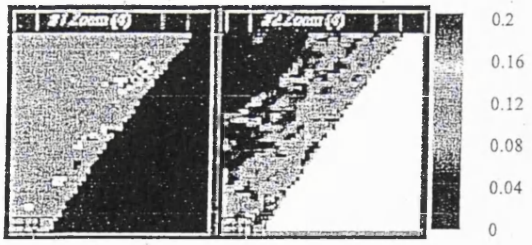

Figure 3. QA (left) and Broadband visible albedo for Florida JD 001-2001

IV. Discussion

The magnitude inverted BRDF parameters fall clearly into distinct classes as would be expected since the available observations are derived from a landcover database of archetypal BRDF shapes[6]. It is encouraging to observe that urban areas are consistently being identified as belonging to the same class. The reason why the result is not replicated with full BRDF inversions may lie with the kernels not being orthogonal. Geometric and volumetric effects are not mutually exclusive, as there are volumetric effects at the canopy level and vice versa [8]. A sparse sampling scheme only aggravates this situation. Terra's sister spacecraft 'Aqua' will be used to augment the sampling with afternoon views and the integration of MISR directional looks will improve the sampling subject to cloud cover considerations.

V. Summary

NDFI has been examined for both retrieval regimes of the MODIS BRDF/Albedo product. Urban areas were only successfully identified when there were magnitude inversions. Full retrievals appear to completely obscure this effect. This is hypothesised to be due to a degree of coupling between the two main kernels. The derived visible albedo produces more homogeneous values and does appear to correlate well with anthropogenic features associated with suburbs and ribbon developments. The global production of this dataset every 16 days should seriously augment current efforts to understand the effect of human activity on the climate system, and land surface dynamics in general.

References

[1] W. Lucht, C.B. Schaaf, and A.H Strahler "An algorithm for the retrieval of albedo from space using semiempirical BRDF models" IEEE Trans. Geoscience and Remote Sensing Vol. 38 No. 2. 977-998 2000.

[2] J.L. Roujean, M.Leroy, and P.Y.Deschamps "A bidirectional reflectance model of the Earth's surface for the correction of remote sensing data" Journal of Geophysical Research, 97, 20 pp.20 455-20 468. 1992.

[3] W.Wanner, X.Li, and A.H. Strahler, "On the derivation of kernels for kernel-driven models of bidirectional reflectance" Journal of Geophysical Research., vol.100 pp. 21 077-21 090, 1995.

[4] D'Entremont, R.P, Schaaf, C.B., Lucht, W., Strahler, A.H. (1999). "Retrieval of red spectral albedo and bidirectional reflectance using AVHRR HRPT and GOES satellite observations of the New England region." Journal of Geophysical Research-Atmospheres Vol.D-104 pp.6229-6239 1999.

[5] W.Lucht and P.Lewis "Theoretical noise sensitivity of BRDF and albedo retrieval from the EOS-MODIS and MISR sensors with respect to angular sampling," Int. J. Remote Sensing, 21, 81-98. 2000.

[6] N.Strugnell, W.Lucht and C.B. Schaaf. "A global albedo data set derived from AVHRR data for use in climate simulations" Geophys. Res. Lett, 28(1), 191-194

[7] C.B. Schaaf. Et al. "Prototyping the moderate resolution imaging spectroradiometer (MODIS) BRDF and Albedo product" IGARSS99 Hamburg pp.1506-1508. 1999.

[8] Lucht, W., Schaaf, C.B., Strahler, A.H., D'Entremont, R.P, "Remote sensing of albedo using the BRDF in relation to land surface properties" in Observing land from Space: Science, Customers and Technology. Ed. M. Verstraete, Kluwer Academic, NL, pp175-186, 2000

15 Estimating non-population activities from night-time satellite imagery

Christopher N. H. Doll

15.1 Introduction

The expansion of global change research has opened a Pandora's box of data requirements of increasingly diverse parameters. Initially, environmental monitoring was confined to the condition of the biosphere with little regard to the overarching agents of change. As we improve our understanding of the interactions of the various processes involved, so too does our identification of the key factors lying at the heart of global change. The ever-broadening remit of global change demands an increasing number of disciplines to be employed to fully describe it.

The global economy is an example of such a key factor. There is a growing realization that it is a major driving force of global change as it influences, first, urbanization and, second, levels of power consumption. Taken together, these two activities spawn serious issues facing human populations, such as increased pollution and its associated health effects, loss of agricultural land and pressure on water resources. Economic activity is not only a driving force of environmental stress, but also a determinant of the adaptability and ameliorative capacity of a society to deal with its impacts. A joint study by the Environment Programme (UNEP) and Development Programme (UNDP) of the United Nations highlighted the economy as one of the top ten high-priority data themes for environmental assessment (UNEP/UNDP 1994). Additionally, the issues of land use change, hydrology, air and water quality are also regarded with the same importance. Many of the major data requirements can be mapped by satellites, increasingly more so with the launch of new sensors and satellite missions such as the National Aeronautics and Space Administration's (NASA) Earth Observing System (Kaufman *et al.* 1998a). This programme will seriously augment current remotely sensed data sets by establishing a database of Earth science products for the land, ocean and atmosphere that is expected to last until at least 2015.

The increasing use of satellite sensor data for the creation of systematic environmental data products stimulates the requirement to provide data at a constant resolution. This is something that is not often available for socio-

economic data since they are often reported at regional, national, sub-national or other irregular spatial units. The question therefore presents itself that assuming night-time lights are representative of human activity, how well do they correlate with facets of human activity such as economic activity and energy consumption? By association they may also serve as indirect tracers of greenhouse gas production (Southwell 1997).

Night-time satellite imagery has provided researchers with a means to push back the boundaries of what is conventionally thought to be the limits of environmental remote sensing. As a data source, it has the potential to offer information on human activity unlike anything that can be derived from other forms of remotely sensed imagery. This chapter is concerned with how night-time satellite imagery as captured from the Defense Meteorological Satellite Programme's Operational Linescan System (DMSP OLS) sensor described in previous chapters can model and map various facets of human activity.

15.2 Global mapping of GDP and CO_2 emissions from DMSP OLS imagery

The potential for night-time light imagery to describe economic activity and energy usage has been noted in early papers written on the subject (Croft 1978; Welch 1980; Sullivan III 1989). Elvidge *et al.* (1997) examined correlations of lit area and Gross Domestic Product (GDP) and lit area and power consumption for twenty countries in the Americas. Doll *et al.* (2000) developed this further by establishing global regression relationships between lit area in a country and GDP, and CO_2 emissions. Global 1-degree resolution maps were created from these relationships.

15.2.1 Mapping methodologies

Producing maps at 1-degree resolution from night-time satellite imagery requires generalization of the existing data, which are at a much finer resolution (30 arcsec in this case). The night-time light data were summarized into 1-degree units by calculating the "percentage lit" value for each new cell. Global maps and models invariably use geographic projection to represent the Earth's surface as it is one of the most convenient for displaying global data at a variety of resolutions and allows easy indexing of any position through the use of latitude/longitude coordinates. This presents a problem when using an empirically derived relationship based on area to distribute data, since it is not an equal area projection. Converging lines of longitude result in a square degree at the equator being larger than the same unit at higher latitudes. Although most of the data of interest are within 60° north or south of the equator, a degree of longitude is still half the length at 60° than it is at the equator.

Table 15.1 Dimensions of the latitudinal zones used to create maps

Latitudinal zone	*Dimension at 30" (E/W × N/S)* (m)	*Area at 1 degree* (km^2)
60°+ (northern hemisphere)	400 × 929	5,351.040
50°–60°	531.25 × 927.5	7,095.375
40°–50°	655 × 926.1	8,734.975
30°–40°	755 × 924.6	10,052.251
10°–30°	850 × 922.5	11,291.400
−10°–10°	920 × 921.5	12,208.032

In order to map onto this system, mean cell areas were calculated for ten latitudinal zones (Table 15.1). The summarized night-time light data could then be calculated directly to a lit area figure for each cell. The relationships between lit area and GDP, and CO_2 emissions calculated are given below:

$$CO_2 = 10^{(1.2508*(\log \text{area})-0.7291)} \quad (15.1)$$

$$GDP = 10^{(0.9735*(\log \text{area})+0.7124)} \quad (15.2)$$

The global product was generated by applying the relationship to each latitudinal band and merging the subgrids.

The CO_2 emissions map was compared with one previously prepared at 1-degree resolution by the Carbon Dioxide Information and Analysis Center (CDIAC) (for method see Andres *et al.* 1996 and ORNL/CDIAC for data location). Their map used a global, gridded, population density map developed by Li (1996) to distribute the emission figures. Human population centres and the location of night-time lights are also very highly correlated, which helps to explain the excellent correspondence of emission locations between the two maps. The two histograms also resemble each other, both exhibiting a bimodal distribution with the largest class in each case belonging to the lowest range of emissions (0–25 kilotonnes of carbon [ktC]) and a second peak in the 100–250-ktC class. This may be interpreted as the division between developing and developed countries since maximum emissions in developing countries rarely exceed this figure.

A difference map CDIAC OLS (Figure 15.1, see colour plates) was used to identify those areas over- and underestimated by CDIAC. The modal class of this histogram centred on the zero value, but generally the night-time light map underestimated emission values. These differences were greatest in those regions that had the highest values. More interesting, however, are those areas that have been overestimated in the DMSP OLS results by applying the global relationship. These areas include parts of Canada, Scandinavia and southern Brazil. This could be indicative of energy generation from non-fossil fuels. The Itaipu Dam in Paraguay for instance

also supplies energy to the neighbouring southern states of Brazil, and Sweden has particularly low relative levels of fossil fuel consumption. The emissions total of the night-time light map is 1.53 billion tonnes of carbon, around 25 per cent of the CDIAC map total. The widespread underestimation of emissions suggests that other factors need to be considered in the model. Certainly issues such as the contribution of fossil fuels to national energy consumption, and its relationship to lighting practices would appear to be appropriate places to start to identify the biasing factors between countries which affect global mapping of CO_2. A more detailed discussion of the assumptions and extra data sources required to refine greenhouse gas emissions mapping from radiance-calibrated night-time imagery is given in Section 15.3.4.

Validation of the GDP map is more speculative as there is no other map of its kind. In terms of a global figure of economic activity, the map sums to 22.1 trillion international dollars (Intl.$), some 80 per cent of the total for the input data. The international dollar is the currency unit for the purchasing power parity GDP statistic, which attempts to account for the purchasing power of different currencies thus making international comparisons more meaningful. There is a much wider range of values in the GDP map due to the higher intercept of the allometric relationship. Even though it has a lower gradient than the CO_2 relationship, the value of the constant is an important feature in log–log space where the gradients are similar as it influences the magnitude of the retrieved anti-log. Features such as the Trans-Siberian Railway are apparent as well as hubs of economic activity within a country such as Moscow and New Delhi. The developed nations on the other hand exhibit less variation between high and low values. Successive night-time light data sets will allow for analysis of the change in relationship parameters, as well as tracking the development of burgeoning economies such as China (see Figure 15.2, colour plates).

Using global relationships to disaggregate data from the country level, national totals, from which the relationships were derived, are not preserved in the maps due to the best fit nature of a regression line. An alternative to this approach was presented by Li *et al.* (1996) who used a political map of the world segmented over a 1-degree grid. The study aimed at mapping concentrations of hexachlorocyclohexane (HCH) an organochlorine insecticide, which was widely employed to improve agricultural yield, protect livestock and eliminate vector-transmitted disease. The figure for usage of this compound was also quoted at the country level. A NASA/GISS (NASA's Goddard Institute for Space Studies) map of cultivation intensity at 1° by 1° resolution (Matthews 1983) was used to disaggregate the country level totals. Five intensity levels were identified from these data. Since the disaggregation data were already at the output resolution of the map, no generalization was required. However, instead of deriving a global correlation between cultivation intensity and HCH concentrations, the segmented 1-degree grid was used to distribute the national total into the grid cells lying

within a national boundary. Where a grid cell was intersected by one or more political units, the relative contribution of the cell for each unit was calculated and then assigned the commensurate proportion of the intensity value according to the following formula:

$$V_{ij} = \frac{C_i R_{ij}}{\sum_i C_i R_{ij}} V_j \qquad (15.3)$$

where for a cell i and political unit j: C is the cultivation intensity value, R_{ij} is the percentage of total area j in cell i and V_j is the total value of the parameter to be mapped (HCH). In this case, C and V_j would be replaced by radiance and GDP/CO_2, respectively. This method assumes that the quantity is evenly distributed within a cell. This is unlikely to be the case for night-time imagery as lights tend to be clustered. The problem of splitting allocated proportions in a cell by intersecting it with a line or polygon coverage is a fundamental problem in geographic information science. The error involved in allocating data to cells is inversely proportional to the resolution of the cells in the grid.

15.3 The potential of radiance-calibrated data

The maps created in the previous section (Figures 15.1 and 15.2, both in colour plate section) were the results of applying an empirical relationship based on area. A radiance-calibrated data set offers an expanded range of possible correlations since the radiance profile within a lit area can be used as weights. Doll and Muller (1999a) used radiance-calibrated data to examine how they could be used to improve its population predictions from the traditional allometric lit area relationships identified by Tobler (1969). In this case, the radiance-calibrated data offered the refinement of modelling intra-urban population density and was found to offer much more robust estimates for the twelve countries in their study. Radiance-calibrated data can be used in much the same way for estimating other parameters. GDP, CO_2 emissions and power consumption have all been shown to be highly correlated with lit area figures at the country level (Doll *et al.* 2000; Elvidge *et al.* 1997). When estimating a parameter like power consumption, a radiance value may be a more useful attribute to take as a proxy than the lit area. This section examines the relationship of "cumulative radiance" to these parameters, and also the nature of relationships at different spatial scales. Cumulative radiance is here defined as the summed radiance value over a number of pixels.

15.3.1 Subnational spatial classifications

The wealth of statistical data for the UK, produced by the Office of National Statistics (ONS), provides a way of assessing how well an approach like this

performs at a smaller subnational scale. Nomenclature of Units for Territorial Statistics (NUTS) is a hierarchical classification of spatial units that provides a breakdown of the EU's territory for reporting regional statistics that are comparable across the Union. Starting at the NUTS-0 (country) level, countries are divided up into broad regions (NUTS-1) and then individual counties or groupings thereof (NUTS-2). There are eleven NUTS-1 regions in the UK and around three NUTS-2 areas in each NUTS-1 region. Many social and economic data sets can be requested and downloaded from their website (ONS 2002).

15.3.2 Radiance and GDP: an analysis for the UK

The established area–GDP relationship developed at the national level appears to be invalid at the subnational scale. Table 15.2 shows the correlation between night-time light parameters and GDP at different spatial units. The cumulative radiance correlates better but the correlation statistic is still low. The Greater London region has an anomalously high GDP for both its cumulative radiance and its area. Although London accounts for just under 2 per cent of the total lit area of the UK, it contributes 15.9 per cent to national GDP (Table 15.3). Conversely, the East Midlands and Scotland have a greater proportion of lit area compared with their proportion of GDP contribution. In this sense sole reliance on an areal relationship between light and economic activity at the subnational regional level is unrealistic, the R^2 value of 0.04 testifying to this. However, when the Greater London region is removed from the data, a positive correlation is apparent.

If one hypothesizes that increasing radiance is linearly related to GDP, then one way to disaggregate the statistic is to divide the GDP by the total

Table 15.2 Correlation coefficients for fourteen European countries (NUTS-0), and NUTS-1/2 regions for the UK between lit area and radiance with GDP (excluding Northern Ireland)

Parameter	R^2 *(linear–linear)*	R^2 *(log–log)*
NUTS-0 Europe lit area	0.84	0.72
NUTS-0 Europe radiance	0.74	0.66
NUTS-1 lit area	0.04	0.01
NUTS-1 total radiance	0.30	0.50
NUTS-1 primary (lit area)	0.66	0.90
NUTS-1 primary (radiance)	0.19	0.33
NUTS-1 secondary (lit area)	0.27	0.18
NUTS-1 secondary (radiance)	0.78	0.71
NUTS-1 tertiary (lit area)	0.01	0.002
NUTS-1 tertiary (radiance)	0.20	0.42
NUTS-2 lit area	0.22	0.14
NUTS-2 radiance	0.61	0.72

Table 15.3 NUTS-1 statistics of lit area, cumulative radiance and GDP for the UK

NUTS-1 region	*Lit area* (km^2)	*Cumulative radiance* ($\times 10^{-10}$ W cm^2 μm^{-1} sr^{-1})	*GDP* (£ millions)
Scotland	11,880	743,420	58,578
North-east	3,403	327,523	24,321
North-west	7,989	618,702	72,475
Yorkshire and the Humber	9,614	686,588	53,002
East Midlands	11,106	544,521	47,289
Wales	5,508	253,741	27,912
West Midlands	7,231	499,110	58,053
East of England	12,695	642,582	72,229
South-east	14,320	678,347	107,630
South-west	8,821	368,894	53,453
Greater London	1,586	505,366	108,645

radiance to establish a "GDP per unit radiance" coefficient and apply this to lit pixels. By doing this, pixels of a given radiance will have the same GDP value and the country total is preserved. Total radiance and GDP at NUTS-1 are not well correlated in normal or logarithmic space ($R^2 = 0.3$ and 0.5, respectively). Comparing coefficients across NUTS-1 regions, there is a difference of a factor of 3 between the lowest (north-east) and the highest (Greater London). A single coefficient was calculated for the UK and applied to the eleven NUTS-1 regions. The resulting graph (Figure 15.3) shows that Greater London and the south-east are not well represented by this approach, both regions being significantly underestimated. In fact there is a general north/south divide with the greatest disparities of over- and underestimation being those regions farthest apart!

The distribution of radiance values over the UK is heavily biased toward the lower radiance values. Forty-one per cent of the land area of England, Scotland and Wales has a light source detectable from space. Of this, 37 per cent of the lit area occupies the five lowest radiance values. The connection between ground level light sources and radiance values in the product is not well established and thresholding out these very low radiance values only marginally improves the strength of the correlation.

Uncertainties exist concerning the manifestation of certain sectors of the economy by the presence of night-time lights; therefore it might be helpful to examine the nature of the light GDP relationship with respect to individual sectors of the GDP. The effect of the relative contributions from the agricultural (primary), industrial (secondary) and service (tertiary) sectors to GDP is also not well understood. The ONS produce NUTS-1 data for the UK split into the various categories of the economy. These can be grouped into the three principal sectors mentioned above. The UK economy is principally service-based, with this accounting for an average of 67 per cent of the GDP across the regions. The agricultural contribution is very

342 *Christopher N. H. Doll*

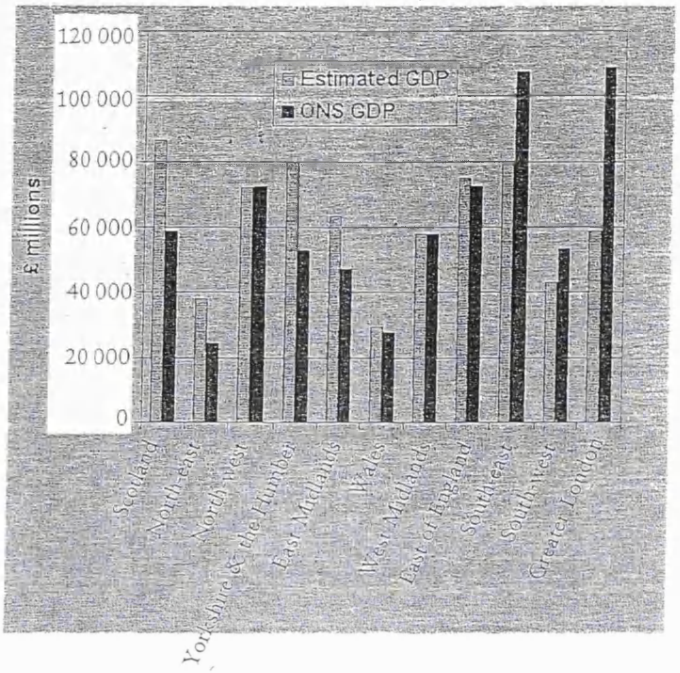

Figure 15.3 Estimation of GDP at NUTS-1 level using a single GDP/radiance coefficient.

low, only accounting for a maximum of 3 per cent (south-west). Nonetheless, the primary sector correlates very well with lit area, but poorly when compared with cumulative radiance. However, the opposite effect is observed when analysing the industrial sector. Here, cumulative radiance is shown to be the better descriptor. The tertiary sector was not well correlated to either measure from night-time light imagery despite being the largest sector of the UK economy.

The GDP to lit area relationship at the NUTS-2 scale is completely uncorrelated, but the cumulative radiance relationship is still good. It appears that the lit area relationships break down much more quickly than the radiance relationships. The strength of the cumulative radiance relationship appears to dip at NUTS-1. The cumulative radiance relationship at NUTS-2 is better than at NUTS-1. This could be due to less aggregation of different economic sectors in NUTS-2. NUTS-1 regions occupy larger areas and therefore have more heterogeneous sector contributions. However, aggregating light and GDP to NUTS-0 (country level GDP from the World Resources Institute) appears to efface these regional disparities and the relationship becomes stronger again. The individual sector figures suggest that NUTS-1 is the scale where confusion between light and GDP is the highest. This is likely to be an example of the modifiable areal unit problem (Openshaw 1984). As such it is not clear

whether this trend would be repeated for other countries, or even different zoning schemes for NUTS-1 sectors in the UK. For instance, a better correlation may be achieved by constructing NUTS-1 regions by grouping NUTS-2 areas by dominant GDP sector. The correlation coefficients listed in Table 15.2 for NUTS-2 excludes London, which was not split into its inner and outer London NUTS-2 regions for this study.

15.3.2.1 Possible solutions

Considering the relative proportions of lit area and radiance to GDP contribution, it is apparent that the Greater London region skews any relationship, which one may seek to draw, because of its anomalously high economic contribution. The relationship between area, radiance and GDP is more complex at NUTS-1 than at the international level. The differences in the regional economy cannot be adequately modelled by a relationship relying on just one parameter. Greater London for instance has some very high radiance pixels over a small area. It would appear that using cumulative radiance as a proxy does not adequately describe the subnational relationship of light to GDP. Figure 15.4 demonstrates that a region can have a larger lit area and greater cumulative radiance than another region, but contribute less GDP. Table 15.2 gives these figures for NUTS-1 in the UK. The splitting of GDP by sector yielded some interesting results and may be helpful when planning a methodology for estimating economic activity in rural areas or countries with a highly agrarian economy.

The use of a single GDP/radiance coefficient assumes, first, an equal GDP generating capacity per unit radiance and, second, no consideration is given to its status with respect to neighbouring pixels. A more sophisticated model could be weighted toward individual pixels of a high radiance. Furthermore, clusters could be defined using some thresholding technique. A large cluster would have greater weighting than a smaller one. In this way, two areas of equal cumulative radiance can have different GDP values depending on the arrangement of pixels with their spatial unit. The Greater London region is a cluster in itself and would therefore be heavily weighted toward a higher GDP. The East Midlands in contrast is composed of a series of smaller clusters. The influence of clustering may help explain why the correlation improves at NUTS-2 level. As spatial units get smaller, there is less chance for larger clusters to develop.

15.3.3 Radiance and power consumption

The relationship between power consumption and lit area, and radiance was tested for different countries in Europe. The relationship could not be tested at subnational scales due to a lack of suitable data at this level. The relationships were found to be very strong in log–log space. Areal relation-

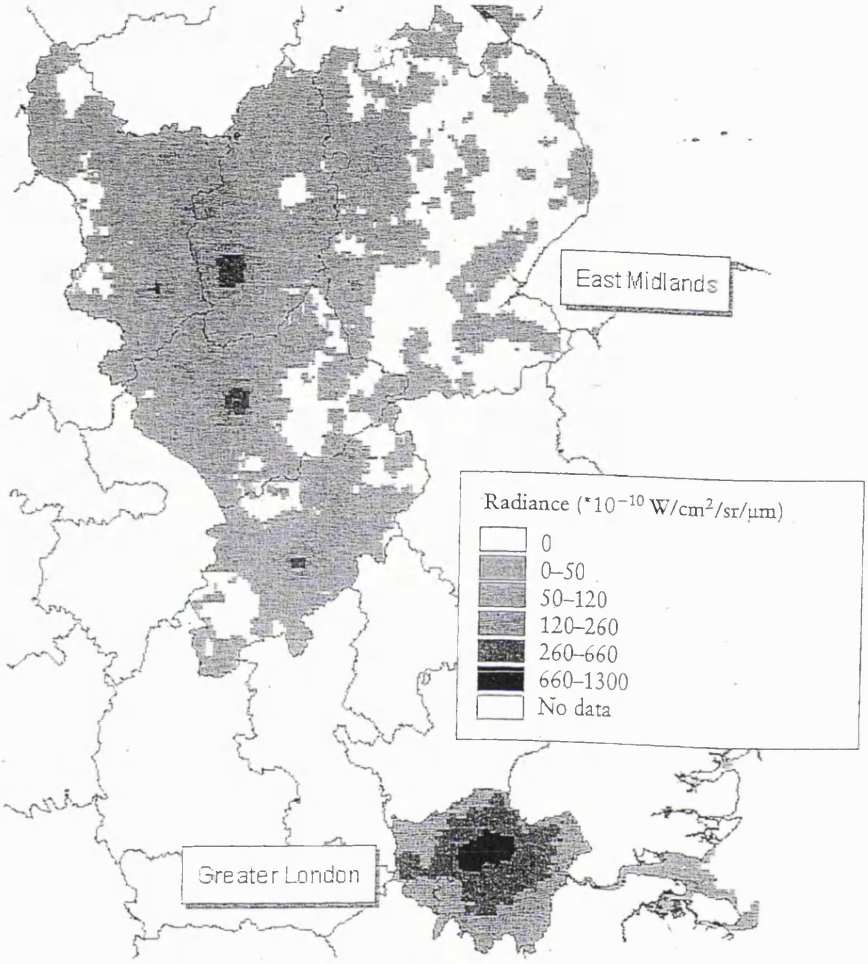

Figure 15.4 Comparison of Greater London with East Midlands. Though the East Midlands has more lit area and total radiance (Table 15.3), it only generates 43.5% of London's GDP.

ships performed marginally better than radiance ones ($R^2 = 0.91$ for area and $R^2 = 0.84$ for radiance). The law of allometric growth is observed in a host of geographic features from river morphology to volcanoes and also densely populated urban areas. Originally developed by biologists, it states that the rate of relative growth of an organ is a constant fraction of the rate of relative growth of the total organism (Nordbeck 1965). Taking 'y' to be the organ and 'x' to be the organism, the law of allometric growth can be expressed as $y = ax^b$. Taking the logarithm of both sides will linearize the equation thus:

$$\log y = b \log x + \log a$$

Welch (1980) previously investigated urban energy utilization patterns in the USA. A selection of US cities was mapped using the early DMSP OLS

sensor, from which three-dimensional surfaces were computed of the illuminated urban area. These volumes were found to correlate highly ($R = 0.89$) with energy consumption (kWh), the regression model again taking the $P = aAb$ allometric form. This suggests that the relationship of radiance to power consumption may be more robust to scale than for GDP. To map power consumption accurately at the subnational level, one has to make an assumption about what proportion of energy is being used for street and industrial/commercial lighting. Often this is not uniform across a country and also dependent on the location of heavy manufacturing and other industrial processes. The assumptions one is required to make are very similar to mapping of a related parameter: CO_2 emissions.

15.3.4 Radiance and CO_2 emissions

The discussion of critical factors concerning the mapping of GDP and power consumption can be extended to the monitoring of fossil fuel trace gas emissions. A first attempt at global mapping of this environmentally important parameter was discussed in Section 15.2 (see also Doll *et al.* 2000). The study confirmed that night-time lights appear to be a highly appropriate data set to use to disaggregate country level data. It was mentioned in the previous section that the poor agreement of the satellite-derived CO_2 map with the CDIAC estimates was possibly due to the mode of energy generation (e.g., nuclear, wind, solar) and how the energy produced was utilized. One has to consider what are the "invisible" energy uses, and how important they are in assessments. The disparate emission magnitudes between the two maps underline the requirement for a far more sophisticated model incorporating many more factors than just the relationship between lit area and emissions. Elvidge *et al.* (2000) described how this might be accomplished using a radiance-calibrated night-time lights data set. In the study Elvidge *et al.* (2000) presented a graph of cumulative brightness vs. energy-related carbon emissions for the forty-eight conterminous states of the USA, which showed that the two parameters are strongly positively correlated. Building on this result, they outlined the extensive ancillary data required to make sensible assumptions about distributing the data. It is likely that countries will also have to be grouped into those that are heavily reliant on fossil fuels, and therefore should have closer agreement with official estimates. It is also likely that GDP will be the key determinant of how to group these countries, as Sutton *et al.* (2001) has shown for population estimation using night-time imagery. Mapping of CO_2 emissions is potentially one of the most valuable applications of using night-time data, if it could be demonstrated to produce reliable and consistent results.

Terrestrial night-time lights can be attributed to three sources: biomass burning, gas flaring and human settlements. Their identification from

satellite imagery is facilitated due to their distinct spatial and temporal features. Biomass burning can be identified in forest areas by lights that have a short temporal duration. Aside from their location, gas flares have a limited spatial extent and are extremely bright. Elvidge *et al.* (2001) used DMSP OLS data to assess the areal extent of biomass burning in Roraima, Brazil, while other studies have sought to establish relationships between the thermal properties of the fire, the rate of biomass consumption (fuel load), and aerosol and trace gas emissions also from satellite sensor data (Kaufman *et al.* 1998b). These figures are not currently included in estimates of fossil fuel consumption.

In addition to the CDIAC data used earlier, the International Energy Agency provides data on national levels of fossil fuel consumption. These data are also broken down into estimates of fossil fuel types used for electrical power generation, industrial, commercial, transportation and residential use. This is a very useful starting point but only addresses part of the problem. These data still have to be disaggregated. This can be done by incorporating further data sets such as power station locations for the electrical power generation component and road networks for the transportation component. In particular, night-time lights can be used to weight this distribution around bright urban centres. The spatial distribution from international air travel may be distributed according to the sectors with the densest traffic (Penner *et al.* 1999). Other emission sources may be distributed according to the location and brightness of night-time light imagery. This results in four emission submaps that may be easily combined in a GIS to produce a global, high spatial resolution emission map.

15.4 Other applications for night-time satellite imagery

Night-time light imagery has been used for a number of other applications besides mapping socio-economic parameters. The examples below represent three of the most recent developments using DMSP OLS data.

15.4.1 DMSP OLS data for urban mapping

Any regional scale image of night-time light data will reveal lit areas extending along transportation networks and along coastlines, which even the untrained observer can associate with human settlement. Using these data as a measure of urban land cover is therefore one of its most obvious applications. Doll and Muller (1999b) have compared it with the Digital Chart of the World's urban polygons, while Elvidge *et al.* (1997) and Imhoff *et al.* (1997) describe how DMSP OLS data relate to urban boundaries from US Census data. Urban land cover is notoriously difficult to map from conventional optical remotely sensed data at the appropriate scale for global applications. There are numerous issues where an accurate map of urban

areas would be hugely beneficial. Night-time imagery acquired from the DMSP OLS sensor has gone a long way to addressing this requirement. Owen *et al.* (1998) used DMSP OLS data for urban categorization in order to correct meteorological records for urban heat island bias. In the same way urban land cover as described by DMSP OLS data have been used by Imhoff *et al.* (2000) to assess the impact of urbanization on primary productivity.

Frequency composite DMSP OLS data from 1994–95 were used to identify urban and peri-urban land cover. Using a technique the authors developed in a previous study (Imhoff *et al.* 1997), wholly urban areas were classified as those being detected as lit 89 per cent of the time from cloud-free observations. Peri-urban areas were classified as those lit 5–88 per cent of the time. This map of urbanized lands was then geo-spatially combined with a US Geological Survey land cover map and a year's worth of Normalized Difference Vegetation Index data (NDVI) within a GIS. The NDVI is defined as the sum of the visible and near-infrared channels divided by its difference and has been shown to provide a reasonable estimate of absorbed photosynthetically active radiation (Asrar *et al.* 1984). Monthly maximum NDVI data sets over a year were averaged within the three classes of urban land cover. Each month's data were multiplied by the number of days in that month to provide a comparable unit (NDVI * days) which when summed over the whole year represents annual primary production. The effect of urbanization at the continental scale is generally found to cause a decrease in photosynthetic activity when compared with surrounding areas. Analysing individual cities, however, revealed that urbanization could in fact have a positive effect on primary productivity especially in cities with a strongly seasonal climate. The urban heat island effect was found to maintain a higher level of photosynthetic production for places like Chicago. Increased primary productivity in urban areas was also attributed to new species introduced and supported by irrigation in cities located in an otherwise resource-limited environment.

The effect of urbanization on primary productivity was found to be related to the climatic and physiographic environment of the city. Peri-urban areas had the highest degree of primary productivity and are also those that lie in the path of urban sprawl. Imhoff *et al.* (2000) estimates a loss of 10 NDVI * days of photosynthetic production should these lands become fully urbanized.

15.4.2 DMSP OLS data for creation of a night-time atlas of light pollution

Probably the most intuitive use of night-time data is to use it to map and quantify the amount of light pollution. Our limited view of the Universe has had a profound influence on human development. It serves as a constant reminder to consider the nature of our existence and begs questions, which we may never be able to answer. However, a clear view of the night sky for

those who live in the developed world is a rapidly disappearing occurrence. Cinzano *et al.* (2001) set about using the DMSP OLS radiance-calibrated night-time light data set to quantify artificial night sky brightness. Light propagation from the top of the atmosphere radiances present in the DMSP OLS product was modelled through Rayleigh scattering by molecules, Mie scattering by aerosols, atmospheric extinction along light paths and Earth curvature. Hence, many areas that appear dark in the night-time light product due the absence of a ground level light source are in fact affected by light pollution from adjacent bright areas. In some cases the source of the pollution is from a neighbouring country. Cinzano *et al.* (2001) intersected their atlas of light pollution with the LandScan2000 global population density database (Dobson *et al.* 2000) to assess the number of people affected. The extent of this pollution is so widespread across the developed world that more than 99 per cent of the population of the EU and USA, and 66 per cent of the entire world population suffer from some degree of light pollution. In particular about half the population of the developed world do not have the possibility of viewing the Milky Way with the naked eye.

15.4.3 Modelling the development of night-time lights

The modelling of the development of night-time light is of use to all the applications discussed in this and previous chapters. The ability to predict future scenarios of the spatial distribution of night-time lights and, by association, economic activity could greatly aid transport and energy infrastructure planning, as well as environmental impact assessments. This would be particularly beneficial for developing countries. Night-time satellite imagery is well suited for cell-based modelling, not only because of its raster format, but also because it is flexible within a range of rules and assumptions that can be incorporated into a model.

Plutzar *et al.* (2000) used a cellular automata model to simulate the growth of night-time lights in China. A cellular automata model consists of a regular, discrete lattice of cells. Each cell is characterized by a state taken from a finite set of states. Evolution takes place at discrete time steps and each cell evolves according to the same rule, which depends only on the state of the cell and a finite number of neighbouring cells (Weimar 1998). The model incorporated not only night-time lights but also terrain, population and transport infrastructure data sets. Probability surfaces were generated and the weighted mean was computed to combine these surfaces. A probability surface was also generated from the night-time light data. This was based on an annular region around a cell. The higher the focal sum of this region, the higher the probability the target cell will change. The focal sum of the region can be weighted such that cells at the edge of the region have less influence in the computation. The model was run to calculate pixels that have both intensified in value, and changed state from being unlit to lit. The generated layers of changed cells are summed with non-changing

cells and compared with a predefined limit to determine whether the layer will serve as an input for the next iteration of the model or be output as the result. The model shows an intensification of night-time light between Beijing and Shanghai, and expansion along the coast and around Hong Kong.

15.5 Prospects

The discussion up to now has exclusively dealt with night-time satellite imagery from the low-resolution DMSP OLS sensor as it is currently the only spaceborne sensor that is sufficiently sensitive to detect anthropogenic lighting activity from space. However, the Airborne Visible/Infrared Imaging Spectrometer (AVIRIS) can also be used to acquire high spatial resolution data over individual cities. The AVIRIS sensor is a hyperspectral imaging system which senses in 224 very narrow bands (~10 nm) from 0.41–2.45 mm. It is designed to fly on board NASA's U2 aircraft where, at an altitude of 20 km, it can image 20-m pixels over a 10-km swathewidth (Porter and Enmark 1987). This additional data source offers not only the advantage of an enhanced spatial resolution, but also of enhanced spectral resolution too. The exclusivity of DMSP OLS data as a source of night-time imagery has forced researchers to use it at the continental–global level without fully understanding the contributions of different light sources at the subpixel level. AVIRIS data could address this issue. A test flight over Las Vegas in 1998 suggests that there are distinctive spectral signatures over the city (Elvidge and Jansen 1999). Combining these two data sources would be of use to help understand what the DMSP OLS data is really showing at the small scale, and therefore aid the assumptions one makes in macroscale models using night-time imagery. There are various types of lighting used in cities. Each has distinct spectral characteristics depending on the element used. Commonly used types of high-intensity discharge light are high-pressure sodium used for street lights, mercury vapour and metal halide used for illuminating car parks and sports stadiums. Figure 15.5 shows a sample spectral plot from a low-altitude (around 4,000 m) acquisition over Las Vegas. Of note is a very strong signal in Band 18 (536 nm). Plots such as these could aid better estimation of energy usage. Mapping spectral patterns over cities could help to identify patterns of residential, commercial and industrial land use (Elvidge and Jansen 1999). This could be one way of filtering out the population component if concerned with assessing areas of high economic activity. In addition to this, the vastly superior spectral resolution of AVIRIS may be of use to correct night-time data atmospherically.

Temporal data sets of night-time lights will permit the analysis of relationships and help to identify urban growth patterns, which will serve as a record on urbanization patterns across the Earth. This will in turn allow

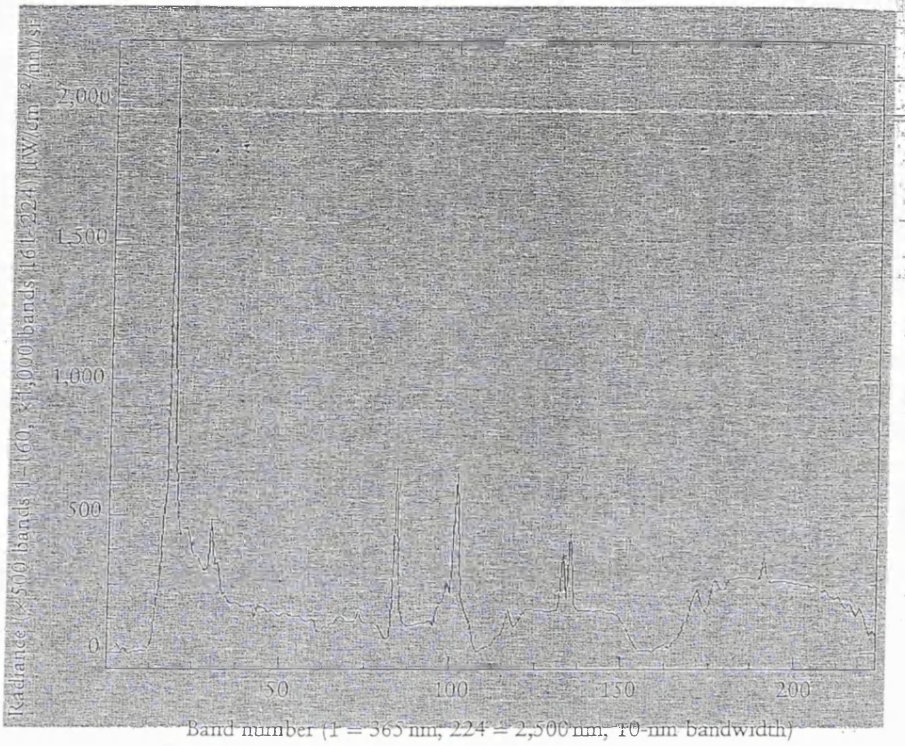

Figure 15.5 Spectral plot for a lit pixel over 224 10-nm bands from AVRIS taken over Las Vegas on the night of 5 October 1998.

more accurate assumptions to be made when setting up the models. Cellular automata modelling techniques provide a useful means to examine the future impacts of urban growth. A study has been carried out to model the urban growth of San Francisco (Clarke *et al.* 1997). In this model, the control parameters (transportation, topography, etc.) were allowed to develop with urban area, thereby providing an extra feedback into the model. It also used a time series of historical boundary data to calibrate the model. Night-time light data could also be used for this application. While the estimation of socio-economic parameters mentioned in this chapter is an important application of night-time imagery, it must also be realized that this can be used in a predictive capacity when coupled to a growth model. Taken together, these activities represent the best chance to advance research and provide better results from DMSP OLS night-time data.

15.6 Conclusions

The research presented here has extended the current body of results showing correlations between night-time lights and various socio-economic

and environmental parameters at the country level to include finer scale relationships. Generally, it was found that the simple relationships built up at the country level are not as strong when compared with data at the subnational level. This has been attributed to the oversimplicity of the model to describe the disparities in the subregional economy. The use of a weighted radiance model is regarded as a possible solution.

If night-time imagery is to be used for mapping, then the conceptual issue of what the lights are actually showing must be considered. High spatial resolution night-time data could help to solve this problem. Once this has been set in a framework one can begin to deal with the range of assumptions for which there is often no data publicly available. Night-time light imagery can be used to estimate a range of parameters, but there is a requirement for much ancillary data, to distribute and calibrate relationships. GIS plays a fundamental role throughout the whole process. Its value is not limited to mapping, but has been shown to be of great help in the development of more complex models where a range of external data sources are required. With these considerations in mind, this unique remotely sensed data source provides the potential to advance mapping beyond what we currently assume to be the remit of environmental remote sensing.

15.7 Acknowledgements

The author wishes to thank Chris Elvidge for supplying the DMSP OLS and AVIRIS data, and Prof. Jan-Peter Muller and Jeremy Morley for their comments and advice in preparing this manuscript. Acknowledgement is also due to the Office of National Statistics for supplying data tables on economic statistics for the UK and European power consumption.

15.8 References

Andres, R. J., Marland, G., Fung, I., Matthews, E. and Brenkert, A. L., 1996, Geographic patterns of carbon dioxide emissions from fossil-fuel burning, hydraulic cement production, and gas flaring on a one degree by one degree grid cell basis: 1950 to 1990. *Global Biogeochemical Cycles*, 10, 419–29.

Asrar, G. S., Fuchs, M., Kanemasu, E. T. and Hatfield, J. L., 1984, Estimating absorbed photosynthetically active radiation and leaf area index from spectral reflectance in wheat. *Agronomy Journal*, 76, 300–6.

Cinzano, P., Falchi, F. and Elvidge, C. D., 2001, The first world atlas of the artificial night sky brightness. *Monthly Notices of the Royal Astronomical Society*, 328(3), 689–707.

Clarke, K. C., Gaydos, L. and Hoppen, S., 1997, A self-modifying cellular automaton model of historical urbanization in the San Francisco bay area. *Environment and Planning B*, 24, 247–61.

Croft, T. A., 1978, Night-time images of the Earth from space. *Scientific American*, 239, 68–79.

Dobson, J. E., Bright, E. A., Coleman, P. R., Durfee, R. C. and Worley, B. A., 2000, LANDSCAN: A global population database for estimating population at risk. *Photogrammetric Engineering and Remote Sensing*, 66, 849–57.

Doll, C. N. H. and Muller, J-P., 1999a, The use of radiance calibrated data to improve remotely sensed population estimation. Paper given at Conference of the Remote Sensing Society, Cardiff, pp. 127–33.

Doll, C. N. H. and Muller, J-P, 1999b, An evaluation of global urban growth via comparison of DCW and DMSP-OLS satellite data. *Proceedings of the IEEE International Geoscience and Remote Sensing Symposium, IGARSS '99*, Hamburg, Germany (Piscataway, NJ: IEEE), 1134–6.

Doll, C. N. H., Muller, J-P. and Elvidge, C. D., 2000, Night-time imagery as a tool for mapping socio-economic parameters and greenhouse gas emissions. *Ambio*, 29, 159–64.

Elvidge, C. D. and Jansen, W. T., 1999, AVIRIS observations of nocturnal lighting. *AVIRIS Airborne Geosciences Workshop Proceedings* (http://popo.jpl.nasa.gov/docs/workshops/99docs/16.pdf).

Elvidge, C. D. and Wlarave, W. T., 1999, AVIRIS observations of nocturnal lighting. *AVIRIS Airborne Geosciences Workshop Proceedings* (http://popo.jpl.nasa.gov/docs/workshops/99_docs/16.pdf).

Elvidge, C. D., Baugh, K. E., Kihn, E. A., Kroehl, H. W., Davis, E. R. and Davis, C. W., 1997, Relation between satellite observed visible–near infrared emissions, population, economic activity and power consumption. *International Journal of Remote Sensing*, 18, 1373–9.

Elvidge, C. D., Imhoff, M. L. and Sutton, P. C., 2000, Relation between fossil fuel trace gas emissions and satellite observations of nocturnal lighting. Paper given at Conference of IAPRS, Vol. XXXIII, Part B7 (Amsterdam: GITC), pp. 397–401.

Elvidge, C. D., Hobson, V. R., Baugh, K. E., Dietz, J. B., Shimabukuro, Y. E., Krug, T., Novo, E. M. L. M. and Echavaria, F. R., 2001, DMSP-OLS estimation of tropical forest area impacted by surface fires in Roraima, Brazil: 1995 versus 1998, *International Journal of Remote Sensing*, 22, 2661–73.

Imhoff, M. L., Lawrence, W. T., Stutzer, D. C. and Elvidge, C. D., 1997, A technique for using composite DMSP/OLS "city lights" satellite data to accurately map urban areas. *Remote Sensing of Environment*, 61, 361–70.

Imhoff, M. L., Tucker, C. J., Lawrence, W. T. and Stutzer, D. C., 2000, The use of multisource satellite and geospatial data to study the effect of urbanization on primary productivity in the United States. *IEEE Trans. Geoscience and Remote Sensing*, 38, 2549–56.

Kaufman, Y. J., Herring, D. D., Ranson, K. J. and Collatz, G. J., 1998a, Earth observing system AM1 mission to Earth. *IEEE Trans. Geoscience and Remote Sensing*, 36, 1045–55.

Kaufman, Y. J., Justice, C. O., Flynn, L. P., Kendall, J. D., Prins, E. M., Giglio, L., Ward, D. E., Menzel, W. P. and Setzer, A. W., 1998b, Potential global fire monitoring from EOS-MODIS. *Journal of Geophysical Research-Atmospheres*, 103, 32215–38.

Li, Y-F., 1996, *Global Population Distribution (1990), Terrestrial Area and Country Name Information on a One by One Degree Grid Cell Basis*, ORNL/CDIAC-96, DB1016 (Oak Ridge, TN: Carbon Dioxide Analysis Center) (http://cdiac.esd.ornl.gov/ndps/db1016.html).

Li, Y-F., McMillan, A. and Scholtz, M. T., 1996, Global HCH with 1° × 1° longitude/latitude resolution. *Environment Science Technology*, 30, 3525–33.

Matthews, E., 1983, Global vegetation and land use – new high-resolution databases for climate studies. *Journal of Climate and Applied Meteorology*, 22, 474–87.

ONS, 2002, The Office of National Statistics (http://www.statistics.gov.uk).

ORNL/CDIAC, NDP-058a. *Carbon Dioxide Emission Estimates from Fossil-fuel Burning, Hydraulic Cement Production, and Gas Flaring for 1995 on a One-Degree Grid Cell Basis*. (Oak Ridge, TN: Carbon Dioxide Analysis Center) (http://cdiac.esd.ornl.gov/ftp/ndp058a/).

Openshaw, S., 1984, *The modifiable areal unit problem. Concepts and Techniques in Modern Geography 38* (Norwich, UK: GeoBooks).

Owen, T. W., Gallo, K. P., Elvidge, C. D. and Baugh, K. E., 1998, Using DMSP-OLS light frequency data to categorize urban environments associated with US climate observing stations, *International Journal of Remote Sensing*, 19, 3451–6.

Penner, J., Lister, D., Griggs, D. J., Dokken, D. and McFarland, M. (eds), 1999, *Aviation and the Global Atmosphere: Special Report on the Intergovernmental Panel on Climate Change* (Cambridge: Cambridge University Press).

Porter, M. and Enmark, H. T., 1987, A system overview of the Airborne Visible/Infrared Imaging Spectrometer (AVIRIS) (http://popo.jpl.nasa.gov/docs/aviris87/A-PORTER.PDF).

Plutzar, C., Grubler, A., Stojanovic, V., Reidl, L. and Pospishil, W., 2000, A GIS approach for modelling the spatial and temporal development of night-time lights. In J. Stobl, T. Blasshke and G. Griesebner (eds) *Angewandte Geographische Informationsverarbeitung XII* (Heidelberg, Germany: Wichman Verlag), pp. 389–94.

Southwell, K., 1997, Remote sensing; night lights. *Nature*, 390, 21.

Sullivan III, W. T., 1989, A 10 km image of the entire night-time Earth based on cloud-free satellite photographs in the 400–1100 nm band. *International Journal of Remote Sensing*, 10, 1–5.

Sutton, P. C., Roberts, D., Elvidge, C. and Baugh, K., 2001, Census from heaven: An estimate of the global human population using night-time light satellite imagery. *International Journal of Remote Sensing*, 22, 3061–76.

Tobler, W. R., 1969, Satellite confirmation of settlement size coefficients. *Area*, 1, 31–4.

UNEP/UNDP, 1994, *Report of the International Symposium on Core Data Needs for Environmental Assessment and Sustainable Development Strategies* (Bangkok, Thailand: UN).

Weimar, J., 1998, Simulations with cellular automata (http://www.tu-bs.de/institute/WiR/weimar/Zascriptnew/intro.html).

Welch, R., 1980, Monitoring urban population and energy utilization patterns from satellite data. *Remote Sensing of Environment*, 9, 1–9.

World Resources Institute, Earthtrends Database (http://earthtrends.wri.org).